PARALLEL SYNTHESIS OF SMALL MOLECULE COMPOUND LIBRARIES: ISOFORM SELECTIVE RHO-KINASE INHIBITORS

by

Safwat Mohamed

B.Pharm., Assiut University, Egypt 2000

M.Sc., Assiut University, Egypt 2006

A THESIS SUBMITTED IN PARTIAL FUFILLMENT OF
THE REQUIREMENTS FOR THE DEGREE OF

DOCTOR OF PHILOSOPHY

in

The Faculty of Graduate and Postdoctoral Studies
(Pharmaceutical Sciences)

THE UNIVERSITY OF BRITISH COLUMBIA

(Vancouver)

August 2015

Abstract

The objective of this thesis was to use parallel synthesis to build small molecule libraries of novel compounds with potential as isoform selective type II rho-kinase (ROCK1/2) inhibitors. Considerable effort is ongoing to identify isoform selective ROCK inhibitors, as hyperactivity of the ROCK is implicated in cardiovascular diseases, cancer, diabetes and many other diseases that affect millions of Canadians, and billions of people worldwide.

In the absence the extensive structural details of the type II kinase inhibitor binding mode, we have used an empirical approach to the design of type II ROCK inhibitors, based on the conception that such molecules correspond to elongated structures with H-bonding functional elements in their central portion, a motif at one end that mimics the adenine ring in ATP, and a hydrophobic moiety at the other end of the molecule that will interact with an allosteric pocket in the ATP binding region of the kinase. Based on these very general structural requirements, eleven different representative libraries of novel compounds (not described in CAS) were designed and synthesized. In the initial series of compounds, a 2-pyridinone motif was employed as the hinge binding element, and the central portion corresponded to carboxamide substituted oxazoline, oxadiazole, or 2-aminothiazole system, joined through the amide bond to a set of structurally diverse aromatic, heteroaromatic and benzylamine subunits, corresponding to the diversity elements. The preliminary assay results demonstrated that, overall, these compounds were weak and non-selective ROCK1/2 inhibitors when compared to H-1152 as a positive control at 10 μM concentration. However, further structural modification revealed the interest in using an indazole motif as the hinge binder in conjunction with the 2-aminothiazole carboxamide linker. Indeed, more potent activities were observed in the single point assay for a significant portion of the libraries of molecules built around these structural components. Further evaluation of 18 active compounds in a 10-point assay, by Invitrogen, to determine IC50's revealed that indazole-based inhibitors are active at low micromolar concentrations (1-10 μM), but do not display any significant isoform selectivity.

Preface

This dissertation is submitted for the degree of Doctor of Philosophy at the University of British Columbia. The research described in this dissertation was performed under the supervision of Professor David Grierson in the Department of Pharmaceutical Sciences, University of British Columbia, between January 2009 and January 2015.

With guidance and supervision from Dr. Grierson, I was responsible for the planning, designing, and conducting all of the chemistry experiments, data analysis, and interpretation of the results. The biological assays were conducted in Dr. Kathleen MacLeod laboratory by Dr. Guorong Lin. To the best of my knowledge, this work is original except where references are made to previous work. The cited figures in my thesis are used with permission from applicable sources.

This work was financia1ly supported by the Egyptian government in the first two years (Jan 2009-Jan 2011) in the form of scholarship (Egyptian Channel System).

Table of Contents

List of Tables

List of Figures

List of Symbols and Abbreviations

ABL1	Abelson murine leukemia viral oncogene homolog 1
ACN	Acetonitrile
ADP	Adenosine diphosphate
AGC	Protein kinases A, G, and C
AIDS	Acquired immunodeficiency syndrome
AMPA	α-Amino-3-hydroxy-5-methyl-4-isoxazolepropionic acid receptor
AKT	Protein kinase B
Ar	Aryl
ATP	Adenosine triphosphate
Bcr-Abl	Breakpoint cluster region- Abelson murine leukemia virus
Boc	*tert*-Butoxy carbonyl
BOP-Cl	Bis-(2-oxo 3-oxazolidinyl)phosphonic chloride
Braf	B-Raf proto-oncogene, serine/threonine kinase
br s	Broad singlet
^{13}C	Carbon NMR
^{o}C	Degrees Celsius
calcd.	Calculated
CAS	Chemical Abstracts Service
CCK	Cholecystokinin
Cdc42	Cell division control gene
CDK	Cyclin-dependent kinase
CML	Chronic myeloid leukemia
CNS	Central nervous system
CRD	Cysteine Rich Domain
CyCl	Cyanuric chloride

d	Doublet
dd	Doublet of doublets
ddd	Doublet of doublet of doublets
DAPK	Death-associated protein kinase
DAST	Bis(2-methoxyethyl) amino-sulfur trifluoride
DBU	1,8-Diazabicyclo[5.4.0]undec-7-ene
DCM	Dichloromethane
DFG	Asp-Phe-Gly
DHA	Diheteroaryl amides
DHP	Dihydropyridine
DIAD	Diisopropyl azodicarboxylate
DIEA	Diisopropylethylamine
DMF	Dimethylformamide
DMF-DMA	*N*,*N*-Dimethylformamide dimethoxyacetal
DMAP	4-(Dimethylamino)pyridine
DMSO-d_6	Deuterated dimethylsulfoxide
DOS	Diversity-oriented synthesis
EDC	1-Ethyl-3-(3-dimethylaminopropyl)carbodiimide
EDCF	Endothelium-derived constricting factors
EDRF	Endothelium-derived relaxing factors
EGFR	Epidermal growth factor receptor
ELISA	Enzyme-linked immunosorbent assay
eNOS	Endothelial nitric oxide synthase
equiv.	equivalents
ESI	Electrospray ionization
et al.	Et alii, and others
EtOAc	Ethyl acetate

EtOH	Ethanol
FDA	US Food and Drug Administration
FGFR	Fibroblast growth factor receptor
FP	Front pocket
FRET	Fluorescence resonance energy transfer
g	Gram(s)
GAPs	GTPase-activating proteins
GDP	Guanosine diphosphate
GDI	Guanine nucleotide dissociation inhibitor
GEF	Guanine nucleotide exchange factor
GTP	Guanosine triphosphate
GTPases	Guanosine triphosphatase
GSK	Glycogen synthase kinase
h	Hour(s)
^{1}H	Proton NMR
HATU	1-[Bis(dimethylamino)methylene]-1H-1,2,3-triazolo[4,5-b]pyridinium 3-oxid hexafluorophosphate
HBTU	O-Benzotriazole-N,N,N`,N`-tetramethyl-uronium-hexafluorophosphate
HCV	Hepatitis C virus
HIV	Human immunodeficiency virus infection
HOAt	1-Hydroxy-7-aza-benzotriazole
HOBT	Hydoxybenzotriazole
HRMS	High resolution mass spectrometry
Hyp	Hydrophobic pocket
HTS	High-throughput screening
Hz	Hertz
IC_{50}	Inhibitory concentration 50

IP3K	Inositol 1,4,5-trisphosphate 3-kinase
J	Coupling constant
K_m	Michaelis constant
L	Liter
LIMK	LIM kinase
LTCC	L-Type Calcium Channel
µ	Micro
µL	Microliter
µM	Micromole
M	Molar
m	Multiplet
MAPK	Mitogen-activated protein kinases
MBS	Myosin binding subunit
MCR	Multi-component reaction
Me	Methyl
MeOH	Methanol
mg	Milligram
MHz	Mega hertz
min	minutes
mL	Milliliter
MLCK	Ca^{2+}-calmodulin-dependent myosin light chain
MLCP	Myosin light chain phosphatase
mmol	Millimole
mol	Mole
MS	Mass spectrometry
MSK	Mitogen and stress activated protein kinase
MW	Microwave irradiation

MYPT	Myosin phosphatase target subunit
m/z	Mass to charge ratio
NMR	Nuclear magnetic resonance
NO	Nitric oxide
P38	P38 mitogen-activated protein kinases
P450	Cytochromes P450
PDE	Phosphodiesterase
Ph	Phenyl
PG	Protecting group
PKA	Protein kinase A
PKC	Protein kinase C
PH	Pleckstrin Homology
ppm	Parts per million
PyBOP	Benzotriazol-1-yl-oxytripyrrolidinophosphonium hexafluorophosphate
q	Quartet
Rac1	Ras-related C3 botulinum toxin substrate 1
RBD	Rho Binding Domain
Rho	Small G protein Rho
ROCK	Rho-Associated, coiled-coil containing protein Kinase
rt	Room temperature
s	Singlet
SAR	Structural activity relationship
SI	Selectivity index
S_NAr	Nucleophilic aromatic substitution
SR	Serine/arginine-rich proteins
Src	Proto-oncogene tyrosine-protein kinase
SRSF1	Serine/arginine-rich splicing factor 1

STZ	Streptozotocin
Syk	Spleen tyrosine kinase
t	Triplet
t	Tert
TBAF	Tetrabutylammonium fluoride
TBS	*tert*-Butyldimethylsilyl
TCDI	1,1'-Thiocarbonyldiimidazole
Tec	Tyrosine-protein kinase Tec
TFA	Triflouoacetic acid
THF	Tetrahydrofuran
TLC	Thin layer chromatography
Ts	Tosyl
*p*TsOH	p-Toluenesulfonic acid
UBC	The University of British Columbia
VEGFR	Vascular endothelial growth factor receptor

Acknowledgments

First and foremost, I would like to express my gratitude to Professor David Grierson, my supervisor, for accepting me as a graduate student in his laboratory, for his constant support and encouragement over the years. Also thank, Dr. Grierson, for giving me the opportunity to be the first doctoral student to graduate from his laboratory at UBC, and most importantly for his patience with me. I am really proud to have worked under his supervision because he taught me invaluable lessons which equipped me with the required basics to be able to start my scientific journey. I hope I will continue to live up to his expectations. Words are inadequate to thank all members of Dr. Grierson lab, past and present, for their friendship and support. I will never forget our insightful discussions every Thursday morning in our lab meetings. I would not have been able to go forward without their help and constructive critiques.

Second, I would like to thank our collaborator Professor Kathleen MacLeod for her willingness to run the biological testing in her lab, and Dr. Guorong Lin, for running the biological assays and troubleshooting when nothing appeared to be working as it should.

A special thanks to the members of my committee, including my chair Professor Wayne Riggs, for their helpful suggestions and constructive comments throughout the years of my thesis. In particular, I would like to thank Professor Glenn Sammis for teaching me advanced organic chemistry topics in his interesting course Chemistry 566.

I would like to thank the Egyptian government, the Mission office, and El-Minia University for funding my research in the first two years.

I am thankful to Dr. Markus Heller from CDRD for his assistance in running NMR samples, and Andras Szeitz for his assistance with mass spectroscopy. I would also like to extend my thank-you's to the administrative office of UBC Pharmaceutical Sciences. Also, I would like to thank Jamal Kurtu for his continuous support. I would like to forward my appreciation to all of my friends, past and present, especially Hesham Soliman who helped me a lot during my journey. Finally, I will close out by thanking my wife for her endless support and encouragement. I am eternally grateful to her for her sacrifices that helped to make my dream come true.

This thesis is dedicated to my mother, my wife, and my two sons (Muhammad and Omar) for their endless support and prayers

Chapter 1

Introduction

1.1 Drug Discovery and Compound Libraries

The development of rapid readout *in vitro* and cellular assay protocols for biological targets of therapeutic interest (e.g. enzyme, receptor, nucleic acids) and their integration into robotic platform technologies for the high-throughput screening (HTS) of large sets of molecules heralded the beginning of a new paradigm in drug discovery.[1,2] Prior to this point, biologically active compounds were almost exclusively discovered using assays designed to test one molecule, or small groups of molecules at a time. The subsequent optimization of an active "hit" to produce a "lead" compound required the synthesis of analogues of the primary hit.[3-5] This process, referred to as a structure-activity relationship (SAR) study, involved making small modifications in the hit structure and evaluation of how these changes impact activity. In this way, making a series of incremental changes in the hit structure helps, on the one hand, to determine what modifications enhance or diminish activity/target affinity, and, on the other hand, it provides crucial information concerning the composition of the active molecule binding site. Although the SAR strategy has proven hugely successful for the development of a large number of therapeutics, in the modern context this iterative activity driven approach to drug discovery is too time consuming and incompatible with the advent of HTS. To respond to the technological challenge HTS represented, industry countered by systematically reevaluating in-house libraries against new therapeutic targets. Further, both industrial and academic laboratories engaged in the development of combinatorial chemistry and parallel synthesis techniques, whereby a sequence of reactions and/or functionalized (privileged) scaffolds could be used to create new and structurally diverse chemical entities imbued with drug-like properties. Small molecule libraries can be used as a chemical-biology tool to explore biology space.[6] Indeed, it was recognized, that traditional drug development programs created molecules around a specific objective, and therefore explored only a tiny part of the supposedly almost infinite number of variations in the nature of interactions that could exist between a protein and small molecules. The underlying tenant in the compound library approach is that testing diversity libraries against all new, and established, targets of therapeutic interest would reveal

new and unimagined molecules displaying biological activity. Importantly, these discoveries serve as the starting point for new drug development programs. In essence, this approach corresponds to the synthetic chemists complement to what nature has achieved through the assembly of complex natural products, which has fueled the development over the past century of a myriad of drugs (antibiotics, anticancer agents, etc.). The fundamental paradigm shift that has occurred following efforts to explore the utility of compound libraries in drug discovery is that, in contrast to the traditional SAR approach, diversity driven small molecule library synthesis generally precedes biological evaluation, rather than being guided by it.

1.2 Pharmaceutical Industry In-House Libraries and HTS

Essentially all pharmaceutical companies have "in-house libraries", which have been built up over decades from directed (SAR driven) medicinal chemistry efforts around particular pharmacophores. Indeed, the process of taking a hit molecule through the drug development pipeline to identify a clinical candidate level generally involves the synthesis and screening of 500 to >1000 molecules. As only one molecule finds application in each case, the other "failed" molecules comprise the in-house library.[7] These libraries, or a selection from these libraries, are systematically retested using HTS against new, or other established therapeutic targets. In this way screening series of phenylaminopyrimidines and anilinoquinazolines ultimately led to the development of kinase inhibitors imatinib **I** (Bcr-Abl inhibitor) and gefitinib **II** (EGFR inhibitor), respectively (**Figure 1**).[8,9] Similarly, HTS was at the origin of discovery of many other drugs and drug candidates such as eltrombopag **III** (thrombopoietin receptor agonist) and BMS-858 **IV** (HCV inhibitor in clinical trials) (**Figure 1**).[9,10]

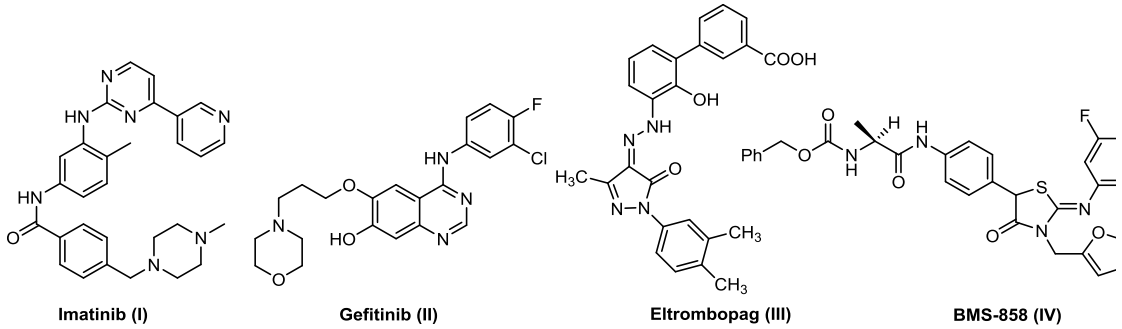

Figure 1: Drugs identified in high-throughput screening.

Interestingly, marketed drugs are often included in new screening programs, as even marketed drugs display "off-target effects" that may be of therapeutic interest.[11] The advantage in finding

a new application for an existing drug is that their *in vivo* properties are already optimized (low molecular weight molecules (<500 Da), ability to cross biological membranes, and good solubility in water and dimethyl sulphoxide, etc.[12] Indeed, most drug candidates (up to 90%) fail to reach the market due to problems encountered during *in vivo* evaluation phase. A potential disadvantage of in house libraries is that they comprise large numbers of analogues of specific hit structures, and although the number of molecules in the library may be large, they are limited in structural diversity, i.e. they explore only a small part of chemical-biology space.

1.3 Combinatorial Chemistry - Parallel Synthesis and Structural Diversity

Under the pressure of HTS, many innovative advances have been made to construct libraries and to optimize their diversity. In concept, "combinatorial library synthesis" refers to the production of mixtures of compounds, obtained by reacting sets of reacting partners (building blocks) with each other in the same reaction vessel.[13] For example, the reaction of a set of amines with a set of carboxylic acids in the presence of a peptide coupling reagent will, in principle, result in the formation of a mixture of all possible amide products. This amide bond forming reaction can also be an integral part of different multi-component reaction (MCR) processes (ex. Ugi reactions) (**Figure 2**).[14]

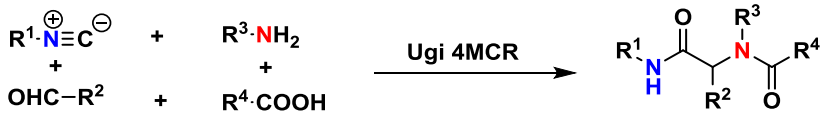

Figure 2: Ugi reaction for the generation of amide bond.

The interest in the combinatorial chemistry strategy is that, even in a single operation, a very diverse set of reaction components can be engaged, and the result is the formation of a complex and equally diverse set of product molecules that are tested together.[15] However, a drawback to the combinatorial approach is the necessity, when biological activity is found, to separate the library constituents from each other in order to identify the active component. Although ingenious strategies have been developed to deconvolute compound libraries, this process is time consuming relative to the alternative parallel synthesis approach to small molecule library construction.[16] In the parallel synthesis version of combinatorial chemistry all combinations of the reactions are carried out simultaneously (i.e. in parallel), but importantly, they are carried out in separate reaction vessels. Thus, in contrast to the combinatorial chemistry, each reaction vessel will contain a single predetermined product. Parallel synthesis can be significantly

accelerated using robotic technology, and when optimally planned, product purification is simplified, and in some cases unnecessary.[17] Today, the combinatorial chemistry approach has been largely surpassed by the use of parallel synthesis strategies to construct small molecule libraries of "drug-like" molecules in a minimum timeline.

In its multiple applications, parallel synthesis has been used to identify new ligands that bind and modulate the function of known families of proteins, such as kinases, G-protein coupled receptors, proteases, and ion channels.[18] Importantly, it finds its full potential in the construction of libraries of molecules for testing against protein targets of therapeutic interest for which there is little or no structural information available. Further, structural comparison of active and no-active molecules in a compound library provides a preliminary glimpse at SAR.[19]

Looking at combinatorial chemistry-parallel synthesis more closely, one sees that large collections of molecules having diverse structure and functionality can be prepared from simple starting materials.[20] In these libraries structural complexity/diversity can be efficiently generated in four ways: a) skeleton (scaffold) diversity by incorporation of different core structures in the library, b) functional group diversity by varying functional groups, c) appendage diversity (or building-block diversity) through variation in structural elements around a common skeleton or functional group, d) stereochemical diversity through variation in the orientation of the elements that interact with the macromolecules.[21-23] Grouping combinatorial chemistry-parallel synthesis together under the term "diversity-oriented synthesis" (DOS), one sees that DOS is a powerful and efficient tool for generating libraries of complex and diverse molecules.[21,22] As practiced in our laboratory, parallel synthesis is used to generate libraries of new chemical entities using primarily the appendage diversity and scaffold diversity approaches.

1.3.1 Parallel Synthesis: Appendage Diversity Strategy

As an example of the appendage diversity strategy, efforts are being directed in our laboratory to define an alternative to the anti-HIV agent IDC16 **V** (**Figure 3**). This tetracyclic indole compound was the first small molecule identified that inhibits the exonic splicing enhancer activity of the human spliceosome SR protein factor SRSF1.[24] It was discovered through random screening of the Institute Curie in house library of 6700 molecules, which was initially synthesized as anti-tumor agents.[24] Our current objective is to construct ring-opened, non-toxic and more synthetically accessible "mimics" of IDC16. This included the parallel synthesis of a library of 240 diheteroarylamide compounds **VI**. In this program, the expectation was that

compound **VII**, containing the right side pyridine ring appendage (ring D in IDC16) would be active (see superposition in **Figure 3**). To our surprise, this molecules was totally inactive. However, the four related molecules **VIIIa-d**, possessing a common benzoisosthiazole appendage in their structure, displayed potent anti-HIV activity. These latter molecules differ significantly in structure from IDC16, and, in fact, in a traditional SAR study, we would never have envisaged their synthesis.[25]

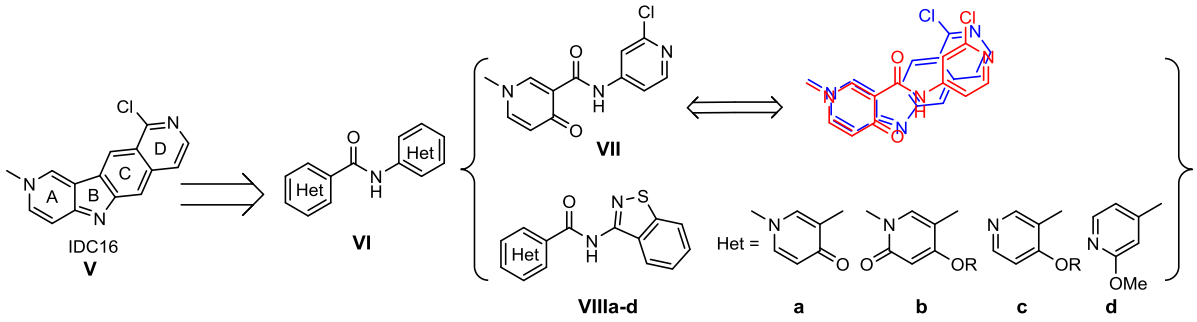

Figure 3: Development of inhibitors of HIV-1 alternative splicing.

1.3.2 Parallel Synthesis: Privileged Scaffolds for Library Design

Chemical library construction is often based on the chemistry of a suitably functionalized (activated) "privileged scaffold". This approach, first coined by Evans in the late 1980s, refers to the idea of using a molecular framework or substructure that has the ability to serve as a ligand for multiple, diverse classes of targets.[26]

The benzodiazepines as anxiolytic drugs were discovered in the 1950s by Hoffman-LaRoche Company. In 1994, Elman and colleagues constructed a library of structurally diverse 1, 4-benzodiazapine-based compounds as antagonists of the cholecystokinin (CCK) receptor A (for treatment of gastrointestinal cancer). The 1,4-benzodiazapine core was further used for a wide array of therapeutic targets (**Figure 4**).[26,27]

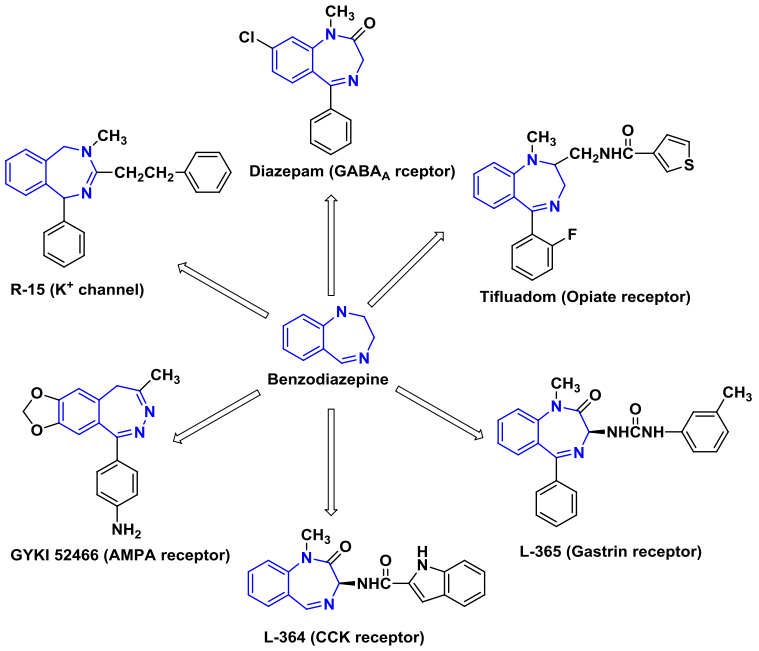

Figure 4: Benzodiazepine as a privileged scaffold.

The chromone scaffold has also been used as a privileged scaffold. Indeed, decorating the chromone scaffold leads to a variety of therapeutic agents used to treat different disorders (**Figure 5**).[26,28-31]

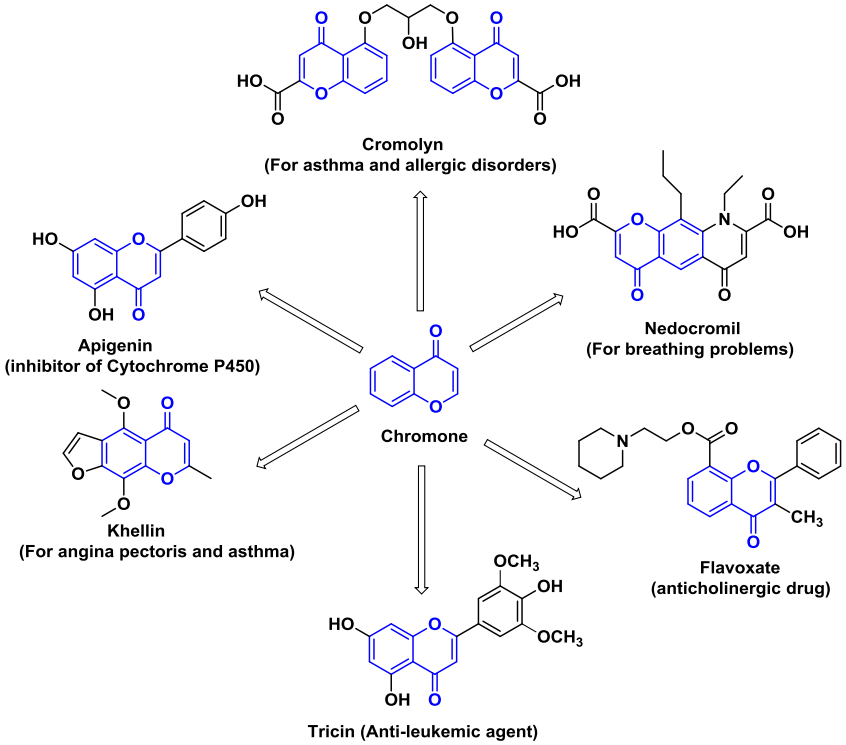

Figure 5: Chromone as a privileged scaffold.

The 1,4-dihydropyridine (1,4-DHP) has been used as a scaffold to construct L-type Calcium Channel (LTCC) blockers for treatment for hypertension. However, structural modifications involving introduction of diverse functionality on the 1,4-DHP scaffold has resulted in the identification of many pharmacological probes for other pathologies (**Figure 6**).[26,32-36]

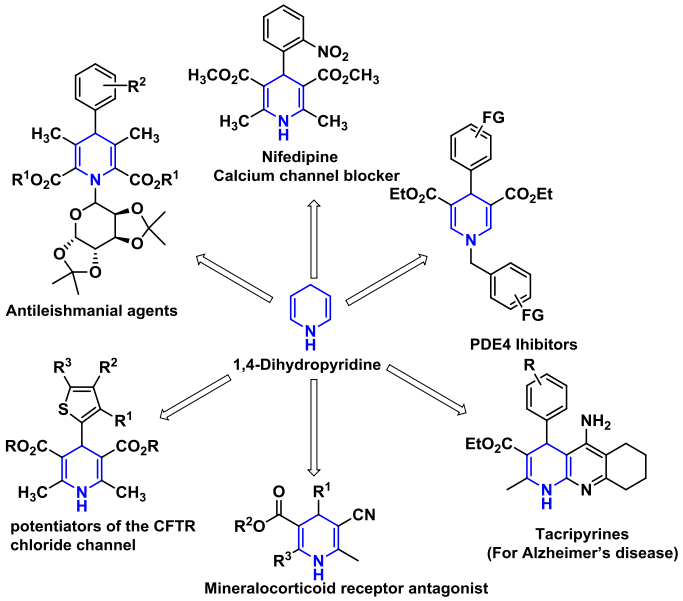

Figure 6: 1,4-Dihydropyridine as a privileged scaffold.

Quinoline-containing compounds are widely used as "parental" compounds to synthesize molecules with diverse biological application, including antimalarial, antibacterial, antiarrhythmic, and irritable bowel syndrome treatment (**Figure 7**).[26,37-40]

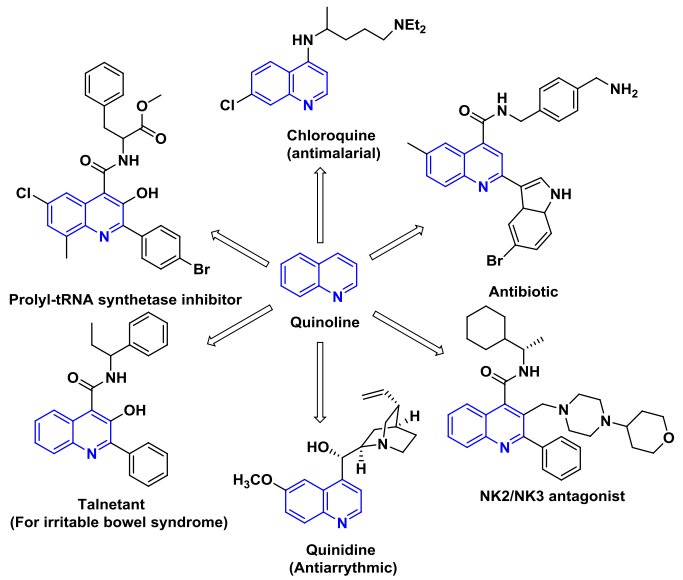

Figure 7: Quinoline as a privileged scaffold.

The 2-aminothiazole motif (fused or non-fused) appears as an integral feature in many compounds of therapeutic interest and marketed drugs. As indicated in **Figure 8**, 2-aminothiazole-based compounds showed broad spectrum of biological activities.[41-46]

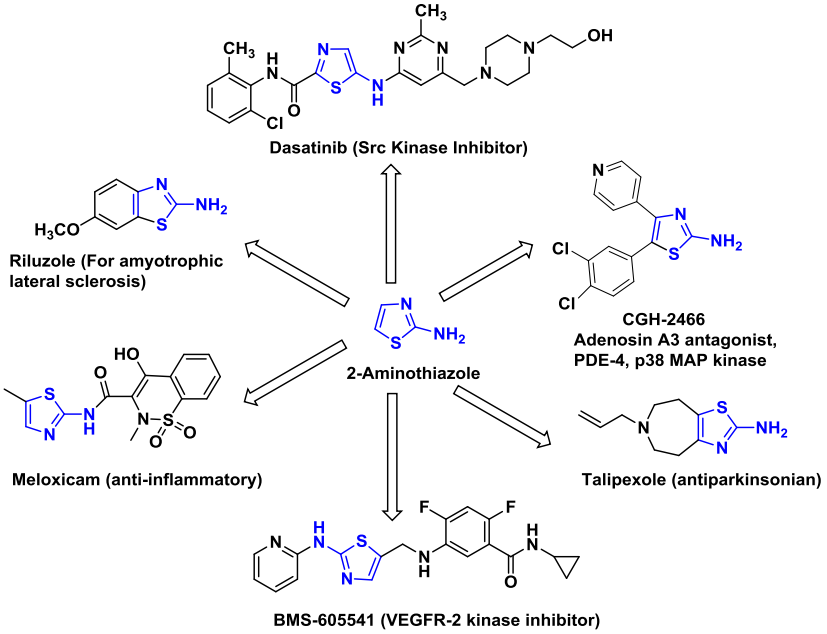

Figure 8: 2-Aminothiazole as a privileged scaffold.

Finally, libraries of purine containing compounds have been screened against a wide variety of biological targets and they resulted in the development of many therapeutic agents. A review by Legraverend and Grierson illustrates the many different applications that arise through changes in the functionality on the purine ring (**Figure 9**).[47]

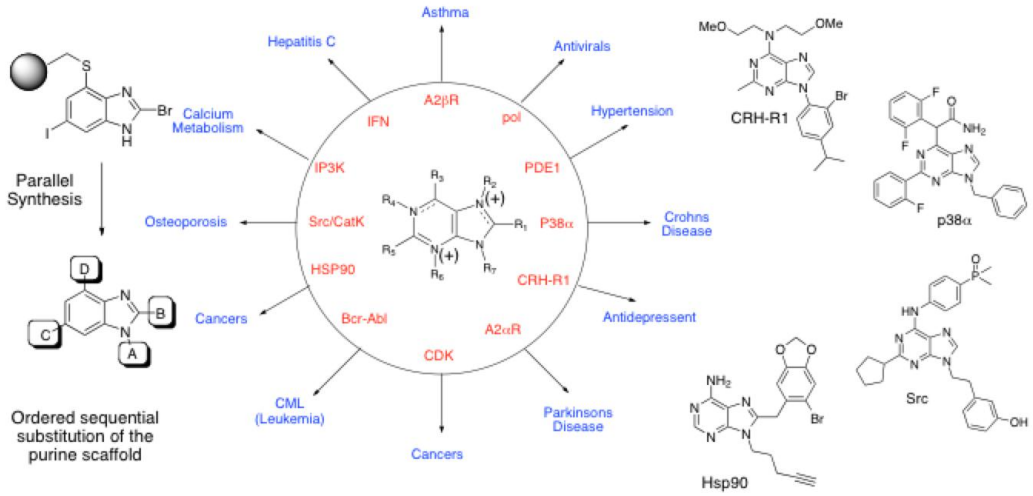

Figure 9: Applications of purine ring-based chemical libraries.

There are many other examples in the literature describing the development of compound libraries based on privileged scaffold structures.

1.4 Thesis Project: Development of Isoform Selective Rho-kinase Inhibitors

In our laboratory the parallel synthesis approach is being used to progressively create a library of "drug-like" small molecules[25] that will be screened to discover biologically active compounds targeting a wide range of systems of therapeutic interest. This is being achieved, using as a starting point the synthesis of targeted libraries for several projects that are aimed at developing molecules as inhibitors of protein-protein interactions and inhibitors of specific classes of enzymes. A particularity of each of these projects is the absence of precise structural knowledge of the nature of the interactions between our compounds and the protein target that we could use to guide the design of new inhibitors. The parallel synthesis strategy is thus well adapted to our objectives. From a fundamental research perspective, the exploration of new therapeutic targets, and the development of new ligands against existing targets implicated in important pathologies, places our effort at the forefront in new areas of biomedical research. As outlined in detail in Chapter 2, the objective of my thesis research is to use a combination of the appendage and scaffold-based parallel synthesis strategies to create a library of selective inhibitors of the two isoforms of Rho-kinase (ROCK1 and ROCK2). The precise role of these two kinase isoforms in cancer and diabetic cardiovascular disease is currently being unfolded. Consequently, there is considerable interest in the pharmaceutical sector to secure isoform selective ROCK1/2 inhibitors in order to determine the pathophysiological role of each isoform, and to validate ROCK as a therapeutic target. The development of kinase inhibitor-based drugs has undergone an exponential growth with the arrival of 23 new, marketed drugs during the past ten years.[48] These drugs are categorized as being either type I or II kinase inhibitors on the basis of their mode of binding in the ATP binding site. Interestingly, although the structural basis for the design of type I kinase inhibitors is very solidly established, there is still an incomplete picture of how to design type II inhibitors, which stabilize the activation loop closed conformation.[49] In fact, despite considerable effort, no type II rho-kinase inhibitors have been described to date. My research project focused on the use of diversity driven parallel synthesis to explore different structural options to identify isoform selective type 1 and type II ROCK inhibitors. Before entering into the foundations of my research and the results obtained, a brief introduction to

kinases and Type 1/2 kinase inhibitors will be given, along with a summary of the biology of our kinase targets, ROCK1/2.

1.5 Protein Kinases

Protein kinases comprise one of the largest families of phosphotransferase enzymes that catalyze the transfer of the terminal, or γ-phosphate moiety of adenosine triphosphate (ATP) to a serine, threonine (serine/threonine kinases), or tyrosine residue (tyrosine kinase) located on a substrate protein (**Figure 10**).[50]

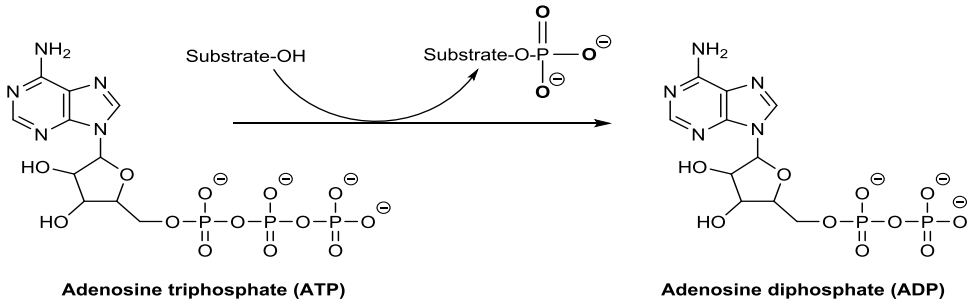

Figure 10: Phosphorylation of protein substrate by kinases.

The human genome has about 518 protein kinase genes, and they represent about 2% of all human genes.[49] Protein kinases are classified into eight major groups according to their sequence similarity in catalytic domain (**Figure 11**).[49]

a)

group[a]	human kinases
AGC	63
CAMK	74
CK1	12
CMGC	61
STE	47
TK	90
TKL	43
other	88

[a]The eight major groups are AGC (PKA, PKG, and PKC containing families), CAMK (calcium/calmodulin-dependent protein kinase), CK1 (casein kinase 1), CMGC (CDK, MAPK, GSK3, and CLK containing families), STE (homologues of yeast sterile 7, sterile 11, sterile 20 kinases), TK (tyrosine kinase), TKL (tyrosine kinase-like), other (protein kinases that do not fit any of the major groups).

b)

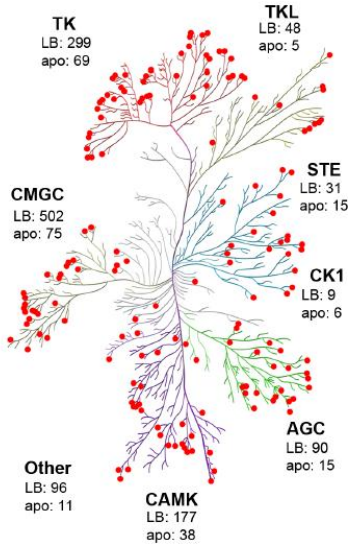

Figure 11: a) Human protein kinases classification, b) Graphical representation of the human kinome tree.[49]

Protein kinases are essential for controlling and modulating many diverse cellular regulatory functions, including signal transduction, gene expression, cell differentiation, and apoptosis.[51-54] Although these enzymes are essential to normal physiology, aberrant expression of protein kinases is associated with major pathologies, including cancers (e.g. EGFR, VEGFR, ABL, CDKs, Braf, c-Kit, AKT), diabetes mellitus and cardiovascular disorders (e.g. PKA, PKC, and ROCK), inflammation (e.g. Src, Tec, and Syk), central nervous system (CNS) diseases (e.g. GSK3, DAPK1, and MAPK), and many others.[51-54]

1.5.1 Rho-associated, Coiled-Coil Containing, Protein Kinase (ROCK)

Rho-associated, coiled-coil containing protein kinase (ROCK) is a kinase enzyme belonging to the AGC family of serine/threonine protein kinases with a molecular mass of ~160 kDa. Rho-kinase is activated by upstream G-protein, as a part of cell signaling, called RhoA. Rho G proteins belong to the Ras superfamily of monomeric GTPases and it contains 20 members of ubiquitously expressed protein in eukaryotes, including RhoA, RhoB, RhoC, Rac1 and Cdc42. Rho G proteins regulate various cellular aspects such as cell shape, cell motility, and cell proliferation. Rho acts as molecular "on-off" switches that cycle between inactive GDP-bound form and active GTP-bound form interacting with different downstream effectors to trigger a series of cellular effects. The activity of Rho is regulated by three regulatory factors (**Figure 12**), including guanine nucleotide exchange factors (GEFs), GTPase-activating proteins (GAPs) and guanine nucleotide dissociation inhibitors (GDIs). GEFs act as a positive modulator and activate Rho proteins by catalyzing the exchange of GDP for GTP while GAPs stimulate the intrinsic GTP hydrolysis activity and inactivate Rho. GDIs suppress the transformation between Rho-GDP and Rho-GTP forms and block the spontaneous activation (Figure 10). Rho-GDP is present in the cytoplasm while Rho-GTP is predominantly bound to the cell membrane. [55-57]

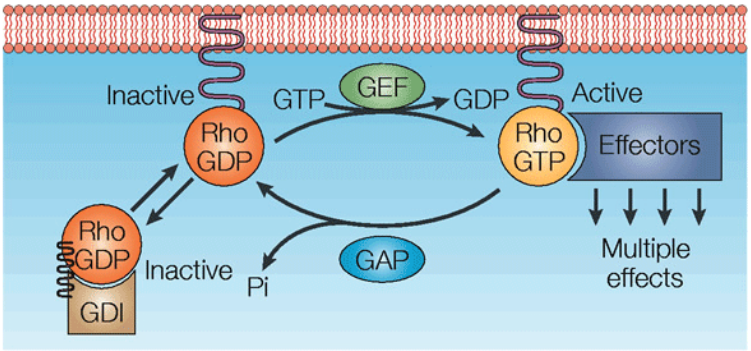

Figure 12: Regulation of Rho-G protein activity.[55]

In the active form, GTP-bound, Rho GTPases activate many downstream effectors. One of the first and best-characterized downstream effectors of the small GTP-binding protein RhoA which is Rho-kinase (ROCK).

1.5.2 ROCK Isoform Homology, Functional Roles, and Tissue Distribution

Identified in 1996, Rho-kinase has two isoforms known as ROCK-1 and ROCK-2 or Rho-kinase β and α, respectively (**Figure 13**).[58] The two isoforms are encoded by two different genes. The ROCK-1 gene is present in chromosome 18 and encodes a 1354 amino acid protein, while the ROCK-2 gene is present in chromosome 2 and encodes a 1388 amino acid protein. ROCK-1 and -2 exhibit an overall 65% homology in amino acid sequence and the two isoforms are almost identical in their kinase domains (92% sequence identity).[59]

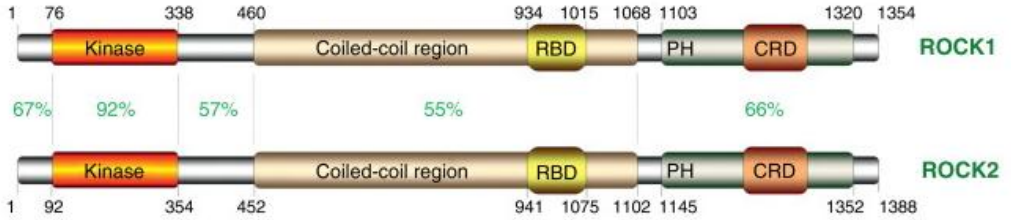

Figure 13: A schematic of the molecular structure of Rho-kinase isoforms.[58]

Activation of ROCK by GTP-bound RhoA leads to phosphorylation of different substrates modulating a wide range of important cellular functions such as vascular smooth muscle contraction, cell adhesion, cell migration, actin cytoskeleton organization, cytokinesis, stress fiber formation, and gene expression.[58,60] In fact, due to the high degree of structural similarity, ROCK1 and ROCK2 are believed to share more than 30 downstream substrates including myosin light chain (MLC), LIM kinases (LIMK), ezrin, radixin, moesin, and adducin (**Figure 14**).[58] ROCK plays a crucial role in regulation of vascular smooth muscle contraction through phosphorylation of the regulatory myosin light chain MLC.[60] Smooth muscle contraction is controlled by the phosphorylation of MLC, which is regulated by the opposing activities of MLC kinase (MLCK) and MLC phosphatase (MLCP). MLCP dephosphorylates MLC, leading to vascular smooth muscle relaxation. A rise in concentration of free Ca^{2+}in the cytosol causes activation of Ca^{2+}-calmodulin-dependent myosin light chain kinase (MLCK) and in turn phosphorylation of MLC and smooth muscle contraction. However, MLC phosphorylation and smooth muscle contraction can be induced in the absence of significant increases in Ca^{2+} (Ca^{2+} -independent smooth muscle contraction or calcium sensitization). This is accomplished through

phosphorylation of the regulatory myosin binding subunit (MBS) of MLCP by ROCK leading to the inhibition of MLCP activity and an increase in the level of phosphorylated MLC.[60]

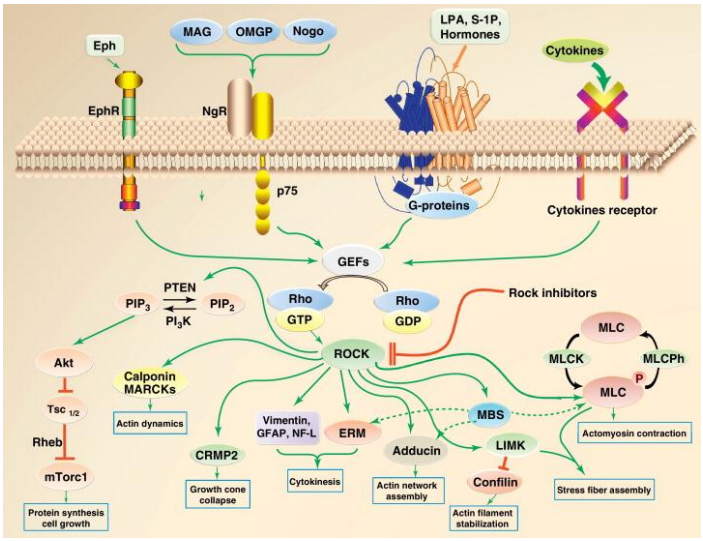

Figure 14: ROCK substrates.[58]

Although the two ROCK isoforms are ubiquitously expressed in most tissues; they have been found to possess differential tissue localization. ROCK1 mRNA was found highly expressed in lung, kidney, liver and spleen; whereas ROCK2 mRNA was found preferentially expressed in the heart, brain and skeletal muscles.[61] It was initially assumed that the two ROCK isoforms would be functionally redundant. However, recent studies have shown that they often have distinct non-redundant physiological roles.[62] Genetic deletion of one ROCK isoform does not exhibit a compensatory up-regulation of the other isoform expression.[62] Genetic deletion, knockout, of ROCK1 ($ROCK1^{-/-}$) in mice resulted in reducing cardiac fibrosis in chronic high blood pressure models, inhibition of cell detachment induced by doxorubicin treatment, and insulin resistance.[59,62,63] Whereas ROCK2-knockout ($ROCK2^{-/-}$) resulted in intrauterine growth retardation, increased fetal death, and impaired motor function.[64,65] Additionally, Both ROCK1 and ROCK2 knockdown resulted in eyelid open at birth (EOB) phenotype, omphalocele phenotype.[66]

The roles of ROCK in many diseases have been studied extensively with the aim to find out a new treatment. In the scope of my thesis, I will focus on the role of ROCK in cardiovascular diseases (collaboration with Dr. Kath MacLeod), diabetes, and cancer.

1.5.3 ROCK and Cardiovascular Diseases

RhoA/ROCK-pathway abnormalities are a central feature of the molecular pathology of arterial hypertension and it is regarded as a promising strategy for the treatment of hypertension.[67] ROCKs influence arterial smooth muscle contraction through inhibition of MLCP activity and thus increased activity of the Rho/Rho-kinase pathway plays a central role in arterial hypercontraction.[68] Rho/Rho-kinase pathway might be also involved in the angiotensin II-induced hypertension since ROCKs are considered one of the downstream effectors for angiotensin II.[69] Dysregulated cell proliferation of vascular smooth muscle cells can be considered as a one feature of hypertension. ROCKs are involved in the regulation of SMC proliferation so ROCKs might also modulate vascular hypertension via increasing cell proliferation.[70] The non-selective ROCK inhibitor, fasudil **IX**, (**Figure 15**) has been shown to lower blood pressure in hypertensive rats versus normotensive rats.[71]

Rho-kinase pathway plays a crucial role in the pathogenesis of coronary vasospasm which in turn favors the development of variant angina, myocardial infarction, and sudden death.[72] Accumulating evidence indicated that the expression of ROCKs has increased in the arteriosclerotic coronary lesions.[73] It was demonstrated that the injection of fasudil **IX** and hydroxyfasudil **X** (**Figure 15**) in the coronary arteries suppress the coronary vasospasm and decrease ischemia/reperfusion (I/R) injury.[74,75]

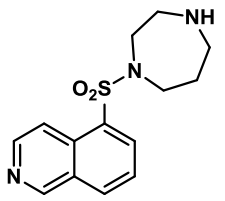

IX

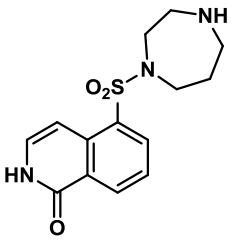

X

Figure 15: Structure of the approved ROCK inhibitor fasudil **IX**, and the experimental drug hydroxyfasudil (keto form) **X**.

The Rho/Rho-kinase-mediated pathway also plays an important role in the pathogenesis of cardiac hypertrophy and heart failure via phosphorylating troponin and inhibiting tension generation in cardiac myocytes.[76] Recent evidence indicated that Rho-kinase abnormalities are substantially involved in the pathogenesis of fatal pulmonary hypertension through multiple mechanisms including vascular smooth muscles hypercontraction, pulmonary cell proliferation leading to vascular remodeling, and inflammatory cell migration.[77] Long-term inhibition of Rho-kinase with fasudil caused a marked improvement of the pulmonary hypertension.[78]

1.5.4 ROCK and Diabetes

Recently, a great deal of attention has been focused on Rho/Rho-kinase pathway in diabetes-related research as a new strategy in the management of diabetic complications. The studies have demonstrated a strong correlation between the overexpression/hyperactivity of Rho-kinase and the development or progression of diabetic complications.[79] The possibility of using Rho-kinase inhibitors for treatment of diabetic neuropathy, sexual dysfunction, cardiomyopathy and other diabetic complications has been suggested.[80] In this context, ongoing research in Dr. Kath MacLeod's laboratory highlighted the role of RhoA/ROCK in the ventricular dysfunction that is associated with diabetic cardiomyopathy.[81] Lin and coworkers found that the activation of the RhoA/ROCK signaling pathway plays a crucial role in the development of diabetic cardiomyopathy, and inhibition of ROCK acutely improved the contractile dysfunction in a rat model of diabetic cardiomyopathy.[82]

Erectile dysfunction (ED), a prevalent complication of diabetes, is associated with an impairment of the relaxation of corporal smooth muscle. It was reported that RhoA/ROCK pathway plays an important role in the erectile dysfunction in the STZ-diabetic rat penis. [83] The mechanism involved the increase in MYPT1phosphorylation and the down-regulation of eNOS expression/activity that both inhibit the corporal smooth muscle relaxation. ROCK and eNOS proteins were found colocalized in the endothelium of the corpus cavernosum in the STZ-diabetic rats. The erectile responsiveness in diabetic animals was significantly improved by intracavernous injection of Y-27632 that caused an increase in the maximal intracavernosal pressure without affecting mean arterial pressure.[84]

Diabetic vascular diseases such as neuropathy, retinopathy and nephropathy are initiated by endothelial dysfunction.[85] The endothelial dysfunction results from an imbalance between the endothelium-derived relaxing factors (EDRF) such as nitric oxide (NO) and endothelium-derived constricting factors (EDCF) such thromboxane A2, and angiotensin II.[85] RhoA/Rho-kinase activation has significant effects on the development of diabetic vascular diseases. ROCK has been implicated in the down-regulation of nitric oxide (NO) synthesis via reducing the endothelial nitric oxide synthase (eNOS) mRNA stability and consequently decreasing expression of the (eNOS).[86] Rho Kinase Inhibitors were found to ameliorate impairment of diabetic endothelial dysfunction in kidney vasculature.[87]

Insulin resistance and obesity play an important role in the development of type II diabetes. RhoA/Rho-kinase pathway has recently been found to modulate insulin signaling through

phosphorylation of serine residue of insulin receptor substrate-1 (IRS-1).[88] Selective deletion of ROCK2 improved insulin sensitivity, suggesting that ROCK2 inhibition may be a novel approach for treatment of diabetes.[81]

1.5.5 ROCK and Cancer

Mounting evidence has suggested that the Rho/ROCK overexpression has a distinct contribution in a number of human cancers. ROCK2 has been found over-expressed in colon, bladder, hepatocellular, and lung tumors.[89-91] Furthermore, elevated levels of ROCKI were reported in hormone-refractory prostate cancer.[92] Aberrant expression of ROCKs plays an important role in the cell migration and metastasis of the tumor cells via regulating assembly/disassembly of actin-cytoskeleton.[93] Moreover, ROCK isoforms mediate vascular endothelial growth factor-A (VEGF)-driven angiogenesis suggesting that the overexpression of ROCK protein plays an important role in the formation of new blood vessels for tumor tissues.[94] Because of this, Rho-kinase might be a potential therapeutic target for cancer therapies in the future and ROCK inhibitors may be a potential treatment of the disease via delaying tumor progression or preventing tumor migration. Y27632, has been reported to reduce human breast cancer cell migration, proliferation and metastasis to human bone.[95] Moreover, Y27632 was reported to inhibit the Rho-mediated activation of actomyosin and the dissemination of MM1 hepatoma cells.[91] In Addition, fasudil and hydroxyfasudil, as Rho-kinase inhibitors, were reported to inhibit tumor cell migration and tumor progression in human and rat tumor models.[96]

The crucial role of Rho-kinase in the pathogenesis of various diseases strongly motivates the discovery of ROCK inhibitor. ROCK is considered as a promising drug target for the search of cure for these diseases. Designing Rho-kinase inhibitors require understanding of the structure of the kinase domain (catalytic site), the binding mode of ATP, and the factors that govern the specific binding of the inhibitor to the catalytic site.[97]

1.6 Design of Kinase Inhibitors

A fundamental step toward designing kinase inhibitors is to understand the composition and geometry of the ATP binding site, the nature of the interactions between ATP and the kinase, and the effect of the activation loop status on the organization of the kinase active site.

1.6.1 ROCK Structure and Catalytic Mechanism

Kinases have the same general structure and they are highly conserved in the ATP binding-catalytic sites. The typical protein kinase domain is composed of two lobes (**Figure 16**): a smaller N-terminal lobe containing a twisted five-stranded anti-parallel β-sheet and the C-helix and a largely α-helical C-terminal lobe. ATP binds in the cleft between the N- and C-terminal lobes, such that the adenine ring forms crucial donor-acceptor hydrogen bonds to the backbone amide NH and CO components in the short segment of amino acids, referred to as "hinge residues", which connect the N- and C-lobes (**Figures 16**, **17**). The ribose ring in ATP binds into a sugar pocket and the triphosphate motif in ATP binds in a hydrophilic channel, which corresponds to the catalytic site.[105,106] Other important features of the ATP binding-catalytic site include the glycine-rich loop, which allows ATP to approach the peptide backbone closely, the activation loop, which (as discussed below) controls entry of ATP and the protein substrate, and the phosphate binding site, where the catalytic reaction occurs (**Figure 16**).[98-100]

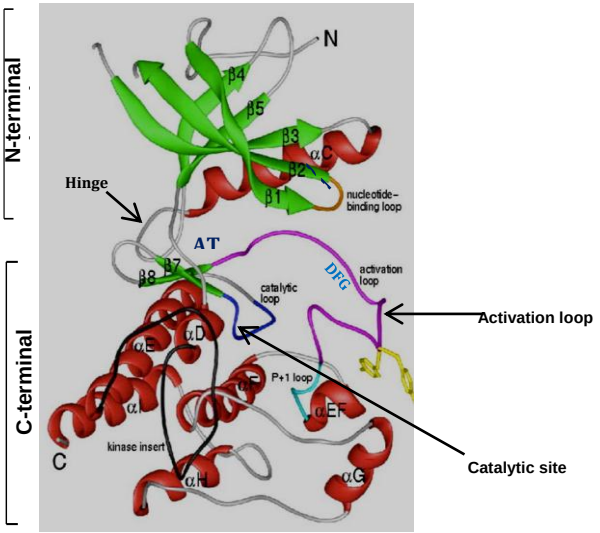

Substructures	ROCK 1	ROCK 2
Hinge:	154-158	170-174
Gatekeeper:	M153	M169
Glycine rich loop:	81-91	97-107
Glu-Lys pair:	E124-K105	E140-K121
DFG motif:	216-218	232-234
Activation loop:	216-231	232-247
Ribose pocket:	D160	D176
Catalytic site:	K105	K121
	D198	D214
	N203	N219
	D216	D232

Figure 16: General kinase domain architecture and residue numbering for the residues of ATP binding site in ROCK1 and ROCK2.[100]

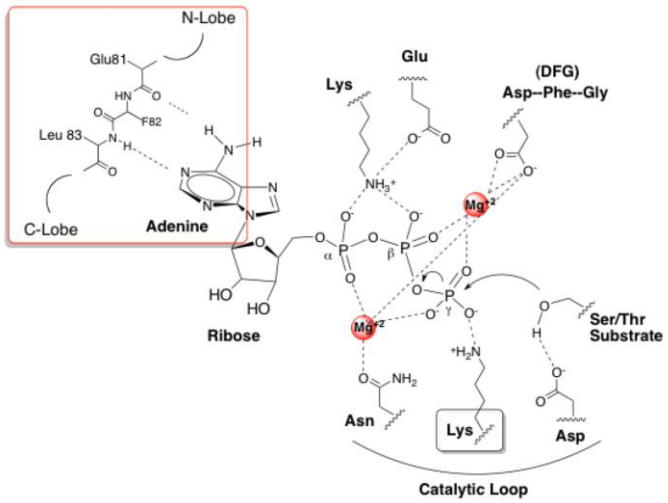

Figure 17: Organization of the kinase active site, ATP binding and catalytic site.

In normally functioning cells, kinase activity is regulated via a number of different mechanisms. The activation loop is a crucial regulatory element as its movement defines the organization of the catalytic site as well as access of ATP and the protein substrate to their respective binding sites. At the N-terminus of the activation loop is a conserved DFG (Asp-Phe-Gly) sequence, which contributes to positioning the triphosphate group in ATP for phosphate transfer. There are two extreme conformations of the activation loop: open and closed (**Figure 18**). When the activation loop adopts the open or "in" conformation, i.e. the DFG active conformation, the catalytic site is correctly structured and substrate/ATP can bind, resulting in catalysis. In the "DFG-in" conformation, the aspartic acid (D) residue points toward the terminal phosphate group of bound ATP and helps to coordinate a catalytically important Mg^{2+} ion. Further, the phenylalanine (F) in the DFG motif points away from the ATP binding sites to the back cleft.[101-104]

Alternatively, when the activation loop adopts the "closed" or "out" conformation (DFG inactive conformation) the catalytic site is disorganized and substrates and ATP cannot access the active site. In the "DFG-out" conformation, the phenylalanine rotates away from the nearby αC helix and projects into the ATP pocket, thereby blocking the accessibility of ATP and protein substrate to their binding sites (**Figure 18**).[102]

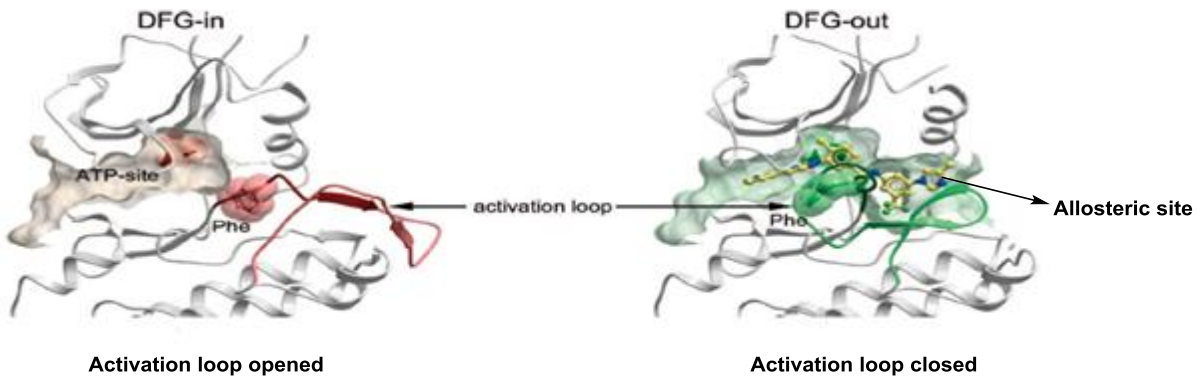

Figure 18: The various conformations of the activation loop.[104]

1.6.2 Type 1 Kinase Inhibitors

The vast majority of kinase inhibitors developed to date (>10,000) are type 1 inhibitors. Type I kinase inhibitors are ATP competitive inhibitors, in that they compete with ATP for occupation of the ATP binding site in the activation loop open (active) conformation.[105] Like ATP, a key feature in type I inhibitors is the presence of a subunit that forms one to three H-bonds to the hinge region residues. However, with few exceptions type 1 kinase inhibitors are not designed such that structural elements project into the sugar and phosphate binding regions. The reason for this is that the ATP binding site and adjoining catalytic site are highly conserved between kinases. Indeed, due to the only minor differences between these sites in kinases, it has proven to not be possible (to date) to develop kinase selective inhibitors that exploit uniquely these binding regions.[106] Fortunately, it has proven possible to develop type 1 kinase inhibitors displaying a good to high level of selectivity between kinase by designing molecules that project structural elements into two hydrophobic pockets (hydrophobic region I and II), which touch the ATP site, but are not involved in ATP binding.[105,106]

Figures **19a** and **b** illustrate the position of these two additional or supplementary hydrophobic binding pockets, relative to the binding regions for ATP. In the 2D representation in **Figure 19a**, the pocket located in the interior of the ATP site is designated as Hyp I and the other pocket, which connects with the solvent (H_2O) exposed surface of the enzyme is referred to as Hyc II. In the more topological representation in **Figure 19b**, the regions corresponding to Hyp I are BP1 and BP2 and the regions making up Hyc II on the front cleft are E0, which serves as the entrance of the ligand and E1,which serves as entrance for solvent-exposed surface.[105] These two pockets have different size, shape, and composition between kinases. The gatekeeper

residue (represented by the "K" motif) is a further selectivity feature, located at the entrance to the Hyp1 pocket. Its size/steric bulk, determines to what extent motifs in the inhibitor structure can access this pocket. In general, the gatekeeper corresponds to alanine/threonine (small) or to phenyl alanine/leucine/methionine (bulky) residues. In ROCK1/2 the gatekeeper is a Met residue at positions 153/169, respectively.[98,105]

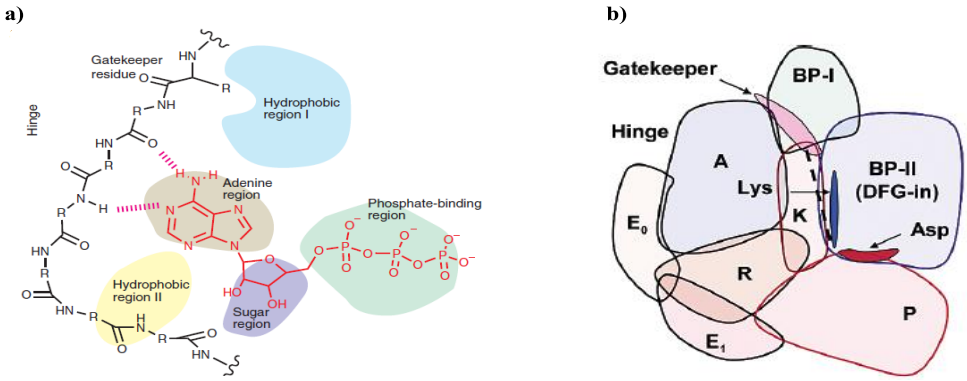

Figure 19: a) ATP binding sites divided into adenine-binding region, ribose-binding region, and phosphate-binding region, hydrophobic pockets I and II around ATP binding site, b) Topological view of ATP binding site in activation loop open conformation.[105,106]

Figure 20 illustrates the structural elements in kinase inhibitor PD166326 (ABL1 inhibitor) that bind to the hinge and interact with the selectivity pockets Hyp I and Hyc II.[103,105]

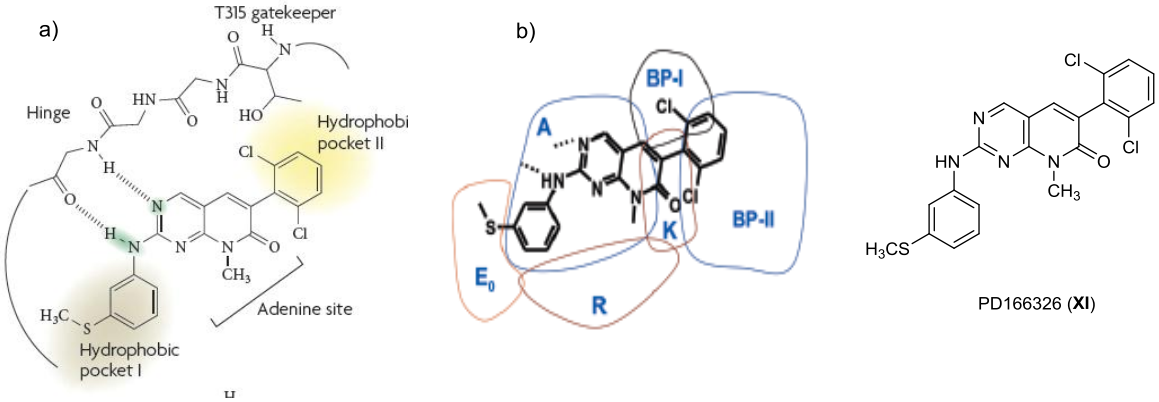

Figure 20: a) Type I inhibitor, PD166326 **XI**, exploiting hydrophobic pockets I and II of ABL1. b) Topological representation of PD166326 **XI** in the ABL1, the aminopyrimidine fragment occupies the adenine pocket, thiomethyl group extends towards E_0, dichlorophenyl inserted into back pocket BP-II.[103,105]

Type 1 inhibitors can accommodate different heterocyclic rings that occupy the purine binding site and serves as a scaffold for appending side chains that interact/bind in the adjacent

hydrophobic regions I and II.[103] Examples of the diversity of functionality and structural motifs that enable the design of kinase selective kinase inhibitors is illustrated in **Figure 21**.[105]

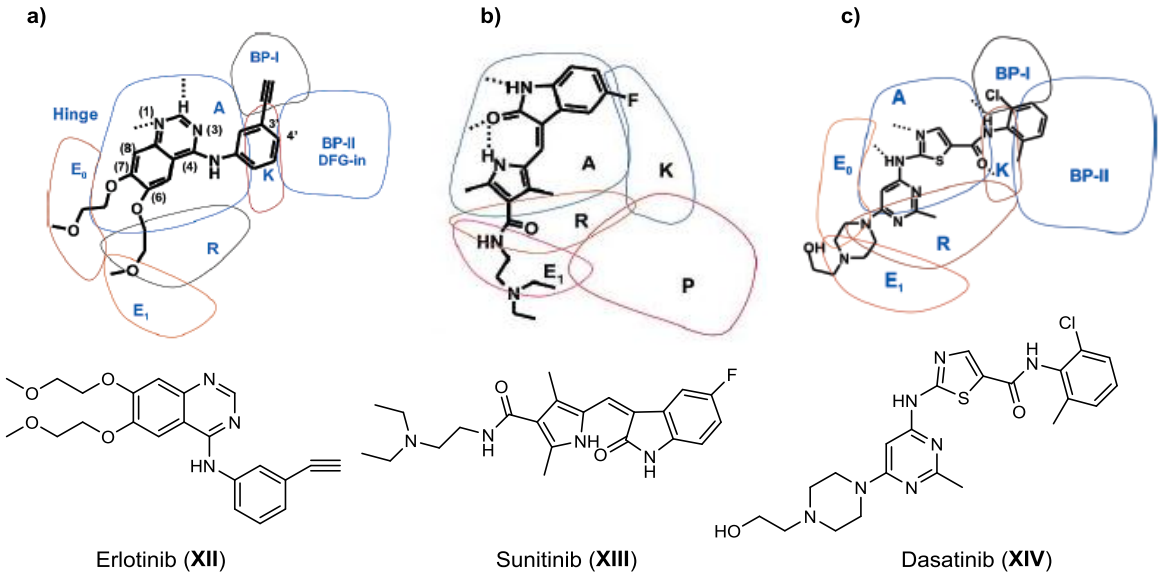

Figure 21: Examples of type 1 inhibitors, a) Erlotinib **XII** in EGFR, quinazoline ring occupies the adenine pocket, the ether functionalities extends towards E_0 and E_1, and the acetylene moiety is extended toward BP-1, b) Sunitinib **XIII** in FGFR1, indolinone ring bound to the adenine region and the 3^o amine extends towards E_1, c) Dasatinib **XIV** in c-Abl, the aminothiazole moiety binds in the adenine pocket, the hydroxyethyl piperidine extends toward E_1, and the substituted phenyl inserted into back pocket BP-II.[105]

1.6.3 Type II Kinase Inhibitors

The Type II kinase inhibition mode was initially revealed from the structure of imatinib (Gleevec®) **I** in complex with Bcr-Abl.[107] Imatinib is a non-ATP competitive inhibitor that binds to the inactive, activation loop closed, form of the enzyme. Schematically, the interactions involved are shown in **Figures 22a** and **b**. The process whereby imatinib ultimately binds to the kinase involves interaction of the drug with the kinase at some point in the equilibrium between the activation loop open (active) and closed (inactive) conformations, such that it captures and stabilizes the inactive conformation (thereby shifting the equilibrium to the inactive state).[108]

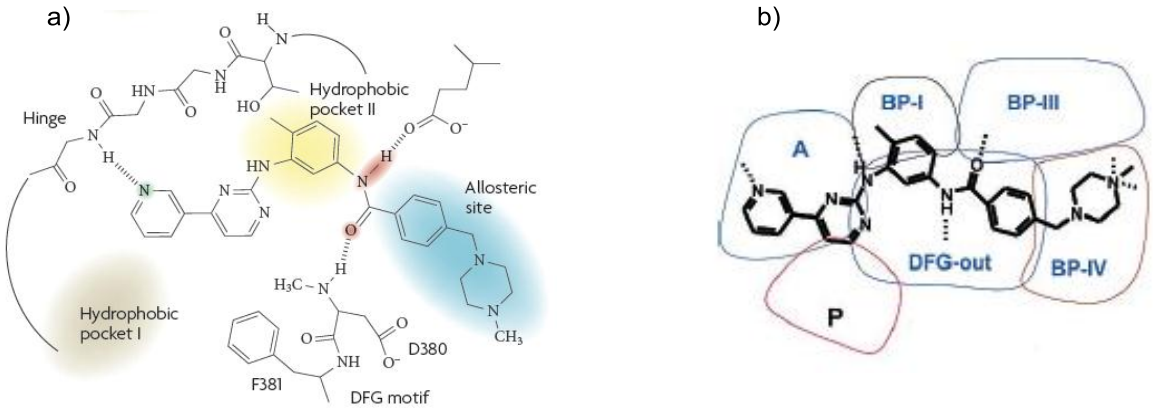

Figure 22: a) Imatinib (type II inhibitor) **I** in complex with c-Abl,[103] b) Topological representation of imatinib **I** in the c-Abl, the 2-aminopyrimidine and the attached pyridine ring occupies the adenine pocket, the substituted benzamide group binds to the back cleft BP-I and DFG pockets. The piperazine moiety occupies the back pocket BP-IV.[103,105]

Important is that the shape adopted by the activation loop in the closed conformation differs considerably to the open state. This movement occludes binding of ATP and the protein substrate, and effectively destroys the organization of the catalytic site. Further, it most frequently results in a significant shift on the position of the DFG sequence to the "DFG-out" position (see Figure 18 above). Indeed, the DFG motif will move up 10 angstrom during the closing of the activation loop, and this is accompanied by a significant increase in the volume of the back pocket (BPI-IV) such that an allosteric site exists beyond the DFG and Lys-Glu residues. The resulting increase in the volume of the PB-I or BP-IV pockets provides the room necessary for large molecules such as imatinib to bind to the kinase.[104] This movement can be pictorially represented in **Figure 23**.

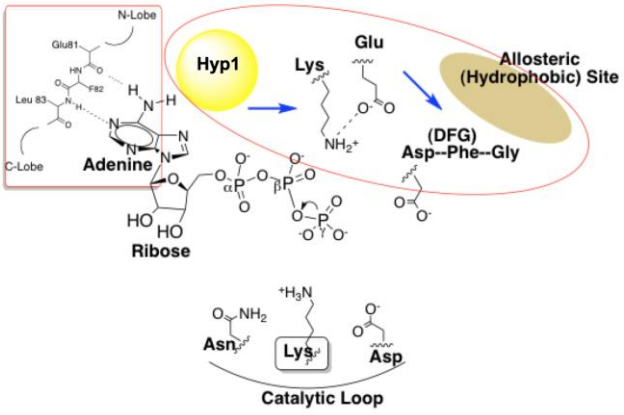

Figure 23: Closed activation loop conformation accompanied by increased size of back "Hyp1" pocket and its involvement in the new allosteric zone.

It has been suggested that, as the ATP binding region has a unique structure for each kinase when the activation loop is closed, type II kinase inhibitors can naturally "select" between kinases.[51,104] However, more recent data points to the possibility that this phenomenon may not be general.[109]

The combination of a hinge binding component, additional functionality that H-bonds to the DFG sequence and/or the Lys-Glu pair and a third component that interacts with the newly exposed hydrophobic region beyond the DFG and Lys/Glu motifs are characteristics found in the currently known Type II kinase inhibitors.[105] In other terms, Type II inhibitors are typically elongated-type structures that contain a head motif designed to interact with the hinge residue, an amide/urea linker functions in the middle of the molecule that harbor hydrogen-bond donor/acceptor groups essential to form H-bonds to the DFG sequence, and a tail (terminal) aromatic ring designed to occupy the allosteric site in the reorganized/restructured ATP binding region (**Figure 24)**.[109] The positioning of these structural elements in the type II binding site are illustrated in the topology diagrams in **Figure 25**.[105]

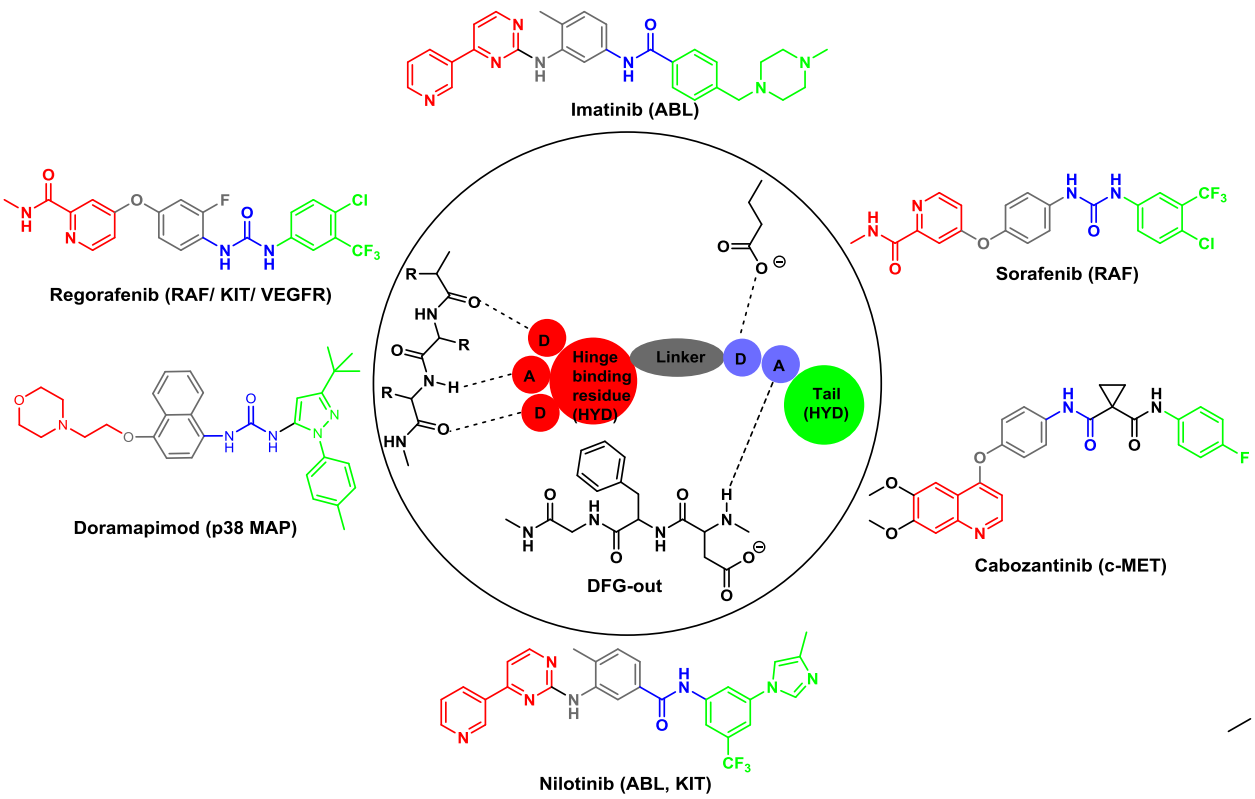

Figure 24: Examples of type II inhibitors: The hinge-binding motif is indicated in red, the linker motif in gray, amide/urea function in blue, and the terminal hydrophobic in green.

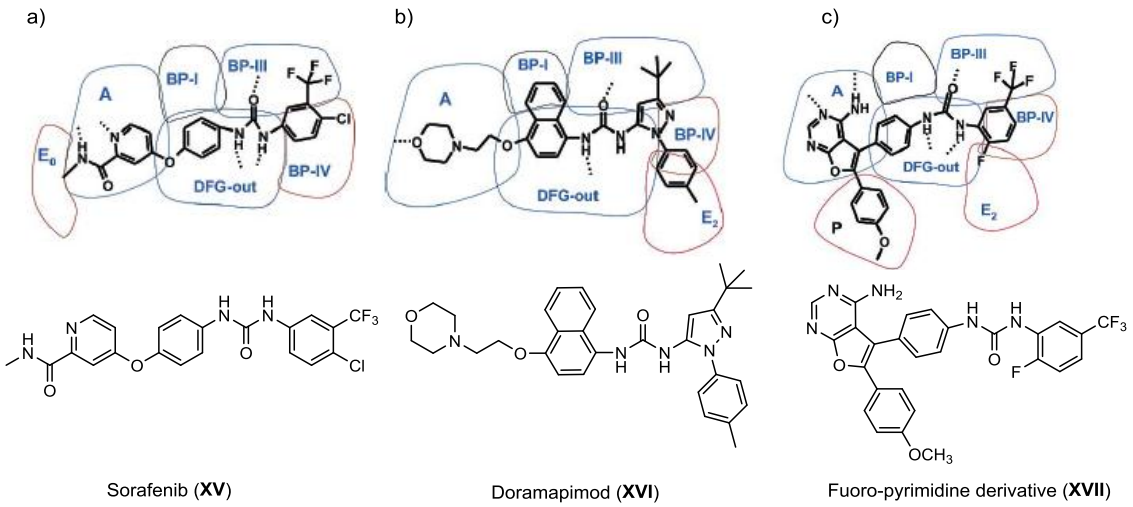

Figure 25: a) Topological representation of sorafenib **XV** in B-Raf, the pyrdinyl-carboxamide moiety occupies the adenine pocket, the phenyl urea fragment binds to the back cleft BP-III and DFG-out pockets. The terminal substituted phenyl moiety inserted into the back pocket BP-IV,[105] b) Doramapimod **XVI** in p38 MAP, and c) Fuoro-pyrimidine derivative **XVII** in VEGFR2.[105]

The number of Type II kinase inhibitors reaching the market is increasing, as they display good to excellent selectivity profiles relative to the target kinase. Further, they possess low association rate constant (k_{on}) and a profoundly lower dissociation rate constant (k_{off}) resulting in a long acting and extended kinase inhibition. The reason for the low k_{off} is assumed to be due to the higher lipophilicity and extra hydrogen bonding of these molecules.[110]

1.6.4 Other Kinase Inhibitors

Additional efforts have been exerted to develop alternative modalities for inhibiting kinases. These efforts paved the way to develop more selective inhibitors, Type III, IV, and V, that can target regions outside the highly conserved ATP-binding. Unfortunately, the rational design of these type of inhibitors is challenged by our incomplete understanding of these binding options and a lack of screening methods.[111]

Type III kinase inhibitors are small molecules, which act as non-ATP site binders (ATP-noncompetitive). They exclusively bind to an allosteric pocket adjacent to the catalytic domain of the kinase and negatively modulate kinase activity (**Figure 26**).[109,111]

Type IV kinase inhibitors also bind to a site apart from the ATP binding pocket, allosteric site (**Figure 26**). Upon binding to the allosteric site, they induce conformational changes of the

active site of the enzyme that make the kinase inactive. The exact location of the allosteric site is not known and may be anywhere on the kinase except for the pocket exploited by type III.[109,111] Type V kinase inhibitors refers to bi-substrate, bivalent, inhibitors that target both the ATP and the substrate binding regions concurrently.[111]

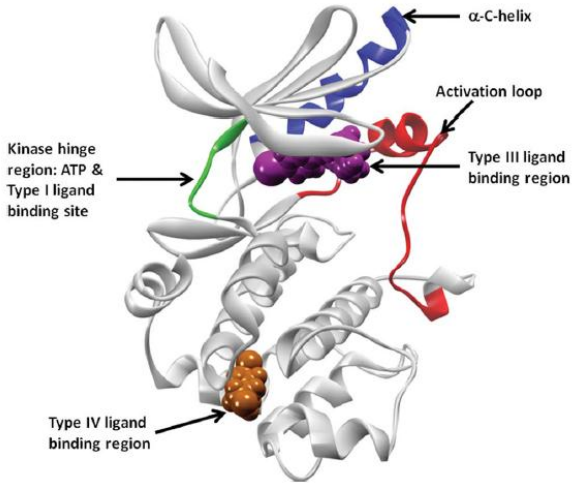

Figure 26: Schematic representation of kinase inhibitors binding modes highlighting type III and type IV binding modes.[111]

1.7 Current Status of ROCK Inhibitor Development

Significant research effort worldwide has been directed towards the discovery of potent and selective ROCK inhibitors. However, as mentioned earlier, due to the high sequence identity between ROCK isoforms in their kinase domain (92%), the development of ROCK-isoform-selective inhibitors has been, and continues to be a challenging task.

1.7.1 First Generation ROCK Inhibitors

Currently, the only ROCK inhibitor clinically approved is fasudil **IX** (HA-1077) (**Figure 15**), which has been used safely in Japan since 1995 for the treatment of cerebral vasospasm after subarachnoid hemorrhage (SAH). Although, fasudil is a more potent Type I inhibitor of ROCK (IC_{50}= 1.2 and 0.82 μM for ROCK1 and ROCK2, respectively) relative to related AGC family kinases, it is a non-selective ROCK kinase inhibitor drug.[71,112] The half-life of fasudil hydrochloride was found very short, less than 15 minutes. However, the long lasting effect has been attributed to its active hydroxylated metabolite, hydroxyfasudil **X**, rather than fasudil itself. Hydroxyfasudil **X** (**Figure 15**) has been prepared and proved to be more potent and selective toward ROCK1/2 relative to other kinases than fasudil.[113] Further optimization of fasudil led to the discovery of the dimethylfasudil **XVIII**, H-1152P, (**Figure 27**), which was found to be more

potent than fasudil as Rho-kinase inhibitor but still retains inhibitory activity against other kinases.[114]

In 1997 Uehata and coworkers discovered a monocyclic pyridine-based compound, Y-27632 **XIX** (**Figure 27**), as slightly more potent (K_i of 220 nM) and more selective for Rho-kinase inhibitor than fasudil.[60,71] Fasudil, hydroxyfasudil, dimethylfasudil (H-1152P), and Y-27632 are widely used as a molecular probes to evaluate the function of Rho-kinases in various diseases. They are further used to study the structure of the enzyme binding site.[99]

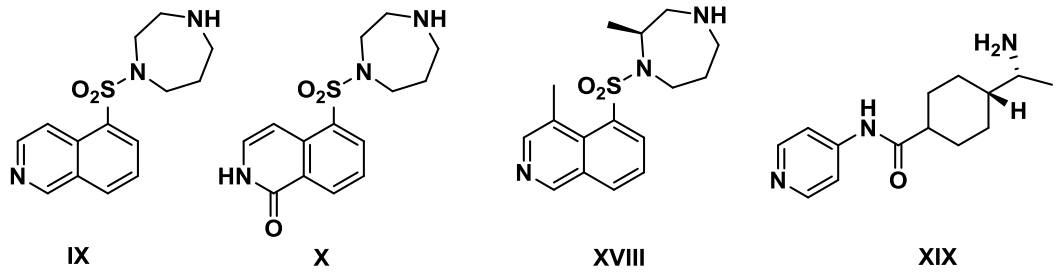

Figure 27: Molecular structures of four Rho-kinase inhibitors. Fasudil (**IX**) and hydroxyfasudil (keto form, **X**) are also presented in Figure 15.

Crystallographic data for fasudil **IX**, and hydroxyfasudil **X** in complex with ROCK (**Figure 28**) reveal that the isoquinoline ring occupies the adenine binding region of ATP and forms typical two hydrogen bonds with the hinge region of the enzyme. In fasudil, the isoquinoline nitrogen and C_1-H form H-bonds with $Met^{156/172}$(NH) and $Glu^{154/170}$(C=O) hinge residues, respectively. Interestingly, the isoquinolone motif in hydroxyfasudil is oriented in a "flipped" orientation relative to fasudil, in order to enable both the isoquinolone NH and C=O motifs to form H-bonds to the main chain of the hinge $Glu^{154/170}$(C=O) and $Met^{156/172}$(NH) residues.[98,99,115]

The weak isoform selectivity observed for these four Type I ROCK1/2 inhibitors is a consequence of the fact that the remaining polar functionality is projected into the sugar (R) or phosphate (P) binding regions (which are the same for all kinases), rather than into one of the two hydrophobic selectivity pockets (HypI or HycII).[99]

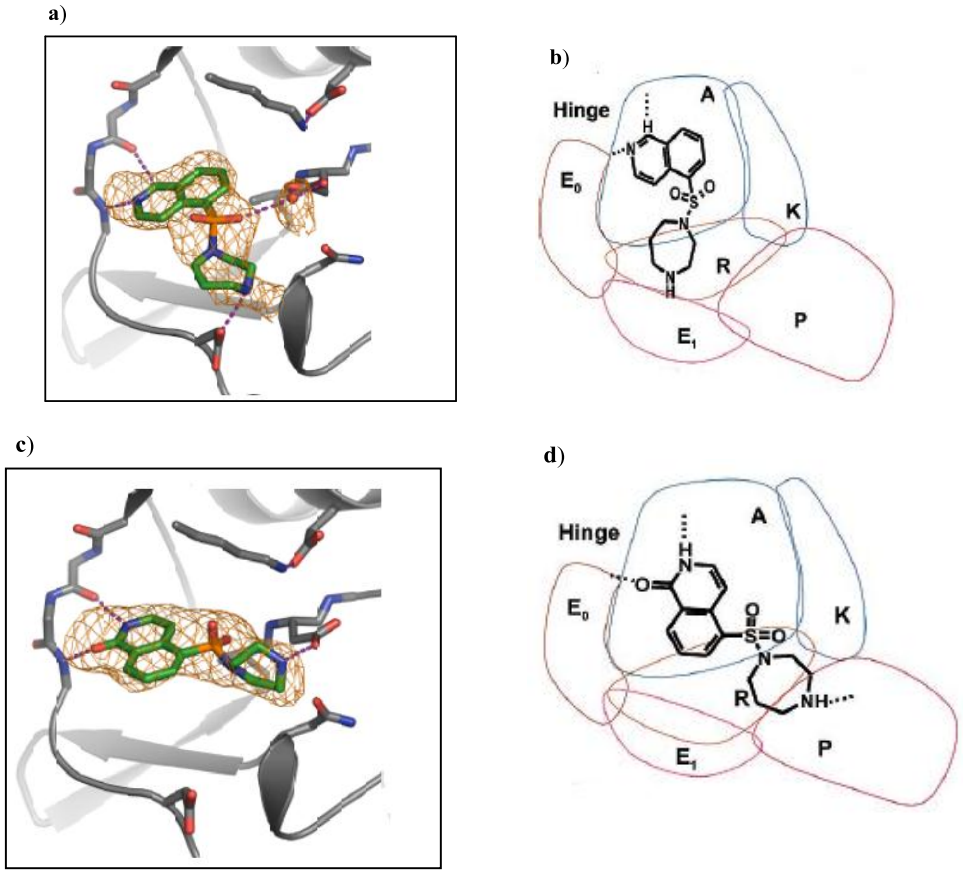

Figure 28: a) Binding interactions of fasudil **IX** within ROCK-ATP site, b) Topological representation of fasudil **IX** in ROCK **c**) Binding interactions of hydroxyfasudil **X** within ROCK-ATP site, d) Topological representation of hydroxyfasudil **X** in ROCK.[99]

Over the past decade, many second generation Rho-kinase inhibitors have been identified, belonging to various chemical classes.

1.7.2 Second Generation Isoquinoline-Based Inhibitors

Building on the isoquinoline scaffold found in fasudil, Iwakubo and coworkers showed that the R-enantiomer of compound **XX** is highly active in a cell-free kinase assay.[116] Ray *et al.* used a fragment-based NMR screening strategy to develop compound **XXI** as ROCK1 inhibitor.[117] Wu and coworkers showed that compound **XXII** displayed 10-fold improvement in potency over fasudil and Y-27632.[118] In another study, the conjugate of 5-isoquinolinsulfonylamide and oligo-D-arginine (ARC-3002 **XXIII**) was reported to possess high affinity toward ROCK2 (ROCK1 not tested) with subnanomolar dissociation constant (K_d= 20 pM) [119] (**Figure 29**).

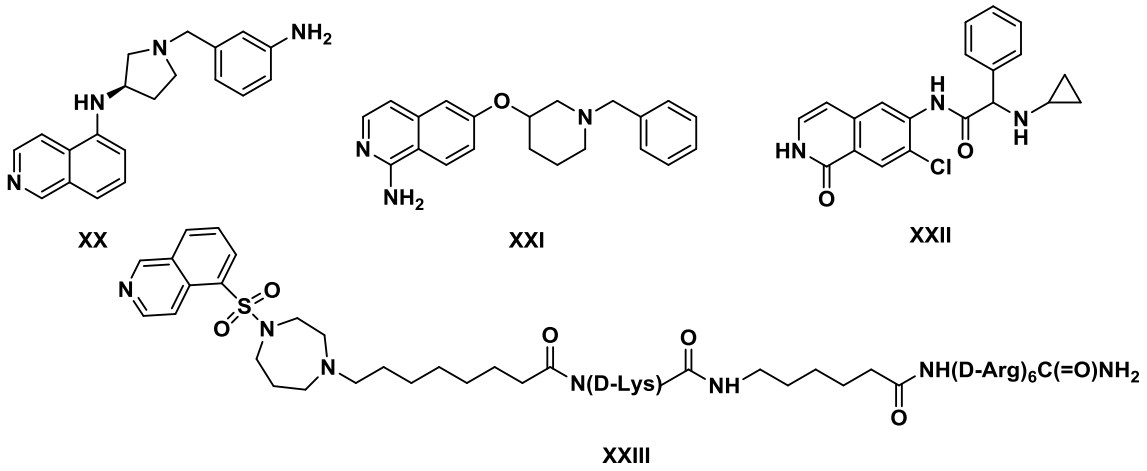

Figure 29: Isoquioline-based ROCK inhibitors.

1.7.3 Pyridine-Based Compounds

The Y-27632 **XIX** analogue Wf536 **XXIV** was reported by Nakajima to inhibit metastasis in animal model systems[120]. Patel *et al* described the pyridine-thiazole-urea RKI-1447 **XXV** as a potent ROCK1 and ROCK2 inhibitor (**Figure 30**) with significant anti-invasive and antitumor activities in breast cancer.[121] As revealed from X-ray diffraction studies (**Figure 31**), the pyridine head group of **XXV** resides in the adenine pocket of the ATP-binding site of ROCK1 forming one key hydrogen bond between the N of the ring and the NH of M[156]. The urea system forms two H-bond interactions with the backbone NH/C=O of Lys[105] and Asp[216] in the DFG motif, respectively.[121] It is important to note that, despite the presence of both a urea functionality and a terminal non-polar aromatic motif in this elongated structure, it binds in ROCK1 as a type-I inhibitor rather than via the type-2 mode.[121]

Boland *et al.* developed ROCK inhibitor **XXVI** with excellent intraocular pressure lowering effect when applied topically to ocular normotensive NZW rabbits (ROCK2 IC_{50} = 2.5 nM). Further development of this compound series by Amakem resulted in the discovery of AMA0076 (undisclosed structure), which is currently in clinical trials for the treatment of glaucoma.[122] Pfizer discovered PF-4950834 **XXVII** as a selective Rho-kinase inhibitor with anti-inflammatory properties (ROCK1/2 (IC_{50}= 8-33 nM)).[123] Finally, Li *et al.* showed that AS 1892802 **XXVIII** decreases both inflammatory and non-inflammatory pain in rat models. Moreover it was found to be slightly more selective for ROCK2 (IC_{50} = 100 nM) than ROCK1 (IC_{50} = 1690 nM) (SI = 17).[124]

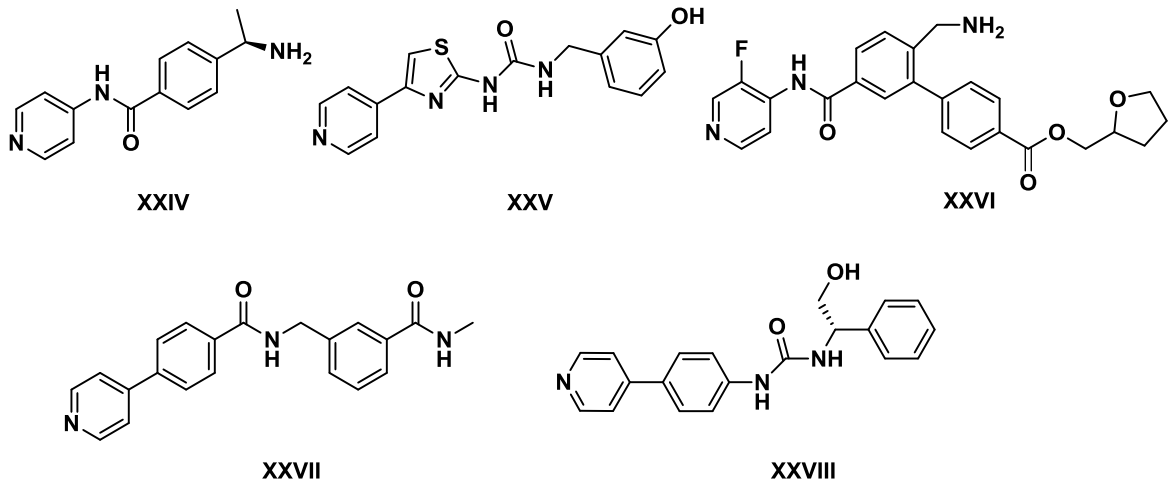

Figure 30: Pyridine-based ROCK inhibitors.

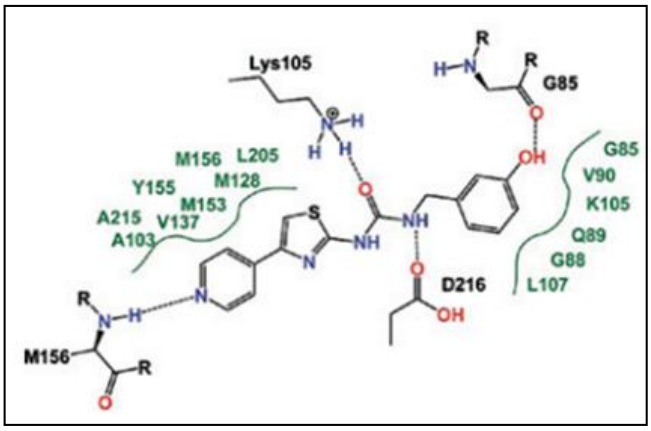

Figure 31: Schematic presentation of RKI-1447 **XXV** interactions with the ROCK1-ATP site.[121]

1.7.4 Azaindole-Based Compounds

Efforts to optimize Y-27632 **XIX** by substituting the pyridine ring with a pyrrolo-pyridine, azaindole, ring system led to the development of Y39983 **XXIX** (ROCK1/2 IC_{50}= 2.5-5.1 nM) and **XXX** (ROCK1/2 IC_{50}= 0.6-1.1 nM) (**Figure 32**) as a more potent Rho-kinase inhibitors. Currently, Y39983 **XXIX** was submitted to phase II clinical trials as a treatment for ocular hypertension or glaucoma. [125,126]

Molecular modeling studies (**Figure 32**) indicated that the replacement of the pyridine ring in Y-27632 **XIX** by an azaindole motif, as in **XXX**, gave rise to an extra hydrogen bond interaction in the hinge region between the azaindole N^1-H and carbonyl O from Glu^{154}. The insertion of a secondary amino group between the central difluorobenzene and terminal pyrimidine ring also

resulted in the second extra hydrogen bond interaction with the side chain carbonyl O of Asp[160].[127,128]

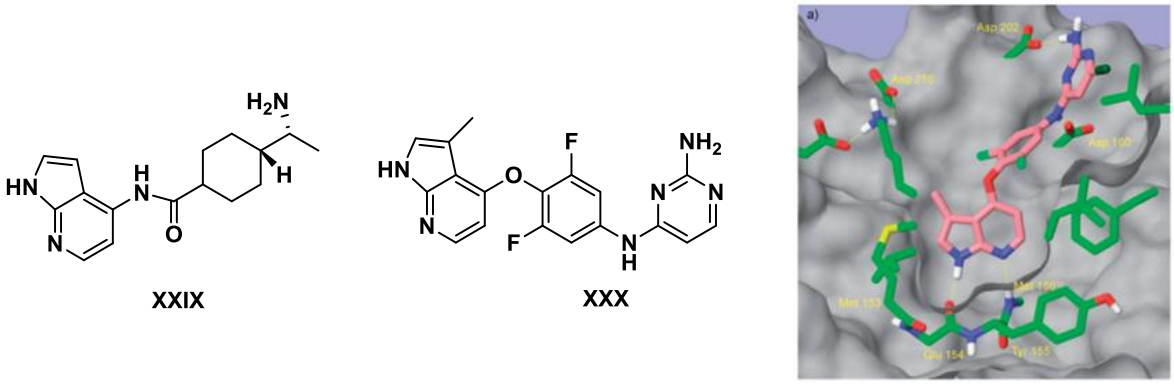

Figure 32: Azaindole-based ROCK inhibitors and a molecular modeling image of **XXX** docked into ROCK1.[127]

1.7.5 Indazole-Based Compounds

Indazole-based compounds GSK429286A **XXXI** and DW 1865 **XXXII** have displayed good potency against ROCK1 (IC_{50}= 14 and 250 nM respectively).[129,130] SR-1459 **XXXIII** and SR-899 **XXXIV** displayed low nanomolar binding affinity against ROCK2 (IC_{50}= 13, 100 nM respectively).[131] Compound **XXXV,** discovered by a fragment-based strategy, also shows moderate potency for ROCK (IC_{50}= 650-670 nM range).[124] Most importantly, KD025 (formerly SLx-2119) **XXXVI** has proven to be a novel and potent ROCK2 inhibitor (IC_{50}= 105 nM), with a 200-fold selectivity (SI) over ROCK1 (IC_{50}= 24000 nM)[132] (**Figure 33**).

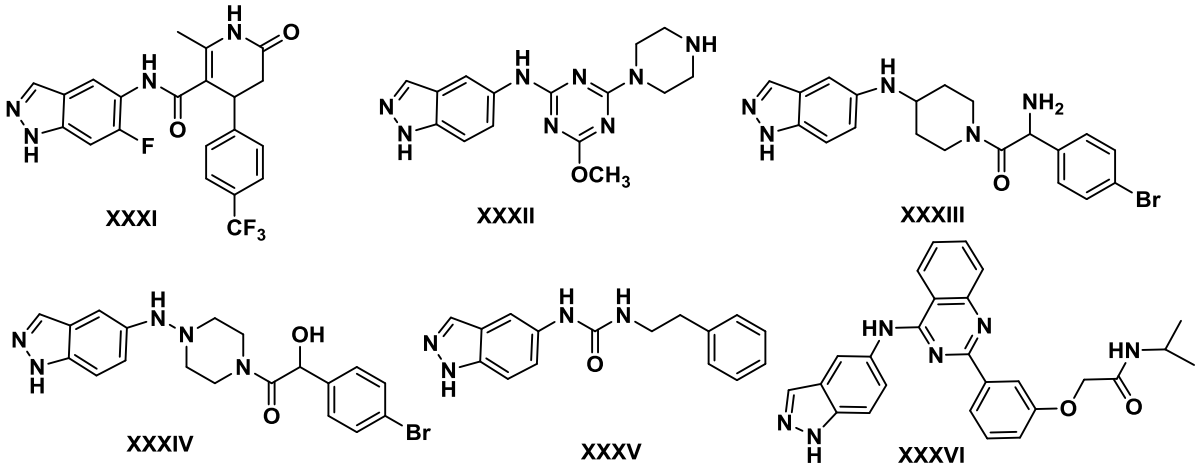

Figure 33: Indazole-based ROCK inhibitors.

Analysis of the data for binding of **XXXV** into the ATP-binding site of ROCK1 (**Figure 34**) revealed that, like the pyridine-thiazole-urea compound **XXV**, it binds as a type-I inhibitor (DFG-in conformation).[49,124] Indeed, although the urea motif captures a key H-bonding interaction with the Asp residue in the DFG sequence, the terminal phenyl ring interacts with the front pocket (Hyp1 or E1) of the ATP binding site. The results for **XXXV** and **XXV** suggests that simply incorporating an amide/urea and a terminal hydrophobic aromatic component behind the hinge scaffold may not be a sufficient condition for the design of a type II ROCK inhibitor.

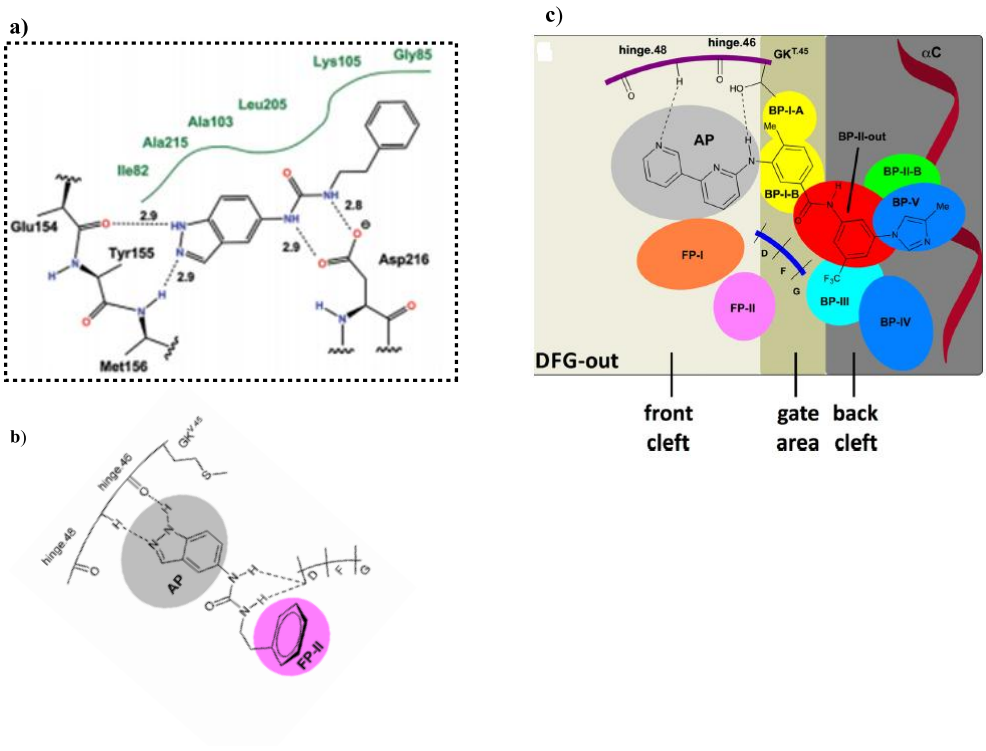

Figure 34: a) Schematic presentation of the key interactions between **XXXV** and ROCK1; b) structural analysis indicates that **XXXV** binds to ROCK1 in the DFG-in conformation and the terminal aromatic ring resides in the front pocket (FP2, also known as E1)[49], c) Imatinib binding in Bcr-Abl in the DFG-out conformation showing a detailed description of the hydrophobic pockets around ATP binding site.[49,124]

It is noteworthy to mention that the variation in the positioning of the motifs on the middle portion of the molecules **XXXI** to **XXXVI** seems acceptable, i.e. compatible with activity. In this context, we find it compelling to imagine, from the superposition of compound **XXXI** on **XXXVI** (KD025) (**Figure 35**), that the origin of the ROCK1/2 selectivity for compound **XXXVI** resides in the presence of the added substituted aromatic motif that is inside the blue box. Whether or not compound **XXXVI** is a type II ROCK inhibitor remains to be determined.

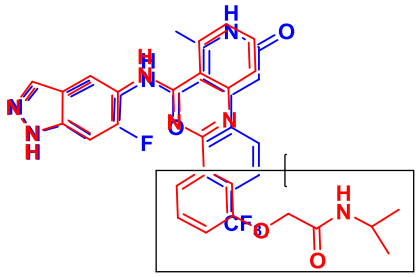

Figure 35: Superposition of **XXXI** (blue) on **XXXVI** (red), note close structural identify,except for aryl motif in black box.

1.7.6 Pyrazole-Based Compounds

SR-3677 **XXXVII** is one of several pyrazole-based inhibitors that have been identified from a high-throughput screen as a selective ROCK2 (ROCK2/ROCK1= 20-fold) (**Figure 36**).[133] Compound **XXXVIII** was identified by Fang and coworkers as ROCK inhibitor and has been used as a starting point for the development of compound **XXXIX** as a potent ROCK2 inhibitor (IC_{50} = 7 nM).[134] Other compounds possessing a pendant side chain have been developed. Of these compounds, **XL-XLIV** with remarkable binding affinity against ROCK2 isoform (IC_{50} ≈1 nM).[135-137]

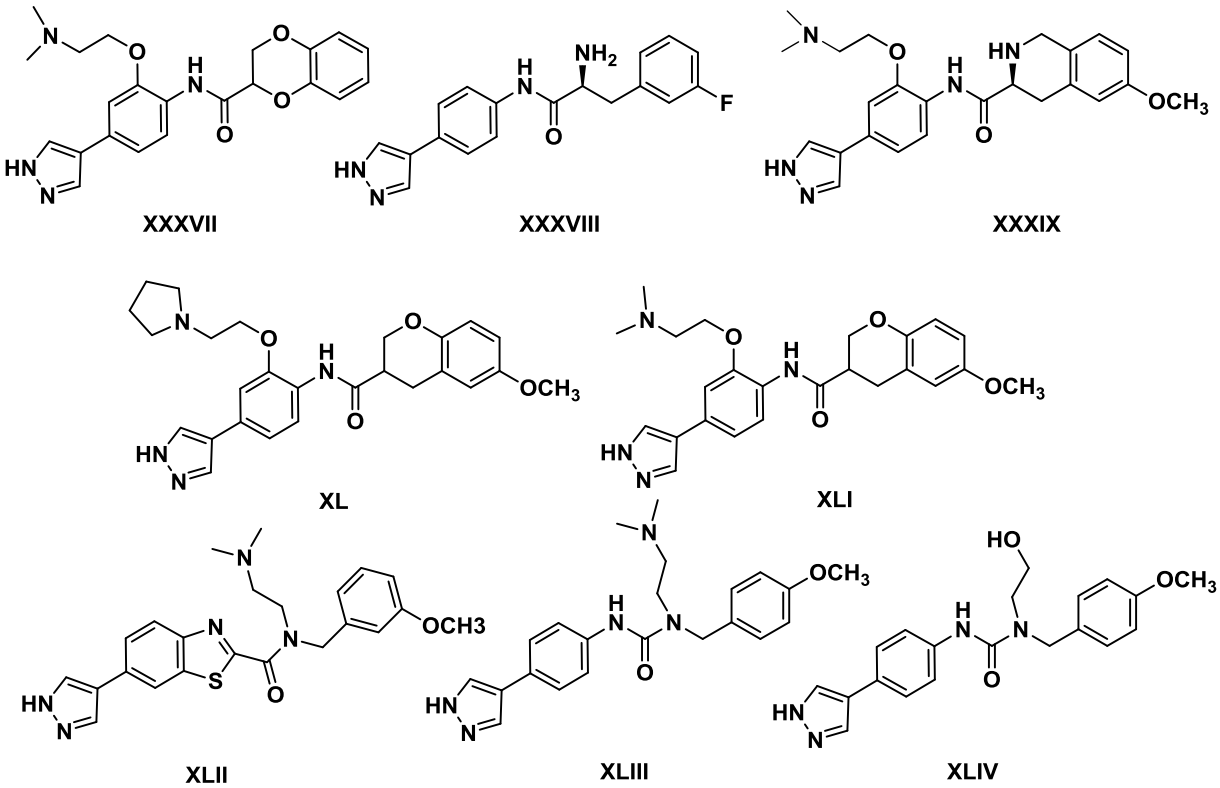

Figure 36: Pyrazole-based ROCK inhibitors.

Compounds **XXXVII** and **XXXIX** were docked into the ATP-binding site of the ROCK2 and the enzyme–ligand complex showed that they all bind as Type-I inhibitors (**Figure 37**). Beyond the interactions of the pyrazole motif with the hinge residues, a third hydrogen bond is formed in the phosphate binding region between the carboxamide C=O and the side chain NH of Lys^{121}. A fourth H-bonding interaction was found between the protonated tertiary amine of the dimethylaminoethyl group and the side chain carbonyl group of Asp^{176}. This interaction is probably the key binding element that contributes for the higher selectivity of these compounds for ROCK over other kinases. Hydrophobic interaction was found between the terminal aromatic ring and a hydrophobic pocket under the P-loop. It is believed that this hydrophobic interaction is the dominant factor that contributes to the high potency of the these compounds.[133,134]

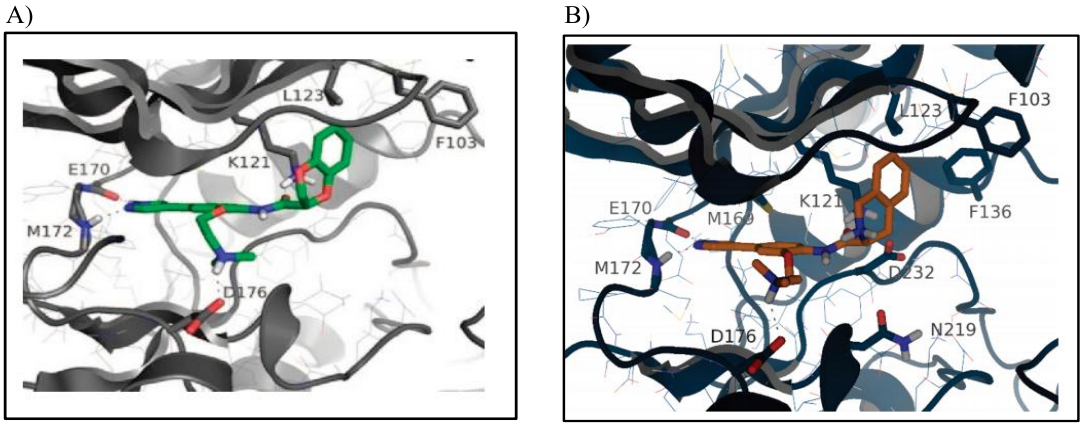

Figure 37: Structure of compounds A) **XXXVII** docked into ROCK2 ATP-binding site**,** B) **XXXIX** docked into ROCK2 ATP-binding site.[133,134]

1.7.7 Aminofurazan-Based Compounds

GlaxoSmithKline described two potent compounds: GSK269962A **XLVI** and SB-772077-B **XLVII** based upon earlier work on compound **XLV**, a MSK-1 inhibitor.[138] Adding extra functionalities/substituents to the prototype molecule **XLV** resulted in loss of affinity for MSK-1, AGC family kinase member, and the development of high affinity for ROCK isoforms. GSK269962A **XLVI** and SB-772077-B **XLVII** have high potency (IC_{50}= 1.6 to 6 nM) and good selectivity for human ROCK1/2 relative to other protein kinases[138-140] (**Figure 38**).

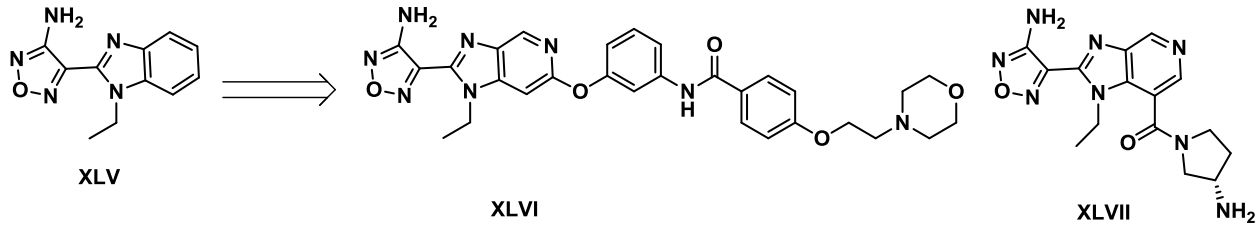

Figure 38: Aminofurazan-based ROCK inhibitors.

1.7.8 Others

Continued medicinal chemistry efforts to develop Rho-kinase inhibitors have resulted in the discovery of numerous other scaffolds that are noteworthy in their ability to inhibit ROCK1/2. These include benzoxaborole[141], benzimidazole[142], phenyl urea[143], and 3-nitropyridine[144]. Other potent and non-isoform selective ROCK inhibitors are undergoing clinical evaluation, but their structures are not disclosed.

1.8 Prospective

The growing evidence of the implication of ROCK isoforms in the pathogenesis of many diseases and knowing that these two isoforms are functionally non-redundant drives the need to synthesize drug-like molecules that are isoform selective, and avoid off-target binding. In view of the high degree (92%) of sequence identity for the kinase domains in ROCK1 and ROCK2, the design of isoform selective inhibitors is going to be challenging. Further, the available data indicates that the currently known ROCK inhibitors bind at the ATP-binding site in the Type I binding mode.[60] At present KD025 remains the only Rho-kinase inhibitor to exhibit significant ROCK2 versus ROCK1 selectivity (200-fold). The structural origin of this selectivity remains obscure.

1.9 Scope of My Work

The work presented in this dissertation aims to develop isoform selective ROCK inhibitors inhibiting ROCK by type II binding mode that can specifically inhibit ROCK isoforms. To accomplish this goal, we have developed the synthesis of 11 different small molecule libraries as outlined in Chapter 2.

Chapter 2

Objectives and Evolution of my Thesis Project

2.1 Starting Point for a Rho-kinase (ROCK) Inhibitor Library

The ultimate aim of my research is to generate a small molecule library based on different scaffolds and appendages that will be tested against different targets of therapeutic interest. In the scope defined for this thesis, the discussion is centralized around one target, ROCK.

The development of rho-kinase inhibitors has been an active field of research over the past 10 years, and will continue to be, due to the escalating evidence of their implication in many pathophysiological disorders. As described in chapter one, the ATP binding sites in ROCK1/2 are 92% identical, which makes the goal of development of isoform-selective inhibitors difficult to achieve. Despite this obstacle, based on experiments using the non-selective inhibitor Y-27632, there is a noted difference between the two sites in their affinity (Km) for ATP binding (Km values for ATP were estimated to be 0.15 μM and 0.25 μM for ROCK1 and ROCK2, respectively).[145] These data suggest that it may, in fact, be possible to design isoform selective type II ROCK inhibitors. Importantly, this small, but significant difference in ATP binding site geometry/composition may accentuate differences in the activation loop closed conformations of the two enzymes, which may further permit the design of type II Rho-kinase inhibitors that select between the two ROCK isoforms.

At the outset of my work, structural data were available for fasudil, hydroxyfasudil, and Y-27632 only in complex with ROCK1 in the activation loop open conformation.[98,99] This enabled us to analyze the binding of these type I kinase inhibitors in the ATP binding site of ROCK. In contrast, no corresponding structural information was available that could provide insight as to the geometry of the activation loop closed conformation of ROCK. Consequently, it was not possible to engage a program to "rationally design" type II isoform selective ROCK inhibitors using structural data. For this reason we leaned heavily toward the use of parallel synthesis to study a wide range of structures as potential type II rho kinase inhibitors. Targeting the ROCK activation loop in a closed conformation was a pioneering idea from the research perspective.

In the conception of our parallel synthesis approach we were guided by the generalized observation that known type II kinase inhibitors (Chapter 1, **Figure 24**) typically have a hinge

binding moiety at one end, which forms at least one H-bonding interaction with the hinge residues, an internal, or central, segment containing an amide or urea motif, which H-bonds to either the DFG activation loop subunit or the C-loop Glu residue, and at the other end a hydrophobic aryl/heteroaryl subunit, which interacts with the allosteric pocket created by the DFG-out flip. In other words, type II inhibitors are elongated molecules, which are just too large (complicated), to fit into the hydrophobic pocket in the ATP binding site in the type I model. This point is illustrated (**Figure 39**) by one tactic that has been developed to transform type I kinase inhibitors to type II inhibitors by simply adding a amide/urea and hydrophobic subunits onto the HYP1 binding pocket motif.[106]

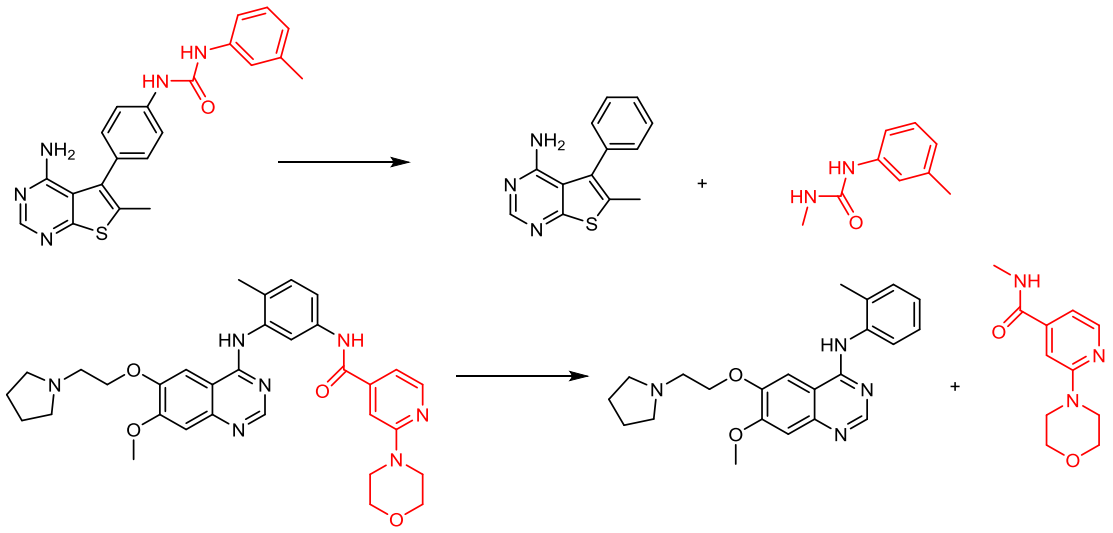

Figure 39: Designing of type II kinase inhibitors by attaching type I head (black) to a type II tail (red).[106]

The crucial choice at the beginning of my project was the selection of the hinge binder motif (head part) that is amenable to more structural modifications and optimization. Inspired by the presence of the cyclic amide function in hydroxyfasudil **X** and several other kinase inhibitors,[146] and considering synthetic accessibility of diversely functionalized 2-pyridinone systems,[147] the 2-pyridinone motif was initially chosen as the hinge binding motif. The 2-pyridinone system has the possibility to bind to the hinge region via two hydrogen bond interactions between the carbonyl oxygen/NH of the ring and the amide NH of Met[156]/ the C=O of Glu[154] respectively or between the carbonyl oxygen/NH of the ring and NH/C=O of Glu[154], respectively (**Figure 40**). Further, in our initial work the decision was taken to connect the spacer to the 2-pyridinone ring via the C-5.

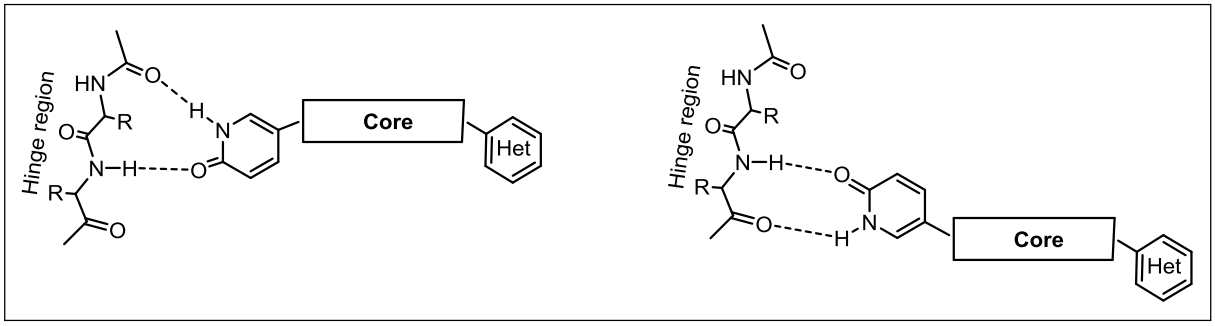

Figure 40: The binding options of 2-pyridinone-based scaffold..

Considering the easy accessibility of the requisite 2-pyridinone-5-carboxylic acid derivatives, the synthesis of a series of diheteroaryl amides (DHA's) **XLVIII** was envisaged (**Figure 41**).

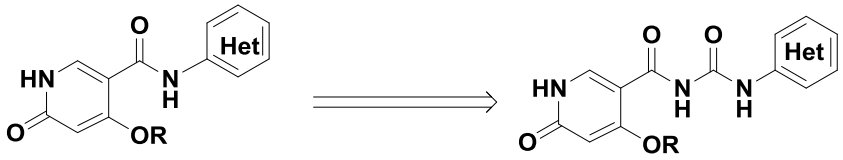

XLVIII **XLIX**

Figure 41: Initial choice of the core motif.

Although the preparation of a diverse library of DHA compounds **XLVIII** could easily be prepared by peptide-type coupling reactions, it was anticipated that such compounds would not be sufficiently elongated for them to act as type II kinase inhibitors. An alternative choice for the spacer-DFG binding element, which would provide a more elongated structure, is the acyl urea motif found in **XLIX**. However, N-acyl ureas are metabolically unstable. For this reason, priority was given, as presented in Figure 42, to incorporate a stable amide bioisostere, such as an oxazole and oxadiazole, in the linker segment.[148] This idea is explored in chapter 3 of my thesis. Indeed, in this chapter, we described our effort to synthesize the oxazoles **22/23a-f**, and the synthesis of oxadiazoles **34a-ah**. Note that right side of the molecules will be varied so as to create a diverse library of analogues that will permit us to explore means to optimize binding to the allosteric site in the type II binding mode. This work is extended to include the isomeric oxadiazole compounds **41a-g**, and the oxadiazoles **45a-f** lacking the central amide motif. These compounds were prepared in order to determine whether such compounds could in fact function as type I ROCK inhibitors.

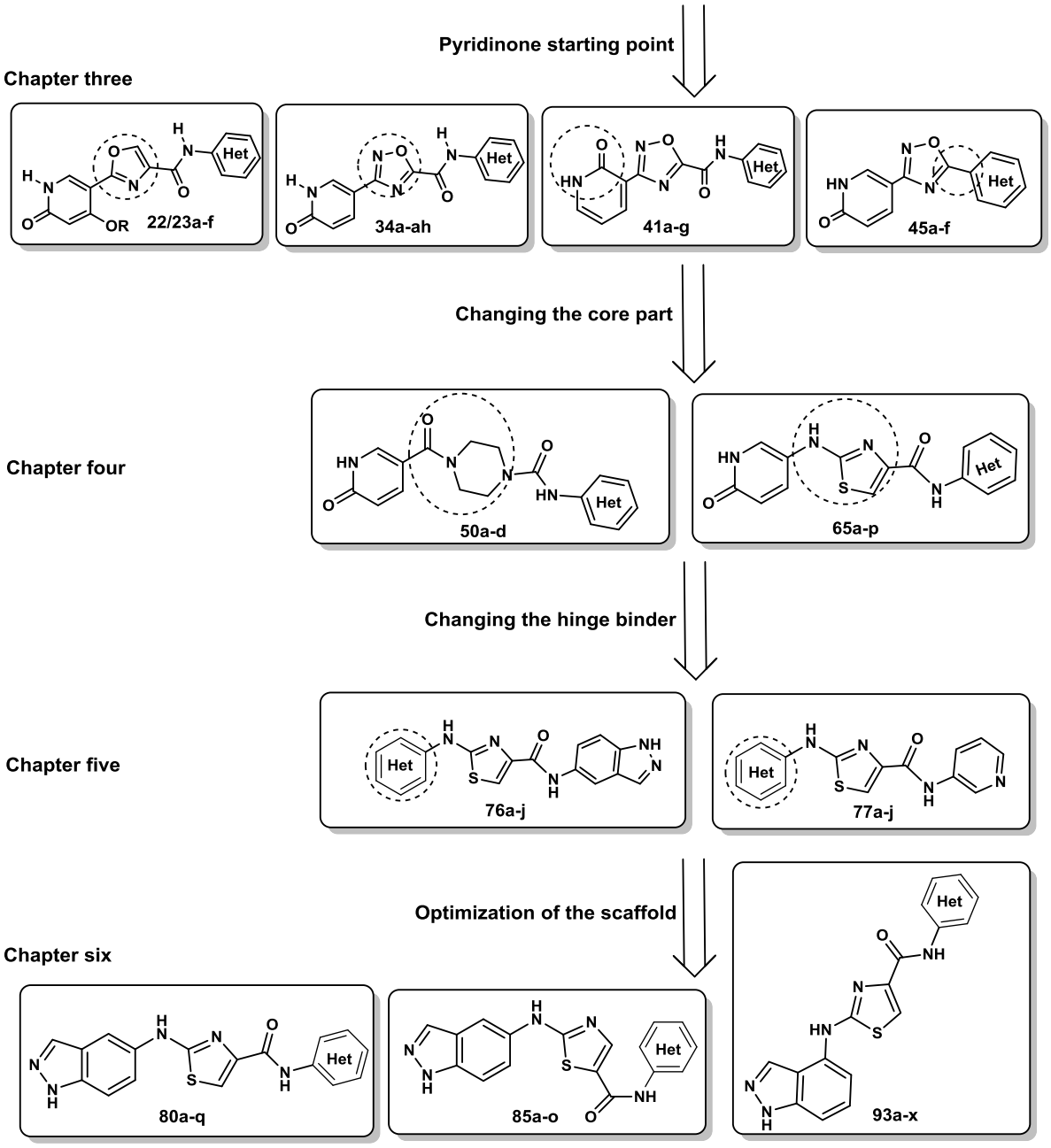

Figure 42: Overall strategy of the thesis.

For simplicity in presenting of this thesis

Het = Alkyl or cycloalkyl or aryl or heteroaryl

In chapter 4 we described different structural modifications to the linker part of the pyridinone based scaffold, which were studied to evaluate the optimal length of the linker. The strategy adopted for these modifications included: 1) incorporating six-membered saturated ring (piperazine) and hydrogen-bond acceptor (C=O), 2) incorporating five-membered hateroaromatic ring (thiazole) and hydrogen-bond donor (NH).

In chapter 5 we described further structural modification that were prompted by the biological results obtained in chapter 4. A different strategy was ultimately employed by changing the lefts side of our scaffold by introducing divergent (hetero)aromatic rings as hinge binder motifs while having either an indazole or a pyridine motif on the right side.

In chapter 6 we described structural optimization to improve upon the established scaffold, indazole-aminothiazole based scaffold, to increase potency and selectivity based on biological results obtained in chapter 5. The design of these analogs acted to closely mimic type-II inhibitors.

In Chapter 7, we discussed the biological results obtained for a selection of the molecules that have been synthesized.

It is important to note, that during the course of these studies, a relatively large number of publications have appeared exploring the potential the different ROCK inhibitor classes described in the introductory chapter (Sections 1.7.1 to 1.7.8). Many of these molecules, illustrated in **Figure 43**, have structural features that satisfy the criteria established for Type II kinase inhibitor binding. However, the structural data and docking studies for complexes of these molecule types with ROCK indicate that they all interact via either the type I inhibitor model (DFG-in), or an intermediate state between the DFG-in and DFG-out, (DFG-out like conformation), where the inhibitors interact with the FP I and/or II pockets, and not the inner pocket as found for essentially all other type II kinase inhibitors (**Figure 34c**, Chapter 1).[49] As surprising as these results are, they underscore the importance and interest of studies, such as ours, to further explore different structural types in an effort to identify type II ROCK Inhibitors. Indeed, the structural features of the activation loop closed conformation of ROCK appear to differ significantly from many of the other kinases investigated. Although there is significant progress made in the development of ROCK inhibitors such as KD025 **XXXVI** (**Chapter 1**), ROCK-isoform-selective inhibitors have not been optimized yet in terms of structural features and binding mode**.**

.

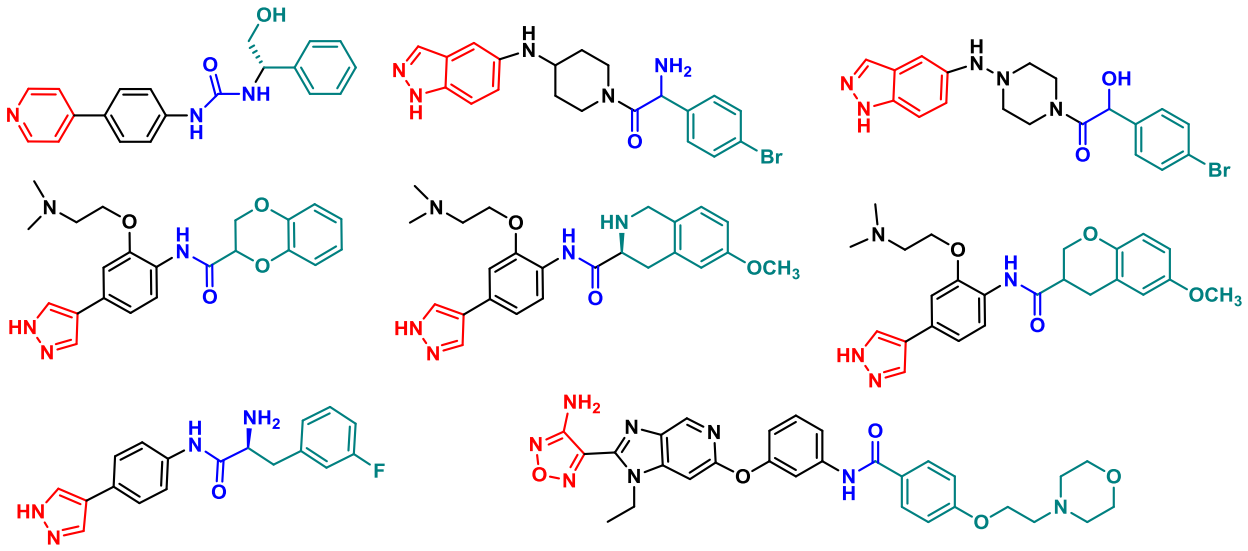

Figure 43: Type II-like rho-kinase inhibitors; hinge binding motif is indicated in red, the linker motif in black, amide/urea function in blue, and the terminal hydrophobic in green.

Chapter 3

Pyridinone-Dihydroxazole/Oxadiazole-Based Compounds

3.1 Introduction

As briefly mentioned in the previous chapter, the first objective fixed was to construct a library of compounds where the separation between the hinge binding 2-pyridinone component and the diverse set of aryl and heteroaryl motifs incorporated on the other extremity is larger than that found in the simple diheteroaryl amide (DHA) analogues **XLVIII** (**Figure 44**). Such molecules can be built by introducing an additional amide motif into the central portion of **XLVIII**. However, it was anticipated that the resulting acylurea-type compounds **XLIX** would be unstable, relative to molecules where an oxazole ring is used as a stable bioisostere of one of the amide functions. Our initial goal was to synthesize a library of 2-pyridinone-oxazole carboxamides **22a-f**/**23a-f** as potential ROCK inhibitors.

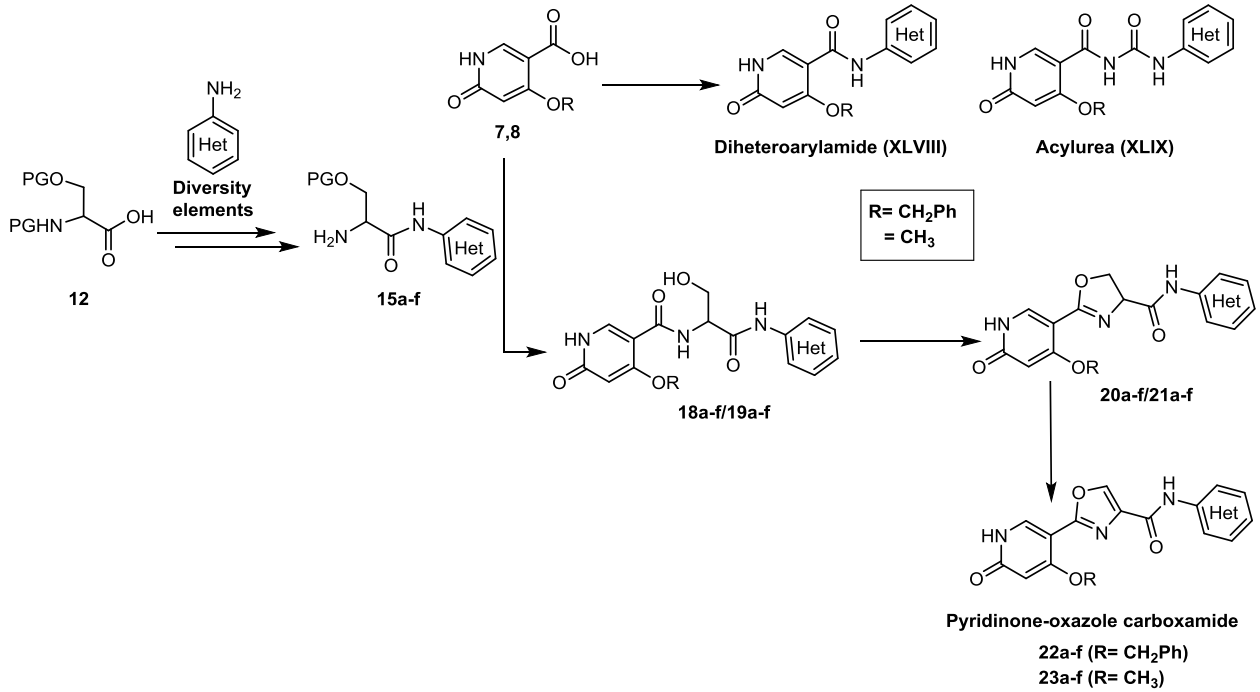

Figure 44: Summary of synthesis of compounds **22a-f** and **23a-f**.

3.2 Synthesis of Pyridinone-Oxazole Carboxamides 22a-f and 23a-f

Based upon the method developed by Pattenden,[149] Wipf,[150] and others[151,152] to construct substituted oxazoles from *l*- or *d*-serine, the synthesis of our target library of compounds **22a-f/23a-f** can be divided into 4 stages (**Figure 44**): i) synthesis of the 2-pyridinone-5 carboxylic acids **7** and **8**, ii) synthesis of the *O*-protected serine carboxamide intermediates **15a-f** iii) condensation of **7** and **8** with **15a-f**, iv) dehydrocyclization of intermediates **18a-f**/**19a-f** followed by oxidation to get the desired oxazole products **22a-f**/**23a-f**.

Note, a key feature in this synthesis is to form the crucial amide bond that introduces the diversity element prior to formation of the oxazole ring. It was anticipated that the acid function in the simple serine derivative **12** would be more reactive than a carboxyl function attached to C-4 of an oxazole.

3.2.1 Synthesis of the 2-Pyridinone-5-Carboxylic Acid Building Blocks 7 and 8

The pyridinone-5-carboxylic acid derivative **3** that we initially chose to use bears an additional OH substituent at C-4, which can be exploited in SAR to improve binding to the ROCK enzyme and/or to improve solubility and other physico-chemical properties. Compounds **7** and **8** were obtained in 5 steps from diethyl 1,3-acetonedicarboxylate **1** (**Figure 45**).[153]

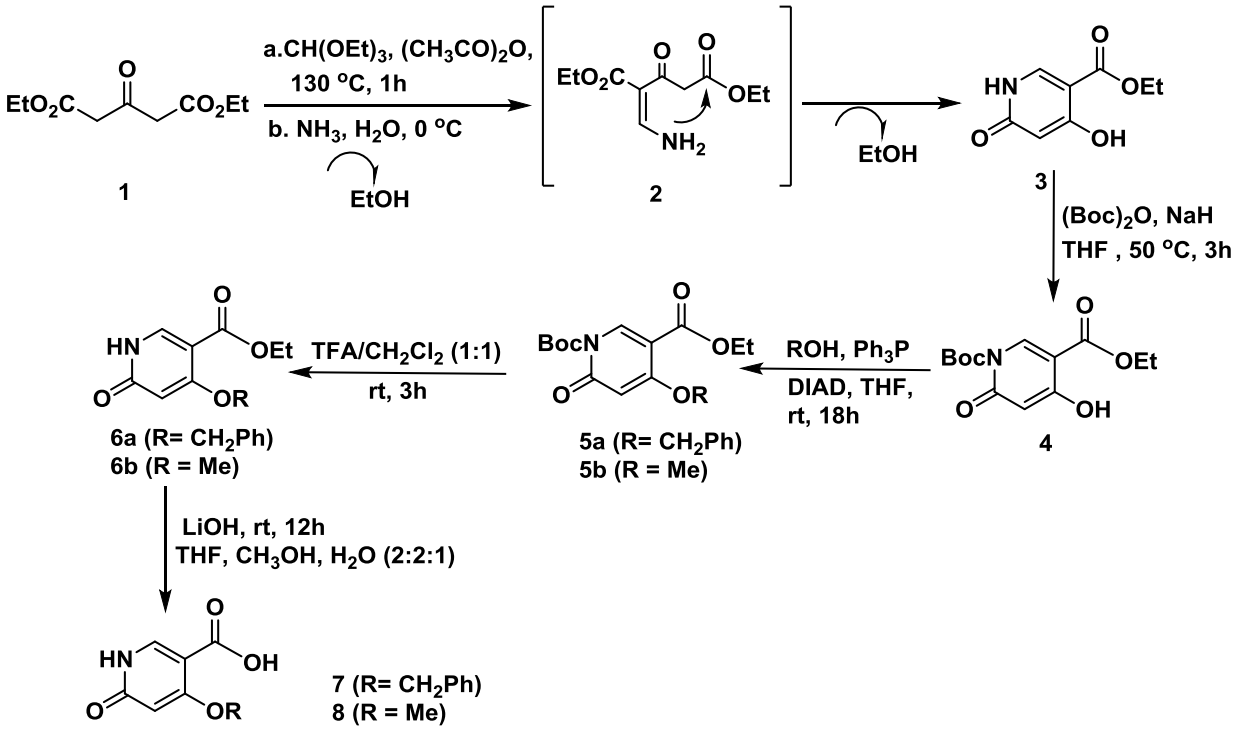

Figure 45: Synthesis of 4-alkoxy-6-oxo-1,6-dihydropyridine-3-carboxylic acids.

In the first step, diester **1** was reacted with triethyl orthoformate in acetic anhydride to give intermediate **2**. Without isolation, this intermediate was reacted with ammonia to give the expected pyridinone product **3** in 68% yield through a 1,4-addition – cyclization process.It was hoped that, in the next step, it would be possible to carry out a selective O-benzylation/methylation of the C-4 OH group in **3** to give compounds **6a** and **b** directly. However, this proved to be challenging, as the lactam NH and lactim OH in the two tautomeric forms of **3** are also reactive. Although X-ray crystallography shows that the 2-pyridinone form **3a** is the largely predominant tautomer in the solid state,[154] it is well known that the desired reaction of the C-4 phenolic OH in **3** can be accompanied by alkylation of at either the NH (lactam tautomer) and OH (lactim tautomer) centers (**Figure 46**).[155]

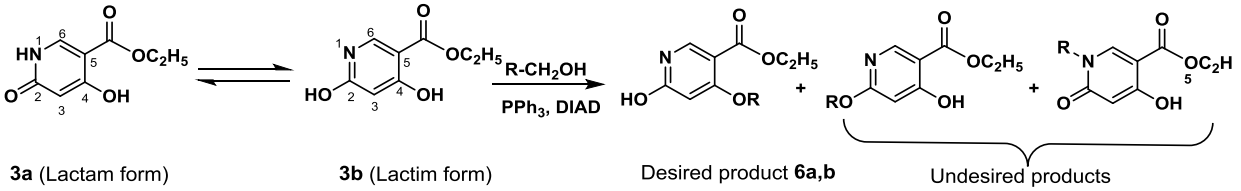

Figure 46: Tautomerism of 2-pyridinone ring system and its effect on alkylation reaction.

Indeed, attempts to selectively O-methylate/benzylate the C-4 OH in **3** using Mitsunobu conditions resulted in the formation of a mixture of N^1-, O^2-, and O^4-alkylated products (**Figure 46**), which could not be separated by flash chromatography.[155] To circumvent this problem, the N^1-Boc protected pyridinone **4** was prepared by reacting **3** with di-*tert*-butyl dicarbonate Boc_2O in THF, using sodium hydride as a catalyst, (68% yield). The chemoselective *N*-protection over *O*-protection results from the greater stability of (*N*-Boc) carbamate versus the O-Boc carbonate in basic medium.[156]

Having protected the lactam nitrogen, the *O*-alkyaltion of the C-4 OH in **4** was attempted under different basic conditions (NaH, cesium and potassium carbonate) in THF. Surprisingly, under the same base conditions used to put the Boc group on nitrogen it was deprotected, and multiple products were formed. A plausible explanation for these results is that the THF was not completely anhydrous, and that adventitious water acted as a nucleophile, which effected hydrolysis of the amide bond. In fact, *N*-Boc protected nitrogen heterocycles are known to be susceptible to base promoted amide hydrolysis, due to the stability of the N-anion that is produced as a leaving group in such reactions.[157] In light of these results, attention was turned to using the Mitsunobu reaction for the aryl-alkyl ether formation step, as base is not included in

the protocol.[158] The Mitsunobu reaction was carried out using benzyl alcohol/methyl alcohol in combination of triphenylphosphine and diisopropyl azodicarboxylate (DIAD) in THF at room temperature. The required O^4-alkylated products **5a,b** were isolated in 51% and 47% yield, respectively. The moderate yields in these reactions was a consequence of difficulties encountered during separation of the products from hydrazine and triphenylphosphine oxide by-products. Formation of the O^4-alkylation products was confirmed by the presence of deshielded protons of O-CH_2, of **5a**, and O-CH_3, of **5b** at 5.23 and 3.51 ppm, respectively in the ^{1}H NMR spectrum.

Mechanistically, the Mitsunobu reaction involves: 1) formation of protonated betaine from the reaction between triphenyl phosphine and DEAD, 2) the activation of an alcoholic hydroxyl group by the protonated betaine to form the oxyphosphonium intermediate, and 3) oxyphosphonium attack by the pyridinone anion, nucleophile, in SN_2 mechanism with carbon-oxygen bond cleavage and formation of the final ether (**Figure 47**). One of the main considerations for the Mitsunobu reaction is the pK_a of nucleophile. The acidic proton in the nucleophile must have a pK_a less than 15 for the reaction to be successful.[158] In our case, 4-hydroxypyridine is sufficiently acidic (Pk_a= 11.12) for its participation in the Mitsunobu reaction.[159]

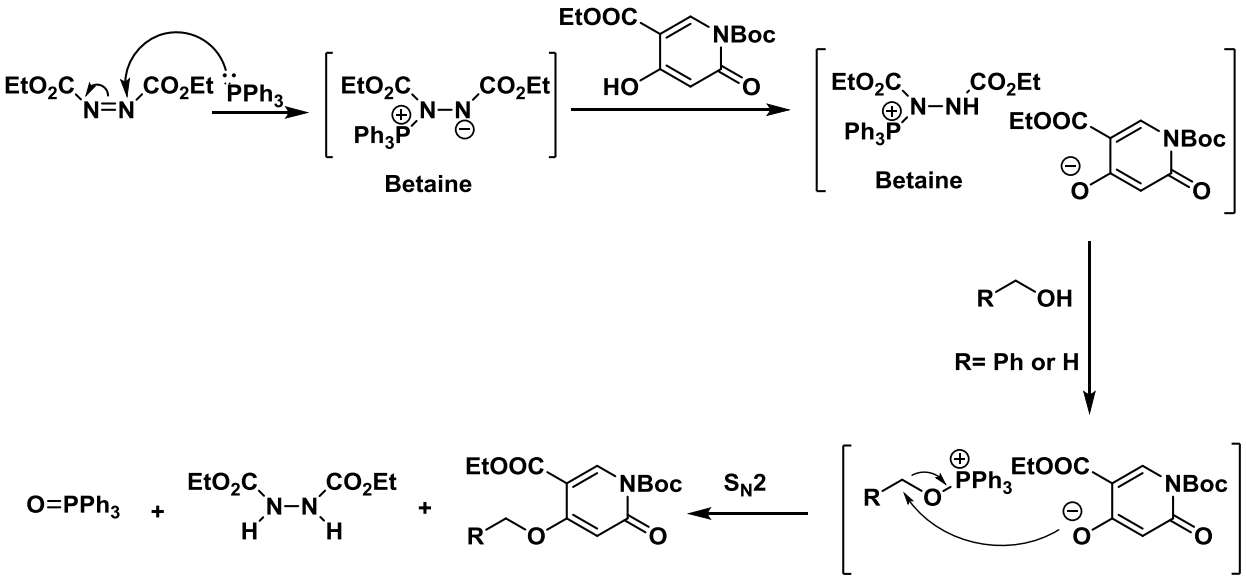

Figure 47: Mitsunobu reaction mechanism.

Subsequent deprotection of the *N*-Boc group in **5a**,**b** was achieved by treatment with trifluoroacetic acid in dichloromethane to give the ester **6a,b** in 90 and 84% yields, respectively. In this deprotection step (**Figure 48**) the *t*-butyl ester group undergoes cleavage in acidic conditions forming carbon dioxide and isobutylene by-products.

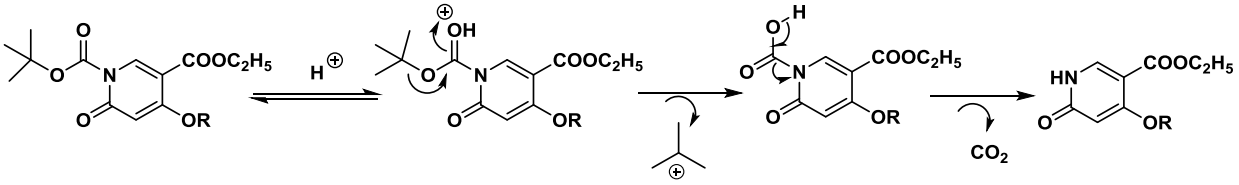

Figure 48: Boc deprotection mechanism.

In the last step, saponification of ester **6a,b** using LiOH in THF:MeOH:H_2O (2:2:1) at room temperature provided the desired acids **7** and **8** in high yield (88% and 84%, respectively).

The structures of compounds **3-8** were confirmed by ^{1}H NMR and mass spectroscopy. For all compounds there are two characteristic peaks in the proton NMR: one peak around 5.8-5.6 ppm for the C-3 H and the other peak at 8.0-7.8 ppm for the C-6 H. The different chemical shifts for these two protons is a function of their chemical environment. The C-6 proton is located on a β-carbon to the exocyclic carboxylate ester or acid which is an electron withdrawing groups while C-3 proton is located on a β-carbon to the exocyclic hydroxyl or alkoxy groups which are electron donating groups.

3.2.2 Synthesis of the Serine Carboxamide Building Blocks 15a-f

The approach adopted for the synthesis of the serine carboxamide components **15a-f** is illustrated in **Figure 49**. The first step involved *N*-Boc protection of L-serine methyl ester **9** (HCl salt) through reaction with Boc_2O in the presence of triethylamine to give **10** in 90% yield.[160] Subsequent conversion of **10** to the fully *O/N*-protected ketal (oxazolidine or Garner's ester) **11** was acheived using DMP in the presence of BF_3-Et_2O as catalyst.[161]

The ester **11** was then saponified to the corresponding acid **12** using aqueous lithium hydroxide in MeOH at room temperature for 12 hours. Acid **12** was then reacted with the library amines under BOP-Cl/Et_3N conditions to produce amides **13a-f** in 51-75% yield. The ^{1}H NMR spectra for compounds **13a-f** showed that the two protons on CH_2 of the serine residue are not equivalent: one multiplet signal for one proton appeared at δ 4.50-4.13 ppm and the other multiplet appeared at δ 4.02-3.85 ppm.

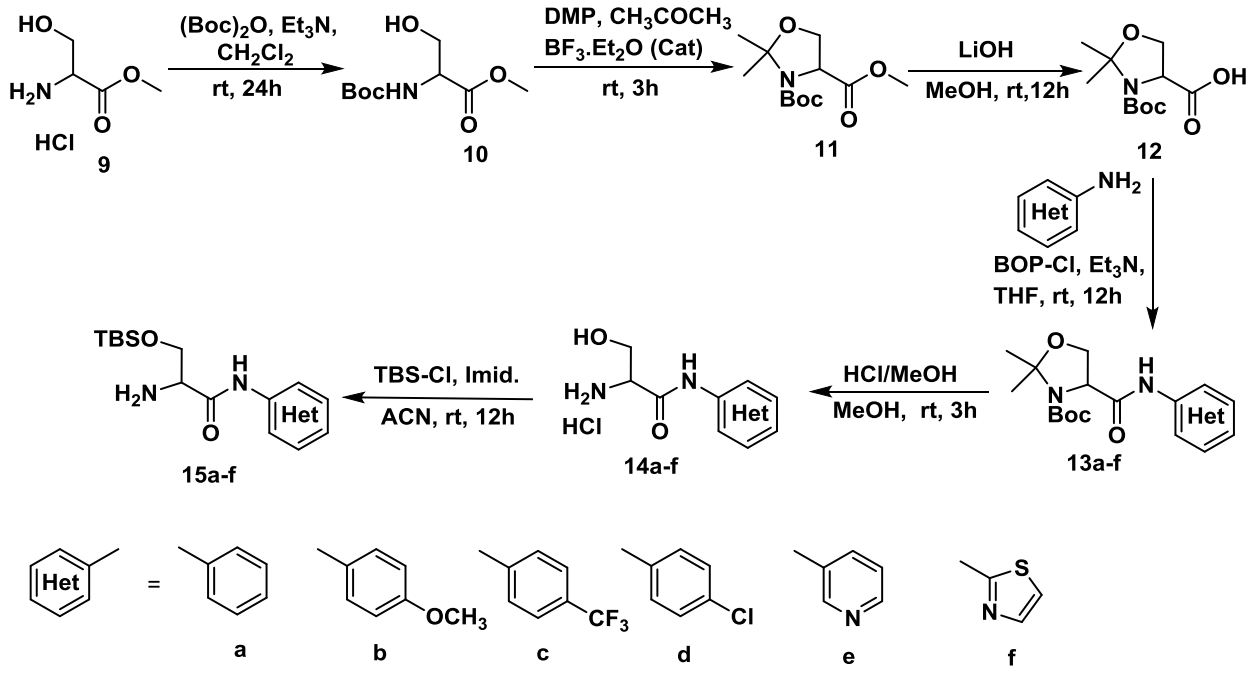

Figure 49: Synthesis of serine carboxamide.

Exploratory experiments were then carried out using aniline as a representative amine component in order to find optimal conditions for the peptide-type coupling reaction that introduce the diversity elements. The results, listed in Table 1, showed that the best (isolated) yield was obtained using BOP-Cl (Table 1, entry 2) so BOP-Cl was applied in the formation of derivatives **13b-f**.

Entry	Coupling agent	Equiv.	Isolated yield (%)
1	BOP	1.2	48%
2	BOP-Cl	1.2	78%
3	PyBOP	1.2	57%
4	HBTU	1.2	28%

Conditions: acid (1 eq), amine (1 eq), Et_3N (3 eq) in THF at room temperature for 12h

Table 1: Selection of peptide coupling agent for **13a-f** synthesis.

BOP-Cl activation of carboxylic acids (**Figure 50)** depends on base-catalyzed formation of a mixed anhydride, which is subsequently attacked by the amine forming the amide.[162]

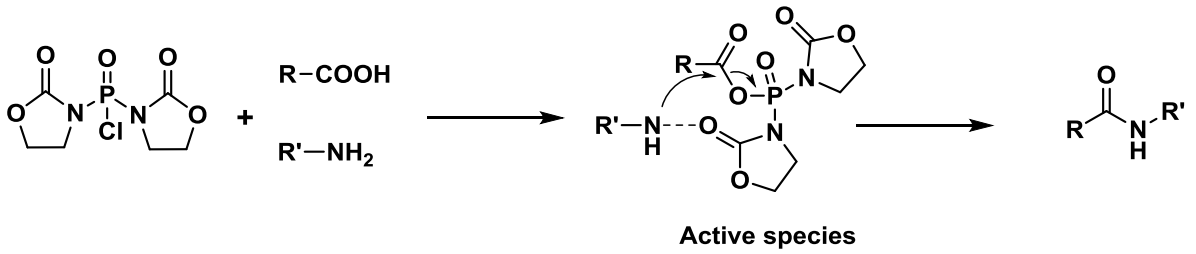

Figure 50: Mechanism of BOP-Cl in amide bond formation.

Cleavage of both the *O,N*-ketal and the Boc group in the following step was initially effected using TFA/CH_2Cl_2 (1:1). However, competing trifluoroacetylation of the liberated amine functionality was observed (**Figure 51**). Even though cleavage of the trifluoroacetyl group could be readily affected by rendering the reaction medium basic prior to work-up, the use of TFA was abandoned in favor of the use of HCl. Indeed, treatment of compounds **13a-f** with methanolic hydrogen chloride at RT for 3 h afforded the *β*-hydroxy amines **14a-f** as hydrochloride salts in good yields (71-84%).

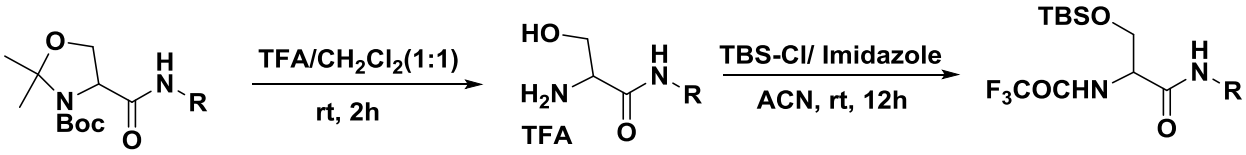

Figure 51: Side reaction from TFA cleavage of *O,N*-ketal.

In the subsequent step, the liberated alcohol function in **14a-f** was *O*-TBS protected, so as to avoid any competing ester formation during the EDC mediated amide coupling reaction. In the experiment, reaction of alcohol **14a-f** with *tert*-butyldimethylsilyl chloride (TBS) in acetonitrile in the presence of imidazole afforded the β-silylated hydroxy amines **15a-f** in 66-75% isolated yields.

3.2.3 Synthesis of Target Compounds 22a-f and 23a-f

The synthetic pathway to access compounds **22**/**23a-f** (**Figure 52**) began with formation of amides **16a-f** and **17a-f**. In cases where racemization is not a concern, one of the most popular ways to form an amide bond is to react an acid chloride with the requisite amine in the presence of a base to trap the HCl generated during the reaction.[163] In our case, formation of the acid chlorides of **7** and **8** through reaction with thionyl chloride was tricky. The reaction was sluggish

and resulted in the formation of many by-products, as shown by TLC. However, the reaction of acids **7** and **8** with amines **15a-f** in the presence of EDC/HOBt/DIEA afforded the desired amides **16a-f** and **17a-f** in moderate to good yields (42-67%).

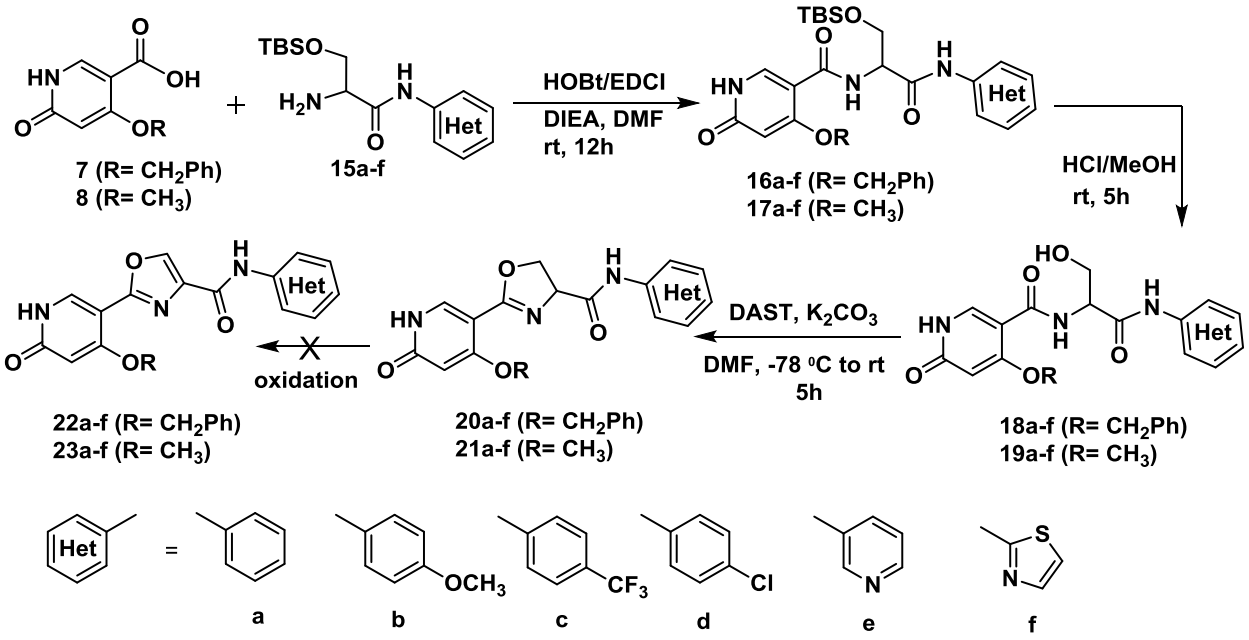

Figure 52: Synthesis of pyridinone oxazole-based compounds.

A problem encountered with this reaction was that considerable quantities of product were lost during the aqueous extraction process. In an attempt to overcome this situation, the concentrated reaction mixture was taken up in a small volume of DCM and applied directly to a silica-gel column. However, even using this strategy purification was difficult, resulting in loss of valuable material.

Intermediates **16a-f** and **17a-f** were initially desilyated using TBAF in THF to give the β-hydroxy amides **18a-f** and **19a-f**. However, again, the aqueous extraction during work up to remove excess TBAF and by-products from TBAF was not ideal because the product had significant water solubility. Efforts to remove excess TBAF with an alternative work-up method using sulfonic acid resin and calcium carbonate also proved unsatisfacory. Ultimately, these problems were circumvented by treating compounds **16** and **17** with methanolic hydrogen chloride, as work-up consisted in simple evaporation of the methanol solvent. The crude product was taken on to the ring closure step without purification.

A variety of reagents and conditions have been developed that effect cyclodehydration of β-hydroxy amides **18a-f** and **19a-f** to oxazolines **20a-f** and **21a-f**, including the use of

diethylaminosulfur trifluoride (DAST) and Burgess reagent (methyl N-(triethylammoniumsulfonyl)carbamate).[164,165] In our hands, the use of DAST at low temperature in the presence of base gave consistently better results.[164] Compounds **20a-f** and **21a-f** were obtained in 16-46% isolated yields (see experimental section, Chapter 8).

Different conditions have also been developed for the oxidation of oxazolines to the corresponding oxazoles.[166-168] However, it was recognized that this transformation can be problematic. Indeed, efforts to dehydrogenate oxazolines **20a-f** and **21a-f** using using $BrCCl_3$/ DBU, MnO_2 or NBS were all unsuccessful. In all cases, formation of multiple products was observed when the reaction was carried out at room temperature, or on mild heating, or at higher temperature (above 80°C).

The structures for the oxazoline derivatives **20a-f** and **21a-f** were confirmed by NMR (Chapter 8, Table 22, and 23) and mass spectroscopy. In the ^{1}H NMR spectra, the disappearance of amide N-H and the O-H protons was noted, and there was a downfield shift in the oxazoline CH (C-4) and CH_2 (C-5) protons. All 12 of the pyridinone-oxazolines **20a-f** and **21a-f** correspond to novel compounds (not described in CAS).

As considerable difficulties were encountered in the conversion of the oxazolines to oxazoles **22a-f** and **23a-f**, the dihydrooxazole derivatives **20a-f** and **21a-f** were instead evaluated as potential ROCK2 inhibitors using the *in vitro* ELISA assay developed in collaboration with Dr. Kath MacLeod's group. The 12 compounds were tested at a single point concentration (10 μM) using Y27632 as a positive control. Disappointingly, eight compounds (**20a**, **20b**, **20c**, **20e**, **21a**, **21b**, **21e**, and **21f**) were only found active (Chapter 7, Table 6) and they exhibited very weak, up to 20%, inhibitory activity against ROCK2 compared to the positive control.

As the synthetic route to the desired oxazoles was long and tedious (purification problems at essentially every step) and it did not prove possible to effect the final oxidation step, we decided abandon further work in this direction.

3.3 Synthesis of Pyridinone-Oxadiazole Carboxamide based series 34a-ah

In view of the difficulty encountered to oxidize the oxazoline intermediates **20/21a-f** to the target oxazoles **22/23a-f**, we turned our attention toward the use of the 1,2,4-oxadiazole ring as an alternative and more readily accessible amide bioisostere. The 1,2,4-oxadiazole motif is found in a number of clinically used drugs, as well as in many molecules currently in late stage clinical trials.[169-171] This amide/ester bioisostere has the advantage of higher metabolic and

hydrolytic stability.[172] Due to the significance of 1,2,4-oxadiazoles in drug development, numerous approaches have been described in literature for the synthesis of this ring system. One of the common methods used involves the condensation of amidoximes with carboxylic acid derivatives (acid chlorides, nitriles, esters, or other activated acid derivatives) (**Figure 53**).[173-175]

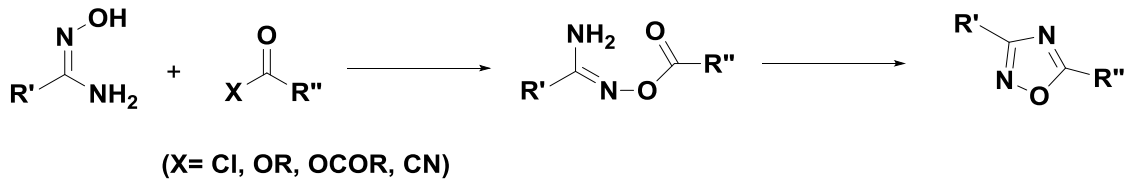

Figure 53: General method for 1,2,4-oxadiazole synthesis.

We have used this approach to synthesize of a series of 34 novel pyridinone-1,2,4-oxadiazoles based compounds **34a-ah** (not described in CAS), incorporating the N-substituted amide function at C-5 of the oxadiazole ring (**Figure 54**).

The synthetic pathway to access compounds **34a-ah** (**Figure 54**) began with the CDI-mediated conversion of the commercially available acid **24** to amide **26.** In this process, the *in situ* generated *N*-acylimidazole **25** intermediate was treated with ammonium hydroxide at room temperature to afford the primary amide **26** in 77% yield.

Examination of the ^{1}H-NMR spectrum of the amide product **26** showed the appearance of new broad singlet at δ12.36 ppm corresponding to NH_2. The peaks corresponding to H-2, H-4, and H-5 in the proton spectrum were observed at 7.9-8.0 ppm, 7.8-7.7 ppm, and 6.4-6.3 ppm respectively.

Dehydration of amide **26** using cyanuric chloride (CyCl) in DMF at 40 ^{o}C subsequently afforded nitrile **27**. The advantage of using these conditions was that it required only one third of equivalent of cyanuric chloride for the reaction to go to completion, and the cyanuric acid by-product was easy to remove by aqueous extraction.

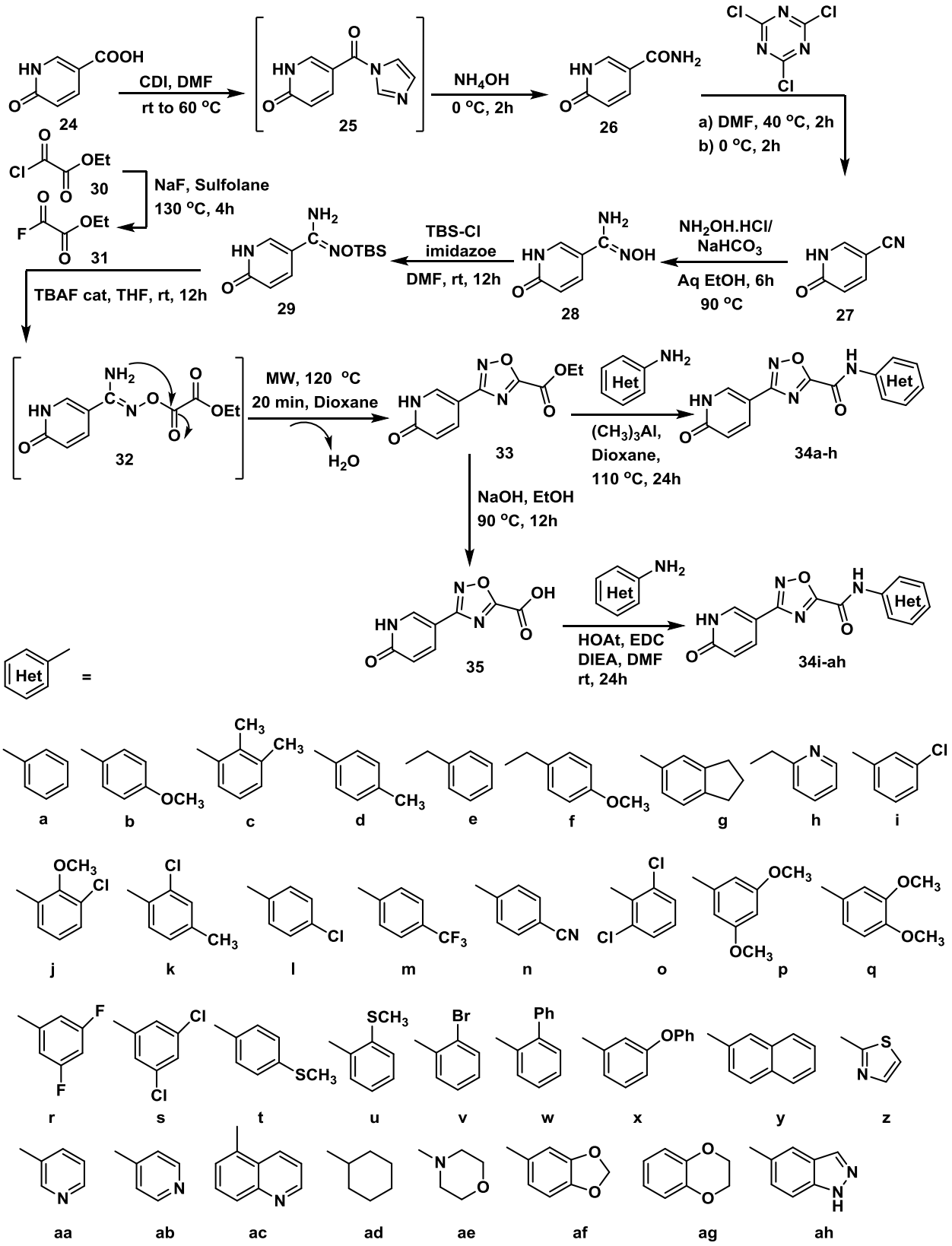

Figure 54: Synthesis of pyridinone oxadiazole carboxamide-based compounds.

The mechanism for the cyanuric chloride-mediated dehydration of amide **26** is depicted in **Figure 55**. In the first step, the hydroxyl group of DMF is activated by a nucleophilic aromatic substitution S_NAr to form the reactive species, a Vilsmeier adduct. The next step involves the dehydration of the amide by the *in-situ* generated Vilsmeier adduct to produce the nitrile function.[176] In the ^{1}H-NMR of nitrile **27** a downfield shift for the H-2 signal occurred relative to the same proton in the spectrum of amide **26**. This was attributed to the more electron-withdrawing effect of nitrile group.

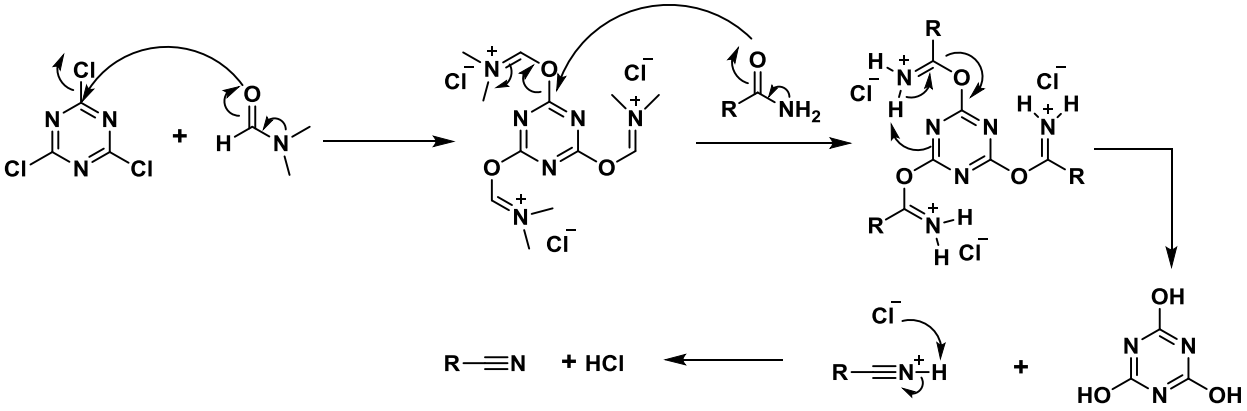

Figure 55: Dehydration of primary amides by CyCl.

Nitrile **27** was converted to amidoxime **28** (an amino oxime) upon reaction with hydroxylamine hydrochloride in the presence of sodium bicarbonate as a base in an ethanol/water mixture (4:1). This involved nucleophilic attack on the nitrile carbon atom by the nitrogen atom of hydroxylamine.[177] One of the challenges encountered during work–up procedures for the amidoxime **28** was its high polarity, which made the purification step difficult.

Efforts to condense amidoxime **28** with the acid chloride of monoethyloxalate **30,** in the presence of triethylamine as a catalyst, to give **32** using different solvent and temperature conditions resulted in the formation of a complex mixture of products (as seen by TLC). This is presumably because there is, once again, competing acylation of NH of lactam and OH of lactim tautomer. However, this situation was effectively circumvented using new conditions we developed, based upon the condensation of the *O*-silylated amidoxime **29** with the acyl fluoride **31**. Acid fluorides have the advantage of being more stable toward oxygen nucleophiles, such as water or methanol, than the corresponding acid chlorides due to the nature of the C-F bond.[163] In addition, acid fluorides react more efficiently with amines than do acid chlorides.[163] Further, reaction of acid fluoride with silylated hydroxyl group would avoid base catalysis since the reaction is driven forward by the formation of strong Si-F bond.[178] The silylated amidoxime **29**

was obtained by silylation of the hydroxyl group of **28** using *tert*-butyldimethylsilyl chloride in DMF in the presence of imidazole as a base, while the acid fluoride **31** was prepared by heating the acid chloride of monoethyloxalate **30** with sodium fluoride in high-boiling polar aprotic solvent, sulfolane, and then distilling off the product.[179] Reaction of the silylated amidoxime **29** with acid fluoride **31** at room temperature in presence of catalytic amount of TBAF afforded *O*-acylated amidoxime **32.** TBAF act as a catalyst initiating the desilylation of oxygen to generate a reactive oxygen anion that attacks the acid fluoride carbonyl group. The fluoride ion released in this step engages in the *O*-desilyaltion process. After solvent change from THF to dioxane, the acyclic intermediate **32** cyclized to ester **33** by heating at 120 ^{o}C for 20 minutes under microwave conditions (61% yield). This involved the intramolecular nucleophilic attack of the amine nitrogen on the carbonyl carbon followed by dehydration and aromatization. The ^{1}H NMR spectrum of compound **33** confirmed the formation of the product (absence of signal of the starting material **29** at 6.05 (s, 2H, NH_2) and the appearance of chemical shift changes of the protons at C-2', and C-4'relative to the starting material **29**. These chemical changes are assumed to be due to the electron-withdrawing effect of the oxadiazole.

Ester **33** was converted directly to amides **34a-h** by reaction with the requisite amines in presence of trimethylaluminium as a catalyst at 110 ^{o}C for 24h (23-41% yields). The mechanism of ester aminolysis is illustrated in **Figure 56**.[180,181] This synthetic strategy was used to synthesize the eight novel compounds **34a-h** (not described in CAS). The structure of these target compounds were confirmed by ^{1}H-NMR (Chapter 8, Table 24) and high resolution mass spectroscopy.

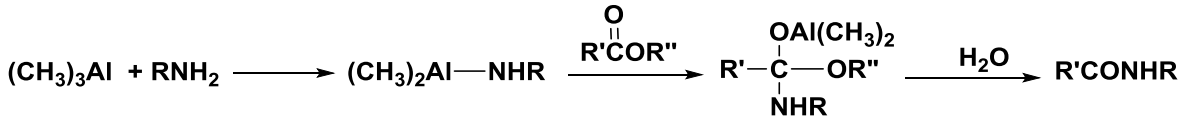

Figure 56: Trimethylaluminium-mediated amide formation.

However, as the amide bond forming conditions were harsh and the yields were not good, we opted to use classical peptide coupling reagents to synthesize the remaining target compounds **34i to 34ah**. In preparation for this operation, ester **33** was hydrolyzed (NaOH, EtOHaq, heat, 12 h) to acid **35**.

3.3.1 Optimization of Peptide Coupling Conditions for the Synthesis of 34i-ah

To find the optimal conditions for the peptide-coupling step, the reaction of the acid **35** with aniline with different coupling reagents was studied (Table 2)

Entry	Coupling agent	Equiv.	Isolated yield (%)
1	EDC	1.2	18%
2	BOP-Cl	1.2	20%
3	PyBOP	1.2	15%
4	EDC/HOBT	1.2/1.2	48%
5	EDC/HOAt	1.2/1.2	58%
6	HOAt/HATU	1.2/1.2	51%

Conditions: Acid (1 eq), amine (1 eq), DIEA (3 eq) in DMF at room temperature for 24h

Table 2: Optimization of peptide coupling agents for **34i-ah** synthesis.

The results showed that reactions using EDC, BOP-Cl, and PyBOP did not go to completion, as the product yields were low (up to 20 %) and most of the starting material was recovered. However, using the coupling agent pairs EDC/HOBT, EDC/HOAt, and HOAt/HATU resulted in greater conversion of the starting material to the product, and the yields were effectively doubled (48-58%). The best yield for the coupling product was observed with EDC/HOAt mixture (Table 2, entry 5).

Having established using HOAt/EDC as coupling mixture, we then explored the optimization of the base used during coupling. We performed a series of experiments (Table 3) using different equivalents of non-nucleophilic Hunig's base DIEA together with of EDC/HOAt (1.2 eq) coupling agents in DMF at room temperature for 24h. The base screen showed that DIEA in 2.5 equivalents (Table 3, entry 2) gave the best conversion so it was selected as the optimal base condition for the coupling reaction.

Entry	Hunig's base	Equiv.	Isolated yield (%)
1	DIEA	1.2	35%
2	DIEA	2.5	56%
3	DIEA	3	56%

Table 3: Optimization of base for **34i-ah** synthesis.

The reaction of the acid **35** (1 eq) with aniline (1 eq) in presence of EDC/HOAt (1.2 eq) and DIEA (2.5 eq) in DMF was monitored, by TLC, at different temperatures (rt, 50 ^{o}C, and 80 ^{o}C). At high temperatures, the reaction failed to provide the full conversion and the yields separated were less than that at room temperature (56%, 18%, and 7% yields obtained at rt, 50 ^{o}C, and 80 ^{o}C respectively). Furthermore, Microwave-assisted peptide coupling was tried at 100 ^{o}C but it was very sluggish and led to the formation of several byproducts.

The peptide coupling reaction of acid **35** with aniline was monitored by TLC over 48h and no change happened in TLC after the first 24h so it was chosen as the optimal time for the reaction. DMF was also chosen as a solvent for the peptide coupling reaction because of the high polarity of the starting acid which made it insoluble in various solvents like DCM, THF, and ACN.

Having established conditions for the coupling reaction, acid **35** was reacted with the set of 26 amines to give pyridinone-oxadiazole carbocamides **34i-ah**. Although the preparation of these amides worked well in most cases, the observed variation in yield from 18%, for the worst cases **34v**, to 56%, for the best case **34ad**, was found to be dependent on the nucleophilicity of the amine. Amines bearing electron-donating substituents, such as amine components in **34ad**, generally behave better than the ones bearing electron-withdrawing substituents, such as amine component in **34v**. It is also a consequence of the limited solubility of amides **34i-ah** in typical organic solvents (DCM, EtOAc, etc), and DMSO, which made it difficult to purify them by flash chromatography. The reason for this insolubility is presumably due to the complimentary hydrogen bond donors and acceptors inside the molecule, which results in strong solute-solute interactions and self-assembly.

The structures of the target compounds **34a-ah**, issuing from both amide bond forming techniques, were confirmed by ^{1}H-NMR (Chapter 8, Table 24) and high resolution mass spectroscopy. As expected, the ^{1}H NMR spectra for compounds **34a-ah** showed that only minor

chemical shift changes occur for the signature peaks for the C-2', and C-4' protons relative to the starting pyridin-6-one-3-carboxylic acid **24**. These chemical shift changes are assumed to reflect the electron-withdrawing effect of the oxadiazole ring as well as the polarity of the (hetero)aromatic substituent on the oxadiazole ring.

The diverse amine components, used to construct the library of molecules **34a-ah**, were chosen amongst different aryl, heteroaryl, benzyl and cycloalkyamines, such that we could identify motifs that productively occupy the type 2 inhibitor allosteric site in the activation loop closed conformation in ROCK1/2. However, due to limited budget resources, only 10 compounds (**34a**, **34f**, **34j**, **34l**, **34n**, **34r**, **34z**, **34aa**, **34ac**, **34af**) were initially submitted for screening in the ROCK2 inhibitory assay developed by Dr. Kath MacLeod's group (see chapter 7). The compounds were tested at a single point concentration (10 μM) using Y-27632 as a positive control. Among the tested compounds, eight compounds (**34a**, **34f**, **34j**, **34l**, **34r**, **34aa**, **34ac**, **34af**) showed a weak Rho-kinase inhibitory activity (Chapter 7, Table 7). After optimizing the test conditions by Dr. MacLeod's group, 24 compounds (**34a-c**, **34e-g**, **34j-n**, **34p-r**, **34u**, **34w-ac**, **34ae**, and **34af**) were tested against ROCK1 and ROCK2 at a single point concentration (10 μM) using H-1152 as a positive control. The results (Chapter 7, Table 8) showed improvement on ROCK inhibitory activity compared to oxazoline compounds **20**/**21a-f**. Additionally, all of active compounds inhibited ROCK1 in preference to ROCK2. In particular, compounds **34g** (71% inhibition), **34q** (55% inhibition), **34af** (62% inhibition), and **34ag** (58% inhibition).

In summary, pyridinone-oxadiazole based scaffold can serve as starting point for further structural optimization to improve inhibitory activity and isoform selectivity.

3.4 Synthesis of Isomeric Pyridinone-Oxadiazole Based Derivatives 41a-g

At this juncture, the decision was made to evaluate whether modifying the geometry of the pyridinone-oxadiazole carboxamide structure, by changing the point of attachment of the oxadiazole ring to the pyridinone scaffold from C-5 to C-3, would enhance binding affinity to ROCK1/2. A series of seven isomeric pyridinone-based derivatives **41a-g** were prepared, where the amine components were chosen amongst those conferring activity to compounds **34a-ah** (**Figure 57**).

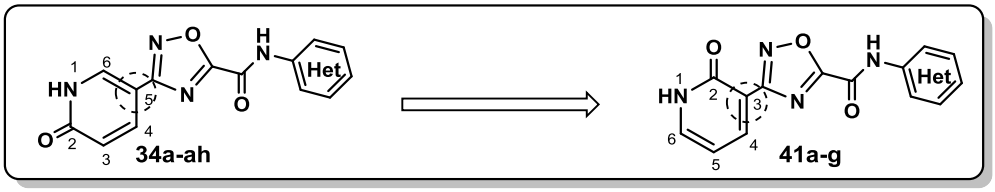

Figure 57: Isomeric modification of 6-pyridinone-based compounds.

In principle, this modification would enable us to explore an alternate arrangement of H-bond donor/acceptor interactions with the hinge residues and whether such molecules more readily access the inner type 1 and type 2 inhibitor selectivity pockets in the ATP binding region (**Figure 58**).

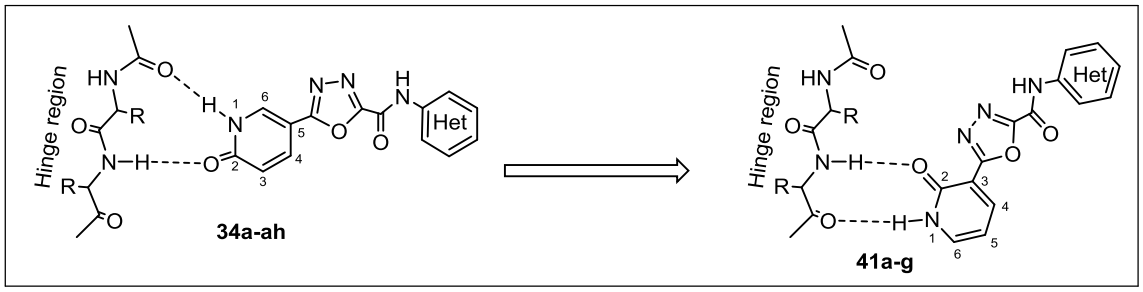

Figure 58: Difference between pyridinones **34a-ah**, and **41a-g** in their orientation within the hinge residue.

The synthesis of compounds **41 a-g** was accomplished by an alternative and more convergent route to that used for compounds **34a-ah**, which involves assembly of the oxadiazole ring through condensation of the amidoxime intermediate **38** with the requisite oxalate amide derivatives **40a-g** (**Figure 59**).[182]

This four-step approach started with the transformation of commercially available 2-chloronicotinonitrile **36** to 2-hydroxylnicotinonitrile **37** in excellent yield (96%) via heating in glacial acetic acid at 125^{o}C for five hours. The derived pyridinone **37** was then transformed into amidoxime **38** by reaction with hydroxylamine hydrochloride and sodium bicarbonate for six hours in refluxing aqueous ethanol. The amidoxime **38** was isolated with a good yield (71%) and was characterized by ^{1}H NMR (Chapter 8, Table 25) and mass spectrometry. The 2-(arylamino)-2-oxoacetates esters **40a-g**, obtained by reacting the set of amines with ethyl chlorooxoacetate **39** in the presence of triethylamine, were coupled with amidoxime **38** in the presence of sodium hydride to provide an intermediate *O*-acylamidoxime, which was heated at 60 ^{o}C in DMF to furnish the target pyridinone-oxadiazoles carboxamide derivatives **41a-g** in yields ranging from 23-44%.

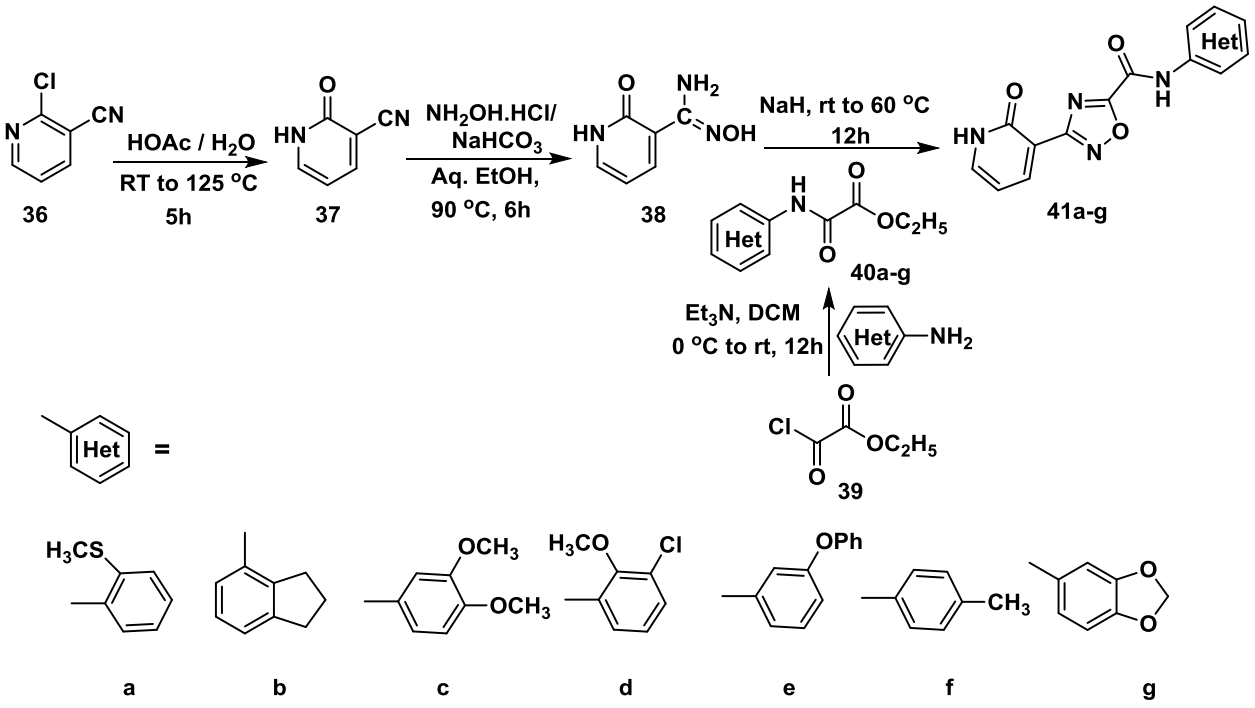

Figure 59: Synthesis of isomeric pyridinone oxadiazole carboxamide-based compounds.

The synthesized compounds were screened *in vitro* against ROCK1 and ROCK2 at a single point concentration (10 μM) using H-1152 as a positive control. To our disappointment, attachment of the oxadiazole ring to the pyridinone scaffold at C-3 did not improve affinity for ROCK. The results (Chapter 7, Table 9) indicated that six compounds, **41a-e**, and **41g**, exhibited weak inhibitory activity (less than 40% inhibition), compared to the positive control, and weak selectivity against ROCK isoforms.

3.5 Synthesis of Modified Pyridinone Oxadiazole-Based Compounds 45a-f

To complete our study of the pyridinone oxadiazole-based compounds, a series of six compounds **45a-f** were prepared to probe the effect of omitting the carboxamide component of the linker. In principle, this should provide us with molecules acting as type I ROCK inhibitors (Figure 60).

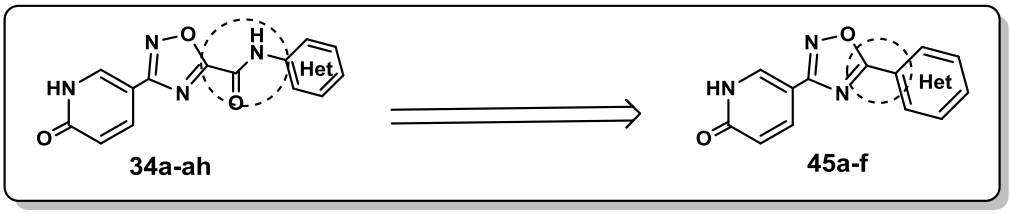

Figure 60: Linker shortening of pyridinone oxadiazole-based compounds.

The synthesis of compounds **45a-f** was achieved by condensing two key building blocks: the silylated amidoxime **28** and the acid fluorides **43a-f** as depicted in **Figure 61**.

The aroyl fluorides **43a-f** were prepared by reacting the corresponding benzoic acid derivatives **42a-f** with cyanuric fluoride in DCM at room temperature. Acylation of the silylated amidoxime **28** with the acid fluoride at room temperature in the presence of catalytic amount of TBAF afforded *O*-acyalted amidoxime **44a-f**. This acyclic intermediate **44a-f** was heated under microwave conditions at 100 ^{0}C for 20 minutes, to accelerate the ring closure reaction rate. The cyclodehydration afforded the target compounds **45a-f** in yields ranging from 25-63%.

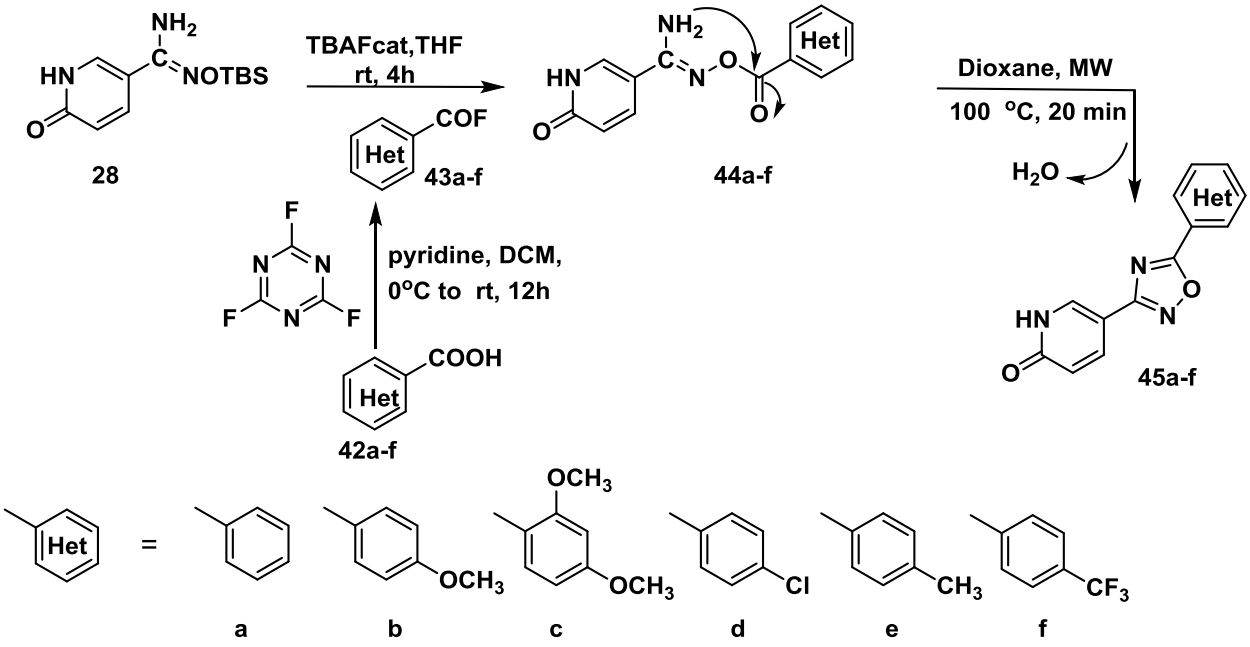

Figure 61: Modified pyridinone oxadiazoles **45a-f**.

The derived tricyclic compounds **45a-f** were assayed for their potential as Rho-kinase inhibitor. Disappointingly, no activity was observed. This suggests that the carboxamide component in the more elongated pyridinone-oxadiazole is beneficial for activity. Although these results obtained for the oxazolines and oxadiazoles compounds were very preliminary (primitive), they did encourage us to move forward in our goal to design and identify isoform selective ROCK inhibitors molecules possessing the essential structural characteristics typical of Type II kinase inhibitors.

Chapter 4

Structural Elongation of the Linker Component

4.1 Introduction

Progressing forward with our goal to identify type II Rho-kinase inhibitors, two modifications to the central linker portion in the pyridinone compounds **34a-ah** were chosen for evaluation of their influence on isoform selective ROCK inhibition. The first option (**Figure 62**) was to replace the oxadiazole ring by an *N*-acylpiperazine motif as found in **50a-d**, and the second was to replace the oxadiazole ring by a 2-aminothiazole motif, as found in molecules with general formula **65a-p**/**66o,p**. Both of these modifications provide novel structure types, which are more elongated relative to the pyridinone-oxadiazoles **34a-ah**. Further, an additional H-bonding option is created in each molecule-type, and both series of molecules are easily adaptable to parallel synthesis of compound libraries. Note, that, once again, it is the right side component of the molecules that corresponds to the diversity element.

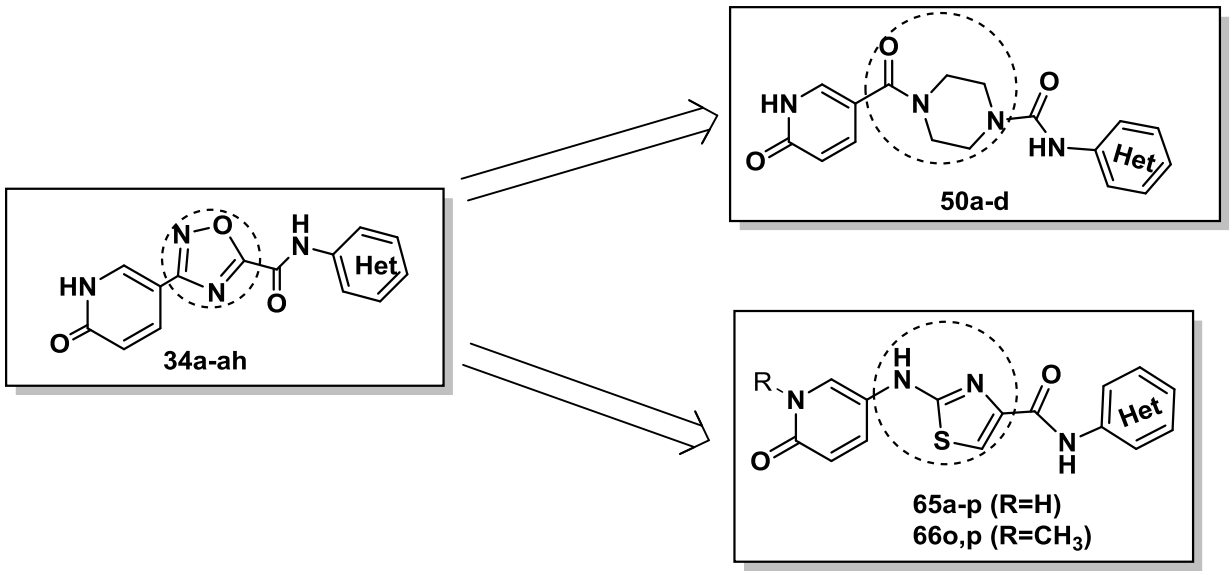

Figure 62: Pyridinone piperazine and pyridinone aminothiazole-based compounds.

4.2 Synthesis of Pyridinone-Piperazine-Based Compounds 50a-d

The rationale behind choosing to incorporate a piperazine ring in compounds **50a-d** derives from literature reports on rho-kinase inhibitors having this substructure (compounds **I**, **XIV**, **XXI**, **XXIII**, **XXIV**, Chapter 1).[105,117,131] Indeed, docking studies on this class of inhibitors showed that cycloalkylamines (piperidine and piperazine), fit into and fully occupy the F region of the ligand-binding pocket of the Rho kinase. Additionally, the presence of the piperazine ring was determined to improve water solubility and oral bioavailability.[131]

We initially envisioned the synthesis of a trial set of four compounds **50a-d** using commercially available aryl isocyanates **47-a-d**, which differ in electron density in the aromatic ring (**Figure 63**). Reaction of these isocyanates with mono Boc-protected piperazine **46** in DCM at room temperature afforded the urea derivatives **48a-d** in good yield (71-88%). Subsequent, *N*-Boc deprotection of **48a-d** under acidic conditions (TFA/CH_2Cl_2) gave the *N*-substituted phenylpiperazine-1-carboxamides **49a-d**. The target compounds **50a-d** were obtained in 38-61% overall yield by coupling acid **23** with amines **49a-d** using HOAt/EDC peptide coupling reagents in DMF at room temperature for 12 hours.

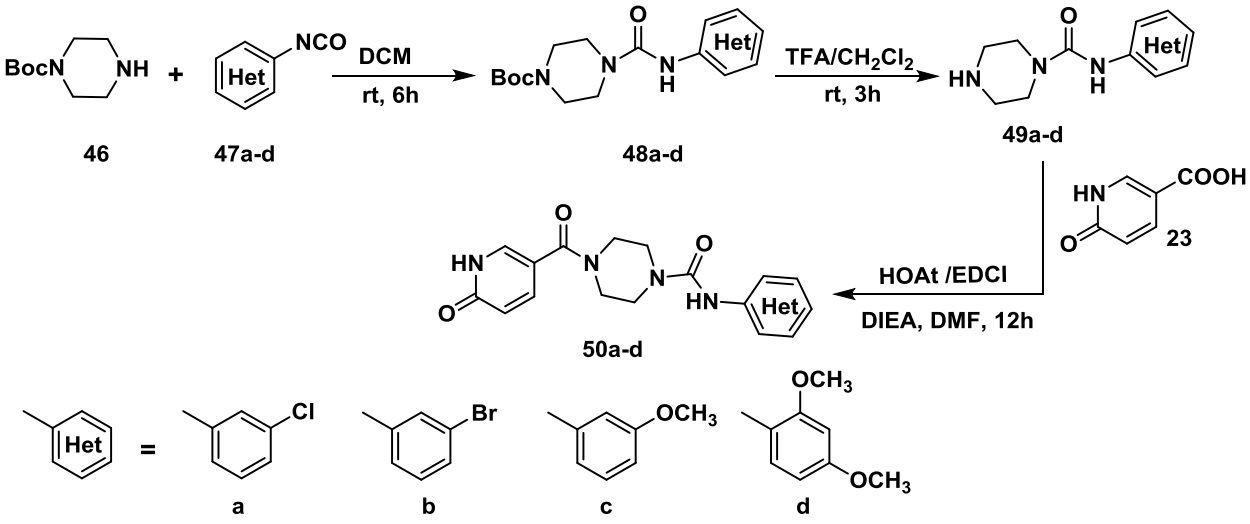

Figure 63: Synthesis of pyridinone piperazine-based compounds.

The preliminary biological results (Chapter 7, Table 10) showed that the substitution of oxadiazole substructure of **34a-ah** with carbonyl-piperazine in **50a-d** resulted in diminished inhibitory activity.

4.3 Synthesis of Pyridinone Aminothiazoles-Based Compounds 65a-p and 66o,p

The 2-aminothiazole motif is frequently encountered in biologically active compounds, including inhibitors of different kinases such as dasatinib (c-Abl kinase inhibitor), BMS-605541 (VEGFR-2 kinase inhibitor), and masatinib (c-kit kinase inhibitor) (**Figure 64**).[105,183,184] Note, that relative to the oxadiazole carboxamides studied in chapter 3 , the longer C-S bond in the thiazole ring was anticipated to alter the geometry and directional orientation of the carboxamide substituents coming off this ring. It was further hoped that this oxadiazole to thiazole modification, plus the added conformational flexibility resulting from incorporation of an NH group between the pyridinone and thiazole rings, would enhance affinity for binding to ROCK. The secondary amino group between the pyridinone head and thiazole ring also provides the opportunity for supplementary H-bonding.[127,128]

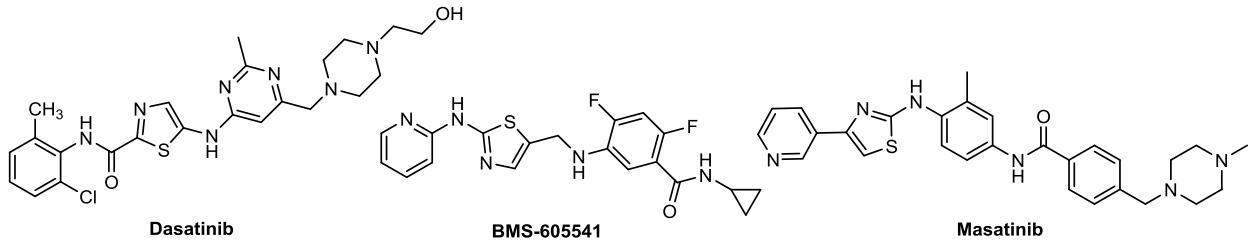

Figure 64: Reported 2-aminothiazole-based kinase inhibitors.

The synthetic route employed to obtain the target pyridinone-aminothiazole-carboxamide compounds **65a-p** is illustrated in **Figure 65**. This six-step reaction sequence, based on the Hantzsch synthesis of 2-aminothiazoles from thioureas and bromopyruvate derivatives,[185] began with reduction of the 5-nitro group in **51** at atmospheric pressure using 10% palladium on carbon as catalyst, to form the corresponding 5-aminopyridinone **53** in 68% yield. These conditions proved vastly superior to the alternate option where nitro compound **51** was heated with a mixture of iron and aqueous hydrochloric acid (Fe-HCl) in methanol. In this instance, the reduction was sluggish and the expected compound was obtained in only 18% yield. The ^{1}H NMR spectrum for compound **53** showed the appearance of broad singlet signal at 4.25-4.15 ppm for the -NH_2- protons.

The next step involved the construction of the thiourea motif. Initially, we attempted to prepare thiourea **57** directly by reacting amine **53** with 1,1'-thiocarbonyldiimidazole (TCDI) followed by quenching with 25% ammonia solution. However, the reaction proceeded in very poor yield (<10%). We also tried another single-step reaction to prepare thiourea **57**, involving reaction of

amine **53** with ammonium thiocyanate in the presence of concentrated hydrochloric acid. To our surprise, the reaction failed to give any product, and the starting material was recovered. However, the reaction of amine **53** with the benzoylisothiocyante in acetonitrile at room temperature for 6 hours afforded the disubstituted thiourea derivative **55** in good yield (75%).[186] The ^{1}H NMR spectrum for this product revealed the appearance of broad singlets at δ 12.01 ppm and δ 11.69-11.64 ppm, attributed to the N-H protons of the thiourea, and a multiplet signal at δ 8.01–7.49 ppm for the phenyl ring protons.

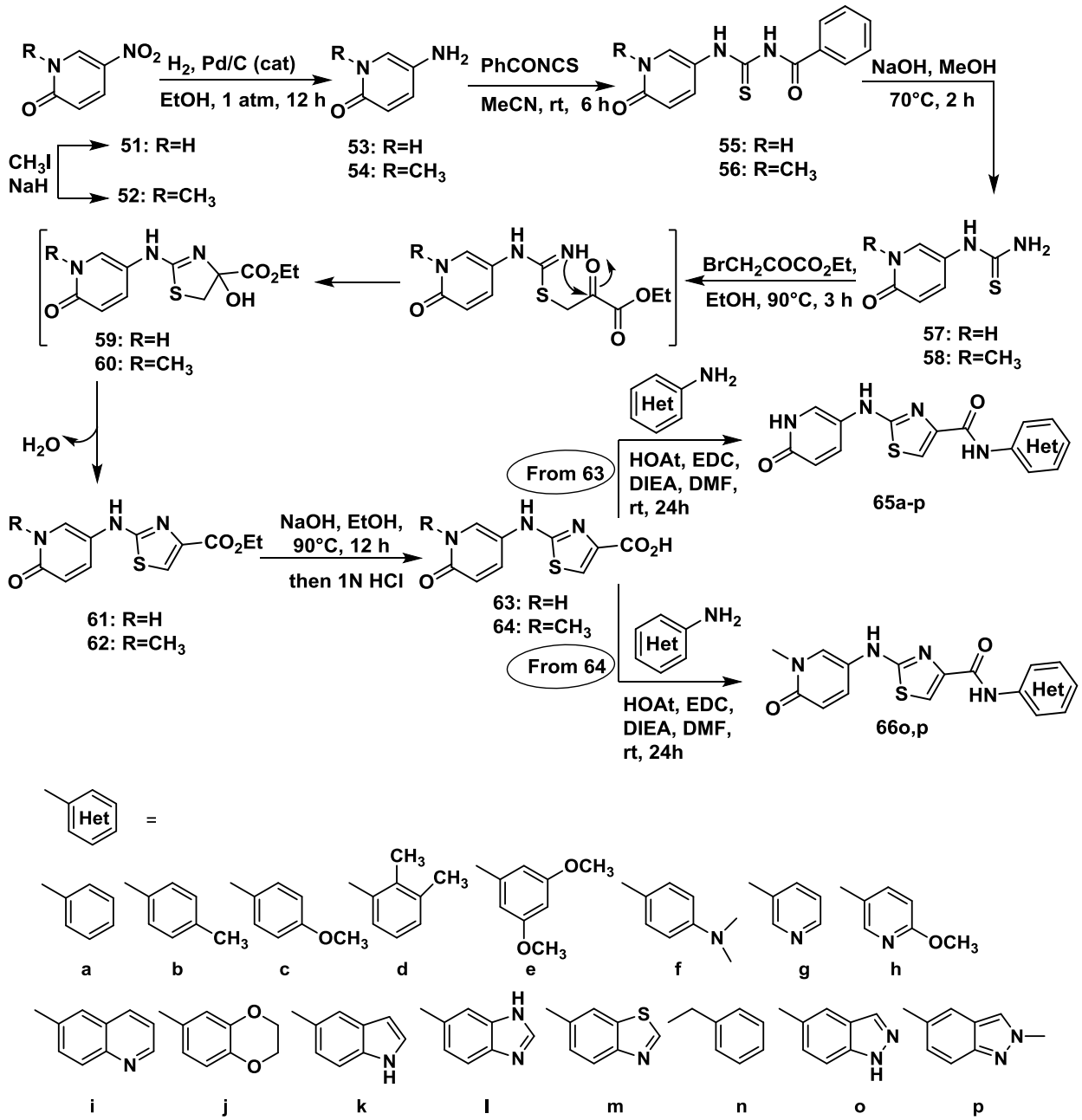

Figure 65: Synthesis of pyridinone aminothiazole-based compounds.

Treatment of *N*-acylthiourea **55** with sodium hydroxide in methanol at 70 ^{o}C readily cleaved the benzoyl group to give the monosubstituted thiourea **57** in good yield (70%). The mechanism for this reaction involves the attack of the hydroxide ion on the electrophilic benzoyl carbonyl group of the *N*-acylthiourea, forming a tetrahedral intermediate which quickly expels benzoic acid.[187] The structure of the hydrolysis product was confirmed by the absence of peaks for the phenyl group in the ^{1}H-NMR spectrum, and the appearance of a broad singlet signal at δ 8.14-6.89 ppm for the NH_2 group.

With thiourea **57** in hand, it was converted to the aminothiazole **61** by reaction with ethyl bromopyruvate in hot EtOH (Hantzsch reaction). This ring forming process is initiated by alkylation of the thiourea sulfur (present in its enethiol form) to form a *S*-alkyl intermediate that cyclizes through nucleophilic attack of the NH at the carbonyl carbon. Elimination of water from the derived thiazoline intermediate **59** then occurs, completing formation of the 2-aminothiazole-4-carboxylate system ring.[185,188] The ^{1}H-NMR spectrum of the product revealed the disappearance of NH_2 signal of thiourea moiety, and the appearance new signals for the C-5 proton of the 1,3-thiazole ring and ethyl group of carboxylate ester.

Ester **61** was subsequently hydrolyzed to the corresponding carboxylic acid **63** (71%) by heating in aqueous sodium hydroxide for 12 hours. Formation of the free acid was confirmed by ^{1}H-NMR (broad singlet signal for the carboxylic proton at δ12.65-12.07 ppm, which disappeared by D_2O exchange).

The last step involved building the library of amide derivatives **65a-o** (13-56% yields) by reacting the set of 15 amines with acid **61** under peptide coupling conditions (HOAt/EDC/DIEA in DMF). Note that, once again reaction work-up and chromatographic purification was complicated by the poor solubility of the amide products in common organic solvents. Note also, that the variation in reaction yields reflected the differences in nucleophilicity of the nitrogen atom in the amines partners (good yields were observed with π-rich (hetero)aromatic amines and vice versa).

Compounds **65a-p** were screened against the two ROCK isoforms. Interestingly, it was observed that the most active analogues were compounds **65g** (ROCK1 % inhibition= 81% and ROCK2 % inhibition= 63%) and **65o** (ROCK1 % inhibition= 91% and ROCK2 % inhibition= 72%) (Chapter 7, Table 11), having 3-aminopyridine and 5-aminoindazole, respectively, as the amine coupling component. Indeed, these results posed the fascinating question as to whether it

was the 2-pyridinone motif or the benzopyrazole (indazole) or pyridine motifs that H-bond to the hinge residues.

To distinguish between these possibilities for compound **65o**, the corresponding analogues **65p**, **66o**, and **66p**, were prepared, where either, or both, the pyridine NH and the indazole N-2 nitrogen are N-methylated. It was envisaged that *N*-methylation would disrupt H-bonding to the hinge C=O, and render the molecules ineffective as ROCK inhibitors.

Compound **65p** was prepared by coupling carboxylic acid intermediate **63** with N^2-methyl aminoindazole. To access compounds **66o,p**, 1-methyl 5-nitropyridin-2-one **52** was prepared from **51** (**Figure 65**) and carried through the steps to give the *N*-methylated carboxylic acid intermediate **64**. It was, in turn, reacted with indazole and N^2-methyl indazole to give the target compounds **66o,p**. Compounds **66o,p** were evaluated against ROCK1 and ROCK2 at a single point concentration (10 μM). According to our initial view that the 2-pyridinone motif binds to the hinge residues, it was anticipated that compounds **66o**, and **66p** would be inactive. However, activity was observed for both compounds and for the N(2)-methylindazole analogue **65p** (Chapter 7, Table 11). That activity was observed for the dimethylated compound **66p**, was particularly surprising. However, pazopanib **L** an N^2-methylated indazole-based kinase inhibitor, (**Figure 66**) is a potent VEGFR tyrosine kinase inhibitor, marketed for treatment of renal cell carcinoma. The drug was found bound to the hinge region of the enzyme via a one hydrogen bond interaction with N^1-H (**Figure 66**).[189] Taking into consideration that *N*-methylation of the indazole ring may not influence activity, these results suggest that binding of compounds **65o,p** and **66o/p** in ATP site of ROCK most likely involves the indazole ring. These result further suggest that central 2-amino-4-carboxythiazole motif that links the two terminal rings can be oriented in either direction. In a similar way, it may be the pyridine nitrogen in compound **64g** that preferentially binds to the hinge residue NH.

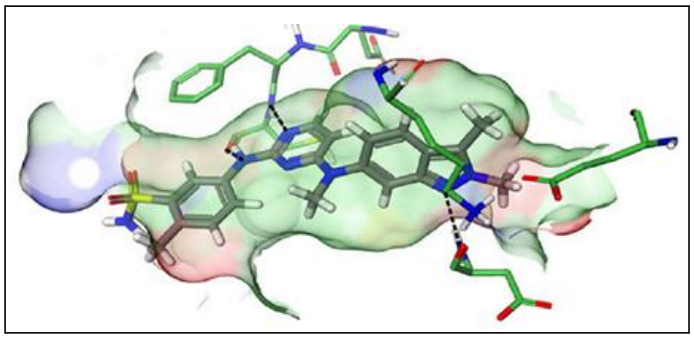

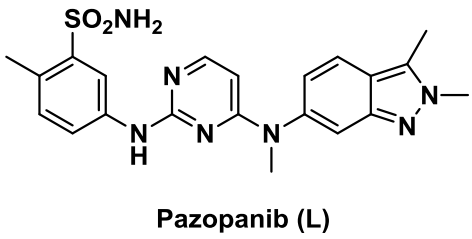

Figure 66: Plausible binding interactions for **66o**, and **66p.**[189]

Based on these observations, it was decided to explore (Chapter 5) the activity of a series of indazole compounds **76a-j**, wherein the indazole is kept on the right side and diversity is introduced on the left side of the molecule by replacing the pyridinone component found in **65a-p** by different aryl and heteroraryl subunits. As the 3-pyridine motif also gave good activity, the corresponding compounds **77a-j** were also included in this study. Further, to complete the investigation of ROCK inhibitors based on indazole hinge binder, we also decided to replace the pyridinone as the hinge binder on the left side by indazole, and to introduce diversity on the right side, as in compounds **80a-q**, **85a-o**, and **93a-x** (Chapter 6).

Chapter 5

Indazole/Pyridine-based ROCK Inhibitors: Introduction of Diversity Elements on the Left Side of the Molecules

5.1 Introduction

The biological data for the *N*-methylated pyridinone-indazole compounds, **65p** and **66o,p**, and pyridinone-pyridine based compound **65g**, suggested that these molecules may display a stronger affinity for ROCK1/2 when it is the indazole and pyridine subunits, rather than the 2-pyridinone motif, that bind H-bond to the hinge residues. To test this idea, the synthesis of a library of compounds **76a-j** and **77a-j** (**Figure 67**) was undertaken, in which the left side of the molecule corresponds to different aromatic/hetero-aromatic motifs and the right side is either an indazole **76a-j** or a pyridine hinge binding motif **77a-j**.

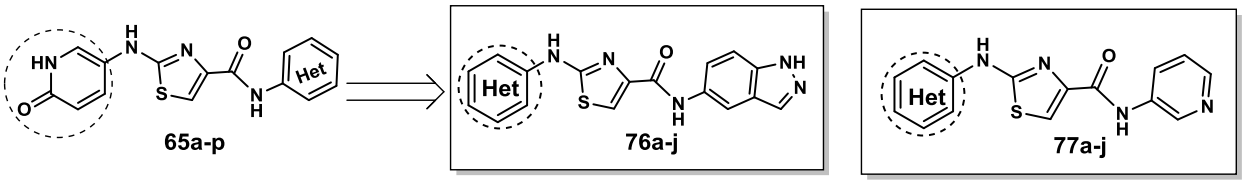

Figure 67: aminothiazole amide-based compound library.

The indazole ring has been successfully used as a building block for the development of ROCK inhibitors (Chapter 1, section 1.7.5). The docking model of **LI** with ROCK (**Figure 68**) showed that the indazole ring resides in the hinge region and forms two hydrogen bond interactions between the N^1-H/N^2 of the pyrazole ring and the backbone C=O group of Glu^{165}/the amide NH of Met^{167} respectively.[190] Additionally, inspired by the binding interactions of compound **XXV** (Chapter 1), we can assume that the 3-pyridine-based compounds we propose can similarily bind via H- bond interactions between the N of the pyridine ring and the NH of Met^{156}.

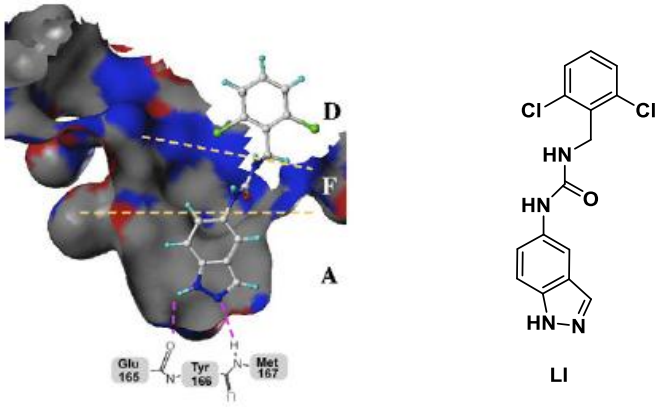

Figure 68: Binding interactions for **LI** with ROCK as determined by homology modeling.[190]

5.2 Preparation of *N*-Aryl Aminothiazole Ester Intermediates 72a-j

5.2.1 Ethyl 2-Bromothiazole-4-Carboxylate as a Common Intermediate to Prepare *N*-Aryl Aminothiazole 72a-j

In the previous chapters, the strategy followed was to introduce the diversity element into the molecule in the last step, through reaction of a suitable activated acid intermediate with a series of aryl and heteroarylamines. To access compounds **76a-j** and **77a-j** an alternate approach was envisaged in which the diverse set of amines is reacted in the first step with ethyl 2-bromothiazole carboxylate, and the two selected hinge binder components are then introduced in an amide bond forming reaction, involving the C-4 acid function in this pivotal thiazole intermediate (**Figure 69**).

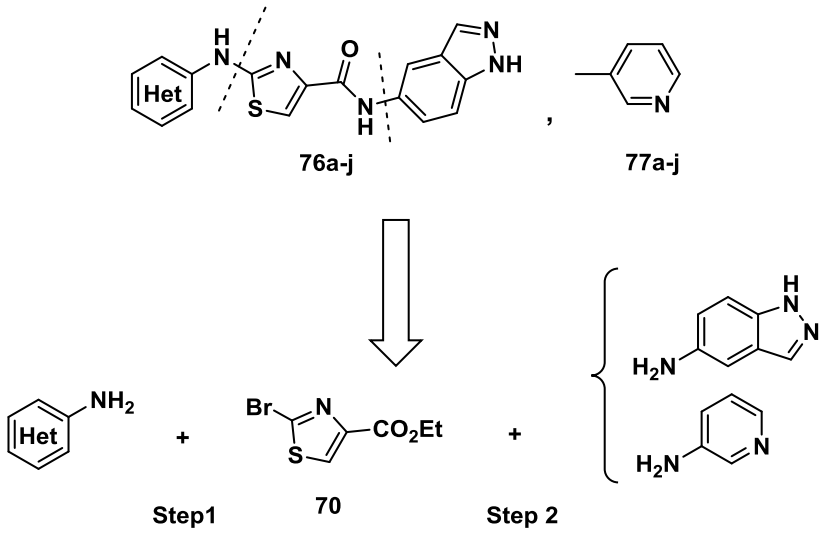

Figure 69: Building compounds **76a-j** and **77a-j** based on 2-bromothiazole ester 70.

The required 2-bromo substituted thiazole intermediate **70** was conveniently prepared in 56% overall yield **Figure 70**), by condensation of thiourea **67** with ethyl bromopyruvate **68**, and reaction of the derived 2-aminothiazole intermediate **69** (obtained in 89% yield) with isoamyl nitrite and copper(II) bromide in acetonitrile at 80°C (Sandmeyer reaction).

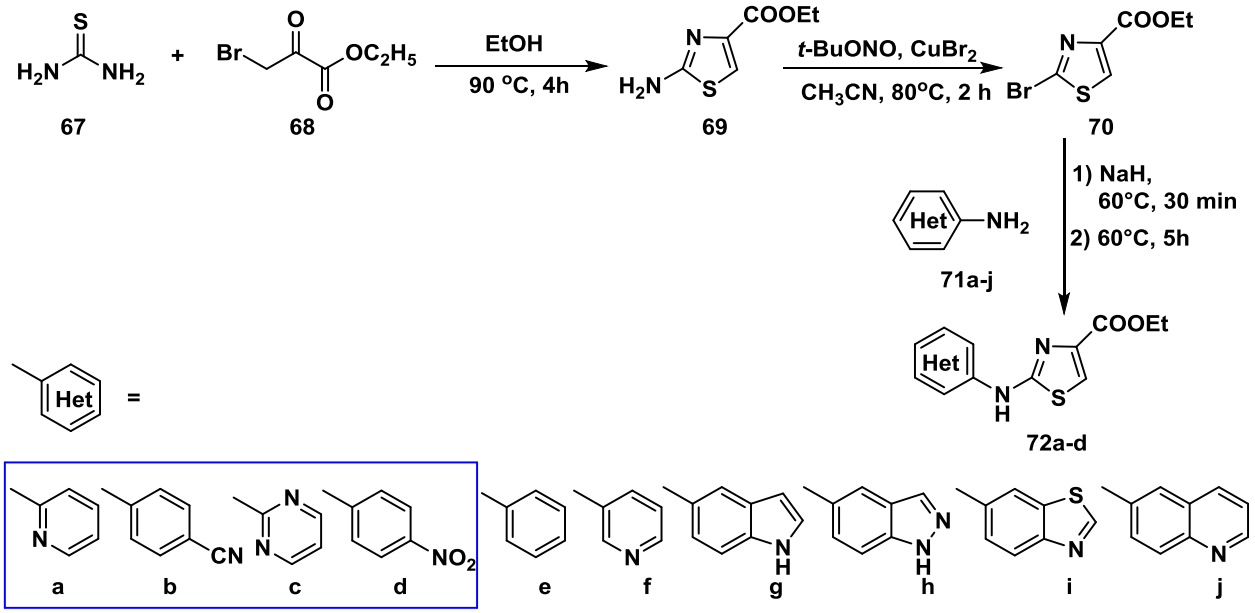

Figure 70: S_NAr reaction of bromothiazole intermediate **70** with (hetero)arylamines **71a-j.**

For the next step two different strategies were studied for *N*-arylation of the thiazole ring at C-2: displacement of the bromo substituent in **70** via an S_NAr reaction,[191] and transition metal (Cu(II)[192,193] and Pd(0)[194,195]) catalyzed coupling processes.

According to the literature, formation of the *N*-arylated thiazoles via S_NAr reactions is considered challenging, due to low nucleophilicity of aniline and other heterocyclic amines.[196] To explore this process, a study of the influence of base on the conversion of **70** to compound **72a** (Table 5) was undertaken using 2-aminopyridine **64a** as a model heterocyclic amine (THF, 60°C, 5 hours). As can be seen, the yields were comparable using either weak or stronger base, but the best result was obtained using sodium hydride as a strong base (Table 4, entry 4).

Entry	Base	Solvent	Yield (%)
1	K_2CO_3	THF	41
2	Cs_2CO_3	DMF	48
3	*t*-BuONa	DMF	51
4	NaH	THF	54

Table 4: S_NAr of bromothiazole under different base conditions.

In this reaction, the idea was to quantitatively convert 3-aminopyridine to the corresponding amide anion, such that the nucleopilicity of the exocyclic amino group would be significantly enhanced.[191] Using these conditions it proved possible to prepare compounds **65a-d**. However, the reaction failed for the other amines **64e-j** studied.

Looking at this substitution reaction from the opposite viewpoint, an alternate way to compensate for poor reactivity of substituted anilines and heteroaromatic amines amines was to activate of thiazole ring toward S_NAr reaction via its protonation under acid conditions.[196] In the experiment, reaction of 2-bromothiazole **70** with amines **71e-j** was studied in the presence of *p*TsOH (**Figure 71**).[196] These conditions worked for the preparation of target compound **72e**, but were unsuccessful for the other aryl and heteroarylamines.

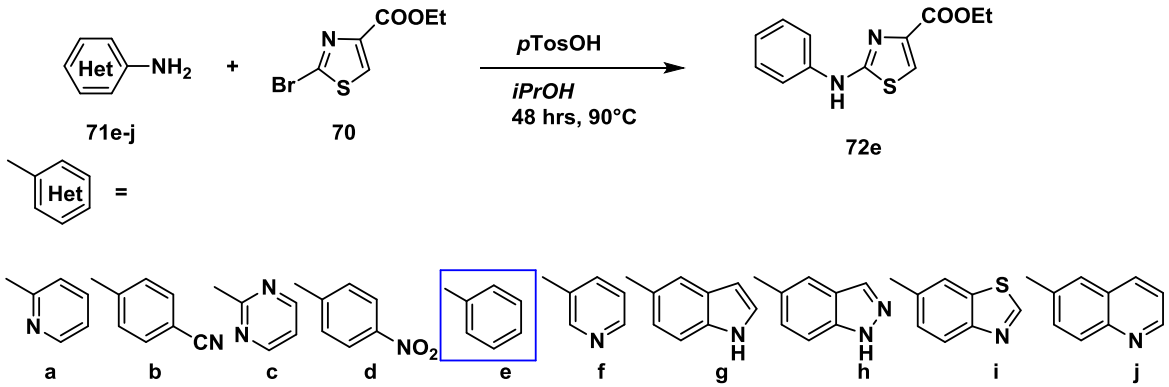

Figure 71: S_NAr reaction of 2-bromothiazole with (hetero)arylamines in acidic medium.

As the S_NAr reaction approach proved to not be readily generalizable to all the (hetero)aromatic amines studied, attention was directed to perfecting copper(II) catalysed C-N cross coupling conditions (Goldberg reaction) for the preparation of the *N*-aryl thiazoles **72f-j** (**Figure 72**).[193] . Indeed, the Goldberg reaction has been used to couple a wide range of (hetero)aromatic amines with (hetero)aryl halides.[192] Based on this, bromothiazole derivative **70** was reacted with 3-aminopyridine **71f** using a catalytic amount (5 mol%) of copper iodide and *N,N'*-dimethylethylamine as the chelating diamine ligand. However, even in experiments where the quantity of ligand is varied considerably (10-50 mol%), product formation was not observed, and the starting material was almost totally recovered.

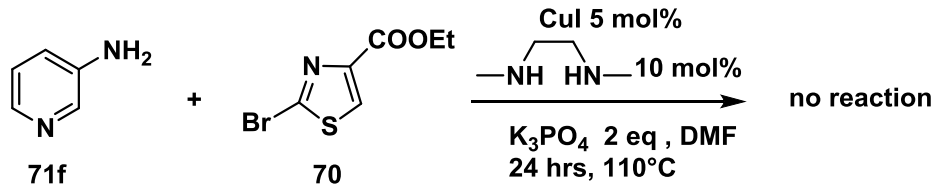

Figure 72: Amination of 2-bromothiazole using Goldberg reaction.

In view of these results, we tried to use another approach for C-N cross coupling based on Buchwald-Hartwig *N*-arylation of 2-bromothiazole **70** (**Figure 73**).[194,195] The reaction was initially studied for 3-amnopyridine **71f** using $Pd_2(dba)_3$ as a catalyst, Xantphos as a ligand, *t*-BuONa as a base in dioxane at 110 ^oC for 24h (nitrogen atmosphere).

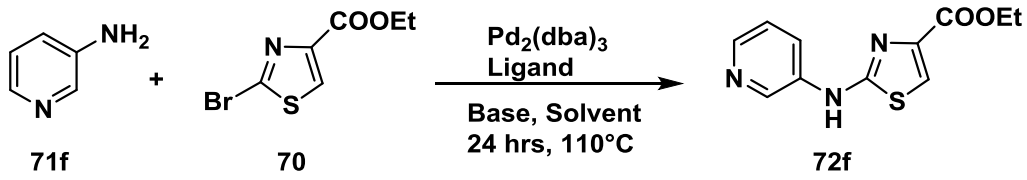

Figure 73: Amination of 2-bromothiazole using Buchwald-Hartwig reaction.

Under these conditions, the product **72f** was obtained in very low (<10%) yield. In order to increase the yield, we ran the reaction in presence of different ligands and different bases as summarized in Table 5. However, the yield remained inferior to 10%. Indeed, 5-membered ring heteroaryl halides containing multiple heteroatoms were found recalcitrant in Pd-catalyzed C–N cross-coupling reactions.[197]

Entry	Pd source	Ligand	Base	Solvent	Yield (%)
1	$Pd_2(dba)_3$	Xantphos	*t*-BuONa	DMF	3%
2	$Pd_2(dba)_3$	XPhos	*t*-BuONa	DMF	5%
3	$Pd_2(dba)_3$	XPhos	Cs_2CO_3	DMF	8%
3	$Pd_2(dba)_3$	Xantphos	Cs_2CO_3	DMF	6%

Table 5: Buchwald-Hartwig cross coupling trials to prepare **72f**.

As for the S_NAr reactions, the origin of the disappointingly poor yields observed for the copper and palladium catalyzed cross-coupling reactions is likely rooted in the low reactivity of both reacting components. We thus decided not to pursue any further use of 2-bromothiazole **70** as a pivotal substructure for the introduction of both sides of the product molecules.

5.2.2 Hantszch Approach to Prepare *N*-Aryl Aminothiazole Esters 72f-j

The more linear approach based on the Hantszch method for the construction of the thiazole ring, enabled the synthesis of the remaining *N*-aryl aminothiazole ester intermeidates **72f-j** required for the preparation our compound library (**Figure 74**).

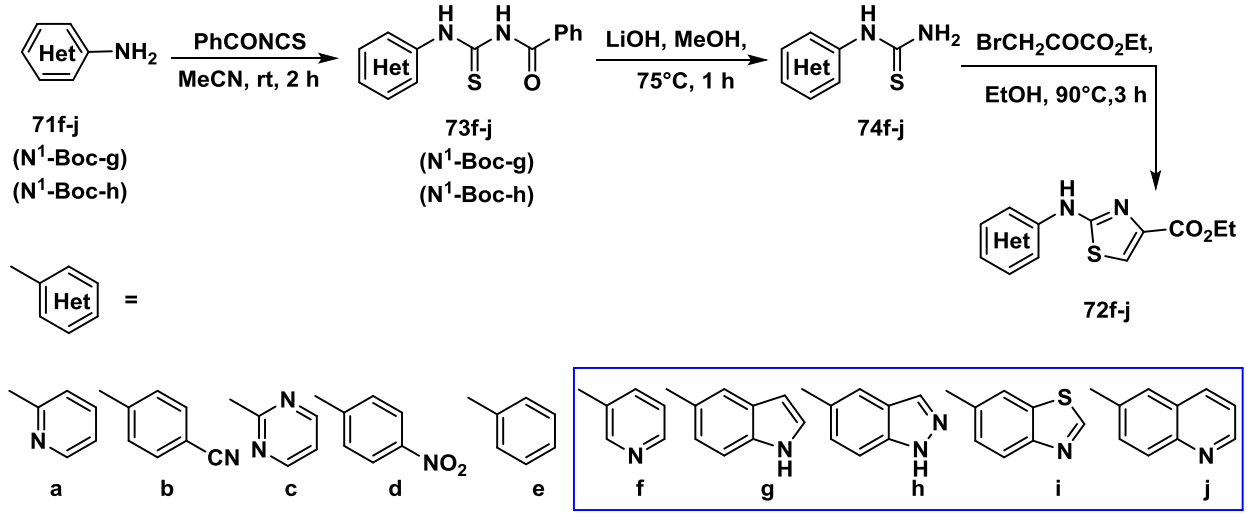

Figure 74: Hantszch synthesis of thiazoles **72f-j.**

In a similar fashion to the synthetic pathway shown in **Figure 65**, The protocol for the synthesis of compounds **72f-j** (**Figure 74**) started with reacting heteroaryl amines **71f-j** (the protected *N*-

Boc-**71g**/**h** were used) with benzoylisothiocyanate in acetonirile at room temperature to form the *N,N'*-disubstituted thiourea **73f-j**. Deacylation of disubstituted thiourea **73f-j** with lithium hydroxide in methanol afforded the key N-substituted thiourea **74f-j** intermediates. Not suprizingly (see earlier) the Boc protecting group on N-Boc-**71g**/**h** was cleaved during the deacylation step. The Boc cleavage in basic medium could happen through the mechanism illustrated in **Figure 75**.[198]

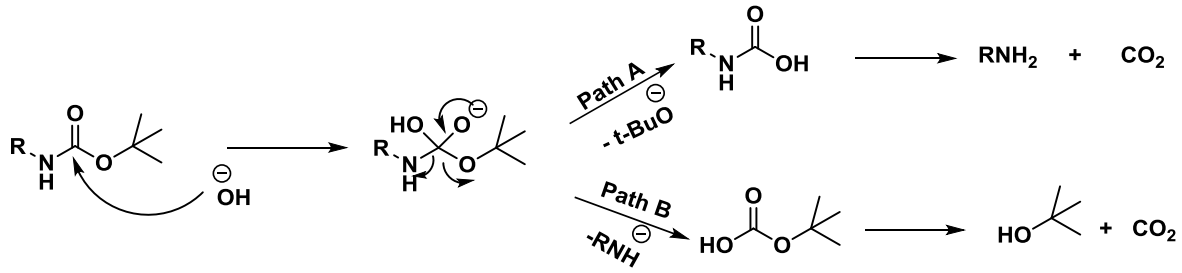

Figure 75: suggested mechanism for Boc cleavage in basic medium.

The cyclocondenastion of thiourea **74f-j** with ethyl bromopyruvate lead to the formation of aminothiazole carboxylate ester **72f-j** in yields ranging from 51%-73.

5.3 Preparation of Compounds 76a-j and 77a-j

The final stage in the synthesis of the library of compounds **76** and **77** was to attach the 3-pyridyl and 5-indazolyl hinge binder components to acids **75** via an amide bond forming reaction, as illustrated in **Figure 76**.

The acid precursors **75a-j** were prepared by hydrolysis of esters **72a-e** (obtained from the S_NAR approach) and **72f-j** (obtained from Hantszch approach) using aqueous lithium hydroxide in methanol for 12 hours (44-76% yields). It should be noted that the separation of two acid derivatives, **75g** and **75j** was troublesome. Unlike the others, these two compounds did not precipitate out of the solution after acidification, and required purification by silica column chromatography (dry adsorbed onto the column).

Coupling acids **75a-j** with 5-aminoindazole and 3-aminopyridine was carried out using HOAt/EDC (DMF at rt for 18 hours) to give a library of 20 novel compounds (not described in CAS) **76a-j** and **77a-j**, respectively in in moderate yields (38-%54%). The structures of these compounds were confirmed by ^{1}H-NMR and high resolution mass spectroscopy as described in the experimental section, Tables 28,29.

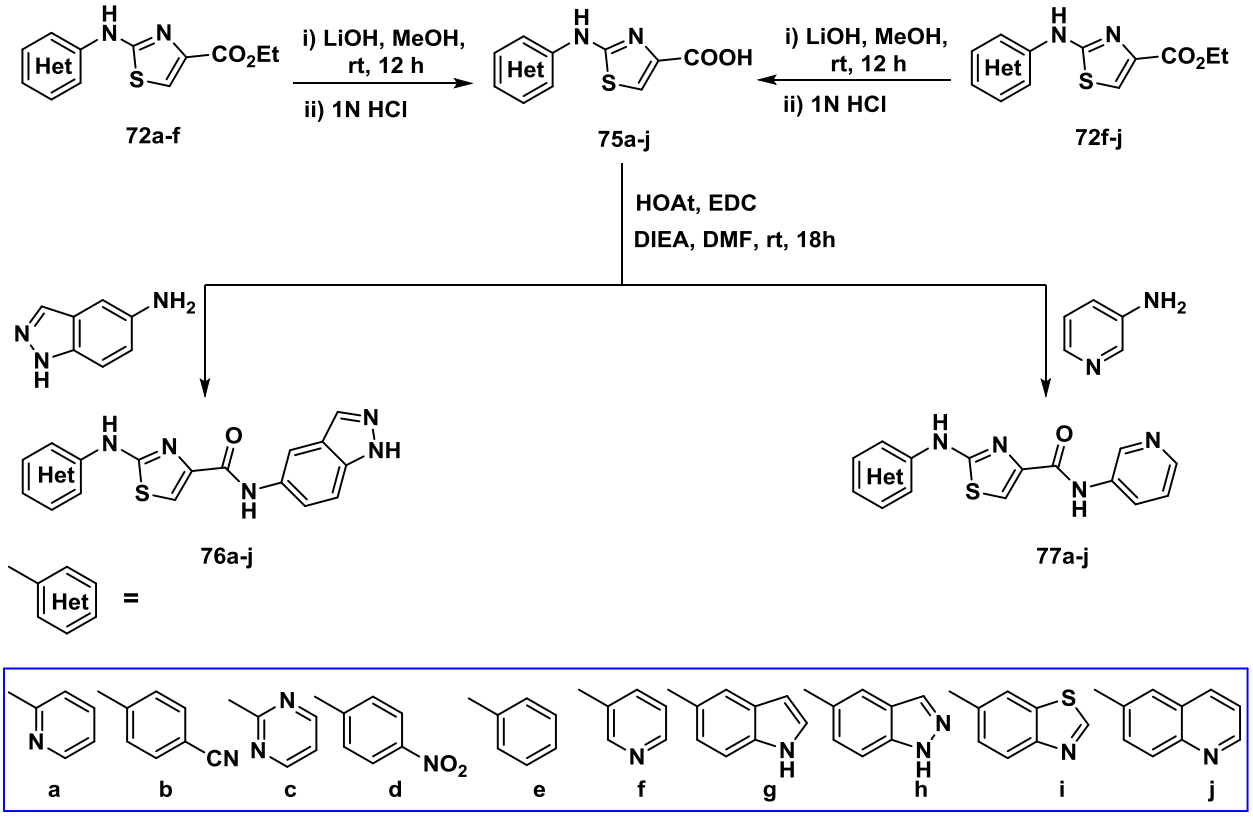

Figure 76: Aminothiazole carboxamide-based compounds **76a-j and 77a-j.**

These compounds were evaluated against ROCK1 and ROCK2 using the ELISA technique in Dr. MacLeod's lab. The compounds were tested at a single point concentration (10 µM) using H1152 as a positive control. Seven compounds showed inhibitory activity against ROCK isoforms (Chapter 7, Table 12). Out of these seven active compounds, four compounds (**76f**, **76g**, **76h**, and **76i**) had high inhibitory activity against ROCK1 (92%, 95%, 105%, and 95%, respectively compared to the positive control) and they all have in common the 5-aminoindazole ring on the right side of the molecule. These results highlight the significance of this ring in our future plans (Chapter 6).

Chapter 6

Indazole-Based ROCK1/ROCK2 Inhibitors

6.1 Introduction

The results described in Chapters 4 and 5 for the aminothiazole compounds **65o** and **76h** (**Figure 77**), which contain an indazole motif as the diversity component on the right and/or left side of their structure, encouraged us to look further into the importance of the indazole ring in our effort to develop isoform selective ROCK inhibitors. For that reason, we undertook the synthesis and evaluation of three sets of isomeric indazole-aminothiazole carboxamide derivatives **80a-q**, **85a-o**, and **93a-x**. All three incorporate the diversity elements on the right side of the molecule, but they differ in either the positioning of the carboxamide substituent on the thiazole ring or the point of attachment of the aminothiazole unit onto the left side indazole nucleus. Although only a single orientation is represented for these molecules, it is clearly apparent from the structures that they will be oriented in the ATP site of rho-kinase in distinctly different ways. In particular, it was hoped that the geometry of one of these systems would be optimal such that right side motif would interrogate the allosteric pocket accessible to type II kinase inhibitors.

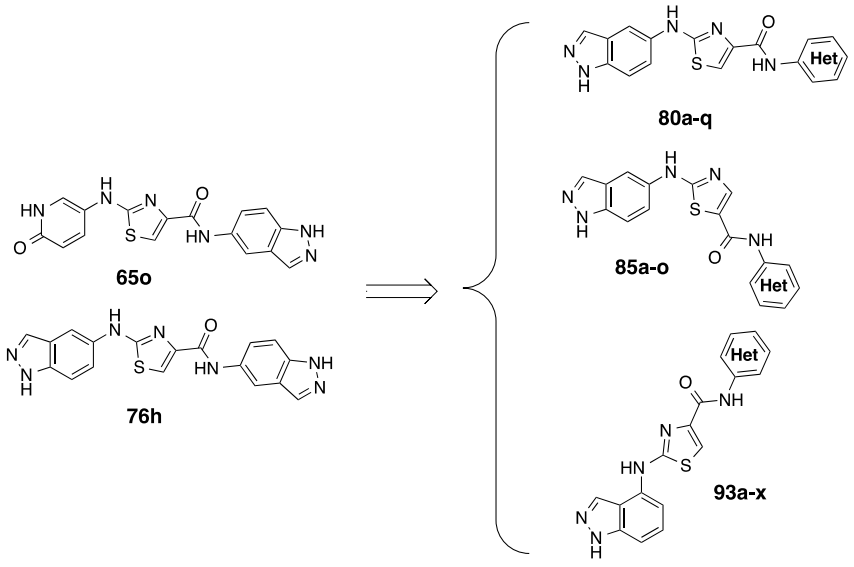

Figure 77: Conception of the three isomeric indazole-aminothiazole carboxamide families of potential type II rho kinase inhibitors: compounds **80a-q**, **85a-o**, and **93a-x**.

6.2 Synthesis of 2-(Indazole-5-yl)aminothiazoles-4-Carboxamide Derivatives 80a-q

The reaction sequence that was elaborated to access compounds **80a-q** (**Figure 78**) required in the first steps that we protect the indazole NH in 5-nitroindazole **78** with a Boc group (Boc_2O, Et_3N, RT; 86%) to give **79**, and reduce the nitro group to give N(1)-Boc-5-aminoindazole **71h** (see chapter 5 for first use of this intermediate).

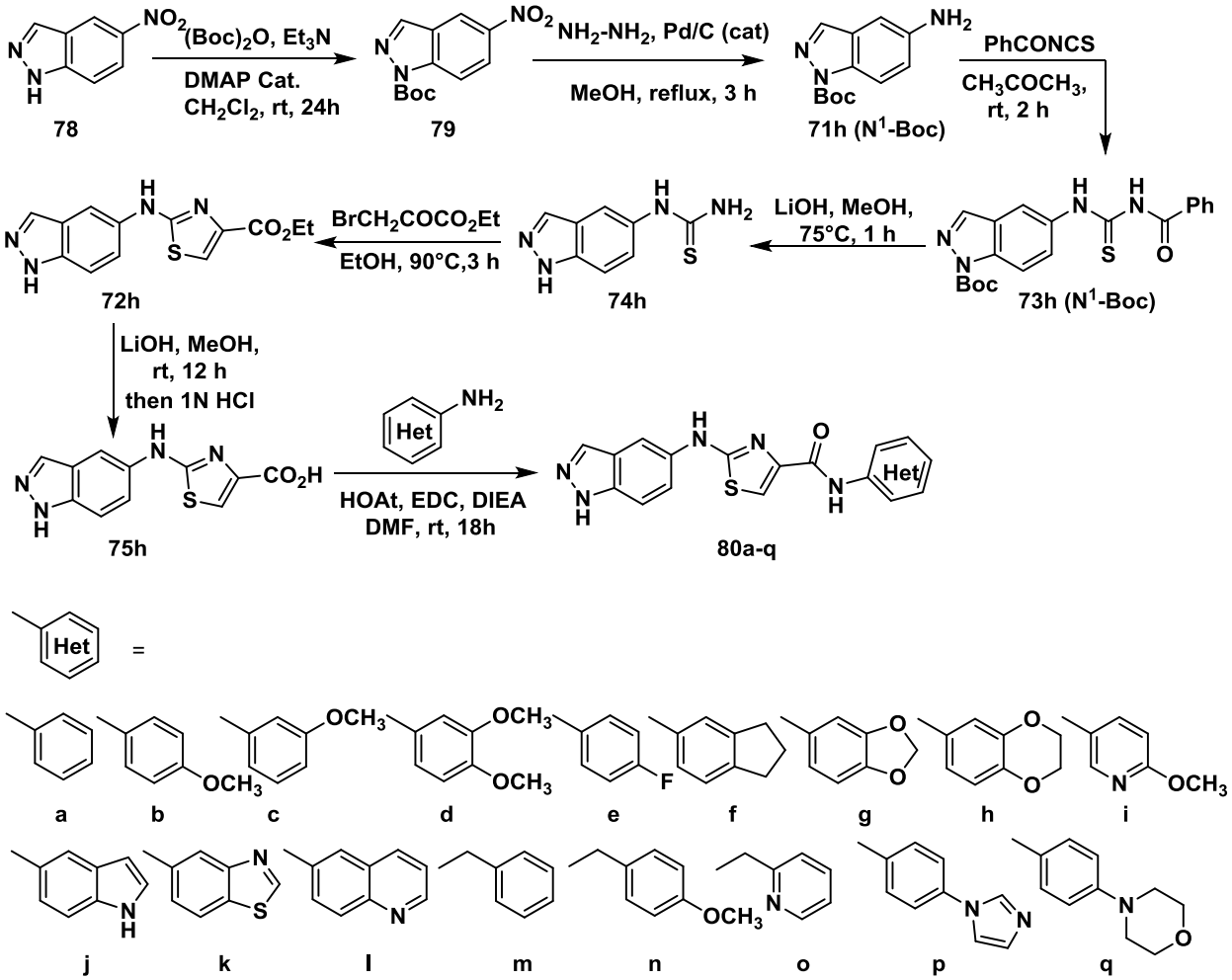

Figure 78: Synthesis of indazole-5-aminothiazole-4-carboxamide derivatives **80a-q**.

Reduction of the nitro compound **79** using hydrazine hydrate in the presence of palladium on carbon as a catalyst afforded **71h** in high yield (81%). The appearance of -NH_2 protons in ^1H NMR spectrum, as well as the shift in the peaks for the aromatic C-H's confirmed the formation of the amine. The mechanism for this reduction (**Figure 79**) involves nucleophilic attack of hydrazine on the nitro group nitrogen atom to form 1-hydroxy-1-aryltriazane 1-oxide. This intermediate loses hydroxide anion, which then abstracts a proton from the terminal NH_2. This is followed by the release diazene and formation of nitroso intermediate. This nitroso intermediate

is then attacked by a second hydrazine molecule forming 1-hydroxy-1-aryltriazane, which rearranges to form the aromatic amine product, water, and nitrogen.[199]

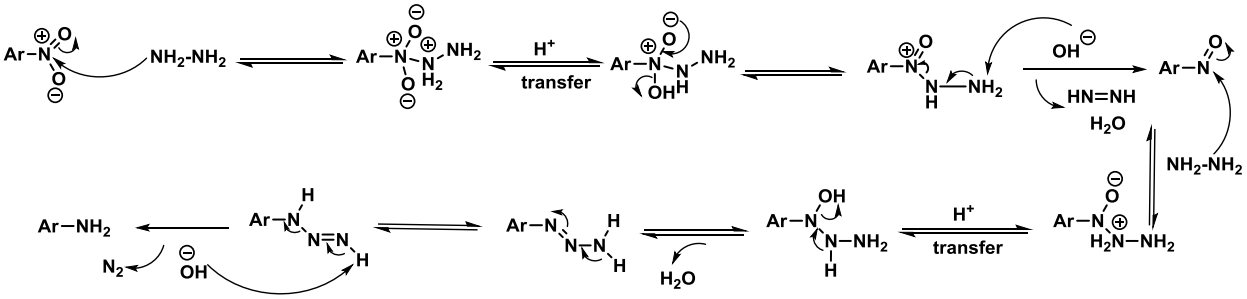

Figure 79: Proposed mechanism for the reduction of the nitro group using hydrazine

Reaction of amine derivative **71h** with benzoylisothiocyanate in acetone at room temperature gave *N*-benzoyl-*N′*-indazolylthiourea **73h**. Deacylation of this *N,N'*-disubstituted thiourea with LiOH resulted in both debenzoylation and *N*-BOC deprotection, affording the monosubstituted thiourea **74h**.[198] Compound **74h** was then converted to the aminothiazole **72h** by S-alkylation of the thiourea function with ethyl bromopyruvate followed by cyclization (Hantzsch approach). The ester **72h** was hydrolyzed by stirring with LiOH in aqueous methanol at room temperature for 12h. This provided the pivotal acid intermediate **75h** in good yield (70%). In the library forming step acid **75h** was reacted with a set of 17 amines under peptide coupling conditions (HOAt-EDC and DIEA in DMF, RT, 18h) to give compounds **80a-q** (not described in CAS) in yields ranging from 22% to 61%. The structures of the library compounds **80a-q** were confirmed by ^{1}H-NMR (Chapter 8, Table 30) and high resolution mass spectroscopy.^{1}H-NMR showed the appearance of new singlet signal belonging to carboxamide NH as well as the appearance of new set aromatic protons in the aromatic region for the diversity elements on the right side of the molecule.

These compounds were submitted as their HCl salts for *in vitro* testing against ROCK1 and ROCK2 in Dr. MacLeod's lab using the ELISA technique. The compounds were tested at a single point concentration (10 μM) using H1152 as a positive control. It was satisfying that most of the synthesized compounds showed a marked improvement in inhibitory activity over pyridinone-based compounds, and a number of these tested compounds were also superior to positive control H1152 (Chapter 7, Table 13).

Additionally, compounds **80b** and **80f-j** were submitted for testing in Invitrogen using fluorescence resonance energy transfer (FRET) technique. These compounds were tested at 10-

point concentrations and the IC_{50} for the tested compound was determined (Chapter 7, Table 15).

6.3 Synthesis of 2-(Indazole-5-yl)aminothiazole-5-Carboxamide Derivatives 85a-o

The alternate strategy to access the isomeric C-5 carboxamide substituted 2-aminothiazole system in compounds **85a-o** is outlined in **Figure 80**.

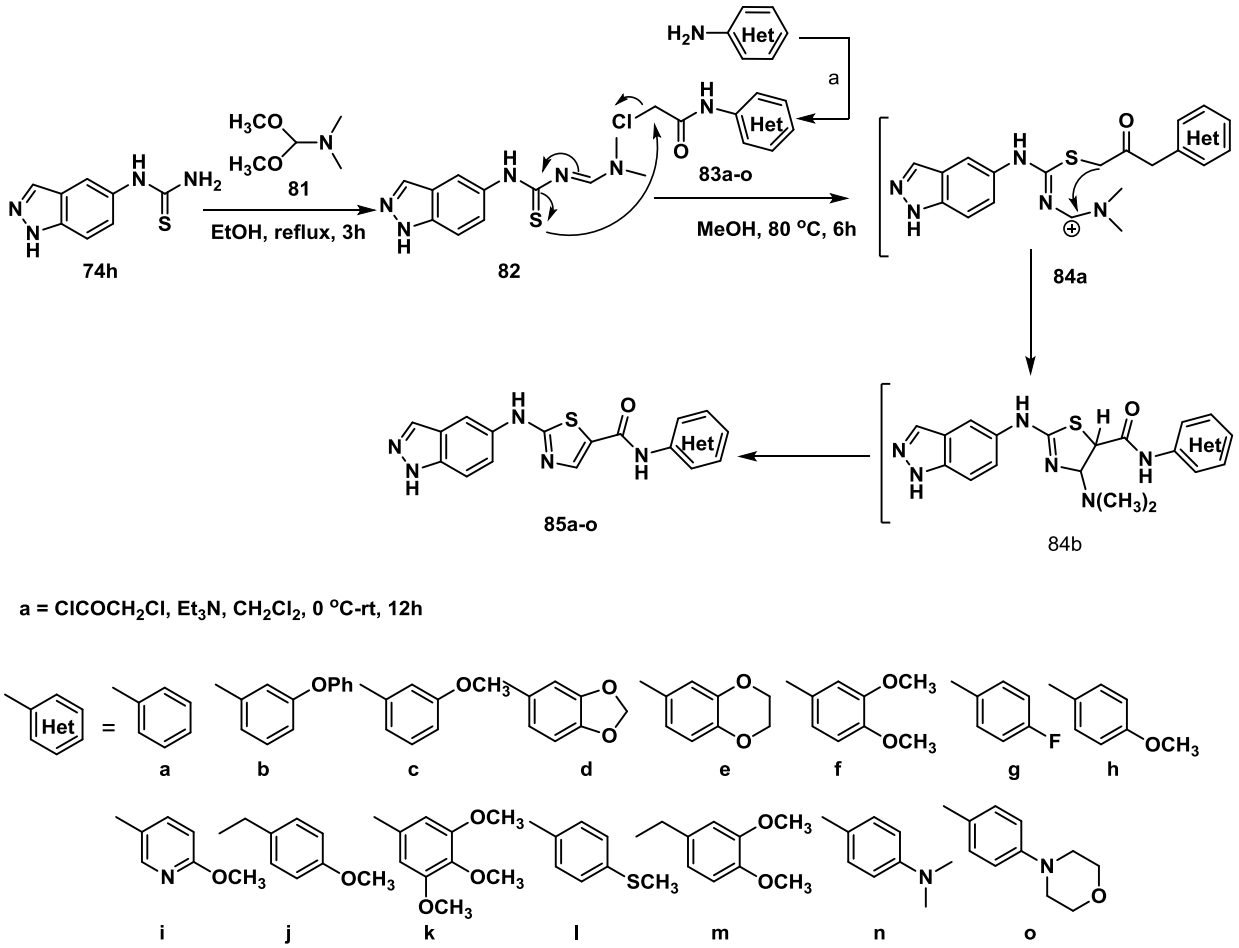

Figure 80: Synthesis of indazole-5-aminothiazole-5-carboxamide derivatives **85a-o**.

Indeed, a novel and convergent two-step synthetic route was developed that permitted us to avoid the tedious peptide coupling step with amines. Treatment of the available *N*^{1}-(indazol-5-yl) thiourea **74h** with *N*,*N*-dimethylformamide dimethoxyacetal (DMF-DMA) **81** in ethanol at reflux for 3h afforded the key intermediate *N,N'*-disubstituted thiourea **82** in excellent yield (91%). In the second step, reaction of **82** with the chloroacetamide derivatives **83a-o** (prepared by reacting set of amines with chloroacetyl chloride in the presence of Et_3N as a base) in

methanol at 80 ^{o}C for 6 h and furnished the 15 novel compounds **85a-o** in overall yields ranging from 29 - 49%. In this sequence, the disubtituted thiourea **82** provided the two ring carbon atoms (C-2 and C-4) and the heteroatoms (S and N) of the resultant thiazole ring, while the remaining carbon atom (C-5) was supplied by the methylene group in the chloroacetamide derivatives **83a-o**. Mechanistically, the reaction is believed to involve S-alkylation of thiourea **82** forming intermediate **84a** followed by nucleophilic attack of the active methylene group on the in situ generated iminium ion. This latter step forms the 5-membered ring intermediate **84b**, which spontaneously loses Me_2NH to give afford the target aminothiazoles **85a-o**.

All of these compounds **85a-o** were tested *In-vitro* against ROCK1 and ROCK2 at a single point concentration (10 µM), using H1152 as a positive control. The results revealed that improved inhibitory activity was achieved by altering the substitution pattern on the thiazole ring and all of the synthesized compounds inhibited ROCK1 more than ROCK2 (Chapter 7, Table 14). Subsequently, compounds **85a**, **85d**, **85i** and **85n** were submitted for testing in Invitrogen using FRET technique. These compounds were tested at 10-point concentrations and the IC_{50} for the tested compound was determined (Chapter 7, Table 15).

6.4 Synthesis of 2-(Indazole-4-yl)aminothiazoles-4-Carboxamide Derivatives 93a-x

In our continuing effort to optimize the activity and selectivity of the synthesized compounds against ROCK isoforms, we turned our attention to shifting the position of the aminothiazole motif on the indazole ring from C-5 to C-4 (**Figure 77**). The desired indazole-aminothiazole-caboxamide based compounds **93a-x** were synthesized following the route outlined in **Figure 81**. Although the 4-nitroindazole **87** is commercially available, an economically practical synthesis was achieved via diazaotization (aqueous sodium nitrite under acidic conditions at 0 ^{o}C) of 2-methyl-3-nitroaniline **86** followed by intraomolecular cyclization to affords **87** in high yield (89%).[200] The strategy followed for the synthesis of **80a-q** was then followed to access the target molecules. Reduction of the nitro group in **87** using hydrazine hydrate and Pd/C (cat) afforded 4-aminoindazole intermediate **88**. The *N*-benzoyl-*N'*-indazolyl thiourea intermediate **89** was then obtained by reacting amine **88** with benzoylisothiocyanate in acetone at room temperature for 2 hours. Hydrolysis of thiourea derivative **89** by heating with lithium hydroxide afforded the monosubstituted derivative **90** in good yield (77%). The reaction of indazole amine **88** with ammonium thiocyanate in acidic medium was also explored as an alternative route to prepare *N*-(indazol-4-yl) thiourea **90**, but it failed to give the desired product (the starting amine

was recovered). Similarily, reaction of amine **88** with 1,1'-thiocarbonyldiimidazole (TCDI) followed by quenching with 25% ammonia solution to form **90** failed.

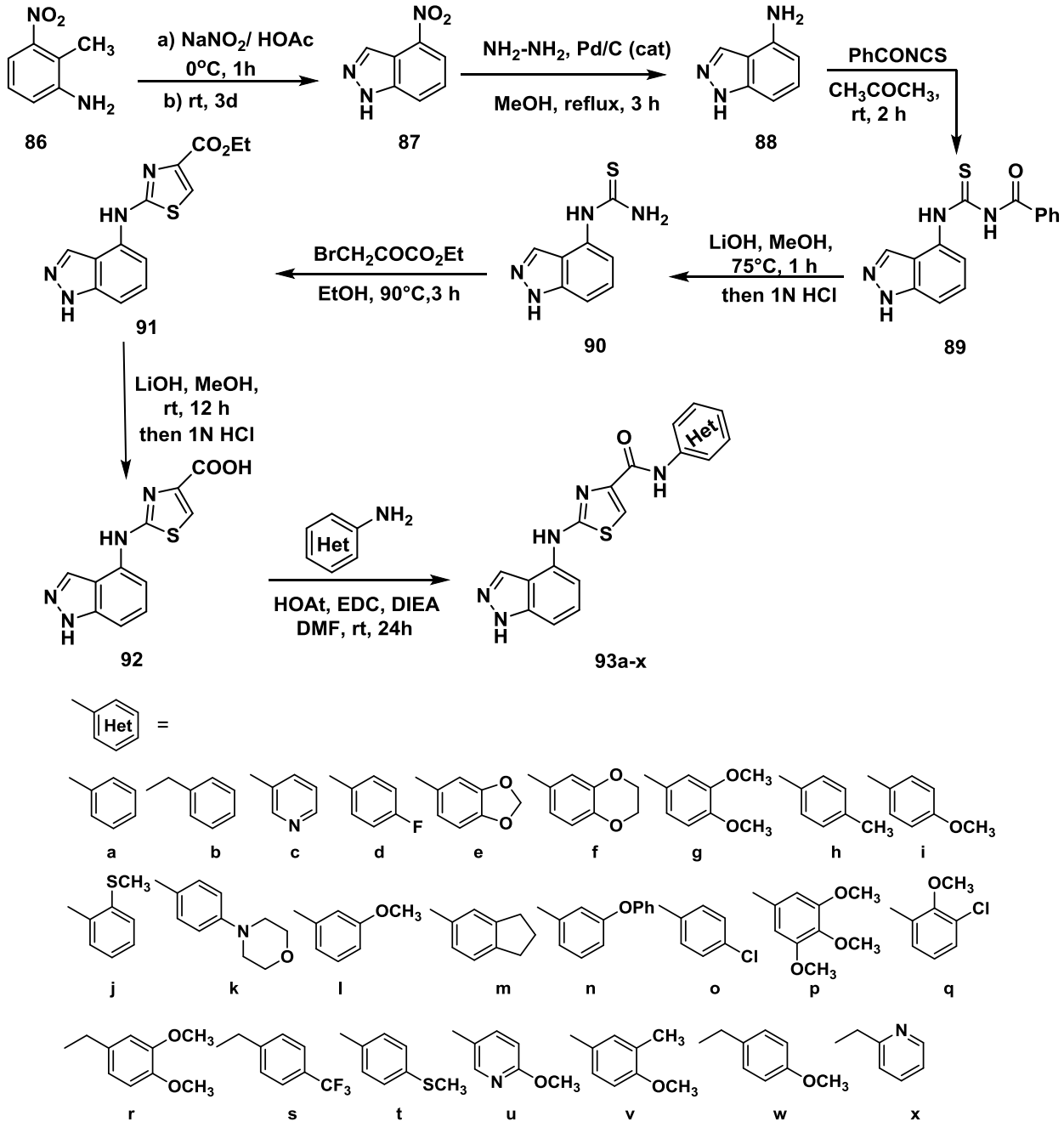

Figure 81: Synthesis of indazole-4-aminothiazole-4-carboxamide derivatives **93a-x**.

Reaction of thiourea derivative **90** with ethyl bromopyruvate proceeded as wanted to give thiazole ester **91** in 72% yield. This ester was saponified to acid **92** by stirring with LiOH in aqueous methanol at room temperature for 12h. Acid **92** was subsequently reacted with the

requisite aryl, heteroaryl and benzylamines to give the 24 membered library novel indazole-aminothiazole carboxamides **93a-x** (not described in CAS) using standard peptide coupling conditions HOAt/ EDC/ DIEA.

The structures of the analogues **93a-x** were confirmed by 1H-NMR spectroscopy (Chapter 8, Table 32) and high resolution mass spectrometry (Chapter 8, Table).

These compounds were submitted for in vitro testing against ROCK1 and ROCK2 at single-point concentration (10 μM) using H1152 as positive control. To our disappointment, this structural modification resulted in complete loss of inhibitory activity against ROCK isoforms. As none of the **93a-x** analogues reached the potency range of congeners **80a-q**, this suggest that position-4 was not the ideal for improving activity and selectivity.

Chapter 7

In Vitro Biological Assays and Results

As described in Chapters 2 to 6, a library synthesis approach has been used to generate molecule-types that incorporate the qualitative characteristics of type II kinase inhibitors. This has been achieved by varying the left (hinge binder) and right side of the molecules, as well as the nature of the linker element. Selected members from each subset of molecules were evaluated for their activity/isoform selectivity using *in vitro* assays developed in Dr. Kath MacLeod's laboratory. Subsequent and independent evaluation of isoform selectivity for the more active compounds was subsequently carried out using the industry standard ROCK1/2 assay developed by Invitrogen™ Life Technologies. The results of these preliminary screens informed us whether a given sub-library of compounds exhibited activity/isoform selectivity. This in turn motivated the study of further iterative modifications to the active skeleton that were summarized in Figure 42, Chapter 2. It must be emphasized that the objective in the library strategy we adopted during this research was to identify structural types that display activity, rather than to establish structure-activity relationships (SAR) within a given set of compounds. In fact, only in the next phase of our project will effort be more specifically directed to optimizing the activity/isoform selectivity for the most active compounds.

The evaluation of the *in vitro* inhibitory activity and selectivity of the ROCK inhibitor libraries described in Chapters 3 to 6 was initially carried out in Dr. MacLeod's laboratory using an Enzyme-Linked Immunosorbent Assay (ELISA) technique. The initial testing focused on ROCK2 activity, as a consequence of the interest of the MacLeod group to have in hand isoform selective ROCK2 inhibitors as probes to study diabetic cardiovascular disease (see Chapter 1). These tests were carried out using the kinase assay kit developed by Cyclex to measure ROCK2 inhibition activity. As the project advanced, an alternative kit supplied by Millipore was employed, as it permitted us to measure both ROCK1 and ROCK2 inhibition by our molecules.

7.1 Enzyme-Linked Immunosorbent Assay (ELISA)

This biochemical method was used for Cyclex® and Millipore® ROCK assay protocols. The method is based on using plates precoated with recombinant ROCK substrate (MYPT1) which contains a Thr^{696} residue as a phosphorylation site for ROCK1 and ROCK2. MYPT1 Thr^{696} phosphorylation is detected by a primary antibody that specifically detects only phosphorylated MYPT1. Subsequently, a horseradish peroxidase (HRP)-conjugated secondary antibody is added followed by the chromogenic substrate tetramethylbenzidine (TMB) which yields a blue color upon conversion to the diimine derivative by HRP. A stop solution is added to change the color to yellow which is read at 450 nm and is proportional to the amount of MYPT1 Thr^{696} phosphorylation (an index of ROCK activity).[202,203]

Compounds were tested in duplicate at single-point concentration (10 μM) to determine the % inhibition against ROCK2, for the Cyclex assay, and against ROCK1 and ROCK2 isoforms, for the Millipore® assay.

7.1.1 Cyclex® ROCK Assay

7.1.1.1 Screening of Pyridinone Oxazoline Carboxamide-Based Compounds 20a-f and 21a-f

Pyridinone-oxazoliine carboxamide derivatives **20a-f** and **21a-f** were tested in vitro for their ROCK2 inhibitory activity. The compounds were tested at single-point concentration (10 μM) using Y-27632 as a positive control. Only eight compounds exhibited weak ROCK2 inhibitory activity as illustrated in Table 6. At this testing concentration, compound **21e** exhibited the highest inhibitory activity (20% inhibition).

Table 6: Inhibitory activity of pyridinone oxazoline carboxamide-based compounds **20a-f** and **21a-f** against ROCK2

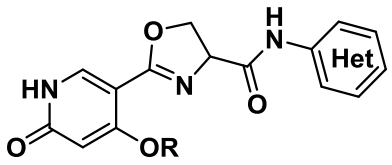

Compound	R		% Inhibition for ROCK2 (at 10 µM)
Y-27632			98
20a	CH_2Ph		4
20b	CH_2Ph	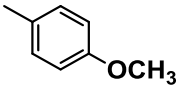	18
20c	CH_2Ph	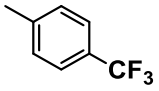	9
20e	CH_2Ph		5
21a	CH_3		10
21b	CH_3	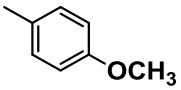	8
21e	CH_3		20
21f	CH_3		3

7.1.1.2 Screening of Pyridinone Oxadiazole Carboxamide-Based Compounds 34a-ah

We tested ten compounds (**34a**, **34f**, **34j**, **34l**, **34n**, **34r**, **34z**, **34aa**, **34ac**, **34af**) from **34a-ah** compounds against ROCK2 using Y-27632 as a positive control. As illustrated in Table 7, these results showed that the replacement of the oxazoline ring by an oxadiazole ring slightly improved ROCK2 inhibitory activity. Eight compounds had weak inhibitory activity against

ROCK2 compared to the positive control (Table 7). Compounds **34j**, **34ac,** and **34af** exhibited the highest inhibitory activity against ROCK2 compared to the other derivatives.

Table 7: Inhibitory activity of pyridinone oxadiazole carboxamide-based compounds **34a-ah** against ROCK2

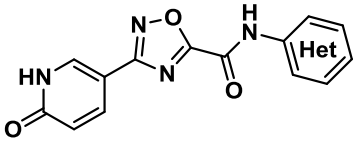

34a-ah

Compound	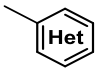	**ROCK2 % Inhibition**
Y-27632		101
34a		2
34f	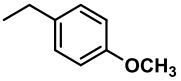	13
34j	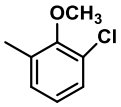	48
34l	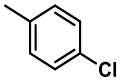	16
34r	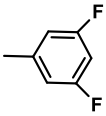	3
34aa		28
34ac	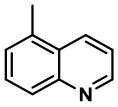	41
34af	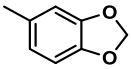	38

As we progressed along, an alternative kit supplied by Millipore was employed that permitted us to measure both ROCK1 and ROCK2 inhibition by our molecules. The conditions were optimized so the inhibition curves, generated by Dr. MacLeod's group, of H-1152 for ROCK1 and ROCK2 correlated with the literature.

7.1.2 Millipore® ROCK Assay

In this assay, compounds were tested against ROCK1/2 at a single-point concentration (10 μM) using H-1152 as a positive control.

7.1.2.1 Screening of Pyridinone Oxadiazole Carboxamide-Based Compounds 34a-ah

Twenty-four compounds (**34a-c**, **34e-g**, **34j-n**, **34p-r**, **34u**, **34w-ac**, **34ae**, and **34af**) were retested against ROCK1 and ROCK2 using H-1152 as a positive control. Out of these derivatives, fifteen compounds were found active (Table 8). The results showed that the replacement of oxazoline ring by oxadiazole ring had a slight improvement on ROCK inhibitory activity. None of the tested compounds had a strong inhibitory activity toward ROCK isoforms compared to the positive control H-1152. As shown in Table 9, compounds **34g**, **34q**, **34u**, **34af**, and **34ag** exhibited the highest inhibitory activity against ROCK1. It should be noted that compounds **34g, 34g, 34ag** had a bicyclic system on the right side, tail segment while **34q** and **34u** share phenyl ring bearing electron-donating on the tail segment.

As for the selectivity between ROCK1 and ROCK2, all of the active compounds inhibited ROCK1 in preference to ROCK2. In particular, compounds **34g**, and **34af** with a bicyclic system on the tail segment displayed 9- to 12-fold more activity against ROCK1 than ROCK2. On the other hand, compound **34ag** bearing 1,4-benzodioxan-6-yl motif at the right side inhibited ROCK1 (58% inhibition) without any effect on ROCK2.

Table 8: Inhibitory activity of pyridinone oxadiazole carboxamide-based compounds **34a-ah** against ROCK1/2

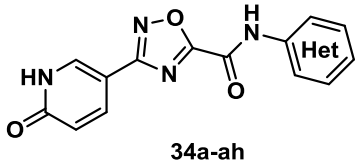

34a-ah

Compound		ROCK1 % Inhibition	ROCK2 %Inhibition
H-1152		96	101
34a		43	12
34e	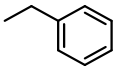	29	10
34f	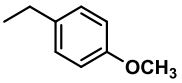	44	9
34g	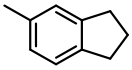	71	6
34j	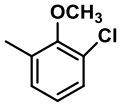	39	10
34l	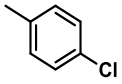	19	8
34n	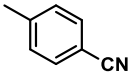	39	13
34q	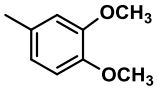	55	7
34u	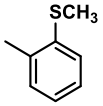	46	37
34x	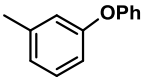	33	22
34aa		41	17
34ac	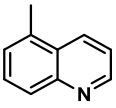	38	4
34ae		22	10
34af	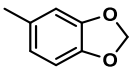	62	7
34ag	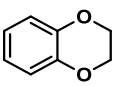	58	0.0

7.1.2.2 Screening of Isomeric Pyridinone Oxadiazole Carboxamide-Based Derivatives 41a-g

Trials to improve inhibitory activity by synthesizing isomeric pyridinone-based derivatives **41a-g** did not succeed in improving either activity or selectivity. The compounds were tested at single-point concentration (10 μM) using H-1152 as a positive control. Six compounds showed activity as illustrated in Table 9. At this testing concentration, compound **41d** exhibited the highest inhibitory activity (37% inhibition) compared to the positive control.

Table 9: Inhibitory activity of isomeric pyridinone oxadiazole carboxamide-based compounds **41a-g** against ROCK1/2

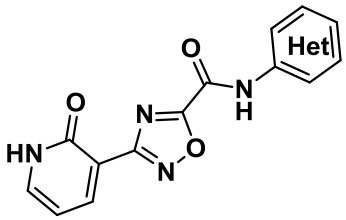

41a-g

Compound		ROCK1 % Inhibition	ROCK2 % Inhibition
H-1152		93	98
41a	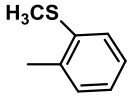	28	2
41b	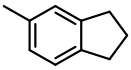	31	11
41c	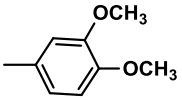	35	14
41d	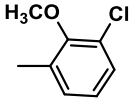	37	17
41e	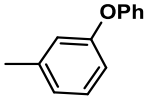	13	17
41g	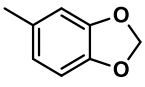	19	8

7.1.2.3 Screening of Pyridinone Piperazine-Based Compounds 50a-d

Derivatives of pyridinone piperazine-based compounds **50a-d** have been tested for inhibitory activity against ROCK1 and ROCK2 at 10 μM concentration using H-1152 as a positive control. The results of these four derivatives, as demonstrated in Table 10, showed that substitution of oxadiazole substructure of **34a-ah** with carbonyl-piperazine in **50a-d** resulted in diminished inhibitory activity.

Table 10: Inhibitory activity of pyridinone piperazine-based compounds **50a-d** against ROCK2

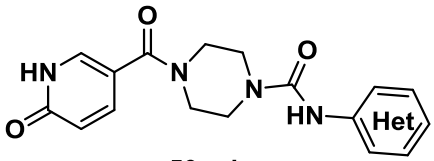

50a-d

Compound	Het	ROCK1 % Inhibition	ROCK2 % Inhibition
H-1152		93	98
45a	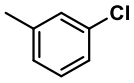	13	17
45b	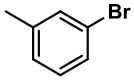	11	3
45c	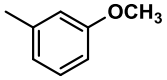	32	12
45d	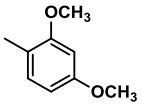	31	11

7.1.2.4 Screening of Pyridinone Aminothiazole Carboxamide-Based Compounds 65a-p and 66o,p

Aminothiazole was chosen as a substitute fragment for the oxadiazole substructure in **34a-ah** to afford compounds **65a-p,** and **66o,p**. These analogues were tested at 10 μM concentration against ROCK1 and ROCK2. Only eight compounds were found active as shown in Table 11. The inhibitory activity of compounds **65o** and **66o** against ROCK1 was found very close to the positive control H-1152 at this testing concentration. Compounds **65c**, **65g**, **65p**, and **66p** moderately inhibited both isoforms at the previously mentioned concentration. Substitutions on

the ring nitrogen of the pyrdinone or indazole ring by methyl group, as found in **65p** and **66o,p**, were well tolerated.

As for the selectivity between ROCK1 and ROCK2, most of the active inhibited ROCK1 more than ROCK2, less than 2-fold more activity against ROCK1 than ROCK2.

In summary, this modification had a positive impact on ROCK inhibitory activity whereas it did not improve selectivity.

Table 11: Inhibitory activity of pyridinone aminothiazole carboxamide-based compounds **65a-p** and **66o,p** against ROCK1/2.

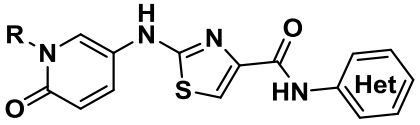

65a-p (R= H)
66o,p (R= CH_3)

Compound	Het	ROCK1 % Inhibition	ROCK2 % Inhibition
H-1152		96	101
65a		32	35
65c	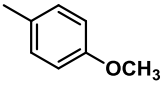	58	51
65g		81	63
65j	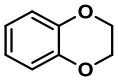	41	40
65o	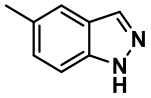	91	72
65p	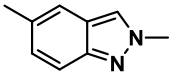	56	51
66o	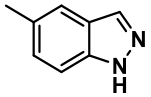	95	91
66p	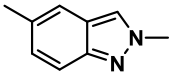	68	54

7.1.2.5 Screening of Aminothiazole Carboxamide-Based Compounds 76a-j and 77a-j

We next turned our attention to change the left side of the molecule by using different aromatic/hetero-aromatic motifs while keeping the 3-pyridyl, of **65g**, or 5-indazolyl moieties, of **65o**, on the right side. Results showed that active compounds, Table 12, maintained the weak isoform selectivity but showed an increase in ROCK inhibitory activity. As shown in Table 12, seven compounds were found active at 10 μM concentration. At this testing concentration, compound **76h**, **77h** exhibited inhibitory activity toward ROCK1 greater than the positive control H-1152. Analogues **76f**, **76i, 77f**, and **77i** potentially inhibited ROCK1 more than ROCK2. Compound **76g** had almost the same inhibitory activity against the two isoforms. Although these structural modifications improved inhibitory activity toward ROCK isoforms as compared with the previous series, they decreased the isoform selectivity. Most of the compounds inhibited ROCK1 more than ROCK2, less than 2-fold.

Out of the six active compounds, four compounds had an indazole ring on the left side of the molecule. Therefore, we hypothesized the importance of this ring as a hinge binder motif.

Table 12: Inhibitory activity of aminothiazole carboxamide-based compounds **76a-j** and **77a-j** against ROCK1/2

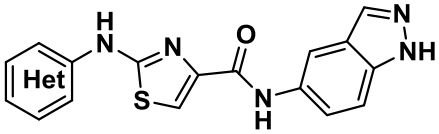

76a-j

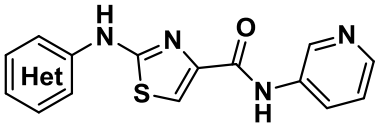

77a-j

Compound	Het	ROCK1 % Inhibition	ROCK2 % Inhibition
H-1152		96	101
76f		92	75
76g	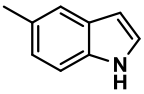	95	93

Compound	Het	ROCK1 % Inhibition	ROCK2 % Inhibition
76h	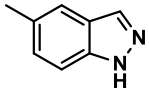	105	85
76i	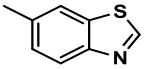	95	68
77f		91	56
77h	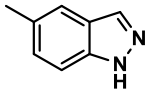	102	70
77i	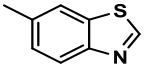	71	28

7.1.2.6 Screening of 2-(Indazole-5-yl)aminothiazole-4-Carboxamide Derivatives 80a-q

To examine the importance of the indazole ring as a hinge binder motif, we prepared compounds **80a-q** and evaluated their ROCK-inhibitory activity. As shown in Table 13, fifteen compounds were tested and all of the tested compounds exhibited remarkable inhibitory activity toward ROCK1. Seven compounds **80b**, **80c**, **80d**, **80h**, **80j**, **80n**, and **80q** exhibited inhibitory activity toward ROCK1 greater than the positive control H-1152 at 10 μM concentrations. Some analogues, **80d**, **80i**, **80o**, **80p**, and **80q**, exhibited weak inhibitory activity against ROCK2.

As for the isoform selectivity, these modifications improved isoform selectivity. Compounds **80a-q** inhibited ROCK1 more than (3- to 11-fold) ROCK2 compared to the previous series. However, the selectivity did not significantly increase to the extent that we can claim that we have good isoform selectivity.

In summary, compounds **80a-q** with a new hinge binder motif, indazole, displayed a remarkable improvement in the inhibitory activity toward ROCK1 whereas a little effect against ROCK2 was exhibited. This suggested that the indazole ring is a good choice for hinge binding but we still need more structural optimization.

Table 13: Inhibitory activity of 2-(indazole-5-yl)aminothiazole-4-carboxamide derivatives **80a-q** against ROCK1/2

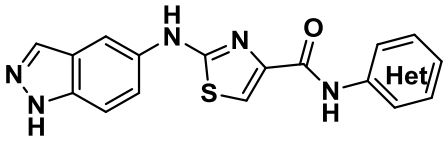

80a-q

Compound		**ROCK1 % Inhibition**	**ROCK2 % Inhibition**
H-1152		94	99
80a		70	13
80b	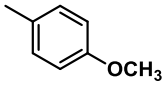	104	19
80c	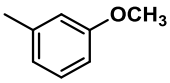	110	11
80d	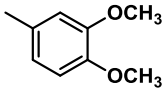	102	24
80e	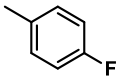	75	7
80g	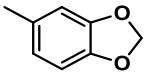	91	22
80h	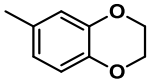	100	15
80i	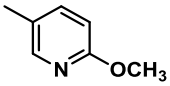	87	24
80j	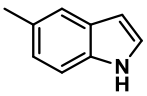	109	12
80k	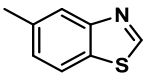	72	17
80l	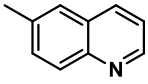	90	29

Compound	Het	ROCK1 % Inhibition	ROCK2 % Inhibition
80n	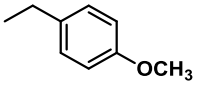	100	15
80o	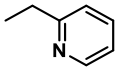	95	23
80p	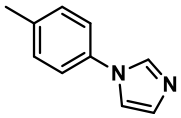	103	49
80q	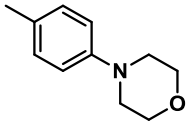	116	25

7.1.2.7 Screening of 2-(Indazole-5-yl)aminothiazole-5-Carboxamide Derivatives 85a-o

Having demonstrated the importance of the indazole ring as a hinge binder motif, we considered it interesting to continue and expand this investigation by synthesizing indazole-aminothiazole carboxamide derivatives **85a-o** having the carboxamide motif at C-5 of the thiazole ring. Improved inhibitory activity was achieved by altering the substitution pattern on the thiazole ring. As displayed in Table 14, all of the synthesized compounds inhibited ROCK1 more than ROCK2. Compounds **85h-j**, and **85l-o** having phenyl ring substituted with electron-donating groups, methoxy and methylthio, exhibited high inhibitory activity against ROCK1 superior to the positive control H-1152 at 10 μM concentration. Furthermore, the unsubstituted phenyl and the 4-fluoro substituted analogues **85a, 85g**, respectively displayed high inhibitory activity toward ROCK1.

For the isoform selectivity, the results showed that compounds **85a-o** inhibited ROCK1 (2- to 7-fold) at the testing concentration which was lower than the previous analogues **80a-q**.

In summary, analogues having carboxamide derivatives at 5-position of thiazole ring, **85a-o**, displayed higher inhibitory activity but less selectivity than those having carboxamide derivatives at 4-position, **80a-q**.

Table 14: Inhibitory activity of 2-(indazole-5-yl)aminothiazole-5-carboxamide derivatives **85a-o** against ROCK1/2

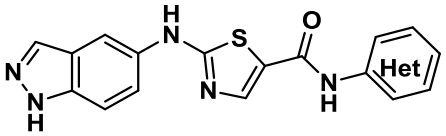

85a-o

Compound	Het	ROCK1 % Inhibition	ROCK2 % Inhibition
H-1152		94	99
85a		104	48
85b	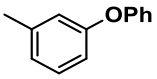	90	31
85c	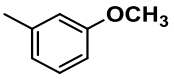	94	18
85d	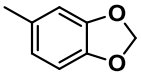	85	15
85e	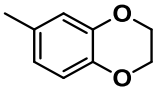	103	14
85f	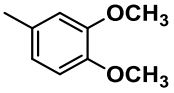	98	14
85g	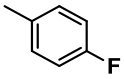	112	31
85h	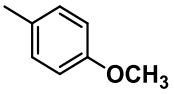	104	40
85i	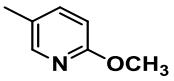	102	20
85j	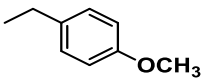	109	20

Compound	Het	ROCK1 % Inhibition	ROCK2 % Inhibition
85k	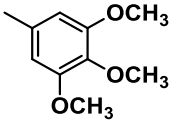	89	18
85l	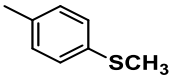	109	44
85m	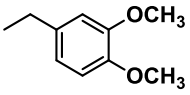	104	27
85n	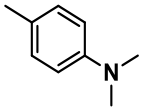	106	36
85o	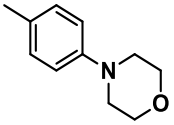	112	41

7.1.2.8 Screening of 2-(Indazole-4-yl)aminothiazole-4-Carboxamide Derivatives 93a-x

Continuing our efforts to develop potent and selective ROCK inhibitors, we next investigated repositioning amionthiazole-carboxamide substructure from 5- to 4-position of indazole ring to form **93a-x**. This structural modification showed a significant reduction in inhibition of ROCK isoforms and almost of compounds were inactive. It may be speculated that the diminished activity displayed by **93a-x** is due partly to unfavorable orientation of the linker and tail segments with respect to their binding sites.

7.2 Rho-Kinase (ROCK) Activity Assay using FRET Technique

Some compounds were submitted for reevaluation in the industry standard assay developed by Invitrogen Life Technologies to ensure the reliability of the results and to determine the IC_{50}. These compounds were tested using FRET-based assay (Z'-LYTE®). The Z'-LYTE® technology is a homogenous biochemical assay based on fluorescence resonance energy transfer (FRET). It is designed to utilize the differential sensitivity of phosphorylated and non-phosphorylated peptides to proteolytic cleavage. The assay uses peptide substrate that is labeled with two fluorophores (coumarin donor and fluorescein acceptor) one at each end and in close proximity to one another (typically 10-100 Å). These two fluorophores make up a FRET pair.[204] In the

initial reaction referred to as the kinase reaction, the Kinase transfers the γ-phosphate of ATP to serine/threonine residue in the synthetic peptide substrate. In the secondary reaction (the development Reaction), a site-specific protease recognizes and cleaves non-phosphorylated peptides.[204] The phosphorylated substrate exhibits suppressed cleavage by the development reagent. The uncleaved phosphorylated peptides maintain FRET whereas cleavage disrupts FRET emission, non-radioactive energy transfer, between the coumarin donor and fluorescein acceptor fluorophores on the peptide. After excitation of the donor fluorophore at 400 nm, The FRET signal is calculated as the ratio between coumarin (i.e., donor) emission at 445-460 nm to fluorescein (i.e., acceptor) emission at 520-535nm.[204,205]

Emission Ratio = Coumarin Emission (445 nm)/ Fluorescein Emission (520 nm)

Eighteen compounds were tested using Z'-LYTE® ROCK assay kit (Table 15). The compounds were tested in duplicate at 10-point concentrations to obtain a dose-response curve. In the retest campaign, compound activity was calculated as percentage inhibition in relation to the positive control, staurosporine. The IC_{50} values for the tested compounds were determined by the company using fitted curves with GraphPad Prism 5 software.

As shown in Table 15, the major finding from these results was that nine compounds, **76e**, **76g**, **76h**, **76i**, **80b**, **80h**, **80i**, **80q**, **85i**, inhibited ROCK1 more than ROCK2. Structural analysis of these compounds showed that all have indazole ring at one side of the molecules, indazole-based compounds. The other side of these molecules was found to contain either a bicyclic system (as in case of **76g**, **76h**, **76i**, **80h**, and **80q**) with hydrogen bond donor and/or acceptor or a monocyclic ring bearing electron-donating groups (as in **80b**, and **80i)**.

On the other hand, compounds, **80j**, **85a**, **85n**, had more ROCK2 inhibitory activity in Invitrogen's test whereas they were more active against ROCK1 in Millipore's test.

Among the tested compounds, compound **76i,** with 6-methoxy pyridine-6-ylat the right side of the molecule, displayed the highest ROCK1 potency (IC_{50}= 1.1 μM) whereas compound **85n** had higher affinity for ROCK2 (IC_{50}= 2.1 μM). Indazole-based compounds **80f**, **80k**, and **85d** with indanyl, benzothiazolyl, and benzodioxolyl moieties, respectively exhibited the weakest ROCK inhibitory activity with IC_{50} >10 μM. Changing the substitution pattern of the linker segment in compound **93d** diminished activity.

With regard to the isoform selectivity, the tested compounds displayed weak isoform selectivity. Analogue **80h** showed the highest selectivity against ROCK1 (≈3.5-fold). On the other hand,

analogues **80g**, **85n, and 85n,** inhibited ROCK2 (3-folds) more than ROCK1. Actually, these results differed from the ones obtained from Millipore's test

Table 15: IC_{50} values of compounds tested in Invitrogen

Compound	**ROCK1** **IC_{50} (µM)**	**ROCK2** **IC_{50} (µM)**
Staurosporin	0.43	0.42
34af	>10	>10
76e	4.6	7.8
76g	6.4	>10
76h	1.7	2.5
76i	1.1	2.6
80b	8.6	>10
80f	>10	>10
80g	>10	3.3
80h	3.7	11
80i	1.3	2.7
80j	7.7	4.6
80k	>10	>10
80q	4.8	>10
85a	9.3	3.5
85d	>10	>10
85i	3.4	7
85n	7.4	2.1
93d	>100	>100

7.3 Factors that may Contribute to the Differences in Biological Results Between the ELISA-Based and FRET-Based ROCK Activity Assay Methods

There are several factors to be considered during ROCK assay design that might affect the results. Herein, I will discuss the major factors that might lead to the differences between the ELISA-based (EMD Millipore) and FRET-based (Z'-LYTE®, Invitrogen) ROCK activity assay results.

7.3.1 ATP Concentration

Optimizing ATP concentration is a key factor in developing a ROCK biochemical assay. Too low ATP concentration will limit enzyme activity whereas high ATP concentration will saturate the enzyme and reduce the chance of inhibitor binding. In order to achieve good linearity between signal and kinase activity, an optimal ATP concentration must be used. There are three different approaches for choosing ATP concentration for the activity assay. The first option relies on using a standard fixed ATP concentration, usually between 10 and 100 μM, for all different protein kinase assays. This option has the advantage of making the experimental procedure easier especially if several protein kinases are involved. However, the disadvantage is that it cannot be used to sort the potency of a given inhibitor between different kinases; in other words, the binding affinity of the inhibitor is not a good measure of the inhibitor selectivity.

According to Cheng–Prusoff equation, the IC_{50}, concentration of inhibitor that results in 50% inhibition of maximal enzyme activity, of an ATP-competitive inhibitor is linearly related to ATP concentration.[206]

Equation of Cheng–Prusoff: $K_i = IC_{50}/(1 + [S]/K_m)$

Where the K_i is the inhibition constant that describes the binding affinity between the inhibitor and the enzyme, K_m is Michaelis–Menten constant that describes the affinity between the ATP and the enzyme and [S] is a fixed substrate concentration.

Here is an example to demonstrate the effect of using a fixed ATP concentration on inhibitor selectivity studies. Consider two hypothetical kinases, kinase 1 with K_{mATP}=10 μM and kinase 2 with K_{mATP}=1.5 μM. An inhibitor X has a K_i of 0.01μM for kinase 1 and 0.002 μM for kinase 2. The IC_{50} for X measured at an ATP concentration of 10 μM for kinase 1 would be larger than that for kinase 2 whereas at ATP concentration of 30 μM, the IC_{50} measured for kinase 1 would be smaller than that for kinase 2. Thus, inhibitor selectivity ranking between different kinases using assays with a fixed ATP concentration may be misleading.[207]

The second option is to use an ATP concentration that mimics the intracellular ATP levels. This option is complicated by the fact that little information about the exact cellular ATP concentrations is known. Moreover, ATP concentrations continuously fluctuate, may differ from one cellular compartment to another, from one cell type to another, and between diseased and normal cells which makes the determination of cellular level of ATP challenging.[207]

The third option for choosing the ATP concentration is to use ATP at a concentration that equals its K_m value, the concentration that allows half maximal reaction velocity, for the investigated kinase. ATP K_m concentration for ROCK2 was determined to be 39.5 µM. At ATP K_m, the IC_{50} equals twice the K_i value and represents a good measure of affinity between the inhibitor and the tested kinase. Thus, the selectivity of a given inhibitor against several different kinases can be ranked on the basis of its intrinsic affinity (potency). [207,208]

In summary, working exactly at ATP K_m concentration is preferred when more than one kinase is tested and will ensure that all types of inhibition are detected.

7.3.2 Enzyme Concentration

A very important aspect of ROCK assay design is the enzyme concentration used. There is a strong correlation between the reaction velocity and enzyme concentration. Too low enzyme concentrations may lead to weak signal and increased error. At optimal kinase concentrations, the assay signal is strong enough to give reproducible data and linearity can be achieved between assay signal and kinase activity. The best approach is to use an enzyme concentration well within the linear region of the curve. At high kinase concentrations, accumulation of phosphorylated substrate after the given reaction time and deviation from linearity between kinase activity and assay signal will be observed (**Figure 82**, nonlinear region). As the concentration of enzyme increases more, depletion of the substrate and the conversion of all ATP into ADP will result in a plateau (insensitive) region (**Figure 82**). In this region, higher kinase concentration cannot increase the reaction velocity further.[207,209, 210]

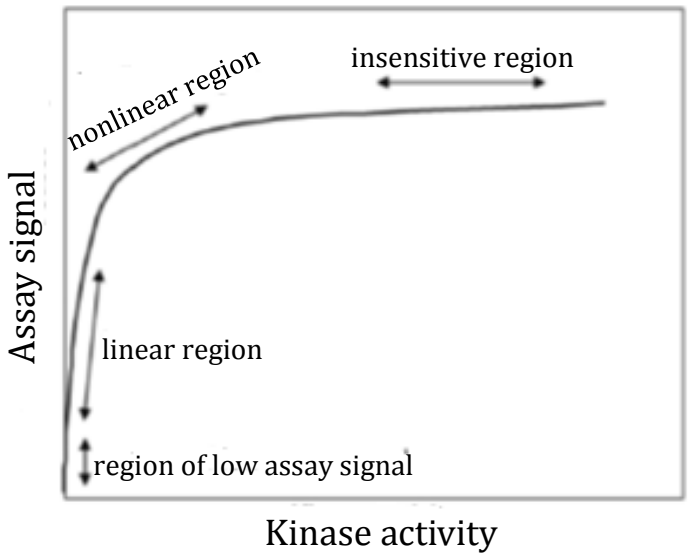

Figure 82: Effect of kinase concentration on assay signal.[207]

7.3.3 Buffer Composition

Typically, *in vitro* biochemical assays are conducted at physiological pH in an attempt to mimic the intracellular environment of the native enzyme. Finding a buffer is an important step in designing a robust and sensitive kinase assay. Buffer components have a major influence on determining the lowest possible kinase concentration that can be used and the maximal enzyme capacity that can be obtained. Compatible assay buffers guarantee the lowest IC_{50} value that can be measured for an inhibitor.[207] It is important to mention that the IC_{50} depends on enzyme concentration in a way that the assay wall equals half the kinase concentration used in the assay. The IC_{50} can never get lower than assay wall even if the tested compound binds tightly to the enzyme. For example, the lowest IC_{50} value that can be measured for an inhibitor in an assay that uses 20 nM kinase is 10 nM even if the real IC_{50} of the inhibitor is less.[207,209,211]

A previous study investigated the influence of different physiological buffers (MES, MOPS, HEPES and Tris) used in kinase assays on enzyme inhibitor screening assays [207]. Buffers were tested at 20 mM, pH=7.5 in the presence of 10 mM $MgCl_2$, 0.01% Triton X-100, and 1 mM DTT. The study found that inhibition of ROCK2 was sensitive to the composition of the assay buffer. MOPS had the least effect on enzyme activity and was recommended to maximize the catalytic activity of ROCK2 in activity assays [207]. The buffer composition provided with ROCK

ELISA assay kit by EMD Millipore is different from that of the Z'-LYTE® kit by Invitrogen. Thus, this may be a reason for the difference in results between the two kits.

To optimize the addition of phospahatase inhibitors to ROCK2 assay, it was found that sodium orthovanadate and β-glycerophosphate decrease enzyme activity. On the basis of these results, sodium orthovanadate and β-glycerophosphate should be avoided.[207]

7.3.4 Detection Method

Various assay detection methods have been used in ROCK activity assays. Herein, I will discuss the differences between ELISA and FRET as methods used for our compound libraries assay.

ELISA is one of the earliest antibody dependent assays used to detect phosphorylated peptides from kinase reaction. This assay offers the advantages of being relatively fast and simple. The main drawback is that it has limited use for Ser/Thr protein kinases because of the possibility of cross-reactivity between the secondary antibody and many substrate sequences. As well, these assays require many washing steps.[212]

FRET-based assay is a non-antibody based format with the advantages of minimizing the absolute and relative errors. With this in mind, the FRET technology is more attractive than ELISA for ROCK assays.

7.3.5 Screening Concentrations

Selection of inhibitor concentrations is an key factor in kinase inhibition assays. Screening inhibitors using a single concentration, as was done using the ELISA activity assay cannot be used to determine the IC_{50}. Thus, the generated data in the form of % inhibition could not be used in inhibitor profiling.[209] In the other hand, screening the inhibitor at several different concentrations (10 inhibitor concentrations) as was done with the FRET-based assay enables the generation of a dose response curve for each test compound.[209] The $IC_{50,}$ can be determined from the curve and used to profile the potency and selectivity of each test compound. Thus, screening strategies for reporting IC_{50} require testing the inhibitor at several different concentrations.

In conclusion, the differences in inhibitory potencies of our compounds between EMD Millipore and Invitrogen's assays is likely due to different assay conditions, substrate concentration, ATP concentration, and buffer components. The preliminary results obtained can form the basis for developing more potent and selective ROCK inhibitors using ligand-based drug design approach.

7.4 Enzyme-Linked Immunosorbent-Based Assay Protocol

1- Active, N-terminal His6-tagged recombinant human ROCK-II residues 11-552 and active, N-terminal His6-tagged, recombinant, human ROCK-I amino acids 17-535 can be used be used directly in the assay or further diluted with kinase buffer. Each sample were assayed in duplicate. Initiate the kinase reaction by adding 50 µL of kinase buffer (50 µM ATP, 15mM $MgCl_2$, 20mM MOPS, pH 7.2, 25mM β-glycerol phosphate, 5mM EGTA, 1mM sodium orthovanadate, 1mM dithiothreitol).

2- Add µL of the diluted solution of ROCK positive control (H-1152) or the different test compounds (10µM).

3- Recombinant ROCK1 or ROCK2 (1 mUnit/µL) was added

4- The mixture was incubated for 30 minutes at 30ºC with medium agitation on an orbital shaker.

5- The mixture was discarded and the wells were washed with wash buffer (0.05% tween 20 in 5% TBS) 2-3 times.

6- After washing and adequate blotting, the precoated wells were incubated with a 100 µL of anti-phospho-MYPT1 (Thr^{696}) antibody for 1 hour at room temperature with medium agitation.

7- The unbound antibody was discarded and the wells were washed 2-3 times.

8- The wells were incubated with a 100 µL of HRP-conjugated secondary antibody for 1 hour at room temperature with continuous agitation, after which the unbound antibody was discarded and wells were washed 2-3 times.

9- 100 µL of TMB/E substrate were added to each well and the plate was placed in the dark for not more than 15 minutes for blue color development with continuous monitoring.

10- The reaction was terminated by adding 100 µL of stop solution (1M sulphuric acid) to each well and the yellow color generated was measured at 450 nm.

7.5 FRET-Based Assay Protocol

Active, N-terminal GST-tagged recombinant human ROCK1$^{(1-535)}$ and ROCK2$^{(1-552)}$ enzymes (Invitrogen, cat. PR7028A and PV3759, respectively) were employed in this study.

The procedure was as follows:

1. In each well, 2.5 μL of 4X test compound solution in 1% DMSO, 5 μL of 2X Peptide/Kinase mixture and 2.5 μL of 4X ATP Solution were mixed and shaken 30 seconds on a plate shaker.
2. The kinase reaction mixture was then incubated at room temperature for 60 minutes.
3. At the end of the kinase reaction, 5 μL of development reagent solution (for proteolytic cleavage of non-phosphorylated peptides) were added and the mixture was shaken for 30 seconds on a plate shaker and then incubated at room temperature for another 60 minutes.
4. Fluorescence developed was read at 445-460 nm (coumarin emission) and 520-535 nm (fluorescein emission) using a fluorescence plate reader.
    - Test compounds were used at 10 different concentrations and a dose-response curve was constructed for each compound.
    - Z-Lyte® Kinase Assay Ser/Thr 07 and 13 peptides (Invitrogen, cat. PV3180 and PV3793) were used as substrates for ROCK1 and ROCK2, respectively, in accordance with the manufacturer's instructions. Final peptide concentration in the reaction mixture was 2 μM for both peptides.
    - Final concentrations of ROCK1 and ROCK2 in the kinase reaction was 378 ng/mL (3.8573 nM) and 116 ng/mL (1.2775 nM), respectively.
    - Final ATP concentration in the reaction mixture was 5 μM for ROCK1 and 50 μM for ROCK2. This was based on a ATP Km of 3.1 μM for ROCK1 and 39.5 μM for ROCK2.
    - The reaction buffer was composed of 50 mM HEPES buffer, pH 7.5, 10 mM $MgCl_2$, 1 mM EGTA, and 0.01% Brij-35.
    - Staurosporine was used as a positive control. IC_{50} of staurosporine for ROCK1 was 4.26 nM and for ROCK2 was 4.15 nM using the substrates mentioned above.
    - Coumarin/fluorescein emission ratio is determined and % phosphorylation of substrate is calculated.

Chapter 8

Experimental

8.1 Materials and methods

All reactions were performed in flame-dried or oven-dried glassware unless otherwise mentioned. DMSO-*d6*, CDCl3, Acetonitrile (anhydrous), and all chemicals were purchased from commercial sources and used as received. THF was pre-dried by refluxing over sodium benzophenone ketyl under nitrogen atmosphere and distilling prior to use. Dimethylformamide (DMF) was distilled under reduced pressure over molecular sieves and degassed prior to use. Dichloromethane (DCM) was pre-dried over CaH_2 and distilled prior to use

Thin layer chromatography (TLC) was done using precoated silica gel 60 F_{254} plates. Flash chromatography was performed using Silica Flash P60 silica gel (230-400 mesh). Biotage Isolera Spektra One flash chromatography was also used in the purification.

Proton nuclear magnetic resonance (^{1}H NMR) spectra and Carbon nuclear magnetic resonance (^{13}C NMR) were measured using a Bruker AV-400 spectrometer (400MHz for ^{1}H and 100MHz for ^{13}C, respectively). Chemical shifts are reported in parts per million (ppm) and are referenced relative to the center line of deuterated dimethylsulfoxide DMSO-*d6* (2.5 ppm ^{1}H NMR; 39.51 ppm ^{13}C NMR), and chloroform-*d* (7.27 ppm ^{1}H NMR; 77.0 ppm ^{13}C NMR). All spectra were performed at room temperature. The splitting patterns (multiplicities) were represented as follows: s = singlet, d = doublet, t = triplet, q = quartet, m = multiplet, dd = doublet of doublets, td = triplet of doublets, and ddd = doublet of doublet of doublets. High resolution mass spectra were measured with Thermo Scientific Q Exactive Orbitrap High Resolution Mass Spectrometer and low resolution mass spectra were recorded using AB Sciex QTRAP 5500-Agilent 1290. Microwave experiments were performed on Biotage Initiator microwave reactor.

8.2 Experimental Details

Ethyl 4-hydroxy-6-oxo-1,6-dihydropyridine-3-carboxylate **3**:

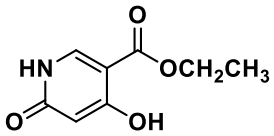

According to reference 213, a mixture of diethyl 1,3-acetonedicarboxylate 1 (25 ml, 138mmol), acetic anhydride (26.05 ml, 276mmol) and triethyl orthoformate (22.9 ml, 138mmol) was heated at 130°C for 1 hr. The reaction mixture was then cooled to room temperature and the solution was concentrated in vacuo to remove excess acetic anhydride. The resulting oily residue was cooled to 0ºC and 30% ammonia (45 ml) was added, followed by water (100 ml). The reaction mixture was allowed to stand in an ice bath for 1h, and the white precipitate that formed was isolated by filtration, washed with water. The filtrate was acidified to pH 4.0 using 1N HCl and cooled to 0ºC. The additional precipitated material filtered off, washed with water and combined with the previously isolated solid. This yellow solid was crystallized from MeOH: H_2O (1:1) to give **3** (17.18 g, 68%) as a yellowish solid.
^{1}H-NMR (400 MHz, DMSO-*d6*): δ 11.78 (1H, br s, OH), 10.74 (1H, br s, N^1-H), 8.02 (1H, br s, H-2), 5.61 (1H, s, H-5), 4.27 (2H, q, J=7.1Hz, CH_2), 1.29 (3H, t, J=7.1Hz, CH_3).
MS ESI (m/z): 182 $[M-H]^-$.

1-(*tert*-Butyl) 3-ethyl 4-hydroxy-6-oxopyridine-1,3(*6H*)-dicarboxylate **4:**

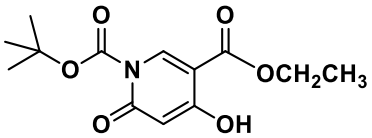

To a suspension of NaH (60% in a mineral oil, 5.35 g, 134 mmol) in dry THF (100 mL), was added compound **3** (6.13 g, 33.5 mmol). The mixture was stirred at 50 °C for 1 h. After cooling to room temperature, a solution of di-Tert-Butyl dicarbonate (29.2 g, 134 mmol) in dry THF (50 mL) was added and the mixture was stirred at 50 °C for 2 h. After cooling, the mixture was quenched slowly with saturated aqueous NH_4Cl (500 mL) and extracted with EtOAc. The combined organic fractions were dried over Na_2SO_4 and the solvent was removed in vacuo. The oily residue was purified by flash column chromatography on silica gel (gradient elution, 0-5% MeOH in CH_2Cl_2) to give **4** (6.64 g, 68%) as a white solid.

^{1}H-NMR (400 MHz, DMSO-*d6*): δ 12.33 (1H, br s, OH), 8.10 (1H, s, H-2), 6.20 (1H, s, H-5), 4.18 (2H, q, J=7.1Hz, CH_2), 1.46 (9H, s, $C(CH_3)_3$), 1.25 (3H, t, J=7.1Hz, CH_3).
MS ESI (m/z): 282 $[M-H]^-$.

1-(*tert*-Butyl) 3-ethyl 4-(benzyloxy)-6-oxopyridine-1,3(*6H*)-dicarboxylate **5a**:

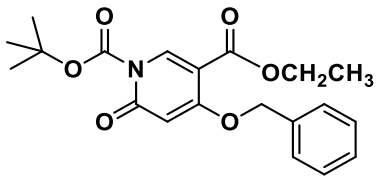

A mixture of *N*-Boc pyridinone **4** (4.6 g, 16.3 mmol), benzyl alcohol (2.7 g, 25 mmol) and PPh_3 (6.82g, 25 mmol) in dry THF (80mL) was stirred under N_2 until complete dissolution. The solution was cooled to 0 ^oC and DIAD (5.12 mL, 26 mmol) was added dropwise. After stirring the mixture at room temperature for 18 hours, it was diluted with water (100-150 ml) and extracted with EtOAc. The combined organic phase was dried over sodium sulfate (Na_2SO_4), filtered and then concentrated *in vacuo*. The crude material was purified by falsh column chromatography on silica gel (gradient elution, 0-3% MeOH in CH_2Cl_2) to give **5a** as white semisolid (3.1 g, 51%).

^{1}H-NMR (400 MHz, DMSO-*d6*): δ 8.70 (1H, s, H-2), 7.39-7.33 (2H, dd, J=6.3Hz, J=7.9Hz, H-3',5'), 7.31-7.27 (3H, m, H-2',4',6'), 6.34 (1H, s, H-5), 5.23 (2H, s, OCH_2Ph), 4.20 (2H, q, J=7.1Hz, CH_2), 1.46 (9H, s, $C(CH_3)_3$), 1.25 (3H, t, J=7.1Hz, CH_3).
MS ESI (m/z): 372 $[M-H]^-$.

1-(*tert*-Butyl) 3-ethyl 4-methoxy-6-oxopyridine-1,3(*6H*)-dicarboxylate **5b**:

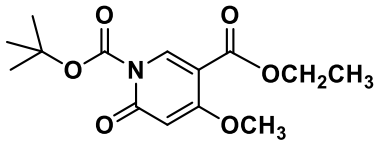

Prepared according to the procedure for **5a**, *N*-Boc pyridinone **4** (4.6 g, 16.3 mmol) was reacted with methanol (0.8 g, 25 mmol mmol). The crude product was purified by flash column chromatography on silica gel (gradient elution, 1-4% MeOH in CH_2Cl_2) to give **5b** as white semisolid (2.28 g, 47%).

^{1}H-NMR (400 MHz, DMSO-*d6*): δ 8.58 (1H, s, H-2), 6.27 (1H, s, H-5), 4.20 (2H, q, J=7.1Hz, CH_2), 3.51 (3H, s, OCH_3), 1.46 (9H, s, $C(CH_3)_3$), 1.26 (3H, t, J=7.1Hz, CH_3).
MS ESI (m/z): 296 $[M-H]^-$.

Ethyl 4-(benzyloxy)-6-oxo-1,6-dihydropyridine-3-carboxylate **6a:**

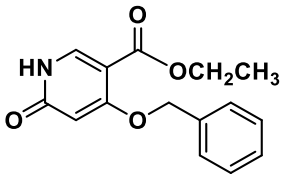

To a solution of **5a** (2.5 g, 6.7 mmol) in dry CH_2Cl_2 (12 mL) was added TFA (12 mL). The solution was stirred at room temperature for 3 h. The reaction mixture was evaporated *in vacuo* and the resulting residue was dissolved in EtOAc, and washed with saturated aqueous $NaHCO_3$. The organic layer was separated and the aqueous layer was extracted with EtOAc. The combined extracts were dried over Na_2SO_4 and the solvent was removed *in vacuo*. The residue was purified by flash column chromatography on silica gel (gradient elution, 1-5% MeOH in CH_2Cl_2) to give **6a** as a white solid (1.65g, 90%).

^{1}H-NMR (400 MHz, DMSO-*d6*): δ 8.53 (1H, s, H-2), 7.37-7.31 (2H, dd, J=6.4Hz, J=7.9Hz, H-3',5'), 7.30-7.24 (3H, m, H-2',4',6'), 5.67 (1H, s, H-5), 5.14 (2H, s, OCH_2Ph), 4.03 (2H, q, J=7.1Hz, CH_2), 1.17 (3H, t, J=7.1Hz, CH_3).

MS ESI (m/z): 272 $[M-H]^-$.

Ethyl 4-methoxy-6-oxo-1,6-dihydropyridine-3-carboxylate **6b**:

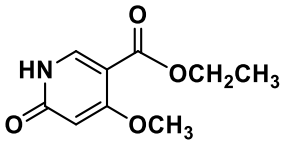

Prepared according to the procedure for **6a**, compound **5b** (2.0 g, 6.7 mmol) was reacted with TFA (10 mL) in in dry CH_2Cl_2 (10 mL). The crude product was purified by flash column chromatography on silica gel (gradient elution, 1-5% MeOH in CH_2Cl_2) to give **6b** as a white solid (1.11g, 84%).

^{1}H-NMR (400 MHz, DMSO-*d6*): δ 10.72 (1H, br s, N^1-H), 8.48 (1H, s, H-2), 5.68 (1H, s, H-5), 4.28 (2H, q, J=7.1Hz, CH_2), 3.43 (3H, s, OCH_3), 1.30 (3H, t, J=7.1Hz, CH_3).

MS ESI (m/z): 196 $[M-H]^-$.

4-(Benzyloxy)-6-oxo-1,6-dihydropyridine-3-carboxylic acid **7**:

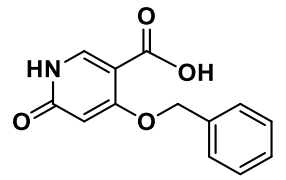

LiOH (0.40 g, 16.74 mmol) in water (5 ml) was added to a solution of ethyl 4-(benzyloxy)-6-oxo-1,6-dihydropyridine-3-carboxylate **6a** (1.52 g, 5.58 mmol) in THF:MeOH:H_2O 2:2:1 (15ml), and the mixture was stirred at ambient temperature for 12 h. The reaction mixture was then concentrated *in vacuo* and the resulting residue was dissolved in water, and the pH was adjusted to pH 4.0 by careful addition of 1N HCl. Upon cooloing in an ice bath, the precipitate formed was isolated by filtration, washed with water and dried *in vacuo* to afford the desired compounds **7** as an off white solid (1.20g, 88%).

^{1}H-NMR (400 MHz, DMSO-*d6*): δ 12.45 (2H, br s, N^1-H, COOH), 8.56 (1H, s, H-2), 7.38-7.31 (2H, dd, J=6.4Hz, J=7.9Hz, H-3',5'), 7.30-7.24 (3H, m, H-2',4',6'), 5.67 (1H, s, H-5), 5.14 (2H, s, OCH_2Ph).

MS ESI (m/z): 244 $[M-H]^-$.

4-Methoxy-6-oxo-1,6-dihydropyridine-3-carboxylic acid **8**:

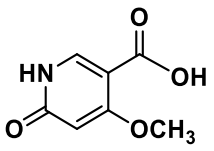

Following the procedure for **7**, compound **6b** (1.1 g, 5.58 mmol) was hydrolyzed to give **8** as an off white solid (0.80 g, 84%).

^{1}H-NMR (400 MHz, DMSO-*d6*): δ 12.34 (2H, br s, N^1-H, COOH), 8.49 (1H, s, H-2), 5.64 (1H, s, H-5), 3.42 (3H, s, OCH_3).

MS ESI (m/z): 168 $[M-H]^-$.

N-(*tert*-Butoxycarbonyl)-L-serine, methyl ester **10**:

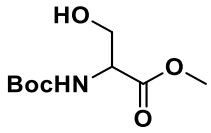

According to reference 214, l-serine methyl ester hydrochloride **9** (15.25 g, 98 mmol) was dissolved in dry CH_2Cl_2 (250 mL). Et_3N (28.5 mL, 196 mmol) and di-tert-Butyl dicarbonate (25.5 g, 117.5 mmol) were added, and the reaction mixture was stirred at room temperature for 24 h under nitrogen. The mixture was diluted with water and extracted with EtOAc. The combined organic layer was washed with saturated $NaHCO_3$ (250 mL) and brine (250 mL), dried over Na_2SO_4 and concentrated *in vacuo* to afford N-Boc-L-serine methyl ester **10** as colourless oil (19.28 g, 90%) which was used in the next step without further purification.

2,2-Dimethyl-oxazolidine-3,4-dicarboxylic acid 3-*tert*-butyl ester 4-methyl ester **11**:

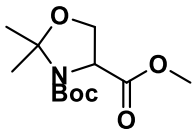

According to reference 214, the crude product **10** (16.24 g, 74.08 mmol) was dissolved in acetone (250mL) and 2,2 dimethoxypropane DMP (80 mL). $BF_3 \cdot Et_2O$ (0.5 mL) was added as a catalyst. The resulting mixture was stirred at room temperature for 3 h or till reaction completion (monitored by TLC). The solvent was removed *in vacuo*, the residual oil is dissolved in CH_2Cl_2 (250 mL) and washed with saturated aqueous $NaHCO_3$, brine (100 mL), The organic phase was dried over Na_2SO_4 and the solvent evaporated *in vacuo* to give compound **11** as a pale yellow oil (16.90g, 88%), which was used in the next step without further purification.

3-(*tert*-Butoxycarbonyl)-2,2-dimethyloxazolidine-4-carboxylic acid **12**:

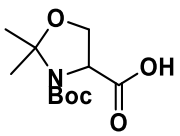

According to reference 214, to an ice cooled solution of methyl ester **11** (13.68 g, 52.77 mmol) in MeOH (200 mL) was added LiOH (3.79 g, 158.31 mmol) in water (15 mL) with stirring. The mixture was allowed to warm to room temperature and stirred for 12h. When the reaction was complete (TLC monitoring) the solvent was removed in vacuo, and the resulting residue was dissolved in water (200 mL) and neutralized with 10% citric acid. The solution was extracted with EtOAc, dried over Na_2SO4, and concentrated to give the acid **12** as a yellow semisolid (11.13 g, 86%), which was used for the next step without further purification. A small amount of the product was purified for ^{1}H-NMR and mass analysis by flash column chromatography on silica gel (gradient elution, 2-5% EtOAc in hexane)

^{1}H-NMR (400 MHz, $CDCl_3$): δ 9.19 (1H, br s, COOH), 4.52–4.40 (1H, m, CH-N), 4.22–4.12 (2H, m, CH_2-O), 1.67-1.51 (15H, m, 5 CH_3).

MS ESI (m/z): 244 $[M-H]^-$.

tert-Butyl 2,2-dimethyl-4-(phenyl carbamoyl)oxazolidine-3-carboxylate **13a**:

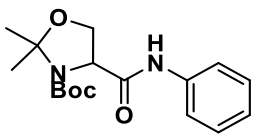

3-(Tert-butoxycarbonyl)-2,2-dimethyloxazolidine-4-carboxylic acid **12** (2.45 g, 10 mmol) and aniline (0.93 g, 10 mmol) in dry THF (25 mL) was treated with BOP-Cl (3.04 g, 12 mmol) and Et_3N (4.17 mL, 30 mmol). The resulting solution was stirred at ambient temperature for 12 h. The mixture was poured in water and extracted with EtOAc. The organic layer was dried over Na_2SO_4, filtered and then concentrated *in vacuo*. The crude material was purified by flash column chromatography on silica gel (gradient elution, 0-2% MeOH in CH_2Cl_2) to give the product **13a** as an off white solid (2.4 g, 75%).

^{1}H-NMR (400 MHz, DMSO-*d6*): see Table 16.

MS ESI (m/z): 319 $[M-H]^-$.

tert-Butyl 4-((4-methoxyphenyl)carbamoyl)-2,2-dimethyloxazolidine-3-carboxylate **13b**:

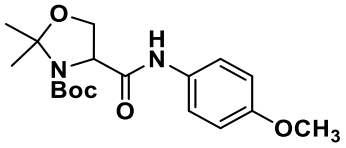

According to procedure for **13a**, compound **12** (2.45 g, 10 mmol) was reacted with *p*-anisidine (1.23 g, 10 mmol). The crude product was purified by flash column chromatography on silica gel (gradient elution, 0-4% MeOH in CH_2Cl_2) to afford **13b** as an off white solid (2.5 g, 71%).

^{1}H-NMR (400 MHz, DMSO-*d6*): see Table 16

MS ESI (m/z): 351 $[M+H]^+$.

tert-Butyl 2,2-dimethyl-4-(4-(4-trifluoromethylphenyl)carbamoyl)oxazolidine-3-carboxylate **13c**:

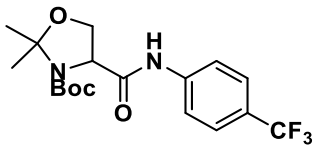

According to procedure for **13a**, compound **12** (2.45 g, 10 mmol) was reacted with 4-trifluromethylaniline (1.62 g, 10 mmol). The crude product was purified by flash column chromatography on silica gel (gradient elution, 0-2% MeOH in CH_2Cl_2) to afford **13c** as an off white solid (1.99 g, 51%).

^{1}H-NMR (400 MHz, DMSO-*d6*): see Table 16.

MS ESI (m/z): 387 $[M-H]^-$.

tert-Butyl 2,2-dimethyl-4-(4-(4-chlorophenyl)carbamoyl)oxazolidine-3-carboxylate **13d**:

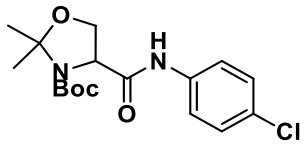

According to procedure for **13a**, compound **12** (2.45 g, 10 mmol) was reacted with 4-chloroaniline (1.27 g, 10 mmol). The crude product was purified by flash column chromatography on silica gel (gradient elution, 0-2% MeOH in CH_2Cl_2) to afford **13d** as a pale yellow solid (1.89 g, 53%).

^{1}H-NMR (400 MHz, DMSO-*d6*): see Table 16.

MS ESI (m/z): 353 $[M-H]^-$.

tert-Butyl 2,2-dimethyl-4-(pyridine-3-yl carbamoyl)oxazolidine-3-carboxylate **13e**:

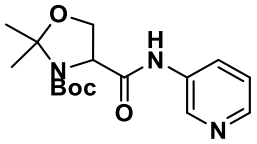

According to procedure for **13a**, compound **12** (2.0 g, 8.16 mmol) was reacted with 3-aminopyridine (0.77 g, 8.16 mmol), dry THF (20 mL), BOP-Cl (2.48 g, 9.78 mmol) and Et_3N (3.4 mL, 24.46 mmol). The crude product was purified by flash column chromatography on silica gel (gradient elution, 0-5% MeOH in CH_2Cl_2) to give the desired product **13e** as a white powder (1.68 g, 64%).

^{1}H-NMR (400 MHz, DMSO-*d6*): see Table 16.

MS ESI (m/z): 320 $[M-H]^-$.

tert-Butyl 2,2-dimethyl-4-(thiazol-2-yl carbamoyl)oxazolidine-3-carboxylate **13f**:

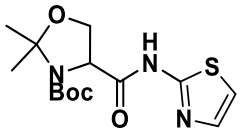

According to procedure for **13a**, compound **12** (1.5 g, 6.12 mmol) was reacted with 2-aminothiazole (0.61 g, 6.12 mmol), dry THF (15 mL), BOP-Cl (1.86 g, 7.33 mmol) and Et_3N (2.55 mL, 18.35 mmol). The crude product was purified by flash column chromatography on silica gel (gradient elution, 0-3% MeOH in CH_2Cl_2) to give the desired product **13f** as a light yellow powder (1.36g, 68%).

^{1}H-NMR (400 MHz, DMSO-*d6*): see Table 16.

MS ESI (m/z): 328 $[M+H]^+$.

Table 16: NMR data of compounds **13a-f**

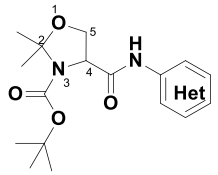

Entry		Scaffold ^{1}H-NMR (400 MHz, DMSO-*d6*) δ ppm	R ^{1}H-NMR (400 MHz, DMSO-*d6*) δ ppm
13a	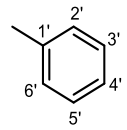	10.07 (1H, d, J=14.1Hz, N-H), 4.48-4.37 (1H, m, CH-N), 4.24-4.13 (1H, m, one of CH_2-O), 3.98-3.85 (1H, m, one of CH_2-O), 1.63-1.22 (15H, m, 5 CH_3)	7.58 (2H, d, J=7.9Hz, H-2',6'), 7.31 (2H, t, J=7.9Hz, H-3',5'), 7.05 (1H, t, J=7.9Hz, H-4')
13b	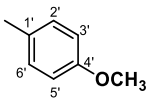	10.13 (1H, d, J=14.1Hz, N-H), 4.45-4.35 (1H, m, CH-N), 4.25-4.13 (1H, m, one of CH_2-O), 3.99-3.86 (1H, m, one of CH_2-O), 1.65-1.20 (15H, m, 5 CH_3)	7.51 (2H, d, J=9.1Hz, H-2',6'), 6.89 (2H, d, J=9.1Hz, H-3',5'), 3.71 (3H, s, OCH_3)
13c	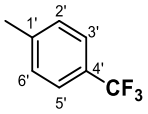	10.47 (1H, d, J=14.6Hz, N-H), 4.51-4.39 (1H, m, CH-N), 4.25-4.16 (1H, m, one of CH_2-O), 4.01-3.90 (1H, m, one of CH_2-O), 1.67-1.22 (15H, m, 5 CH_3)	7.81 (2H, dd, J=8.4Hz, H-3',5'), 7.7 (2H, dd, J=8.4Hz, H-2',6')
13d	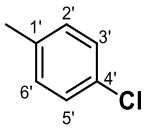	10.22 (1H, d, J=14.6Hz, N-H), 4.45-4.35 (1H, m, CH-N), 4.22-4.14 (1H, m, one of CH_2-O), 3.97-3.87 (1H, m, one of CH_2-O), 1.62-1.19 (15H, m, 5 CH_3)	7.61 (2H, dd, J=8.4Hz, H-3',5'), 7.38 (2H, dd, J=8.4Hz, H-2',6')
13e	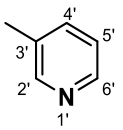	10.32 (1H, d, J=13.9Hz, N-H), 4.50-4.38 (1H, m, CH-N), 4.26-4.14 (1H, m, one of CH_2-O), 4.02-3.88 (1H, m, one of CH_2-O), 1.67-1.17 (15H, m, 5 CH_3).	8.72 (1H, s, H-2'), 8.28 (1H, d, J=4.5Hz, H-6'), 8.05 (1H, d, J=8.2Hz, H-4'), 7.37 (1H, dd, J=4.5Hz, J=8.2Hz, H-5')

Entry	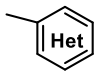	Scaffold ^{1}H-NMR (400 MHz, DMSO-*d6*) δ ppm	R ^{1}H-NMR (400 MHz, DMSO-*d6*) δ ppm
13f	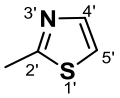	12.31 (1H, d, J=30.1Hz, N-H), 4.61-4.52 (1H, m, CH-N), 4.24-4.13 (1H, m, one of CH_2-O), 4.01-3.88 (1H, m, one of CH_2-O), 1.64-1.18 (15H, m, 5 CH_3).	7.48 (1H, d, J=4.0Hz, H-4'), 7.36 (1H, d, J=4.0Hz, H-5')

2-Amino-3-hydroxy-*N*-phenylpropanamide hydrochloride **14a**:

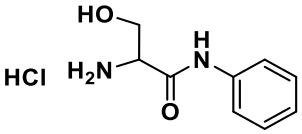

To **13a** (2 g, 6.24 mmol) in MeOH (12 mL) was added methanolic HCl (5 mL, 3M), and the reaction was stirred for 3h at room temperature. When the reaction was complete (TLC monitoring) the solvent was removed *in vacuo*. The resulting residue was then washed with ethyl ether and collected by filtration to the give the product **14a** as a white powder (1.1 g, 81%).

^{1}H-NMR (400 MHz, DMSO-*d6*): see Table 17.

MS ESI (m/z): 217 $[M+H]^+$.

2-Amino-3-hydroxy-*N*-(4-methoxyphenyl)propanamide hydrochloride **14b**:

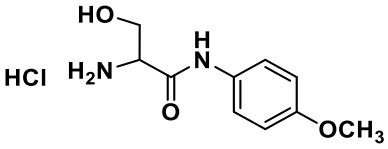

According to the procedure for **14a**, oxazolidine **13b** (2.5 g, 7.13 mmol) was converted to **14b**, isolated as a white powder (1.48 g, 84%).

^{1}H-NMR (400 MHz, DMSO-*d6*): see Table 17.

MS ESI (m/z): 211 $[M+H]^+$.

2-Amino-3-hydroxy-*N*-(4-(trifluoromethyl)phenyl)propanamide hydrochloride **14c**:

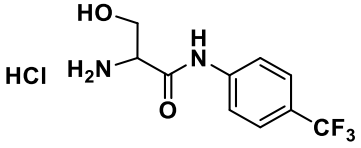

According to the procedure for **14a**, oxazolidine **13c** (2.0 g, 5.15 mmol) was converted to **14c**, isolated as a white powder (1.07 g, 73%).

^{1}H-NMR (400 MHz, DMSO-*d6*): see Table 17.

MS ESI (m/z): 249 $[M+H]^+$.

2-Amino-*N*-(4-chlorophenyl)-3-hydroxypropanamide hydrochloride **14d**:

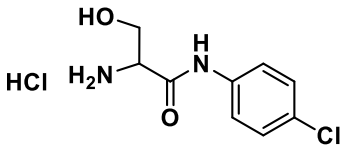

According to the procedure for **14a**, oxazolidine **13d** (2.0 g, 5.64 mmol) was converted to **14d**, isolated as a white powder (1.0 g, 71%).

^{1}H-NMR (400 MHz, DMSO-*d6*): see Table 17.

MS ESI (m/z): 252 $[M+H]^+$.

2-Amino-3-hydroxy-*N*-(pyridin-3-yl)propanamide hydrochloride **13e**:

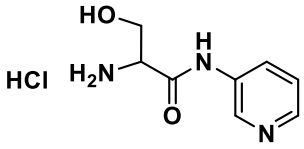

According to the procedure for **14a**, oxazolidine **13e** (2.5 g, 7.78 mmol) was converted to **14e**, isolated as a white powder (1.34 g, 79%).

^{1}H-NMR (400 MHz, DMSO-*d6*): see Table 17.

MS ESI (m/z): 218 $[M+H]^+$.

2-Amino-3-hydroxy-*N*-(thiazol-2-yl)propanamide hydrochloride **14f**:

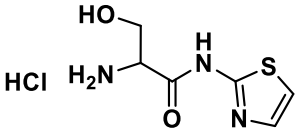

According to the procedure for **14a**, oxazolidine **13f** (2.0 g, 6.11 mmol) was converted to **14f**, isolated as a white powder (1.05 g, 77%).

^{1}H-NMR (400 MHz, DMSO-*d6*): see Table 17.

MS ESI (m/z): 224 $[M+H]^+$.

Table 17: NMR data of compounds **14a-f**

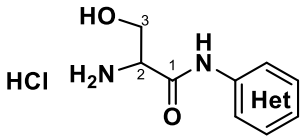

Entry		Scaffold ^{1}H-NMR (400 MHz, DMSO-*d6*) δ ppm	R ^{1}H-NMR (400 MHz, DMSO-*d6*) δ ppm
14a	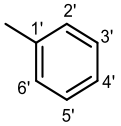	10.45 (1H, s, CONH), 8.22 (2H, s, NH_2), 5.60 (1H, t, J=4.8Hz, OH), 3.99 (1H, t, J=4.8Hz, CH-N), 3.84 (2H, t, J=4.8Hz, CH_2-O)	7.60 (2H, d, J=7.7Hz, H-2',6'), 7.35 (2H, t, J=7.7Hz, H-3',5'), 7.11 (1H, t, J=7.7Hz, H-4')
14b	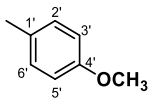	10.52 (1H, s, CONH), 8.26 (2H, s, NH_2), 5.55 (1H, t, J=5.0Hz, OH), 3.98 (1H, t, J=5.0Hz, CH-N), 3.83 (2H, t, J=5.0Hz, CH_2-O)	7.54 (2H, d, J=9.1Hz, H-2',6'), 6.92 (2H, d, J=9.1Hz, H-3',5'), 3.73 (3H, s, OCH_3)
14c	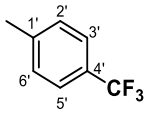	11.06 (1H, s, CONH), 8.30 (2H, s, NH_2), 5.60 (1H, t, J=4.5Hz, OH), 4.10 (1H, t, J=4.5Hz, CH-N), 3.95-3.83 (2H, m, CH_2-O)	7.88 (2H, d, J=8.5Hz, H-2',6'), 7.75 (2H, d, J=8.5Hz, H-3',5')
14d	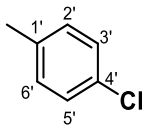	11.06 (1H, s, CONH), 8.35 (2H, s, NH_2), 5.60 (1H, s, OH), 4.08 (1H, s, CH-N), 3.96-3.83 (2H, m, CH_2-O)	7.88 (2H, d, J=8.9Hz, H-2',6'), 7.75 (2H, d, J=8.9Hz, H-3',5')
14e	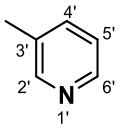	10.73 (1H, s, CONH), 8.27 (2H, s, NH_2), 5.59 (1H, s, OH), 4.09-4.0 (1H, m, CH-N), 3.92-3.82 (2H, m, CH_2-O)	8.81 (1H, d, J=2.4Hz, H-2'), 8.36 (1H, dd, J=1.4Hz, J=4.8Hz, H-6'), 8.06 (1H, ddd, J=1.4Hz, J=2.4Hz, J=8.5Hz, H-4'), 7.45 (1H, dd, J=4.8Hz, J=8.5Hz, H-5')
14f		12.68 (1H, s, CONH), 8.56 (2H, s, NH_2), 4.20-4.09 (1H, m, CH-N), 3.99-3.84 (2H, m, CH_2-O).	7.53 (1H, d, J=3.6Hz, H-4'), 7.32 (1H, d, J=3.6Hz, H-5')

2-Amino-3-((*tert*-butyldimethylsilyl)oxy)-*N*-phenylpropanamide **15a**:

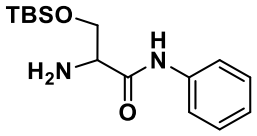

To a solution of **14a** (1.08 g, 5 mmol) in acetonitrile (12 mL) was added imidazole (0.85 g, 12.5 mmol). The mixture was stirred for 30 minutes before the addition of tert-butylchlorodimethylsilane (1.13 g, 7.5 mmol). The mixture was stirred at room temperature for 12h., then concentrated *in vacuo*. The oily residue was purified by flash column chromatography on silica gel (gradient elution, 0-6% MeOH in CH_2Cl_2) to give the desired product **15a** as a semi-solid (73%).

^{1}H-NMR (400 MHz, DMSO-*d6*): see Table 18.

MS ESI (m/z): 295 $[M+H]^+$.

2-Amino-3-((*tert*-butyldimethylsilyl)oxy)-*N*-(4-methoxyphenyl)propanamide **15b**:

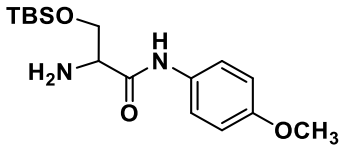

According to the procedure for **15a**, aminoalcohol **14b** (1.23 g, 5 mmol) was converted to **15b**, isolated as a semi-solid (1.22 g, 75%).

^{1}H-NMR (400 MHz, DMSO-*d6*): see Table 18.

MS ESI (m/z): 325 $[M+H]^+$.

2-Amino-3-((*tert*-butyldimethylsilyl)oxy)-*N*-(4-(trifluoromethyl)phenyl)propanamide **15c**:

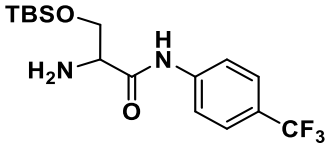

According to the procedure for **15a**, aminoalcohol **14c** (1.42 g, 5 mmol) was converted to **15b**, isolated as a semi-solid (1.2 g, 66%).

^{1}H-NMR (400 MHz, DMSO-*d6*): see Table 18 .

MS ESI (m/z): 363 $[M+H]^+$.

2-Amino-3-((*tert*-butyldimethylsilyl)oxy)-*N*-(4-chlorophenyl)propanamide **15d**:

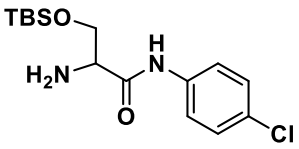

According to the procedure for **15a**, aminoalcohol **14d** (1.25 g, 5 mmol) was converted to **15d**, isolated as a semi-solid (1.09 g, 66%).

^{1}H-NMR (400 MHz, DMSO-*d6*): see Table 18.

2-Amino-3-((*tert*-butyldimethylsilyl)oxy)-*N*-(pyridin-3-yl)propanamide **15e**:

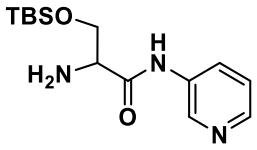

According to the procedure for **15a**, aminoalcohol **14e** (1.09 g, 5 mmol) was converted to **15e**, isolated as a white powder (1.05 g, 71%).

^{1}H-NMR (400 MHz, DMSO-*d6*): see Table 18.

MS ESI (m/z): 296 $[M+H]^+$.

2-Amino-3-((*tert*-butyldimethylsilyl)oxy)-*N*-(thiazol-2-yl)propanamide **15f**:

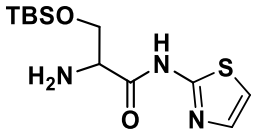

According to the procedure for **15a**, aminoalcohol **14f** (1.12 g, 5 mmol) was converted to **15f**, isolated as a white powder (1.03 g, 68%).

^{1}H-NMR (400 MHz, DMSO-*d6*): see Table 18.

MS ESI (m/z): 302 $[M+H]^+$.

Table 18: NMR data of compounds **15a-f**

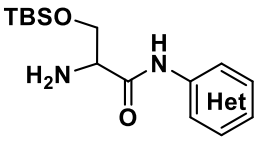

Entry	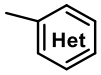	**Scaffold** ^{1}H-NMR (400 MHz, DMSO-*d6*) δ ppm	**R** ^{1}H-NMR (400 MHz, DMSO-*d6*) δ ppm
15a	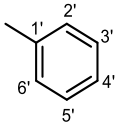	9.84 (1H, s, CONH), 3.77-3.64 (2H, m, CH_2-O), 3.41(1H, t, J=5.5Hz, CH-N), 0.81 (9H, s, $SiC(CH_3)_3$), -0.01 (6H, s, $SiCH_3CH_3$)	7.63 (2H, d, J=7.6Hz, H-2',6'), 7.29 (2H, t, J=7.6Hz, H-3',5'), 7.03 (1H, t, J=7.6Hz, H-4')

Entry	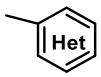	Scaffold ^{1}H-NMR (400 MHz, DMSO-*d6*) δ ppm	R ^{1}H-NMR (400 MHz, DMSO-*d6*) δ ppm
15b	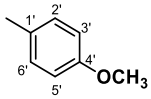	9.66 (1H, s, CONH), 3.74-3.63 (5H, m, CH_2-O, OCH_3), 3.37(1H, t, J=5.2Hz, CH-N), 0.82 (9H, s, $SiC(CH_3)_3$), -0.01 (6H, s, $SiCH_3CH_3$)	7.53 (2H, d, J=8.9Hz, H-2',6'), 6.86 (2H, d, J=8.9Hz, H-3',5'), 3.74-3.63 (5H, m, OCH_3)
15c	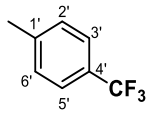	9.66 (1H, s, CONH), 3.80-3.63 (2H, m, CH_2-O), 3.37(1H, t, J=5.4Hz, CH-N), 0.8 (9H, s, $SiC(CH_3)_3$), -0.01 (6H, s, $SiCH_3CH_3$)	7.86 (2H, d, J=8.4Hz, H-2',6'), 7.75 (2H, d, J=8.4Hz, H-3',5')
15d	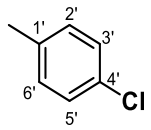	9.96 (1H, s, CONH), 3.78-3.62 (2H, m, CH_2-O), 3.4 (1H, t, J=5.2Hz, CH-N), 0.81 (9H, s, $SiC(CH_3)_3$), -0.01 (6H, s, $SiCH_3CH_3$)	7.68 (2H, d, J=8.7Hz, H-2',6'), 7.35 (2H, d, J=8.7Hz, H-3',5')
15e	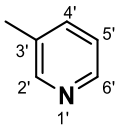	3.92-3.74 (2H, m, CH_2-O), 3.68 (1H, t, J=5.3Hz, CH-N), 0.81 (9H, s, $SiC(CH_3)_3$), -0.01 (6H, s, $SiCH_3CH_3$).	8.79 (1H, d, J=2.5Hz, H-2'), 8.27 (1H, dd, J=1.4Hz, J=4.7Hz, H-6'), 8.07 (1H, ddd, J=1.4Hz, J=2.5Hz, J=8.5Hz, H-4'), 7.36 (1H, dd, J=4.7Hz, J=8.5Hz, H-5')
15f	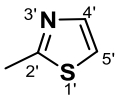	5.24 (2H, br s, NH_2), 3.79-3.64 (2H, m, CH_2-O), 3.68 (1H, dd, J=4.9 Hz, J= 6.2Hz, CH-N), 0.78 (9H, s, $SiC(CH_3)_3$), -0.03 (6H, s, $SiCH_3CH_3$).	7.46 (1H, d, J=3.7Hz, H-4'), 7.19 (1H, d, J=3.7Hz, H-5')

4-(Benzyloxy)-*N*-(3-((*tert*-butyldimethylsilyl)oxy)-1-oxo-1-(phenylamino)propan-2-yl)-6-oxo-1,6-dihydropyridine-3-carboxamide **16a:**

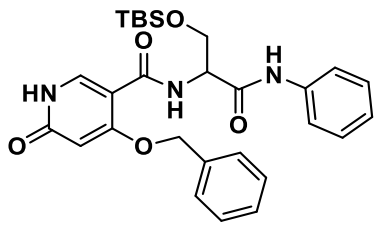

To a solution of 4-benzyloxy-6-oxo-1,6-dihydropyridine-3-carboxylic acid **7** (0.12 g, 0.5 mmol) and 2-amino-3-hydroxy-N-phenyl propanamide **15a** (0.15 g, 0.5 mmol) in DMF (5

ml) was added HOBt (0.08 g, 0.6 mmol), EDC (0.12 g, 0.6 mmol), and DIEA (0.19 g, 1.5 mmol) at room temperature. The mixture was stirred at ambient temperature for 12 h. The solvent was evaporated under vacuum. The resulting oily residue was flash column chromatographed on silica gel (gradient elution, 3-10% MeOH in CH_2Cl_2) to give **16a** (0.17g, 67%) as a colorless oil.

^{1}H-NMR (400 MHz, DMSO-*d6*): see Table 19.

MS ESI (m/z): 520 $[M-H]^-$.

4-(Benzyloxy)-*N*-(3-((*tert*-butyldimethylsilyl)oxy)-1-((4-methoxyphenyl)amino)-1-oxopropan-2-yl)-6-oxo-1,6-dihydropyridine-3-carboxamide **16b**:

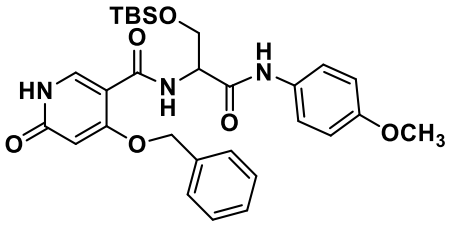

According to the procedure for **16a**, amine **15b** (0.16 g, 0.5 mmol) was converted to **16b**, isolated as a as a colorless oil (0.17 g, 63%).

^{1}H-NMR (400 MHz, DMSO-*d6*): see Table 19.

MS ESI (m/z): 550 $[M-H]^-$.

4-(Benzyloxy)-*N*-(3-((*tert*-butyldimethylsilyl)oxy)-1-oxo-1-((4(trifluoromethyl)phenyl)amino) propan-2-yl)-6-oxo-1,6-dihydropyridine-3-carboxamide **16c**:

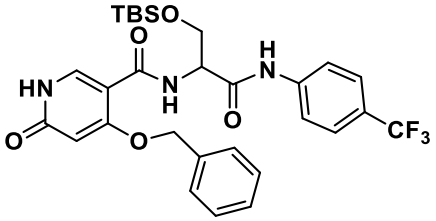

According to the procedure for **16a**, amine **15c** (0.18 g, 0.5 mmol) was converted to **16c**, isolated as a colorless oil (0.14 g, 49%).

^{1}H-NMR (400 MHz, DMSO-*d6*): see Table 19.

MS ESI (m/z): 588 $[M-H]^-$.

4-(Benzyloxy)-*N*-(3-((*tert*-butyldimethylsilyl)oxy)-1-((4-chlorophenyl)amino)-1-oxopropan-2-yl)-6-oxo-1,6-dihydropyridine-3-carboxamide **16d**:

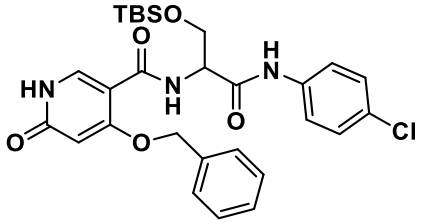

According to the procedure for **16a**, amine **15d** (0.16 g, 0.5 mmol) was converted to **16d**, isolated as a colorless oil (0.15 g, 53%).

^{1}H-NMR (400 MHz, DMSO-*d6*): see Table 19.

MS ESI (m/z): 555 $[M-H]^-$.

4-(Benzyloxy)-*N*-(3-((*tert*-butyldimethylsilyl)oxy)-1-oxo-1-(pyridin-3-ylamino)propan-2-yl)-6-oxo-1,6-dihydropyridine-3-carboxamide **16e**:

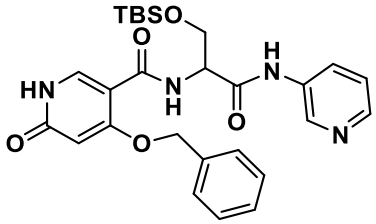

According to the procedure for **16a**, amine **15e** (0.15 g, 0.5 mmol) was converted to **16e**, isolated as a colorless oil (0.15 g, 58%).

^{1}H-NMR (400 MHz, DMSO-*d6*): see Table 19.

MS ESI (m/z): 521 $[M-H]^-$.

4-(Benzyloxy)-*N*-(3-((*tert*-butyldimethylsilyl)oxy)-1-oxo-1-(thiazol-2-ylamino)propan-2-yl)-6-oxo-1,6-dihydropyridine-3-carboxamide **16f**:

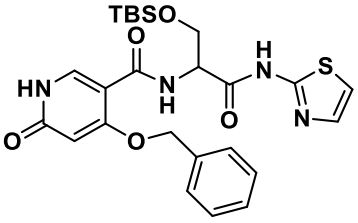

According to the procedure for **16a**, amine **15f** (0.15 g, 0.5 mmol) was converted to **16f**, isolated as a colorless oil (0.17 g, 65%).

^{1}H-NMR (400 MHz, DMSO-*d6*): see Table 19.

MS ESI (m/z): 527 $[M-H]^-$.

Table 19: NMR data of compounds **16a-f**

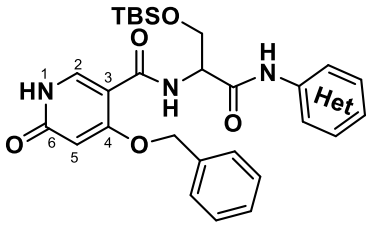

Entry		Scaffold ^{1}H-NMR (400 MHz, DMSO-*d6*) δ ppm	R ^{1}H-NMR (400 MHz, DMSO-*d6*) δ ppm
16a	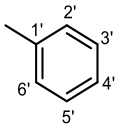	10.13 (1H, s, CONH), 8.61 (1H, s, H-2), 7.41-7.22 (8H, m , Ar-H, CONH), 5.21 (1H, s, H-5), 5.18 (2H, s, CH_2Ph), 4.83-4.70 (1H, m, CH-N), 4.06-3.87 (2H, m, CH_2-O), 0.61 (9H, s, $SiC(CH_3)_3$), -0.12 (6H, s, $SiCH_3CH_3$).	7.58 (2H,d, J=7.2Hz H-2',6'), 7.41-7.22 (8H, m, H-3',5'), 7.05 (1H, t, J=7.2Hz, H-4')
16b	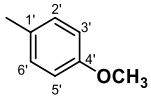	12.31 (1H, s, N^1-H), 9.97 (1H, s, CONH), 8.64 (1H, s, CONH), 8.46 (1H, s, H-2), 7.37-7.22 (5H, m , Ar-H), 5.75 (1H, s, H-5), 5.13 (2H, s, CH_2Ph), 4.74-4.66 (1H, m, CH-N), 3.96-3.78 (2H, m, CH_2-O), 0.81 (9H, s, $SiC(CH_3)_3$), -0.02 (6H, s, $SiCH_3CH_3$).	7.49 (2H, d, J=8.8Hz, H-2',6'), 6.87 (2H, d, J=8.8Hz, H-3',5'), 3.71 (3H, s, OCH_3)
16c	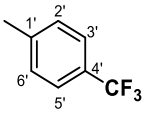	12.35 (1H, s, N^1-H), 10.49 (1H, s, CONH), 8.65 (1H, s, CONH), 8.47 (1H, s, H-2), 7.37-7.22 (5H, m , Ar-H), 5.75 (1H, s, H-5), 5.13 (2H, s, CH_2Ph), 4.74-4.66 (1H, m, CH-N), 3.96-3.78 (2H, m, CH_2-O), 0.81 (9H, s, $SiC(CH_3)_3$), -0.02 (6H, s, $SiCH_3CH_3$).	7.81 (2H, d, J=8.8Hz, H-3',5'), 7.68 (2H, d, J=8.8Hz, H-2',6')
16d	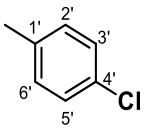	12.37 (1H, s, N^1-H), 10.26 (1H, s, CONH), 8.67 (1H, s, CONH), 8.44 (1H, s, H-2), 7.35-7.21 (5H, m , Ar-H), 5.75 (1H, s, H-5), 5.13 (2H, s, CH_2Ph), 4.77-4.67 (1H, m, CH-N), 3.99-3.79 (2H, m,	7.62 (2H, d, J=8.9Hz, H-2',6'), 7.37 (2H, d, J=8.9Hz, H-3',5')

Entry		Scaffold ^{1}H-NMR (400 MHz, DMSO-*d6*) δ ppm	R ^{1}H-NMR (400 MHz, DMSO-*d6*) δ ppm
		CH_2-O), 0.79 (9H, s, $SiC(CH_3)_3$), -0.03 (6H, s, $SiCH_3CH_3$).	
16e	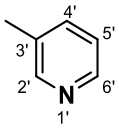	12.36 (1H, s, N^1-H), 10.36 (1H, s, CONH), 8.63 (1H, d, J=7.2Hz, CONH), 8.48 (1H, s, H-2), 7.38-7.23 (6H, m , Ar-H), 5.75 (1H, s, H-5), 5.14 (2H, s, CH_2Ph), 4.80-4.70 (1H, m, CH-N), 4.03-3.83 (2H, m, CH_2-O), 0.81 (9H, s, $SiC(CH_3)_3$), -0.03 (6H, s, $SiCH_3CH_3$).	8.75 (1H, d, J=2.5Hz, H-2'), 8.27 (1H, dd, J=1.4Hz, J=4.7Hz, H-6'), 8.02 (1H, ddd, J=1.4Hz, J=2.5Hz, J=8.5Hz, H-4'), 7.38-7.23 (6H, m , H-5')
16f	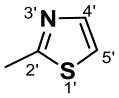	12.35 (1H, s, N^1-H), 8.73 (1H, s, CONH), 8.43 (1H, s, H-2), 7.36-7.21 (7H, m , Ar-H, CONH), 5.75 (1H, s, H-5), 5.13 (2H, s, CH_2Ph), 4.84-4.77 (1H, m, CH-N), 4.07-3.85 (2H, m, CH_2-O), 0.78 (9H, s, $SiC(CH_3)_3$), -0.04 (6H, s, $SiCH_3CH_3$).	7.47 (1H, d, J=4.2Hz, H-4'), 7.36-7.21 (7H, m , H-5')

N-(3-((*tert-Butyl*dimethylsilyl)oxy)-1-oxo-1-(phenylamino)propan-2-yl)-4-methoxy-6-oxo-1,6-dihydropyridine-3-carboxamide **17a:**

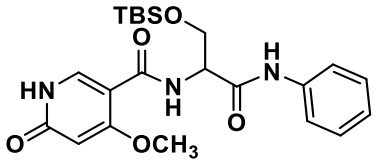

To a solution of 4-methoxy-6-oxo-1,6-dihydropyridine-3-carboxylic acid **8** (0.07 g, 0.4 mmol) and 2-amino-3-hydroxy-N-phenyl propanamide **15a** (0.12 g, 0.4 mmol) in DMF (5 ml) was added HOBt (0.06 g, 0.48 mmol), EDC (0.1 g, 0.48 mmol), and DIEA (0.15 g, 1.2 mmol) at room temperature. The mixture was stirred at ambient temperature for 12 h, and concentrated *in vacuo*. The resulting oily residue was flash column chromatographed on silica gel (gradient elution, 4-12% MeOH in CH_2Cl_2) to give **17a** as a white powder (0.11 g, 61%).

^{1}H-NMR (400 MHz, DMSO-*d6*): see Table 20.

MS ESI (m/z): 444 $[M-H]^-$.

N-(3-((*tert-Butyl*dimethylsilyl)oxy)-1-((4-methoxyphenyl)amino)-1-oxopropan-2-yl)-4-methoxy-6-oxo-1,6-dihydropyridine-3-carboxamide **17b**:

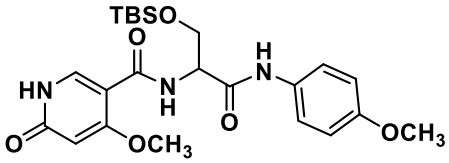

According to the procedure for **17a**, amine **15b** (0.13 g, 0.4 mmol) was reacted with acid **8** (0.07 g, 0.4 mmol) to give **17b**, isolated as a white powder (0.1 g, 53%) after flash column chromatography on silica gel (gradient elution, 6-15% MeOH in CH_2Cl_2).

^{1}H-NMR (400 MHz, DMSO-*d6*): see Table 20.

MS ESI (m/z): 474 $[M-H]^-$.

N-(3-((*tert-Butyl*dimethylsilyl)oxy)-1-oxo-1-((4-(trifluoromethyl)phenyl)amino)propan-2-yl)-4-methoxy-6-oxo-1,6-dihydropyridine-3-carboxamide **17c**:

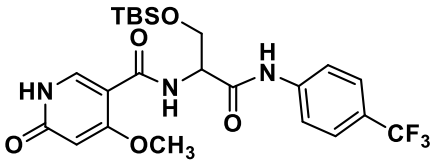

According to the procedure for **17a**, amine **15c** (0.18 g, 0.5 mmol) was reacted with acid 8 (0.09 g, 0.5 mmol) to give **17c**, isolated as a white powder (0.11 g, 43%) after flash column chromatography on silica gel (gradient elution, 2-11% MeOH in CH_2Cl_2).

^{1}H-NMR (400 MHz, DMSO-*d6*): see Table 20.

MS ESI (m/z): 512 $[M-H]^-$.

N-(3-((*tert-Butyl*dimethylsilyl)oxy)-1-((4-chlorophenyl)amino)-1-oxopropan-2-yl)-4-methoxy-6-oxo-1,6-dihydropyridine-3-carboxamide **17d**:

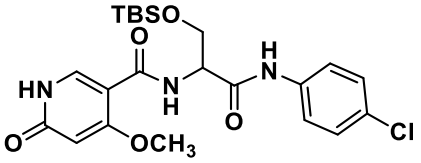

According to the procedure for **17a**, amine **15d** (0.16 g, 0.5 mmol) was reacted with acid **8** (0.09 g, 0.5 mmol) to give **17d**, isolated as a yellowish powder (0.099 g, 41%) after flash column chromatography on silica gel (gradient elution, 2-11% MeOH in CH_2Cl_2).

^{1}H-NMR (400 MHz, DMSO-*d6*): see Table 20.

MS ESI (m/z): 479 $[M-H]^-$.

N-(3-((*tert-Butyl*dimethylsilyl)oxy)-1-oxo-1-(pyridin-3-ylamino)propan-2-yl)-4-methoxy-6-oxo-1,6-dihydropyridine-3-carboxamide **17e**:

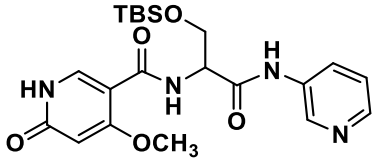

According to the procedure for **17a**, amine **15e** (0.12 g, 0.4 mmol) was reacted with acid **8** (0.07 g, 0.4 mmol) to give **17e**, isolated as a white powder (0.1 g, 55%) after flash column chromatography on silica gel (gradient elution, 4-15% MeOH in CH_2Cl_2).

^{1}H-NMR (400 MHz, DMSO-*d6*): see Table 20.

MS ESI (m/z): 445 $[M-H]^-$.

N-(3-((*tert-Butyl*dimethylsilyl)oxy)-1-oxo-1-(thiazol-2-ylamino)propan-2-yl)-4-methoxy-6-oxo-1,6-dihydropyridine-3-carboxamide **17f**:

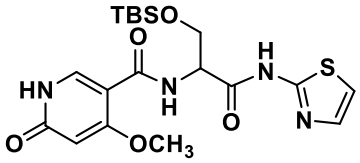

According to the procedure for **17a**, amine **15f** (0.12 g, 0.4 mmol) was reacted with acid **8** (0.07 g, 0.4 mmol) to give **17f**, isolated as a yellowish powder (0.09 g, 57%) after flash column chromatography on silica gel (gradient elution, 3-12% MeOH in CH_2Cl_2).

^{1}H-NMR (400 MHz, DMSO-*d6*): see Table 20.

MS ESI (m/z): 451 $[M-H]^-$.

Table 20: NMR data of compounds **17a-f**

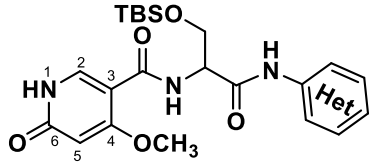

Entry	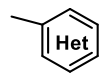	**Scaffold** ^{1}H-NMR (400 MHz, DMSO-*d6*) δ ppms	**R** ^{1}H-NMR (400 MHz, DMSO-*d6*) δ ppm
17a	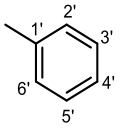	12.23 (1H, s, N^1-H), 10.13 (1H, s, CONH), 8.60 (1H, s, CONH), 8.41 (1H, s, H-2), 5.69 (1H, s, H-5), 4.81-4.71 (1H, m, CH-N), 3.99-3.81 (2H, m, CH_2-O), 3.42 (3H, s, OCH_3), 0.81 (9H, s, $SiC(CH_3)_3$), -0.01 (6H, s, $SiCH_3CH_3$).	7.59 (2H, d, J=8.2Hz H-2',6'), 7.34-7.27 (2H, m, H-3',5'), 7.05 (1H, t, J=8.2Hz, H-4')

Entry		Scaffold ^{1}H-NMR (400 MHz, DMSO-*d6*) δ ppms	R ^{1}H-NMR (400 MHz, DMSO-*d6*) δ ppm
17b	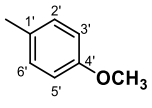	12.19 (1H, s, N^1-H), 9.99 (1H, s, CONH), 8.58 (1H, s, CONH), 8.41 (1H, s, H-2), 5.69 (1H, s, H-5), 4.76-4.67 (1H, m, CH-N), 3.97-3.80 (2H, m, CH_2-O), 3.41 (3H, s, OCH_3), 0.81 (9H, s, $SiC(CH_3)_3$), -0.01 (6H, s, $SiCH_3CH_3$).	7.50 (2H, d, J=8.7Hz, H-2',6'), 6.88 (2H, d, J=8.7Hz, H-3',5'), 3.72 (3H, s, OCH_3)
17c	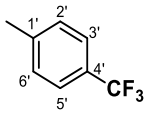	12.22 (1H, s, N^1-H), 10.51 (1H, s, CONH), 8.61 (1H, s, CONH), 8.41 (1H, s, H-2), 5.70 (1H, s, H-5), 4.81-4.73 (1H, m, CH-N), 3.97-3.80 (2H, m, CH_2-O), 3.42 (3H, s, OCH_3), 0.80 (9H, s, $SiC(CH_3)_3$), -0.02 (6H, s, $SiCH_3CH_3$).	7.81 (2H, d, J=8.7Hz, H-3',5'), 7.69 (2H, d, J=8.7Hz, H-2',6')
17d	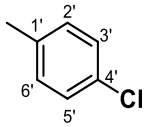	12.22 (1H, s, N^1-H), 10.28 (1H, s, CONH), 8.60 (1H, s, CONH), 8.40 (1H, s, H-2), 5.69 (1H, s, H-5), 4.80-4.69 (1H, m, CH-N), 3.99-3.79 (2H, m, CH_2-O), 3.41 (3H, s, OCH_3), 0.80 (9H, s, $SiC(CH_3)_3$), -0.02 (6H, s, $SiCH_3CH_3$).	7.63 (2H, d, J=8.8Hz, H-2',6'), 7.37 (2H, d, J=8.8Hz, H-3',5')
17e	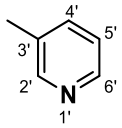	12.29 (1H, s, N^1-H), 10.40 (1H, s, CONH), 8.65 (1H, s, CONH), 8.41 (1H, s, H-2), 5.71 (1H, s, H-5), 4.81-4.72 (1H, m, CH-N), 4.03-3.83 (2H, m, CH_2-O), 3.41 (3H, s, OCH_3), 0.80 (9H, s, $SiC(CH_3)_3$), -0.02 (6H, s, $SiCH_3CH_3$).	8.76 (1H, d, J=2.4Hz, H-2'), 8.27 (1H, dd, J=1.4Hz, J=4.6Hz, H-6'), 8.03 (1H, ddd, J=1.4Hz, J=2.4Hz, J=8.5Hz, H-4'), 7.34 (1H, dd, J=4.6Hz, J=8.5Hz, H-5')
17f	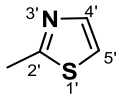	12.36 (1H, s, N^1-H), 12.18 (1H, s, CONH), 8.62 (1H, br s, CONH), 8.39 (1H, s, H-2), 5.71 (1H, s, H-5), 4.90-4.78 (1H, m, CH-N), 4.11-3.85 (2H, m, CH_2-O), 3.41 (3H, s, OCH_3), 0.79 (9H, s, $SiC(CH_3)_3$), -0.04 (6H, d, J=11.9Hz, $SiCH_3CH_3$).	7.48 (1H, d, J=3.9Hz, H-4'), 7.23 (1H, d, J=3.9Hz, H-5')

4-(Benzyloxy)-*N*-(3-hydroxy-1-oxo-1-(phenylamino)propan-2-yl)-6-oxo-1,6-dihydropyridine-3-carboxamide **18a:**

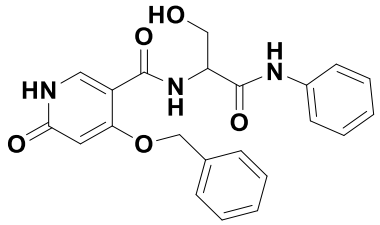

To **16a** (0.21g, 0.4 mmol) in methanol (5 mL) was added methanolic HCl (1 mL, 3M), and the reaction was stirred for 5h (complete by TLC analysis), then concentrate *in vacuo*. The residue was washed with ethyl ether to give **18a** as a white solid (0.13 g, 82%), which was used without further purification.

MS ESI (m/z): 406 $[M-H]^-$.

4-(Benzyloxy)-*N*-(3-hydroxy-1-((4-methoxyphenyl)amino)-1-oxopropan-2-yl)-6-oxo-1,6-dihydropyridine-3-carboxamide **18b**:

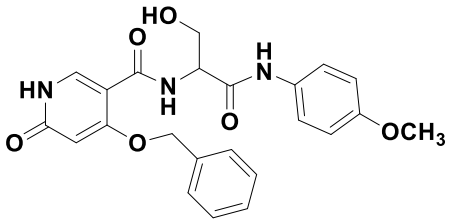

According to the procedure for **18a**, intermediate **16b** (0.22 g, 0.4 mmol) was converted to **18b (**white solid; 0.14 g, 79%).

MS ESI (m/z): 436 $[M-H]^-$.

4-(Benzyloxy)-*N*-(3-hydroxy-1-oxo-1-((4-(trifluoromethyl)phenyl)amino)propan-2-yl)-6-oxo-1,6-dihydropyridine-3-carboxamide **18c**:

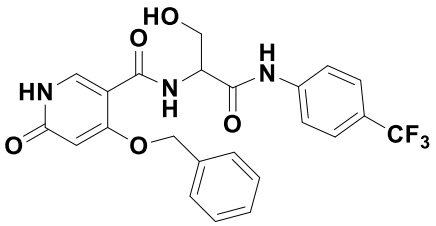

According to the procedure for **18a**, intermediate **16c** (0.21 g, 0.36 mmol) was converted to **18c (**yellowish solid; 0.12 g, 72%).

MS ESI (m/z): 474 $[M-H]^-$.

4-(Benzyloxy)-*N*-(1-((4-chlorophenyl)amino)-3-hydroxy-1-oxopropan-2-yl)-6-oxo-1,6-dihydropyridine-3-carboxamide **18d**:

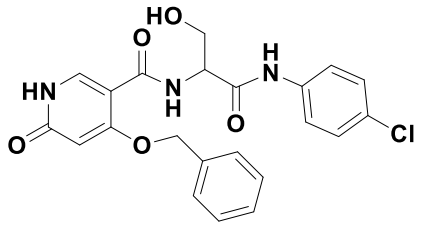

According to the procedure for **18a**, intermediate **16d** (0.2 g, 0.36 mmol) was converted to **18d (**yellowish solid; 0.11 g, 68%).

MS ESI (m/z): 440 $[M-H]^-$.

4-(Benzyloxy)-*N*-(3-hydroxy-1-oxo-1-(pyridin-3-ylamino)propan-2-yl)-6-oxo-1,6-dihydropyridine-3-carboxamide **18e**:

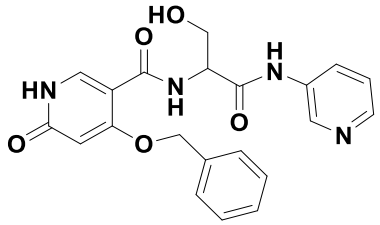

According to the procedure for **18a**, intermediate **16e** (0.21 g, 0.4 mmol) was converted to **18e** (white solid; 0.11 g, 69%).

MS ESI (m/z): 407 $[M-H]^-$.

4-(Benzyloxy)-*N*-(3-hydroxy-1-oxo-1-(thiazol-2-ylamino)propan-2-yl)-6-oxo-1,6-dihydropyridine-3-carboxamide **18f**:

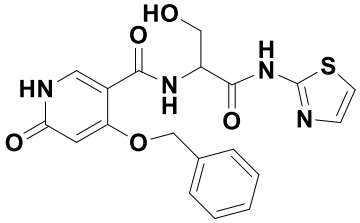

According to the procedure for **18a**, intermediate **16f** (0.18 g, 0.34 mmol) was converted to **18c (**white solid; 0.08 g, 56%).

MS ESI (m/z): 413 $[M-H]^-$.

N-(3-Hydroxy-1-oxo-1-(phenylamino)propan-2-yl)-4-methoxy-6-oxo-1,6-dihydropyridine-3-carboxamide **19a:**

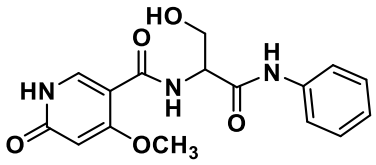

To **17a** (0.14 g, 0.32 mmol) in methanol (4 mL) was added methanolic HCl (1 mL, 2M) and the reaction was stirred for 3h. After completion of the reaction (TLC monitoring), the precipitated compound was collected, washed with methanol, and dried in vacuo to give product **19a** as a white solid (0.9 g, 84%).

^{1}H-NMR (400 MHz, DMSO-*d6*): see Table 21.
MS ESI (m/z): 330 $[M-H]^-$.

N-(3-Hydroxy-1-((4-methoxyphenyl)amino)-1-oxopropan-2-yl)-4-methoxy-6-oxo-1,6-dihydropyridine-3-carboxamide **19b**;

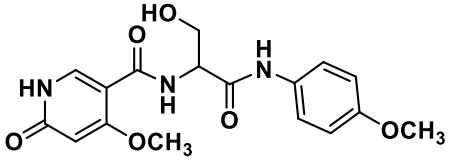

According to the procedure for **19a**, intermediate **17b** (0.14 g, 0.30 mmol) was converted to **19b** (white solid; 0.09 g, 80%).
^{1}H-NMR (400 MHz, DMSO-*d6*): see Table 21.
MS ESI (m/z): 360 $[M-H]^-$.

N-(3-Hydroxy-1-oxo-1-((4-(trifluoromethyl)phenyl)amino)propan-2-yl)-4-methoxy-6-oxo-1,6-dihydropyridine-3-carboxamide **19c**:

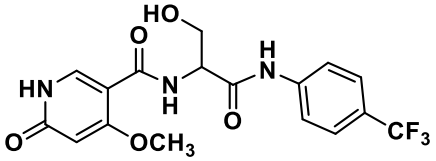

According to the procedure for **19a**, intermediate **17c** (0.15 g, 0.30 mmol) was converted to **19c** (white solid; 0.09 g, 74%).
^{1}H-NMR (400 MHz, DMSO-*d6*): see Table 21.
MS ESI (m/z): 398 $[M-H]^-$.

N-(1-((4-Chlorophenyl)amino)-3-hydroxy-1-oxopropan-2-yl)-4-methoxy-6-oxo-1,6-dihydropyridine-3-carboxamide **19d**:

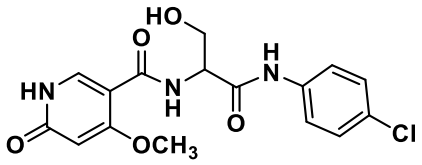

According to the procedure for **19a**, intermediate **17d** (0.14 g, 0.30 mmol) was converted to **19d** (white solid; 0.08 g, 71%).

^{1}H-NMR (400 MHz, DMSO-*d6*): see Table 21.

MS ESI (m/z): 364 $[M-H]^-$.

N-(3-Hydroxy-1-oxo-1-(pyridin-3-ylamino)propan-2-yl)-4-methoxy-6-oxo-1,6-dihydropyridine-3-carboxamide **19e**:

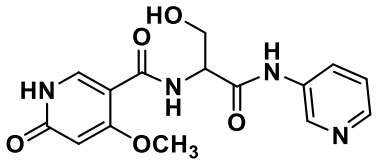

According to the procedure for **19a**, intermediate **17e** (0.13 g, 0.30 mmol) was converted to **19c** (white solid; 0.08 g, 85%).

^{1}H-NMR (400 MHz, DMSO-*d6*): see Table 21.

MS ESI (m/z): 331 $[M-H]^-$.

N-(3-Hydroxy-1-oxo-1-(thiazol-2-ylamino)propan-2-yl)-4-methoxy-6-oxo-1,6-dihydropyridine-3-carboxamide **19f**:

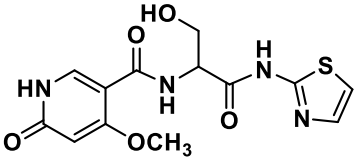

According to the procedure for **19a**, intermediate **17f** (0.14 g, 0.31 mmol) was converted to **19f** (white solid; 0.07 g, 69%).

^{1}H-NMR (400 MHz, DMSO-*d6*): see Table 21.

MS ESI (m/z): 337 $[M-H]^-$.

Table 21: NMR data of compounds **19a-f**

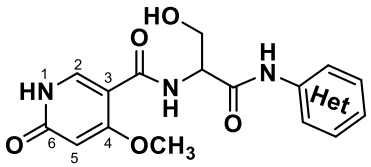

Entry	Het	Scaffold ^{1}H-NMR (400 MHz, DMSO-*d6*) δ ppm	R ^{1}H-NMR (400 MHz, DMSO-*d6*) δ ppm
19a	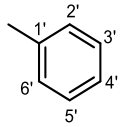	10.13 (1H, s, CONH), 8.63 (1H, d, J=7.4Hz, CONH), 8.49 (1H, s, H-2), 5.70 (1H, s, H-5), 5.37 (1H, br s, OH), 4.70-4.62 (1H, m, CH-N), 3.82-3.69 (2H, m, CH_2-O), 3.43 (3H, s, OCH_3).	7.62 (2H, d, J=8.4Hz H-2',6'), 7.34-7.27 (2H, m, H-3',5'), 7.05 (1H, t, J=7.4Hz, H-4')
19b	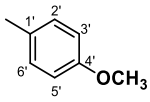	12.24 (1H, s, N^1-H), 9.96 (1H, s, CONH), 8.58 (1H, d, J=7.3Hz, CONH), 8.46 (1H, s, H-2), 5.67 (1H, s, H-5), 4.66-4.59 (1H, m, CH-N), 3.78-3.68 (5H, m, CH_2-O), 3.42 (3H, s, OCH_3).	7.52 (2H, d, J=8.6Hz, H-2',6'), 6.88 (2H, d, J=8.6Hz, H-3',5'), 3.78-3.68 (5H, m, OCH_3)
19c	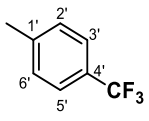	10.55 (1H, s, CONH), 8.68 (1H, d, J=7.4Hz, CONH), 8.54 (1H, s, H-2), 5.67 (1H, s, H-5), 4.71-4.62 (1H, m, CH-N), 3.89-3.70 (2H, m, CH_2-O), 3.43 (3H, s, OCH_3).	7.85 (2H, d, J=8.5Hz, H-3',5'), 7.68 (2H, d, J=8.5Hz, H-2',6')
19d	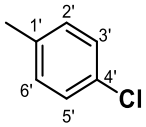	12.70 (1H, s, N^1-H), 10.24 (1H, s, CONH), 8.81 (1H, s, CONH), 8.42 (1H, s, H-2), 5.64 (1H, s, H-5), 5.20 (1H, br s, OH), 4.70-4.59 (1H, m, CH-N), 3.84-3.66 (2H, m, CH_2-O), 3.40 (3H, s, OCH_3).	7.65 (2H, d, J=8.7Hz, H-2',6'), 7.36 (2H, d, J=8.7Hz, H-3',5')
19e	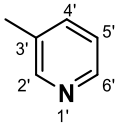	11.33 (1H, s, CONH), 8.76 (1H, d, J=7.4Hz, CONH), 8.65-8.55 (3H, m, H-2), 5.76 (1H, s, H-5), 5.20 (1H, br s, OH), 4.72-4.65 (1H, m, CH-N), 3.97-3.73 (2H, m, CH_2-O), 3.42 (3H, s, OCH_3).	9.25 (1H, d, J=2.5Hz, H-2'), 8.65-8.55 (3H, m, H-4',6'), 8.00 (1H, dd, J=4.6Hz, J=8.5Hz, H-5')

Entry	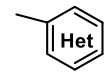	Scaffold ^{1}H-NMR (400 MHz, DMSO-*d6*) δ ppm	R ^{1}H-NMR (400 MHz, DMSO-*d6*) δ ppm
19f	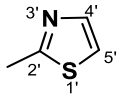	12.31 (1H, s, N^1-H), 10.24 (1H, s, CONH), 8.71 (1H, d, J=7.4Hz, CONH), 8.52 (1H, s, H-2), 5.76 (1H, s, H-5), 4.77-4.70 (1H, m, CH-N), 3.89-3.72 (2H, m, CH_2-O), 3.43 (3H, s, OCH_3).	7.48 (1H, d, J=3.9Hz, H-4'), 7.24 (1H, d, J=3.9Hz, H-5')

2-(4-Benzyloxy-6-oxo-1,6-dihydropyridin-3-yl)-*N*-phenyl-4,5-dihydrooxazole-4-carboxamide **20a:**

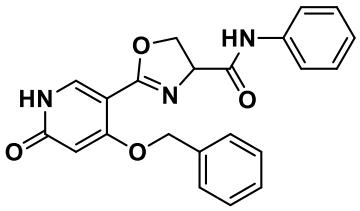

To a solution of **18a** (0.04 g, 0.1 mmol) in DMF (3 mL) at −78°C (dry ice-acetone), was slowly added bis(2-methoxyethyl) amino-sulfur trifluoride (DAST) (0.016 g, 0.12 mmol) under nitrogen. The reaction was stirred at −78°C for 1h. Anhydrous K_2CO_3, (0.04 g, 0.28 mmol,) was added and the reaction was allowed to warm to room temperature and stirred for 5h. Once the reaction has completed (monitored by TLC) the reaction mixture was quenched by addition of 10% aqueous $NaHCO_3$ solution and extracted with EtOAc. The combined organic layers were dried over Na_2SO_4, and concentrated *in vacuo*. The resulting residue was purified by flash column chromatography on silica gel (gradient elution, 2-8% MeOH in CH_2Cl_2) to give the product **20a** as a white solid (0.018 g, 46%).

^{1}H-NMR (400 MHz, DMSO-*d6*): see Table 22.

MS ESI (m/z): 388 $[M-H]^-$.

2-(4-(Benzyloxy)-6-oxo-1,6-dihydropyridin-3-yl)-*N*-(4-methoxyphenyl)-4,5-dihydrooxazole-4-carboxamide **20b**:

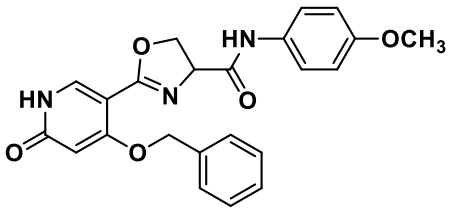

According to the procedure for **20a**, intermediate **18b** (0.05 g, 0.12 mmol) was reacted with DAST to give **20b** as a white solid (0.020 g, 41%) after silica flash chromatography (gradient elution, 3-12% MeOH in CH_2Cl_2).

^{1}H-NMR (400 MHz, DMSO-*d6*): see Table 22.

MS ESI (m/z): 418 $[M-H]^-$, **HRMS:** m/z calculated for $C_{23}H_{21}N_3O_5^-$: 418.14084, found: 418.14127.

2-(4-(Benzyloxy)-6-oxo-1,6-dihydropyridin-3-yl)-*N*-(4-(trifluoromethyl)phenyl)-4,5-dihydrooxazole-4-carboxamide **20c**:

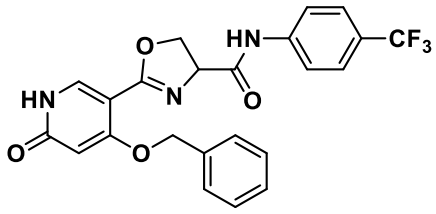

According to the procedure for **20a**, intermediate **18c** (0.05 g, 0.12 mmol) was reacted with DAST to give **20c** as a pale yellow solid (0.014 g, 32%) after silica flash chromatography (gradient elution, 2-8% MeOH in CH_2Cl_2).

^{1}H-NMR (400 MHz, DMSO-*d6*): see Table 22.

MS ESI (m/z): 456 $[M-H]^-$.

2-(4-(Benzyloxy)-6-oxo-1,6-dihydropyridin-3-yl)-*N*-(4-chlorophenyl)-4,5-dihydrooxazole-4-carboxamide **20d**:

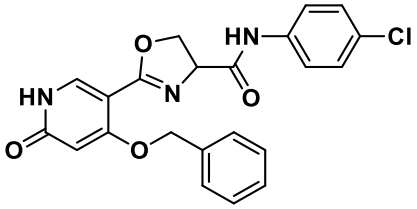

According to the procedure for **20a**, intermediate **18d** (0.044 g, 0.10 mmol) was reacted with DAST to give **20d** as a white solid (0.012 g, 29%) after silica flash chromatography (gradient elution, 3-8% MeOH in CH_2Cl_2).

^{1}H-NMR (400 MHz, DMSO-*d6*): see Table 22.

MS ESI (m/z): 422 $[M-H]^-$.

2-(4-(Benzyloxy)-6-oxo-1,6-dihydropyridin-3-yl)-*N*-(pyridin-3-yl)-4,5-dihydrooxazole-4-carboxamide **20e**:

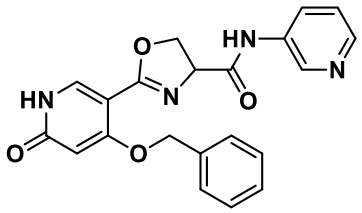

According to the procedure for **20a**, intermediate **18e** (0.041 g, 0.10 mmol) was reacted with DAST to give **20e** as a white solid (0.014 g, 35%) after silica flash chromatography (gradient elution, 5-12% MeOH in CH_2Cl_2).

^{1}H-NMR (400 MHz, DMSO-*d6*): see Table 22.

MS ESI (m/z): 389 $[M-H]^-$, **HRMS:** m/z calculated for $C_{21}H_{18}N_4O_4^-$: 389.12553, found: 389.12592.

2-(4-(Benzyloxy)-6-oxo-1,6-dihydropyridin-3-yl)-*N*-(thiazol-2-yl)-4,5-dihydrooxazole-4-carboxamide **20f**:

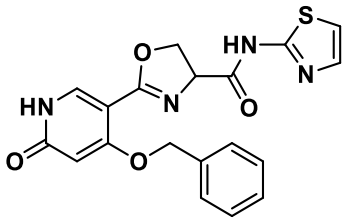

According to the procedure for **20a**, intermediate **18f** (0.054 g, 0.13 mmol) was reacted with DAST to give **20f** as a white solid (0.014 g, 28%) after silica flash chromatography (gradient elution, 3-12% MeOH in CH_2Cl_2).

^{1}H-NMR (400 MHz, DMSO-*d6*): see Table 22.

MS ESI (m/z): 395 $[M-H]^-$, **HRMS:** m/z calculated for $C_{19}H_{16}N_4O_4S^-$: 395.08195, found: 395.08197.

Table 22: NMR data of compounds **20a-f**

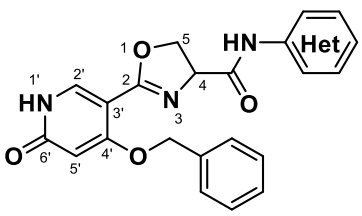

Entry		Scaffold ^{1}H-NMR (400 MHz, DMSO-*d6*) δ ppm	R ^{1}H-NMR (400 MHz, DMSO-*d6*) δ ppm
20a	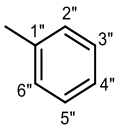	11.83 (1H, s, N$^{1'}$-H), 10.31 (1H, s, CONH), 8.47 (1H, s, H-2'), 7.37-7.21 (5H, m , Ar-H), 5.76 (1H, s, H-5'), 5.16 (2H, s, CH_2Ph), 5.04 (1H, dd, J=7.2Hz, 9.9Hz, H-4), 4.68-4.59 (2H, m, H-5).	7.61 (2H, d, J=8.4Hz H-2',6'), 7.33-7.26 (2H, m, H-3',5'), 7.04 (1H, t, J=7.4Hz, H-4')
20b	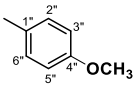	12.00 (1H, s, N$^{1'}$-H), 10.20 (1H, s, CONH), 8.48 (1H, s, H-2'), 7.36-7.23 (5H, m , Ar-H), 5.78 (1H, s, H-5'), 5.16 (2H, s, CH_2Ph), 5.01 (1H, dd, J=7.2Hz, 9.9Hz, H-4), 4.68-4.59 (2H, m, H-5).	7.53 (2H, d, J=8.7Hz, H-2",6"), 6.90 (2H, d, J=8.7Hz, H-3",5"), 3.72 (3H, s, OCH_3)
20c	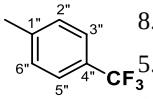	12.02 (1H, s, N$^{1'}$-H), 10.68 (1H, s, CONH), 8.45 (1H, s, H-2'), 7.40-7.22 (5H, m , Ar-H), 5.77 (1H, s, H-5'), 5.16 (2H, s, CH_2Ph), 5.08 (1H, dd, J=7.1Hz, 9.9Hz, H-4), 4.68-4.59 (2H, m, H-5).	7.86 (2H, d, J=8.6Hz, H-3",5"), 7.71 (2H, d, J=8.6Hz, H-2",6")
20d	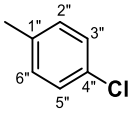	11.87 (1H, s, N$^{1'}$-H), 10.49 (1H, s, CONH), 8.45 (1H, s, H-2'), 7.37-7.22 (5H, m , Ar-H), 5.76 (1H, s, H-5'), 5.16 (2H, s, CH_2Ph), 5.04 (1H, dd, J=7.1Hz, 9.9Hz, H-4), 4.68-4.59 (2H, m, H-5).	7.67 (2H, d, J=8.6Hz, H-2",6"), 7.39 (2H, d, J=8.6Hz, H-3",5")
20e	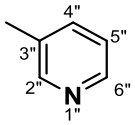	10.55 (1H, s, CONH), 8.49 (1H, s, H-2'), 7.40-7.25 (6H, m, Ar-H), 5.78 (1H, s, H-5'), 5.16 (2H, s, CH_2Ph), 5.08 (1H, dd, J=6.9Hz, 9.9Hz, H-4), 4.72-4.60 (2H, m, H-5).	8.80 (1H, d, J=2.5Hz, H-2"), 8.30 (1H, dd, J=1.4Hz, J=4.6Hz, H-6"), 8.06 (1H, ddd, J=1.4Hz, J=2.5Hz, J=8.5Hz, H-4"), 7.40-7.25 (6H, m , H-5")
20f	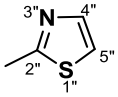	11.71 (1H, s, N$^{1'}$-H), 8.47 (1H, s, H-2'), 7.37-7.21 (6H, m, Ar-H), 5.76 (1H, s, H-5'), 5.16 (2H, s, CH_2Ph), 5.04 (1H, dd, J=7.2Hz, 9.9Hz, H-4), 4.75-4.50 (2H, m, H-5).	7.53 (1H, d, J=3.8Hz, H-4"), 7.28 (1H, d, J=3.8Hz, H-5")

2-(4-Methoxy-6-oxo-1,6-dihydropyridin-3-yl)-*N*-phenyl-4,5-dihydrooxazole-4-carboxamide **21a**:

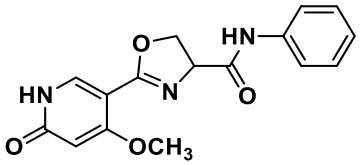

To **19a** (0.05 g, 0.15 mmol) in DMF (4 mL) at −78°C (dry ice-acetone), was slowly added bis(2-methoxyethyl) amino-sulfur trifluoride DAST (0.024 g, 0.18 mmol) under nitrogen. The reaction was stirred at −78°C for 1h. Anhydrous K_2CO_3, (0.04 g, 0.28 mmol,) was then added, and the reaction was allowed to warm to room temperature and stirred for 5h. Once the reaction has completed (monitored by TLC) the reaction mixture was quenched by addition of 10% aqueous $NaHCO_3$ solution and extracted with EtOAc. The combined organic layers were dried over Na_2SO_4, filtered and concentrated *in vacuo*. The resulting residue was purified by flash column chromatography on silica gel (gradient elution, 4-10% MeOH in CH_2Cl_2) to give the desired product **21a** as a white solid (0.018 g, 39%).

^{1}H-NMR (400 MHz, DMSO-*d6*): see Table 23.

MS ESI (m/z): 312 $[M-H]^-$, **HRMS:** m/z calculated for $C_{16}H_{15}N_3O_4^-$: 312.09898, found: 312.09903.

2-(4-Methoxy-6-oxo-1,6-dihydropyridin-3-yl)-*N*-(4-methoxyphenyl)-4,5-dihydrooxazole-4-carboxamide **21b**:

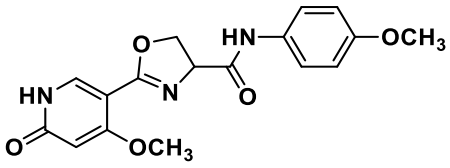

According to the procedure for **21a**, intermediate **19b** (0.05 g, 0.14 mmol) was reacted with DAST to give **21b** as a white solid (0.015 g, 31%) after silica flash chromatography (gradient elution, 2-12% MeOH in EtOAc).

^{1}H-NMR (400 MHz, DMSO-*d6*): see Table 23.

MS ESI (m/z): 342 $[M-H]^-$, **HRMS:** m/z calculated for $C_{17}H_{17}N_3O_5^-$: 342.10954, found: 342.10956.

2-(4-Methoxy-6-oxo-1,6-dihydropyridin-3-yl)-*N*-(4-(trifluoromethyl)phenyl)-4,5-dihydrooxazole-4-carboxamide **21c**:

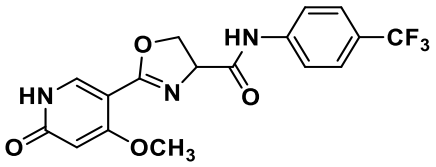

According to the procedure for **20a**, intermediate **19c** (0.052 g, 0.13 mmol) was reacted with DAST to give **21c** as a white solid (0.009 g, 18%) after silica flash chromatography (gradient elution, 2-10% MeOH in CH_2Cl_2).

^{1}H-NMR (400 MHz, DMSO-*d6*): see Table 23.

MS ESI (m/z): 380 $[M-H]^-$, **HRMS:** m/z calculated for $C_{17}H_{14}N_3O_4F_3^-$: 380.08636, found: 380.08658.

N-(4-Chlorophenyl)-2-(4-methoxy-6-oxo-1,6-dihydropyridin-3-yl)-4,5-dihydrooxazole-4-carboxamide **21d:**

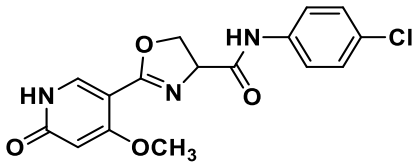

According to the procedure for **20a**, intermediate **19d** (0.047 g, 0.13 mmol) was reacted with DAST to give **21d** as a white solid (0.009 g, 22%) after silica flash chromatography (gradient elution, 3-12% MeOH in CH_2Cl_2).

^{1}H-NMR (400 MHz, DMSO-*d6*): see Table 23.

MS ESI (m/z): 346 $[M-H]^-$, **HRMS:** m/z calculated for $C_{16}H_{14}N_3O_4Cl^-$: 346.06001, found: 346.06003.

2-(4-Methoxy-6-oxo-1,6-dihydropyridin-3-yl)-*N*-(pyridin-3-yl)-4,5-dihydrooxazole-4-carboxamide **21e**:

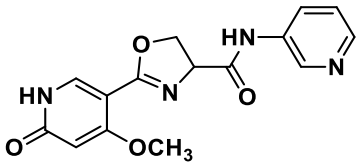

According to the procedure for **20a**, intermediate **19e** (0.05 g, 0.15 mmol) was reacted with DAST to give **21e** as an off white solid (0.01 g, 22%) after silica flash chromatography (gradient elution, 3-12% MeOH in EtOAc).

^{1}H-NMR (400 MHz, DMSO-*d6*): see Table 23.

MS ESI (m/z): 313 $[M-H]^-$, **HRMS:** m/z calculated for $C_{15}H_{14}N_4O_4^-$: 313.09423, found: 313.09445.

2-(4-Methoxy-6-oxo-1,6-dihydropyridin-3-yl)-*N*-(thiazol-2-yl)-4,5-dihydrooxazole-4-carboxamide **21f**:

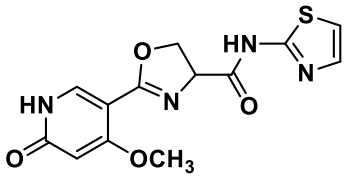

According to the procedure for **20a**, intermediate **19f** (0.05 g, 0.15 mmol) was reacted with DAST to give **21f** as a white solid (0.008 g, 16%) after silica flash chromatography (gradient elution, 3-12% MeOH in CH_2Cl_2).

^{1}H-NMR (400 MHz, DMSO-*d6*): see Table 23.

MS ESI (m/z): 319 $[M-H]^-$, **HRMS:** m/z calculated for $C_{13}H_{12}N_4O_4S^-$: 319.05065, found: 319.05084.

Table 23: NMR data of compounds **21a-f**

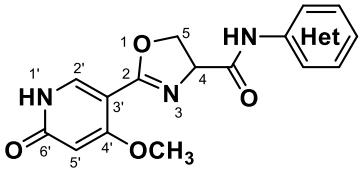

Entry		Scaffold ^{1}H-NMR (400 MHz, DMSO-*d6*) δ ppm	R ^{1}H-NMR (400 MHz, DMSO-*d6*) δ ppm
21a	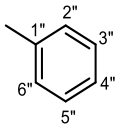	11.94 (1H, s, N$^{1'}$-H), 10.36 (1H, s, CONH), 8.38 (1H, s, H-2'), 5.73 (1H, s, H-5'), 5.05 (1H, dd, J=7.0Hz, 10.0Hz, H-4), 4.74-4.59 (2H, m, H-5), 3.44 (3H, s, OCH_3).	7.62 (2H, dd, J=8.6Hz, 1.2Hz, H-2",6"), 7.37-7.28 (2H, m, H-3",5"), 7.12-7.03 (1H, m, H-4")
21b	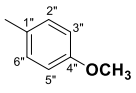	11.84 (1H, s, N$^{1'}$-H), 10.41 (1H, s, CONH), 8.38 (1H, s, H-2'), 5.73 (1H, s, H-5'), 5.05 (1H, dd, J=7.0Hz, 10.0Hz, H-4), 4.73-4.59 (2H, m, H-5), 3.44 (3H, s, OCH_3).	7.52 (2H, d, J=8.7Hz, H-2",6"), 6.89 (2H, d, J=8.7Hz, H-3",5"), 3.73 (3H, s, OCH_3)

Entry		Scaffold ^{1}H-NMR (400 MHz, DMSO-*d6*) δ ppm	R ^{1}H-NMR (400 MHz, DMSO-*d6*) δ ppm
21c	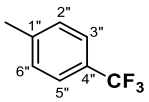	11.89 (1H, s, $N^{1'}$-H), 10.69 (1H, s, CONH), 8.37 (1H, s, H-2'), 5.73 (1H, s, H-5'), 5.09 (1H, dd, J=7.0Hz, 10.0Hz, H-4), 4.75-4.59 (2H, m, H-5), 3.44 (3H, s, OCH_3).	7.86 (2H, d, J=8.6Hz, H-3",5"), 7.71 (2H, d, J=8.6Hz, H-2",6")
21d	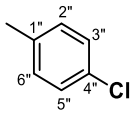	11.89 (1H, s, $N^{1'}$-H), 10.48 (1H, s, CONH), 8.37 (1H, s, H-2'), 5.73 (1H, s, H-5'), 5.05 (1H, dd J=7.0Hz, 10.0Hz, H-4), 4.72-4.59 (2H, m, H-5), 3.44 (3H, s, OCH_3).	7.67 (2H, d, J=8.6Hz, H-2",6"), 7.39 (2H, d, J=8.6Hz, H-3",5")
21e	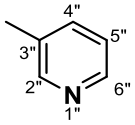	10.57 (1H, s, CONH), 8.38 (1H, s, H-2'), 5.74 (1H, s, H-5'), 5.09 (1H, dd J=7.0Hz, 10.0Hz, H-4), 4.72-4.60 (2H, m, H-5), 3.44 (3H, s, OCH_3).	8.80 (1H, d, J=2.6Hz, H-2"), 8.30 (1H, dd, J=1.4Hz, J=4.6Hz, H-6"), 8.07 (1H, ddd, J=1.4Hz, J=2.6Hz, J=8.5Hz, H-4"), 7.38 (1H, dd, J=4.6Hz, J=8.5Hz, H-5")
21f	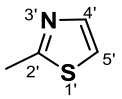	12.68 (1H, s, $N^{1'}$-H), 8.42 (1H, s, H-2'), 5.75 (1H, s, H-5'), 5.22 (1H, dd J=7.0Hz, 10.0Hz, H-4), 4.80-4.63 (2H, m, H-5), 3.52 (3H, s, OCH_3).	7.53 (1H, d, J=3.8Hz, H-4"), 7.28 (1H, d, J=3.8Hz, H-5")

6-Oxo-1,6-dihydropyridine-3-carboxamide **26**:

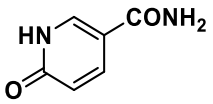

To a solution of 6-oxo-1,6-dihydropyridine-3-carboxylic acid **24** (13.91 g, 100 mmol) in dry DMF (120 mL), 1,1-carbonyldiimidazole (17.84 g, 110 mmol) was added portionwise at room temperature. The mixture was heated to 60 ^oC until bubbling ceased, then cooled to room temperature. Concentrated 28% ammonium hydroxide (60 mL) was added and the mixture stirred at 0 ^oC for 2h. The precipitate that formed was isolated by filteration, washed with water and dried under vacuum at 50 ^oC to give **26** as a white solid (10.64 g, 77%).

^{1}H-NMR (400 MHz, DMSO-*d6*): δ 12.37 (3H, s, N^1-H, $CONH_2$), 7.98 (1H, d, J=2.6Hz, H-2), 7.78 (1H, dd, J=2.6Hz, J=9.6Hz, H-4), 6.34 (1H, d, J=9.6Hz, H-5).

MS ESI (m/z): 137 $[M-H]^-$.

6-Oxo-1,6-dihydropyridine-3-carbonitrile **27**:

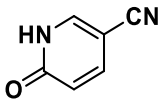

To a solution of 6-oxo-1,6-dihydropyridine-3-carboxamide **26** (10 g, 72.4 mmol) in DMF (100 mL) was added cyanuric chloride (6.68 g, 36.2 mmol) portionwise at room temperature. Then the mixture was stirred at 40 ºC for 2h, and the suspension was then poured into ice water (60 mL) and stirred at 0 ºC for 2h. The precipitate that formed was isolated by filtration, washed with water and dried under vacuum at 50 ºC to give **27** as a pale yellow solid (5.91 g, 68%).

^{1}H-NMR (400 MHz, DMSO-*d6*): δ 12.43 (1H, s, N^1-H), 8.25 (1H, d, J=2.5Hz, H-2), 7.65 (1H, dd, J=2.5Hz, J=9.6Hz, H-4), 6.41 (1H, d, J=9.6Hz, H-5).

MS ESI (m/z): 119 $[M-H]^-$.

N'-Hydroxy-6-oxo-1,6-dihydropyridine-3-carboximidamide **28**:

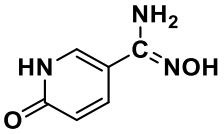

To a hot solution of 6-oxo-1,6-dihydropyridine-3-carbonitrile **27** (7 g, 58.33 mmol) in EtOH (100 mL), was added a solution of hydroxylamine hydrochloride (8.1 g, 116.66 mmol) and $NaHCO_3$ (9.8 g, 116.66 mmol) in water (80 mL). The reaction mixture was heated to reflux for 6h and then concentrate *in vacuo*. The resulting residue was dry loaded onto silica gel and flash column chromatographed (gradient elution, 10-30% MeOH in EtOAc) to give **28** as a white solid (6.96 g, 78%).

^{1}H-NMR (400 MHz, DMSO-*d6*): δ 11.71 (1H, s, N^1-H), 9.50 (1H, s, OH), 7.72 (1H, dd, J=2.3Hz, J=9.6Hz, H-4), 7.65 (1H, d, J=2.3Hz, H-2), 6.31 (1H, d, J=9.6Hz, H-5), 5.72 (2H, br s, NH_2).

MS ESI (m/z): 154 $[M+H]^+$.

N'-((*tert-Butyl*dimethylsilyl)oxy)-6-oxo-1,6-dihydropyridine-3-carboximid-amide **29**:

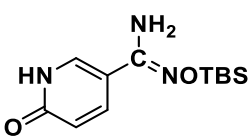

Amidoxime **28** (6.5 g, 42.44 mmol) was dissolved in DMF (100 mL) and imidazole (4.29 g, 63.66 mmol) was added. The mixure was cooled to 0°C and *tert*-butyldimethylsilyl chloride (8.06 g, 55.55 mmol) was added. The reaction mixture was stirred for 12h at ambient temperature, and concentrated *in vacuo*. The resulting crude oil was purified by flash column chromatography on silica gel (gradient elution, 2-8% MeOH in CH_2Cl_2) to afford **29** as a white solid (7.5 g, 66%).

^{1}H-NMR (400 MHz, DMSO-*d6*): δ 11.80 (1H, s, N^1-H), 7.75-7.65 (2H, m, H-2,4), 6.34 (1H, d, J=9.6Hz, H-5), 6.05 (2H, br s, NH_2), 0.92 (9H, s, $SiC(CH_3)_3$), 0.12 (6H, s, $SiCH_3CH_3$).

MS ESI (m/z): 266 $[M-H]^-$.

Ethyl fluorooxoacetate **31**:

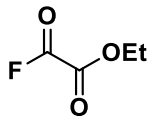

A mixture of ethyl chloroxoacetate **30** (12.2 g, 89.4 mmol) and dry sodium fluoride (3.8g, 89.4 mmol) in sulfolane (80 mL) was refluxed at 130 °C for 4h. The reaction mixture was distilled under reduced pressure to give compound **31** as colorless oil (5.8g, 54%).

Ethyl 3-(6-oxo-1,6-dihydropyridin-3-yl)-1,2,4-oxadiazole-5-carboxylate **33**:

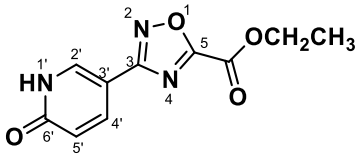

To the O-silylated amidoxime **29** (1.03g, 3.85 mmol) solution in dry THF (12 mL), was added ethyl fluoroxoacetate **31** (0.45g, 3.85 mmol) and a catalytic amount of TBAF (0.2 µL, 0.21 mmol). The reaction mixture was stirred overnight at ambient temperature, and the solvent was then removed *in vacuo*. The residue was dissolved in dioxane (5 mL) in a microwave vial and irradiated for 20 minutes at 120 °C. The solvent was evaporated and the residue was silica flash column chromatographed (gradient elution, 2-8% MeOH in CH_2Cl_2) to give compound **33** as white solid (0.38 g, 61%).

^{1}H-NMR (400 MHz, DMSO-*d6*): δ 12.18 (1H, s, $N^{1'}$-H), 8.09 (1H, d, J=2.6Hz, H-2'), 7.94 (1H, dd, J=2.6Hz, J=9.6Hz, H-4'), 6.52 (1H, d, J=9.6Hz, H-5'), 4.45 (2H, q, J=7.1Hz, CH_2), 1.36 (3H, t, J=7.1Hz, CH_3).

MS ESI (m/z): 236 $[M+H]^+$.

3-(6-Oxo-1,6-dihydropyridin-3-yl)-*N*-phenyl-1,2,4-oxadiazole-5-carboxamide **34a:**

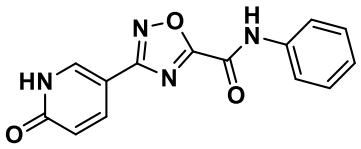

Under nitrogen atmosphere, trimethylaluminium (2 M solution in heptane; 0.63 ml, 1.27mmol) was added to a stirred solution of aniline (0.12 g, 1.27 mmol) in dioxane (4 ml) at ambient temperature. The mixture was stirred at room temperature for 2 h. A solution of ester **33** (0.08 g, 0.32 mmol) in dioxane (3 mL) was then added. The mixture was heated to 110 ^oC for 24h. The mixture was cooled to room temperature and quenched with water (2 mL). After 15 minutes stirring, Na_2SO_4 was added and stirring was continued for another 15 minutes. The mixture was then filtered and the cake was washed with dioxane. The filtrate was concentrated *in vacuo* and the residue was silica flash column chromatographed (gradient elution, 3-10% MeOH in CH_2Cl_2) to give **34a** as a white solid (0.027 g, 30%).

^{1}H-NMR (400 MHz, DMSO-*d6*): see Table 24.

MS ESI (m/z): 281 $[M-H]^-$, **HRMS:** m/z calculated for $C_{14}H_{10}N_4O_3^-$: 281.06801, found: 281.06805.

N-(4-Methoxyphenyl)-3-(6-oxo-1,6-dihydropyridin-3-yl)-1,2,4-oxadiazole-5-carboxamide **34b**:

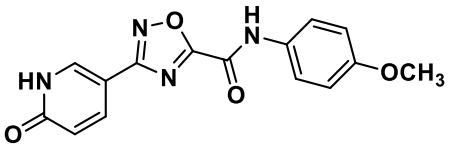

Following the procedure described for **34a**, ester **33** (0.08 g, 0.32 mmol) was condensed with *p*-anisidine (0.16 g, 1.27 mmol). The crude product mixture was separated by flash column chromatography on silica gel (gradient elution, 2-12 % MeOH in CH_2Cl_2) to give **34b** as an off white solid (0.028 g, 29%).

^{1}H-NMR (400 MHz, DMSO-*d6*): see Table 24.

^{13}C NMR (100MHz, DMSO-*d6*): δ 169.5, 166.2, 162.6, 157.0, 151.4, 145.3, 140.9, 138.1, 130.7, 122.9, 121.5, 117.7, 114.4, 104.7, 55.7.

MS ESI (m/z): 311 $[M-H]^-$, **HRMS:** m/z calculated for $C_{15}H_{12}N_4O_4^-$: 311.07858, found: 311.07874.

N-(2,3-Dimethylphenyl)-3-(6-oxo-1,6-dihydropyridin-3-yl)-1,2,4-oxadiazole-5-carboxamide **34c**:

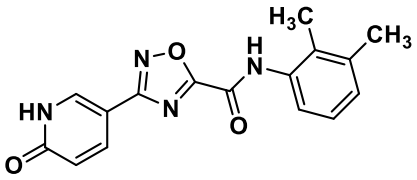

Following the procedure described for **34a**, ester **33** (0.08 g, 0.32 mmol) was condensed with 2,3-dimethylaniline (0.15 g, 1.27 mmol). The crude product mixture was separated by flash column chromatography on silica gel (gradient elution, 2-10 % MeOH in CH_2Cl_2) to give **34c** as an off white solid (0.037 g, 38%).

^{1}H-NMR (400 MHz, DMSO-*d6*): see Table 24.

MS ESI (m/z): 309 $[M-H]^-$, **HRMS:** m/z calculated for $C_{16}H_{14}N_4O_3^-$: 309.09931, found: 309.09949.

3-(6-Oxo-1,6-dihydropyridin-3-yl)-*N*-(*p*-tolyl)-1,2,4-oxadiazole-5-carboxamide **34d**:

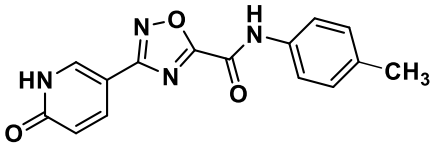

Following the procedure described for **34a**, ester **33** (0.08 g, 0.32 mmol) was condensed with *p*-toludine (0.16 g, 1.28 mmol). The crude product mixture was separated by flash column chromatography on silica gel (gradient elution, 2-12 % MeOH in CH_2Cl_2) to give **34d** as a white solid (0.025 g, 26%).

^{1}H-NMR (400 MHz, DMSO-*d6*): see Table 24.

^{13}C NMR (100MHz, DMSO-*d6*): δ 166.2, 159.2, 151.9, 149.9, 144.7, 142.4, 140.2, 135.3, 129.8, 121.3, 116.8, 106.5, 105.7, 103.8, 21.0.

MS ESI (m/z): 295 $[M-H]^-$, **HRMS:** m/z calculated for $C_{15}H_{12}N_4O_3^-$: 295.08366, found: 295.08368.

N-Benzyl-3-(6-oxo-1,6-dihydropyridin-3-yl)-1,2,4-oxadiazole-5-carboxamide **34e**:

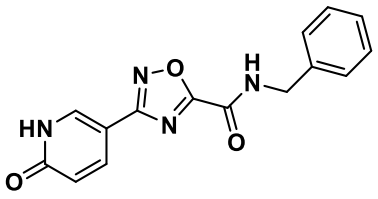

Following the procedure described for **34a**, ester **33** (0.08 g, 0.32 mmol) was condensed with benzylamine (0.14 g, 1.28 mmol). The crude product mixture was separated by flash column chromatography on silica gel (gradient elution, 2-8 % MeOH in CH_2Cl_2) to give **34e** as a white solid (0.039 g, 41%).

^{1}H-NMR (400 MHz, DMSO-*d6*): see Table 24.

^{13}C NMR (100MHz, DMSO-*d6*): δ 169.3, 166.1, 162.5, 153.4, 138.5, 138.1, 137.6, 128.8, 128.0, 127.6, 122.9, 121.4, 104.6, 43.1.

MS ESI (m/z): 295 $[M-H]^-$, **HRMS:** m/z calculated for $C_{15}H_{12}N_4O_3^-$: 295.08366, found: 295.08380.

N-(4-Methoxybenzyl)-3-(6-oxo-1,6-dihydropyridin-3-yl)-1,2,4-oxadiazole-5-carboxamide **34f**:

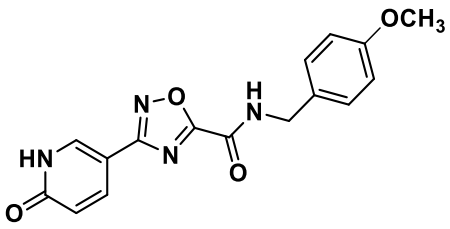

Following the procedure described for **34a**, ester **33** (0.08 g, 0.32 mmol) was condensed with 4-methoxybenzylamine (0.17 g, 1.28 mmol). The crude product mixture was separated by flash column chromatography on silica gel (gradient elution, 2-10 % MeOH in CH_2Cl_2) to give **34f** as a white solid (0.04 g, 39%).

^{1}H-NMR (400 MHz, DMSO-*d6*): see Table 24.

^{13}C NMR (100MHz, DMSO-*d6*): δ 169.4, 166.1, 162.5, 158.9, 153.3, 138.1, 137.5, 130.5, 129.5, 122.8, 121.4, 114.2, 104.7, 55.5, 42.6.

MS ESI (m/z): 325 $[M-H]^-$, **HRMS:** m/z calculated for $C_{16}H_{14}N_4O_4^-$: 325.09423, found: 325.09415.

N-(2,3-Dihydro-*1H*-inden-5-yl)-3-(6-oxo-1,6-dihydropyridin-3-yl)-1,2,4-oxadiazole-5-carboxamide **34g**:

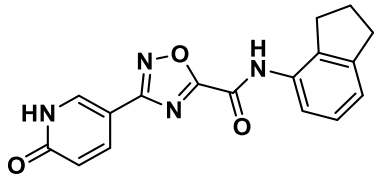

Following the procedure described for **34a**, ester **33** (0.08 g, 0.32 mmol) was condensed with 4-methoxybenzylamine (0.17 g, 1.28 mmol). The crude product mixture was separated by flash column chromatography on silica gel (gradient elution, 2-6 % MeOH in CH_2Cl_2) to give **34g** as a white solid (0.03 g, 30%).

^{1}H-NMR (400 MHz, DMSO-*d6*): see Table 24.

MS ESI (m/z): 321 $[M-H]^-$, **HRMS:** m/z calculated for $C_{17}H_{14}N_4O_3^-$: 321.09931, found: 321.09930.

3-(6-Oxo-1,6-dihydropyridin-3-yl)-*N*-(pyridin-2-ylmethyl)-1,2,4-oxadiazole-5-carboxamide **34h**:

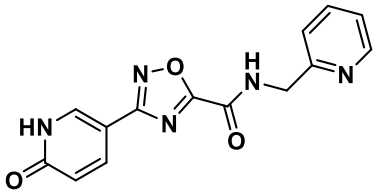

Following the procedure described for **34a**, ester **33** (0.08 g, 0.32 mmol) was condensed with 2-picolyamine (0.14 g, 1.28 mmol). The crude product mixture was separated by flash column chromatography on silica gel (gradient elution, 2-6 % MeOH in CH_2Cl_2) to give **34h** as white solid (0.02 g, 23%).

^{1}H-NMR (400 MHz, DMSO-*d6*): see Table 24.

^{13}C NMR (100MHz, DMSO-*d6*): δ 169.2, 166.1, 162.5, 157.4, 153.6, 149.4, 138.1, 137.5, 137.3, 122.9, 121.7, 121.5, 104.7, 45.0.

MS ESI (m/z): 296 $[M-H]^-$, **HRMS:** m/z calculated for $C_{14}H_{11}N_5O_3^-$: 296.07891, found: 296.07895.

3-(6-Oxo-1,6-dihydropyridin-3-yl)-1,2,4-oxadiazole-5-carboxylic acid **35**:

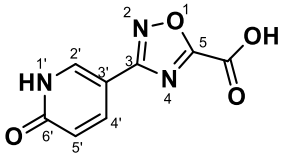

NaOH (2M; 16 mL) was added to a stirred suspension of **33** (2.5g, 10.62 mmol) in ethanol (50ml), and the mixture was heated at 90 ^oC for 12 h. The reaction mixture was then concentrated *in vacuo*, and the residue was dissolved in water and acidified to pH 4.0 by careful addition of 1N HCl. After cooling, the precipitate was isolated by filtration and dried *in vacuo* to afford the desired compound **35** as a white powder (1.6 g, 73%). The product was taken forward to the next step without further purification.

^{1}H-NMR (400 MHz, DMSO-*d6*): δ 11.51 (2H, s, $N^{1'}$-H, COOH), 8.25 (1H, d, J=2.6Hz, H-2'), 7.65 (1H, dd, J=2.6Hz, J=9.6Hz, H-4'), 6.41 (1H, d, J=9.6Hz, H-5').
MS ESI (m/z): 206 $[M-H]^-$.

N-(3-Chlorophenyl)-3-(6-oxo-1,6-dihydropyridin-3-yl)-1,2,4-oxadiazole-5-carboxamide **34i**:

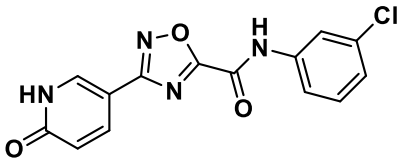

To a solution of 3-(6-oxo-1,6-dihydropyridin-3-yl)-1,2,4-oxadiazole-5-carboxylic acid **35** (0.07 g, 0.33 mmol) in DMF (5 mL) was added HOAt (0.055 g, 0.4 mmol), EDC (0.076 g, 0.4 mmol) and DIEA (0.11 g, 0.83 mmol) . After stirring for 30 minutes, 3-chloroaniline (0.04 g, 0.33 mmol) was added and stirring was continued at room temperature for 24h. The solvent was removed, and the concentrate was azeotroped twice with CH_2Cl_2. The residue was silica flash column chromatographed (gradient elution, 3-10% MeOH in CH_2Cl_2) to afford **34i** as a white solid (0.027 g, 26%).
^{1}H-NMR (400 MHz, DMSO-*d6*): see Table 24.
MS ESI (m/z): 315 $[M-H]^-$, **HRMS:** m/z calculated for $C_{14}H_9ClN_4O_3^-$: 315.02904, found: 315.02921.

N-(3-Chloro-2-methoxyphenyl)-3-(6-oxo-1,6-dihydropyridin-3-yl)-1,2,4-oxadiazole-5-carboxamide **34j**:

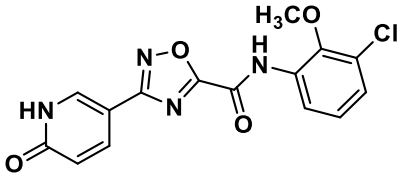

Following the procedure described for **34i**, acid **35** (0.07 g, 0.33 mmol) was condensed with 3-chloro-*o*-anisidine (0.052 g, 0.33 mmol). The crude product mixture was separated by flash column chromatography on silica gel (gradient elution, 2-12 % MeOH in CH_2Cl_2) to give **34j** as a white solid (0.032 g, 28%).
^{1}H-NMR (400 MHz, DMSO-*d6*): see Table 24.
MS ESI (m/z): 345 $[M-H]^-$, **HRMS:** m/z calculated for $C_{15}H_{11}ClN_4O_4^-$: 345.03961, found: 345.03989.

N-(2-Chloro-4-methylphenyl)-3-(6-oxo-1,6-dihydropyridin-3-yl)-1,2,4-oxadiazole-5-carboxamide **34k**:

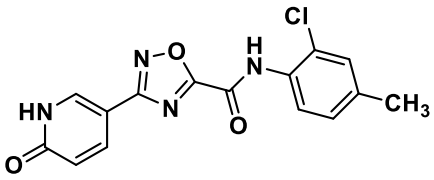

Following the procedure described for **34i**, acid **35** (0.07 g, 0.33 mmol) was condensed with 2-chloro-4-methylaniline (0.047 g, 0.33 mmol). The crude product mixture was separated by flash column chromatography on silica gel (gradient elution, 2-9 % MeOH in CH_2Cl_2) to give **34k** as pale yellow solid (0.03 g, 28%).

^{1}H-NMR (400 MHz, DMSO-*d6*): see Table 24.

^{13}C NMR (100MHz, DMSO-*d6*): δ 169.0, 166.3, 162.5, 152.1, 139.0, 138.1, 137.7, 130.8, 130.4, 129.2, 128.9, 127.9, 121.5, 104.5, 20.8.

MS ESI (m/z): 329 $[M-H]^-$, **HRMS:** m/z calculated for $C_{15}H_{11}N_4O_3Cl^-$: 329.04469, found: 329.04529.

N-(4-Chlorophenyl)-3-(6-oxo-1,6-dihydropyridin-3-yl)-1,2,4-oxadiazole-5-carboxamide **34l**:

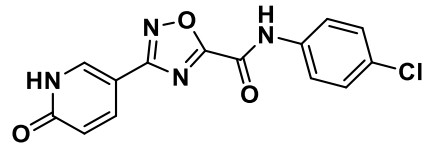

Following the procedure described for **34i**, acid **35** (0.07 g, 0.33 mmol) was condensed with 4-chloroaniline (0.04 g, 0.33 mmol). The crude product mixture was separated by flash column chromatography on silica gel (gradient elution, 2-10 % MeOH in CH_2Cl_2) to give **34l** as a pale green coloured solid (0.022 g, 21%).

^{1}H-NMR (400 MHz, DMSO-*d6*): see Table 24.

MS ESI (m/z): 315 $[M-H]^-$, **HRMS:** m/z calculated for $C_{14}H_9N_4O_3Cl^-$: 315.02904, found: 315.02911.

3-(6-Oxo-1,6-dihydropyridin-3-yl)-*N*-(4-(trifluoromethyl)phenyl)-1,2,4-oxadiazole-5-carboxamide **34m**:

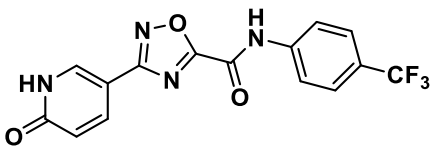

Following the procedure described for **34i**, acid **35** (0.07 g, 0.33 mmol) was condensed with 4-(trifluoromethyl)aniline (0.053 g, 0.33 mmol). The crude product mixture was separated by flash column chromatography on silica gel (gradient elution, 2-10 % MeOH in CH_2Cl_2) to give **34m** as an off white solid (0.022 g, 21%).

^{1}H-NMR (400 MHz, DMSO-*d6*): see Table 24.

MS ESI (m/z): 349 $[M-H]^-$, **HRMS:** m/z calculated for $C_{15}H_9N_4O_3F_3^-$: 349.0554, found: 349.05542.

N-(4-Cyanophenyl)-3-(6-oxo-1,6-dihydropyridin-3-yl)-1,2,4-oxadiazole-5-carboxamide **34n**:

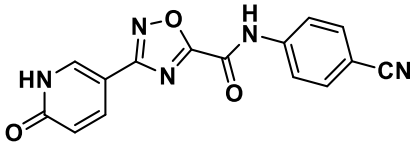

Following the procedure described for **34i**, acid **35** (0.09 g, 0.43 mmol) was condensed with 4-aminobenzonitrile (0.051 g, 0.43 mmol). The crude product mixture was separated by flash column chromatography on silica gel (gradient elution, 2-10 % MeOH in CH_2Cl_2) to give **34n** as an off white solid (0.025 g, 19%).

^{1}H-NMR (400 MHz, DMSO-*d6*): see Table 24.

MS ESI (m/z): 306 $[M-H]^-$, **HRMS:** m/z calculated for $C_{15}H_9N_5O_3^-$: 306.06326, found: 306.06326.

N-(2,6-dichlorophenyl)-3-(6-oxo-1,6-dihydropyridin-3-yl)-1,2,4-oxadiazole-5-carboxamide **34o**:

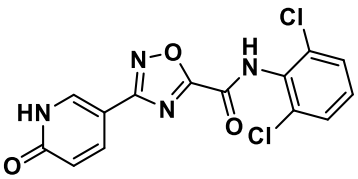

Following the procedure described for **34i**, acid **35** (0.09 g, 0.43 mmol) was condensed with 2,6-dichloroaniline (0.07 g, 0.43 mmol). The crude product mixture was separated by flash column chromatography on silica gel (gradient elution, 2-8 % MeOH in CH_2Cl_2) to give **34o** as a yellowish white solid (0.035 g, 23%).

^{1}H-NMR (400 MHz, DMSO-*d6*): see Table 24.

MS ESI (m/z): 348 $[M-H]^-$, **HRMS:** m/z calculated for $C_{14}H_8N_4O_3Cl_2^-$: 348.99007, found: 348.99011.

N-(3,5-Dimethoxyphenyl)-3-(6-oxo-1,6-dihydropyridin-3-yl)-1,2,4-oxadiazole-5-carboxamide **34p**:

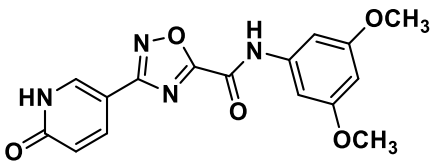

Following the procedure described for **34i**, acid **35** (0.07 g, 0.33 mmol) was condensed with 3,5-dimethoxyaniline (0.05 g, 0.33 mmol). The crude product mixture was separated by flash column chromatography on silica gel (gradient elution, 3-15 % MeOH in CH_2Cl_2) to give **34p** as an off white solid (0.047 g, 42%).

^{1}H-NMR (400 MHz, DMSO-*d6*): see Table 24.

MS ESI (m/z): 341 $[M-H]^-$, **HRMS:** m/z calculated for $C_{16}H_{14}N_4O_5^-$: 341.08914, found: 341.08917.

N-(3,4-Dimethoxyphenyl)-3-(6-oxo-1,6-dihydropyridin-3-yl)-1,2,4-oxadiazole-5-carboxamide **34q**:

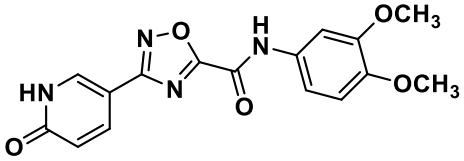

Following the procedure described for **34i**, acid **35** (0.07 g, 0.33 mmol) was condensed with 3,4-dimethoxyaniline (0.05 g, 0.33 mmol). The crude product mixture was separated by flash column chromatography on silica gel (gradient elution, 2-14 % MeOH in CH_2Cl_2) to give **34q** as an off white solid (0.05 g, 45%).

^{1}H-NMR (400 MHz, DMSO-*d6*): see Table 24.

MS ESI (m/z): 341 $[M-H]^-$, **HRMS:** m/z calculated for $C_{16}H_{14}N_4O_5^-$: 341.08914, found: 341.08939.

N-(3,5-Difluorophenyl)-3-(6-oxo-1,6-dihydropyridin-3-yl)-1,2,4-oxadiazole-5-carboxamide **34r**:

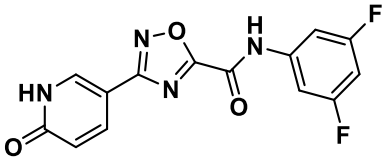

Following the procedure described for **34i**, acid **35** (0.09 g, 0.43 mmol) was condensed with 3,5-difluoroaniline (0.055 g, 0.43 mmol). The crude product mixture was separated by flash

column chromatography on silica gel (gradient elution, 2-10 % MeOH in CH_2Cl_2) to give to give **34r** as a white solid (0.04 g, 30%).

^{1}H-NMR (400 MHz, DMSO-*d6*): see Table 24.

MS ESI (m/z): 317 $[M-H]^-$, **HRMS:** m/z calculated for $C_{14}H_8F_2N_4O_3^-$: 317.04917, found: 317.04916.

N-(3,5-Dichlorophenyl)-3-(6-oxo-1,6-dihydropyridin-3-yl)-1,2,4-oxadiazole-5-carboxamide **34s**:

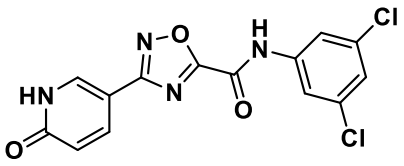

Following the procedure described for **34i**, acid **35** (0.09 g, 0.43 mmol) was condensed with 3,5-dichloroaniline (0.07 g, 0.43 mmol). The crude product mixture was separated by flash column chromatography on silica gel (gradient elution, 2-10 % MeOH in CH_2Cl_2) to give **34s** as a pale yellow solid (0.035 g, 23%).

^{1}H-NMR (400 MHz, DMSO-*d6*): see Table 24.

^{13}C NMR (100MHz, DMSO-*d6*): δ 169.0, 166.3, 162.6, 152.3, 145.3, 140.9, 138.1, 137.7, 134.6, 124.8, 121.5, 119.6, 117.7, 104.6.

MS ESI (m/z): 348 $[M-H]^-$, **HRMS:** m/z calculated for $C_{14}H_8N_4O_3Cl_2^-$: 348.99007, found: 348.99048.

N-(4-(Methylthio)phenyl)-3-(6-oxo-1,6-dihydropyridin-3-yl)-1,2,4-oxadiazole-5-carboxamide **34t**:

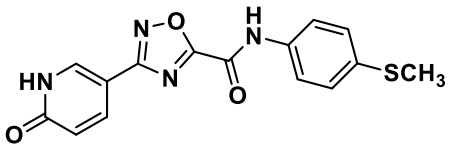

Following the procedure described for **34i**, acid **35** (0.07 g, 0.33 mmol) was condensed with 4-(methylthio)aniline (0.046 g, 0.33 mmol). The crude product mixture was separated by flash column chromatography on silica gel (gradient elution, 2-12 % MeOH in CH_2Cl_2) to give **34t** as pale red solid (0.055 g, 51%).

^{1}H-NMR (400 MHz, DMSO-*d6*): see Table 24.

^{13}C NMR (100MHz, DMSO-*d6*): δ 169.3, 166.2, 162.6, 151.6, 140.8, 138.1, 137.8, 135.0, 129.2, 127.0, 122.0, 121.5, 104.7, 15.5.

MS ESI (m/z): 327 $[M-H]^-$, **HRMS:** m/z calculated for $C_{15}H_{12}N_4O_3S^-$: 327.05573, found: 327.05573.

N-(2-(Methylthio)phenyl)-3-(6-oxo-1,6-dihydropyridin-3-yl)-1,2,4-oxadiazole-5-carboxamide **34u**:

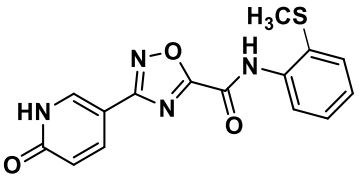

Following the procedure described for **34i**, acid **35** (0.07 g, 0.33 mmol) was condensed with 2-(methylthio)aniline (0.046 g, 0.33 mmol). The crude product mixture was separated by flash column chromatography on silica gel (gradient elution, 2-10 % MeOH in CH_2Cl_2) to give **34u** as a white solid (0.051 g, 48%).

^{1}H-NMR (400 MHz, DMSO-*d6*): see Table 24.

^{13}C NMR (100MHz, DMSO-*d6*): δ 169.1, 166.2, 162.6, 152.0, 138.1, 137.7, 134.6, 134.1, 128.2, 126.4, 122.5, 121.5, 104.5, 16.0.

MS ESI (m/z): 327 $[M-H]^-$, **HRMS:** m/z calculated for $C_{15}H_{12}N_4O_3S^-$: 327.05573, found: 327.05591.

N-(2-Bromophenyl)-3-(6-oxo-1,6-dihydropyridin-3-yl)-1,2,4-oxadiazole-5-carboxamide **34v**:

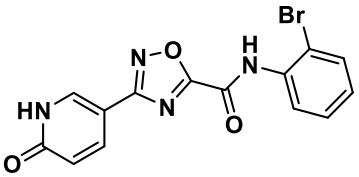

Following the procedure described for **34i**, acid **35** (0.07 g, 0.33 mmol) was condensed with 2-bromoaniline (0.057 g, 0.33 mmol). The crude product mixture was separated by flash column chromatography on silica gel (gradient elution, 2-6 % MeOH in CH_2Cl_2) to give **34v** as a white solid (0.021 g, 18%).

^{1}H-NMR (400 MHz, DMSO-*d6*): see Table 24.

^{13}C NMR (100MHz, DMSO-*d6*): δ 169.1, 166.3, 162.6, 152.1, 138.2, 137.8, 135.1, 133.4, 129.3, 128.9, 128.4, 121.5, 120.2, 104.6.

MS ESI (m/z): 358 $[M-H]^-$, **HRMS:** m/z calculated for $C_{14}H_9N_4O_3Br^-$: 358.97853, found: 358.97894.

N-([1,1'-Biphenyl]-2-yl)-3-(6-oxo-1,6-dihydropyridin-3-yl)-1,2,4-oxadiazole-5-carboxamide **34w**:

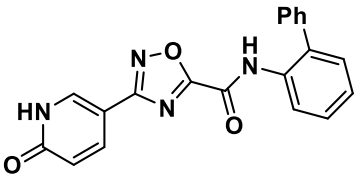

Following the procedure described for **34i**, acid **35** (0.07 g, 0.33 mmol) was condensed with 2-aminobiphenyl (0.057 g, 0.33 mmol). The crude product mixture was separated by flash column chromatography on silica gel (gradient elution, 2-8 % MeOH in CH_2Cl_2) to give **34w** as a white solid (0.057 g, 48%).

^{1}H-NMR (400 MHz, DMSO-*d6*): see Table 24.

MS ESI (m/z): 357 $[M-H]^-$, **HRMS:** m/z calculated for $C_{20}H_{14}N_4O_3^-$: 357.09931, found: 357.09982.

3-(6-Oxo-1,6-dihydropyridin-3-yl)-*N*-(3-phenoxyphenyl)-1,2,4-oxadiazole-5-carboxamide **34x**:

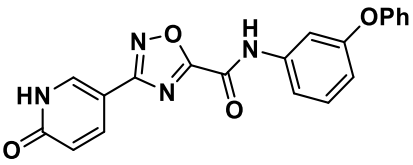

Following the procedure described for **34i**, acid **35** (0.07 g, 0.33 mmol) was condensed with 3-phenoxyaniline (0.06 g, 0.33 mmol). The crude product mixture was separated by flash column chromatography on silica gel (gradient elution, 2-10 % MeOH in CH_2Cl_2) to give **34x** as a white solid (0.057 g, 46%).

^{1}H-NMR (400 MHz, DMSO-*d6*): see Table 24.

^{13}C NMR (100MHz, DMSO-*d6*): δ 169.2, 166.2, 162.5, 157.6, 156.6, 151.8, 139.3, 138.1, 137.7, 130.8, 130.6, 124.3, 122.7, 121.5, 119.6, 116.0, 115.5, 111.1, 104.6.

MS ESI (m/z): 373 $[M-H]^-$, **HRMS:** m/z calculated for $C_{20}H_{14}N_4O_4^-$: 373.09423, found: 373.09427.

N-(Naphthalen-2-yl)-3-(6-oxo-1,6-dihydropyridin-3-yl)-1,2,4-oxadiazole-5-carboxamide **34y**:

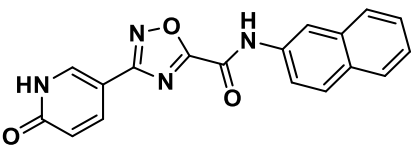

Following the procedure described for **34i**, acid **35** (0.07 g, 0.33 mmol) was condensed with 2-naphthylamine (0.047 g, 0.33 mmol). The crude product mixture was separated by flash column chromatography on silica gel (gradient elution, 2-6 % MeOH in CH_2Cl_2) to give **34y** as an off white solid (0.05 g, 50%).

^{1}H-NMR (400 MHz, DMSO-*d6*): see Table 24.

MS ESI (m/z): 331 $[M-H]^-$, **HRMS:** m/z calculated for $C_{18}H_{12}N_4O_3^-$: 331.08366, found: 331.08368.

3-(6-Oxo-1,6-dihydropyridin-3-yl)-*N*-(thiazol-2-yl)-1,2,4-oxadiazole-5-carboxamide **34z**:

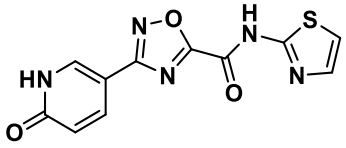

Following the procedure described for **34i**, acid **35** (0.07 g, 0.33 mmol) was condensed with 2-aminothiazole (0.033 g, 0.33 mmol). The crude product mixture was separated by flash column chromatography on silica gel (gradient elution, 2-10 % MeOH in CH_2Cl_2) to give **34z** as a pale yellow solid (0.04 g, 42%).

^{1}H-NMR (400 MHz, DMSO-*d6*): see Table 24.

MS ESI (m/z): 288 $[M-H]^-$, **HRMS:** m/z calculated for $C_{11}H_7N_5O_3S^-$: 288.01968, found: 288.01968.

3-(6-Oxo-1,6-dihydropyridin-3-yl)-*N*-(pyridin-3-yl)-1,2,4-oxadiazole-5-carboxamide **34aa**:

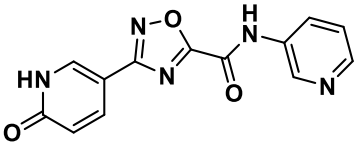

Following the procedure described for **34i**, acid **35** (0.07 g, 0.33 mmol) was condensed with 3-aminopyridine (0.031 g, 0.33 mmol). The crude product mixture was separated by flash column chromatography on silica gel (gradient elution, 2-15 % MeOH in CH_2Cl_2) to give **34aa** as an off white solid (0.036 g, 38%).

^{1}H-NMR (400 MHz, DMSO-*d6*): see Table 24.

MS ESI (m/z): 282 $[M-H]^-$, **HRMS:** m/z calculated for $C_{13}H_9N_5O_3^-$: 282.06326, found: 282.06323.

3-(6-Oxo-1,6-dihydropyridin-3-yl)-*N*-(pyridin-4-yl)-1,2,4-oxadiazole-5-carboxamide **34ab**:

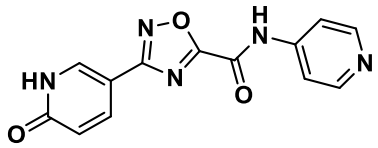

Following the procedure described for **34i**, acid **35** (0.07 g, 0.33 mmol) was condensed with 4-aminopyridine (0.031 g, 0.33 mmol). The crude product mixture was separated by flash column chromatography on silica gel (gradient elution, 2-15 % MeOH in CH_2Cl_2) to give **34ab** as a white solid (0.017 g, 18%).

^{1}H-NMR (400 MHz, DMSO-*d6*): see Table 24.

MS ESI (m/z): 282 $[M-H]^-$, **HRMS:** m/z calculated for $C_{13}H_9N_5O_3^-$: 282.06326, found: 282.06348.

3-(6-Oxo-1,6-dihydropyridin-3-yl)-*N*-(quinolin-6-yl)-1,2,4-oxadiazole-5-carboxamide **34ac**:

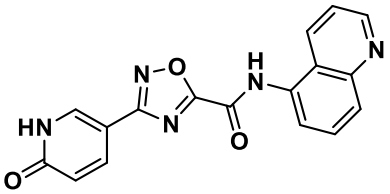

Following the procedure described for **34i**, acid **35** (0.07 g, 0.33 mmol) was condensed with 6-aminoquinoline (0.048 g, 0.33 mmol). The crude product mixture was separated by flash column chromatography on silica gel (gradient elution, 2-15 % MeOH in CH_2Cl_2) to give **34ac** as a white solid (0.023 g, 21%).

^{1}H-NMR (400 MHz, DMSO-*d6*): see Table 24.

^{13}C NMR (100MHz, DMSO-*d6*): δ 169.4, 166.3, 162.6, 153.1, 151.3, 148.5, 138.1, 137.7, 132.7, 132.5, 129.5, 128.8, 124.8, 124.6, 121.9, 121.5, 104.7.

MS ESI (m/z): 332 $[M-H]^-$, **HRMS:** m/z calculated for $C_{17}H_{11}N_5O_3^-$: 332.07891, found: 332.07904.

N-Cyclohexyl-3-(6-oxo-1,6-dihydropyridin-3-yl)-1,2,4-oxadiazole-5-carboxamide **34ad**:

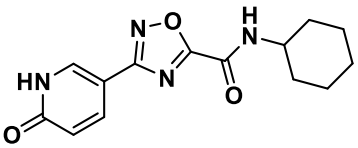

Following the procedure described for **34i**, acid **35** (0.07 g, 0.33 mmol) was condensed with cyclohexylamine (0.033 g, 0.33 mmol). The crude product mixture was separated by flash

column chromatography on silica gel (gradient elution, 2-5 % MeOH in CH_2Cl_2) to give **34ad** as a white solid (0.054 g, 56%).

^{1}H-NMR (400 MHz, DMSO-*d6*): see Table 24.

MS ESI (m/z): 287 $[M-H]^-$, **HRMS:** m/z calculated for $C_{14}H_{16}N_4O_3^-$: 287.11496, found: 287.11523.

3-(6-Oxo-1,6-dihydropyridin-3-yl)-5-(5-(morpholine-1-carbonyl)-1,2,4-oxadiazole **34ae**:

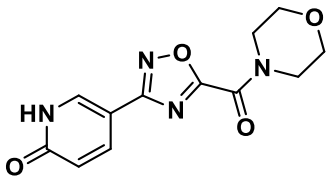

Following the procedure described for **34i**, acid **35** (0.07 g, 0.33 mmol) was condensed with morpholine (0.029 g, 0.33 mmol). The crude product mixture was separated by flash column chromatography on silica gel (gradient elution, 2-8 % MeOH in CH_2Cl_2) to give **34ae** as a white solid (0.027 g, 30%).

^{1}H-NMR (400 MHz, DMSO-*d6*): see Table 24.

MS ESI (m/z): 275 $[M-H]^-$, **HRMS:** m/z calculated for $C_{12}H_{12}N_4O_4^-$: 275.07858, found: 275.07858.

N-(Benzo[d][1,3]dioxol-5-yl)-3-(6-oxo-1,6-dihydropyridin-3-yl)-1,2,4-oxadiazole-5-carboxamide **34af**:

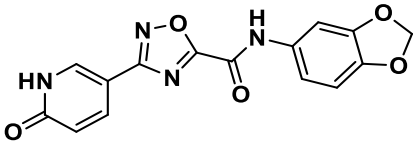

Following the procedure described for **34i**, acid **35** (0.07 g, 0.33 mmol) was condensed with 3,4-(methylenedioxy)aniline (0.045 g, 0.33 mmol). The crude product mixture was separated by flash column chromatography on silica gel (gradient elution, 2-12 % MeOH in CH_2Cl_2) to give **34af** as a white solid (0.058 g, 54%).

^{1}H-NMR (400 MHz, DMSO-*d6*): see Table 24.

^{13}C NMR (100MHz, DMSO-*d6*): δ 169.4, 166.2, 162.6, 151.4, 147.6, 144.9, 138.1, 137.7, 131.9, 121.4, 114.7, 108.6, 104.7, 103.2, 101.8.

MS ESI (m/z): 325 $[M-H]^-$, **HRMS:** m/z calculated for $C_{15}H_{10}N_4O_5^-$: 325.05784, found: 325.05774.

N-(2,3-Dihydrobenzo[b][1,4]dioxin-6-yl)-3-(6-oxo-1,6-dihydropyridin-3-yl)-1,2,4-oxadiazole-5-carboxamide **34ag**:

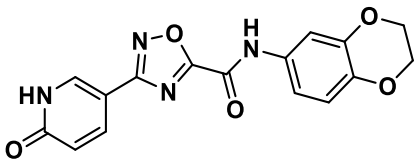

Following the procedure described for **34i**, acid **35** (0.07 g, 0.33 mmol) was condensed with 1,4-benzodioxane-6-amine (0.05 g, 0.33 mmol). The crude product mixture was separated by flash column chromatography on silica gel (gradient elution, 2-12 % MeOH in CH_2Cl_2) to give **34ag** as a yellow solid (0.057 g, 51%).

^{1}H-NMR (400 MHz, DMSO-*d6*): see Table 24.

MS ESI (m/z): 337 $[M-H]^-$, **HRMS:** m/z calculated for $C_{16}H_{10}N_4O_5^-$: 337.05784, found: 339.07330.

N-(*1H*-Indazol-5-yl)-3-(6-oxo-1,6-dihydropyridin-3-yl)-1,2,4-oxadiazole-5-carboxamide **34ah**:

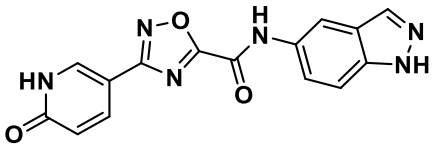

Following the procedure described for **34i**, acid **35** (0.07 g, 0.33 mmol) was condensed with 5-aminoindazole (0.044 g, 0.33 mmol). The crude product mixture was separated by flash column chromatography on silica gel (gradient elution, 2-15 % MeOH in CH_2Cl_2) to give **34ah** as an off white solid (0.015 g, 14%).

^{1}H-NMR (400 MHz, DMSO-*d6*): see Table 24.

MS ESI (m/z): 321 $[M-H]^-$, **HRMS:** m/z calculated for $C_{15}H_{10}N_6O_3^-$: 321.07416, found: 321.07413.

Table 24: NMR of compounds **34a-ah**

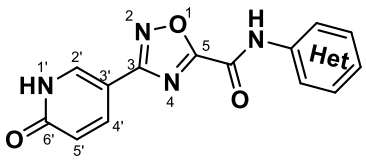

Entry	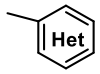	Scaffold ^{1}H-NMR (400 MHz, DMSO-*d6*) δ ppm	R ^{1}H-NMR (400 MHz, DMSO-*d6*) δ ppm
34a	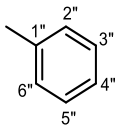	12.22 (1H, s, N$^{1'}$-H), 11.22 (1H, s, CONH), 8.16 (1H, d, J=2.6Hz, H-2'), 7.98 (1H, dd, J=2.6Hz, J=9.6Hz, H-4'), 6.55 (1H, d, J=9.6Hz, H-5')	7.81 (2H,d, J=7.6Hz H-2",6") 7.36 (2H, t, J=7.6Hz, H-3",5"), 7.20 (1H, t, J=7.6Hz, H-4")
34b	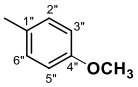	12.22 (1H, s, N$^{1'}$-H), 11.12 (1H, s, CONH), 8.15 (1H, d, J=2.5Hz, H-2'), 7.98 (1H, dd, J=2.5Hz, J=9.6Hz, H-4'), 6.54 (1H, d, J=9.6Hz, H-5')	7.73 (2H, d, J=9.0Hz, H-2",6"), 6.98 (2H, d, J=9.0Hz, H-3",5"), 3.76 (3H, s, OCH_3)
34c	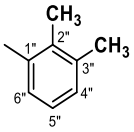	12.24 (1H, s, N$^{1'}$-H), 10.93 (1H, s, CONH), 8.15 (1H, d, J=2.3Hz, H-2'), 7.98 (1H, dd, J=2.3Hz, J=9.4Hz, H-4'), 6.54 (1H, d, J=9.4Hz, H-5')	7.21-7.11(3H, m, H-4",5",6")
34d	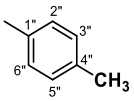	12.24 (1H, s, N$^{1'}$-H), 11.16 (1H, s, CONH), 8.15 (1H, d, J=2.5Hz, H-2'), 7.98 (1H, dd, J=2.5Hz, J=9.6Hz, H-4'), 6.54 (1H, d, J=9.6Hz, H-5')	7.69 (2H, d, J=9.0Hz, H-2",6"), 7.21 (2H, d, J=9.0Hz, H-3",5"), 2.30 (3H, s, CH_3)
34e	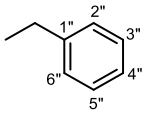	12.21 (1H, s, N$^{1'}$-H), 9.98 (1H, t, J=6.4Hz, CO-NH), 8.08 (1H, d, J=2.5Hz, H-2'), 7.94 (1H, dd, J=2.5Hz, J=9.6Hz, H-4'), 6.52 (1H, d, J=9.6Hz, H-5')	7.35 (4H, d, J=4.4Hz, H-2",3",5",6"), 7.31-7.24 (1H, m, H-4"), 4.48 (1H, d, J=6.4Hz, CH_2)
34f	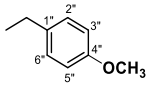	12.19 (1H, s, N$^{1'}$-H), 9.88 (1H, t, J=6.4Hz, CO-NH), 8.07 (1H, d, J=2.5Hz, H-2'), 7.93 (1H, dd, J=2.5Hz, J=9.6Hz, H-4'), 6.52 (1H, d, J=9.6Hz, H-5')	7.27 (2H, d, J=8.7Hz, H-2",6"), 6.90 (2H, d, J=8.7Hz, H-3",5"), 4.40 (2H, d, J=6.3Hz, CH_2), 3.73 (3H, s, OCH_3)

Entry		Scaffold ^{1}H-NMR (400 MHz, DMSO-*d6*) δ ppm	R ^{1}H-NMR (400 MHz, DMSO-*d6*) δ ppm
34g	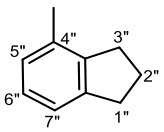	12.22 (1H, s, $N^{1'}$-H), 10.87 (1H, s, CONH), 8.15 (1H, d, J=2.4Hz, H-2'), 7.98 (1H, dd, J=2.4Hz, J=9.6Hz, H-4'), 6.54 (1H, d, J=9.6Hz, H-5')	7.26 (1H, dd, J=2.9Hz, J=6.1Hz, H-5"), 7.24-7.13 (2H, m, H-6",7"), 2.92 (2H, t, J=7.4Hz, benzylic CH_2), 2.84 (2H, t, J=7.4Hz, benzylic CH_2), 2.01 (2H, p, J=7.4Hz, CH_2)
34h	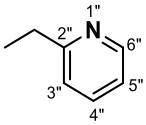	12.19 (1H, s, $N^{1'}$-H), 9.93 (1H, t, J=6.4Hz, CO-NH), 8.09 (1H, d, J=2.5Hz, H-2'), 7.95 (1H, dd, J=2.5Hz, J=9.6Hz, H-4'), 6.53 (1H, d, J=9.6Hz, H-5')	8.53 (1H, dd, J=1.7Hz, J=4.8Hz, H-6"), 7.79 (1H, dt, J=1.7Hz, J=7.7Hz, H-3"), 7.40 (1H, d, J=7.7Hz, H-4"), 7.32-7.26 (1H, m, H-5"), 4.59 (2H, d, J=5.9Hz, CH_2)
34i	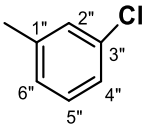	12.22 (1H, s, $N^{1'}$-H), 11.39 (1H, s, CONH), 8.16 (1H, d, J=2.4Hz, H-2'), 7.98 (1H, dd, J=2.4Hz, J=9.5Hz, H-4'), 6.54 (1H, d, J=9.5Hz, H-5')	7.96 (1H, d, J=2.1Hz, H-2"), 7.78 (1H, ddd, J=0.8Hz, J=2.1Hz, J=8.2Hz, H-6"), 7.45 (1H, t, J=8.1Hz, H-5"), 7.28 (1H, ddd, J=0.8Hz, J=2.1Hz, J=8.1Hz, H-4")
34j	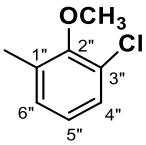	12.22 (1H, s, $N^{1'}$-H), 10.55 (1H, s, CONH), 8.15 (1H, d, J=2.4Hz, H-2'), 7.98 (1H, dd, J=2.4Hz, J=9.5Hz, H-4'), 6.55 (1H, d, J=9.5Hz, H-5')	7.79 (1H, dd, J=1.5Hz, J=8.1Hz, H-4"), 7.43 (1H, dd, J=1.5Hz, J=8.1Hz, H-6"), 7.24 (1H, t, J=8.1Hz, H-5"), 3.82 (3H, s, OCH_3)
34k	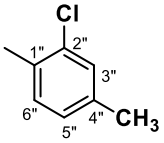	12.21 (1H, s, $N^{1'}$-H), 10.91 (1H, s, CONH), 8.14 (1H, d, J=2.6Hz, H-2'), 7.97 (1H, dd, J=2.6Hz, J=9.5Hz, H-4'), 6.55 (1H, d, J=9.5Hz, H-5')	7.52 (1H, d, J=8.1Hz, H-6"), 7.43 (1H, d, J=1.1Hz, H-3"), 7.24 (1H, dd, J=1.1Hz, J=8.1Hz, H-5"), 2.34 (3H, s, CH_3)
34l	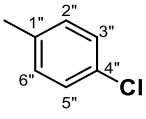	12.25 (1H, s, $N^{1'}$-H), 11.37 (1H, s, CONH), 8.16 (1H, d, J=2.6Hz, H-2'), 7.98 (1H, dd, J=2.6Hz, J=9.5Hz, H-4'), 6.54 (1H, d, J=9.5Hz, H-5')	7.86 (2H, d, J=8.9Hz, H-2",6"), 6.98 (2H, d, J=8.9Hz, H-3",5")

Entry		Scaffold ^{1}H-NMR (400 MHz, DMSO-*d6*) δ ppm	R ^{1}H-NMR (400 MHz, DMSO-*d6*) δ ppm
34m	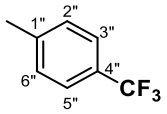	12.21 (1H, s, N$^{1'}$-H), 11.56 (1H, s, CONH), 8.16 (1H, d, J=2.6Hz, H-2'), 7.98 (1H, dd, J=2.6Hz, J=9.5Hz, H-4'), 6.55 (1H, d, J=9.5Hz, H-5')	8.06 (2H, d, J=9.0Hz, H-2",6"), 7.80 (2H, d, J=9.0Hz, H-3",5")
34n	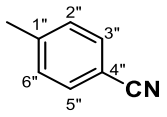	12.23 (1H, s, N$^{1'}$-H), 11.57 (1H, s, CONH), 8.16 (1H, d, J=2.5Hz, H-2'), 7.98 (1H, dd, J=2.5Hz, J=9.5Hz, H-4'), 6.54 (1H, d, J=9.5Hz, H-5')	8.04 (2H, d, J=9.0Hz, H-2",6"), 7.89 (2H, d, J=9.0Hz, H-3",5")
34o	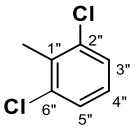	12.23 (1H, s, N$^{1'}$-H), 11.49 (1H, s, CONH), 8.14 (1H, d, J=2.6Hz, H-2'), 7.98 (1H, dd, J=2.6Hz, J=9.5Hz, H-4'), 6.55 (1H, d, J=9.5Hz, H-5')	7.64 (2H, d, J=8.1Hz, H-3",5"), 7.47 (1H, t, J=8.1Hz, H-4")
34p	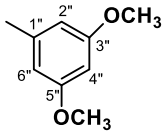	12.27 (1H, s, N$^{1'}$-H), 11.10 (1H, s, CONH), 8.15 (1H, d, J=2.5Hz, H-2'), 7.97 (1H, dd, J=2.5Hz, J=9.6Hz, H-4'), 6.54 (1H, d, J=9.6Hz, H-5')	7.11 (2H, d, J=2.2Hz, H-2",6"), 6.37 (1H, t, J=2.2Hz, H-4"), 3.76 (6H, s, 2 OCH_3)
34q	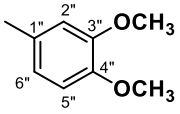	12.23 (1H, s, N$^{1'}$-H), 11.06 (1H, s, CONH), 8.15 (1H, d, J=2.5Hz, H-2'), 7.98 (1H, dd, J=2.5Hz, J=9.6Hz, H-4'), 6.54 (1H, d, J=9.6Hz, H-5')	7.48 (1H, d, J=2.3Hz, H-2"), 7.42 (1H, dd, J=2.3Hz, J=8.8Hz, H-6"), 6.98 (1H, d, J=8.8Hz, H-5"), 3.76 (6H, s, 2 OCH_3)
34r	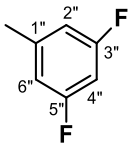	12.27 (1H, s, N$^{1'}$-H), 11.10 (1H, s, CONH), 8.15 (1H, d, J=2.5Hz, H-2'), 7.97 (1H, dd, J=2.5Hz, J=9.6Hz, H-4'), 6.54 (1H, d, J=9.6Hz, H-5')	7.62 (2H, d, J=2.2Hz, H-2"), 7.60 (2H, d, J=2.2Hz, H-6"), 7.10 (1H, t, J=2.2Hz, H-4").
34s		12.24 (1H, s, N$^{1'}$-H), 11.52 (1H, s, CONH), 8.15 (1H, d, J=2.4Hz, H-2'), 7.98 (1H, dd, J=2.4Hz, J=9.5Hz, H-4'), 6.55 (1H, d, J=9.5Hz, H-5')	7.92 (2H, d, J=1.8Hz, H-2", 6"), 7.46 (1H, t, J=1.8Hz, H-4")

Entry		Scaffold ^{1}H-NMR (400 MHz, DMSO-*d6*) δ ppm	R ^{1}H-NMR (400 MHz, DMSO-*d6*) δ ppm
34t	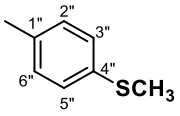	11.75 (2H, d, N$^{1'}$-H, CONH), 8.15 (1H, d, J=2.3Hz, H-2'), 7.98 (1H, dd, J=2.3Hz, J=9.5Hz, H-4'), 6.54 (1H, d, J=9.5Hz, H-5')	7.78 (2H, d, J=8.7Hz, H-2",6"), 7.31 (2H, d, J=8.7Hz, H-3",5"), 2.48 (3H, s, SCH_3)
34u	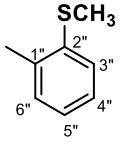	12.22 (1H, s, N$^{1'}$-H), 10.78 (1H, s, CONH), 8.13 (1H, d, J=2.5Hz, H-2'), 7.97 (1H, dd, J=2.5Hz, J=9.6Hz, H-4'), 6.55 (1H, d, J=9.6Hz, H-5')	7.56 (1H, dd, J=1.4Hz, J=7.9Hz, H-3"), 7.47 (1H, dd, J=1.4Hz, J=7.9Hz, H-6"), 7.36 (1H, dt, J=1.4Hz, J=7.6Hz, H-5"), 7.29 (1H, dt, J=1.4Hz, J=7.6Hz, H-4"), 2.51(3H, s, SCH_3)
34v	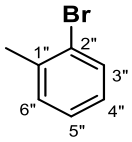	12.23 (1H, s, N$^{1'}$-H), 10.95 (1H, s, CONH), 8.14 (1H, d, J=2.6Hz, H-2'), 7.98 (1H, dd, J=2.6Hz, J=9.5Hz, H-4'), 6.55 (1H, d, J=9.5Hz, H-5')	7.77 (1H, dd, J=1.1Hz, J=8.1Hz, H-3"), 7.65 (1H, dd, J=1.2Hz, J=7.8Hz, H-6"), 7.49 (1H, dt, J=1.1Hz, J=7.8Hz, H-5"), 7.30 (1H, dt, J=1.2Hz, J=7.8Hz, H-4")
34w	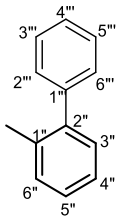	12.20 (1H, s, N$^{1'}$-H), 10.65 (1H, s, CONH), 8.01 (1H, d, J=2.6Hz, H-2'), 7.90 (1H, dd, J=2.4Hz, J=9.4Hz, H-4'), 6.52 (1H, d, J=9.6Hz, H-5')	7.68 (1H, d, J=7.6Hz), 7.51-7.34 (8H, m, Ar-H)
34x	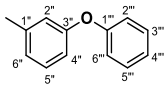	12.22 (1H, s, N$^{1'}$-H), 11.27 (1H, s, CONH), 8.14 (1H, d, J=2.4Hz, H-2'), 7.96 (1H, dd, J=2.4Hz, J=9.4Hz, H-4'), 6.53 (1H, d, J=9.4Hz, H-5')	7.63 (1H, ddd, J=0.9Hz, J=2.7Hz, J=8.1Hz, Ar-H) 7.53 (1H, t, J=2.7Hz, H-2"), 7.47-7.37 (3H, m, Ar-H), 7.22-7.14 (1H, m, Ar-H), 7.10-7.03 (2H, m, Ar-H), 6.89-6.84 (1H, ddd, J=0.9Hz, J=2.7Hz, J=8.1Hz, Ar-H)
34y	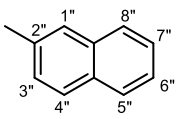	12.27 (1H, s, N$^{1'}$-H), 11.37 (1H, s, CONH), 8.19 (1H, d, J=2.6Hz, H-2'), 8.08-7.96* (3H, m, H-4'), 6.57 (1H, d, J=9.6Hz, H-5')	8.08-7.96* (3H, m, Ar-H), 7.95 (1H, d, J=7.5Hz, Ar-H), 7.68-7.55 (4H, m, Ar-H)

Entry		Scaffold ^{1}H-NMR (400 MHz, DMSO-*d6*) δ ppm	R ^{1}H-NMR (400 MHz, DMSO-*d6*) δ ppm
34z	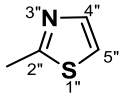	12.70 (2H, s, N$^{1'}$-H, CONH), 8.25 (1H, d, J=2.6Hz, H-2'), 7.65 (1H, dd, J=2.6Hz, J=9.6Hz, H-4'), 6.41 (1H, d, J=9.6Hz, H-5')	7.53 (1H, d, J=4.2Hz, H-4"), 7.36 (1H, d, J=4.2Hz, H-5")
34aa	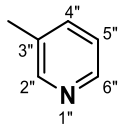	12.00 (1H, s, N$^{1'}$-H), 8.15 (1H, d, J=2.5Hz, H-2'), 7.98 (1H, dd, J=2.5Hz, J=9.6Hz, H-4'), 6.54 (1H, d, J=9.6Hz, H-5')	8.92 (1H, d, J=2.3Hz, H-2"), 8.35 (1H, dd, J=1.4Hz, J=4.7Hz, H-6"), 8.19 (1H, ddd, J=1.4Hz, J=2.3Hz, J=8.2Hz, H-4"), 7.42 (1H, dd, J=4.7Hz, J=8.2Hz, H-5")
34ab	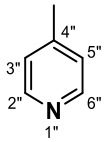	12.21 (1H, s, N$^{1'}$-H), 11.53 (1H, s, CONH), 8.15 (1H, d, J=2.5Hz, H-2'), 7.98 (1H, dd, J=2.5Hz, J=9.6Hz, H-4'), 6.54 (1H, d, J=9.6Hz, H-5')	8.56 (2H, d, J=6.3Hz, H-2",6"), 7.84 (2H, d, J=6.3Hz, H-3",5")
34ac	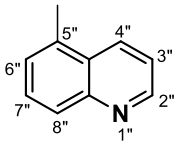	12.23 (1H, s, N$^{1'}$-H), 11.49 (1H, s, CONH), 8.19 (1H, d, J=2.4Hz, H-2'), 8.08-7.97* (m, 2H, H-4'), 6.57 (1H, d, J=9.6Hz, H-5')	8.96 (1H, dd, J=1.5Hz, J=4.2Hz, H-2"), 8.49 (1H, dd, J=1.5Hz, J=8.6Hz, H-4"), 8.08-7.97* (2H, m, H-6"), 7.84 (1H, t, J=7.3Hz, H-7"), 7.71 (1H, dd, J=1.0Hz, J=7.3Hz, H-8"), 7.59 (1H, dd, J=4.2Hz, J=8.6Hz, H-3")
34ad	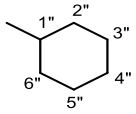	12.21 (1H, s, N$^{1'}$-H), 9.24 (1H, d, J=8.4Hz, CO-NH), 8.09 (1H, d, J=2.5Hz, H-2'), 7.93 (1H, dd, J=2.5Hz, J=9.6Hz, H-4'), 6.51 (1H, d, J=9.6Hz, H-5')	1.90-1.02 (10H, m, H-2",3",4",5",6"), 3.81-3.67 (1H, m, H-1")
34ae	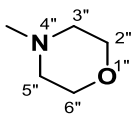	12.00 (1H, s, N$^{1'}$-H), 8.08 (1H, d, J=2.5Hz, H-2'), 7.93 (1H, dd, J=2.5Hz, J=9.6Hz, H-4'), 6.52 (1H, d, J=9.6Hz, H-5')	3.80-3.75 (2H, m, CH_2), 3.69 (4H, s, 2 CH_2), 3.67-3.62 (2H, m, CH_2)

Entry		Scaffold ^{1}H-NMR (400 MHz, DMSO-*d6*) δ ppm	R ^{1}H-NMR (400 MHz, DMSO-*d6*) δ ppm
34af	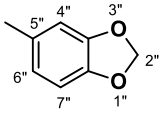	12.21 (1H, s, N$^{1'}$-H), 11.17 (1H, s, CONH), 8.14 (1H, d, J=2.4Hz, H-2'), 7.97 (1H, dd, J=2.4Hz, J=9.4Hz, H-4'), 6.54 (1H, d, J=9.4Hz, H-5')	7.42 (1H, d, J=2.1Hz, H-4"), 7.30 (1H, dd, J=2.1Hz, J=8.4Hz, H-6"), 6.95 (1H, d, J=8.4Hz, H-7"), 6.04 (2H, s, OCH_2O)
34ag	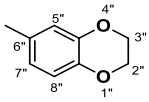	12.22 (1H, s, N$^{1'}$-H), 11.07 (1H, s, CONH), 8.15 (1H, d, J=2.5Hz, H-2'), 7.97 (1H, dd, J=2.5Hz, J=9.6Hz, H-4'), 6.54 (1H, d, J=9.6Hz, H-5')	7.40 (1H, d, J=2.5Hz H-5"), 7.27 (1H, dd, J=2.5Hz, J=8.8Hz, H-7"), 6.88 (1H, d, J=8.8Hz, H-8"), 4.24 (4H, d, J=1.0Hz, 2 OCH_2)
34ah	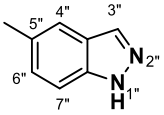	12.26 (1H, br s, N$^{1'}$-H), 11.28 (1H, br s, CONH), 8.17 (1H, d, J=2.4Hz, H-2'), 7.99 (1H, dd, J=2.4Hz, J=9.4Hz, H-4'), 6.55 (1H, d, J=9.4Hz, H-5')	8.29 (1H, d, J=1.7Hz, H-4"), 8.12 (1H, s, H-3"), 7.70 (1H, dd, J=1.7Hz, J=8.8Hz, H-6"), 7.58 (1H, d, J=8.8Hz, H-7")

2-Oxo-1,2-dihydropyridine-3-carbonitrile **37**:

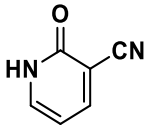

According to reference 215, a solution of 2-chloronicotinonitrile **36** (5.00 g, 36.1mmol) in AcOH (100 mL) and H_2O (10 mL) was heated at 125 ºC for 5 h. The cooled suspension was then poured onto ice. The solid was collected, washed with water and dried under vacuum to give **37** (4.16 g, 96%) which was used in the next step without further purification.

^{1}H-NMR (400 MHz, DMSO-*d6*): δ ppm 12.56 (1H, br s, N^1-H), 8.14 (1H, dd, J=1.7Hz, J=6.8Hz, H-4), 7.78 (1H, dd, J=1.7Hz, J=6.8Hz, H-6), 6.34 (1H, t, J=6.8Hz, H-5).

MS ESI (m/z): 119 $[M-H]^-$.

N'-Hydroxy-2-oxo-1,2-dihydropyridine-3-carboximidamide **38**:

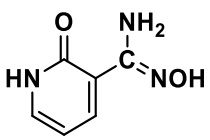

To a hot solution of 2-oxo-1,2-dihydropyridine-3-carbonitrile **37** (3.50 g, 29.17 mmol) in EtOH (50 mL), was added a solution of hydroxylamine hydrochloride (4.05 g, 58.33 mmol) and $NaHCO_3$ (4.9 g, 58.33 mmol) in water (40 mL). The reaction mixture was heated at reflux for 6h. The solvent was then removed *in vacuo* and the resulting residue was dry-loaded silica gel flash column chromatographed (10-20% MeOH in EtOAc) to give the **38** as a white solid (6.33 g, 71%).

^{1}H-NMR (400 MHz, DMSO-*d6*): δ ppm 12.07 (1H, br s, N^1-H), 9.48 (1H, s, OH), 7.94 (1H, dd, J=1.4Hz, J=6.8Hz, H-4), 7.50 (1H, dd, J=1.4Hz, J=6.8Hz, H-6), 6.30 (3H, t, J=7.8Hz, H-5, NH_2).

MS ESI (m/z): 154 $[M+H]^+$.

Ethyl 2-((2-(methylthio)phenyl)amino)-2-oxoacetate **40a**:

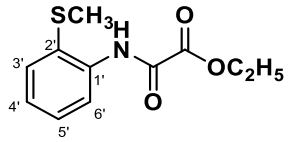

Ethyl chlorooxoacetate **39** (0.5 mL, 4.48 mmol) was added dropwise to a mixture of 2-methylthioaniline (0.62 g, 4.48 mmol) and Et_3N (0.75 mL, 5.37 mmol) in CH_2Cl_2 (8 mL) at 0 ^oC. The reaction mixture was allowed to warm slowly to room temperature and stirred for 12 h. The mixture was then filtered to remove the ammonium salts, and the filtrate was washed with water. The organic layer was dried over Na_2SO_4, filtered, and concentrated *in vacuo*. The crude oil was flash column chromatographed on silica gel (gradient elution, 5-10% EtOAc in hexane) to afford **40a** as an off white solid (0.95 g, 89%).

^{1}H-NMR (400 MHz, DMSO-*d6*): δ ppm 10.22 (1H, br s, N-H), 7.66-7.61 (1H, m, H-3'), 7.49-7.43 (1H, m, H-6'), 7.30-7.24 (2H, m, H-4', H-5'), 4.32 (2H, q, J=7.1Hz, CH_2), 2.43 (3H, s, SCH_3), 1.32 (3H, t, J=7.1Hz, CH_3).

MS ESI (m/z): 240 $[M+H]^+$.

Ethyl 2-((2,3-dihydro-*1H*-inden-4-yl)amino)-2-oxoacetate **40b**:

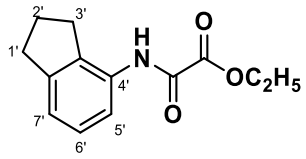

Indan-4-amine (0.6 g, 4.48 mmol) was reacted with ethyl chlorooxoacetate **39** (0.5 mL, 4.48 mmol) according to the procedure for **40a**. The crude product was flash column

chromatographed on silica gel (gradient elution, 3-10% EtOAc in hexane) to afford **40b** as a brown solid (0.87 g, 83%).

^{1}H-NMR (400 MHz, DMSO-*d6*): δ ppm 10.28 (1H, br s, N-H), 7.26 (1H, dd, J=2.9Hz, J=6.1Hz, H-5'), 7.18-7.09 (2H, m, H-6',7'), 4.30 (2H, q, J=7.1Hz, ethyl CH_2), 2.92 (2H, t, J=7.4Hz, benzylic-H), 2.84 (2H, t, J=7.4Hz, benzylic-H), 2.01 (2H, p, J=7.4Hz, CH_2(2')), 1.31 (3H, t, J=7.1Hz, CH_3).

MS ESI (m/z): 234 $[M+H]^+$.

Ethyl 2-((3,4-dimethoxyphenyl)amino)-2-oxoacetate **40c**:

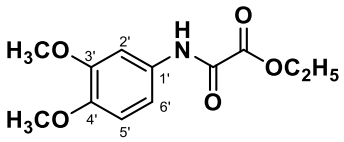

3,4-Dimethoxyaniline (0.69 g, 4.48 mmol) was reacted with ethyl chlorooxoacetate **39** (0.5 mL, 4.48 mmol) according to the procedure for **40a**. The crude product was flash column chromatographed on silica gel (gradient elution, 3-15% EtOAc in hexane) to afford **40c** as a white solid (1.03 g, 91%).

^{1}H-NMR (400 MHz, DMSO-*d6*): δ ppm 10.61 (1H, br s, N-H), 7.40 (1H, d, J=2.2Hz, H-2'), 7.33 (1H, dd, J=2.2Hz, J=8.8Hz, H-6'), 6.93 (1H, d, J=8.8Hz, H-5'), 4.29 (2H, q, J=7.1Hz, CH_2), 3.73 (6H, d, J=2.7Hz, 2 OCH_3), 1.31 (3H, t, J=7.1Hz, CH_3).

MS ESI (m/z): 253 $[M+H]^+$.

Ethyl 2-((3-chloro-2-methoxyphenyl)amino)-2-oxoacetate **40d**:

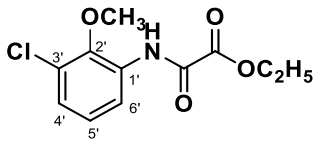

3-Choloro-4-methoxyaniline (0.71 g, 4.48 mmol) was reacted with ethyl chlorooxoacetate **39** (0.5 mL, 4.48 mmol) according to the procedure for **40a**. The crude product was flash column chromatographed on silica gel (gradient elution, 3-12% EtOAc in hexane) to afford **40d** as a yellowish white solid (0.82 g, 71%).

^{1}H-NMR (400 MHz, DMSO-*d6*): δ ppm 10.01 (1H, br s, N-H), 7.87 (1H, dd, J=1.6Hz, J=8.1Hz, H-4'), 7.34 (1H, dd, J=1.6Hz, J=8.1Hz, H-6'), 7.19 (1H, t, J=8.1Hz, H-5'), 4.32 (2H, q, J=7.3Hz, CH_2), 3.82 (3H, s, OCH_3), 1.31 (3H, t, J=7.3Hz, CH_3).

MS ESI (m/z): 258 $[M+H]^+$.

Ethyl 2-oxo-2-((3-phenoxyphenyl)amino)acetate **40e**:

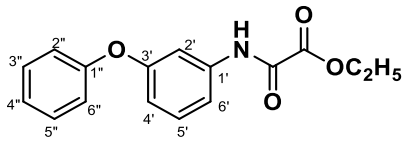

3-Phenoxyaniline (0.83 g, 4.48 mmol) was reacted with ethyl chlorooxoacetate **39** (0.5 mL, 4.48 mmol) according to the procedure for **40a**. The crude product was flash column chromatographed on silica gel (gradient elution, 3-12% EtOAc in hexane) to afford **40e** as off white solid (1.0 g, 78%).

^{1}H-NMR (400 MHz, DMSO-*d6*): δ ppm 10.84 (1H, br s, N-H), 7.53 (1H, ddd, J=0.9Hz, J=2.6Hz, J=8.1Hz, Ar-H) 7.47 (1H, t, J=2.6Hz, H-2'), 7.44-7.32 (3H, m, Ar-H), 7.20-7.13 (1H, m, Ar-H), 7.07-7.00 (2H, m, Ar-H), 6.83-6.73 (1H, ddd, J=0.9Hz, J=2.6Hz, J=8.1Hz, Ar-H), 4.29 (2H, q, J=7.2Hz, CH_2), 3.82 (3H, s, OCH_3), 1.30 (3H, t, J=7.2Hz, CH_3).

Ethyl 2-oxo-2-(*p*-tolylamino)acetate **40f**:

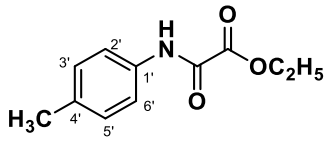

4-Methylaniline (0.48 g, 4.48 mmol) was reacted with ethyl chlorooxoacetate **39** (0.5 mL, 4.48 mmol) according to the procedure for **40a**. The crude product was flash column chromatographed on silica gel (gradient elution, 3-12% EtOAc in hexane) to afford **40f** as a white solid (0.84 g, 90%).

^{1}H-NMR (400 MHz, DMSO-*d6*): δ ppm 10.67 (1H, br s, N-H), 7.61 (2H, d, J=8.9Hz, H-2',6'), 7.16 (2H, d, J=8.9Hz, H-3',5'), 4.29 (2H, q, J=7.2Hz, CH_2), 3.82 (3H, s, OCH_3), 2.27 (3H, s, CH_3), 1.30 (3H, t, J=7.2Hz, ethyl CH_3).

MS ESI (m/z): 208 $[M+H]^+$.

Ethyl 2-(benzo[*d*][1,3]dioxol-5-ylamino)-2-oxoacetate **40g**:

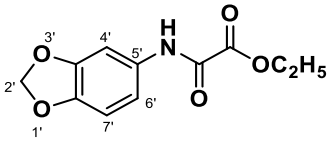

3,4-(Methylenedioxy)aniline (0.61 g, 4.48 mmol) was reacted with ethyl chlorooxoacetate **39** (0.5 mL, 4.48 mmol) according to the procedure for **40a**. The crude product was flash

column chromatographed on silica gel (gradient elution, 3-15% EtOAc in hexane) to afford **40g** as a white solid (0.98 g, 92%).

^{1}H-NMR (400 MHz, DMSO-*d6*): δ ppm 10.68 (1H, br s, N-H), 7.36 (1H, d, J=2.3Hz, H-4'), 7.22 (1H, dd, J=2.3Hz, J=8.9Hz, H-6'), 6.90 (1H, d, J=8.9Hz, H-7'), 6.01 (2H, s, OCH_2O), 4.29 (2H, q, J=7.1Hz, CH_2), 1.30 (3H, t, J=7.1Hz, CH_3).

MS ESI (m/z): 238 $[M+H]^+$.

N-(2-(Methylthio)phenyl)-3-(2-oxo-1,2-dihydropyridin-3-yl)-1,2,4-oxadiazole-5-carboxamide **41a**:

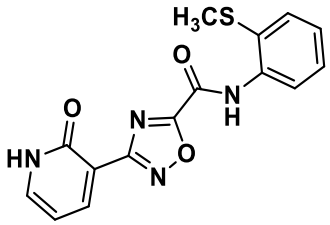

Sodium hydride 60% suspension in oil (200 mg, 5.0 mmol) was added to a stirred solution of ethyl 2-((2-(methylthio)phenyl)amino)-2-oxoacetate **40a** (0.31 g, 1.31mmol) and amidoxime **38** (0.2g, 1.31mmol) in dry DMF (6 mL) at 0 ^oC under nitrogen. After stirring for 2 hours at room temperature, then the reaction mixture was stirred at 60 ^oC for 12 hours. The solvent was removed *in vacuo* and the crude oil silica flash column chromatographed (gradient elution, 3-10% MeOH in CH_2Cl_2) to afford **41a** as a white solid (0.18 g, 43%).

^{1}H-NMR (400 MHz, DMSO-*d6*): see Table 25.

^{13}C NMR (100MHz, DMSO-*d6*): δ 169.1, 166.4, 162.6, 152.0, 138.2, 137.7, 134.6, 134.3, 128.2, 126.7, 122.5, 121.1, 104.8, 16.1.

MS ESI (m/z): 327 $[M-H]^-$, **HRMS:** m/z calculated for $C_{15}H_{12}N_4O_3S^-$: 327.05573, found: 327.05597.

N-(2,3-Dihydro-*1H*-inden-4-yl)-3-(2-oxo-1,2-dihydropyridin-3-yl)-1,2,4-oxadiazole-5-carboxamide **41b**:

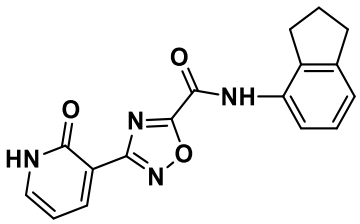

Following the procedure for **41a**, ethyl 2-((2,3-dihydro-1H-inden-4-yl)amino)-2-oxoacetate **40b** (0.31 g, 1.31 mmol) was reacted with amidoxime **38** (0.2g, 1.31mmol). The crude

product was silica flash column chromatographed (gradient elution, 3-8% MeOH in CH_2Cl_2) to afford **41b** as a white solid (0.17 g, 40%).

^{1}H-NMR (400 MHz, DMSO-*d6*): see Table 25.

MS ESI (m/z): 321 $[M-H]^-$, **HRMS:** m/z calculated for $C_{17}H_{14}N_4O_3^-$: 321.09931, found: 321.09930.

N-(3,4-Dimethoxyphenyl)-3-(2-oxo-1,2-dihydropyridin-3-yl)-1,2,4-oxadiazole-5-carboxamide **41c**:

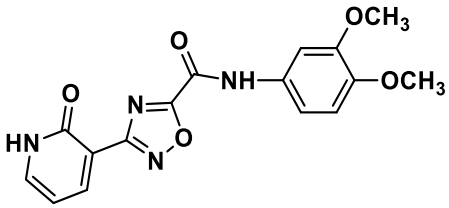

Following the procedure for **41a**, ethyl 2-((3,4-dimethoxyphenyl)amino)-2-oxoacetate **40c** (0.33 g, 1.31 mmol) was reacted with amidoxime **38** (0.2g, 1.31mmol). The crude product was silica flash column chromatographed (gradient elution, 3-15% MeOH in CH_2Cl_2) to afford **41c** as white solid (0.16 g, 36%).

^{1}H-NMR (400 MHz, DMSO-*d6*): see Table 25.

MS ESI (m/z): 341 $[M-H]^-$.

N-(3-Chloro-2-methoxyphenyl)-3-(2-oxo-1,2-dihydropyridin-3-yl)-1,2,4-oxadiazole-5-carboxamide **41d**:

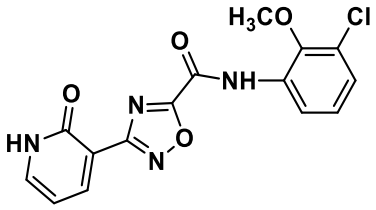

Following the procedure for **41a**, ethyl 2-((3-chloro-2-methoxyphenyl)amino)-2-oxoacetate **40d** (0.34 g, 1.31 mmol) was reacted with amidoxime **38** (0.2g, 1.31mmol). The crude product was silica flash column chromatographed (gradient elution, 3-10% MeOH in CH_2Cl_2) to afford **41d** as a white solid (0.1 g, 23%).

^{1}H-NMR (400 MHz, DMSO-*d6*): see Table 25.

MS ESI (m/z): 345 $[M-H]^-$, **HRMS:** m/z calculated for $C_{15}H_{11}ClN_4O_4^-$: 345.03961, found: 345.03992.

3-(2-Oxo-1,2-dihydropyridin-3-yl)-*N*-(3-phenoxyphenyl)-1,2,4-oxadiazole-5-carboxamide **41e**:

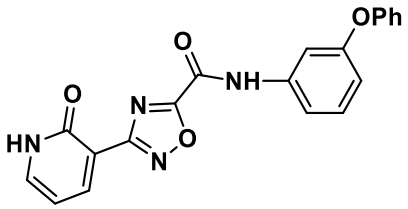

Following the procedure for **41a**, ethyl 2-oxo-2-((3-phenoxyphenyl)amino)acetate **40e** (0.37 g, 1.31 mmol) was reacted with amidoxime **38** (0.2g, 1.31mmol). The crude product was silica flash column chromatographed (gradient elution, 3-10% MeOH in CH_2Cl_2) to afford **41e** as an off white solid (0.19 g, 37%).

^{1}H-NMR (400 MHz, DMSO-*d6*): see Table 25.

^{13}C NMR (100MHz, DMSO-*d6*): δ 168.1, 166.2, 159.2, 157.6, 156.6, 152.1, 144.3, 140.2, 139.3, 130.8, 130.6, 124.3, 122.7, 121.2, 119.6, 116.7, 116.0, 115.5, 111, 105.3.

MS ESI (m/z): 373 $[M-H]^-$, **HRMS:** m/z calculated for $C_{20}H_{14}N_4O_4^-$: 373.09423, found: 373.09406.

3-(2-Oxo-1,2-dihydropyridin-3-yl)-*N*-(*p*-tolyl)-1,2,4-oxadiazole-5-carboxamide **41f**:

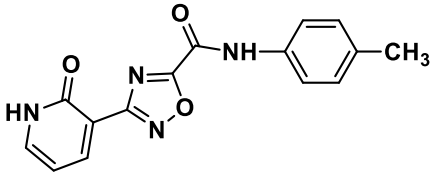

Following the procedure for **41a**, ethyl 2-oxo-2-(p-tolylamino)acetate **40f** (0.27 g, 1.31 mmol) was reacted with amidoxime **38** (0.2g, 1.31mmol). The crude product was silica flash column chromatographed (gradient elution, 3-10% MeOH in CH_2Cl_2) to afford **41f** as an off white solid (0.16 g, 41%).

^{1}H-NMR (400 MHz, DMSO-*d6*): see Table 25.

^{13}C NMR (100MHz, DMSO-*d6*): δ 166.1, 159.1, 151.9, 149.9, 144.9, 142.4, 140.2, 134.3, 129.6, 121.3, 116.8, 106.5, 104.7, 101.8, 21.2.

MS ESI (m/z): 295 $[M-H]^-$, **HRMS:** m/z calculated for $C_{15}H_{12}N_4O_3^-$: 295.08366, found: 295.08368.

N-(Benzo[*d*][1,3]dioxol-5-yl)-3-(2-oxo-1,2-dihydropyridin-3-yl)-1,2,4-oxadiazole-5-carboxamide **41g**:

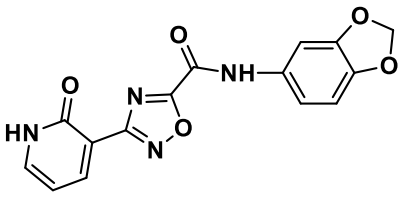

Following the procedure for **41a**, ethyl 2-(benzo[d][1,3]dioxol-5-ylamino)-2-oxoacetate **40g** (0.31 g, 1.31 mmol) was reacted with amidoxime **38** (0.2g, 1.31mmol). The crude product was silica flash column chromatographed (gradient elution, 3-10% MeOH in CH_2Cl_2) to afford**41g** as an off white solid (0.19 g, 44%).

^{1}H-NMR (400 MHz, DMSO-*d6*): see Table 25.

MS ESI (m/z): 325 $[M-H]^-$, **HRMS:** m/z calculated for $C_{15}H_{10}N_4O_5^-$: 325.05784, found: 325.05817.

Table 25: NMR data of compounds **41a-g**

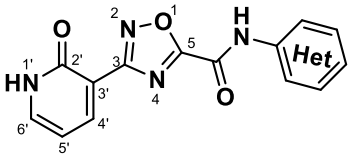

Entry	Het	Scaffold ^{1}H-NMR (400 MHz, DMSO-*d6*) δ ppm	R ^{1}H-NMR (400 MHz, DMSO-*d6*) δ ppm
41a	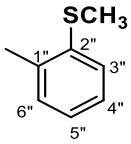	12.32 (1H, s, N$^{1'}$-H), 10.76 (1H, s, CONH), 8.30 (1H, dd, J=2.1Hz, J=7.1Hz, H-4'), 7.72 (1H, dd, J=2.1Hz, J=6.5Hz, H-6'), 6.45 (1H, t, J=6.8Hz, H-5')	7.58 (1H, dd, J=1.4Hz, J=7.9Hz, H-3"), 7.47 (1H, dd, J=1.4Hz, J=7.9Hz, H-6"), 7.35 (1H, dt, J=1.4Hz, J=7.6Hz, H-5"), 7.29 (1H, dt, J=1.4Hz, J=7.6Hz, H-4"), 2.46 (3H, s, SCH_3)
41b	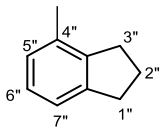	12.38 (1H, s, N$^{1'}$-H), 10.86 (1H, s, CONH), 8.31 (1H, dd, J=2.2Hz, J=7.1Hz, H-4'), 7.71 (1H, dd, J=2.2Hz, J=6.5Hz, H-6'), 6.44 (1H, t, J=6.8Hz, H-5')	7.28 (1H, dd, J=2.9Hz, J=6.1Hz, H-5"), 7.13-7.22 (2H, m, H-6",7"), 2.92 (2H, t, J=7.4Hz, benzylic-H), 2.85 (2H, t, J=7.4Hz, benzylic-H), 2.01 (2H, p, J=7.4Hz, CH_2)

Entry		Scaffold ^{1}H-NMR (400 MHz, DMSO-*d6*) δ ppm	R ^{1}H-NMR (400 MHz, DMSO-*d6*) δ ppm
41c	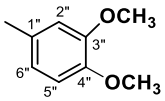	12.31 (1H, s, N$^{1'}$-H), 11.08 (1H, s, CONH), 8.33 (1H, dd, J=2.1Hz, J=7.2Hz, H-4'), 7.71 (1H, dd, J=2.1Hz, J=6.4Hz, H-6'), 6.44 (1H, t, J=6.8Hz, H-5')	7.48 (1H, d, J=2.3Hz, H-2"), 7.43 (1H, dd, J=2.3Hz, J=8.8Hz, H-6"), 6.98 (1H, d, J=8.8Hz, H-5"), 3.76 (6H, s, 2 OCH_3)
41d	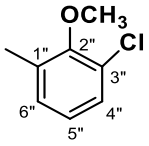	12.35 (1H, s, N$^{1'}$-H), 10.54 (1H, s, CONH), 8.33 (1H, dd, J=2.1Hz, J=7.2Hz, H-4'), 7.73 (1H, dd, J=2.1Hz, J=6.4Hz, H-6'), 6.44 (1H, t, J=6.8Hz, H-5')	7.82 (1H, dd, J=1.6Hz, J=8.0Hz, H-4"), 7.43 (1H, dd, J=1.6Hz, J=8.0Hz, H-6"), 7.24 (1H, t, J=8.0Hz, H-5"), 3.82 (3H, s, OCH_3)
41e	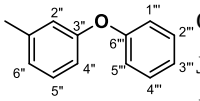	12.33 (1H, s, N$^{1'}$-H), 11.30 (1H, s, CONH), 8.32 (1H, dd, J=2.2Hz, J=7.1Hz, H-4'), 7.72 (1H, dd, J=2.2Hz, J=6.5Hz, H-6'), 6.44 (1H, t, J=6.8Hz, H-5')	7.63 (1H, ddd, J=0.9Hz, J=2.6Hz, J=8.1Hz, Ar-H) 7.53 (1H, t, J=2.6Hz, H-2"), 7.47-7.37 (3H, m, Ar-H), 7.22-7.15 (1H, m, Ar-H), 7.13-7.02 (2H, m, Ar-H), 6.89-6.84 (1H, ddd, J=0.9Hz, J=2.6Hz, J=8.1Hz, Ar-H)
41f	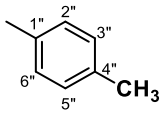	12.34 (1H, s, N$^{1'}$-H), 11.18 (1H, s, CONH), 8.33 (1H, dd, J=2.2Hz, J=7.1Hz, H-4'), 7.72 (1H, dd, J=2.2Hz, J=6.5Hz, H-6'), 6.45 (1H, t, J=6.8Hz, H-5')	7.70 (2H, d, J=9.0Hz, H-2",6"), 7.21 (2H, d, J=9.0Hz, H-3",5"), 2.30 (3H, s, CH_3)
41g	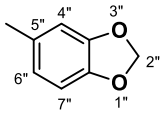	12.34 (1H, s, N$^{1'}$-H), 11.17 (1H, s, CONH), 8.32 (1H, dd, J=2.1Hz, J=7.2Hz, H-4'), 7.72 (1H, dd, J=2.1Hz, J=6.4Hz, H-6'), 6.44 (1H, t, J=6.8Hz, H-5')	7.43 (1H, d, J=2.2Hz, H-4"), 7.30 (1H, dd, J=2.2Hz, J=8.3Hz, H-6"), 6.95 (1H, d, J=8.3Hz, H-7"), 6.04 (2H, s, OCH_2O)

Benzoyl fluoride derivatives **43a**:

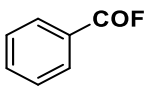

Cyanuric fluoride (0.3 mL, 5 mmol) was added dropwise to a mixture of benzoic acid **42a** (0.41 g, 3.33 mmol) and pyridine (0.81 mL, 10 mmol) in CH_2Cl_2 (8 mL) at 0 ^oC. The

reaction mixture was allowed to warm slowly to room temperature and stirred for 12 h. After completion of the reaction (monitored by TLC) the mixture was poured onto water and extracted with CH_2Cl_2. The combined organic layer was dried over Na_2SO_4, filtered and concentrated *in vacuo*. The residue was silica flash column chromatographed (gradient elution, 2-6% EtOAc in hexane) to afford benzoyl fluoride **43a** as a colourless oil (0.29 g, 71%).

^{19}F-NMR (400 MHz, $CDCl_3$): δ + 18.00 ppm.

4-Methoxybenzoyl fluoride **43b**:

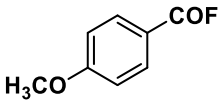

Prepared according to the procedure followed in **43a**, 4-methoxybenzoic acid **42b** (0.51 g, 3.34 mmol) was reacted with cyanuric fluoride (0.3 mL, 5 mmol). The crude product was silica flash column chromatographed (gradient elution, 2-8% EtOAc in hexane) to afford **43b** as white semisolid (0.37 g, 73%).

2,4-Dimethoxybenzoyl fluoride **43c**:

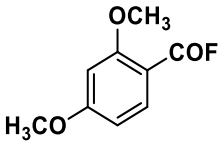

Prepared according to the procedure followed in **43a** 2,4-dimethoxybenzoic acid **42c** (0.61 g, 3.34 mmol) was reacted with cyanuric fluoride (0.3 mL, 5 mmol). The crude product was silica flash column chromatographed (gradient elution, 2-10% EtOAc in hexane) to afford **43c** as white powder (0.46 g, 75%).

4-Chlorobenzoyl fluoride **43d**:

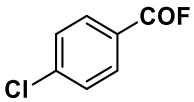

Prepared according to the procedure followed in **43a**, 4-chlorobenzoic acid **42d** (0.52 g, 3.33 mmol) was reacted with cyanuric fluoride (0.3 mL, 5 mmol). The crude product was silica flash column chromatographed (gradient elution, 2-6% EtOAc in hexane) to afford **43d** as a colourless oil (0.34 g, 64%).

4-Methylbenzoyl fluoride **43e**:

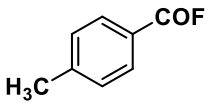

Prepared according to the procedure followed in **43a** using *p*-toluic acid **42e** (0.45 g, 3.33 mmol). The crude product was purified by flash column chromatography on silica gel (gradient elution, 2-5% EtOAc in hexane) to afford **43e** as a colourless oil (0.33 g, 73%).

4-(Trifluoromethyl)benzoyl fluoride **43f**:

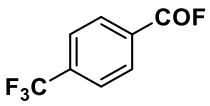

Prepared according to the procedure followed in **43a**, 4-(trifluoromethyl)benzoic acid **42f** (0.63 g, 3.33 mmol) was reacted with cyanuric fluoride (0.3 mL, 5 mmol). The crude product was purified by flash column chromatography on silica gel (gradient elution, 2-5% EtOAc in hexane) to afford **43f** as a colourless oil (0.38 g, 59%).

N'-(Benzoyloxy)-6-oxo-1,6-dihydropyridine-3-carboximidamide **44a:**

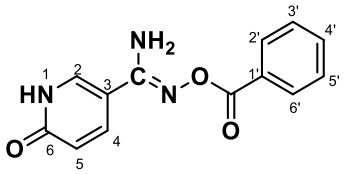

To a stirred solution` of amidoxime **28** (0.25g, 1.64 mmol) and benzoyl fluoride **43a** (0.2 g, 1.64 mmol) in dry THF (6 mL) was added a catalytic amount of TBAF (15 µL). The reaction mixture was stirred at ambient temperature for 4h. After removal of the THF *in vacuo*, the residue was silica flash column chromatographed (gradient elution, 3-8% MeOH in CH_2Cl_2) to afford **44a** as a white solid (0.33 g, 79%).

^{1}H-NMR (400 MHz, DMSO-*d6*): δ 11.96 (1H, s, N-H), 8.18-8.13 (2H, m, H-2',6'), 7.87 (1H, d, J=2.4Hz, H-2), 7.79 (1H, dd, J=2.4Hz, J=9.6Hz, H-4), 7.69-7.63 (1H, m, H-4'), 7.56-7.49 (2H, m, H-3',5'), 6.84 (2H, br s, NH_2), 6.39 (1H, d, J=9.6Hz, H-5).

MS ESI (m/z): 256 $[M-H]^-$.

N'-((4-Methoxybenzoyl)oxy)-6-oxo-1,6-dihydropyridine-3-carboximidamide **44b**:

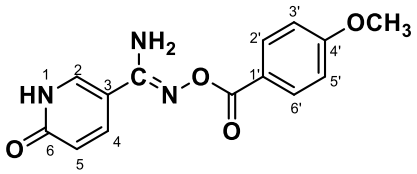

According to the procedure for **44a**, 4-methoxybenzoyl fluoride **43b** (0.25 g, 1.64 mmol) was reacted with amidoxime **28** (0.25g, 1.64 mmol). The crude product was silica flash column chromatographed (gradient elution, 3-10% MeOH in CH_2Cl_2) to afford **44b** as an off white solid (0.34 g, 73%).

^{1}H-NMR (400 MHz, DMSO-*d6*): δ 11.94 (1H, s, N-H), 8.11 (2H, d, J=9.0Hz, H-2',6'), 7.86 (1H, d, J=2.3Hz, H-2), 7.78 (1H, dd, J=2.3Hz, J=9.5Hz, H-4), 7.04 (2H, d, J=9.0Hz, H-3',5'), 6.80 (2H, br s, NH_2), 6.38 (1H, d, J=9.5Hz, H-5), 3.85 (3H, s, OCH_3).
MS ESI (m/z): 285 $[M-H]^-$.

N'-((2,4-Dimethoxybenzoyl)oxy)-6-oxo-1,6-dihydropyridine-3-carboximidamide **44c:**

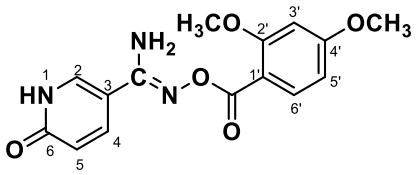

According to the procedure for **44a**, 2,4-dimethoxybenzoyl fluoride **43c** (0.30 g, 1.64 mmol) was reacted with amidoxime **28** (0.25g, 1.64 mmol). The crude product was silica flash column chromatographed (gradient elution, 3-10% MeOH in CH_2Cl_2) to afford **44c** as an off white solid (0.37 g, 71%).
^{1}H-NMR (400 MHz, DMSO-*d6*): δ 11.92 (1H, s, N-H), 7.86 (1H, d, J=2.3Hz, H-2), 7.77 (1H, dd, J=2.3Hz, J=9.5Hz, H-4), 7.46 (1H, d, J=8.1Hz, H-6"), 6.68 (1H, d, J=2.2Hz, H-3"), 6.64 (1H, dd, J=2.2Hz, J=8.1Hz, H-5"), 6.68 (2H, br s, NH_2), 6.39 (1H, d, J=9.5Hz, H-5), 3.87 (3H, s, OCH_3), 3.76 (3H, s, OCH_3).
MS ESI (m/z): 316 $[M-H]^-$.

N'-((4-Chlorobenzoyl)oxy)-6-oxo-1,6-dihydropyridine-3-carboximidamide **44d**:

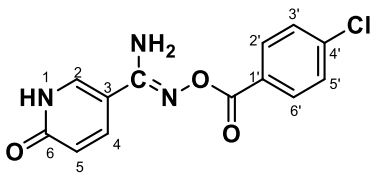

According to the procedure for **44a**, 4-chlorobenzoyl fluoride **43d** (0.26 g, 1.64 mmol) was reacted with amidoxime **28** (0.25g, 1.64 mmol). The crude product was silica flash column chromatographed (gradient elution, 2-8% MeOH in CH_2Cl_2) to afford **44d** as an off white solid (0.37 g, 79%).

^{1}H-NMR (400 MHz, DMSO-*d6*): δ 11.98 (1H, s, N-H), 8.18 (2H, d, J=8.9Hz, H-2',6'), 7.87 (1H, d, J=2.4Hz, H-2), 7.77 (1H, dd, J=2.4Hz, J=9.5Hz, H-4), 7.60 (2H, d, J=8.9Hz, H-3',5'), 6.89 (2H, br s, NH_2), 6.39 (1H, d, J=9.5Hz, H-5).

MS ESI (m/z): 290 $[M-H]^-$.

<u>*N'*-((4-Methylbenzoyl)oxy)-6-oxo-1,6-dihydropyridine-3-carboximidamide **44e**:</u>

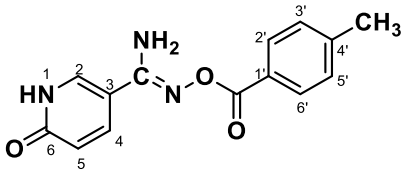

According to the procedure for **44a**, 4-methylbenzoyl fluoride **43e** (0.23 g, 1.66 mmol) was reacted with amidoxime **28** (0.25g, 1.66 mmol). The crude product was silica flash column chromatographed (gradient elution, 2-6% MeOH in CH_2Cl_2) to afford **44e** as a pale yellow solid (0.30 g, 69%).

^{1}H-NMR (400 MHz, DMSO-*d6*): δ 11.95 (1H, s, N-H), 8.05 (2H, d, J=8.5Hz, H-2',6'), 7.87 (1H, d, J=2.4Hz, H-2), 7.78 (1H, dd, J=2.4Hz, J=9.6Hz, H-4), 7.33 (2H, d, J=8.5Hz, H-3',5'), 6.81 (2H, br s, NH_2), 6.39 (1H, d, J=9.6Hz, H-5), 2.39 (3H, s, CH_3).

MS ESI (m/z): 270 $[M-H]^-$.

<u>6-Oxo-*N'*-((4-(trifluoromethyl)benzoyl)oxy)-1,6-dihydropyridine-3-carboximidamide **44f**:</u>

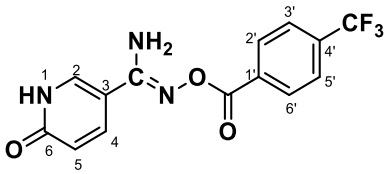

According to the procedure for **44a**, 4-(trifluoromethyl)benzoyl fluoride **43f** (0.32 g, 1.66 mmol) was reacted with amidoxime **28** (0.25g, 1.66 mmol). The crude product was silica flash column chromatographed (gradient elution, 2-8% MeOH in CH_2Cl_2) to afford **44f** as an off white solid (0.40 g, 75%).

^{1}H-NMR (400 MHz, DMSO-*d6*): δ 12.03 (1H, s, N-H), 8.36 (2H, d, J=8.3Hz, H-2',6'), 7.93-7.86 (3H, m, H-2,3',5'), 7.78 (1H, dd, J=2.4Hz, J=9.5Hz, H-4), 6.95 (2H, br s, NH_2), 6.40 (1H, d, J=9.5Hz, H-5).

MS ESI (m/z): 324 $[M-H]^-$.

5-(5-Phenyl-1,2,4-oxadiazol-3-yl)pyridin-2(*1H*)-one **45a**:

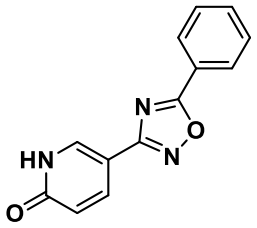

N'-(Benzoyloxy)-6-oxo-1,6-dihydropyridine-3-carboximidamide **44a** (0.13 g, 0.5 mmol) was dissolved in dioxane (4 mL) and irradiated for 20 minutes at 100 ^oC under microwave conditions. The solvent was then evaporated and the residue was silica flash column chromatographed (gradient elution, 2-10% MeOH in CH_2Cl_2) to give compound **45a** as a white solid (0.07 g, 58%).

^{1}H-NMR (400 MHz, DMSO-*d6*): see Table 26.

MS ESI (m/z): 238 $[M-H]^-$, **HRMS:** m/z calculated for $C_{13}H_9N_3O_2^-$: 238.06220, found: 238.0621.

5-(5-(4-Methoxyphenyl)-1,2,4-oxadiazol-3-yl)pyridin-2(*1H*)-one **45b**:

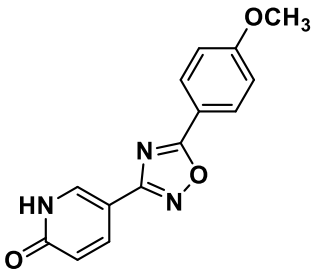

Following the procedure for **45a,** compound **44b** (0.14 g, 0.5 mmol) was converted to **45b**, obtained as a white solid (0.08 g, 61%) after silica flash column chromatography (gradient elution, 2-10% MeOH in CH_2Cl_2).

^{1}H-NMR (400 MHz, DMSO-*d6*): see Table 26.

MS ESI (m/z): 268 $[M-H]^-$.

5-(5-(2,4-Dimethoxyphenyl)-1,2,4-oxadiazol-3-yl)pyridin-2(*1H*)-one **45c**:

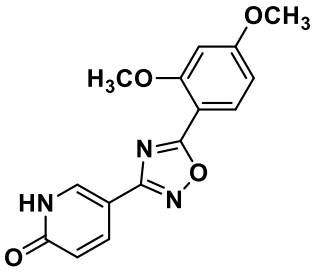

Following the procedure for **45a,** compound **44c** (0.16 g, 0.5 mmol) was converted to **45c**, obtained as a white solid (0.08 g, 53%) after silica flash column chromatography (gradient elution, 2-12% MeOH in CH_2Cl_2).

^{1}H-NMR (400 MHz, DMSO-*d6*): see Table 26.

MS ESI (m/z): 298 $[M-H]^-$.

5-(5-(4-Chlorophenyl)-1,2,4-oxadiazol-3-yl)pyridin-2(*1H*)-one **45d**:

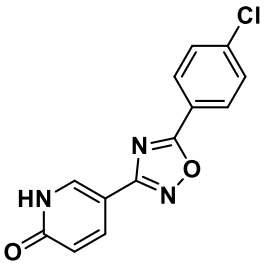

Following the procedure for **45a,** compound **44d** (0.15 g, 0.51 mmol) was converted to **45d**, obtained as an off white solid (0.05 g, 38%) after silica flash column (gradient elution, 2-6% MeOH in CH_2Cl_2).

^{1}H-NMR (400 MHz, DMSO-*d6*): see Table 26.

MS ESI (m/z): 272 $[M-H]^-$, **HRMS:** m/z calculated for $C_{13}H_8ClN_3O_2^-$: 272.02323, found: 272.02344.

5-(5-(*p*-Tolyl)-1,2,4-oxadiazol-3-yl)pyridin-2(*1H*)-one **45e**:

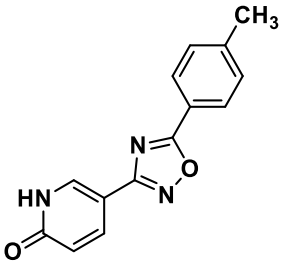

Following the procedure for **45a,** compound **44e** (0.14 g, 0.51 mmol) was converted to **45e**, obtained as a white solid (0.08 g, 63%) after silica flash column chromatography (gradient elution, 2-6% MeOH in CH_2Cl_2).

^{1}H-NMR (400 MHz, DMSO-*d6*): see Table 26.

MS ESI (m/z): 252 $[M-H]^-$, **HRMS:** m/z calculated for $C_{14}H_{11}N_3O_2^-$: 252.07785, found: 252.07779.

5-(5-(4-(Trifluoromethyl)phenyl)-1,2,4-oxadiazol-3-yl)pyridin-2(*1H*)-one **45f**:

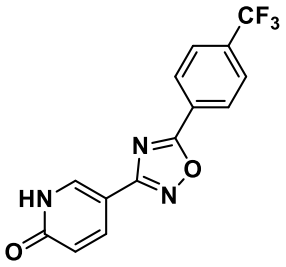

Following the procedure for **45a,** compound **44f** (0.16 g, 0.5 mmol) was converted to **45f**, obtained as a white solid (0.04 g, 25%) after silica flash column (gradient elution, 2-6% MeOH in CH_2Cl_2) to afford **45f**.

^{1}H-NMR (400 MHz, DMSO-*d6*): see Table 26.

MS ESI (m/z): 306 $[M-H]^-$.

Table 26: NMR data of **45a-f**

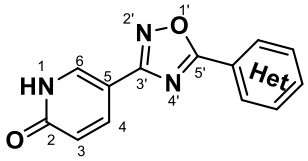

Entry		Scaffold ^{1}H-NMR (400 MHz, DMSO-*d6*) δ ppm	R ^{1}H-NMR (400 MHz, DMSO-*d6*) δ ppm
45a	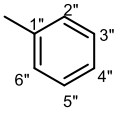	12.16 (1H, s, N-H), 8.12 (1H, d, J=2.4Hz, H-6), 7.97 (1H, dd, J=2.4Hz, J=9.6Hz, H-4), 6.53 (1H, d, J=9.6Hz, H-3)	8.16 (2H, m, H-2",6"), 7.77-7.71 (1H, m, H-4"), 7.69-7.63 (2H, m, H-3",5")

Entry		Scaffold ^{1}H-NMR (400 MHz, DMSO-*d6*) δ ppm	R ^{1}H-NMR (400 MHz, DMSO-*d6*) δ ppm
45b	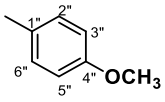	12.14 (1H, s, N-H), 8.15-8.06* (3H, m, H-6), 7.95 (1H, dd, J=2.5Hz, J=9.6Hz, H-4), 6.52 (1H, d, J=9.6Hz, H-3)	8.15-8.06* (3H, m, H-2",6"), 7.19 (2H, d, J=9.0Hz, H-3",5"), 3.88 (3H, s, OCH_3)
45c	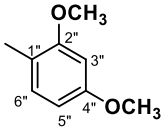	8.03-7.98 (1H, m, H-6), 7.58-7.53 (1H, m, H-4), 7.10-7.04 (1H, m, H-3)	7.50 (1H, d, J=8.1Hz, H-6"), 6.75 (1H, d, J=2.2Hz, H-3"), 6.70 (1H, dd, J=2.2Hz, J=8.1Hz, H-5"), 3.87 (3H, s, OCH_3), 3.76 (3H, s, OCH_3)
45e	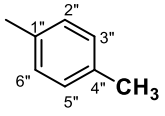	12.13 (1H, s, N-H), 8.10 (1H, d, J=2.2Hz, H-6), 7.96 (1H, dd, J=2.2Hz, J=9.5Hz, H-4), 6.52 (1H, d, J=9.5Hz, H-3)	8.05 (2H, d, J=8.7Hz, H-2",6"), 7.46 (2H, d, J=8.7Hz, H-3",5"), 2.42 (3H, s, CH_3)
45f	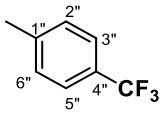	12.19 (1H, s, N-H), 8.15 (1H, d, J=2.0Hz, H-6), 7.99 (1H, dd, J=2.0Hz, J=9.2Hz, H-4), 6.54 (1H, d, J=9.2Hz, H-3)	8.37 (2H, d, J=8.4Hz, H-2",6"), 8.04 (2H, d, J=8.4Hz, H-3",5")

tert-Butyl 4-((3-methoxyphenyl)carbamoyl)piperazine-1-carboxylate **48a**:

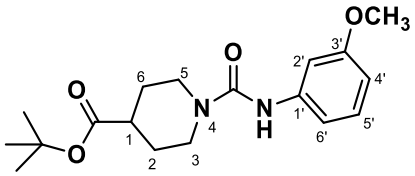

3-Methoxyphenyl isocayante **47a** (0.26 g, 1.75 mmol) was added dropwise to a solution of *N-Boc*-piperazine **46** (0.33 g, 1.75 mmol) in CH_2Cl_2 (5 mL) under N_2. The reaction mixture was stirred at ambient temperature for 6 h. After completion of the reaction (monitored by TLC) the mixture was poured onto water and extracted with CH_2Cl_2. The combined organic layer was dried over Na_2SO_4, filtered and concentrated *in vacuo*. The residue was silica flash column chromatographed (gradient elution, 5-15% EtOAc in hexane) to afford **48a** as colourless oil (0.51 g, 88%).

^{1}H-NMR (400 MHz, DMSO-*d6*): δ 8.53 (1H, br s, CONH), 7.14 (1H, t, J=2.4Hz, H-2'), 7.11 (1H, d, J=8.2Hz, H-5'), 7.03 (1H, ddd, J=0.8Hz, J=2.4Hz, J=8.2Hz, H-6'), 6.51 (1H,

ddd, J=0.8Hz, J=2.4Hz, J=8.2Hz, H-4'), 3.70 (3H, s, OCH_3), 3.45–3.32 (m, 8H, NCH_2), 1.42 (9H, s, $C(CH_3)_3$).

MS ESI (m/z): 334 $[M-H]^-$.

tert-Butyl 4-((3-bromophenyl)carbamoyl)piperazine-1-carboxylate **48b**:

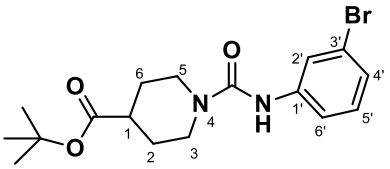

Prepared according to the procedure for **48a**, 3-bromophenyl isocyanate **47b** (0.35 g, 1.75 mmol) was reacted with *N-Boc*-piperazine **46** (0.33 g, 1.75 mmol). The residue was silica flash column chromatographed (gradient elution, 5-10% EtOAc in hexane) to afford **48b** as colourless oil (0.48 g, 71%).

^{1}H-NMR (400 MHz, DMSO-*d6*): δ 8.73 (1H, br s, CONH), 7.78 (1H, t, J=2.1Hz, H-2'), 7.43 (1H, ddd, J=0.8Hz, J=2.1Hz, J=8.1Hz, H-6'), 7.19 (1H, t, J=8.1Hz, H-5'), 7.10 (1H, ddd, J=0.8Hz, J=2.1Hz, J=8.1Hz, H-4'), 3.46–3.33 (m, 8H, NCH_2), 1.42 (9H, s, $C(CH_3)_3$).

MS ESI (m/z): 407 $[M^+ +2]^+$.

tert-Butyl 4-((3-chlorophenyl)carbamoyl)piperazine-1-carboxylate **48c**:

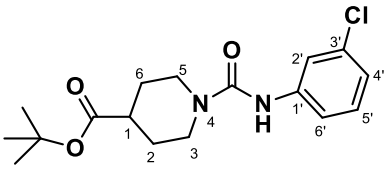

Prepared according to the procedure for **48a**, 3-chlorophenyl isocyanate **47c** (0.27 g, 1.75 mmol) was reacted with *N-Boc*-piperazine **46** (0.33 g, 1.75 mmol). The residue was silica flash column chromatographed (gradient elution, 5-10% EtOAc in hexane) to afford **48c** as colourless oil (0.43 g, 72%).

^{1}H-NMR (400 MHz, DMSO-*d6*): δ 8.74 (1H, br s, CONH), 7.64 (1H, t, J=2.1Hz, H-2'), 7.38 (1H, ddd, J=0.8Hz, J=2.1Hz, J=8.1Hz, H-6'), 7.25 (1H, t, J=8.1Hz, H-5'), 6.97 (1H, ddd, J=0.8Hz, J=2.1Hz, J=8.1Hz, H-4'), 3.46–3.32 (m, 8H, NCH_2), 1.42 (9H, s, $C(CH_3)_3$).

tert-Butyl 4-((2,4-dimethoxyphenyl)carbamoyl)piperazine-1-carboxylate **48d**:

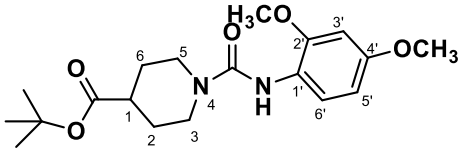

Prepared according to the procedure for **48a**, 2,4-dimethoxyphenyl isocyanate **47d** (0.31 g, 1.75 mmol) was reacted with *N-Boc*-piperazine **46** (0.33 g, 1.75 mmol). The residue was silica flash column chromatographed (gradient elution, 5-15% EtOAc in hexane) to afford **48d** as colourless oil (0.49 g, 77%).

^{1}H-NMR (400 MHz, DMSO-*d6*): δ 7.61 (1H, br s, CONH), 7.32 (1H, d, J=8.8Hz, H-6'), 6.57 (1H, d, J=2.7Hz, H-3'), 6.44 (1H, d, J=2.7Hz, J=8.8Hz, H-5'), 3.76 (3H, s, OCH_3), 3.73 (3H, s, OCH_3), 3.41–3.32 (m, 8H, NCH_2), 1.42 (9H, s, $C(CH_3)_3$).

N-(3-Methoxyphenyl)piperazine-1-carboxamide **49a:**

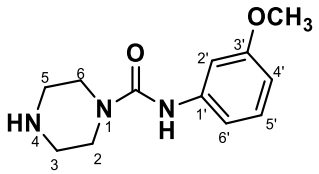

To a solution of **48a** (0.4 g, 1.2 mmol) in dry CH_2Cl_2 (3 mL) was added TFA (3 mL). The solution was stirred at room temperature for 3 h. The mixture was evaporated *in vacuo* and the residue was dissolved in EtOAc, and washed with saturated aqueous $NaHCO_3$. The organic layer was separated and the aqueous layer was extracted with EtOAc. The combined EtOAc extracts were dried over Na_2SO_4 and concentrated *in vacuo*. The residue was silica flash column chromatographed (gradient elution, 2-6% MeOH in CH_2Cl_2) to give **49a** as a colourless semi-solid (0.2 g, 72%).

^{1}H-NMR (400 MHz, DMSO-*d6*): δ 8.88 (1H, br s, NH), 8.70 (1H, br s, NH), 7.15 (1H, d, J=7.8Hz, H-5'), 7.12 (1H, t, J=2.2Hz, H-2'), 7.03 (1H, ddd, J=0.8Hz, J=2.2Hz, J=7.8Hz, H-6'), 6.54 (1H, ddd, J=0.8Hz, J=2.2Hz, J=7.8Hz, H-4'), 3.70 (3H, s, OCH_3), 3.67–3.61 (m, 4H, NCH_2), 3.18–3.10 (m, 4H, NCH_2).

MS ESI (m/z): 236 $[M+H]^+$.

N-(3-Bromophenyl)piperazine-1-carboxamide **49b**:

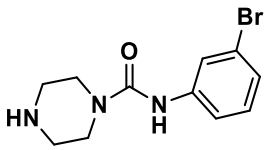

Prepared according to the procedure for **49a,** compound **48b** (0.42 g, 1.1 mmol) was reacted with TFA. The residue was silica flash column chromatographed (gradient elution, 2-4% MeOH in CH_2Cl_2) to give **49b** as a colourless semi-solid (0.21 g, 68%).

^{1}H-NMR (400 MHz, DMSO-*d6*): δ 8.97 (1H, br s, NH), 8.91 (1H, br s, NH), 7.77 (1H, t, J=2.1Hz, H-2'), 7.43 (1H, ddd, J=0.8Hz, J=2.1Hz, J=8.1Hz, H-6'), 7.21 (1H, t, J=8.1Hz, H-5'), 7.13 (1H, ddd, J=0.8Hz, J=2.1Hz, J=8.1Hz, H-4'), 3.70–3.60 (m, 4H, NCH_2), 3.20–3.09 (m, 4H, NCH_2).

MS ESI (m/z): 286 $[M+2]^+$.

N-(3-Chlorophenyl)piperazine-1-carboxamide **49c**:

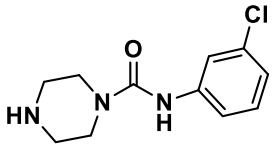

Prepared according to the procedure for **49a**, compound **48c** (0.41 g, 1.2 mmol) was reacted with TFA. The residue was silica flash column chromatographed (gradient elution, 2-4% MeOH in CH_2Cl_2) to give **49c** as a colourless semi-solid (0.19 g, 65%).

^{1}H-NMR (400 MHz, DMSO-*d6*): δ 9.02 (1H, br s, NH), 8.94 (1H, br s, NH), 7.63 (1H, t, J=2.0Hz, H-2'), 7.38 (1H, ddd, J=0.8Hz, J=2.0Hz, J=7.8Hz, H-6'), 7.27 (1H, t, J=7.8Hz, H-5'), 7.13 (1H, ddd, J=0.8Hz, J=2.0Hz, J=7.8Hz, H-4'), 3.70–3.60 (m, 4H, NCH_2), 3.20–3.09 (m, 4H, NCH_2).

MS ESI (m/z): 240 $[M+H]^+$.

N-(2,4-Dimethoxyphenyl)piperazine-1-carboxamide **49d**:

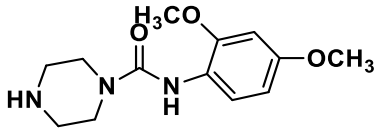

Prepared according to the procedure for **49a**, compound **48d** (0.4 g, 1.1 mmol) was reacted with TFA. The residue was silica flash column chromatographed (gradient elution, 2-6% MeOH in CH_2Cl_2) to give **49d** as a colourless semi-solid (0.21 g, 73%).

^{1}H-NMR (400 MHz, DMSO-*d6*): δ 8.87 (1H, br s, NH), 7.85 (1H, br s, NH), 7.27 (1H, d, J=8.8Hz, H-6'), 6.58 (1H, d, J=2.7Hz, H-3'), 6.46 (1H, d, J=2.7Hz, J=8.8Hz, H-5'), 3.76 (3H, s, OCH_3), 3.74 (3H, s, OCH_3), 3.64–3.50 (m, 4H, NCH_2), 3.15–3.07 (m, 4H, NCH_2).

MS ESI (m/z): 266 $[M+H]^+$.

N-(3-Methoxyphenyl)-4-(6-oxo-1,6-dihydropyridine-3-carbonyl)piperazine-1-carboxamide **50a**:

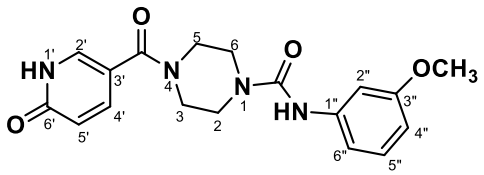

To a solution of 6-oxo-1,6-dihydropyridine-3-carboxylic acid **23** (0.1 g, 0.72 mmol) and *N*-(3-methoxyphenyl)piperazine-1-carboxamide **49a** (0.17 g, 0.72 mmol) in DMF (5 mL) was added HOAt (0.12 g, 0.86 mmol), EDC (0.17 g, 0.86 mmol) and DIEA (0.19 g, 1.44 mmol). The mixture was stirred at room temperature for 12h. The solvent was evaporated *in vacuo* and azeotroped twice with CH_2Cl_2. The residue was silica flash chromatographed (gradient elution, 5-10% MeOH in CH_2Cl_2) to afford **50a** as a colourless semisolid (0.14 g, 54%).

^{1}H-NMR (400 MHz, DMSO-*d6*): δ 11.88 (1H, br s, $N^{1'}$-H), 8.66 (1H, br s, NH), 7.62 (1H, d, J=2.4Hz, H-2'), 7.51 (1H, dd, J=2.4Hz, J=9.4Hz, H-4'), 7.11 (1H, t, J=2.2Hz, H-2"), 7.05 (1H, ddd, J=0.8Hz, J=2.2Hz, J=7.8Hz, H-6"), 6.54 (1H, ddd, J=0.8Hz, J=2.2Hz, J=7.8Hz, H-4"), 6.35 (1H, d, J=9.4Hz, H-5'), 3.74 (3H, s, OCH_3), 3.58–3.44 (m, 8H, NCH_2).

MS ESI (m/z): 357 $[M+H]^+$.

N-(3-Bromophenyl)-4-(6-oxo-1,6-dihydropyridine-3-carbonyl)piperazine-1-carboxamide **50b**:

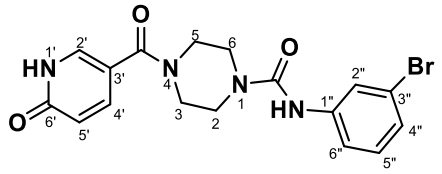

Prepared according to the procedure for **50a**, compound **49b** (0.2 g, 0.72 mmol) was reacted with acid **23** (0.1 g, 0.72 mmol). The residue was silica flash column chromatographed (gradient elution, 2-6% MeOH in CH_2Cl_2) to afford **50b** as a colourless semisolid (0.12 g, 41%).

^{1}H-NMR (400 MHz, DMSO-*d6*): δ 11.88 (1H, br s, $N^{1'}$-H), 8.79 (1H, s, NH), 7.78 (1H, t, J=2.1Hz, H-2"), 7.61 (1H, d, J=2.4Hz, H-2'), 7.52 (1H, dd, J=2.4Hz, J=9.5Hz, H-4'), 7.44 (1H, ddd, J=0.8Hz, J=2.1Hz, J=8.1Hz, H-6"), 7.20 (1H, t, J=8.1Hz, H-5"), 7.11 (1H, ddd, J=0.8Hz, J=2.1Hz, J=8.1Hz, H-4"), 6.36 (1H, d, J=9.5Hz, H-5'), 3.58–3.45 (m, 8H, NCH_2).

MS ESI (m/z): 407 $[M+2]^+$.

N-(3-Chlorophenyl)-4-(6-oxo-1,6-dihydropyridine-3-carbonyl)piperazine-1-carboxamide **50c**:

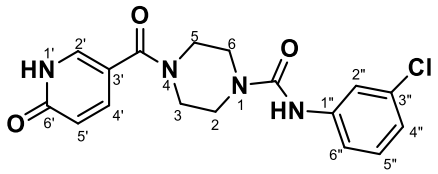

Prepared according to the procedure for **50a**, compound **50c** (0.17 g, 0.72 mmol) was reacted with acid **23** (0.1 g, 0.72 mmol). The residue was silica flash column chromatographed (gradient elution, 2-6% MeOH in CH_2Cl_2) to afford **50c** as a colorless semisolid (0.1 g, 38%).

^{1}H-NMR (400 MHz, DMSO-*d6*): δ 11.88 (1H, br s, $N^{1'}$-H), 8.78 (1H, br s, NH), 7.64 (1H, t, J=2.2Hz, H-2"), 7.61 (1H, d, J=2.4Hz, H-2'), 7.52 (1H, dd, J=2.4Hz, J=9.4Hz, H-4'), 7.39 (1H, ddd, J=0.8Hz, J=2.2Hz, J=8.4Hz, H-6"), 7.26 (1H, t, J=8.4Hz, H-5"), 6.98 (1H, ddd, J=0.8Hz, J=2.2Hz, J=8.4Hz, H-4"), 6.36 (1H, d, J=9.4Hz, H-5'), 3.60–3.45 (m, 8H, NCH_2).
MS ESI (m/z): 361 $[M+H]^+$.

N-(2,4-Dimethoxyphenyl)-4-(6-oxo-1,6-dihydropyridine-3-carbonyl)piperazine-1-carboxamide **50d**:

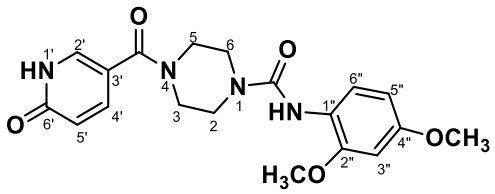

Prepared according to the procedure followed in **50a** compound **50d** (0.19 g, 0.72 mmol) was reacted with acid 23 (0.1 g, 0.72 mmol). The residue was silica flash column chromatographed (gradient elution, 2-10% MeOH in CH_2Cl_2) to afford **50d** as a white semisolid (0.17 g, 61%).

^{1}H-NMR (400 MHz, DMSO-*d6*): δ 11.89 (1H, br s, $N^{1'}$-H), 8.65 (1H, br s, NH), 7.60 (1H, d, J=2.4Hz, H-2'), 7.52 (1H, dd, J=2.4Hz, J=9.4Hz, H-4'), 7.27 (1H, d, J=8.8Hz, H-6"), 6.57 (1H, d, J=2.6Hz, H-3"), 6.45 (1H, dd, J=2.6Hz, J=8.8Hz, H-5"), 6.36 (1H, d, J=9.4Hz, H-5'), 3.77 (3H, s, OCH_3), 3.71 (3H, s, OCH_3), 3.57–3.41 (m, 8H, NCH_2).
MS ESI (m/z): 387 $[M+H]^+$.

1-Methyl-5-nitropyridin-2(*1H*)-one **52**:

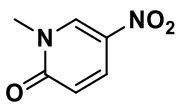

To a solution of 5-nitropyridin-2(1H)-one **51** (2.0 g, 14.28 mmol) in DMF (25 mL) was added NaH (0.74 g, 18.56 mmol) at 0 ^{o}C, and the suspension was stirred at room temperature for 1h. CH_3I (2.2 g, 15.71 mmol) was then added dropwise at 0 ^{o}C, and the mixture was allowed to warm to room temperature and stirred for 6h. Upon reaction completion (monitored by TLC) the solvent was evaporated *in vacuo*. The residue was dissolved in EtOAc and washed with saturated $NaHCO_3$ and water. The organic layer was dried over Na_2SO_4 and concentrated under reduced pressure. The residue was silica flash column chromatographed (gradient elution, 0-4% MeOH in CH_2Cl_2) to afford **52** as a pale yellow solid (1.41 g, 64%).

^{1}H-NMR (400 MHz, DMSO-*d6*): δ 9.20 (1H, d, J=2.9Hz, H-6), 8.13 (1H, dd, J=2.9Hz, J=9.4Hz, H-4), 6.47 (1H, d, J=9.4Hz, H-3), 3.55 (3H, s, CH_3).

MS ESI (m/z): 153 $[M-H]^-$.

5-Aminopyridin-2(*1H*)-one **53:**

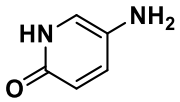

A mixture of **51** (2.0 g, 14.28 mmol) and Pd/C (500mg, 10% w/w) in ethanol (50 mL) was degassed and purged with N_2. The mixture was then hydrogenated at 1 atmosphere pressure for 12 h at room temperature. The mixture was then filtered through a small pad of celite, and concentrated. The residue was silica flash column chromatographed (gradient elution, 10-20% MeOH in CH_2Cl_2) to give **53** as a white solid (1.07 g, 68%).

^{1}H-NMR (400 MHz, DMSO-*d6*): 10.55 (1H, s, N^1-H), 7.03 (1H, dd, J=2.9Hz, J=9.4Hz, H-4), 6.74 (1H, d, J=2.9Hz, H-6), 6.21 (1H, d, J=9.4Hz, H-3), 4.25 (2H, s, NH_2).

MS ESI (m/z): 111 $[M+H]^+$.

1-Methyl-5-nitropyridin-2(*1H*)-one **54**:

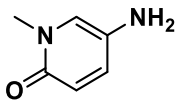

Prepared following the procedure for **53**, compound **52** (2.2 g, 14.28 mmol) was hydrogenated. The crude mixture was silica flash column chromatographed (gradient elution, 5-10% MeOH in CH_2Cl_2) to afford **54** as a white solid (1.3 g, 74%).

^{1}H-NMR (400 MHz, DMSO-*d6*): δ 7.04 (1H, dd, J=2.9Hz, J=9.4Hz, H-4), 6.38 (1H, d, J=2.9Hz, H-6), 6.23 (1H, d, J=9.4Hz, H-3), 4.31 (2H, s, NH_2), 3.32 (3H, s, CH_3).

MS ESI (m/z): 125 $[M+H]^+$.

1-Benzoyl-3-(6-oxo-1,6-dihydropyridin-3-yl) thiourea **55**

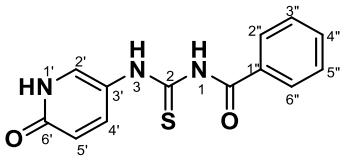

To a solution of **53** (1.0 g, 9.08 mmol) in acetonitrile (12 mL) was added benzoyl isothiocyanate (1.34 mL, 9.97 mmol). The mixture was stirred at ambient temperature for 6h. After completion of reaction (TLC monitoring) the precipitate was filtered, washed with acetonitrile, and dried to afford the product **55** as a brick red solid (1.86 g, 75%).

^{1}H-NMR (400 MHz, DMSO-*d6*): δ 12.01 (1H, br s, NH), 11.64 (2H, br s, NH), 8.01-7.92 (2H, m, H-2",6"), 7.70-7.62 (2H, m, H-4', 4"), 7.58-7.49 (3H, m, H-2',3",5"), 6.36 (1H, d, J=9.4Hz, H-5').

MS ESI (m/z): 272 $[M-H]^-$.

1-Benzoyl-3-(1-methyl-6-oxo-1,6-dihydropyridin-3-yl) thiourea **56**:

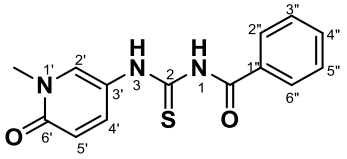

Prepared according to the procedure for **55**, compound **54** (1.13 g, 9.08 mmol) was reacted with benzoyl isothiocyanate (1.34 mL, 9.97 mmol) to afford **56** as a brick red solid (2.04 g, 78%).

^{1}H-NMR (400 MHz, DMSO-*d6*): δ 12.01 (1H, br s, NH), 11.69 (1H, br s, NH), 7.99-7.94 (3H, m, H-4',2",6"), 7.70-7.63 (1H, m, H-4"), 7.58-7.50 (3H, m, H-2',3",5"), 6.40 (1H, d, J=9.5Hz, H-5'), 3.43 (3H, s, CH_3).

MS ESI (m/z): 286 $[M-H]^-$.

1-(6-Oxo-1,6-dihydropyridin-3-yl)thiourea **57:**

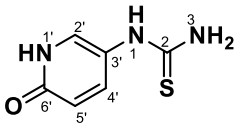

To a suspension of **55** (1.0 g, 3.66 mmol) in MeOH (10 mL) was added aqueous NaOH (0.1 g in 1 mL H_2O) at room temperature. The reaction mixture was heated to 70 ^oC for 2h. After completion of reaction (TLC monitoring), the precipitated compound was separated and

washed on the filter with water and dried under high vacuum to give **57** as a white solid (0.43 g, 70%). The obtained product was taken to the next step without further purification.

^{1}H-NMR (400 MHz, DMSO-*d6*): δ 11.47 (1H, br s, NH), 9.09 (1H, br s, NH), 7.67-7.04 (4H, m, H-2',4', NH_2), 6.30 (1H, d, J=8.9Hz, H-5').

MS ESI (m/z): 168 $[M-H]^-$.

1-(1-Methyl-6-oxo-1,6-dihydropyridin-3-yl)thiourea **58**:

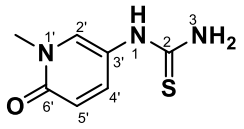

Prepared according to the procedure followed in **57,** treatment of compound **56** (1.05 g, 3.66 mmol) with aqueous NaOH afforded **58** as a white solid (0.5 g, 75%).

^{1}H-NMR (400 MHz, DMSO-*d6*): δ 9.09 (1H, s, NH), 8.14-6.89 (4H, m, H-2',4', NH_2), 6.33 (1H, d, J=8.9Hz, H-5'), 3.38 (3H, s, CH_3).

MS ESI (m/z): 182 $[M-H]^-$.

Ethyl 2-((6-oxo-1,6-dihydropyridin-3-yl)amino)thiazole-4-carboxylate **61:**

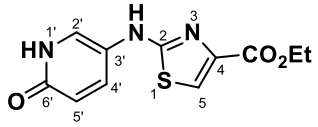

To a suspension of 1-(6-oxo-1,6-dihydropyridin-3-yl) thiourea **57** (1.5 g, 8.87 mmol) in EtOH (15 ml), ethyl bromopyruvate (1.11 mL, 8.87 mmol) was added, and the mixture was heated at 90 ^oC for 3 h. After cooling to room temperature, the solvent was removed under reduced pressure. The resulting crystalline solid was collected by filtration, washed with cold ethanol and dried to give **61** as an off white solid (1.6 g, 68%). The obtained product was taken forward to the next step without further purification.

^{1}H-NMR (400 MHz, DMSO-*d6*): δ 10.26 (1H, br s, NH), 8.30 (1H, d, J=2.3Hz, H-2'), 7.75 (1H, s, H-5), 7.62 (1H, dd, J=2.3Hz, J=9.5Hz, H-4'), 6.63 (1H, d, J=9.5Hz, H-5'), 4.25 (2H, q, J=7.1Hz, CH_2), 1.28 (t, 3H, J=7.1Hz, CH_3).

MS ESI (m/z): 266 $[M+H]^+$.

Ethyl 2-((1-methyl-6-oxo-1,6-dihydropyridin-3-yl)amino)thiazole-4-carboxylate **62**:

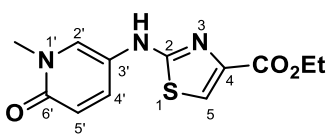

Prepared according to the procedure followed in **61** compound **58** (1.63 g, 8.87 mmol) was converted to tiazole **62**, isolated as an off white solid (1.81 g, 73%).

^{1}H-NMR (400 MHz, DMSO-*d6*): δ 9.91 (1H, br s, NH), 8.21 (1H, d, J=2.4Hz, H-2'), 7.70 (1H, s, H-5), 7.46 (1H, dd, J=2.4Hz, J=9.4Hz, H-4'), 6.46 (1H, d, J=9.4Hz, H-5'), 4.24 (2H, q, J=7.1Hz, CH_2), 3.43 (3H, s, NCH_3), 1.28 (t, 3H, J=7.1Hz, CH_3).

MS ESI (m/z): 279 $[M+H]^+$.

2-((6-Oxo-1,6-dihydropyridin-3-yl)amino)thiazole-4-carboxylic acid **63:**

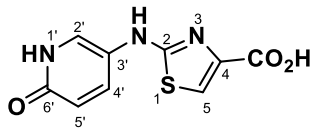

To a stirred suspension of **61** (1.0 g, 3.77 mmol) in ethanol (10ml), sodium hydroxide (0.45g, 11.31 mmol) in water (5 mL) was added. The mixture was heated at 90 ºC for 12 h. The mixture was then concentrated *in vacuo*, and the residue was dissolved in water (10 mL), and the pH was adjusted to PH-4 by careful addition of 1N HCl. The precipitate was isolated by filtration, washed by water then MeOH, and dried *in vacuo* to afford the compound **63** as a brick red solid (0.63 g, 71%). The obtained product was taken forward to the next step without further purification.

^{1}H-NMR (400 MHz, DMSO-*d6*): δ 12.07 (1H, br s, COOH), 9.98 (1H, br s, NH), 8.15 (1H, d, J=2.8Hz, H-2'), 7.65 (1H, s, H-5), 7.45 (dd, 1H, J=2.8Hz, J=9.7Hz, H-4'), 6.41 (1H, d, J=9.7Hz, H-5').

MS ESI (m/z): 236 $[M-H]^-$, **HRMS:** m/z calculated for $C_9H_7N_3O_3S^-$: 236.01354, found: 236.01328.

2-((1-Methyl-6-oxo-1,6-dihydropyridin-3-yl)amino)thiazole-4-carboxylic acid **64**:

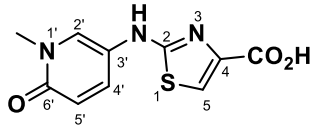

Prepared according to the procedure for **63** compound **62** (1.05 g, 3.77 mmol) was hydrolyzed to afford **64** as a brick red solid (0.69 g, 73%).

^{1}H-NMR (400 MHz, DMSO-*d6*): δ 12.65 (1H, br s, COOH), 9.83 (1H, br s, NH), 8.19 (1H, d, J=2.5Hz, H-2'), 7.64 (1H, s, H-5), 7.45 (dd, 1H, J=2.5Hz, J=9.5Hz, H-4'), 6.43 (1H, d, J=9.5Hz, H-5'), 3.43 (3H, s, NCH_3).

MS ESI (m/z): 250 $[M-H]^-$.

2-((6-Oxo-1,6-dihydropyridin-3-yl)amino)-*N*-phenylthiazole-4-carboxamide **65a**:

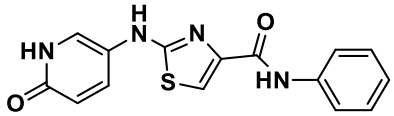

To a solution of the acid **63** (0.07 g, 0.3 mmol) and aniline (0.044 g, 0.48 mmol) in DMF (5 mL), was added HOAt (0.04 g, 0.32 mmol), EDC (0.06 g, 0.32 mmol) and DIEA (0.12 g, 0.9 mmol). The mixture was stirred at ambient temperature for 24h, and then concentrated *in vacuo.* The residue was dry-loaded onto a silica column and column chromatographed (gradient elution, 2-10% MeOH in CH_2Cl_2) to afford **65a** as a pale yellow solid (0.04 g, 44%).

^{1}H-NMR (400 MHz, DMSO-*d6*): see Table 27.

^{13}C NMR (100MHz, DMSO-*d6*): δ 164.5, 160.8, 159.7, 146.3, 138.8, 136.2, 135.0, 129.1, 128.8, 125.6, 124.3, 122.7, 120.8, 120.0, 114.4.

MS ESI (m/z): 311 $[M-H]^-$, **HRMS:** m/z calculated for $C_{15}H_{12}N_4O_2S^-$: 311.06082, found: 311.06113.

2-((6-Oxo-1,6-dihydropyridin-3-yl)amino)-*N*-(*p*-tolyl)thiazole-4-carboxamide **65b**:

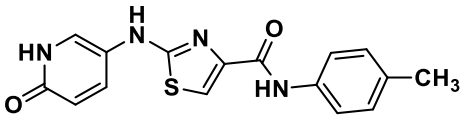

Following the procedure for **65a**, *p*-toluidine (0.05 g, 0.48 mmol) was reacted with acid **63** (0.07 g, 0.3 mmol). The crude product mxture was separated by silica flash column chromatography (gradient elution, 2-10% MeOH in CH_2Cl_2) to afford **65b** as a beige solid (0.07 g, 46%).

^{1}H-NMR (400 MHz, DMSO-*d6*): see Table 27.

MS ESI (m/z): 325 $[M-H]^-$, **HRMS:** m/z calculated for $C_{16}H_{14}N_4O_2S^-$: 325.07647, found: 325.07657.

N-(4-Methoxyphenyl)-2-((6-oxo-1,6-dihydropyridin-3-yl)amino)thiazole-4-carboxamide **65c**:

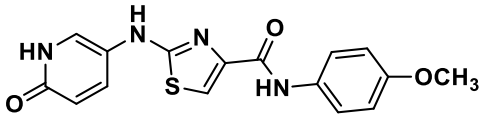

Following the procedure for **65a**, *p*-anisidine (0.06 g, 0.48 mmol) was reacted with acid **63** (0.07 g, 0.3 mmol). The crude product mxture was separated by silica flash column chromatography (gradient elution, 2-12% MeOH in CH_2Cl_2) to afford **65c** as a white solid (0.076 g, 48%).

^{1}H-NMR (400 MHz, DMSO-*d6*): see Table 27.

MS ESI (m/z): 341 $[M-H]^-$, **HRMS:** m/z calculated for $C_{16}H_{14}N_4O_3S^-$: 341.07138, found: 341.07138.

N-(2,3-Dimethylphenyl)-2-((6-oxo-1,6-dihydropyridin-3-yl)amino)thiazole-4-carboxamide **65d**:

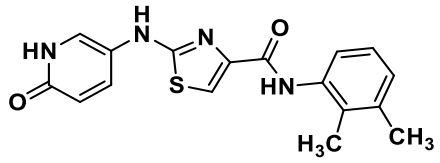

Following the procedure for **65a**, 2,3-dimethylaniline (0.06 g, 0.5 mmol) was reacted with acid **63** (0.073 g, 0.31 mmol). The crude product mxture was separated by silica flash column chromatography (gradient elution, 2-10% MeOH in CH_2Cl_2) to afford **65d** as a beige solid (0.095 g, 56%).

^{1}H-NMR (400 MHz, DMSO-d6): see Table 27.

MS ESI (m/z): 339 $[M-H]^-$, **HRMS:** m/z calculated for $C_{17}H_{16}N_4O_2S^-$: 339.09212, found: 339.09213.

N-(3,5-Dimethoxyphenyl)-2-((6-oxo-1,6-dihydropyridin-3-yl)amino)thiazole-4-carboxamide **65e**:

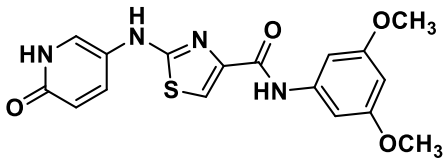

Following the procedure for **65a**, 3,5-dimethoxyaniline (0.076 g, 0.5 mmol) was reacted with acid **63** (0.073 g, 0.31 mmol). The crude product mxture was separated by silica flash column chromatography (gradient elution, 4-14% MeOH in CH_2Cl_2) to afford **65e** as a pale beige solid (0.1 g, 55%).

^{1}H-NMR (400 MHz, DMSO-d6): see Table 27.

^{13}C NMR (100MHz, DMSO-*d6*): δ 164.5, 160.9, 160.8, 159.7, 146.2, 140.5, 136.2, 132.5, 125.5, 122.6, 120.1, 117.2, 114.5, 99.0, 96.2, 55.6, 54.0.

MS ESI (m/z): 371 $[M-H]^-$, **HRMS:** m/z calculated for $C_{17}H_{16}N_4O_4S^-$: 371.08195, found: 371.08191.

N-(4-(Dimethylamino)phenyl)-2-((6-oxo-1,6-dihydropyridin-3-yl)amino)thiazole-4-carboxamide **65f**:

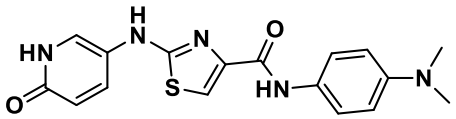

Following the procedure for **65a**, *N*,*N*-dimethyl-*p*-phenylenediamine (0.076 g, 0.5 mmol) was reacted with acid **63** (0.073 g, 0.31 mmol). The crude product mxture was separated by silica flash column chromatography (gradient elution, 2-8% MeOH in CH_2Cl_2) to afford **65f** as dark green solid (0.08 g, 47%).

^{1}H-NMR (400 MHz, DMSO-d6): see Table 27.

MS ESI (m/z): 354 $[M-H]^-$, **HRMS:** m/z calculated for $C_{17}H_{17}N_5O_2S^-$: 354.10302, found: 354.10336.

2-((6-Oxo-1,6-dihydropyridin-3-yl)amino)-*N*-(pyridin-3-yl)thiazole-4-carboxamide **65g**:

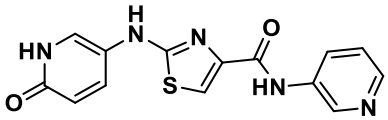

Following the procedure for **65a**, 3-aminopyridine (0.044 g, 0.48 mmol) was reacted with acid **63** (0.07 g, 0.3 mmol). The crude product mxture was separated by silica flash column chromatography (gradient elution, 4-15% MeOH in CH_2Cl_2) to afford **65g** as a white solid (0.046 g, 31%).

^{1}H-NMR (400 MHz, DMSO-d6): see Table 27.

MS ESI (m/z): 312 $[M-H]^-$, **HRMS:** m/z calculated for $C_{14}H_{11}N_5O_2S^-$: 312.05607, found: 312.05637.

N-(6-Methoxypyridin-3-yl)-2-((6-oxo-1,6-dihydropyridin-3-yl)amino)thiazole-4-carboxamide **65h**:

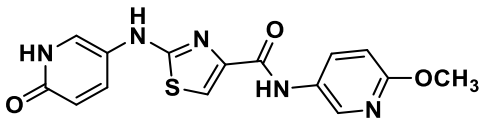

Following the procedure for **65a**, 5-amino-2-methoxypyridine (0.06 g, 0.48 mmol) was reacted with acid **63** (0.07 g, 0.3 mmol). The crude product mxture was separated by silica

flash column chromatography (gradient elution, 4-15% MeOH in CH_2Cl_2) to afford **65h** as pale beige solid (0.05 g, 30%).

^{1}H-NMR (400 MHz, DMSO-d6): see Table 27.

^{13}C NMR (100MHz, DMSO-*d6*): δ 164.5, 160.8, 160.5, 159.9, 146.0, 139.7, 136.2, 133.3, 129.8, 125.6, 122.8, 120.0, 114.5, 110.4, 53.9.

MS ESI (m/z): 342 $[M-H]^-$, **HRMS:** m/z calculated for $C_{15}H_{13}N_5O_3S^-$: 342.06663, found: 342.06683.

2-((6-Oxo-1,6-dihydropyridin-3-yl)amino)-*N*-(quinolin-6-yl)thiazole-4-carboxamide **65i**:

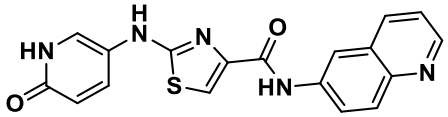

Following the procedure for **65a**, 6-aminoquinoline (0.07 g, 0.48 mmol) was reacted with acid **63** (0.07 g, 0.3 mmol). The crude product mxture was separated by silica flash column chromatography (gradient elution, 4-15% MeOH in CH_2Cl_2) to afford **65j** as a pale beige solid (0.03 g, 18%).

^{1}H-NMR (400 MHz, DMSO-d6): see Table 27.

MS ESI (m/z): 362 $[M-H]^-$, **HRMS:** m/z calculated for $C_{18}H_{13}N_5O_2S^-$: 362.07172, found: 362.07202.

N-(2,3-Dihydrobenzo[*b*][1,4]dioxin-6-yl)-2-((6-oxo-1,6-dihydropyridin-3-yl)amino)thiazole-4-carboxamide **65j**:

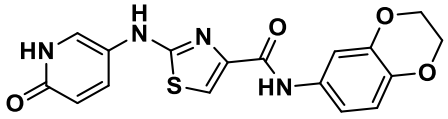

Following the procedure for **65a**, 1,4-benzodioxan-6-amine (0.07 g, 0.48 mmol) was reacted with acid **63** (0.07 g, 0.3 mmol). The crude product mxture was separated by silica flash column chromatography (gradient elution, 2-10% MeOH in CH_2Cl_2) to afford **65j** as an off white solid (0.06 g, 35%).

^{1}H-NMR (400 MHz, DMSO-d6): see Table 27.

^{13}C NMR (100MHz, DMSO-*d6*): δ 164.4, 160.7, 159.4, 146.4, 143.4, 140.2, 136.2, 132.5, 125.5, 122.6, 120.1, 117.2, 114.0, 109.8, 64.7, 64.4.

MS ESI (m/z): 369 $[M-H]^-$, **HRMS:** m/z calculated for $C_{17}H_{14}N_4O_4S^-$: 369.06630, found: 369.06662.

N-(*1H*-Indol-5-yl)-2-((6-oxo-1,6-dihydropyridin-3-yl)amino)thiazole-4-carboxamide **65k**:

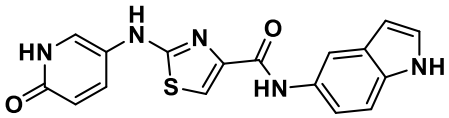

Following the procedure for **65a**, 6-aminoindole (0.06 g, 0.48 mmol) was reacted with acid **63** (0.07 g, 0.3 mmol). The crude product mxture was separated by silica flash column chromatography (gradient elution, 4-15% MeOH in CH_2Cl_2) to afford **65k** as a pale brown solid (0.03 g, 19%).

^{1}H-NMR (400 MHz, DMSO-d6): see Table 27.

MS ESI (m/z): 350 $[M-H]^-$, **HRMS:** m/z calculated for $C_{17}H_{13}N_5O_2S^-$: 350.07172, found: 350.07196.

N-(*1H*-Benzo[*d*]imidazol-6-yl)-2-((6-oxo-1,6-dihydropyridin-3-yl)amino)thiazole-4-carboxamide **65l**:

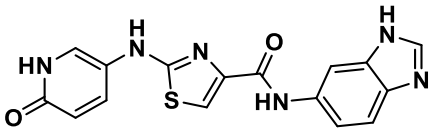

Following the procedure for **65a**, 6-aminobenzimidazole (0.06 g, 0.48 mmol) was reacted with acid **63** (0.07 g, 0.3 mmol). The crude product mxture was separated by silica flash column chromatography (gradient elution, 4-15% MeOH in CH_2Cl_2) to afford **65l** as a pale pink solid (0.02 g, 13%).

^{1}H-NMR (400 MHz, DMSO-d6): see Table 27.

MS ESI (m/z): 351 $[M-H]^-$, **HRMS:** m/z calculated for $C_{16}H_{12}N_6O_2S^-$: 351.06697, found: 351.06711.

N-(Benzo[*d*]thiazol-6-yl)-2-((6-oxo-1,6-dihydropyridin-3-yl)amino)thiazole-4-carboxamide **65m**:

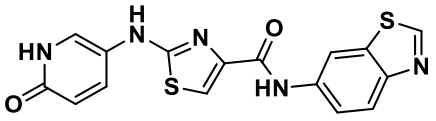

Following the procedure for **65a**, 6-aminobenzothiazole (0.07 g, 0.48 mmol) was reacted with acid **63** (0.07 g, 0.3 mmol). The crude product mxture was separated by silica flash column chromatography (gradient elution, 2-8% MeOH in CH_2Cl_2) to afford **65m** as an off white solid (0.06 g, 34%).

^{1}H-NMR (400 MHz, DMSO-d6): see Table 27.

MS ESI (m/z): 368 $[M-H]^-$, **HRMS:** m/z calculated for $C_{16}H_{11}N_5O_2S_2^-$: 368.02814, found: 368.02817.

N-Benzyl-2-((6-oxo-1,6-dihydropyridin-3-yl)amino)thiazole-4-carboxamide **65n**:

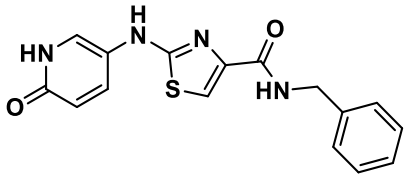

Following the procedure for **65a**, benzylamine (0.05 g, 0.48 mmol) was reacted with acid **63** (0.07 g, 0.3 mmol). The crude product mxture was separated by silica flash column chromatography (gradient elution, 2-8% MeOH in CH_2Cl_2) to afford **65n** as a pale green solid (0.087 g, 56%).

^{1}H-NMR (400 MHz, DMSO-d6): see Table 27.

MS ESI (m/z): 325 $[M-H]^-$, **HRMS:** m/z calculated for $C_{16}H_{14}N_4O_2S^-$: 325.07647, found: 325.07666.

N-(*1H*-Indazol-5-yl)-2-((6-oxo-1,6-dihydropyridin-3-yl)amino)thiazole-4-carboxamide **65o**:

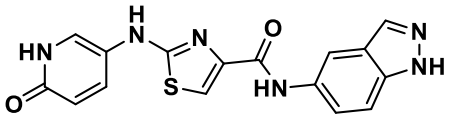

Following the procedure for **65a**, 5-aminoindazole (0.06 g, 0.47 mmol) was reacted with acid **63** (0.07 g, 0.3 mmol). The crude product mxture was separated by silica flash column chromatography (gradient elution, 2-14% MeOH in CH_2Cl_2) to afford **65o** as a pale beige solid (0.03 g, 20%).

^{1}H-NMR (400 MHz, DMSO-d6): see Table 27.

MS ESI (m/z): 351 $[M-H]^-$, **HRMS:** m/z calculated for $C_{16}H_{12}N_6O_2S^-$: 351.06697, found: 351.0672.

N-(2-Methyl-*2H*-indazol-5-yl)-2-((6-oxo-1,6-dihydropyridin-3-yl)amino)thiazole-4-carboxamide **65p**:

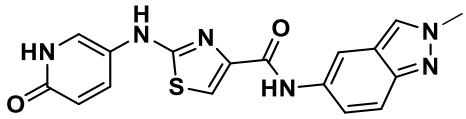

Following the procedure for **65a**, 2-methyl-2H-indazol-5-amine (0.07 g, 0.48 mmol) was reacted with acid (0.07 g, 0.3 mmol). The crude product mxture was separated by silica flash

column chromatography (gradient elution, 2-10% MeOH in CH_2Cl_2) to afford **65p** as a pale green solid (0.046 g, 26%).

^{1}H-NMR (400 MHz, DMSO-d6): see Table 27.

MS ESI (m/z): 365 $[M-H]^-$, **HRMS:** m/z calculated for $C_{17}H_{14}N_6O_2S^-$: 365.08262, found: 365.08252.

Table 27: NMR data of compounds **65a-p**

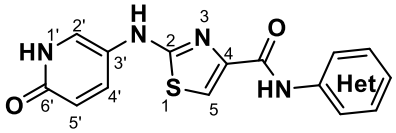

Entry		Scaffold ^{1}H-NMR (400 MHz, DMSO-d6) δ ppm	R ^{1}H-NMR (400 MHz, DMSO-d6) δ ppm
65a	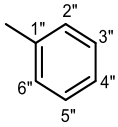	11.37 (1H, br s, N$^{1'}$-H), 9.92 (1H, br s, C_2-NH), 9.68 (1H, br s, CO-NH), 8.10 (1H, d, J=2.9Hz, H-2'), 7.57 (1H, s, H-5) 7.55-7.32* (3H, m, H-4'), 6.40 (1H, d, J=9.6Hz, H-5')	7.78-7.72 (2H, m, H-2",6") 7.55-7.32* (3H, m, H-3",5"), 7.11 (1H, t, J=7.4Hz, H-4")
65b	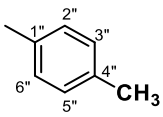	11.32 (1H, br s, N$^{1'}$-H), 9.93 (1H, br s, C_2-NH), 9.61 (1H, s, CO-NH), 8.11 (1H, d, J=2.9Hz, H-2'), 7.57 (1H, s, H-5), 7.53 (1H, dd, J=2.9Hz, J=9.6Hz, H-4'), 6.40 (1H, d, J=9.6Hz, H-5')	7.63 (2H, d, J=8.2Hz, H-2",6"), 7.16 (2H, d, J=8.2Hz, H-3",5"), 2.28 (3H, s, CH_3)
65c	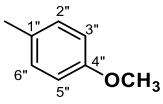	11.30 (1H, br s, N$^{1'}$-H), 9.91 (1H, br s, C_2-NH), 9.60 (1H, s, CO-NH), 8.10 (1H, d, J=2.9Hz, H-2'), 7.55-7.52 (2H, m, H-5,4'), 6.40 (1H, d, J=9.7Hz, H-5')	7.65 (2H, d, J=9.1Hz, H-2",6"), 6.93 (2H, d, J=9.1Hz, H-3",5"), 3.75 (3H, s, OCH_3)
65d	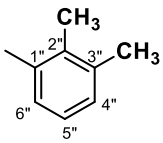	11.34 (1H, br s, N$^{1'}$-H), 9.97 (1H, br s, C_2-NH), 9.41 (1H,br s, CO-NH), 8.01 (1H, d, J=2.7Hz, H-2'), 7.67-7.50* (3H, m, H-5,4'), 6.40 (1H, d, J=9.6Hz)	7.67-7.50* (3H, m, H-6"), 7.11 (1H, t, J=7.7Hz, H-5"), 7.03 (1H, d, J=7.7Hz, H-4"), 2.29 (3H, s, CH_3), 2.16 (3H, s, CH_3)

Entry		Scaffold ^{1}H-NMR (400 MHz, DMSO-d6) δ ppm	R ^{1}H-NMR (400 MHz, DMSO-d6) δ ppm
65e	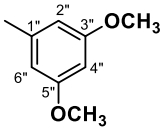	11.39 (1H, br s, $N^{1'}$-H), 9.96 (1H, br s, C_2-NH), 9.65 (1H, br s, CO-NH), 8.14 (1H, d, J=2.9Hz, H-2'), 7.60 (1H, s, H-5), 7.51 (1H, dd, J=2.9Hz, J=9.6Hz, H-4'), 6.41 (1H, d, J=9.6Hz, H-5')	7.06 (2H, d, J=2.2Hz, H-2",6"), 6.29 (1H, t, J=2.2Hz, H-4"), 3.74 (6H, s, 2 OCH_3)
65f	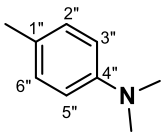	11.30 (1H, br s, $N^{1'}$-H), 9.91 (1H, br s, C_2-NH), 9.60 (1H, br s, CO-NH), 8.10 (1H, d, J=2.9Hz, H-2'), 7.61-7.45* (4H, m, H-5,4'), 6.40 (1H, d, J=9.7Hz, H-5')	7.61-7.45* (4H, m, H-2",6"), 6.72 (2H, d, J=9.1Hz, H-3",5"), 3.33 (6H, s, 2 CH_3)
65g	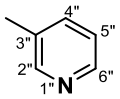	11.34 (1H, br s, $N^{1'}$-H), 9.99 (1H, br s, C_2-NH), 9.95 (1H, br s, CO-NH), 8.13 (1H, d, J=2.9Hz, H-2'), 7.64 (1H, s, H-5), 7.53 (1H, dd, J=2.9Hz, J=9.6Hz, H-4'), 6.40 (1H, d, J=9.6Hz, H-5')	8.91 (1H, d, J=2.3Hz, H-2"), 8.32 (1H, dd, J=1.4Hz, J=4.7Hz, H-6"), 8.20 (1H, ddd, J=1.4Hz, J=2.3Hz, J=8.2Hz, H-4"), 7.40 (1H, dd, J=4.7Hz, J=8.2Hz, H-5")
65h	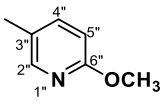	11.34 (1H, br s, $N^{1'}$-H), 9.90 (1H, br s, C_2-NH), 9.83 (1H, br s, CO-NH), 8.11 (1H, d, J=2.9Hz, H-2'), 7.59 (1H, s, H-5), 7.55 (1H, dd, J=2.9Hz, J=9.2Hz, H-4'), 6.40 (1H, d, J=9.2Hz, H-5')	8.50 (1H, d, J=2.7Hz, H-2"), 8.05 (1H, dd, J=2.7Hz, J=8.9Hz, H-4"), 6.84 (1H, d, J=8.9Hz, H-5"), 3.84 (3H, s, OCH_3)
65i	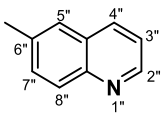	11.34 (1H, br s, $N^{1'}$-H), 10.14 (1H, br s, C_2-NH), 10.03 (1H, br s, CO-NH), 8.09 (1H, d, J=2.9Hz, H-2'), 7.59 (1H, s, H-5), 7.77-7.70* (2H, m, H-4'), 6.43 (1H, d, J=9.2Hz, H-5')	8.68 (1H, dd, J=1.6Hz, J=4.2Hz, H-2"), 8.58 (1H, d, J=9.0Hz, H-7"), 8.47 (1H, dd, J=1.6Hz, J=8.6Hz, H-4"), 8.03 (1H, d, J=9.0Hz, H-8"), 7.77-7.70* (2H, m, H-5"), 7.46 (1H, dd, J=4.2Hz, J=8.6Hz, H-3")
65j	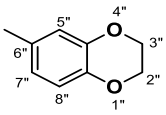	11.32 (1H, br s, $N^{1'}$-H), 9.91 (1H, br s, C_2-NH), 9.55 (1H, br s, CO-NH), 8.10 (1H, d, J=2.9Hz, H-2'), 7.67 (1H, s, H-5), 7.52 (1H, dd, J=2.9Hz, J=9.6Hz, H-4'), 6.39 (1H, d, J=9.6Hz, H-5')	7.37 (1H, d, J=2.5Hz H-5"), 7.18 (1H, dd, J=2.5Hz, J=8.8Hz, H-7"), 6.83 (1H, d, J=8.8Hz, H-8"), 4.24 (4H, dd, J=5.1Hz, J=8.8Hz, 2 OCH_2)

Entry		Scaffold ^{1}H-NMR (400 MHz, DMSO-d6) δ ppm	R ^{1}H-NMR (400 MHz, DMSO-d6) δ ppm
65k	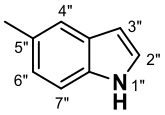	11.34 (1H, br s, $N^{1'}$-H), 10.02 (1H, br s, C_2-NH), 9.51 (1H, br s, CO-NH), 8.15 (1H, d, J=2.7Hz, H-2'), 7.55 (1H, s, H-5), 7.40-7.32* (3H, m, H-4'), 6.44-6.38* (2H, m, H-5')	11.07 (1H, br s, $N^{1''}$-H) 7.95 (1H, s, H-2"), 7.57 (1H, d, J=2.7Hz, H-4"), 7.40-7.32* (3H, m, H-6",7"), 6.44-6.38* (2H, m, H-3")
65l	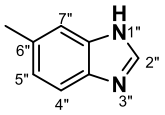	11.33 (1H, br s, $N^{1'}$-H), 9.95 (1H, br s, C_2-NH), 9.71 (1H, s, CO-NH), 8.14 (1H, d, J=2.7Hz, H-2'), 7.59 (1H, s, H-5), 7.58-7.50* (2H, m, H-4'), 6.41 (1H, d, J=9.2Hz, H-5')	12.44 (1H, s, $N^{1''}$-H) 8.18 (1H, s, H-2"), 8.16 (1H, s, H-7") 7.58-7.50* (2H, m, H-4"), 7.45 (1H, d, J=8.6Hz, H-5")
65m	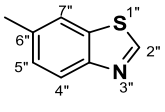	11.37 (1H, br s, $N^{1'}$-H), 10.01 (1H, br s, C_2-NH), 9.97 (1H, br s, CO-NH), 8.15 (1H, d, J=2.9Hz, H-2'), 7.65 (1H, s, H-5), 7.55 (1H, dd, J=2.9Hz, J=9.6Hz, H-4'), 6.41 (1H, d, J=9.6Hz, H-5')	9.31 (1H, s, H-2"), 8.64 (1H, d, J=2.1Hz, H-7"), 8.07 (1H, d, J=8.8Hz, H-4"), 7.86 (1H, dd, J=2.1Hz, J=8.8Hz, H-5")
65n	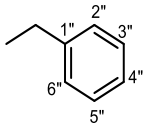	11.22 (1H, br s, $N^{1'}$-H), 9.82 (1H, br s, C_2-NH), 8.57 (1H, t, J=6.3Hz, CO-NH), 7.99 (1H, d, J=2.8Hz, H-2'), 7.58 (1H, dd, J=2.8Hz, J=9.6Hz, H-4'), 7.44 (1H, s, H-5), 6.38 (d, 1H, J=9.6Hz, H-5')	7.36-7.27 (4H, m, H-2",3",5",6"), 7.26-7.19 (1H, m, H-4"), 4.51 (1H, d, J=6.4Hz, CH_2)
65o	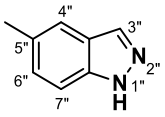	11.37 (1H, br s, $N^{1'}$-H), 9.94 (1H, br s, C_2-NH), 9.74 (1H, br s, CO-NH), 8.13 (1H, d, J=2.8Hz, H-2'), 7.59 (1H, s, H-5), 7.58-7.49* (2H,m, H-4'), 6.41 (1H, d, J=9.6Hz, H-5')	13.03 (1H, s, $N^{1''}$-H), 8.21 (1H, d, J=1.9Hz, H-4"), 8.06 (1H, s, H-3"), 7.62 (1H, dd, J=1.9Hz, J=8.9Hz, H-6"), 7.58-7.49* (2H, m, H-7")
65p	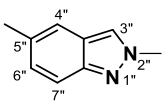	11.37 (1H, br s, $N^{1'}$-H), 9.95 (1H, br s, C_2-NH), 9.65 (1H, br s, CO-NH), 8.13 (1H, d, J=2.9Hz, H-2'), 7.62-7.51* (3H, m, H-5), 7.46 (1H, dd, J=2.0Hz, J=9.6Hz, H-4'), 6.42 (1H, d, J=9.6Hz, H-5')	8.30 (1H, s, H-3"), 8.20 (1H, d, J=1.8Hz, H-4") 7.62-7.51* (3H, m, H-6", 7"), 4.16 (3H, s, CH_3)

N-(*1H*-Indazol-5-yl)-2-((1-methyl-6-oxo-1,6-dihydropyridin-3-yl)amino)thiazole-4-carboxamide **66o**:

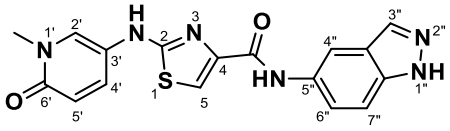

To a solution of the acid **64** (0.12 g, 0.5 mmol) and the 5-aminoindazole (0.07 g, 0.51 mmol) in DMF (5 mL), was added HOAt (0.074 g, 0.55 mmol), EDC (0.11 g, 0.55 mmol) and DIEA (0.16 g, 1.25 mmol). The mixture was stirred at ambient temperature for 24h. The solvent was removed *in vacuo* and the residue was silica flash column chromatographed (gradient elution, 2-12% MeOH in CH_2Cl_2) to afford **66o** as a pale green solid (0.03 g, 18%).

^{1}H-NMR (400 MHz, DMSO-d6): δ 13.03 (1H, s, $N^{1"}$-H), 9.99 (1H, s, C_2-NH), 9.89 (1H, s, CO-NH), 8.58 (1H, d, J=2.9Hz, H-2'), 8.27 (1H, d, J=1.8Hz, H-4"), 8.06 (1H, s, H-3"), 7.65 (1H, dd, J=1.8Hz, J=8.9Hz, H-6"), 7.61 (1H, s, H-5), 7.43 (1H, dd, J=2.9Hz, J=9.6Hz, H-4'), 7.53 (1H, d, J=8.9Hz, H-7"), 6.45 (1H, d, J=9.6Hz, H-5'), 3.53 (3H, s, N^1-CH_3).

^{13}C NMR (100MHz, DMSO-*d6*): δ 164.1, 160.4, 159.6, 146.5, 140.1, 137.6, 135.4, 134.0, 131.8, 128.9, 123.1, 122.0, 121.1, 114.5, 111.6, 110.5, 37.7.

MS ESI (m/z): 365 $[M-H]^-$, **HRMS:** m/z calculated for $C_{17}H_{14}N_6O_2S^-$: 365.08262, found: 365.08279.

N-(2-Methyl-*2H*-indazol-5-yl)-2-((1-methyl-6-oxo-1,6-dihydropyridin-3-yl)amino)thiazole-4-carboxamide **66p**:

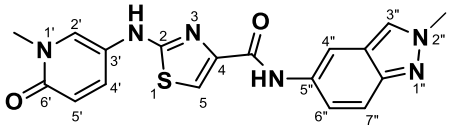

Prepared according to the procedure for **66o**, acid **64** was reacted with 2-methyl-2H-indazol-5-amine (0.073 g, 0.5 mmol). The residue was silica flash column chromatographed (gradient elution, 2-10% MeOH in CH_2Cl_2) to afford **66p** as a dark green solid (0.042 g, 24%).

^{1}H-NMR (400 MHz, DMSO-d6): δ 9.99 (1H, s, C_2-NH), 9.80 (1H, s, CO-NH), 8.58 (1H, d, J=2.9Hz, H-2'), 8.30 (1H, s, H-3"), 8.27 (1H, d, J=1.8Hz, H-4"), 7.61 (1H, s, H-5), 7.54 (1H, d, J=8.9Hz, H-7"), 7.48 (1H, dd, J=1.8Hz, J=8.9Hz, H-6"), 7.43 (1H, dd, J=2.9Hz, J=9.6Hz, H-4'), 6.44 (1H, d, J=9.6Hz, H-5'), 4.15 (3H, s, $N^{2"}$-CH_3), 3.53 (3H, s, N^1-CH_3).

^{13}C NMR (100MHz, DMSO-*d6*): δ 164.1, 160.4, 159.6, 146.5, 146.3, 135.4, 132.1, 129.0, 124.9, 122.4, 121.8, 121.75, 120.0, 117.5, 114.4, 110.1, 37.7.

MS ESI (m/z): 379 $[M-H]^-$, **HRMS:** m/z calculated for $C_{18}H_{16}N_6O_2S^-$: 379.09827, found: 379.09875.

Ethyl 2-aminothiazole-4-carboxylate **69**:

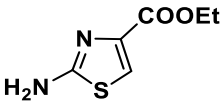

To a suspension of thiourea **67** (5.0 g, 65.69 mmol) in ethanol (30 mL), was slowly added ethyl bromopyruvate **68** (8.25 mL, 65.69 mmol). The mixture was heated to 90 °C for 4 h. After reaction completion (monitored by TLC) the mixture was cooled to room temperature, and concentrated *in vacuo*. The crystalline solid was collected by filtration, washed with ethanol and dried. The crude product was recrystallized from ethylacetate/hexane to afford **69** (10.07 g, 89%) as an off white solid.

^{1}H-NMR (400 MHz, DMSO-d6): δ 7.24 (1H, s, H-5), 7.45 (2H, br s, NH_2), 4.19 (1H, q, J=7.1Hz, CH_2), 1.25 (1H, t, J=7.1Hz, CH_3).

MS ESI (m/z): 173 $[M+H]^+$.

Ethyl 2-bromothiazole-4-carboxylate **70**:

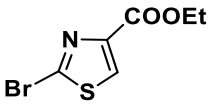

Tert-Butyl nitrite (3.42 mL, 25.8 mmol) was added dropwise to a solution of ethyl 2-aminothiazole-4-carboxylate **69** (3 g, 17.22 mmol) and copper(II)-bromide (5.77 g, 25.86 mmol) in MeCN (75 mL) The mixture was heated at 80 °C for 2 h, then cooled and partitioned between CH_2Cl_2, 1N HCl, and water. The aqueous layer was further extracted with CH_2Cl_2 and the combined organic layers were dried over Na_2SO_4 and concentrated *in vacuo* The residue was silica flash column chromatographed (gradient elution, 5-15% EtOAc in hexane) to afford **70** as a yellow solid (2.3 g, 56%).

^{1}H-NMR (400 MHz, DMSO-d6): δ 7.28 (1H, s, H-5), 4.21 (1H, q, J=7.1Hz, CH_2), 1.25 (1H, t, J=7.1Hz, CH_3).

MS ESI (m/z): 238 $[M+2]^+$.

tert-Butyl tert-butyl 5-nitro-1H-indole-1-carboxylate **71g-NO_2 (N^1-Boc)**:

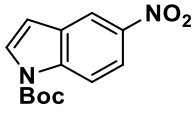

To a stirred solution of 5-nitroindole (5g, 30.65 mmol) in CH_2Cl_2 (60 mL) were successively added Et_3N (5.31 mL, 38.31 mmol), $(Boc)_2O$ (8.36 g, 38.31 mmol), and DMAP (0.38 g, 3.1 mmol). The mixture was stirred for 24 h at room temperature before addition of saturated aqueous NH_4Cl and extraction with CH_2Cl_2. The combined organic layers were dried over Na_2SO_4, filtered, and concentrated under reduced pressure. The residue was purified by flash column chromatography (gradient elution, 1-3% MeOH in CH_2Cl_2) to give the product **71g-NO_2** (**N^1-Boc**) as a yellow solid (7.34g, 91%).

^{1}H-NMR (400 MHz, DMSO-d6): δ 8.61 (1H, d, J=2.3Hz, H-4), 8.26-8.18 (2H, m, H-6,7), 7.90 (1H, d, J=3.5Hz, H-2), 6.96 (1H, d, J=3.5Hz, H-3), 1.64 (9H, s, $C(CH_3)_3$).

tert-Butyl 5-amino-*1H*-indole-1-carboxylate **71g** (**N^1-Boc**):

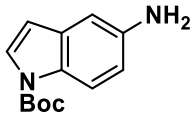

Palladium on carbon (0.8 g, 10% w/w) and $NH_2NH_2.H_2O$ (1.7 mL, 34 mmol) were added to a solution of *tert*-butyl 5-nitro-*1H*-indole-1-carboxylate **71g-NO_2** (**N^1-Boc**) (6.82 g, 26 mmol) in MeOH (70 mL). The mixture was heated under reflux for 3h, then filtered while hot through a bed of celite and washed with hot MeOH. The solvent was evaporated *in vacuo* and the residue was silica flash column chromatographed (gradient elution, 2-5 % MeOH in CH_2Cl_2) to afford **71g** (**N^1-Boc**) as a white powder (4.92g, 81%).

^{1}H-NMR (400 MHz, DMSO-d6): δ 7.70 (1H, d, J=8.6Hz, H-7), 7.46 (1H, d, J=3.7Hz, H-2), 6.70 (1H, d, J=2.3Hz, H-4), 6.61 (1H, dd, J=8.6Hz, J=2.3Hz, H-6), 6.45 (1H, d, J=3.5Hz, H-3), 4.86 (2H, br s, NH_2), 1.56 (9H, s, $C(CH_3)_3$).

MS ESI (m/z): 233 $[M+H]^+$.

tert-Butyl 5-amino-*1H*-indazole-1-carboxylate **71h** (**N^1-Boc**):

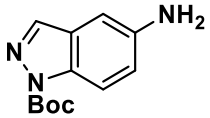

Following the procedure **71g** (**N^1-Boc**), the nitro group in *tert*-butyl 5-nitro-*1H*-indazole-1-carboxylate **79** (6.6 g, 25 mmol) was reduced. The crude mixture was silica flash column chromatographed (gradient elution, 2-6% MeOH in CH_2Cl_2) to afford **71h** (**N^1-Boc**) as an orange solid (4.3g, 74%).

^{1}H-NMR (400 MHz, DMSO-d6): δ 8.11 (1H, s, H-3), 7.75 (1H, d, J=8.9Hz, H-7), 6.91 (1H, dd, J=2.2Hz, J=8.9Hz, H-6), 6.83 (1H, d, J=2.2Hz, H-4), 5.18 (2H, br s, NH_2), 1.62 (s, 9H, $C(CH_3)_3$).

MS ESI (m/z): 234 $[M+H]^+$.

Ethyl 2-(pyridin-2-ylamino)thiazole-4-carboxylate **72a:**

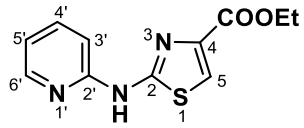

To a suspension of NaH (60% in a mineral oil, 0.54 g, 13.4 mmol) in dry THF (10 mL) 2-aminopyridine **71a** (0.42 g, 4.47 mmol) was added. The mixture was stirred at 60 °C for 30 minutes. Then ethyl 2-bromothiazole-4-carboxylate **70** (1.05 g, 4.47 mmol) was added and the reaction was stirred at 60 °C for an additional 5h. After cooling, the mixture was quenched slowly with saturated aqueous NH_4Cl and extracted with EtOAc. The combined organic extracts were dried over Na_2SO_4 and concentrated *in vacuo*. The oily residue was silica flash column chromatographed (gradient elution, 2-10% MeOH in CH_2Cl_2) to afford **72a** as an off white solid (0.34 g, 31%).

^{1}H-NMR (400 MHz, DMSO-d6): δ 9.64 (1H, br s, NH), 8.36 (1H, dd, 1H, J=1.3Hz, J=4.9Hz, H-6'), 8.18 (1H, d, J=8.3Hz, H-4'), 7.96 (1H, s, H-5), 7.87 (1H, dt, J=1.5Hz, J=8.3Hz, H-3'), 7.19 (ddd, 1H, J=1.5Hz, J=4.9Hz, J=8.3Hz, H-5'), 4.56 (1H, q, J=7.2Hz, CH_2), 1.41 (1H, t, J=7.2Hz, CH_3).

MS ESI (m/z): 250 $[M+H]^+$.

Ethyl 2-((4-cyanophenyl)amino)thiazole-4-carboxylate **72b**:

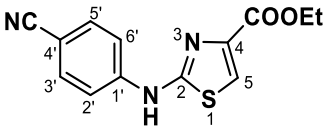

Following the protocol for **72a**, the sodium anion of 4-aminobenzonitrile (0.53 g, 4.74 mmol) was reacted with bromothiazole **70** (1.05 g, 4.47 mmol). The crude product was silica flash column chromatographed (gradient elution, 2-10% MeOH in CH_2Cl_2) to afford **72b** as an off white solid (0.34 g, 31%).

^{1}H-NMR (400 MHz, DMSO-d6): δ 10.92 (1H, br s, NH), 7.90 (1H, s, H-5), 7.81 (2H, d, J=9.0Hz, H-3',5'), 7.77 (2H, d, J=9.0Hz, H-2',6'), 4.27 (1H, q, J=7.2Hz, CH_2), 1.29 (1H, t, J=7.2Hz, CH_3).

MS ESI (m/z): 274 $[M+H]^+$.

Ethyl 2-(pyrimidin-2-ylamino)thiazole-4-carboxylate **72c**:

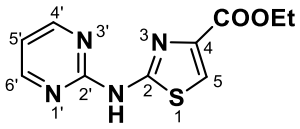

Following the protocol for **72a**, the sodium anion of 2-aminopyrimidine (0.42 g, 4.47 mmol) was reacted with bromothiazole **70** (1.05 g, 4.47 mmol). The crude product was silica flash column chromatographed (gradient elution, 2-10% MeOH in CH_2Cl_2) to afford **72c** as an off white solid (0.27 g, 24%).

^{1}H-NMR (400 MHz, DMSO-d6): ^{1}H-NMR (400 MHz, DMSO-d6): δ 10.64 (1H, br s, NH), 8.64 (2H, d, J=4.9Hz, H-4',6'), 7.96 (1H, s, H-5), 7.08 (1H, t, J=4.9Hz, H-5'), 4.58 (1H, q, J=7.2Hz, CH_2), 1.41 (1H, t, J=7.2Hz, CH_3).

MS ESI (m/z): 251 $[M+H]^+$.

Ethyl 2-((4-nitrophenyl)amino)thiazole-4-carboxylate **72d**:

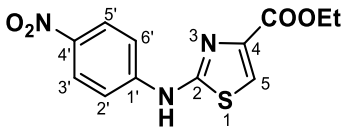

Following the protocol for **72a**, the sodium anion of 4-nitroaniline (0.62 g, 4.47 mmol) was reacted with bromothiazole **70** (1.05 g, 4.47 mmol). The crude product was silica flash column chromatographed (gradient elution, 2-8% MeOH in CH_2Cl_2) to afford **72d** as an orange solid (0.27 g, 24%).

^{1}H-NMR (400 MHz, DMSO-d6): δ 11.02 (1H, br s, NH), 8.21 (2H, d, J=9.0Hz, H-3',5'), 7.92 (1H, s, H-5), 7.82 (2H, d, J=9.0Hz, H-2',6'), 4.25 (1H, q, J=7.2Hz, CH_2), 1.28 (1H, t, J=7.2Hz, CH_3).

MS ESI (m/z): 294 $[M+H]^+$.

Ethyl 2-(phenylamino)thiazole-4-carboxylate **72e**:

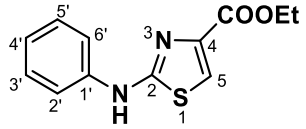

To a solution of aniline (0.51 g, 5.46 mmol) in *i*PrOH (10 mL) was added ethyl 2-bromothiazole-4-carboxylate **70** (0.86 g, 3.64 mmol) and *p*TosOH (0.62 g, 3.64 mmol). The mixture was stirred at 90 °C for 48h, then cooled, diluted with EtOAc, and washed with saturated $NaHCO_3$ and water. The organic layer was dried over Na_2SO_4 and concentrated *in vacuo*. The oily residue was silica flash column chromatographed (gradient elution, 2-10% MeOH in CH_2Cl_2) to give **72e** (0.4 g, 44%) as a white solid.

^{1}H-NMR (400 MHz, DMSO-d6): δ 9.84 (1H, br s, NH), 7.90 (1H, s, H-5), 7.71-7.67 (2H, m, H-2',6'), 7.31-7.250 (2H, m, H-3',5'), 7.01-6.94 (1H, m, H-4'), 4.24 (1H, q, J=7.2Hz, CH_2), 1.23 (1H, t, J=7.2Hz, CH_3).

MS ESI (m/z): 249 $[M+H]^+$.

1-Benzoyl-3-(pyridin-3-yl) thiourea **73f:**

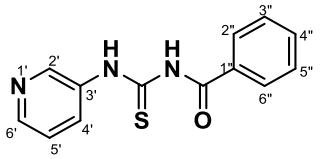

To a solution of 3-aminopyridine **71f** (1.7 g, 18 mmol) in acetonitrile (20 mL) was added benzoyl isothiocyanate (2.37 mL, 18 mmol). The mixture was stirred at ambient temperature for 2h, and then concentrated. The residue was silica flash column chromatographed (gradient elution, 2-5% MeOH in CH_2Cl_2) to afford the product **73f** as a pale red solid (3.6 g, 77%).

MS ESI (m/z): 256 $[M-H]^-$.

tert-Butyl 5-(3-benzoylthioureido)-*1H*-indole-1-carboxylate **73g (N^1-Boc):**

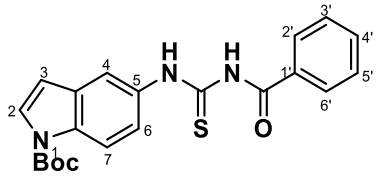

To a solution of **71g** (**N^1-Boc**) (4.18 g, 18 mmol) in acetonitrile (20 mL) was added benzoyl isothiocyanate (2.37 mL, 18 mmol). The mixture was stirred at ambient temperature for 2h,

and then concentrated. The residue was silica flash column chromatographed (gradient elution, 2-7% MeOH in CH_2Cl_2) to afford **73g** (**N^1-Boc**) as pale red solid (5.05 g, 71%).

^{1}H-NMR (400 MHz, DMSO-d6): δ 12.66 (1H, br s, NH), 11.59 (1H, br s, NH), δ 8.08 (1H, d, J=8.6Hz, H-7), 8.05-7.98 (3H, m, H-4,2',6'), 7.74 (1H, d, J=3.7Hz, H-2), 7.69 (1H, t, J=7.5Hz, H-4'), 7.57 (2H, t, J=7.5Hz, H-3',5'), 7.52 (1H, dd, J=8.6Hz, J=2.3Hz, H-6), 6.78 (1H, d, J=3.5Hz, H-3), 1.56 (9H, s, $C(CH_3)_3$).

MS ESI (m/z): 394 $[M-H]^-$.

<u>*tert*-Butyl 5-(3-benzoylthioureido)-*1H*-indazole-1-carboxylate **73h** (**N^1-Boc**):</u>

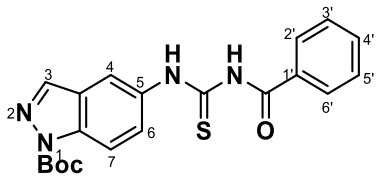

To a solution of **71h** (**N^1-Boc**) (4.2 g, 18 mmol) in acetonitrile (20 mL) was added benzoyl isothiocyanate (2.37 mL, 18 mmol). The mixture was stirred at ambient temperature for 2h, and then concentrated. The residue was silica flash column chromatographed (gradient elution, 2-8% MeOH in CH_2Cl_2) to afford **73h** (**N^1-Boc**) as pale red solid (5.2 g, 73%).

^{1}H-NMR (400 MHz, DMSO-d6): δ 12.66 (1H, br s, NH), 11.65 (1H, br s, NH), 8.46 (1H, s, H-3), 8.27 (1H, d, J=1.9Hz, H-4), 8.09 (1H, d, J=8.9Hz, H-7), 8.00 (2H, d, J=7.4Hz, H-2',6'), 7.76 (1H, dd, J=1.9Hz, J=8.9Hz, H-6), 7.68 (1H, t, J=7.4Hz, H-4'), 7.55 (2H, t, J=7.4Hz, H-3',5'), 1.66 (9H, s, $C(CH_3)_3$).

MS ESI (m/z): 395 $[M-H]^-$.

<u>1-Benzoyl-3-(benzo[*d*]thiazol-6-yl) thiourea **73i:**</u>

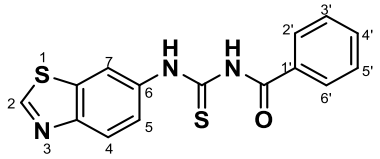

To a solution of **71i** (2.7 g, 18 mmol) in acetonitrile (20 mL) was added benzoyl isothiocyanate (2.37 mL, 18 mmol). The mixture was stirred at ambient temperature for 2h,

and then concentrated. The residue was silica flash column chromatographed (gradient elution, 2-8% MeOH in CH_2Cl_2) to afford **73i** as yellow solid (3.8 g, 68%).

^{1}H-NMR (400 MHz, DMSO-d6): δ 12.71 (1H, br s, NH), 11.67 (1H, br s, NH), 9.41 (1H, s, H-2), 8.57 (1H, d, J=1.9Hz, H-7), 8.11 (1H, d, J=8.9Hz, H-4), 8.00 (2H, d, J=7.4Hz, H-2',6'), 7.74 (1H, dd, J=1.9Hz, J=8.9Hz, H-5), 7.68 (1H, t, J=7.4Hz, H-4'), 7.55 (2H, t, J=7.4Hz, H-3',5').

MS ESI (m/z): 312 $[M-H]^-$.

1-Benzoyl-3-(quinolin-6-yl) thiourea **73j:**

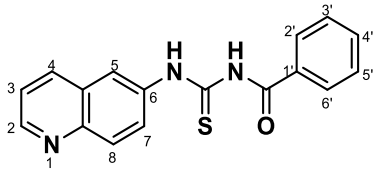

To a solution of **71j** (2.6 g, 18 mmol) in acetonitrile (20 mL) was added benzoyl isothiocyanate (2.37 mL, 18 mmol). The mixture was stirred at ambient temperature for 2h, and then concentrated. The residue was silica flash column chromatographed (gradient elution, 2-10% MeOH in CH_2Cl_2) to afford **73j** as yellow solid (3.5 g, 63%).

^{1}H-NMR (400 MHz, DMSO-d6): δ 12.83 (1H, br s, NH), 11.72 (1H, br s, NH), 8.92 (1H, dd, J=1.6Hz, J=4.2Hz, H-2), 8.46-8.38 (2H, m, Ar-H), 8.09-7.98 (4H, m, Ar-H), 7.70 (1H, t, J=7.4Hz, H-4'), 7.61-7.53 (3H, m, Ar-H).

MS ESI (m/z): 306 $[M-H]^-$.

1-(Pyridin-3-yl)thiourea **74f**:

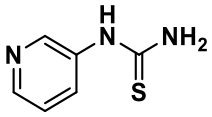

To a solution of **73f** (3.1 g, 12 mmol) in MeOH (30 mL) at room temperature was added LiOH (0.2 g) in water 2 mL. The reaction mixture was heated up to 75 ^oC for 1h. After completion of reaction (TLC monitoring), the precipitate was separated, washed with water and dried in vacuo to give **74f** as a white solid (1.26 g, 69%).

^{1}H-NMR (400 MHz, DMSO-d6): δ 9.97 (1H, br s, NH), 8.94 (1H, d, J=2.3Hz, H-2), 8.35 (1H, dd, J=1.4Hz, J=5.1Hz, H-6), 8.19 (1H, ddd, J=1.4Hz, J=2.3Hz, J=8.4Hz, H-4), 7.54 (1H, d, J=5.1Hz, J=8.4Hz, H-5).

MS ESI (m/z): 154 $[M+H]^+$.

1-(*1H*-Indol-5-yl)thiourea **74g**:

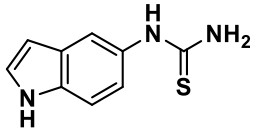

As described for **74f**, intermediate **73g** (**N^1-Boc**) (4.35 g, 11 mmol) was hydrolyzed to afford **74g** as an off white solid (1.5 g, 71%).

^{1}H-NMR (400 MHz, DMSO-d6): δ 11.1 (1H, br s, NH), 9.49 (1H, br s, NH), δ 7.43-7.33 (3H, m, H-2,4,7), 6.93 (1H, dd, J=8.6Hz, J=2.3Hz, H-6), 6.44-6.39 (1H, m, H-3).

MS ESI (m/z): 192 $[M+H]^+$.

1-(*1H*-Indazol-5-yl)thiourea **74h**:

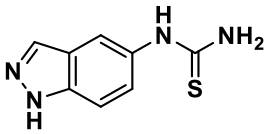

As described for **74f** , intermediate **73h** (**N^1-Boc**) (4.75 g, 12 mmol) was hydrolyzed to afford **74h** as an off white solid (1.73 g, 75%).

^{1}H-NMR (400 MHz, DMSO-d6): δ 13.04 (1H, br s, NH), 9.61 (1H, s, NH), 8.04 (1H, s, H-3), 7.68 (1H, s, H-4), 7.49 (1H, d, J=8.8Hz, H-7), 7.23 (1H, dd, J=1.7Hz, J=8.8Hz, H-6).

MS ESI (m/z): 193 $[M+H]^+$.

1-(Benzo[*d*]thiazol-6-yl)thiourea **74i**;

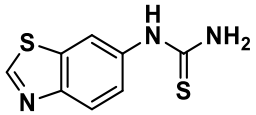

As described for **74f**, intermediate **73i** (3.76 g, 12 mmol) was hydrolyzed to afford **74i** as an off white solid (1.58 g, 63%).

^{1}H-NMR (400 MHz, DMSO-d6): δ 9.87 (1H, br s, NH), 9.31 (1H, s, H-2), 8.25 (1H, d, J=1.9Hz, H-7), 8.01 (1H, d, J=8.8Hz, H-4), 7.46 (1H, dd, J=1.9Hz, J=8.8Hz, H-5).

MS ESI (m/z): 210 $[M+H]^+$.

1-(Quinolin-6-yl)thiourea **74j**:

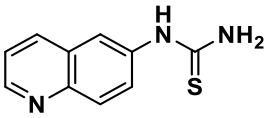

As described for **74f**, itermediate **63j** (3.69 g, 12 mmol) was hydrolyzed to afford **74j** as an off white solid (1.32 g, 54%).

^{1}H-NMR (400 MHz, DMSO-d6): δ 9.97 (1H, br s, NH), 8.81 (1H, dd, J=1.6Hz, J=4.2Hz, H-2), 8.29 (1H, dd, J=1.7Hz, J=8.6Hz, H-4), 8.06 (1H, d, J=2.4Hz, H-5), 7.95 (1H, d, J=9.1Hz, H-8), 7.75 (1H, dd, J=2.4Hz, J=9.1Hz, H-7), 7.49 (1H, dd, J=4.2Hz, J=8.6Hz, H-3).

MS ESI (m/z): 204 $[M+H]^+$.

Ethyl 2-(pyridin-3-ylamino)thiazole-4-carboxylate **72f:**

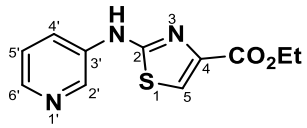

To a suspension of 1-(pyridin-3-yl)thiourea **74f** (1.07 g, 7 mmol) in ethanol (12 mL), was added ethyl 2-bromopyruvate (0.88 mL, 7 mmol). The reaction was heated at 90 ºC for 3h and then allowed to cool to room temperature. The solvent was removed *in vacuo*, and the residue was silica flash column chromatographed (gradient elution, 2−10% MeOH in CH_2Cl_2) to give ester **72f** as an off white solid (1.57 g, 63%).

^{1}H-NMR (400 MHz, DMSO-d6): δ 10.38 (1H, br s, NH), 9.04 (1H, d, J=2.3Hz, H-2'), 8.37 (1H, dd, J=1.4Hz, J=4.9Hz, H-6'), 8.29 (1H, ddd, J=1.4Hz, J=2.3Hz, J=8.3Hz, H-4'), 7.83 (1H, s, H-5), 7.61 (1H, d, J=4.9Hz, J=8.3Hz, H-5'), 4.28 (2H, q, J=7.1Hz, CH_2), 1.29 (3H, t, J=7.1Hz, CH_3).

MS ESI (m/z): 248 $[M-H]^-$.

Ethyl 2-((*1H*-indol-5-yl)amino)thiazole-4-carboxylate **72g**:

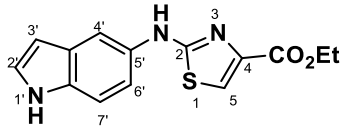

Prepared according to **72f**, compound **74g** (1.33 g, 7 mmol) was reacted with ethyl 2-bromopyruvate (0.88 mL, 7 mmol). The crude mixture was silica flash column chromatographed (gradient elution, 2−8% MeOH in CH_2Cl_2) to afford ester **72g** as pale brown solid (1.43 g, 71%).

^{1}H-NMR (400 MHz, DMSO-d6): δ 11.04 (1H, br s, $N^{1'}$-H), 10.08 (1H, br s, C_2-NH), 7.81 (1H, d, J=2.1Hz, H-4'), 7.62 (1H, s, H-5), 7.36 (1H, d, J=8.5Hz, H-7'), 7.33 (1H, t, J=3.1Hz, H-2'), 7.13 (1H, dd, J=2.1Hz, J=8.5Hz, H-6'), 6.39 (1H, t, J=3.1Hz, H-3'), 4.26 (2H, q, J=7.1Hz, CH_2), 1.30 (3H, t, J=7.1Hz, CH_3).

MS ESI (m/z): 286 $[M-H]^-$.

Ethyl 2-((*1H*-indazol-5-yl)amino)thiazole-4-carboxylate **72h**:

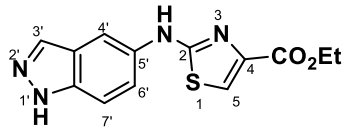

Prepared according to **72f**, compound **74h** (1.34 g, 7 mmol) was reacted with ethyl 2-bromopyruvate (0.88 mL, 7 mmol). The crude mixture was silica flash column chromatographed (gradient elution, 2−10% MeOH in CH_2Cl_2) to afford ester **72h** as an off white solid (1.23 g, 61%).

^{1}H-NMR (400 MHz, DMSO-d6): δ 12.98 (1H, br s, $N^{1'}$-H), 10.33 (1H, br s, C_2-NH), 8.18 (1H, d, J=1.9Hz, H-4'), 8.02 (1H, s, H-3'), 7.72 (1H, s, H-5), 7.52 (1H, d, J=8.9Hz, H-7'), 7.37 (1H, dd, J=1.9Hz, J=8.9Hz, H-6'), 4.27 (2H, q, J=7.1Hz, CH_2), 1.30 (3H, t, J=7.1Hz, CH_3).

MS ESI (m/z): 287 $[M-H]^-$.

Ethyl 2-(benzo[*d*]thiazol-6-ylamino)thiazole-4-carboxylate **72i**:

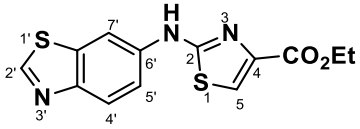

Prepared according to **72f**, compound **74i** (1.46 g, 7 mmol) was reacted with ethyl 2-bromopyruvate (0.88 mL, 7 mmol). The crude mixture was silica flash column chromatographed (gradient elution, 2−6% MeOH in CH_2Cl_2) to afford ester **72i** as a grrenish white solid (1.56 g, 73%).

^{1}H-NMR (400 MHz, DMSO-d6): δ 10.70 (1H, br s, C_2-NH), 9.22 (1H, s, H-2'), 8.62 (1H, d, J=2.2Hz, H-7'), 8.03 (1H, d, J=8.6Hz, H-4'), 7.83 (1H, s, H-5), 7.60 (1H, dd, J=2.2Hz, J=8.6Hz, H-5'), 4.29 (2H, q, J=7.1Hz, CH_2), 1.31 (3H, t, J=7.1Hz, CH_3).

MS ESI (m/z): 304 $[M-H]^-$.

Ethyl 2-(quinolin-6-ylamino)thiazole-4-carboxylate **72j**:

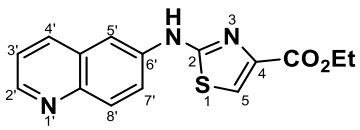

Prepared according to **72f**, compound **74j** (1.42 g, 7 mmol) was reacted with ethyl 2-bromopyruvate (0.88 mL, 7 mmol). The crude mixture was silica flash column chromatographed (gradient elution, 2−10% MeOH in CH_2Cl_2) to afford ester **72j** as a white solid (1.07 g, 51%).

^{1}H-NMR (400 MHz, DMSO-d6): δ 11.19 (1H, br s, C_2-NH), 9.05 (1H, dd, J=1.6Hz, J=4.2Hz, H-2'), 8.85 (1H, d, J=8.6Hz, H-4'), 8.67 (1H, d, J=2.4Hz, H-5'), 8.20 (1H, d, J=8.8Hz, H-8'), 8.10 (1H, dd, J=2.4Hz, J=8.8Hz, H-7'), 7.92 (1H, dd, J=4.2Hz, J=8.6Hz, H-3'), 7.81 (1H, s, H-5), 4.31 (2H, q, J=7.1Hz, CH_2), 1.34 (3H, t, J=7.1Hz, CH_3).

MS ESI (m/z): 298 $[M-H]^-$.

2-(Pyridin-2-ylamino)thiazole-4-carboxylic acid **75a**:

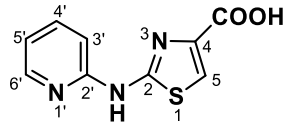

A solution of LiOH (0.29g, 12 mmol) in water (3mL) was added to a stirred suspension of ester **72a** (1.0 g, 4 mmol) in MeOH (12ml). The mixture was stirred at room temperature for 12 h, and then concentrated *in vacuo*. The residue was dissolved in water (10 mL), and the pH was adjusted to 4 by careful addition of 1N HCl. The resulting precipitate was isolated by filtration, washed by water, and dried *in vacuo* to afford **75a** as an off white solid (0.51 g, 58%).

^{1}H-NMR (400 MHz, DMSO-d6): δ 12.66 (1H, br s, COOH), 11.61 (1H, br s, NH), 8.32 (1H, dd, J=1.5Hz, J=4.9Hz, H-6'), 8.14 (1H, d, J=8.3Hz, H-4'), 7.79 (1H, s, H-5), 7.74 (1H, dt, J=1.5Hz, J=8.3Hz, H-3'), 7.03 (ddd, 1H, J=1.5Hz, J=4.9Hz, J=8.3Hz, H-5').

MS ESI (m/z): 220 $[M-H]^-$.

2-((4-Cyanophenyl)amino)thiazole-4-carboxylic acid **75b**:

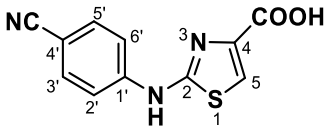

Prepared by the procedure for **75a**, ester **72b** (1.1 g, 4 mmol) was hydrolyzed to afford **75b** as an off white solid (0.6 g, 61%).

^{1}H-NMR (400 MHz, DMSO-d6): δ 12.95 (1H, br s, COOH), 11.07 (1H, br s, NH), 7.90 (1H, s, H-5), 7.84 (2H, d, J=9.0Hz, H-3',5'), 7.79 (2H, d, J=9.0Hz, H-2',6').

MS ESI (m/z): 244 $[M-H]^-$.

2-(Pyrimidin-2-ylamino)thiazole-4-carboxylic acid **75c**:

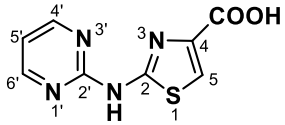

Prepared by the procedure for **75a**, ester **72c** (1.0 g, 4 mmol) was hydrolyzed to afford **75c** as an off white solid (0.47 g, 54%).

^{1}H-NMR (400 MHz, DMSO-d6): δ 11.95 (1H, br s, NH), 8.67 (2H, d, J=4.9Hz, H-4',6'), 7.91 (1H, s, H-5), 7.08 (1H, t, J=4.9Hz, H-5').

MS ESI (m/z): 221 $[M-H]^-$.

2-((4-Nitrophenyl)amino)thiazole-4-carboxylic acid **75d**:

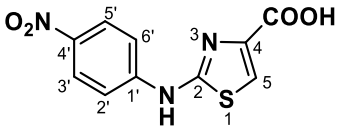

Prepared by the procedure for **75a**, ester **72d** (1.17 g, 4 mmol) was hydrolyzed to afford **75d** as a yellow solid (0.6 g, 57%).

^{1}H-NMR (400 MHz, DMSO-d6): δ 13.05 (1H, br s, COOH), 11.17 (1H, br s, NH), 8.26 (2H, d, J=9.1Hz, H-3',5'), 7.95-7.84 (3H, m, H-5,2',6').

MS ESI (m/z): 264 $[M-H]^-$.

2-(Phenylamino)thiazole-4-carboxylic acid **75e**:

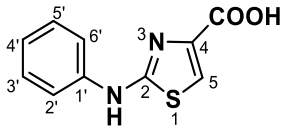

Prepared by the procedure for **75a**, ester **72e** (1.0 g, 4 mmol) was hydrolyzed to afford **75e** as an off white solid (0.72 g, 68%).

^{1}H-NMR (400 MHz, DMSO-d6): δ 12.68 (1H, br s, COOH), 10.41 (1H, br s, NH), 7.84 (1H, s, H-5), 7.68-7.61 (2H, m, H-2',6'), 7.31-7.25 (2H, m, H-3',5'), 6.98-6.94 (1H, m, H-4').

MS ESI (m/z): 219 $[M-H]^-$.

2-(Pyridin-3-ylamino)thiazole-4-carboxylic acid **72f**:

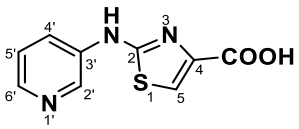

Prepared by the procedure for **75a**, ester **72f** (1.0 g, 4 mmol) was hydrolyzed to afford **75f** as an off white solid (0.58 g, 66%).

^{1}H-NMR (400 MHz, DMSO-d6): δ 12.92 (1H, br s, COOH), 11.09 (1H, br s, NH), 9.12 (1H, d, J=2.1Hz, H-2'), 8-41-8.34 (2H, m, H-4',6'), 7.85 (1H, s, H-5), 7.68 (1H, d, J=5.1Hz, J=8.4Hz, H-5').

MS ESI (m/z): 220 $[M-H]^-$.

2-((*1H*-Indol-5-yl)amino)thiazole-4-carboxylic acid **75g**:

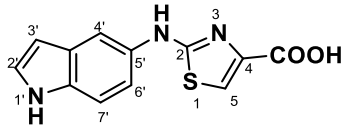

Prepared by the procedure for **75a**, ester **72g** (1.15 g, 4 mmol) was hydrolyzed. Note, the crude product mixture was dry loaded onto a silica column and chromatographed (gradient elution, 10-30% MeOH in EtOAc). Compound **75g** was isolated as a yellow solid (0.49 g, 47%).

^{1}H-NMR (400 MHz, DMSO-d6): δ 12.75 (1H, br s, COOH), 11.02 (1H, br s, $N^{1'}$-H), 10.03 (1H, br s, C_2-NH), 7.87 (1H, d, J=2.1Hz, H-4'), 7.57 (1H, s, H-5), 7.35 (1H, d, J=8.5Hz, H-7'), 7.32 (1H, t, J=3.1Hz, H-2'), 7.16 (1H, dd, J=2.1Hz, J=8.5Hz, H-6'), 6.39 (1H, t, J=3.1Hz, H-3').

MS ESI (m/z): 258 $[M-H]^-$.

2-((*1H*-Indazol-5-yl)amino)thiazole-4-carboxylic acid **75h**:

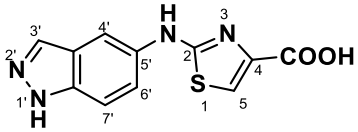

Prepared by the procedure for **75a**, ester **72h** (1.15 g, 4 mmol) was hydrolyzed to afford **75h** as a reddish solid (0.73g, 70%).

^{1}H-NMR (400 MHz, DMSO-d6): δ 12.89 (2H, s, COOH, $N^{1'}$-H), 10.28 (1H, s, C_2-NH), 8.25 (1H, d, J=1.8Hz, H-4'), 8.03 (1H, s, H-3'), 7.66 (1H,s, H-5), 7.51 (1H, d, J=8.9Hz, H-7'), 7.38 (1H, dd, J=1.8Hz, J=8.9Hz, H-6').

MS ESI (m/z): 259 $[M-H]^-$, **HRMS:** m/z calculated for $C_{11}H_8N_4O_2S^-$: 259.02952, found: 259.02951.

2-(Benzo[*d*]thiazol-6-ylamino)thiazole-4-carboxylic acid **75i**:

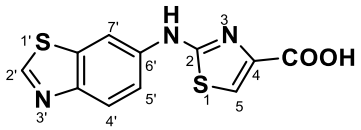

Prepared by the procedure for **75a**, ester **72i** (1.22 g, 4 mmol) was hydrolyzed to afford **75i** as a yellow solid (0.84g, 76%).

^{1}H-NMR (400 MHz, DMSO-d6): δ 12.77 (1H, br s, COOH), 10.65 (1H, br s, C_2-NH), 9.19 (1H, s, H-2'), 8.68 (1H, d, J=2.2Hz, H-7'), 8.02 (1H, d, J=8.6Hz, H-4'), 7.77 (1H, s, H-5), 7.61 (1H, dd, J=2.2Hz, J=8.6Hz, H-5').

MS ESI (m/z): 276 $[M-H]^-$.

2-(Quinolin-6-ylamino)thiazole-4-carboxylic acid **75j**:

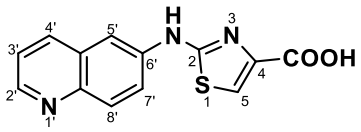

Prepared by the procedure followed in **75a**, ester **72j** (1.19 g, 4 mmol) was hydrolyzed. Note, the crude product mixture was dry loaded onto a silica column and flash chromatographed (gradient elution, 10-30% MeOH in EtOAc). Compound **75j** was isolated as a yellow solid (0.48g, 44%).

^{1}H-NMR (400 MHz, DMSO-d6): δ 13.03 (1H, br s, COOH), 10.75 (1H, br s, C_2-NH), 8.75 (1H, dd, J=1.6Hz, J=4.2Hz, H-2'), 8.40 (1H, d, J=2.4Hz, H-5'), 8.23 (1H, dd, J=1.6Hz, J=8.6Hz, H-4'), 7.99 (1H, d, J=8.8Hz, H-8'), 7.85 (1H, dd, J=2.4Hz, J=8.8Hz, H-7'), 7.81 (1H, s, H-5), 7.48 (1H, dd, J=4.2Hz, J=8.6Hz, H-3').

MS ESI (m/z): 270 $[M-H]^-$.

N-(*1H*-Indazol-5-yl)-2-(pyridin-2-ylamino)thiazole-4-carboxamide 7**6a**:

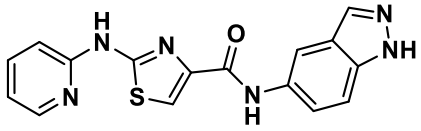

To a solution of acid **75a** (0.11 g, 0.5 mmol) in DMF (5 mL) was added HOAt (0.09 g, 0.55 mmol), EDC (0.11 g, 0.55 mmol) and DIEA (0.22 mL, 1.25 mmol). After stirring for 30 minutes, 5-aminoindazole (0.066 g, 0.5 mmol) was added and stirring was continued at room temperature for 18h. The mixture was then concentrated *in vacuo* and azeotroped twice with

CH_2Cl_2. The resulting residue was silica flash column chromatographed (gradient elution, 3−15% MeOH in CH_2Cl_2) to afford **76a** as an off white solid (0.045 g, 27%).

^{1}H-NMR (400 MHz, DMSO-d6): see Table 28.

MS ESI (m/z): 335 $[M-H]^-$, **HRMS:** m/z calculated for $C_{16}H_{12}N_6OS^-$: 335.07205, found: 335.07251.

2-((4-Cyanophenyl)amino)-*N*-(*1H*-indazol-5-yl)thiazole-4-carboxamide **76b**:

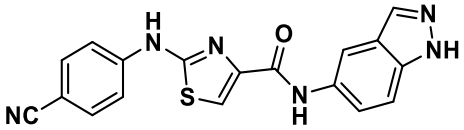

Prepared according to **76a**, acid **75b** (0.14 g, 0.5 mmol) was reacted with 5-aminoindazole (0.066 g, 0.5 mmol). The crude mixture was silica flash column chromatographed (gradient elution, 2−10% MeOH in CH_2Cl_2) to afford **76b** as an off white solid (0.1 g, 31%).

^{1}H-NMR (400 MHz, DMSO-d6): see Table 28.

MS ESI (m/z): 359 $[M-H]^-$, **HRMS:** m/z calculated for $C_{18}H_{12}N_6OS^-$: 359.07205, found: 359.07230.

N-(*1H*-Indazol-5-yl)-2-(pyrimidin-2-ylamino)thiazole-4-carboxamide **76c**:

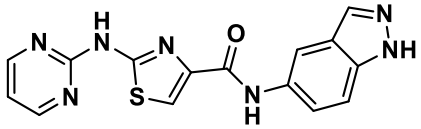

Prepared according to **76a**, acid **75c** (0.11 g, 0.5 mmol) was reacted with 5-aminoindazole (0.066 g, 0.5 mmol). The crude mixture was silica flash column chromatographed (gradient elution, 2−14% MeOH in CH_2Cl_2) to afford **76c** as a white solid (0.04 g, 24%).

^{1}H-NMR (400 MHz, DMSO-d6): see Table 28.

MS ESI (m/z): 336 $[M-H]^-$, **HRMS:** m/z calculated for $C_{15}H_{11}N_7OS^-$: 336.06730, found: 336.06778.

N-(*1H*-Indazol-5-yl)-2-((4-nitrophenyl)amino)thiazole-4-carboxamide **76d**:

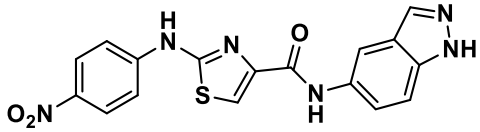

Prepared according to **76a**, acid **75d** (0.13 g, 0.5 mmol) was reacted with 5-aminoindazole (0.066 g, 0.5 mmol). The crude mixture was silica flash column chromatographed (gradient elution, 2−10% MeOH in CH_2Cl_2) to afford **76d** as a pale yellow solid (0.04 g, 21%).

^{1}H-NMR (400 MHz, DMSO-d6): see Table 28.

MS ESI (m/z): 379 $[M-H]^-$, **HRMS:** m/z calculated for $C_{17}H_{12}N_6O_3S^-$: 379.06188, found: 379.06219.

N-(*1H*-Indazol-5-yl)-2-(phenylamino)thiazole-4-carboxamide **76e**:

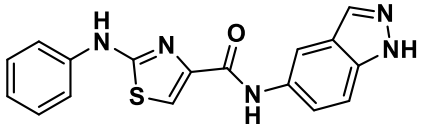

Prepared according to **76a**, acid **75e** (0.11 g, 0.5 mmol) was reacted with 5-aminoindazole (0.066 g, 0.5 mmol). The crude mixture was silica flash column chromatographed (gradient elution, 2−10% MeOH in CH_2Cl_2) to afford **76e** as an off white solid (0.09g, 54%).

^{1}H-NMR (400 MHz, DMSO-d6): see Table 28.

MS ESI (m/z): 334 $[M-H]^-$, **HRMS:** m/z calculated for $C_{17}H_{13}N_5OS^-$: 334.07680, found: 334.07721.

N-(*1H*-Indazol-5-yl)-2-(pyridin-3-ylamino)thiazole-4-carboxamide **76f**:

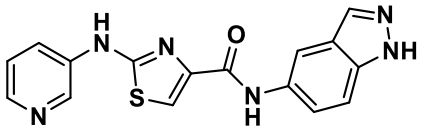

Prepared according to **76a**, acid **75f** (0.11 g, 0.5 mmol) was reacted with 5-aminoindazole (0.066 g, 0.5 mmol). The crude mixture was silica flash column chromatographed (gradient elution, 2−15% MeOH in CH_2Cl_2) to afford **76f** as an off white solid (0.03 g, 18%).

^{1}H-NMR (400 MHz, DMSO-d6): see Table 28.

^{13}C NMR (100MHz, DMSO-*d6*): δ 163.3, 159.8, 150.7, 146.5, 142.7, 140.1, 138.0, 135.0, 131.6, 128.9, 124.4, 123.1, 120.7, 115.4, 112.4, 110.5.

MS ESI (m/z): 335 $[M-H]^-$, **HRMS:** m/z calculated for $C_{16}H_{12}N_6OS^-$: 335.07205, found: 335.07211.

2-((*1H*-Indol-5-yl)amino)-*N*-(*1H*-indazol-5-yl)thiazole-4-carboxamide **76g**:

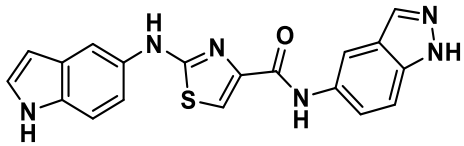

Prepared according to **76a**, acid **75g** (0.13 g, 0.5 mmol) was reacted with 5-aminoindazole (0.066 g, 0.5 mmol). The crude mixture was silica flash column chromatographed (gradient elution, 2−15% MeOH in CH_2Cl_2) to afford **76g** as an orange solid (0.09 g, 48%).

^{1}H-NMR (400 MHz, DMSO-d6): see Table 28.

MS ESI (m/z): 373 $[M-H]^-$, **HRMS:** m/z calculated for $C_{19}H_{14}N_6OS^-$: 373.08770, found: 373.08798.

2-((*1H*-Indazol-5-yl)amino)-*N*-(*1H*-indazol-5-yl)thiazole-4-carboxamide **76h**:

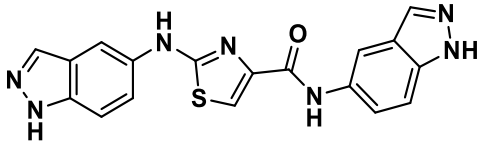

Prepared according to **76a**, acid **75g** (0.13 g, 0.5 mmol) was reacted with 5-aminoindazole (0.066 g, 0.5 mmol). The crude mixture was silica flash column chromatographed (gradient elution, 2−15% MeOH in CH_2Cl_2) to afford **76h** as a brown solid (0.08 g, 43%).

^{1}H-NMR (400 MHz, DMSO-d6): see Table 28.

MS ESI (m/z): 374 $[M-H]^-$, **HRMS:** m/z calculated for $C_{18}H_{13}N_7OS^-$: 374.08295, found: 374.08292.

2-(Benzo[*d*]thiazol-6-ylamino)-*N*-(*1H*-indazol-5-yl)thiazole-4-carboxamide **76i**:

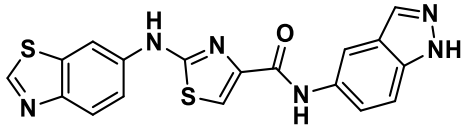

Prepared according to **76a**, acid **75i** (0.14 g, 0.5 mmol) was reacted with 5-aminoindazole (0.066 g, 0.5 mmol). The crude mixture was silica flash column chromatographed (gradient elution, 2−10% MeOH in CH_2Cl_2) to afford **76i** as an off white solid (0.1 g, 51%).

^{1}H-NMR (400 MHz, DMSO-d6): see Table 28.

^{13}C NMR (100MHz, DMSO-*d6*): δ 163.5, 159.8, 154.3, 148.6, 146.6, 138.9, 137.8, 135.4, 134.0, 131.7, 123.5, 122.7, 117.7, 115.1, 112.5, 110.5, 110.0, 49.

MS ESI (m/z): 391 $[M-H]^-$, **HRMS:** m/z calculated for $C_{18}H_{12}N_6OS_2^-$: 391.04412, found: 391.04462.

N-(*1H*-Indazol-5-yl)-2-(quinolin-6-ylamino)thiazole-4-carboxamide **76j**:

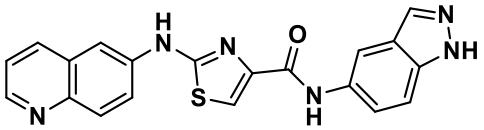

Prepared according to **76a**, acid **75j** (0.14 g, 0.5 mmol) was reacted with 5-aminoindazole (0.066 g, 0.5 mmol). The crude mixture was silica flash column chromatographed (gradient elution, 2−15% MeOH in CH_2Cl_2) to afford **76j** as a pale yellow solid (0.04 g, 21%).

^{1}H-NMR (400 MHz, DMSO-d6): see Table 28.

^{13}C NMR (100MHz, DMSO-*d6*): δ 163.3, 159.7, 148.6, 146.7, 144.6, 138.8, 137.8, 135.9, 134.0, 131.8, 130.2, 129.5, 123.2, 122.8, 122.5, 122.2, 115.4, 112.2, 112.1, 110.5.

MS ESI (m/z): 385 $[M-H]^-$, **HRMS:** m/z calculated for $C_{20}H_{14}N_6OS^-$: 385.08770, found: 385.08795.

Table 28: NMR data of compounds **76a-j**:

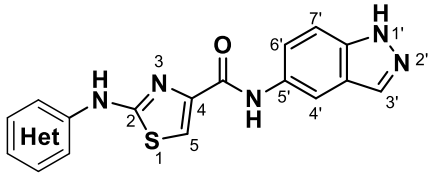

Entry	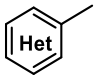	Scaffold ^{1}H-NMR (400 MHz, DMSO-d6) δ ppm	R ^{1}H-NMR (400 MHz, DMSO-d6) δ ppm
76a	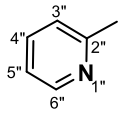	13.03 (1H, br s, $N^{1'}$-H), 11.52 (1H, br s, C_2-NH), 9.75 (1H, br s, CO-NH), 8.27 (1H, d, J=1.7Hz, H-4'), 8.06 (1H, s, H-3'), 7.77 (1H, s, H-5), 7.60 (1H, dd, J=1.7Hz, J=8.8Hz, H-6'), 7.53 (1H, d, J=8.8Hz, H-7')	8.34 (1H, ddd, J=0.8Hz J=1.8Hz, J=4.9Hz, H-6"), 7.75 (1H, ddd, J=1.8Hz, J=7.2Hz, J=8.3Hz, H-4"), 7.13 (1H, dd, J=1.8Hz, J=8.3Hz, H-3"), 6.98 (1H, ddd, J=1.8Hz, J=4.9Hz, J=7.2Hz, H-5")
76b	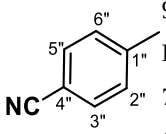	13.04 (1H, s, $N^{1'}$-H), 10.93 (1H, s, C_2-NH), 9.90 (1H, s, CO-NH), 8.20 (1H, d, J=1.8Hz, H-4'), 8.07 (1H, s, H-3'), 7.81 (1H, s, H-5), 7.65 (1H, dd, J=1.8Hz, J=9.0Hz, H-6'), 7.54 (1H, d, J=9.0Hz, H-7')	7.95 (2H, d, J=7.7Hz, H3",5"), 7.77 (2H, d, J=7.7Hz, H-2",6")
76c	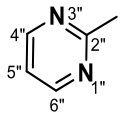	13.04 (1H, br s, $N^{1'}$-H), 11.94 (1H, br s, C_2-NH), 9.80 (1H, s, CO-NH), 8.25 (1H, d, J=1.7Hz, H-4'), 8.06 (1H, s, H-3'), 7.88 (1H, s, H-5), 7.59 (1H, dd, J=1.7Hz, J=8.8Hz, H-6'), 7.53 (1H, d, J=8.8Hz, H-7')	8.68 (2H, d, J=4.9Hz, H-4",6"), 7.09 (1H, t, J=4.9Hz, H-5")
76d	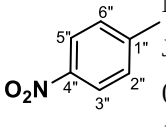	13.06 (1H, br s, $N^{1'}$-H), 11.19 (1H, br s, C_2-NH), 9.90 (1H, br s, CO-NH), 8.21 (1H, d, J=1.7Hz, H-4'), 8.08 (1H, s, H-3'), 7.86 (1H, s, H-5), 7.67 (1H, dd, J=1.7Hz, J=8.6Hz, H-6'), 7.54 (1H, d, J=8.6Hz, H-7')	8.25 (2H, d, J=8.8Hz, H3",5"), 8.02 (2H, d, J=8.8Hz, H-2",6")

Entry		Scaffold ^{1}H-NMR (400 MHz, DMSO-d6) δ ppm	R ^{1}H-NMR (400 MHz, DMSO-d6) δ ppm
76e	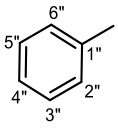	13.03 (1H, br s, $N^{1'}$-H), 10.37 (1H, br s, C_2-NH), 9.80 (1H, br s, CO-NH), 8.21 (1H, d, J=1.7Hz, H-4'), 8.07 (1H, s, H-3'), 7.66 (1H, s, H-5), 7.64 (1H, dd, J=1.7Hz, J=8.9Hz, H-6'), 7.53 (1H, d, J=8.9Hz, H-7')	7.77-7.72 (2H, m, H-2",6"), 7.38-7.32 (2H, m, H-3",5"), 7.05-6.95 (1H, m, H-4")
76g	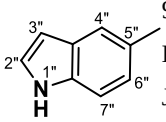	13.04 (1H, s, $N^{1'}$-H), 11.04 (1H, s, C_2-NH), 9.77 (1H, s, CO-NH), 8.25 (1H, d, J=1.9Hz, H-4'), 8.07 (1H, s, H-3'), 7.63 (1H, dd, J=1.9Hz, J=8.5Hz, H-6'), 7.53 (1H, s, H-5), 7.54 (1H, d, J=8.5Hz, H-7')	10.04 (1H, s, $N^{1"}$-H), 7.91 (1H, d, J=2.0Hz, H-4"), 7.54 (1H, d, J=8.3Hz, H-7"), 7.34 (1H, t, J=2.5Hz, H-2"), 7.25 (1H, dd, J=2.0Hz, J=8.7Hz, H-6"), 6.44 (1H, t, J=2.5Hz, H-3")
76h	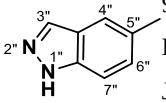	13.05 (1H, s, $N^{1'}$-H), 10.33 (1H, s, C_2-NH), 9.84 (1H, s, CO-NH), 8.26 (1H, d, J=1.9Hz, H-4'), 8.07 (1H, s, H-3'), 7.68 (1H, dd, J=1.9Hz, J=8.7Hz, H-6'), 7.64 (1H, s, H-5), 7.55* (2H, t, J=8.0Hz, H-7')	12.98 (1H, s, $N^{1"}$-H), 8.38 (1H, d, J=1.8Hz, H-4"), 8.09 (1H, s, H-3"), 7.55* (2H, t, J=8.6Hz, H-7"), 7.48 (1H, dd, J=1.8Hz, J=8.6Hz, H-6")
76i		13.05 (1H, s, $N^{1'}$-H), 10.69 (1H, s, C_2-NH), 10.00 (1H, s, CO-NH), 8.25 (1H, d, J=1.8Hz, H-4'), 8.09 (1H, s, H-3'), 7.73 (1H, s, H-5), 7.68 (1H, dd, J=1.8Hz, J=8.6Hz, H-6'), 7.57 (1H, d, J=8.6Hz, H-7')	9.21 (1H, s, H-2"), 9.03(1H, d, J=2.2Hz, H-7"), 8.02(1H, d, J=8.8Hz, H-4"), 7.55(1H, dd, J=2.2Hz, J=8.8Hz, H-5")
76j	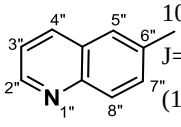	13.05 (1H, s, $N^{1'}$-H), 10.78 (1H, s, C_2-NH), 10.00 (1H, s, CO-NH), 8.29 (1H, d, J=1.8Hz, H-4'), 8.09 (1H, s, H-3'), 7.78 (1H, s, H-5), 7.71 (1H, dd, J=1.8Hz, J=8.6Hz, H-6'), 7.57 (1H, d, J=8.6Hz, H-7')	8.82 (1H, dd, J=1.6Hz, J=4.2Hz, H-2"), 8.73 (1H, d, J=2.3Hz, H-5"), 8.43 (1H, dd, J=1.6Hz, J=8.6Hz, H-4"), 7.98 (1H, d, J=9.1Hz, H-8"), 7.79 (1H, dd, J=2.3Hz, J=9.1Hz, H-7"), 7.50 (1H, dd, J=4.2Hz, J=8.6Hz, H-3")

2-(Pyridin-2-ylamino)-*N*-(pyridin-3-yl)thiazole-4-carboxamide **77a**:

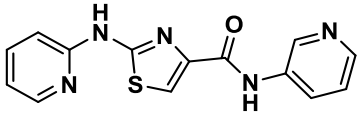

To a solution of acid **75a** (0.11 g, 0.5 mmol) in DMF (5 mL) was added HOAt (0.09 g, 0.55 mmol), EDC (0.11 g, 0.55 mmol) and DIEA (0.22 mL, 1.25 mmol). After stirring for 30 minutes, 3-aminopyridine (0.047 g, 0.5 mmol) was added and stirring continued at room temperature for 18h. The mixture was then concentrated *in vacuo* and azeotroped twice with CH_2Cl_2. The residue was silica flash column chromatogrpahed (gradient elution, 2−10% MeOH in CH_2Cl_2 to afford **77a** as an off white solid (0.046 g, 31%).

^{1}H-NMR (400 MHz, DMSO-d6): see Table 29.

MS ESI (m/z): 296 $[M-H]^-$, **HRMS:** m/z calculated for $C_{14}H_{11}N_5OS^-$: 296.06115, found: 296.06119.

2-((4-Cyanophenyl)amino)-*N*-(pyridin-3-yl)thiazole-4-carboxamide **77b:**

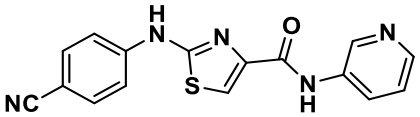

Prepared according to **77a**, acid **75b** (0.12 g, 0.5 mmol) was reacted with 3-aminopyridine (0.047 g, 0.5 mmol). The crude mixture was silica flash column chromatographed (gradient elution, 2−10% MeOH in CH_2Cl_2) to afford **77b** as an off white solid (0.014 g, 12%).

^{1}H-NMR (400 MHz, DMSO-d6): see Table 29.

MS ESI (m/z): 320 $[M-H]^-$, **HRMS:** m/z calculated for $C_{16}H_{11}N_5OS^-$: 320.06115, found: 320.06119.

N-(Pyridin-3-yl)-2-(pyrimidin-2-ylamino)thiazole-4-carboxamide **77c**:

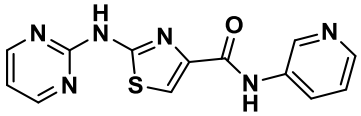

Prepared according to **77a**, acid **75c** (0.11 g, 0.5 mmol) was reacted with 3-aminopyridine (0.047 g, 0.5 mmol). The crude mixture was silica flash column chromatographed (gradient elution, 2−14% MeOH in CH_2Cl_2) to afford **77c** as an off white solid (0.04 g, 28%).

^{1}H-NMR (400 MHz, DMSO-d6): see Table 29.

MS ESI (m/z): 297 $[M-H]^-$, **HRMS:** m/z calculated for $C_{13}H_{10}N_6OS^-$: 297.05640, found: 297.05643.

2-((4-Nitrophenyl)amino)-*N*-(pyridin-3-yl)thiazole-4-carboxamide **77d**:

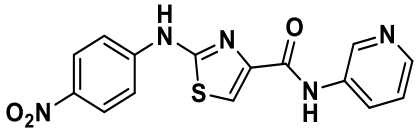

Prepared according to **77a**, acid **75d** (0.13 g, 0.5 mmol) was reacted with 3-aminopyridine (0.047 g, 0.5 mmol). The crude mixture was silica flash column chromatographed (gradient elution, 2−10% MeOH in CH_2Cl_2) to afford **77d** as a yellow solid (0.04 g, 28%).

^{1}H-NMR (400 MHz, DMSO-d6): see Table 29.

^{13}C NMR (100MHz, DMSO-*d6*): δ 162.5, 159.9, 151.3, 146.8, 145.9, 143.3, 141.1, 140.1, 135.1, 129.2, 128.7, 126.0, 124.0, 121.0, 117.3.

MS ESI (m/z): 340 $[M-H]^-$, **HRMS:** m/z calculated for $C_{15}H_{11}N_5O_3S^-$: 340.05098, found: 340.05099.

2-(Phenylamino)-*N*-(pyridin-3-yl)thiazole-4-carboxamide **77e**:

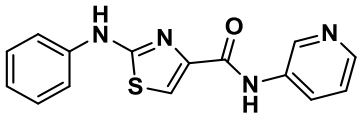

Prepared according to **77a**, acid **75e** (0.11 g, 0.5 mmol) was reacted with 3-aminopyridine (0.047 g, 0.5 mmol). The crude mixture was silica flash column chromatographed (gradient elution, 2−10% MeOH in CH_2Cl_2) to afford **77e** as a pale yellow solid (0.074 g, 50%).

^{1}H-NMR (400 MHz, DMSO-d6): see Table 29.

MS ESI (m/z): 295 $[M-H]^-$, **HRMS:** m/z calculated for $C_{15}H_{12}N_4OS^-$: 295.06591, found: 295.06595.

N-(Pyridin-3-yl)-2-(pyridin-3-ylamino)thiazole-4-carboxamide **77f**:

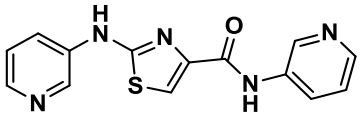

Prepared according to **77a**, acid **75f** (0.11 g, 0.5 mmol) was reacted with 3-aminopyridine (0.047 g, 0.5 mmol). The crude mixture was silica flash column chromatographed (gradient elution, 2−15% MeOH in CH_2Cl_2) to afford **77f** as a pale pink solid (0.068 g, 46%).

^{1}H-NMR (400 MHz, DMSO-d6): see Table 29.

MS ESI (m/z): 296 $[M-H]^-$, **HRMS:** m/z calculated for $C_{14}H_{11}N_5OS^-$: 296.06115, found: 296.06116.

2-((*1H*-Indol-5-yl)amino)-*N*-(pyridin-3-yl)thiazole-4-carboxamide **77g**:

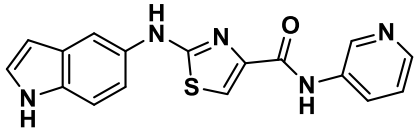

Prepared according to **77a**, acid **75g** (0.13 g, 0.5 mmol) was reacted with 3-aminopyridine (0.047 g, 0.5 mmol). The crude mixture was silica flash column chromatographed (gradient elution, 2−12% MeOH in CH_2Cl_2) to afford **77g** as a pale yellow solid (0.045 g, 47%).

^{1}H-NMR (400 MHz, DMSO-d6): see Table 29.

MS ESI (m/z): 334 $[M-H]^-$, **HRMS:** m/z calculated for $C_{17}H_{13}N_5OS^-$: 334.07680, found: 334.07675.

2-((*1H*-Indazol-5-yl)amino)-*N*-(pyridin-3-yl)thiazole-4-carboxamide **77h**:

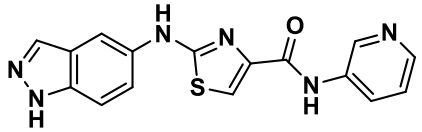

Prepared according to **77a**, acid **75h** (0.13 g, 0.5 mmol) was reacted with 3-aminopyridine (0.047 g, 0.5 mmol). The crude mixture was silica flash column chromatographed (gradient elution, 2−16% MeOH in CH_2Cl_2) to afford **77h** as an off white solid (0.079 g, 47%).

^{1}H-NMR (400 MHz, DMSO-d6): see Table 29.

MS ESI (m/z): 335 $[M-H]^-$, **HRMS:** m/z calculated for $C_{16}H_{12}N_6OS^-$: 335.07205, found: 335.07211.

2-(Benzo[*d*]thiazol-6-ylamino)-*N*-(pyridin-3-yl)thiazole-4-carboxamide **77i**:

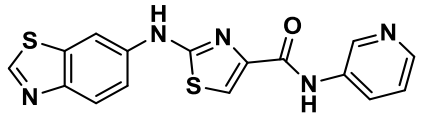

Prepared according to **77a**, acid **75i** (0.14 g, 0.5 mmol) was reacted with 3-aminopyridine (0.047 g, 0.5 mmol). The crude mixture was silica flash column chromatographed (gradient elution, 2−10% MeOH in CH_2Cl_2) to afford **77i** as a yellowish green solid (0.1 g, 57%).

^{1}H-NMR (400 MHz, DMSO-d6): see Table 29.

MS ESI (m/z): 352 $[M-H]^-$, **HRMS:** m/z calculated for $C_{16}H_{11}N_5OS_2^-$: 352.03322, found: 352.03329.

N-(Pyridin-3-yl)-2-(quinolin-6-ylamino)thiazole-4-carboxamide **77j**:

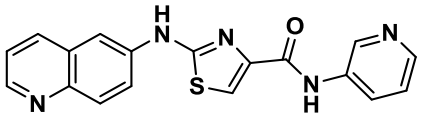

Prepared according to **77a**, acid **75j** (0.14 g, 0.5 mmol) was reacted with 3-aminopyridine (0.047 g, 0.5 mmol). The crude mixture was silica flash column chromatographed (gradient elution, 2−16% MeOH in CH_2Cl_2) to afford **77j** as a yellow solid (0.048 g, 28%).

^{1}H-NMR (400 MHz, DMSO-d6): see Table 29.

^{13}C NMR (100MHz, DMSO-*d6*): δ 163.4, 160.1, 148.6, 145.9, 144.6, 143.0, 138.8, 135.9, 134.8, 130.2, 129.4, 128.4, 127.2, 124.0, 122.8, 118.8, 116.2, 112.3.

MS ESI (m/z): 346 $[M-H]^-$, **HRMS:** m/z calculated for $C_{18}H_{13}N_5OS^-$: 346.07680, found: 346.07730.

Table 29: NMR data of compounds **77a-j**

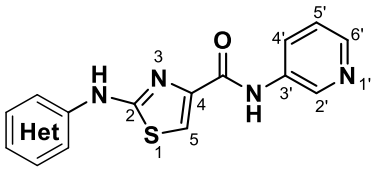

Entry		Scaffold ^{1}H-NMR (400 MHz, DMSO-d6) δ ppm	R ^{1}H-NMR (400 MHz, DMSO-d6) δ ppm
77a	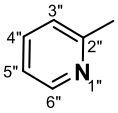	11.51 (1H, br s, C_2-NH), 10.00 (1H, s, CO-NH), 8.92 (1H, d, J=2.3Hz, H-2'), 8.32 (1H, dd, J=1.5Hz, J=4.8Hz, H-6'), 8.13 (1H, ddd, J=1.5Hz, J=2.3Hz, J=8.5Hz, H-4'), 7.82 (1H, s, H-5),7.40 (1H, dd, J=4.8Hz, J=8.5Hz, H-5')	8.34 (1H, ddd, J=0.8Hz J=1.8Hz, J=4.9Hz, H-6"), 7.75 (1H, ddd, J=1.8Hz, J=7.2Hz, J=8.3Hz, H-4"), 7.14 (1H, dd, J=1.8Hz, J=8.3Hz, H-3"), 6.98 (1H, ddd, J=1.8Hz, J=4.9Hz, J=7.2Hz, H-5")
77b	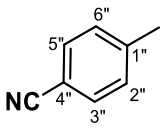	10.95 (1H, br s, C_2-NH), 10.10 (1H, s, CO-NH), 8.95 (1H, d, J=2.3Hz, H-2'), 8.34 (1H, dd, J=1.5Hz, J=4.6Hz, H-6'), 8.19 (1H, ddd, J=1.5Hz, J=2.3Hz, J=8.5Hz, H-4'), 7.87 (1H, s, H-5), 7.42 (1H, dd, J=4.6Hz, J=8.5Hz, H-5')	7.94 (2H, d, J=7.7Hz, H3",5"), 7.77 (2H, d, J=7.7Hz, H-2",6")
77c	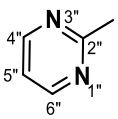	11.91 (1H, br s, C_2-NH), 10.05 (1H, s, CO-NH), 8.92 (1H, s, H-2'), 8.32 (1H, dd, J=1.3Hz, J=4.0Hz, H-6'), 8.21 (1H, dd, J=1.3Hz, J=8.5Hz, H-4'), 7.82 (1H, s, H-5), 7.40 (1H, dd, J=4.0Hz, J=8.5Hz, H-5')	8.68 (2H, d, J=4.9Hz, H-4",6"), 7.09 (1H, t, J=4.9Hz, H-5")

Entry		Scaffold ^{1}H-NMR (400 MHz, DMSO-d6) δ ppm	R ^{1}H-NMR (400 MHz, DMSO-d6) δ ppm
77d	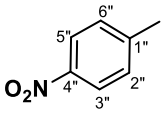	11.23 (1H, br s, C_2-NH), 10.08 (1H, s, CO-NH), 8.98 (1H, d, J=2.3Hz, H-2'), 8.37 (1H, dd, J=1.5Hz, J=4.6Hz, H-6'), 8.22 (1H, ddd, J=1.5Hz, J=2.3Hz, J=8.5Hz, H-4'), 7.95 (1H, s, H-5),7.45 (1H, dd, J=4.6Hz, J=8.5Hz, H-5')	8.27 (2H, d, J=8.7Hz, H3",5"), 8.02 (2H, d, J=8.7Hz, H-2",6")
77e	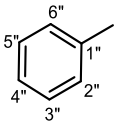	10.39 (1H, br s, C_2-NH), 10.00 (1H, s, CO-NH), 8.95 (1H, d, J=2.3Hz, H-2'), 8.33 (1H, dd, J=1.5Hz, J=4.7Hz, H-6'), 8.20 (1H, ddd, J=1.5Hz, J=2.3Hz, J=8.3Hz, H-4'), 7.73 (1H, s, H-5), 7.41 (1H, dd, J=4.7Hz, J=8.3Hz, H-5')	7.77-7.72 (2H, m, H-2",6"), 7.38-7.32 (2H, m, H-3",5"), 7.05-6.95 (1H, m, H-4")
77f	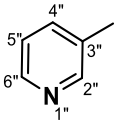	10.63 (1H, br s, C_2-NH), 10.09 (1H, s, CO-NH), 8.94 (1H, d, J=2.3Hz, H-2'), 8.34 (1H, dd, J=1.4Hz, J=4.7Hz, H-6'), 8.18 (1H, ddd, J=1.4Hz, J=2.3Hz, J=8.5Hz, H-4'), 7.80 (1H, s, H-5),7.41 (1H, dd, J=4.7Hz, J=8.5Hz, H-5')	8.81 (1H, d, J=2.3Hz, H-2"), 8.43 (1H, ddd, J=1.4Hz, J=2.3Hz, J=8.5Hz, H-4"), 8.21 (1H, dd, J=1.4Hz, J=4.7Hz, H-6"), 7.38 (1H, dd, J=4.7Hz, J=8.5Hz, H-5")
77g	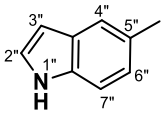	10.70 (1H, br s, C_2-NH), 9.77 (1H, s, CO-NH), 8.92 (1H, d, J=2.2Hz, H-2'), 8.30 (1H, dd, J=1.5Hz, J=4.7Hz, H-6'), 8.19 (1H, ddd, J=1.5Hz, J=2.2Hz, J=8.5Hz, H-4'), 7.46 (1H, s, H-5), 7.39 (1H, dd, J=4.7Hz, J=8.5Hz, H-5')	9.88 (1H, s, $N^{1"}$-H), 7.30 (1H, d, J=1.9Hz, H-4"), 7.27 (1H, d, J=8.3Hz, H-7"), 7.23 (1H, d, J=2.5Hz, H-2"), 7.08 (1H, dd, J=1.9Hz, J=8.7Hz, H-6"), 6.44 (1H, d, J=2.5Hz, H-3")
77h	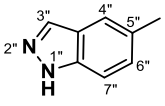	10.70 (1H, br s, C_2-NH), 10.16 (1H, s, CO-NH), 8.99 (1H, d, J=2.2Hz, H-2'), 8.35 (1H, dd, J=1.5Hz, J=4.7Hz, H-6'), 8.24 (1H, ddd, J=1.5Hz, J=2.2Hz, J=8.5Hz, H-4'), 7.80 (1H, s, H-5), 7.44 (1H, dd, J=4.7Hz, J=8.5Hz, H-5')	12.97 (1H, s, $N^{1"}$-H), 8.38 (1H, d, J=1.8Hz, H-4"), 8.06 (1H, s, H-3"), 7.55 (1H, d, J=8.6Hz, H-7"), 7.46 (1H, dd, J=1.8Hz, J=8.6Hz, H-6")
77i	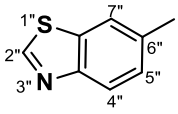	10.70 (1H, br s, C_2-NH), 10.16 (1H, s, CO-NH), 8.99 (1H, d, J=2.2Hz, H-2'), 8.35 (1H, dd, J=1.5Hz, J=4.7Hz, H-6'), 8.24 (1H, ddd, J=1.5Hz, J=2.2Hz, J=8.5Hz, H-4'), 7.80 (1H, s, H-5), 7.44	9.21 (1H, s, H-2"), 9.02(1H, d, J=2.1Hz, H-7"), 8.02(1H, d, J=8.7Hz, H-4"), 7.54(1H, dd, J=2.1Hz, J=8.7Hz, H-5")

Entry		Scaffold ^{1}H-NMR (400 MHz, DMSO-d6) δ ppm	R ^{1}H-NMR (400 MHz, DMSO-d6) δ ppm
		(1H, dd, J=4.7Hz, J=8.5Hz, H-5')	
77j	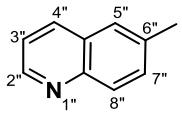	10.83 (1H, br s, C_2-NH), 10.19 (1H, s, CO-NH), 9.03 (1H, d, J=2.2Hz, H-2'), 8.35 (1H, dd, J=1.5Hz, J=4.7Hz, H-6'), 8.27 (1H, ddd, J=1.5Hz, J=2.2Hz, J=8.5Hz, H-4'), 7.84 (1H, s, H-5), 7.44 (1H, dd, J=4.7Hz, J=8.5Hz, H-5')	8.76 (1H, d, J=2.2Hz, H-5"), 8.74 (1H, dd, J=1.6Hz, J=4.2Hz, H-2"), 8.41 (1H, dd, J=1.6Hz, J=8.6Hz, H-4"), 7.98 (1H, d, J=9.0Hz, H-8"), 7.76 (1H, dd, J=2.2Hz, J=9.0Hz, H-7"), 7.50 (1H, dd, J=4.2Hz, J=8.6Hz, H-3")

tert-Butyl 5-nitro-1H-indazole-1-carboxylate **79**:

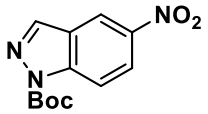

To a stirred solution of 5-nitroindazole **78** (5g, 30.65 mmol) in CH_2Cl_2 (60 mL) were successively added Et_3N (5.31 mL, 38.31 mmol), $(Boc)_2O$ (8.36 g, 38.31 mmol), and DMAP (0.38 g, 3.1 mmol). The mixture was stirred for 24 h at room temperature before addition of saturated aqueous NH_4Cl and extraction with CH_2Cl_2. The combined organic layers were dried over Na_2SO_4, filtered, and concentrated under reduced pressure. The residue was purified by flash column chromatography (gradient elution, 1-5% MeOH in CH_2Cl_2) to give the product **79** as an orange solid (6.94g, 86%).

^{1}H-NMR (400 MHz, DMSO-d6): δ 8.89 (1H, d, J=2.3Hz, H-4), 8.65 (1H, s, H-3), 8.44 (1H, dd, J=2.3Hz, J=9.2Hz, H-6), 8.26 (1H, d, J=9.2Hz, H-7), 1.67 (9H, s, $C(CH_3)_3$).

2-((*1H*-Indazol-5-yl)amino)-*N*-phenylthiazole-4-carboxamide **80a**:

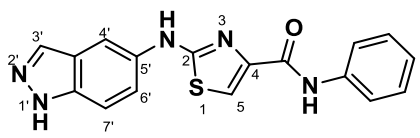

To a solution of acid **75h** (0.1g, 0.38 mmol) in DMF (5 mL), was added HOAt (0.07 g, 0.42 mmol), EDC (0.081 g, 0.42 mmol) and DIEA (0.2 mL, 1.14 mmol). After stirring for 30 minutes, aniline was added (0.035 g, 0.38 mmol) and stirring was continued at room temperature for 18h. The mixture was then concentrated *in vacuo* and azeotroped twice with CH_2Cl_2. The residue was silica flash column chromatographed (gradient elution, 2−12% MeOH in CH_2Cl_2) to afford **80a** as an off white solid (0.065 g, 51%).

^{1}H-NMR (400 MHz, DMSO-d6): see Table 30.

^{13}C NMR (100MHz, DMSO-*d6*): δ 164.8, 159.6, 145.7, 138.8, 137.0, 134.6, 133.5, 129.1, 124.3, 123.4, 121.0, 120.4, 117.2, 114.1, 111.3, 108.2.

MS ESI (m/z): 334 $[M-H]^-$, **HRMS:** m/z calculated for $C_{17}H_{13}N_5OS^-$: 334.07680, found: 334.07721.

2-((*1H*-Indazol-5-yl)amino)-*N*-(4-methoxyphenyl)thiazole-4-carboxamide **80b**:

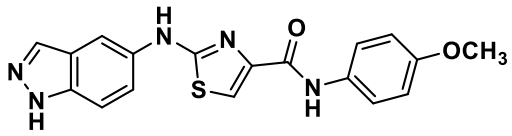

Prepared according to **80a**, acid **75h** (0.1g, 0.38 mmol) was reacted with *p*-anisidine (0.047 g, 0.38 mmol). The crude mixture was silica flash column chromatographed (gradient elution, 2−14% MeOH in CH_2Cl_2) to afford **80b** as a white solid (0.076 g, 56%).

^{1}H-NMR (400 MHz, DMSO-d6): see Table 30.

MS ESI (m/z): 364 $[M-H]^-$, **HRMS:** m/z calculated for $C_{18}H_{15}N_5O_2S^-$: 364.08737, found: 364.08786.

2-((*1H*-Indazol-5-yl)amino)-*N*-(3-methoxyphenyl)thiazole-4-carboxamide **80c**:

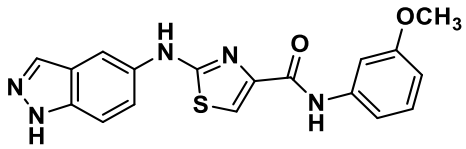

Prepared according to **80a**, acid **75h** (0.1g, 0.38 mmol) was reacted with *m*-anisidine (0.047 g, 0.38 mmol). The crude mixture was silica flash column chromatographed (gradient elution, 2−14% MeOH in CH_2Cl_2) to afford **80c** as an off white solid (0.079 g, 58%).

^{1}H-NMR (400 MHz, DMSO-d6): see Table 30.

^{13}C NMR (100MHz, DMSO-*d6*): δ 164.8, 159.9, 159.6, 145.5, 140.0, 137.0, 134.6, 133.4, 129.9, 123.4, 120.6, 114.2, 113.2, 111.4, 109.8, 108.4, 106.6, 55.5.

MS ESI (m/z): 364 $[M-H]^-$, **HRMS:** m/z calculated for $C_{18}H_{15}N_5O_2S^-$: 364.08737, found: 364.08832.

2-((*1H*-Indazol-5-yl)amino)-*N*-(3,4-dimethoxyphenyl)thiazole-4-carboxamide **80d**:

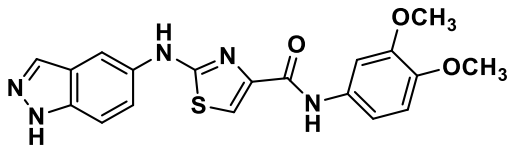

Prepared according to **80a**, acid **75h** (0.1g, 0.38 mmol) was reacted with 3,4-dimethoxyaniline (0.058 g, 0.38 mmol). The crude mixture was silica flash column chromatographed (gradient elution, 2−16% MeOH in CH_2Cl_2) to afford **80d** as a pale yellow solid (0.074 g, 49%).

^{1}H-NMR (400 MHz, DMSO-d6): see Table 30.

MS ESI (m/z): 394 $[M-H]^-$, **HRMS:** m/z calculated for $C_{19}H_{17}N_5O_3S^-$: 394.09793, found: 394.09818.

2-((*1H*-Indazol-5-yl)amino)-*N*-(4-fluorophenyl)thiazole-4-carboxamide **80e**:

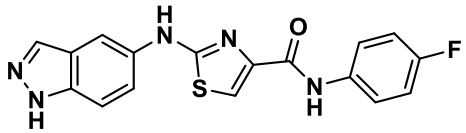

Prepared according to **80a**, acid **75h** (0.1g, 0.38 mmol) was reacted with 4-fluoroaniline (0.042 g, 0.38 mmol). The crude mixture was silica flash column chromatographed (gradient elution, 2−12% MeOH in CH_2Cl_2) to afford **80e** as an off white solid (0.07 g, 52%).

^{1}H-NMR (400 MHz, DMSO-d6): see Table 30.

^{13}C NMR (100MHz, DMSO-*d6*): δ 160.1, 159.7, 157.7, 145.7, 137.0, 135.3, 134.6, 133.5, 123.4, 123.1, 123.0, 120.4, 115.8, 115.6, 114.3, 111.3, 108.2.

MS ESI (m/z): 352 $[M-H]^-$, **HRMS:** m/z calculated for $C_{17}H_{12}N_5OSF^-$: 352.06738, found: 352.06772.

2-((*1H*-Indazol-5-yl)amino)-*N*-(2,3-dihydro-*1H*-inden-4-yl)thiazole-4-carboxamide **80f**:

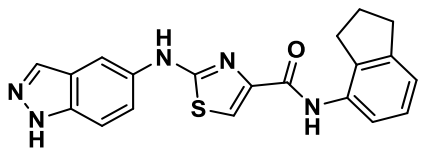

Prepared according to **80a**, acid **75h** (0.1g, 0.38 mmol) was reacted with 4-aminoindan (0.05 g, 0.38 mmol). The crude mixture was silica flash column chromatographed (gradient elution, 2−10% MeOH in CH_2Cl_2) to afford **80f** as a pale yellow solid (0.067 g, 47%).

^{1}H-NMR (400 MHz, DMSO-d6): see Table 30.

MS ESI (m/z): 374 $[M-H]^-$, **HRMS:** m/z calculated for $C_{20}H_{17}N_5OS^-$: 374.10810, found: 374.10831.

2-((*1H*-Indazol-5-yl)amino)-*N*-(benzo[*d*][1,3]dioxol-5-yl)thiazole-4-carboxamide **80g**:

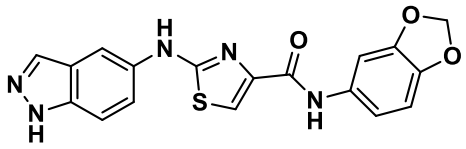

Prepared according to **80a**, acid **75h** (0.1g, 0.38 mmol) was reacted with 3,4-(methylenedioxy) aniline (0.052 g, 0.38 mmol). The crude mixture was silica flash column chromatographed (gradient elution, 2−14% MeOH in CH_2Cl_2) to afford **80g** as an off white solid (0.083 g, 58%).

^{1}H-NMR (400 MHz, DMSO-d6): see Table 30.

MS ESI (m/z): 378 $[M-H]^-$, **HRMS:** m/z calculated for $C_{18}H_{13}N_5O_3S^-$: 378.06663, found: 378.06705.

2-((*1H*-Indazol-5-yl)amino)-*N*-(2,3-dihydrobenzo[*b*][1,4]dioxin-6-yl)thiazole-4-carboxamide **80h**:

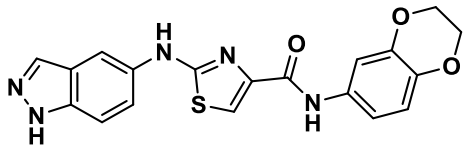

Prepared according to **80a**, acid **75h** (0.1g, 0.38 mmol) was reacted with 1,4-benzodioxan-6-amine (0.052 g, 0.38 mmol). The crude mixture was silica flash column chromatographed (gradient elution, 2−14% MeOH in CH_2Cl_2) to afford **80h** as an off white solid (0.077 g, 52%).

^{1}H-NMR (400 MHz, DMSO-d6): see Table 30.

^{13}C NMR (100MHz, DMSO-*d6*): δ 159.4, 151.6, 146.0, 143.3, 140.3, 137.0, 135.1, 133.5, 132.5, 129.3, 121.2, 117.1, 114.4, 113.8, 111.3, 110.1, 108.2, 64.7, 64.4.

MS ESI (m/z): 392 $[M-H]^-$, **HRMS:** m/z calculated for $C_{19}H_{15}N_5O_3S^-$: 392.08228, found: 392.08270.

2-((*1H*-Indazol-5-yl)amino)-*N*-(6-methoxypyridin-3-yl)thiazole-4-carboxamide **80i**:

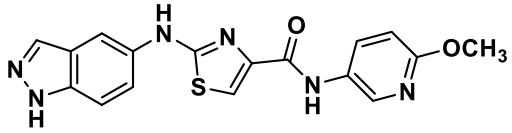

Prepared according to **80a**, acid **75h** (0.1g, 0.38 mmol) was reacted with 5-amino-2-methoxypyridine (0.047 g, 0.38 mmol). The crude mixture was silica flash column chromatographed (gradient elution, 2−14% MeOH in CH_2Cl_2) to afford **80i** as a pale pink solid (0.067 g, 48%).

^{1}H-NMR (400 MHz, DMSO-d6): see Table 30.

^{13}C NMR (100MHz, DMSO-*d6*): δ 164.6, 160.5, 160.0, 146.1, 140.0, 136.9, 134.6, 133.8, 133.6, 129.8, 123.6, 119.9, 114.2, 111.1, 110.4, 108.0, 53.7.

MS ESI (m/z): 365 $[M-H]^-$, **HRMS:** m/z calculated for $C_{17}H_{14}N_6O_2S^-$: 365.08262, found: 365.08301.

2-((*1H*-Indazol-5-yl)amino)-*N*-(1H-indol-5-yl)thiazole-4-carboxamide **80j**:

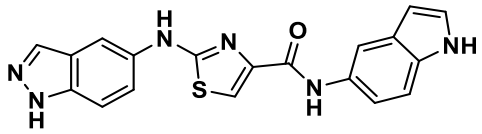

Prepared according to **80a**, acid **75h** (1 equiv) was reacted with 6-aminoindole (0.05 g, 0.38 mmol). The crude mixture was silica flash column chromatographed (gradient elution, 2−12% MeOH in CH_2Cl_2) to afford **80j** as a pale beige solid (0.055 g, 39%).

^{1}H-NMR (400 MHz, DMSO-d6): see Table 30.

^{13}C NMR (100MHz, DMSO-*d6*): δ 164.8, 159.2, 145.8, 137.1, 134.6, 133.6, 133.4, 130.5, 127.9, 126.5, 123.4, 120.6, 116.6, 113.3, 112.7, 111.7, 111.4, 108.4, 101.6.

MS ESI (m/z): 373 $[M-H]^-$, **HRMS:** m/z calculated for $C_{19}H_{14}N_6OS^-$: 373.08770, found: 373.08792.

2-((*1H*-Indazol-5-yl)amino)-*N*-(benzo[*d*]thiazol-6-yl)thiazole-4-carboxamide **80k**:

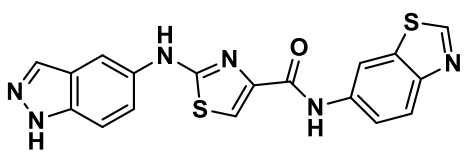

Prepared according to **80a**, acid **75h** (0.1g, 0.38 mmol) was reacted with 6-aminobenzothiazole (0.057 g, 0.38 mmol). The crude mixture was silica flash column chromatographed (gradient elution, 2−12% MeOH in CH_2Cl_2) to afford **80k** as an off white solid (0.077 g, 52%).

^{1}H-NMR (400 MHz, DMSO-d6): see Table 30.

MS ESI (m/z): 391 $[M-H]^-$, **HRMS:** m/z calculated for $C_{18}H_{12}N_6OS_2^-$: 391.04412, found: 391.04434.

2-((*1H*-Indazol-5-yl)amino)-*N*-(quinolin-6-yl)thiazole-4-carboxamide **80l**:

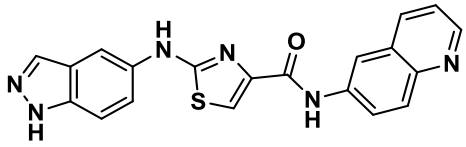

Prepared according to **80a**, acid **75h** (0.1g, 0.38 mmol) was reacted with 6-aminoquinoline (0.055 g, 0.38 mmol). The crude mixture was silica flash column chromatographed (gradient elution, 2−18% MeOH in CH_2Cl_2) to afford **80l** as off whit solid (0.032 g, 22%).

^{1}H-NMR (400 MHz, DMSO-d6): see Table 30.

MS ESI (m/z): 385 $[M-H]^-$, **HRMS:** m/z calculated for $C_{20}H_{14}N_6OS^-$: 385.08770, found: 385.08804.

2-((*1H*-Indazol-5-yl)amino)-*N*-benzylthiazole-4-carboxamide **80m**:

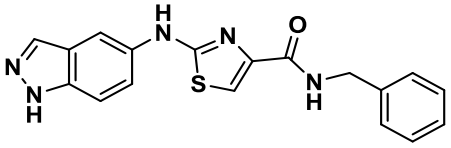

Prepared according to **80a**, acid **75h** (0.1g, 0.38 mmol) was reacted with benzylamine (0.04 g, 0.38 mmol). The crude mixture was silica flash column chromatographed (gradient elution, 2−10% MeOH in CH_2Cl_2) to afford **80m** as white solid (0.08 g, 61%).

^{1}H-NMR (400 MHz, DMSO-d6): see Table 30.

^{13}C NMR (100MHz, DMSO-*d6*): δ 164.4, 161.4, 146.4, 140.2, 136.8, 134.7, 133.7, 128.7, 127.6, 127.2, 123.6, 119.8, 117.3, 113.0, 111.0, 107.6, 42.7.

MS ESI (m/z): 348 $[M-H]^-$, **HRMS:** m/z calculated for $C_{18}H_{15}N_5OS^-$: 348.09245, found: 348.09277.

2-((*1H*-Indazol-5-yl)amino)-*N*-(4-methoxybenzyl)thiazole-4-carboxamide **80n**:

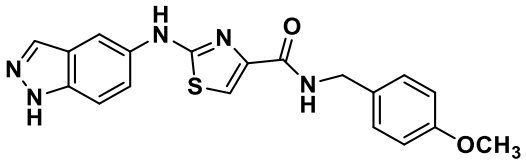

Prepared according to **80a**, acid **75h** (0.1g, 0.38 mmol) was reacted with 4-methoxy benzylamine (0.04 g, 0.38 mmol). The crude mixture was silica flash column chromatographed (gradient elution, 2−12% MeOH in CH_2Cl_2) to afford **80n** as a white solid (0.09 g, 64%).

^{1}H-NMR (400 MHz, DMSO-d6): see Table 30.

MS ESI (m/z): 378 $[M-H]^-$, **HRMS:** m/z calculated for $C_{19}H_{17}N_5O_2S^-$: 378.10302, found: 378.10309.

2-((*1H*-Indazol-5-yl)amino)-*N*-(pyridin-2-ylmethyl)thiazole-4-carboxamide **80o**:

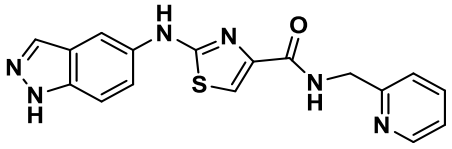

Prepared according to **80a**, acid **75h** (0.1g, 0.38 mmol) was reacted with 2-picolylamine (0.04 g, 0.38 mmol). The crude mixture was silica flash column chromatographed (gradient elution, 2−10% MeOH in CH_2Cl_2) to afford **80o** as an off white solid (0.077 g, 58%).

^{1}H-NMR (400 MHz, DMSO-d6): see Table 30.

^{13}C NMR (100MHz, DMSO-*d6*): δ 164.3, 162.0, 154.7, 146.8, 145.2, 141.7, 136.8, 134.7, 133.5, 126.1, 125.9, 123.5, 120.1, 114.3, 111.1, 107.6, 44.7.

MS ESI (m/z): 349 $[M-H]^-$, **HRMS:** m/z calculated for $C_{17}H_{14}N_6OS^-$: 349.08770, found: 349.08792.

N-(4-(*1H*-Imidazol-1-yl)phenyl)-2-((*1H*-indazol-5-yl)amino)thiazole-4-carboxamide **80p**:

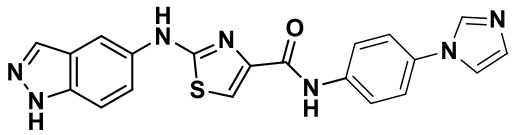

Prepared according to **80a**, acid **75h** (0.1g, 0.38 mmol) was reacted with 4-(1H-Imidazol-1-yl)aniline (0.06 g, 0.38 mmol). The crude mixture was silica flash column chromatographed

(gradient elution, 2−10% MeOH in CH_2Cl_2) to afford **80p** as an off white solid (0.06 g, 40%).

^{1}H-NMR (400 MHz, DMSO-d6): see Table 30.

MS ESI (m/z): 400 $[M-H]^-$, **HRMS:** m/z calculated for $C_{20}H_{15}N_7OS^-$: 400.09860, found: 400.09882.

2-((*1H*-Indazol-5-yl)amino)-*N*-(4-morpholinophenyl)thiazole-4-carboxamide **80q**:

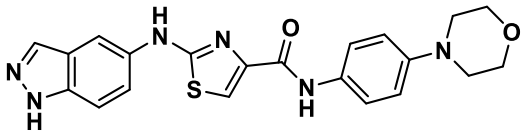

Prepared according to **80a**, acid **75h** (0.1g, 0.38 mmol) was reacted with 4-morpholinoaniline (0.067 g, 0.38 mmol). The crude mixture was silica flash column chromatographed (gradient elution, 2−12% MeOH in CH_2Cl_2) to afford **80q** as an off white solid (0.084 g, 54%).

^{1}H-NMR (400 MHz, DMSO-d6): see Table 30.

MS ESI (m/z): 419 $[M-H]^-$, **HRMS:** m/z calculated for $C_{21}H_{20}N_6O_2S^-$: 419.12957, found: 419.13062.

was reduced. The crude mixture was silica flash column chromatographed (gradient elution, 2-8% MeOH in CH_2Cl_2) to afford **71h** (**N^1-Boc**) as an orange solid (4.3g, 74%).

^{1}H-NMR (400 MHz, DMSO-d6): δ 8.11 (1H, s, H-3), 7.75 (1H, d, J=8.9Hz, H-7), 6.91 (1H, dd, J=2.2Hz, J=8.9Hz, H-6), 6.83 (1H, d, J=2.2Hz, H-4), 5.18 (2H, br s, NH_2), 1.62 (s, 9H, $C(CH_3)_3$).

MS ESI (m/z): 234 $[M+H]^+$.

Table 30: NMR data of compounds **80a-q**

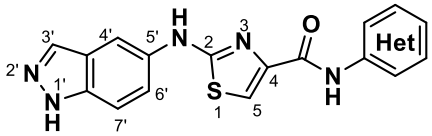

Entry		Scaffold ^{1}H-NMR (400 MHz, DMSO-d6) δ ppm	R ^{1}H-NMR (400 MHz, DMSO-d6) δ ppm
80a		12.97 (1H, br s, N$^{1'}$-H), 10.31 (1H, br s, C_2-NH), 9.77 (1H, s, CO-NH), 8.33 (1H, d, J=1.7Hz, H-4'), 8.04 (1H, s, H-3'),	7.84-7.75 (2H, m, H-2",6"), 7.41-7.33 (2H, m, H-3",5"), 7.17-7.07 (1H, m, H-4")

Entry		Scaffold ^{1}H-NMR (400 MHz, DMSO-d6) δ ppm	R ^{1}H-NMR (400 MHz, DMSO-d6) δ ppm
	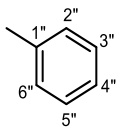	7.63 (1H, s, H-5), 7.53 (1H, d, J=8.9Hz, H-7'), 7.44 (1H, dd, J=1.7Hz, J=8.9Hz, H-6')	
80b	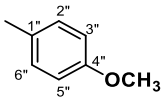	12.96 (1H, br s, $N^{1'}$-H), 10.29 (1H, br s, C_2-NH), 9.68 (1H, br s, CO-NH), 8.34 (1H, d, J=1.8Hz, H-4'), 8.03 (1H, s, H-3'), 7.59 (1H, s, H-5), 7.52 (1H, d, J=8.8Hz, H-7'), 7.43 (1H, dd, J=1.8Hz, J=8.8Hz, H-6')	7.69 (2H, d, J=9.0Hz, H-2",6"), 6.95 (2H, d, J=9.0Hz, H-3",5"), 3.76 (3H, s, OCH_3)
80c	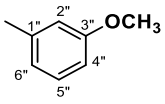	12.96 (1H, br s, $N^{1'}$-H), 10.30 (1H, br s, C_2-NH), 9.74 (1H, br s, CO-NH), 8.32 (1H, d, J=1.9Hz, H-4'), 8.04 (1H, s, H-3'), 7.63 (1H, s, H-5), 7.53 (1H, d, J=8.9Hz, H-7'), 7.44 (1H, dd, J=1.9Hz, J=8.9Hz, H-6')	7.51 (1H, d, J=1.2Hz, H-2"), 7.37 (1H, dd, J=1.2Hz, J=7.9Hz, H-6"), 7.27 (1H, t, J=7.9Hz, H-5"), 6.71 (1H, dd, J=1.2Hz, J=7.9Hz, H-4"), 3.77 (3H, s, OCH_3)
80d	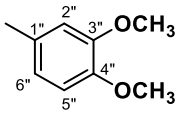	12.96 (1H, br s, $N^{1'}$-H), 10.29 (1H, br s, C_2-NH), 9.66 (1H, br s, CO-NH), 8.35 (1H, d, J=2.0Hz, H-4'), 8.04 (1H, s, H-3'), 7.59 (1H, s, H-5), 7.55-7.48* (2H, m, H-7'), 7.43 (1H, dd, J=2.0Hz, J=8.9Hz, H-6')	7.55-7.48* (2H, m, H-2"), 7.34 (1H, dd, J=2.4Hz, J=8.7Hz, H-6"), 6.95 (1H, d, J=8.7Hz, H-5"), 3.77 (6H, d, J=11.5Hz, OCH_3)
80e	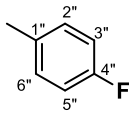	12.96 (1H, br s, $N^{1'}$-H), 10.30 (1H, br s, C_2-NH), 9.88 (1H, br s, CO-NH), 8.36 (1H, d, J=1.7Hz, H-4'), 8.03 (1H, s, H-3'), 7.63 (1H, s, H-5), 7.52 (1H,d, J=8.9Hz, H-7'), 7.44 (1H, dd, J=1.7Hz, J=8.9Hz, H-6')	7.88-7.81 (2H, m, H2",6"), 7.27-7.19 (2H, m, H-3",5")
80f	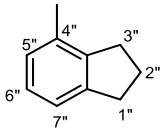	13.00 (1H, br s, N-$H^{1'}$), 10.43 (1H, br s, C_2-NH), 9.42 (1H, br s, CO-NH), 8.44 (1H, d, J=2.0Hz, H-4'), 7.97 (1H, s, H-3'), 7.65 (1H, s, H-5), 7.53 (1H, d, J=9.0Hz, H-7'), 7.38 (1H, dd, J=2.0Hz, J=9.0Hz, H-6')	7.92 (1H, d, J=8.2Hz, H-5") 7.18 (1H, t, J=7.8Hz H-6"), 7.05 (1H, d, J=7.4Hz, H-7"), 2.99 (4H, td, J=7.2Hz, J=22.3Hz, benzylic CH_2), 2.14 (2H, p, J=7.2Hz, CH_2)

Entry		Scaffold ^{1}H-NMR (400 MHz, DMSO-d6) δ ppm	R ^{1}H-NMR (400 MHz, DMSO-d6) δ ppm
80g	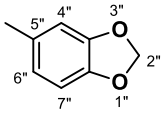	12.96 (1H, br s, $N^{1'}$-H), 10.28 (1H, br s, C_2-NH), 9.71 (1H, br s, CO-NH), 8.33 (1H, d, J=2.0Hz, H-4'), 8.03 (1H, s, H-3'), 7.59 (1H, s, H-5), 7.52 (1H, d, J=8.9Hz, H-7'), 7.44 (1H, dd, J=2.0Hz, J=8.9Hz, H-6')	7.47 (1H, d, J=2.1Hz, H-4"), 7.23 (1H, dd, J=2.1Hz, J=8.4Hz, H-6"), 6.92 (1H, d, J=8.4Hz, H-7"), 6.02 (2H, s, OCH_2O)
80h	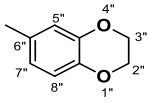	12.96 (1H, br s, $N^{1'}$-H), 10.28 (1H, br s, C_2-NH), 9.64 (1H, br s, CO-NH), 8.32 (1H, d, J=1.8Hz, H-4'), 8.03 (1H, s, H-3'), 7.58 (1H, s, H-5), 7.52 (1H, d, J=8.9Hz, H-7'), 7.45 (1H, dd, J=1.8Hz, J=8.9Hz, H-6')	7.44 (1H, d, J=2.5Hz, H-5"), 7.20 (1H, dd, J=2.5Hz, J=8.8Hz, H-7"), 6.84 (1H, d, J=8.8Hz, H-8"), 4.24 (4H, dd, J=5.1Hz, J=8.6Hz, 2 OCH_2)
80i	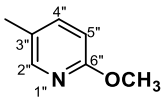	12.97 (1H, br s, $N^{1'}$-H), 10.31 (1H, br s, C_2-NH), 9.90 (1H, br s, CO-NH), 8.40 (1H, d, J=1.8Hz, H-4'), 8.05 (1H, s, H-3'), 7.65 (1H, s, H-5), 7.53 (1H, d, J=8.9Hz, H-7'), 7.45 (1H, dd, J=1.8Hz, J=8.9Hz, H-6')	8.57 (1H, d, J=2.7Hz, H-2"), 8.10 (1H, dd, J=2.7Hz, J=8.9Hz, H-4"), 6.88 (d, 1H, J=8.9Hz, H-5"), 3.87 (3H, s, OCH_3)
80j	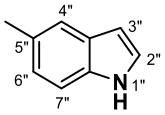	12.96 (1H, br s, $N^{1'}$-H), 11.06 (1H, br s, C_2-NH), 9.60 (1H, br s, CO-NH), 8.33 (1H, d, J=1.9Hz, H-4'), 8.05 (1H, s, H-3'), 7.58 (1H, s, H-5), 7.53 (1H,d, J=9.0Hz, H-7'), 7.46 (1H, dd, J=1.9Hz, J=9.0Hz, H-6')	10.32 (1H, s, $N^{1"}$-H), 7.99 (1H, d, J=1.5Hz, H-4"), 7.36-7.41 (2H, m, H-6",7"), 7.35 (1H, t, J=2.5Hz, H-2"), 6.43 (1H, t, J=2.5Hz, H-3")
80k	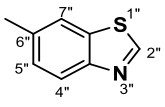	12.97 (1H, br s, N-$H^{1'}$), 10.33 (1H, br s, C_2-NH), 10.06 (1H, br s, CO-NH), 8.36 (1H, d, J=1.9Hz, H-4'), 8.06 (1H, s, H-3'), 7.68 (1H, s, H-5), 7.53 (1H,d, J=9.0Hz, H-7'), 7.46 (1H, dd, J=1.9Hz, J=9.0Hz, H-6')	9.32 (1H, s, H-2"), 8.69 (1H, d, J=2.1Hz, H-7"), 8.08 (1H, d, J=8.9Hz, H-4"), 7.90 (1H, dd, J=2.1Hz, J=8.9Hz H-5")
80l	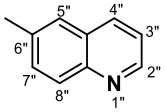	12.98 (1H, br s, $N^{1'}$-H), 10.34 (1H, br s, C_2-NH), 10.13 (1H, br s, CO-NH), 8.38 (1H, d, J=2.0Hz, H-4'), 8.07 (1H, s, H-3'), 7.70 (1H, s, H-5), 7.56 (1H, d, J=9.0Hz, H-7'), 7.47 (1H, dd, J=2.0Hz,	8.74 (1H, dd, J=1.7Hz, J=4.1Hz, H-2"), 8.55 (1H, d, J=2.2Hz, H-5"), 8.34 (1H, dd, J=1.6Hz, J=8.3Hz, H-4"), 8.10 (1H, dd, J=2.2Hz, J=9.1Hz, H-7"), 8.03 (1H, d, J=9.1Hz, H-8"), 7.54 (1H, dd,

Entry		Scaffold ^{1}H-NMR (400 MHz, DMSO-d6) δ ppm	R ^{1}H-NMR (400 MHz, DMSO-d6) δ ppm
		J=8.9Hz, H-6')	J=4.1Hz, J=8.3Hz, H-3")
80m	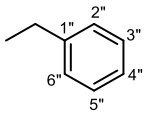	12.93 (1H, br s, N$^{1'}$-H), 10.23 (1H, br s, C_2-NH), 8.61 (1H, t, J=6.4Hz, CO-NH), 8.32 (1H, d, J=2.0Hz, H-4'), 7.97 (1H,s, H-3'), 7.49 (2H, m, H-5, H-7'), 7.42 (1H, dd, J=2.0Hz, J=8.9Hz, H-6')	7.34 (4H, d, J=4.4Hz, H-2",3",5",6"), 7.28-7.20 (1H, m, H-4"), 4.51 (1H, d, J=6.4Hz, CH_2)
80n	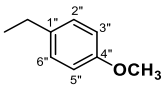	12.93 (1H, br s, N$^{1'}$-H), 10.22 (1H, br s, C_2-NH), 8.52 (1H, t, J=6.3Hz, CO-NH), 8.30 (1H, d, J=2.0Hz, H-4'), 7.97 (1H, s, H-3'), 7.49 (1H, d, J=8.9Hz, H-7'), 7.46 (1H, s, H-5), 7.41 (1H, dd, J=2.0Hz, J=8.9Hz, H-6')	7.20 (2H, d, J=8.7Hz, H-2",6"), 6.90 (2H, d, J=8.7Hz, H-3",5"), 4.43 (2H, d, J=6.3Hz, CH_2), 3.72 (3H, s, OCH_3)
80o	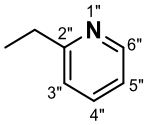	12.95 (1H, br s, N$^{1'}$-H), 10.28 (1H, br s, C_2-NH), 8.73 (1H, t, J=5.9Hz, CO-NH) 8.35 (1H, d, J=1.6Hz, H-4'), 7.98 (1H, s, H-3'), 7.52-7.47 (2H, m, H-5,7'), 7.43 (1H, dd, J=2.0Hz, J=8.9Hz, H-6')	8.55 (1H, dd, J=1.7Hz, J=4.8Hz, H-6"), 7.79 (1H, dt, J=2.2Hz, J=7.7Hz, H-3"), 7.38-7.34 (1H, m, H-4"), 7.32-7.28 (1H, m, H-5"), 4.62 (2H, d, J=5.9Hz, CH_2)
80p	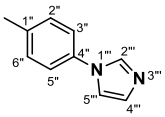	12.97 (1H, br s, N$^{1'}$-H), 10.31 (1H, br s, C_2-NH), 9.98 (1H, br s, CO-NH), 8.37 (1H, d, J=1.9Hz, H-4'), 8.04 (1H, s, H-3'), 7.74 (1H, s, H-5), 7.53 (1H, d, J=8.8Hz, H-7'), 7.44 (1H, dd, J=1.9Hz, J=8.9Hz, H-6')	8.25 (1H, s, H-2"'), 7.96 (2H, d, J=8.9Hz, H-3",5"), 7.70-7.63 (3H, m, H-2",6", 4"'), 7.12 (1H, s, H-5"')
80q	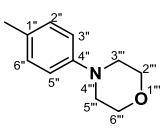	12.96 (1H, br s, N$^{1'}$-H), 10.29 (1H, br s, C_2-NH), 9.60 (1H, br s, CO-NH), 8.33 (1H, d, J=1.9Hz, H-4'), 8.03 (1H, s, H-3'), 7.57 (1H, s, H-5), 7.52 (1H, d, J=8.8Hz, H-7'), 7.43 (1H, dd, J=1.9Hz, J=8.9Hz, H-6')	7.65 (2H, d, J=9.0Hz, H-2",6"), 6.96 (2H, d, J=9.0Hz, H-3",5"), 3.79-3.69 (4H, m, H-2"',6"'), 3.13-3.03 (4H, m, H-3"',5"').

N'-((1H-indazol-5-yl)carbamothioyl)-N,N-dimethylformimidamide **82**:

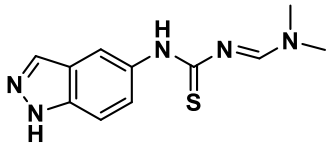

N,*N*-Dimethylformamide dimethoxyacetal **81** (2.5 mL, 18.75 mmol) was added to a suspension of indazolyl thiourea **74h** (3.0g, 15.61 mmol) in EtOH (25 mL). The mixture was heated under reflux for 3h. The reaction was concentrated in vacuo to remove solvent and excess DMF-DMA. The resulting crude product was purified by flash column chromatography (gradient elution, 1-10% MeOH in CH_2Cl_2) to afford **81** as a white solid (3.5 g, 91%).

^{1}H-NMR (400 MHz, DMSO-d6): δ 12.98 (1H, d, J=4.5Hz, NH), 10.49 (1H, d, J=4.5Hz, NH), 8.77 (1H, d, H-3), 8.24-7.85 (2H, m, H-4,7), 7.55 (1H, dd, J=1.7Hz, J=8.8Hz, H-6), 7.47-7.39 (1H, m, N=CH), 3.23-2.95 (6H, m, 2 CH_3).

MS ESI (m/z): 246 $[M-H]^-$.

2-Chloro-*N*-phenylacetamide **83a**:

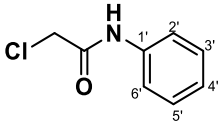

Aniline (0.3 g, 3.22 mmol) was dissolved in dry CH_2Cl_2 (8 mL) and Et_3N (0.54 mL, 3.87 mmol) was added. The reaction mixture was cooled to 0 ^oC, and then 2-chloroacetyl chloride (0.31 mL, 3.87 mmol) was added dropwise. The reaction mixture was warmed to room temperature and stirred for an additional 12 h. The solvent was removed in vacuo and the residue was purified by flash column chromatography (gradient elution, 2-8% EtOAc in hexane) to afford **83a** as an off white solid (0.5 g, 91%).

^{1}H-NMR (400 MHz, DMSO-d6): δ 10.28 (1H, br s, NH), 7.61-7.55 (2H, m, H-2',6'), 7.36-7.30 (2H, m, H-3',5'), 7.12-7.05 (1H, m, H-4'), 4.25 (2H, s, CH_2).

MS ESI (m/z): 168 $[M-H]^-$.

2-Chloro-*N*-(3-phenoxyphenyl)acetamide **83b**:

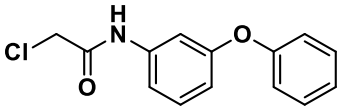

Prepared according to the procedure followed in **83a** using 3-phenoxyaniline (0.6 g, 3.22 mmol). The crude product was purified by flash column chromatography (gradient elution, 2-12% EtOAc in hexane) to afford **83b** as an off white solid (0.73 g, 87%).

MS ESI (m/z): 260 $[M-H]^-$.

2-Chloro-*N*-(3-methoxyphenyl)acetamide **83c**:

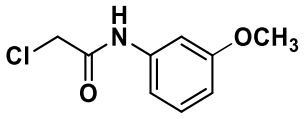

Prepared according to the procedure followed in **83a** using *m*-anisidine (0.4 g, 3.22 mmol). The crude product was purified by flash column chromatography (gradient elution, 3-14% EtOAc in hexane) to afford **83c** as an off white solid (0.57 g, 89%).

^{1}H-NMR (400 MHz, DMSO-d6): δ 10.29 (1H, br s, NH), 7.27 (1H, t, J=2.1Hz H-2'), 7.23 (1H, t, J=8.0Hz H-5'), 7.12 (1H, dd, J=2.1Hz, J=8.0Hz, H-6'), 6.67 (1H, td, J=2.1Hz, J=8.0Hz, H-4'), 4.23 (2H, s, CH_2), 3.75 (3H, s, OCH_3).

MS ESI (m/z): 198 $[M-H]^-$.

N-(Benzo[*d*][1,3]dioxol-5-yl)-2-chloroacetamide **83d**:

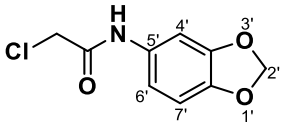

Prepared according to the procedure followed in **83a** using 3,4-(methylenedioxy) aniline (0.44 g, 3.22 mmol). The crude product was purified by flash column chromatography (gradient elution, 3-14% EtOAc in hexane) to afford **83d** as an off white solid (0.64 g, 93%).

^{1}H-NMR (400 MHz, DMSO-d6): δ 10.20 (1H, br s, NH), 7.27 (1H, d, J=2.1Hz, H-4'), 6.96 (1H, dd, J=2.1Hz, J=8.4Hz, H-6'), 6.87 (1H, d, J=8.4Hz, H-7'), 5.98 (2H, s, OCH_2O), 4.21 (2H, s, $COCH_2$).

MS ESI (m/z): 212 $[M-H]^-$.

2-Chloro-*N*-(2,3-dihydrobenzo[*b*][1,4]dioxin-6-yl)acetamide **83e**:

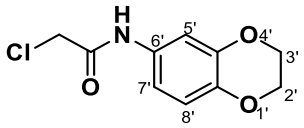

Prepared according to the procedure followed in **83a** using 1,4-benzodioxan-6-amine (0.44 g, 3.22 mmol). The crude product was purified by flash column chromatography (gradient elution, 2-14% EtOAc in hexane) to afford **83e** as an off white solid (0.65 g, 89%).

^{1}H-NMR (400 MHz, DMSO-d6): δ 10.11 (1H, br s, NH), 7.21 (1H, d, J=2.1Hz, H-5'), 6.96 (1H, dd, J=2.1Hz, J=8.4Hz, H-7'), 6.80 (1H, d, J=8.4Hz, H-8'), 4.24-4.18 (6H, m, 2 OCH_2, $COCH_2$).

MS ESI (m/z): 226 $[M-H]^-$.

2-Chloro-*N*-(3,4-dimethoxyphenyl)acetamide **83f**:

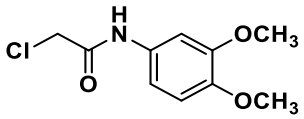

Prepared according to the procedure followed in **83a** using 3,4-dimethoxyaniline (0.49 g, 3.22 mmol). The crude product was purified by flash column chromatography (gradient elution, 5-20% EtOAc in hexane) to afford **83f** as an off white solid (0.68 g, 92%).

^{1}H-NMR (400 MHz, DMSO-d6): δ 10.13 (1H, br s, NH), 7.26 (1H, d, J=2.3Hz, H-2'), 7.10 (1H, dd, J=2.3Hz, J=8.7Hz, H-6'), 6.90 (1H, d, J=8.7Hz, H-5'), 4.21 (2H, s, $COCH_2$), 3.72 (6H, d, J=7.8Hz, 2 OCH_3).

MS ESI (m/z): 228 $[M-H]^-$.

2-Chloro-*N*-(4-fluorophenyl)acetamide **83g**:

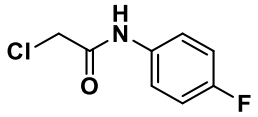

Prepared according to the procedure followed in **83a** using 4-fluoroaniline (0.49 g, 3.22 mmol). The crude product was purified by flash column chromatography (gradient elution, 2-12% EtOAc in hexane) to afford **83g** as an off white solid (0.5 g, 83%).

^{1}H-NMR (400 MHz, DMSO-d6): δ 10.31 (1H, br s, NH), 7.66-7.56 (2H, m, H-2',6'), 7.21-7.12 (2H, m, H-3',5'), 4.25 (2H, s, $COCH_2$).

MS ESI (m/z): 186 $[M-H]^-$.

2-Chloro-*N*-(4-methoxyphenyl)acetamide **83h**:

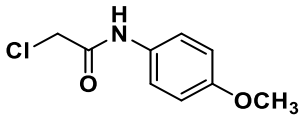

Prepared according to the procedure followed in **83a** using *p*-anisidine (0.4 g, 3.22 mmol). The crude product was purified by flash column chromatography (gradient elution, 4-14% EtOAc in hexane) to afford **83h** as an off white solid (0.58 g, 91%).

^{1}H-NMR (400 MHz, DMSO-d6): δ 10.16 (1H, br s, NH), 7.50 (2H, d, J=9.0Hz, H-2',6'), 6.90 (2H, d, J=9.0Hz, H-3',5'), 4.21 (2H, s, $COCH_2$), 3.72 (3H, s, OCH_3).
MS ESI (m/z): 198 $[M-H]^-$.

2-Chloro-*N*-(6-methoxypyridin-3-yl)acetamide **83i**:

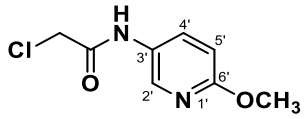

Prepared according to the procedure followed in **83a** using 5-amino-2-methoxypyridine (0.4 g, 3.22 mmol). The crude product was purified by flash column chromatography (gradient elution, 5-18% EtOAc in hexane) to afford **83i** as a pale pink solid (0.56 g, 87%).
^{1}H-NMR (400 MHz, DMSO-d6): δ 10.31 (1H, br s, NH), 8.34 (1H, d, J=2.6Hz, H-2'), 7.89 (1H, dd, J=2.6Hz, J=8.9Hz, H-4'), 6.82 (1H, d, J=8.9Hz, H-5'), 4.25 (2H, s, $COCH_2$), 3.82 (3H, s, OCH_3).
MS ESI (m/z): 199 $[M-H]^-$.

2-Chloro-*N*-(4-methoxybenzyl)acetamide **83j**:

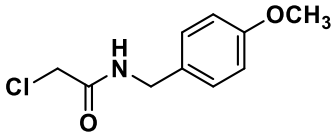

Prepared according to the procedure followed in **83a** using 4-methoxybenzylamine (0.4 g, 3.22 mmol). The crude product was purified by flash column chromatography (gradient elution, 2-12% EtOAc in hexane) to afford **83j** as an off white solid (0.65 g, 95%).
^{1}H-NMR (400 MHz, DMSO-d6): δ 8.64 (1H, t, J=6.1Hz, NH), 7.19 (2H, d, J=8.8Hz, H-2',6'), 6.88 (2H, d, J=8.8Hz, H-3',5'), 4.22 (2H, d, J=6.1Hz, NCH_2), 4.09 (2H, s, $COCH_2$), 3.72 (3H, s, OCH_3).
MS ESI (m/z): 212 $[M-H]^-$.

2-Chloro-*N*-(3,4,5-trimethoxyphenyl)acetamide **83k**:

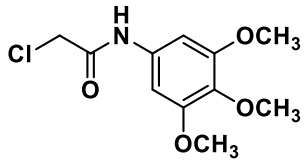

Prepared according to the procedure followed in **83a** using 3,4,5-trimethoxyaniline (0.59 g, 3.22 mmol). The crude product was purified by flash column chromatography (gradient elution, 5-18% EtOAc in hexane) to afford **83k** as an off white solid (0.72 g, 86%).

^{1}H-NMR (400 MHz, DMSO-d6): δ 10.24 (1H, br s, NH), 6.98 (2H, s, H-2',6'), 4.24 (2H, s, $COCH_2$), 3.76 (6H, s, 2 OCH_3), 3.63 (3H, s, OCH_3).

MS ESI (m/z): 258 $[M-H]^-$.

2-Chloro-*N*-(4-(methylthio)phenyl)acetamide **83l**:

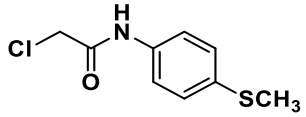

Prepared according to the procedure followed in **83a** using 4-(methylthio)aniline (0.45 g, 3.22 mmol). The crude product was purified by flash column chromatography (gradient elution, 2-12% EtOAc in hexane) to afford **83l** as a pale yellow solid (0.65 g, 94%).

^{1}H-NMR (400 MHz, DMSO-d6): δ 10.29 (1H, br s, NH), 7.54 (2H, d, J=9.0Hz, H-2',6'), 7.24 (2H, d, J=9.0Hz, H-3',5'), 4.23 (2H, s, $COCH_2$), 2.44 (3H, s, SCH_3).

2-Chloro-*N*-(3,4-dimethoxybenzyl)acetamide **83m**:

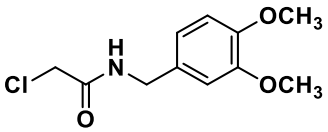

Prepared according to the procedure followed in **83a** using 3,4-dimethoxybenzylamine (0.54 g, 3.22 mmol). The crude product was purified by flash column chromatography (gradient elution, 5-15% EtOAc in hexane) to afford **83m** as an off white solid (0.69 g, 88%).

^{1}H-NMR (400 MHz, DMSO-d6): δ 8.63 (1H, t, J=6.1Hz, NH), 6.92-6.82 (2H, m, H-2',5'), 6.78 (1H, dd, J=1.5Hz, J=8.2Hz, H-6'), 4.23 (2H, d, J=6.1Hz, NCH_2), 4.10 (2H, s, $COCH_2$), 3.73 (6H, d, J=7.8Hz, 2 OCH_3).

MS ESI (m/z): 242 $[M-H]^-$.

2-Chloro-*N*-(4-(dimethylamino)phenyl)acetamide **83n**:

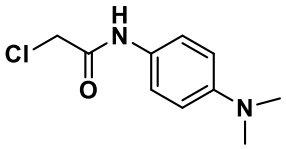

Prepared according to the procedure followed in **83a** using *N*,*N*-dimethyl-*p*-phenylenediamine (0.44 g, 3.22 mmol). The crude product was purified by flash column

chromatography (gradient elution, 5-18% EtOAc in hexane) to afford **83n** as a pale green solid (0.55 g, 81%).

^{1}H-NMR (400 MHz, DMSO-d6): δ 7.12 (2H, d, J=9.0Hz, H-2',6'), 6.75 (2H, d, J=9.0Hz, H-3',5'), 4.53 (2H, s, $COCH_2$), 2.95 (6H, s, 2 CH_3).

MS ESI (m/z): 213 $[M+H]^+$.

2-Chloro-*N*-(4-morpholinophenyl)acetamide **79o**:

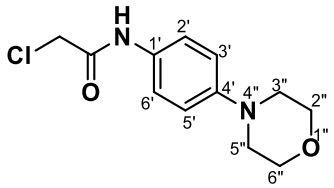

Prepared according to the procedure followed in **83a** using 4-morpholinoaniline (0.57 g, 3.22 mmol). The crude product was purified by flash column chromatography (gradient elution, 4-16% EtOAc in hexane) to afford **83o** as a pale yellow solid (0.67 g, 82%).

^{1}H-NMR (400 MHz, DMSO-*d6*): δ 10.05 (1H, br s, NH), 7.44 (2H, d, J=9.0Hz, H-2',6'), 6.91 (2H, d, J=9.0Hz, H-3',5'), 4.19 (2H, s, $COCH_2$), 3.76-369 (4H, m, H-2",6"), 3.08-3.00 (4H, m, H-3",5").

MS ESI (m/z): 253 $[M-H]^-$.

2-((*1H*-Indazol-5-yl)amino)-*N*-phenylthiazole-5-carboxamide **85a**:

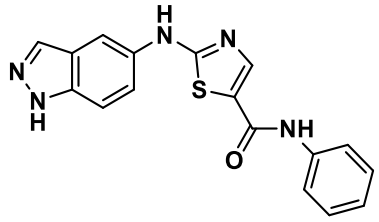

Chloroacetamide derivative **83a** (0.068 g, 0.4 mmol) was added to a suspension of disubstituted thiourea derivative **82** (0.1 g, 0.4 mmol) in MeOH (5 mL). The mixture was heated under reflux for 6h. The completion of the reaction was monitored by TLC, and then the solvent was evaporated under vacuum. The resulting residue was silica flash column chromatographed (gradient elution, 3−12% MeOH in CH_2Cl_2) to afford **85a** as an off white solid (0.05 g, 37%).

^{1}H-NMR (400 MHz, DMSO-*d6*): see Table 31.

MS ESI (m/z): 334 $[M-H]^-$, **HRMS:** m/z calculated for $C_{17}H_{13}N_5OS^-$: 334.0768, found: 334.07709.

2-((*1H*-Indazol-5-yl)amino)-*N*-(3-phenoxyphenyl)thiazole-5-carboxamide **85b**:

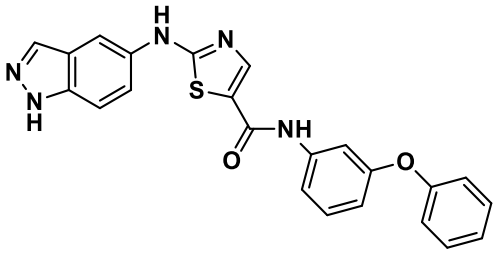

Prepared according to **85a**, disubstituted thiourea derivative **82** (0.1 g, 0.4 mmol) was reacted with chloroacetamide derivative **83b** (0.1 g, 0.4 mmol). The resulting residue was silica flash column chromatographed (gradient elution, 2−12% MeOH in CH_2Cl_2) to afford **85b** as an off white solid (0.068 g, 40%).

^{1}H-NMR (400 MHz, DMSO-d6): see Table 31.

MS ESI (m/z): 426 $[M-H]^-$, **HRMS:** m/z calculated for $C_{23}H_{17}N_5O_2S^-$: 426.10302, found: 426.10345.

2-((*1H*-Indazol-5-yl)amino)-*N*-(3-methoxyphenyl)thiazole-5-carboxamide **85c**:

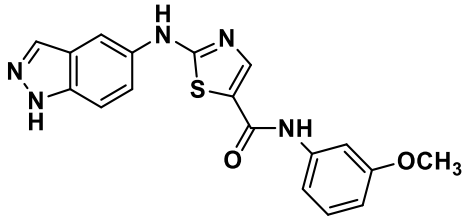

Prepared according to **85a**, disubstituted thiourea derivative **82** (0.1 g, 0.4 mmol) was reacted with chloroacetamide derivative **83c** (0.08 g, 0.4 mmol). The resulting residue was silica flash column chromatographed (gradient elution, 2−15% MeOH in CH_2Cl_2) to afford **85c** as an off white solid (0.057 g, 39%).

^{1}H-NMR (400 MHz, DMSO-d6): see Table 31.

MS ESI (m/z): 364 $[M-H]^-$, **HRMS:** m/z calculated for $C_{18}H_{15}N_5O_2S^-$: 364.08737, found: 364.08783.

2-((*1H*-Indazol-5-yl)amino)-*N*-(benzo[*d*][1,3]dioxol-5-yl)thiazole-5-carboxamide **85d**:

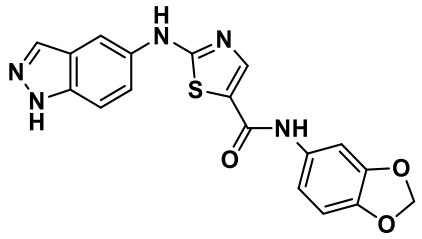

Prepared according to **85a**, disubstituted thiourea derivative **82** (0.1 g, 0.4 mmol) was reacted with chloroacetamide derivative **83d** (0.085 g, 0.4 mmol). The resulting residue was silica flash column chromatographed (gradient elution, 2−15% MeOH in CH_2Cl_2) to afford **85d** as an off white solid (0.065 g, 43%).

^{1}H-NMR (400 MHz, DMSO-d6): see Table 31.

MS ESI (m/z): 378 $[M-H]^-$, **HRMS:** m/z calculated for $C_{18}H_{13}N_5O_3S^-$: 378.06663, found: 378.06729.

2-((*1H*-Indazol-5-yl)amino)-*N*-(2,3-dihydrobenzo[*b*][1,4]dioxin-6-yl)thiazole-5-carboxamide **85e**:

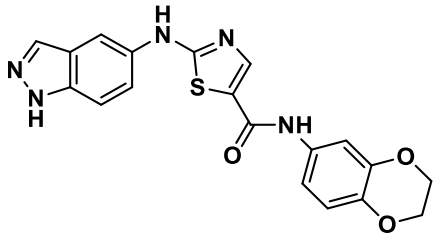

Prepared according to **85a**, disubstituted thiourea derivative **82** (0.1 g, 0.4 mmol) was reacted with chloroacetamide derivative **83e** (0.09 g, 0.4 mmol). The resulting residue was silica flash column chromatographed (gradient elution, 2−15% MeOH in CH_2Cl_2) to afford **85e** as a pale yellow solid (0.075 g, 48%).

^{1}H-NMR (400 MHz, DMSO-d6): see Table 31.

^{13}C NMR (100MHz, DMSO-*d6*): δ 168, 159.4, 143.3, 142.5, 140.0, 137.0, 134.2, 133.8, 132.9, 123.4, 123.2, 120.2, 117.2, 113.8, 111.2, 109.7, 108.4, 64.6, 64.4.

MS ESI (m/z): 392 $[M-H]^-$, **HRMS:** m/z calculated for $C_{19}H_{15}N_5O_3S^-$: 392.08228, found: 392.08325.

2-((*1H*-Indazol-5-yl)amino)-*N*-(3,4-dimethoxyphenyl)thiazole-5-carboxamide **85f**:

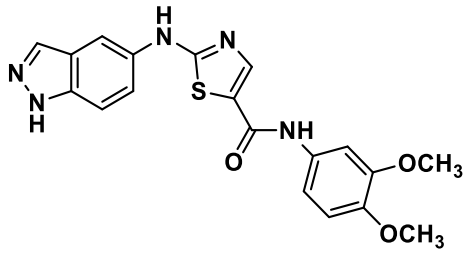

Prepared according to **85a**, disubstituted thiourea derivative **82** (0.1 g, 0.4 mmol) was reacted with chloroacetamide derivative **83f** (0.092 g, 0.4 mmol). The resulting residue was silica flash column chromatographed (gradient elution, 5−18% MeOH in CH_2Cl_2) to afford **85f** as a beige solid (0.055 g, 35%).

^{1}H-NMR (400 MHz, DMSO-d6): see Table 31.

^{13}C NMR (100MHz, DMSO-*d6*): δ 167.9, 159.4, 148.9, 145.5, 142.4, 138.3, 137.8, 134.3, 133.9, 132.8, 123.5, 121.0, 112.6, 111.9, 111.2, 108.4, 105.8, 56.2, 55.8.

MS ESI (m/z): 394 $[M-H]^-$, **HRMS:** m/z calculated for $C_{19}H_{17}N_5O_3S^-$: 394.09793, found: 394.09866.

2-((*1H*-Indazol-5-yl)amino)-*N*-(4-fluorophenyl)thiazole-5-carboxamide **85g**:

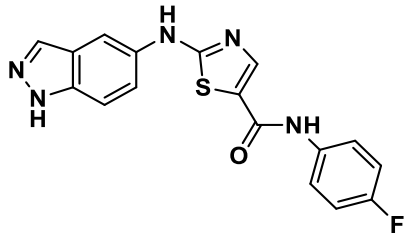

Prepared according to **85a**, disubstituted thiourea derivative **82** (0.1 g, 0.4 mmol) was reacted with chloroacetamide derivative **83g** (0.075 g, 0.4 mmol). The resulting residue was silica flash column chromatographed (gradient elution, 2−12% MeOH in CH_2Cl_2) to afford **85g** as a yellow solid (0.04 g, 29%).

^{1}H-NMR (400 MHz, DMSO-d6): see Table 31.

^{13}C NMR (100MHz, DMSO-*d6*): δ 168.2, 159.8, 157.4, 143.0, 135.7, 135.0, 134.1, 133.8, 129.0, 123.4, 122.9, 122.4, 120.8, 120.3, 115.8, 115.6, 111.2, 108.6.

MS ESI (m/z): 352 $[M-H]^-$, **HRMS:** m/z calculated for $C_{17}H_{12}N_5OSF^-$: 352.06738, found: 352.06812.

2-((*1H*-Indazol-5-yl)amino)-*N*-(4-methoxyphenyl)thiazole-5-carboxamide **85h**:

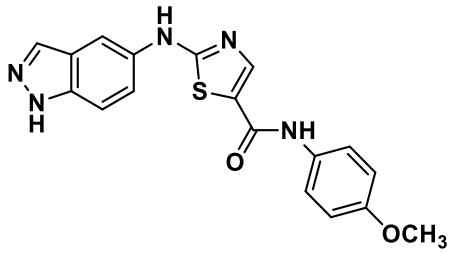

Prepared according to **85a**, disubstituted thiourea derivative **82** (0.1 g, 0.4 mmol) was reacted with chloroacetamide derivative **83h** (0.08 g, 0.4 mmol). The resulting residue was silica flash column chromatographed (gradient elution, 3−15% MeOH in CH_2Cl_2) to afford **85h** as an off white solid (0.067 g, 46%).

^{1}H-NMR (400 MHz, DMSO-d6): see Table 31.

MS ESI (m/z): 364 $[M-H]^-$, **HRMS:** m/z calculated for $C_{18}H_{15}N_5O_2S^-$: 364.08737, found: 364.08804.

2-((*1H*-Indazol-5-yl)amino)-*N*-(6-methoxypyridin-3-yl)thiazole-5-carboxamide **85i**:

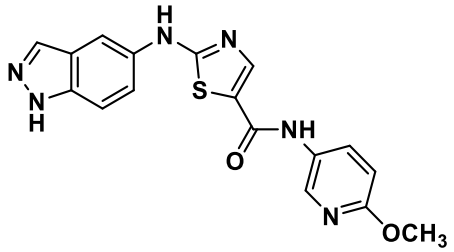

Prepared according to **85a**, disubstituted thiourea derivative **82** (0.1 g, 0.4 mmol) was reacted with chloroacetamide derivative **83i** (0.08 g, 0.4 mmol). The resulting residue was silica flash column chromatographed (gradient elution, 3−15% MeOH in CH_2Cl_2) to afford **85i** as a pale brown solid (0.048 g, 33%).

^{1}H-NMR (400 MHz, DMSO-d6): see Table 31.

MS ESI (m/z): 365 $[M-H]^-$, **HRMS:** m/z calculated for $C_{17}H_{14}N_6O_2S^-$: 365.08262, found: 365.08337.

2-((*1H*-Indazol-5-yl)amino)-*N*-(4-methoxybenzyl)thiazole-5-carboxamide **85j**:

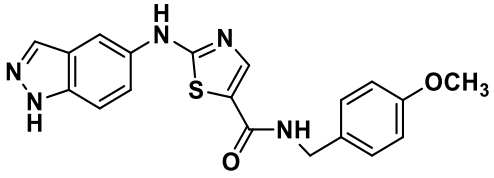

Prepared according to **85a**, disubstituted thiourea derivative **82** (0.1 g, 0.4 mmol) was reacted with chloroacetamide derivative **83j** (0.085 g, 0.4 mmol). The resulting residue was silica flash column chromatographed (gradient elution, 2−10% MeOH in CH_2Cl_2) to afford **85j** as a yellow solid (0.074 g, 49%).

^{1}H-NMR (400 MHz, DMSO-d6): see Table 31.

^{13}C NMR (100MHz, DMSO-*d6*): δ 167.5, 161, 158.7, 141.7, 141.5, 137.0, 134.3, 133.7, 132.0, 129.1, 123.4, 123.0, 120.1, 114.2, 111.1, 108.2, 55.5, 42.3.

MS ESI (m/z): 378 $[M-H]^-$, **HRMS:** m/z calculated for $C_{19}H_{17}N_5O_2S^-$: 378.10302, found: 378.10342.

2-((*1H*-Indazol-5-yl)amino)-*N*-(3,4,5-trimethoxyphenyl)thiazole-5-carboxamide **85k**:

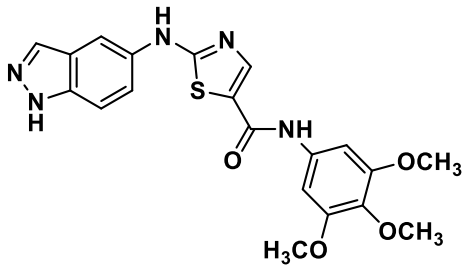

Prepared according to **85a**, disubstituted thiourea derivative **82** (0.1 g, 0.4 mmol) was reacted with chloroacetamide derivative **83k** (0.1 g, 0.4 mmol). The resulting residue was silica flash column chromatographed (gradient elution, 3−18% MeOH in CH_2Cl_2) to afford **85k** as a pale brown solid (0.064 g, 38%).

^{1}H-NMR (400 MHz, DMSO-d6): see Table 31.

^{13}C NMR (100MHz, DMSO-*d6*): δ 168.1, 159.6, 153.1, 142.7, 137.1, 135.5, 134.1, 134.0, 133.8, 129.0, 123.4, 123.2, 120.9, 120.3, 111.2, 108.5, 98.2, 60.6, 56.2.

MS ESI (m/z): 424 $[M-H]^-$, **HRMS:** m/z calculated for $C_{20}H_{19}N_5O_4S^-$: 424.10850, found: 424.10950.

2-((*1H*-Indazol-5-yl)amino)-*N*-(4-(methylthio)phenyl)thiazole-5-carboxamide **85l**:

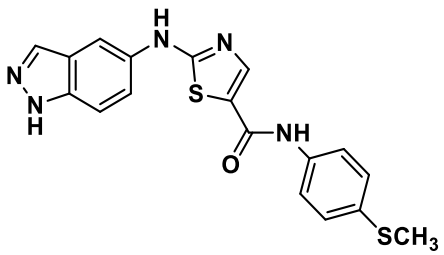

Prepared according to **85a**, disubstituted thiourea derivative **82** (0.1 g, 0.4 mmol) was reacted with chloroacetamide derivative **83l** (0.086 g, 0.4 mmol). The resulting residue was silica flash column chromatographed (gradient elution, 2−10% MeOH in CH_2Cl_2) to afford **85l** as a beige solid (0.07 g, 47%).

^{1}H-NMR (400 MHz, DMSO-d6): see Table 31.

MS ESI (m/z): 380 $[M-H]^-$, **HRMS:** m/z calculated for $C_{18}H_{15}N_5OS_2^-$: 380.06452, found: 380.06528.

2-((*1H*-Indazol-5-yl)amino)-*N*-(3,4-dimethoxybenzyl)thiazole-5-carboxamide **85m**:

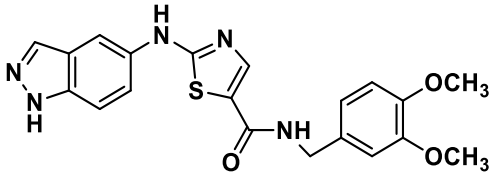

Prepared according to **85a**, disubstituted thiourea derivative **82** (0.1 g, 0.4 mmol) was reacted with chloroacetamide derivative **83m** (0.097 g, 0.4 mmol). The resulting residue was silica flash column chromatographed (gradient elution, 3−12% MeOH in CH_2Cl_2) to afford **85m** as a pale green solid (0.08 g, 49%).

^{1}H-NMR (400 MHz, DMSO-d6): see Table 31.

MS ESI (m/z): 408 $[M-H]^-$, **HRMS:** m/z calculated for $C_{20}H_{19}N_5O_3S^-$: 408.11358, found: 408.11441.

2-((*1H*-Indazol-5-yl)amino)-*N*-(4-(dimethylamino)phenyl)thiazole-5-carboxamide **85n**:

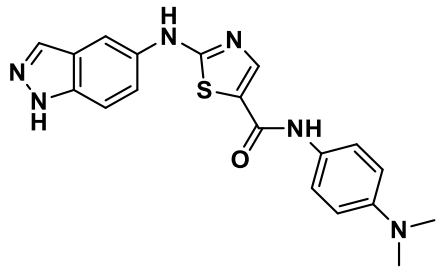

Prepared according to **85a**, disubstituted thiourea derivative **82** (0.1 g, 0.4 mmol) was reacted with chloroacetamide derivative **83n** (0.085 g, 0.4 mmol). The resulting residue was silica flash column chromatographed (gradient elution, 3−15% MeOH in CH_2Cl_2) to afford **85n** as a pale green solid (0.047 g, 31%).

^{1}H-NMR (400 MHz, DMSO-d6): see Table 31.

MS ESI (m/z): 377 $[M-H]^-$, **HRMS:** m/z calculated for $C_{19}H_{18}N_6OS^-$: 377.11900, found: 377.11948.

2-((*1H*-Indazol-5-yl)amino)-*N*-(4-morpholinophenyl)thiazole-5-carboxamide **85o**:

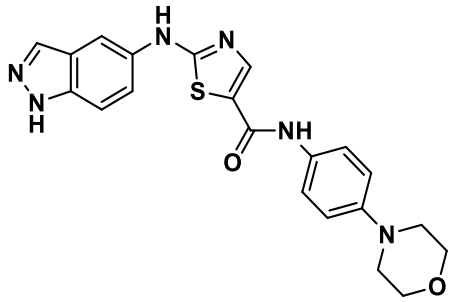

Prepared according to the procedure followed in **85a** using chloroacetamide derivatives **83o** (0.1 g, 0.4 mmol). The resulting residue was silica flash column chromatographed (gradient elution, 3−15% MeOH in CH_2Cl_2) to afford **85o** as an off white solid (0.072 g, 43%).

^{1}H-NMR (400 MHz, DMSO-d6): see Table 31.

MS ESI (m/z): 419 $[M-H]^-$, **HRMS:** m/z calculated for $C_{21}H_{20}N_6O_2S^-$: 419.12957, found: 419.13022.

Table 31: NMR data of compounds **85a-o**

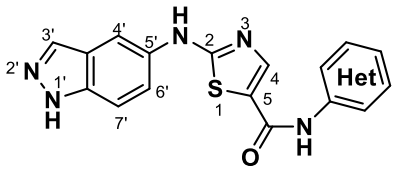

Entry		Scaffold	R
		^{1}H-NMR (400 MHz, DMSO-d6) δ ppm	^{1}H-NMR (400 MHz, DMSO-d6) δ ppm
85a	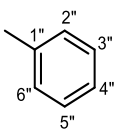	13.02 (1H, br s, $N^{1'}$-H), 10.59 (1H, br s, C_2-NH), 10.05 (1H, br s, CO-NH), 8.19 (1H, d, J=1.7Hz, H-4'), 8.13 (1H, s, H-4), 8.06 (1H, s, H-3'), 7.54 (1H, d, J=8.9Hz, H-7'), 7.41 (1H, dd, J=1.7Hz, J=8.9Hz, H-6')	7.70-7.64 (2H, m, H-2",6"), 7.36-7.29 (2H, m, H-3",5"), 7.11-7.04 (1H, m, H-4")

Entry	Het	Scaffold ^{1}H-NMR (400 MHz, DMSO-d6) δ ppm	R ^{1}H-NMR (400 MHz, DMSO-d6) δ ppm
85b	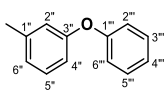	13.02 (1H, br s, $N^{1'}$-H), 10.63 (1H, br s, C_2-NH), 10.02 (1H, br s, CO-NH), 8.19 (1H, d, J=1.9Hz, H-4'), 8.14 (1H, s, H-4), 8.05 (1H, s, H-3'), 7.53 (1H, d, J=9.1Hz, H-7'), 7.42 (1H, dd, J=1.9Hz, J=9.1Hz, H-6')	7.63 (1H, ddd, J=0.9Hz, J=2.6Hz, J=8.1Hz, Ar-H) 7.51 (1H, t, J=2.6Hz, H-2"), 7.44-7.33 (3H, m, Ar-H), 7.21-7.12 (1H, m, Ar-H), 7.12-7.05 (2H, m, Ar-H), 6.87-6.79 (1H, ddd, J=0.9Hz, J=2.6Hz, J=8.1Hz, Ar-H)
85c	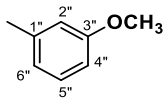	13.03 (1H, br s, $N^{1'}$-H), 10.61 (1H, br s, C_2-NH), 10.04 (1H, br s, CO-NH), 8.20 (1H, d, J=1.9Hz, H-4'), 8.14 (1H, s, H-4), 8.07 (1H, s, H-3'), 7.55 (1H, d, J=9.1Hz, H-7'), 7.42 (1H, dd, J=1.9Hz, J=9.1Hz, H-6')	7.38 (1H, t, J=2.1Hz H-2"), 7.27-7.25 (2H, m, H-5",6"), 6.68 (1H, td, J=2.1Hz, J=7.9Hz, H-4"), 3.77 (3H, s, OCH_3)
85d	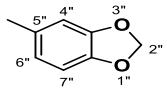	13.01 (1H, br s, $N^{1'}$-H), 10.57 (1H, br s, C_2-NH), 9.97 (1H, br s, CO-NH), 8.18 (1H, d, J=2.0Hz, H-4'), 8.08 (1H, s, H-4), 8.05 (1H, s, H-3'), 7.53 (1H, d, J=8.9Hz, H-7'), 7.40 (1H, dd, J=2.0Hz, J=8.9Hz, H-6')	7.33 (1H, d, J=2.1Hz, H-4"), 7.06 (1H, dd, J=2.1Hz, J=8.4Hz, H-6"), 6.88 (1H, d, J=8.4Hz, H-7"), 6.01 (2H, s, OCH_2O)
85e	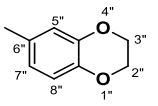	13.10 (1H, br s, $N^{1'}$-H), 11.67 (1H, br s, C_2-NH), 11.18 (1H, br s, CO-NH), 8.22 (1H, d, J=1.9Hz, H-4'), 8.11 (1H, s, H-3'), 8.04 (1H, s, H-4), 7.61-7.48* (3H, m, J=8.9Hz, H-6',7')	7.61-7.48* (3H, m, H-7"), 7.41 (1H, s, H-5"), 7.07 (1H, d, J=8.5Hz, H-8"), 4.04 (2H, s, OCH_2), 3.94 (2H, s, OCH_2)
85f	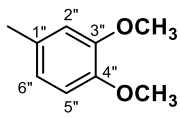	13.01 (1H, br s, $N^{1'}$-H), 10.55 (1H, br s, C_2-NH), 9.94 (1H, br s, CO-NH), 8.19 (1H, d, J=2.0Hz, H-4'), 8.09 (1H, s, H-4), 8.05 (1H, s, H-3'), 7.53 (1H, d, J=8.9Hz, H-7'), 7.41 (1H, dd, J=2.0Hz, J=8.9Hz, H-6')	7.35 (1H, d, J=2.3Hz, H-2"), 7.20 (1H, dd, J=2.3Hz, J=8.7Hz, H-6"), 6.92 (1H, d, J=8.7Hz, H-5"), 3.75 (3H, s, OCH_3), 3.73 (3H, s, OCH_3)

Entry	Het	Scaffold ^{1}H-NMR (400 MHz, DMSO-d6) δ ppm	R ^{1}H-NMR (400 MHz, DMSO-d6) δ ppm
85g	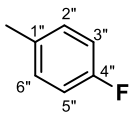	13.01 (1H, br s, $N^{1'}$-H), 10.30 (1H, br s, C_2-NH), 10.11 (1H, br s, CO-NH), 8.18 (1H, d, J=1.8Hz, H-4'), 8.11 (1H, s, H-4), 8.05 (1H, s, H-3'), 7.53 (1H, d, J=9.0Hz, H-7'), 7.40 (1H, dd, J=1.8Hz, J=9.0Hz, H-6')	7.72-7.65 (2H, m, H2",6"), 7.23-7.13 (2H, m, H-3",5")
85h	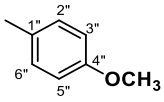	13.01 (1H, br s, $N^{1'}$-H), 10.55 (1H, br s, C_2-NH), 9.95 (1H, br s, CO-NH), 8.19 (1H, d, J=1.8Hz, H-4'), 8.08 (1H, s, H-4), 8.05 (1H, s, H-3'), 7.53 (1H, d, J=9.1Hz, H-7'), 7.40 (1H, dd, J=1.8Hz, J=9.1Hz, H-6')	7.56 (2H, d, J=9.0Hz, H-2",6"), 6.91 (2H, d, J=9.0Hz, H-3",5"), 3.74 (3H, s, OCH_3)
85i	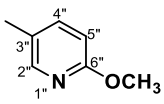	13.01 (1H, br s, $N^{1'}$-H), 10.60 (1H, br s, C_2-NH), 10.11 (1H, br s, CO-NH), 8.19 (1H, d, J=2.1Hz, H-4'), 8.09 (1H, s, H-4), 8.05 (1H, s, H-3'), 7.54 (1H, d, J=9.1Hz, H-7'), 7.40 (1H, dd, J=2.1Hz, J=9.1Hz, H-6')	8.41 (1H, d, J=2.6Hz, H-2"), 7.95 (1H, dd, J=2.6Hz, J=8.9Hz, H-4"), 6.83 (1H, d, J=8.9Hz, H-5"), 3.83 (3H, s, OCH_3)
85j	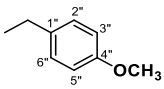	12.98 (1H, br s, $N^{1'}$-H), 10.45 (1H, br s, C_2-NH), 8.77 (1H, t, J=6.5Hz, CO-NH), 8.18 (1H, d, J=1.8Hz, H-4'), 8.03 (1H, s, H-3'), 7.90 (1H, s, H-4), 7.51 (1H, d, J=8.9Hz, H-7'), 7.38 (1H, dd, J=1.8Hz, J=8.9Hz, H-6')	7.23 (2H, d, J=8.8Hz, H-2",6"), 6.90 (2H, d, J=8.8Hz, H-3",5"), 4.34 (2H, d, J=6.1Hz, CH_2), 3.73 (3H, s, OCH_3)
85k	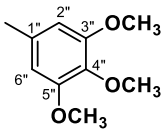	13.01 (1H, br s, $N^{1'}$-H), 10.59 (1H, br s, C_2-NH), 9.99 (1H, br s, CO-NH), 8.20 (1H, d, J=2.1Hz, H-4'), 8.11 (1H, s, H-4), 8.05 (1H, s, H-3'), 7.53 (1H, d, J=9.0Hz, H-7'), 7.41 (1H, dd, J=2.1Hz, J=9.0Hz, H-6')	7.10 (2H, s, H-2",6"), 3.76 (6H, s, 2 OCH_3), 3.63 (3H, s, OCH_3)
85l	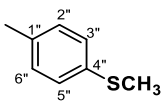	13.03 (1H, br s, $N^{1'}$-H), 10.61 (1H, br s, C_2-NH), 10.08 (1H, br s, CO-NH), 8.20 (1H, d, J=1.9Hz, H-4'), 8.13 (1H, s, H-4), 8.07 (1H, s, H-3'), 7.55 (1H, d, J=9.1Hz, H-7'), 7.42 (1H, dd, J=1.9Hz, J=9.1Hz, H-6')	7.65 (2H, d, J=9.0Hz, H-2",6"), 7.27 (2H, d, J=9.0Hz, H-3",5"), 2.46 (3H, s, SCH_3)

Entry		Scaffold ^{1}H-NMR (400 MHz, DMSO-d6) δ ppm	R ^{1}H-NMR (400 MHz, DMSO-d6) δ ppm
85m	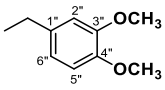	12.98 (1H, br s, $N^{1'}$-H), 10.45 (1H, br s, C_2-NH), 8.75 (1H, t, J=6.4Hz, CO-NH), 8.18 (1H, d, J=1.9Hz, H-4'), 8.03 (1H, s, H-3'), 7.91 (1H, s, H-4), 7.51 (1H, d, J=8.9Hz, H-7'), 7.38 (1H, dd, J=1.9Hz, J=8.9Hz, H-6')	6.92 (1H, d, J=1.5Hz, H-2"), 6.91 (1H, d, J=8.2Hz, H-5"), 6.82 (1H, dd, J=1.5Hz, J=8.2Hz, H-6"), 4.34 (2H, d, J=6.1Hz, CH_2), 3.74 (3H, s, OCH_3), 3.72 (3H, s, OCH_3)
85n	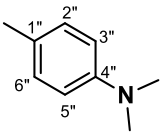	13.00 (1H, br s, $N^{1'}$-H), 10.52 (1H, br s, C_2-NH), 9.82 (1H, br s, CO-NH), 8.20 (1H, d, J=2.0Hz, H-4'), 8.08-8.02 (2H, m, H-4, 3'), 7.53 (1H, d, J=8.9Hz, H-7'), 7.40 (1H, dd, J=2.0Hz, J=8.9Hz, H-6')	7.45 (d, 1H, J=9.1Hz, H-2",6"), 6.72 (1H, d, J=9.1Hz, H-3",5"), 2.86 (6H, s, 2 CH_3)
85o	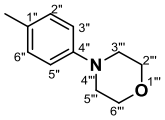	13.01 (1H, br s, $N^{1'}$-H), 10.54 (1H, br s, C_2-NH), 9.90 (1H, br s, CO-NH), 8.19 (1H, d, J=1.8Hz, H-4'), 8.07 (1H, s, H-4), 8.05 (1H, s, H-3'), 7.53 (1H, d, J=8.8Hz, H-7'), 7.40 (1H, dd, J=1.8Hz, J=8.8Hz, H-6')	7.51 (2H, d, J=9.0Hz, H-2",6"), 6.93 (2H, d, J=9.0Hz, H-3",5"), 3.78-3.70 (4H, m, 2 OCH_2), 3.10-3.03 (4H, m, 2 NCH_2)

4-Nitroindazole **87:**

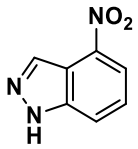

To a cooled solution of 2-methyl-3-nitroaniline **86** (5.0 g, 32.9 mmol) in glacial acetic acid (75 mL) at 0 °C, was added dropwise a cooled solution of sodium nitrite (2.72 g, 38.63 mmol) in water (12 mL). The resulting solution was stirred at 0 °C for 1h then allowed to warm to room temperature. Then, the reaction mixture is allowed to stand at room temperature for 3 days. The solution was concentrated under reduced pressure. The residue was diluted with EtOAc and washed thoroughly with saturated aqueous $NaHCO_3$, brine, and water. The organic layer was dried over Na_2SO_4, filtered, and the solvent was removed *in vacuo*. The resulting residue was silica flash column chromatographed (gradient elution, 2-10% EtOAc in hexane) to afford **87** as a yellow powder in 89% yield.

^{1}H-NMR (400 MHz, DMSO-d6): δ 13.91 (1H, br s, N^1-H), 8.54 (1H, s, H-3), 8.16 (1H, dd, J=0.5Hz, J=7.7Hz, H-5), 8.09 (1H, d, J=8.3Hz, H-7), 7.61 (1H, t, J=7.9Hz, H-6).

4-Amino-*1H*-indazole **88**:

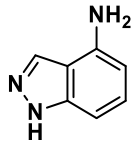

To a solution of 4-nitroindazole **87** (3.26 g, 20 mmol) in MeOH (50 mL), Pd/C (0.5 g, 10% w/w) and $NH_2NH_2.H_2O$ (1.3 mL, 26.15 mmol) were added. The reaction mixture was heated under reflux for 3h. The solution was filtered hot through a bed of Celite then washed with hot MeOH. The solvent was removed under reduced pressure and the resulting residue was purified by flash column chromatography (gradient elution, 1-6% MeOH in CH_2Cl_2) to afford **88** as a white powder (5.04g, 83%).

^{1}H-NMR (400 MHz, DMSO-d6): δ 12.59 (1H, br s, N^1-H), 8.07 (1H, s, H-3), 6.97 (1H, t, J=7.9Hz, H-6), 6.60 (1H, d, J=8.2Hz, H-7), 6.11 (1H, d, J=7.4Hz, H-5), 5.68 (2H, br s, NH_2).

MS ESI (m/z): 134 $[M+H]^+$.

N-((*1H*-Indazol-4-yl)carbamothioyl)benzamide **89**:

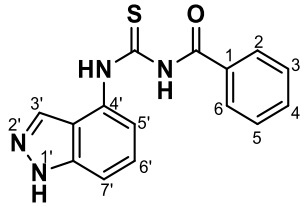

To a solution of 4-amino-*1H*-indazole **88** (4 g, 30.04 mmol) in acetone (40 mL) was added benzoyl isothiocyanate (4.43 mL, 30.67 mmol). The reaction mixture was stirred at ambient temperature for 2h. After completion of reaction (TLC monitoring), the precipitate was filtered, washed with acetone, and dried to afford the product **89** as a white reddish crystalline solid (6.68 g, 75%) which was used for the next step without further purification.

^{1}H-NMR (400 MHz, DMSO-d6): δ 13.30 (1H, br s, NH), 13.14 (1H, br s, NH), 11.73 (1H, br s, NH), 8.08 (1H, s, H-3'), 8.03 (2H, d, J=7.5Hz, H-2,6), 7.96 (1H, d, J=7.0Hz, H-5'), 7.68 (1H, t, J=7.3Hz, H-4), 7.56 (2H, t, J=7.7Hz, H-3,5), 7.47 (1H, d, J=8.3Hz, H-7'), 7.40 (1H, t, J=7.8Hz, H-6').

MS ESI (m/z): 295 $[M-H]^-$.

1-(*1H*-Indazol-4-yl)thiourea **90**:

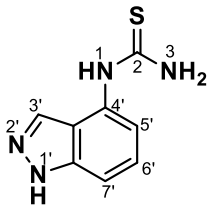

To a suspension of **89** (5g, 16.87 mmol) in MeOH (50 mL) was added LiOH solution (0.13 g, 5.6 mmol) in H_2O (2 mL) at room temperature, a clear solution resulted in 15 minutes. The reaction mixture was heated up to 75 ^oC for 1h. After completion of reaction (TLC monitoring), the solvent was concentrated and the precipitated compound was separated and washed on the filter with methanol and dried under high vacuum to get the desired product **90** as a white solid (2.5g, 77%). The product was used for the next step without further purification.

^{1}H-NMR (400 MHz, DMSO-d6): δ 13.12 (1H, br s, NH), 9.88 (1H, br s, NH), 8.02 (1H, s, H-3'), 7.31 (5H, m, H-5',6',7', NH_2).

Ethyl 2-((*1H*-indazol-4-yl)amino)thiazole-4-carboxylate **91:**

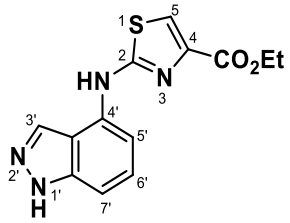

To a suspension of thiourea derivative **90** (2.0 g, 10.4 mmol) in ethanol (20 mL) was added ethyl 2-bromopyruvate (1.31 mL, 10.4 mmol). The reaction was heated at 90 ^oC for 3h and allowed to cool to room temperature. The solvent was evaporated under vacuum, and the resulting crude oil was purified by flash column chromatography (gradient elution, 2-8% MeOH in CH_2Cl_2) to afford **91** as a white powder (2.06g, 72%).

^{1}H-NMR (400 MHz, DMSO-d6): δ 13.08 (1H, br s, $N^{1'}$-H), 10.57 (1H, br s, C_2-NH), 8.36 (1H, s, H-3'), 7.90 (1H, d, J=7.6Hz, H-7'), 7.85 (1H, s, H-5), 7.31 (1H, t, J=8.0Hz, H-6'), 7.15 (1H, d, J=8.3Hz, H-5'), 4.29 (2H, q, J=7.1Hz, CH_2), 1.31 (3H, t, J=7.1Hz, CH_3).

MS ESI (m/z): 287 $[M-H]^-$.

2-((*1H*-Indazol-4-yl)amino)thiazole-4-carboxylic acid **92**:

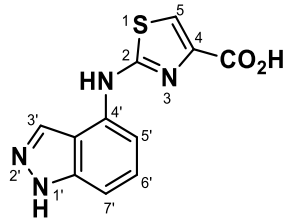

To a stirred suspension of ester **91** (2.0g, 6.94 mmol) in MeOH (20ml), LiOH (0.5g, 20.81 mmol) in water (5mL) was added. The mixture was stirred at room temperature for 12 h. The solvent was evaporated *in vacuo*. The resulting residue was dissolved in water, and the pH was adjusted to 4 by careful addition of 1N HCl. The resulting precipitate was isolated by filtration, washed by water then MeOH, and dried *in vacuo* to afford the desired compounds **92** as an off white powder (1.5g, 78%) which was used for the next step without further purification.

^{1}H-NMR (400 MHz, DMSO-d6): δ 13.05 (2H, br s, $N^{1'}$-H, COOH), 10.52 (1H, br s, C_2-NH), 8.38 (1H, s, H-3'), 7.99 (1H, d, J=7.6Hz, H-7'), 7.79 (1H, s, H-5), 7.31 (1H, t, J=8.0Hz, H-6'), 7.14 (1H, d, J=8.3Hz, H-5').

MS ESI (m/z): 261 $[M+H]^+$, **HRMS:** m/z calculated for $C_{11}H_8N_4O_2S^+$: 261.04407, found: 261.04428.

2-((*1H*-Indazol-4-yl)amino)-*N*-phenylthiazole-4-carboxamide **93a**:

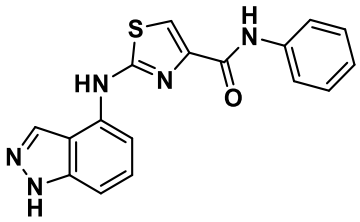

To a solution of acid **92** (0.1g, 0.38 mmol) and aniline (0.035 g, 0.38 mmol) in DMF (6 mL) was added HOAt (0.07 g, 0.42 mmol), EDC (0.081 g, 0.42 mmol) and DIEA (0.2 mL, 1.14 mmol). The reaction mixture was stirred at ambient temperature for 24h. The solvent was evaporated under vacuum and azeotroped twice with CH_2Cl_2. The resulting residue was silica flash column chromatographed (gradient elution, 2−12% MeOH in CH_2Cl_2) to afford **93a** as an off white solid (0.065 g, 51%).

^{1}H-NMR (400 MHz, DMSO-d6): see Table 32.

^{13}C NMR (100MHz, DMSO-*d6*): δ 163.6, 159.7, 151.6, 146.2, 141.5, 140.1, 138.8, 133.5, 131.8, 129.3, 127.9, 124.4, 121.2, 115.5, 115.0, 107.3, 104.3.

MS ESI (m/z): 334 $[M-H]^-$, **HRMS:** m/z calculated for $C_{17}H_{13}N_5OS^-$: 334.07680, found: 334.07727.

2-((*1H*-Indazol-4-yl)amino)-*N*-benzylthiazole-4-carboxamide **93b**:

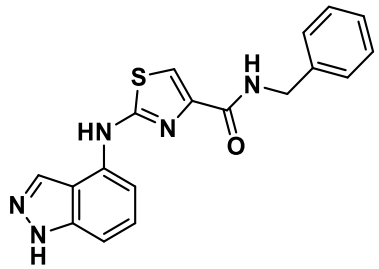

Prepared according to **93a**, acid **92** (0.1g, 0.38 mmol) was reacted with benzylamine (0.04 g, 0.38 mmol). The resulting residue was silica flash column chromatographed (gradient elution, 2−10% MeOH in CH_2Cl_2) to afford **93b** as an off white solid (0.074 g, 56%).

^{1}H-NMR (400 MHz, DMSO-d6): see Table 32.

^{13}C NMR (100MHz, DMSO-*d6*): δ 163.4, 161.3, 146.3, 141.4, 140.2, 133.5, 131.8, 128.7, 127.9, 127.6, 127.2, 121.1, 114.8, 114.6, 107.1, 104.0, 42.7.

MS ESI (m/z): 348 $[M-H]^-$, **HRMS:** m/z calculated for $C_{18}H_{15}N_5OS^-$: 348.09245, found: 348.09244.

2-((*1H*-Indazol-4-yl)amino)-*N*-(pyridin-3-yl)thiazole-4-carboxamide **93c**:

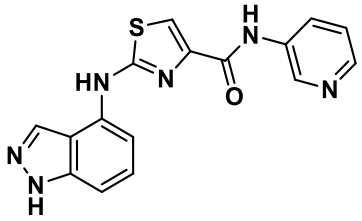

Prepared according to **93a**, acid **92** (0.1g, 0.38 mmol) was reacted with 3-aminopyridine (0.035 g, 0.38 mmol). The resulting residue was silica flash column chromatographed (gradient elution, 2−14% MeOH in CH_2Cl_2) to afford **93c** as a creamy white solid (0.062 g, 49%).

^{1}H-NMR (400 MHz, DMSO-d6): see Table 32.

^{13}C NMR (100MHz, DMSO-*d6*): δ 163.7, 160.3, 150.6, 145.7, 141.5, 140.0, 135.0, 133.4, 131.8, 128.9, 124.0, 120.7, 116.3, 114.9, 107.4, 104.3.

MS ESI (m/z): 335 $[M-H]^-$, **HRMS:** m/z calculated for $C_{16}H_{12}N_6OS^-$: 335.07205, found: 335.07248.

2-((*1H*-Indazol-4-yl)amino)-*N*-(4-fluorophenyl)thiazole-4-carboxamide **93d**:

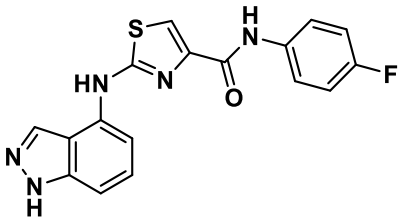

Prepared according to **93a**, acid **92** (0.1g, 0.38 mmol) was reacted with 4-fluoroaniline (0.042 g, 0.38 mmol). The resulting residue was silica flash column chromatographed (gradient elution, 2−12% MeOH in CH_2Cl_2) to afford **93d** as an off white solid (0.067 g, 50%).

^{1}H-NMR (400 MHz, DMSO-d6): see Table 32.

^{13}C NMR (100MHz, DMSO-*d6*): δ 163.5, 160.1, 159.8, 157.8, 146.2, 141.4, 135.2, 133.5, 131.8, 127.9, 123.1, 115.8, 115.7, 115.6, 114.9, 107.3, 104.2.

MS ESI (m/z): 352 $[M-H]^-$, **HRMS:** m/z calculated for $C_{17}H_{12}FN_5OS^-$: 352.06738, found: 352.06760.

2-((*1H*-indazol-4-yl)amino)-*N*-(benzo[*d*][1,3]dioxol-5-yl)thiazole-4-carboxamide **93e**:

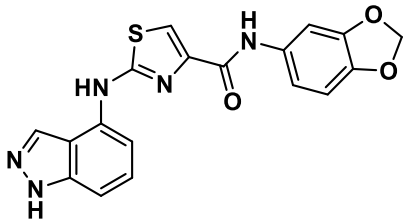

Prepared according to **93a**, acid **92** (0.1g, 0.38 mmol) was reacted with 3,4-(methylenedioxy) aniline (0.052 g, 0.38 mmol). The resulting residue was silica flash column chromatographed (gradient elution, 2−14% MeOH in CH_2Cl_2) to afford **93e** as a green solid (0.08 g, 57%).

^{1}H-NMR (400 MHz, DMSO-d6): see Table 32.

^{13}C NMR (100MHz, DMSO-*d6*): δ 163.5, 159.6, 147.5, 146.2, 144.0, 141.4, 133.4, 133, 131.8, 127.9, 115.4, 114.9, 114.2, 108.4, 107.3, 104.2, 103.2, 101.5.

MS ESI (m/z): 378 $[M-H]^-$, **HRMS:** m/z calculated for $C_{18}H_{13}N_5O_3S^-$: 378.06663, found: 378.06720.

2-((*1H*-Indazol-4-yl)amino)-*N*-(2,3-dihydrobenzo[*b*][1,4]dioxin-6-yl)thiazole-4-carboxamide **93f**:

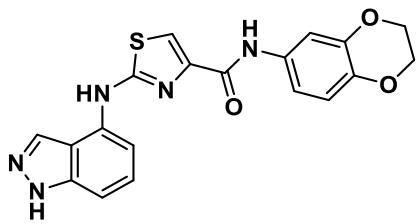

Prepared according to **93a**, acid **92** (0.1g, 0.38 mmol) was reacted with 1,4-benzodioxan-6-amine (0.052 g, 0.38 mmol). The resulting residue was silica flash column chromatographed (gradient elution, 2−15% MeOH in CH_2Cl_2) to afford **93f** as a beige solid (0.087 g, 58%).

^{1}H-NMR (400 MHz, DMSO-d6): see Table 32.

^{13}C NMR (100MHz, DMSO-*d6*): δ 163.5, 159.5, 146.3, 143.3, 141.4, 140.3, 133.5, 132.4, 131.8, 127.9, 117.1, 115.3, 115.0, 114.4, 110.2, 107.3, 104.2, 64.6, 64.4.

MS ESI (m/z): 392 $[M-H]^-$, **HRMS:** m/z calculated for $C_{19}H_{15}N_5O_3S^-$: 392.08228, found: 392.08249.

2-((*1H*-Indazol-4-yl)amino)-*N*-(3,4-dimethoxyphenyl)thiazole-4-carboxamide **93g**:

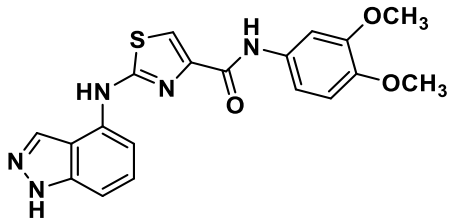

Prepared according to **93a**, acid **92** (0.1g, 0.38 mmol) was reacted with 3,4-dimethoxyaniline (0.058 g, 0.38 mmol). The resulting residue was silica flash column chromatographed (gradient elution, 4−15% MeOH in CH_2Cl_2) to afford **93g** as a green solid (0.078 g, 52%).

^{1}H-NMR (400 MHz, DMSO-d6): see Table 32.

^{13}C NMR (100MHz, DMSO-*d6*): δ 163.6, 159.5, 148.9, 146.3, 145.8, 141.5, 133.5, 132.2, 131.9, 128.0, 115.2, 114.9, 113.2, 112.3, 107.3, 106.3, 104.3, 56.1, 49.1.

MS ESI (m/z): 394 $[M-H]^-$, **HRMS:** m/z calculated for $C_{19}H_{17}N_5O_3S^-$: 394.09793, found: 394.09824.

2-((*1H*-Indazol-4-yl)amino)-*N*-(*p*-tolyl)thiazole-4-carboxamide **93h**:

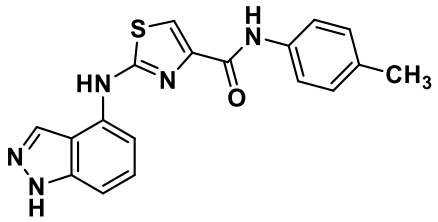

Prepared according to **93a**, acid **92** (0.1g, 0.38 mmol) was reacted with *p*-toluidine (0.04 g, 0.38 mmol). The resulting residue was silica flash column chromatographed (gradient elution, 2−10% MeOH in CH_2Cl_2) to afford **93h** as a beige solid (0.082 g, 62%).

^{1}H-NMR (400 MHz, DMSO-d6): see Table 32.

^{13}C NMR (100MHz, DMSO-*d6*): δ 163.5, 159.6, 151.40, 146.30, 141.5, 140.1, 136.3, 135.1, 133.5, 133.4, 131.8, 129.5, 127.8, 121.1, 115.3, 107.3, 104.3, 21.0.

MS ESI (m/z): 348 $[M-H]^-$, **HRMS:** m/z calculated for $C_{18}H_{15}N_5OS^-$: 348.09245, found: 348.09283.

2-((*1H*-Indazol-4-yl)amino)-*N*-(4-methoxyphenyl)thiazole-4-carboxamide **93i**:

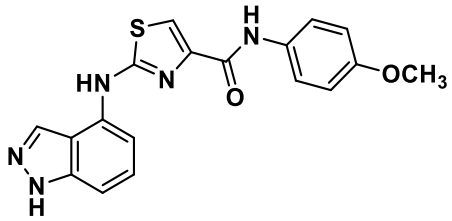

Prepared according to **93a**, acid **92** (0.1g, 0.38 mmol) was reacted with *p*-anisidine (0.047 g, 0.38 mmol). The resulting residue was silica flash column chromatographed (gradient elution, 3−14% MeOH in CH_2Cl_2) to afford **93i** as a beige solid (0.077 g, 56%).

^{1}H-NMR (400 MHz, DMSO-d6): see Table 32.

MS ESI (m/z): 364 $[M-H]^-$.

2-((*1H*-Indazol-4-yl)amino)-*N*-(2-(methylthio)phenyl)thiazole-4-carboxamide **93j**:

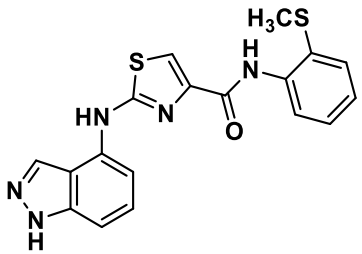

Prepared according to **93a**, acid **92** (0.1g, 0.38 mmol) was reacted with 2-(methylthio)aniline (0.053 g, 0.38 mmol). The resulting residue was silica flash column chromatographed

(gradient elution, 3−12% MeOH in CH_2Cl_2) to afford **93j** as an off white solid (0.068 g, 47%).

^{1}H-NMR (400 MHz, DMSO-d6): see Table 32.

MS ESI (m/z): 380 $[M-H]^-$, **HRMS:** m/z calculated for $C_{18}H_{15}N_5OS_2^-$: 380.06452, found: 380.06494.

2-((*1H*-Indazol-4-yl)amino)-*N*-(4-morpholinophenyl)thiazole-4-carboxamide **93k**:

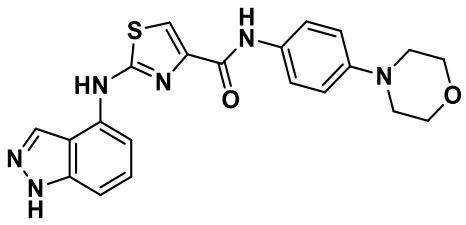

Prepared according to **93a**, acid **92** (0.1g, 0.38 mmol) was reacted with 4-morpholinoaniline (0.067 g, 0.38 mmol). The resulting residue was silica flash column chromatographed (gradient elution, 3−14% MeOH in CH_2Cl_2) to afford **93k** as a pale green solid (0.086 g, 54%).

^{1}H-NMR (400 MHz, DMSO-d6): see Table 32.

^{13}C NMR (100MHz, DMSO-*d6*): δ 163.50, 159.41, 156.20, 151.40, 146.40, 141.40, 140.10, 135.1, 133.5, 131.90, 129.30, 127.90, 122.90, 121.10, 115.10, 114.90, 114.20, 107.20, 104.2, 55.70, 49.0.

MS ESI (m/z): 419 $[M-H]^-$, **HRMS:** m/z calculated for $C_{21}H_{20}N_6O_2S^-$: 419.12957, found: 419.13004.

2-((*1H*-Indazol-4-yl)amino)-*N*-(3-methoxyphenyl)thiazole-4-carboxamide **93l**:

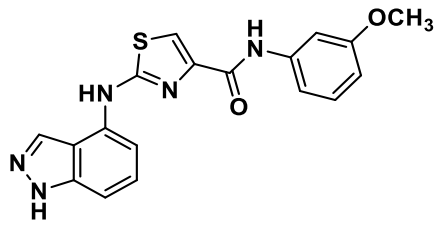

Prepared according to **93a**, acid **92** (0.1g, 0.38 mmol) was reacted with g *m*-anisidine (0.047 g, 0.38 mmol). The resulting residue was silica flash column chromatographed (gradient elution, 3−14% MeOH in CH_2Cl_2) to afford **93l** as a pale beige solid (0.07 g, 51%).

^{1}H-NMR (400 MHz, DMSO-d6): see Table 32.

MS ESI (m/z): 364 $[M-H]^-$, **HRMS:** m/z calculated for $C_{18}H_{15}N_5O_2S^-$: 364.08737, found: 364.08786.

2-((*1H*-Indazol-4-yl)amino)-*N*-(2,3-dihydro-*1H*-inden-5-yl)thiazole-4-carboxamide **93m**:

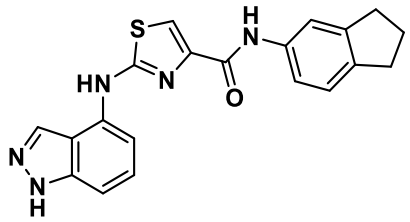

Prepared according to **93a**, acid **92** (0.1g, 0.38 mmol) was reacted with 5-aminoindan (0.05 g, 0.38 mmol). The resulting residue was silica flash column chromatographed (gradient elution, 2−10% MeOH in CH_2Cl_2) to afford **93m** as a beige solid (0.07 g, 49%).

^{1}H-NMR (400 MHz, DMSO-d6): see Table 32.

MS ESI (m/z): 374 $[M-H]^-$, **HRMS:** m/z calculated for $C_{20}H_{17}N_5OS^-$: 374.1081, found: 374.10815.

2-((*1H*-Indazol-4-yl)amino)-*N*-(3-phenoxyphenyl)thiazole-4-carboxamide **93n**:

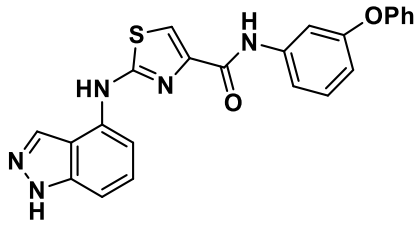

Prepared according to **93a**, acid **92** (0.1g, 0.38 mmol) was reacted with 3-phenoxyaniline (0.07 g, 0.38 mmol). The resulting residue was silica flash column chromatographed (gradient elution, 2−12% MeOH in CH_2Cl_2) to afford **93n** as a greenish white solid (0.087 g, 54%).

^{1}H-NMR (400 MHz, DMSO-d6): see Table 32.

^{13}C NMR (100MHz, DMSO-*d6*): δ 163.6, 159.9, 157.3, 156.96, 151.5, 146.1, 141.43, 133.47, 131.8, 130.5, 130.4, 129.2, 127.7, 124.0, 121.2, 119.2, 115.9, 115.8, 115.0, 114.3, 111.0, 107.3, 104.3.

MS ESI (m/z): 426 $[M-H]^-$, **HRMS:** m/z calculated for $C_{23}H_{17}N_5O_2S^-$: 426.10302, found: 426.10355.

2-((*1H*-Indazol-4-yl)amino)-*N*-(4-chlorophenyl)thiazole-4-carboxamide **93o**:

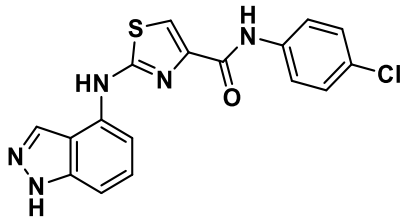

Prepared according to **93a**, acid **92** (0.1g, 0.38 mmol) was reacted with 4-chloroaniline (0.048 g, 0.38 mmol). The resulting residue was silica flash column chromatographed (gradient elution, 2−12% MeOH in CH_2Cl_2) to afford **93o** as an off white solid (0.053 g, 38%).

^{1}H-NMR (400 MHz, DMSO-d6): see Table 32.

^{13}C NMR (100MHz, DMSO-*d6*): δ 163.6, 159.9, 151.2, 146.0, 141.5, 140.0, 137.9, 135.1, 133.4, 131.9, 129.2, 127.8, 127.8, 115.9, 114.9, 107.3, 104.2.

MS ESI (m/z): 368 $[M-H]^-$, **HRMS:** m/z calculated for $C_{17}H_{12}N_5OSCl^-$: 368.03783, found: 368.03784.

2-((*1H*-Indazol-4-yl)amino)-*N*-(3,4,5-trimethoxyphenyl)thiazole-4-carboxamide **93p**:

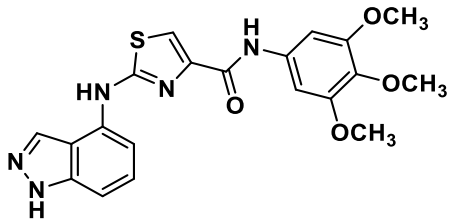

Prepared according to **93a**, acid **92** (0.1g, 0.38 mmol) was reacted with 3,4,5-trimethoxyaniline (0.07 g, 0.38 mmol). The resulting residue was silica flash column chromatographed (gradient elution, 4−18% MeOH in CH_2Cl_2) to afford **93p** as a whitish green solid (0.07 g, 44%).

^{1}H-NMR (400 MHz, DMSO-d6): see Table 32.

^{13}C NMR (100MHz, DMSO-*d6*): δ 163.5, 159.7, 153.1, 146.2, 141.4, 134.9, 134.3, 133.4, 131.8, 127.8, 115.4, 115.0, 107.2, 104.2, 98.8, 60.6, 56.2.

MS ESI (m/z): 424 $[M-H]^-$, **HRMS:** m/z calculated for $C_{20}H_{19}N_5O_4S^-$: 424.10850, found: 424.10944.

2-((*1H*-Indazol-4-yl)amino)-*N*-(3-chloro-2-methoxyphenyl)thiazole-4-carboxamide **93q**:

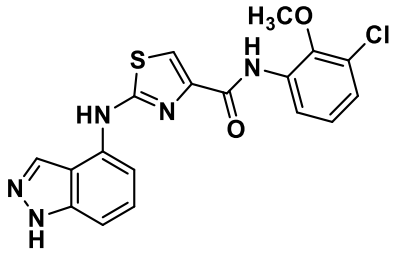

Prepared according to **93a**, acid **92** (0.1g, 0.38 mmol) was reacted with 3-choloro-4-methoxyaniline (0.06 g, 0.38 mmol). The resulting residue was silica flash column chromatographed (gradient elution, 4−15% MeOH in CH_2Cl_2) to afford **93q** as an off white solid (0.044 g, 29%).

^{1}H-NMR (400 MHz, DMSO-d6): see Table 32.

MS ESI (m/z): 398 $[M-H]^-$, **HRMS:** m/z calculated for $C_{18}H_{14}N_5O_2SCl^-$: 398.04840, found: 398.04846.

2-((*1H*-Indazol-4-yl)amino)-*N*-(3,4-dimethoxybenzyl)thiazole-4-carboxamide **93r**:

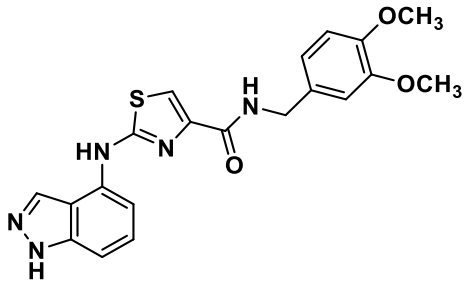

Prepared according to **93a**, acid **92** (0.1g, 0.38 mmol) was reacted with 3,4-dimethoxybenzylamine (0.063 g, 0.38 mmol). The resulting residue was silica flash column chromatographed (gradient elution, 2−12% MeOH in CH_2Cl_2) to afford **93r** as an off white solid solid (0.11 g, 69%).

^{1}H-NMR (400 MHz, DMSO-d6): see Table 32.

^{13}C NMR (100MHz, DMSO-*d6*): δ 163.4, 161.1, 149.0, 148.2, 146.4, 141.4, 133.5, 132.6, 131.8, 127.8, 119.9, 114.8, 114.4, 112.1, 111.9, 107.0, 104.0, 56.0, 55.9, 42.5.

MS ESI (m/z): 408 $[M-H]^-$, **HRMS:** m/z calculated for $C_{20}H_{19}N_5O_3S^-$: 408.11358, found: 408.11380.

2-((*1H*-Indazol-4-yl)amino)-*N*-(4-(trifluoromethyl)benzyl)thiazole-4-carboxamide **93s**:

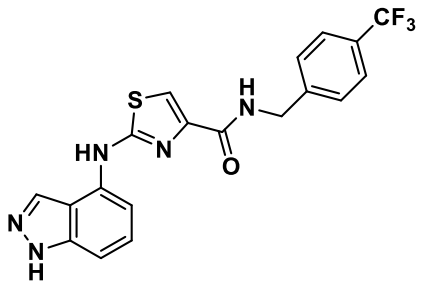

Prepared according to **93a**, acid **92** (0.1g, 0.38 mmol) was reacted with 4-(trifluoromethyl)benzylamine (0.066 g, 0.38 mmol). The resulting residue was silica flash column chromatographed (gradient elution, 2−12% MeOH in CH_2Cl_2) to afford **93s** as an off white solid solid (0.066 g, 42%).

^{1}H-NMR (400 MHz, DMSO-d6): see Table 32.

^{13}C NMR (100MHz, DMSO-*d6*): δ 163.4, 161.5, 146.1, 145.2, 141.4, 133.4, 131.66, 128.6, 128.0, 127.9, 127.7, 126.2, 125.7, 125.6, 114.9, 114.8, 107.1, 104.0, 42.5.

MS ESI (m/z): 416 $[M-H]^-$, **HRMS:** m/z calculated for $C_{19}H_{14}N_5OSF_3^-$: 416.07984, found: 416.08020.

2-((*1H*-Indazol-4-yl)amino)-*N*-(4-(methylthio)phenyl)thiazole-4-carboxamide **93t**:

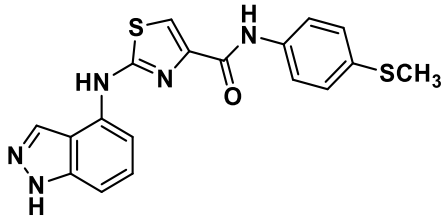

Prepared according to **93a**, acid **92** (0.1g, 0.38 mmol) was reacted with 4-(methylthio)aniline (0.053 g, 0.38 mmol). The resulting residue was silica flash column chromatographed (gradient elution, 2−12% MeOH in CH_2Cl_2) to afford **93t** as an off white solid (0.088 g, 61%).

^{1}H-NMR (400 MHz, DMSO-d6): see Table 32.

^{13}C NMR (100MHz, DMSO-*d6*): δ 163.5, 159.7, 146.2, 141.5, 136.2, 133.5, 133.1, 131.8, 127.9, 127.2, 121.8, 115.5, 114.9, 107.3, 104.3, 15.8.

MS ESI (m/z): 335 $[M-H]^-$, **HRMS:** m/z calculated for $C_{18}H_{15}N_5OS_2^-$: 335.07205, found: 335.07248.

2-((*1H*-Indazol-4-yl)amino)-*N*-(6-methoxypyridin-3-yl)thiazole-4-carboxamide **93u**:

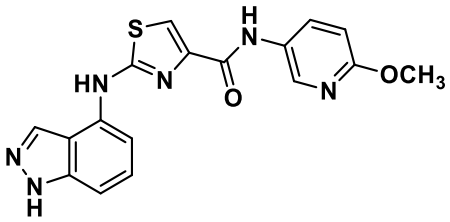

Prepared according to **93a**, acid **92** (0.1g, 0.38 mmol) was reacted with 5-amino-2-methoxypyridine (0.047 g, 0.38 mmol). The resulting residue was silica flash column chromatographed (gradient elution, 3−18% MeOH in CH_2Cl_2) to afford **93u** as a pink solid (0.088 g, 61%).

^{1}H-NMR (400 MHz, DMSO-d6): see Table 32.

^{13}C NMR (100MHz, DMSO-*d6*): δ 163.5, 160.6, 160.0, 146.0, 141.4, 140.1, 133.8, 133.4, 131.8, 129.7, 127.8, 115.8, 114.9, 110.4, 107.3, 104.2, 53.7.

MS ESI (m/z): 365 $[M-H]^-$, **HRMS:** m/z calculated for $C_{17}H_{14}N_6O_2S^-$: 365.08262, found: 365.08301.

2-((*1H*-Indazol-4-yl)amino)-*N*-(4-methoxy-3-methylphenyl)thiazole-4-carboxamide **93v**:

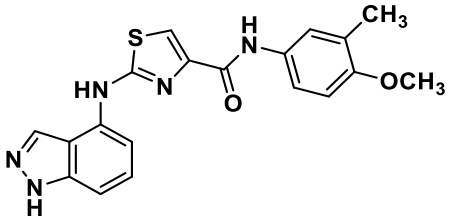

Prepared according to **93a**, acid **92** (0.1g, 0.38 mmol) was reacted with 4-methoxy-3-methylaniline (0.052 g, 0.38 mmol). The resulting residue was silica flash column chromatographed (gradient elution, 2−12% MeOH in CH_2Cl_2) to afford **93v** as a pale brown solid (0.086 g, 60%).

^{1}H-NMR (400 MHz, DMSO-d6): see Table 32.

^{13}C NMR (100MHz, DMSO-*d6*): δ 163.5, 159.4, 154.3, 146.4, 141.3, 133.5, 131.8, 131.3, 127.9, 125.9, 123.9, 120.0, 115.0, 114.9, 110.6, 107.2, 104.1, 55.4, 16.4.

MS ESI (m/z): 378 $[M-H]^-$, **HRMS:** m/z calculated for $C_{19}H_{17}N_5O_2S^-$: 378.10302, found: 378.10342.

2-((*1H*-Indazol-4-yl)amino)-*N*-(4-methoxybenzyl)thiazole-4-carboxamide **93w**:

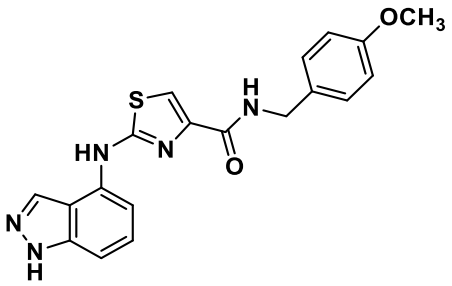

Prepared according to **93a**, acid **92** (0.1g, 0.38 mmol) was reacted with 4-methoxybenzylamine (0.052 g, 0.38 mmol). The resulting residue was silica flash column chromatographed (gradient elution, 2−12% MeOH in CH_2Cl_2) to afford **93w** as an off white solid (0.096 g, 67%).

^{1}H-NMR (400 MHz, DMSO-d6): see Table 32.

^{13}C NMR (100MHz, DMSO-*d6*): δ 163.4, 162.7, 161.1, 158.6, 146.4, 141.4, 133.5, 132.2, 131.7, 129.1, 127.85, 114.8, 114.4, 114.1, 107.0, 103.9, 55.5, 42.1.

MS ESI (m/z): 378 $[M-H]^-$, **HRMS:** m/z calculated for $C_{19}H_{17}N_5O_2S^-$: 378.10302, found: 378.10330.

2-((*1H*-Indazol-4-yl)amino)-*N*-(pyridin-2-ylmethyl)thiazole-4-carboxamide **93x**:

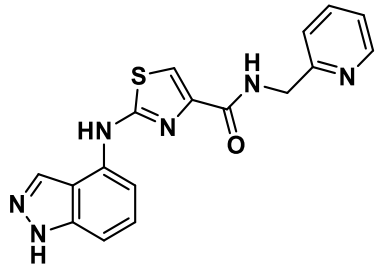

Prepared according to **93a**, acid **92** (0.1g, 0.38 mmol) was reacted with 2-picolylamine (0.041 g, 0.38 mmol). The resulting residue was silica flash column chromatographed (gradient elution, 2−12% MeOH in CH_2Cl_2) to afford **93x** as an off white solid (0.073 g, 55%).

^{1}H-NMR (400 MHz, DMSO-d6): see Table 32.

^{13}C NMR (100MHz, DMSO-*d6*): δ 162.9, 160.8, 158.1, 148.9, 145.6, 140.9, 136.8, 133.1, 131.3, 127.4, 122.1, 121.1, 114.4, 114.1, 106.7, 103.6, 44.1.

MS ESI (m/z): 349 $[M-H]^-$, **HRMS:** m/z calculated for $C_{17}H_{14}N_6OS^-$: 349.08770, found: 349.08792.

Table 32: NMR data of compounds **93a-x**

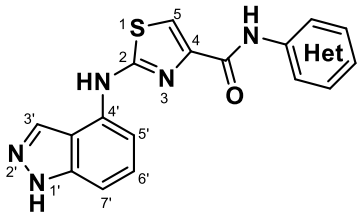

Entry		Scaffold ^{1}H-NMR (400 MHz, DMSO-d6) δ ppm	R ^{1}H-NMR (400 MHz, DMSO-d6) δ ppm
93a	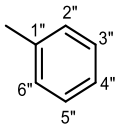	13.08 (1H, br s, H-1'), 10.54 (1H, br s, C_2-NH), 9.78 (1H, br s, CO-NH), 8.38 (1H, s, H-3'), 8.08 (1H, d, J=7.6Hz, H-7'), 7.86-7.68* (3H, m, H-5), 7.45-7.30* (3H, m, H-6'), 7.17 (1H, d, J=8.3Hz, H-5')	7.86-7.68* (3H, m, H-2",6") 7.45-7.30* (3H, m, H-3",5"), 7.13 (1H, t, J=7.4Hz, H-4")
93b	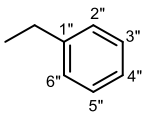	13.06 (1H, br s, H-1'), 10.44 (1H, br s, C_2-NH), 8.65 (1H, t, J=6.4Hz, CO-NH), 8.37 (1H, s, H-3'), 8.14 (1H, d, J=7.6Hz, H-7'), 7.62 (1H, s, H-5), 7.37-7.27* (5H, m, H-6'), 7.13 (1H, d, J=8.3Hz, H-5')	7.37-7.27* (5H, m, H-2",3",5",6"), 7.26-7.20 (1H, m, H-4"), 4.51 (1H, d, J=6.4Hz, CH_2)
93c	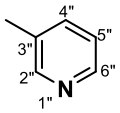	13.10 (1H, br s, H-1'), 10.55 (1H, br s, C_2-NH), 10.07 (1H, br s, CO-NH), 8.40 (1H, s, H-3'), 8.16 (1H, d, J=7.8 Hz, H-7'), 7.84 (1H, s, H-5), 7.38 (1H, t, J=8.0Hz, H-6'), 7.19 (1H, d, J=8.2Hz, H-5')	8.97 (1H, d, J=2.3Hz, H-2"), 8.35 (1H, dd, J=1.4Hz, J=4.7Hz, H-6"), 8.23 (1H, ddd, J=1.4Hz, J=2.3Hz, J=8.2Hz, H-4"), 7.43 (1H, dd, J=4.7Hz, J=8.2Hz, H-5")
93d	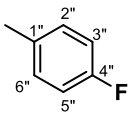	13.08 (1H, br s, H-1'), 10.52 (1H, br s, C_2-NH), 9.89 (1H, br s, CO-NH), 8.38 (1H, s, H-3'), 8.11 (1H, d, J=7.6Hz, H-7'), 7.77 (1H, s, H-5), 7.35 (1H, t, J=8.0Hz, H-6'), 7.26-7.13* (3H, m, H-5')	7.87-7.78 (2H, m, H2",6"), 7.26-7.13* (3H, m, H-3",5")

Entry		Scaffold ^{1}H-NMR (400 MHz, DMSO-d6) δ ppm	R ^{1}H-NMR (400 MHz, DMSO-d6) δ ppm
93e	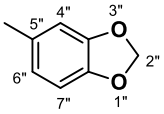	13.08 (1H, br s, H-1'), 10.51 (1H, br s, C_2-NH), 9.72 (1H, br s, CO-NH), 8.37 (1H, s, H-3'), 8.09 (1H, d, J=7.6Hz, H-7'), 7.73 (1H, s, H-5), 7.35 (1H, t, J=8.0Hz, H-6'), 7.16 (1H, d, J=8.3Hz, H-5')	7.46 (1H, d, J=2.1Hz, H-4"), 7.21 (1H, dd, J=2.1Hz, J=8.4Hz, H-6"), 6.91 (1H, d, J=8.4Hz, H-7"), 6.02 (2H, s, OCH_2O)
93f	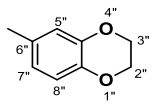	13.09 (1H, br s, H-1'), 10.52 (1H, br s, C_2-NH), 9.65 (1H, br s, CO-NH), 8.37 (1H, s, H-3'), 8.08 (1H, d, J=7.6Hz, H-7'), 7.72 (1H, s, H-5), 7.35 (1H, t, J=7.9Hz, H-6'), 7.26-7.10* (2H, m, H-5')	7.41 (1H, s, H-5"), 7.26-7.10* (2H, m, H-7"), 6.84 (1H, d, J=8.5Hz, H-8"), 4.24 (4H, s, 2 OCH_2)
93g	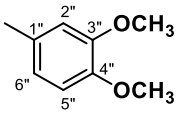	13.08 (1H, br s, H-1'), 10.52 (1H, br s, C_2-NH), 9.66 (1H, br s, CO-NH), 8.38 (1H, s, H-3'), 8.08 (1H, d, J=7.6Hz, H-7'), 7.72 (1H, s, H-5), 7.35 (1H, t, J=7.9Hz, H-6'), 7.17 (1H, d, J=8.3Hz, H-5')	7.48 (1H, d, J=2.4Hz, H-2"), 7.33 (1H, dd, J=2.4Hz, J=8.7Hz, H-6"), 6.95 (1H, d, J=8.7Hz, H-5"), 3.76 (3H, s, OCH_3), 3.74 (3H, s, OCH_3)
93h	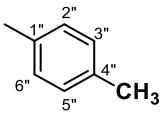	13.08 (1H, br s, H-1'), 10.52 (1H, br s, C_2-NH), 9.70 (1H, br s, CO-NH), 8.37 (1H, s, H-3'), 8.08 (1H, d, J=7.5Hz, H-7'), 7.74 (1H, s, H-5), 7.36 (1H, t, J=7.9Hz, H-6'), 7.22-7.09* (3H, m, H-5')	7.66 (2H, d, J=8.0Hz, H-2",6"), 7.22-7.09* (3H, m, H-3",5"), 2.29 (s, 3H, CH_3)
93i	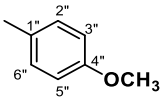	13.09 (1H, br s, H-1'), 10.53 (1H, br s, C_2-NH), 9.70 (1H, br s, CO-NH), 8.38 (1H, s, H-3'), 8.11 (1H, d, J=7.6Hz, H-7'), 7.73 (1H, s, H-5), 7.35 (1H, t, J=8.0Hz, H-6'), 7.16 (1H, d, J=8.3Hz, H-5')	7.68 (2H, d, J=9.0Hz, H-2",6"), 6.94 (2H, d, J=9.0Hz, H-3",5"), 3.75 (3H, s, OCH_3)
93j	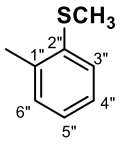	13.12 (1H, br s, H-1'), 10.66 (1H, br s, C_2-NH), 10.27 (1H, br s, CO-NH), 8.44-8.36* (2H, m, H-3'), 8.32 (1H, d, J=7.6Hz, H-7'), 7.83 (1H, s, H-5), 7.29 (1H, t, J=8.0Hz, H-6'), 7.19 (1H, d, J=8.3Hz, H-5')	8.44-8.36* (2H, m, H-3"), 7.60 (dd, 1H, J=1.4Hz, J=7.6Hz, H-6"), 7.37 (dt, 1H, J=1.4Hz, J=7.6Hz, H-5"), 7.18 (dt, 1H, J=1.4Hz, J=7.6Hz, H-4"), 2.51(3H, s, SCH_3)

Entry		Scaffold ^{1}H-NMR (400 MHz, DMSO-d6) δ ppm	R ^{1}H-NMR (400 MHz, DMSO-d6) δ ppm
93k	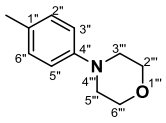	13.08 (1H, br s, H-1'), 10.51 (1H, br s, C_2-NH), 9.61 (1H, br s, CO-NH), 8.37 (1H, s, H-3'), 8.08 (1H, d, J=7.6Hz, H-7'), 7.71 (1H, s, H-5), 7.35 (1H, t, J=7.9Hz, H-6'), 7.16 (1H, d, J=8.2Hz, H-5')	7.63 (2H, d, J=9.1Hz, H-2",6"), 6.96 (2H, d, J=9.1Hz, H-3",5"), 3.75 (4H, m, 2 OCH_2), 3.08 (4H, m, 2 NCH_2)
93l	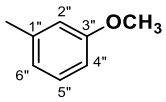	13.10 (1H, br s, H-1'), 10.55 (1H, br s, C_2-NH), 9.77 (1H, br s, CO-NH), 8.37 (1H, s, H-3'), 8.07 (1H, d, J=7.6Hz, H-7'), 7.77 (1H, s, H-5), 7.27 (1H, t, J=8.0Hz, H-6'), 7.17 (1H, d, J=8.3Hz, H-5')	7.49 (1H, t, J=2.2Hz, H-2"), 7.41-7.33 (2H, m, H-5",6"), 6.71 (1H, ddd, J=1.8Hz, J=2.2Hz, J=8.2Hz, H-4"), 3.77 (3H, s, OCH_3)
93m	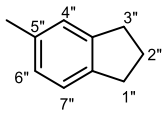	13.09 (1H, br s, H-1'), 10.54 (1H, br s, C_2-NH), 9.66 (1H, br s, CO-NH), 8.38 (1H, s, H-3'), 8.08 (1H, d, J=7.6Hz, H-7'), 7.74 (1H, s, H-5), 7.36 (1H, t, J=7.9Hz, H-6'), 7.17 (1H, d, J=8.3Hz, H-5')	7.67 (1H, s, H-4"), 7.49 (1H, dd, J=1.8Hz, J=8.1Hz, H-6"), 7.20 (1H, d, J=8.1Hz, H-7"), 2.85 (4H, td, J=7.4Hz, J=15.0Hz, 2 benzylic CH_2), 2.03 (2H, p, J=7.4Hz, H-2")
93n	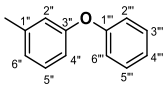	13.10 (1H, br s, H-1'), 10.54 (1H, br s, C_2-NH), 9.91 (1H, br s, CO-NH), 8.38 (1H, s, H-3'), 8.08 (1H, d, J=7.6Hz, H-7'), 7.78 (1H, s, H-5), 7.46-7.32* (4H, m, H-6'), 7.22-7.14* (2H, m, H-5')	7.63 (1H, t, J=2.1Hz, H-2"), 7.56 (1H, dd, J=2.1Hz, J=8.1Hz, H-6") 7.46-7.32* (4H, m, Ar-H), 7.22-7.14* (2H, m, Ar-H),), 7.08 (2H, d, J=7.7Hz, Ar-H), 6.79 (1H, dd, J=2.1Hz, J=8.1Hz, H-4")
93o	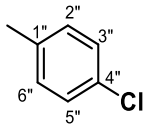	13.09 (1H, br s, H-1'), 10.54 (1H, br s, C_2-NH), 9.97 (1H, br s, CO-NH), 8.38 (1H, s, H-3'), 8.11 (1H, d, J=7.6Hz, H-7'), 7.79 (1H, s, H-5), 7.35 (1H, t, J=8.0Hz, H-6'), 7.17 (1H, d, J=8.4Hz, H-5')	7.85 (2H, d, J=8.9Hz, H-2",6"), 7.43 (2H, d, J=8.9Hz, H-3",5")

Entry		Scaffold ^{1}H-NMR (400 MHz, DMSO-d6) δ ppm	R ^{1}H-NMR (400 MHz, DMSO-d6) δ ppm
93p	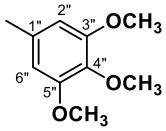	13.08 (1H, br s, H-1'), 10.53 (1H, br s, C_2-NH), 9.70 (1H, br s, CO-NH), 8.37 (1H, s, H-3'), 8.05 (1H, d, J=7.6Hz, H-7'), 7.74 (1H, s, H-5), 7.36 (1H, t, J=7.9Hz, H-6'), 7.17 (1H, d, J=8.3Hz, H-5')	7.23 (2H, s, H-2",6"), 3.79 (6H, s, 2 OCH_3), 3.65 (3H, s, OCH_3)
93q	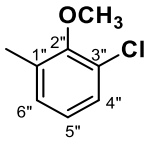	13.14 (1H, br s, H-1'), 10.67 (1H, br s, C_2-NH), 9.83 (1H, br s, CO-NH), 8.37 (1H, s, H-3'), 8.06 (1H, d, J=7.6Hz, H-7'), 7.85 (1H, s, H-5), 7.38 (1H, t, J=7.9Hz, H-6'), 7.26-7.18* (3H, m, H-5')	8.39 (1H, dd, J=1.9Hz, J=7.8Hz, H-6"), 7.26-7.18* (3H, m, H-4",5"), 3.95 (3H, s, OCH_3)
93r	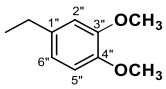	13.08 (1H, br s, H-1'), 10.47 (1H, br s, C_2-NH), 8.56 (1H, t, J=6.3Hz, CO-NH), 8.37 (1H, s, H-3'), 8.12 (1H, d, J=7.6Hz, H-7'), 7.62 (1H, s, H-5), 7.30 (1H, t, J=8.0Hz, H-6'), 7.14 (1H, d, J=8.4Hz, H-5')	6.99 (1H, d, J=1.7Hz, H-2"), 6.91 (1H, d, J=8.2Hz, H-5"), 6.86 (1H, dd, J=1.7Hz, J=8.2Hz, H-6"), 4.44 (2H, d, J=6.2Hz, CH_2), 3.73 (6H, d, J=7.8Hz, 2 OCH_3)
93s	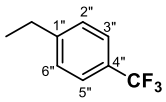	13.01 (1H, br s, H-1'), 10.45 (1H, br s, C_2-NH), 8.79 (1H, t, J=6.2Hz, CO-NH), 8.35 (1H, s, H-3'), 8.12 (1H, d, J=6.9Hz, H-7'), 7.60 (1H, s, H-5), 7.30 (1H, t, J=8.0Hz, H-6'), 7.12 (1H, d, J=8.2Hz, H-5')	7.70 (2H, d, J=8.2Hz, H-3",5"), 7.54 (2H, d, J=8.2Hz, H-2",6"), 4.59 (1H, d, J=6.3Hz, CH_2)
93t	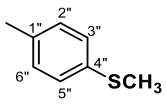	13.08 (1H, br s, H-1'), 10.53 (1H, br s, C_2-NH), 9.81 (1H, br s, CO-NH), 8.38 (1H, s, H-3'), 8.09 (1H, d, J=7.6Hz, H-7'), 7.78 (1H, s, H-5), 7.35 (1H, t, J=8.0Hz, H-6'), 7.17 (1H, d, J=8.3Hz, H-5')	7.78 (2H, d, J=8.7Hz, H-2",6"), 7.29 (2H, d, J=8.7Hz, H-3",5"), 2.48 (3H, s, SCH_3)
93u	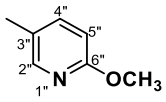	13.07 (1H, br s, H-1'), 10.51 (1H, br s, C_2-NH), 9.89 (1H, br s, CO-NH), 8.38 (1H, s, H-3'), 8.15 (1H, d, J=7.5Hz, H-7'), 7.76 (1H, s, H-5), 7.35 (1H, t, J=7.9Hz, H-6'), 7.16 (1H, d, J=8.4Hz, H-5')	8.53 (1H, d, J=1.6Hz, H-2"), 8.05 (1H, dd, J=1.6Hz, J=8.8Hz, H-4"), 6.86 (1H, d, J=8.8Hz, H-5"), 3.85 (3H, s, OCH_3)

Entry		Scaffold ^{1}H-NMR (400 MHz, DMSO-d6) δ ppm	R ^{1}H-NMR (400 MHz, DMSO-d6) δ ppm
93v	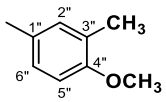	13.09 (1H, br s, H-1'), 10.52 (1H, br s, C_2-NH), 9.60 (1H, br s, 1H, CO-NH), 8.38 (1H, s, H-3'), 8.10 (1H, d, J=7.6Hz, H-7'), 7.71 (1H, s, H-5), 7.36 (1H, t, J=7.8Hz, H-6'), 7.16 (1H, d, J=8.2Hz, H-5')	7.56 (1H, dd, J=2.0Hz, J=8.8Hz, H-6"), 7.52 (1H, s, H-2"), 6.93 (1H, d, J=8.8Hz, H-5"), 3.78 (3H, s, OCH_3), 2.17 (3H, s, CH_3)
93w	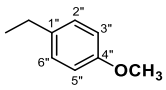	13.07 (1H, br s, H-1'), 10.48 (1H, br s, C_2-NH), 8.57 (1H, t, J=6.5Hz, CO-NH), 8.38 (1H, s, H-3'), 8.11 (1H, d, J=7.4Hz, H-7'), 7.60 (1H, s, H-5), 7.29 (1H, t, J=7.8Hz, H-6'), 7.14 (1H, d, J=8.3Hz, H-5')	7.26 (2H, d, J=8.7Hz, H-2",6"), 6.91 (2H, d, J=8.7Hz, H-3",5"), 4.45 (2H, d, J=6.2Hz, CH_2), 3.74 (3H, s, OCH_3)
93x	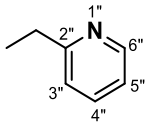	13.02 (1H, br s, H-1'), 10.51 (1H, br s, C_2-NH), 8.77 (1H, t, J=5.9Hz, CO-NH), 8.37 (1H, s, H-3'), 8.13 (1H, d, J=7.4Hz, H-7'), 7.60 (1H, s, H-5), 7.37-7.25* (3H, m, H-6'), 7.13 (1H, d, J=8.3Hz, H-5')	8.55 (1H, m, H-6"), 7.78 (1H, dt, J=1.8Hz, J=7.7Hz, H-3"), 7.37-7.25* (3H, m, H-4",5"), 4.61 (2H, d, J=5.9Hz, CH_2)

Conclusions and Future Directions

During the course of this project, my research has focused on the use of the parallel synthesis approach for the design and synthesis of exploratory libraries of heterocyclic molecules, which have the potential to be isoform selective type II rho-kinase (ROCK1/2) inhibitors. There is considerable interest in both academic and industrial laboratories to identify and develop isoform selective ROCK inhibitors for application in a number of therapeutic areas, and in particular diabetic cardiovascular diseases.

There are several approved drugs (such as Imatinib, Sorafenib, Regorafenib, and Nilotinib) that function as type II kinase inhibitors. However, the design of type II kinase inhibitors is a challenging endeavor, as structural details on kinases in their activation loop closed conformation are lacking. This is particularly true for the two ROCK isoforms that possess 92% identity in their ATP binding domain. Basically, the only guidelines available are that the inhibitor should have an elongated structure (i.e. be too large to bind in type I inhibitor mode), and that it should contain a polar neutral amide/urea function in the middle of its structure, and a non-polar aromatic/heteroaromatic motif at the opposite extremity to the subunit that binds to the hinge residues, such that interaction with an allosteric pocket is favored. In our project, these structural features were included in the different libraries of molecules we have prepared (Chapters 3-6).

Building on the fact that hydroxyfasudil (a metabolite of the approved ROCK inhibitor fasudil) is a potent (but non selective) ROCK inhibitor, a 2-pyridinone-based molecule was initially chosen as the hinge binding component, and our objective was to evaluate the influence of adding different appendages to this scaffold on isoform selective ROCK inhibition. Indeed, in chapters 3 to 6, we successively created libraries of larger and more geometrically modified structures, by altering the nature of the linker element (oxazoline-carboxamides, oxadiazole, oxadiazle-carboxamides, and 4- or 5-carboxamide substituted 2-aminothiazoles) and the nature of the diversity elements.

Due to budget limitations, only selected molecules in these libraries were evaluated as ROCK inhibitors, using a single point assay where % inhibition relative to a control molecule (H-1152) was measured. However, even with these relatively primitive means, we were able to identify structural families (libraries) that displayed activity against ROCK. These results encouraged us to move forward, and did guide us in the choice of structural modifications that were described

in each chapter of the thesis. Most pertinent, was the observation that the indazole motif proved to be superior to the 2-pyridinone system as a hinge binding element. In fact, it was determined that the indazole ring conferred activity when it was positioned on either the left or the right side of the inhibitor. This suggested that considerable options still exist to further modify the linker portion in these types of molecules. To have an accurate picture of the potency and isoform selectivity for the most interesting compounds, 18 selected molecules were tested in a 10-point assay (Invitrogen). It was found that the most potent inhibitors were active in the low micromolar range (IC_{50}), and that none of the compounds exhibited significant isoform selectivity.

These results demonstrated that we could design ROCK inhibitors based only on the general knowledge of what structural elements such molecules should contain in their structure. They also indicated to us the likelihood that more potent molecules based on the indazole hinge binding motif could be identified through further modifications of the linker portion of the molecule. Strategies that merit investigation are the incorporation of appending functionality that seeks out supplementary binding interactions (**Figure 35**, Chapter 1), and the use of entities (splitters) that send functionality into different zones in the inhibitor binding site (**Figure 33**, Chapter 1). Of greatest importance to any future continuation of our project to identify isoform selective kinase inhibitors, will be to have in hand a simple and inexpensive assay that provides rapid IC_{50} data against both ROCK enzymes.

Bibliography

1) Michael, S.; Auld, D.; Klumpp, C.; Jadhav, A.; Zheng, W.; Thorne, N.; Austin, C. P.; Inglese, J.; Simeonov, A. A robotic platform for quantitative high-throughput screening. *Assay Drug Dev. Technol.* **2008**, 6, 637- 657.
2) Zang, R.; Li, D.; Tang, I.; Wang, J.; Yang, S. Cell-based assays in high-throughput screening for drug discovery. *Int. J. Biotech. Well. Indus.* **2012**, 1, 31-51.
3) Hughes, J. P.; Rees, S.; Kalindjian, S. B.; Philpott, K. L. Principles of early drug discovery. *Br. J. Pharmacol.* **2011**, 162, 1239-1249.
4) Keseru, G. M.; Makara, G. M. Hit discovery and hit-to-lead approaches. *Drug Discovery Today*. **2006**, 11, 741-748.
5) Bleicher, K. H.; Böhm, H.; Müller, K.; Alanine, A. Hit and lead generation: beyond high-throughput screening. *Nat. Rev. Drug Discovery.* **2003**, 2, 369-378.
6) Kawasumi, M.; Nghiem, P. Chemical Genetics: Elucidating Biological Systems with Small-Molecule Compounds. J. Invest. Dermatol. **2007**, 127, 1577–1584.
7) Inglese, J.; Shamu, C. E.; Guy, R. K. Reporting data from high-throughput screening of small-molecule libraries. *Nat. Chem. Biol.* **2007**, 3, 438-441.
8) Deininger, M.; Buchdunger, E.; Druker, B. J. The development of imatinib as a therapeutic agent for chronic myeloid leukemia. *Blood.* **2005**, 105, 2640-2653.
9) Macarron, R.; Banks, M. N.; Bojanic, D.; Burns, D. J.; Cirovic, D. A.; Garyantes, T.; Green, D. V. S.; Hertzberg, R. P.; Janzen, W. P.; Paslay, J. W.; Schopfer, U.; Sittampalam, G. S. Impact of high-throughput screening in biomedical research. *Nat. Rev. Drug Discovery.* **2011**, 10, 188-195.
10) Gao, M.; Nettles, R. E.; Belema, M.; Snyder, L. B.; Nguyen, V. N.; Fridell, R. A.; Serrano-Wu, M. H.; Langley, D.R.; Sun, J.; O'Boyle, D. R.; Lemm, J. A.; Wang, C.; Knipe, J. O.; Chien, C.; Colonno, R. J.; Grasela, D. M.; Meanwell, N. A.; Hamann, L. G. Chemical genetics strategy identifies an HCV NS5A inhibitor with a potent clinical effect. *Nature.* **2010**, 465, 96-100.
11) Patel, G.; Karver, C. E.; Behera, R.; Guyett, P. J.; Sullenberger, C.; Edwards, P.; Roncal, N. E.; Mensa-Wilmot, K.; Pollastri, M. P. Kinase scaffold repurposing for neglected disease

drug discovery: discovery of an efficacious, lapatanib-derived lead compound for trypanosomiasis. *J. Med. Chem.* **2013**, 56, 3820-3832.

12) Lipinski, C. A.; Franco, L.; Dominy, B. W.; Feeney, P. J. Experimental and computational approaches to estimate solubility and permeability in drug discovery and development settings. *Adv. Drug Deliv. Rev.* **2001**, 46, 3-26.
13) Geysen, H. M.; Schoenen, F.; Wagner, D.; Wagner, R. Combinatorial compound libraries for drug discovery: an ongoing challenge. *Nat. Rev. Drug Discovery*. **2003**, 2, 222-230.
14) Weber, L.; Wallbaum, S.; Broger, C.; Gubernator, K. Optimization of the biological activity of combinatorial compound libraries by a genetic algorithm. *Angew*. *Chem. Int. Ed. Engl.* **1995**, 34, 2280-2282.
15) Carell, T.; Wintner, E. A.; Sutherland, A. J.; Rebek, J.; Dunayevskiy, Y. M.; Vouros, P. New promise in combinatorial chemistry: synthesis, characterization, and screening of small-molecule libraries in solution. *Chem. biol*. **1995**, 2, 171-183.
16) Wentworth, P.; Janda, K. D. Generating and analyzing combinatorial chemistry libraries. *Curr. Opin. Biotechnol.* **1998**, 9, 109-115
17) Miertus, S.; Fassina, G. Combinatorial chemistry and technologies: Methods and applications, Taylor&Francis group. **2005**, Second edition, p 250
18) Thompson, L. A.; Ellman, J. A. Synthesis and applications of small molecule libraries. *Chem. Rev*. **1996**, 96, 555-600.
19) Ohlstein, E. H.; Ruffolo, R. R.; Elliott, J. D. Drug discovery in the next millennium. *Annu. Rev. Pharmacol. Toxicol.* **2000**, 40, 177-91.
20) Kurti, L.; Czako, B. Strategic applications of named reactions in organic synthesis. Elsevier Inc. **2005**, p 330.
21) Schreiber, S. L. Target-oriented and diversity-oriented organic synthesis in drug discovery. *Science*. **2000**, 287, 1964-1969.
22) Galloway, W. R. D.; Liobet, A. I.; Spring, D. R. Diversity-oriented synthesis as a tool for the discovery of novel biologically active small molecule. *Nat. Commun.* **2010**, 1, 1-13.
23) Tan, D. S.; Foley, M. A.; Stockwell, B. R.; Shair, M. D.; Schreiber, S. Synthesis and preliminary evaluation of a library of polycyclic small molecules for use in chemical genetic assays. *J. Am. Chem. Soc.* **1999**, 121, 9073-9087.
24) Bakkour, N.; Lin, Y.; Maire, S.; Ayadi, L.; Mahuteau-Betzer, F.; Nguyen, C. H.; Mettling, C.; Portales, P.; Grierson, D.; Chabot, B.; Jeanteur, P.; Branlant, C.; Corbeau, P.; Tazi, J.

Small-Molecule inhibition of HIV pre-mRNA splicing as a novel antiretroviral therapy to overcome drug resistance. *PLoS Pathog*. **2007**, 3, 1530-1539.

25) An ongoing project in our laboratory.
26) Welsch, M. E.; Snyder, S. A.; Stockwel, B. R. Privileged scaffolds for library design and drug discovery. *Curr. Opin. Chem. Biol.* **2010**, 14, 347-361.
27) Bunin, B. A.; Plunkett, M. J.; Ellman, J. A. The combinatorial synthesis and chemical and biological evaluation of a 1,4-benzodiazepine library. *Proc. Natl. Acad. Sci.* **1994**, 91, 4708-4712.
28) Keri, R. S.; Budagumpi, S.; Pai, R. K.; Balakrishna, R. G. Chromones as a privileged scaffold in drug discovery: A review. *Eur. J. Med. Chem.* **2014**, 78, 340-374.
29) Machado, N. F. L.; Marques, M. P. M. Bioactive chromone derivatives-structural diversity. *Curr. Bioact. Compd.* **2010**, 6, 76-89.
30) Galietta, L. J. V.; Springsteel, M. F.; Eda, M.; Niedzinski, E. J.; By, K.; Haddadin, M. J.; Kurth, M. J.; Nantz, M. H.; Verkman, A. S. Novel CFTR chloride channel activators identified by screening of combinatorial libraries based on flavone and benzoquinolizinium lead compounds. *J. Biol. Chem*. **2001**, 276, 19723-19728.
31) Gabor, M. Anti-inflammatory and anti-allergic properties of flavonoids. *Prog. Clin. Biol. Res*. **1986**, 213, 471-480.
32) Poondra, R. R.; Nallamelli, R. V.; Meda, C. L. T.; Srinivas, B. N. V.; Grover, A.; Muttabathula, J.; Voleti, S. R.; Sridhar, B.; Pal, M.; Parsa, K. V. L. Discovery of novel 1,4-dihydropyridine-based PDE4 inhibitors. *Bioorg. Med. Chem. Lett.* **2013**, 23, 1104-1109.
33) Bossert, F.; Meyer, H.; Wehinger, E. 4-Aryldihydropyridines, a new class of highly active calcium antagonists. *Angew. Chem. Int. Ed. Engl.* **1981**, 20, 762-769.
34) Pandey, V. P.; Bisht, S. S.; Mishra, M. M.; Kumar, A. A.; Siddiqi, M. I.; Verma, A.; Mittal, M.; Sane, S. A.; Gupta, S.; Tripathi, R. P. Synthesis and molecular docking studies of 1-phenyl-4-glycosyl-dihydropyridines as potent antileishmanial agents. *Eur. J. Med. Chem.* **2010**, 45, 2381-2388.
35) Marco-Contelles, J.; Leon, R.; De los Rios, C.; Samadi, A.; Bartolini, M.; Andrisano, V.; Huertas, O.; Barril, X.; Luque, F. J.; Rodriguez-Franco, M. I.; Lopez, B.; Lopez, M. G.; Garcia, A. G.; Carreiras, M. C.; Villarroya, M. Tacripyrines, the first tacrine-dihydropyridine hybrids, as multitarget-directed ligands for the treatment of Alzheimer's disease. *J. Med. Chem.* **2009**, 52, 2724-2732.

36) Cateni, F.; Zacchigna, M.; Pedemonte, N.; Galietta, J. V.; Mazzei, M. T.; Fossa, P.; Giampieri, M.; Mazzei, M. Synthesis of 4-thiophen-20-yl-1,4-dihydropyridines as potentiators of the CFTR chloride channel. *Bioorg. Med. Chem.* **2009**, 17, 7894-7903.

37) Graves, P. R.; Kwiek, J.; Fadden, P.; Ray, R.; Hardeman, K.; Coley, A. M.; Foley, M. Discovery of novel targets of quinoline drugs in the human purine binding proteome. *Mol. Pharmacol.* **2002**, 62, 1364-1372.

38) Madapa, S.; Tusi, Z.; Batra, S. Advances in the syntheses of quinoline and quinoline-annulated ring systems. *Curr. Org. Chem.* **2008**, 12, 1116-1183.

39) Blaney, F. E.; Raveglia, L. F.; Artico, M.; Cavagnera, S.; Dartois, C.; Farina, C.; Grugni, M.; Gagliardi, S.; Luttmann, M. A.; Martinelli, M.; Nadler, G. M.; Parini, C.; Petrillo, P.; Sarau, H. M.; Scheideler, M. A.; Hay, D. W.; Giardina, G. A. Stepwise modulation of neurokinin-3 and neurokinin-2 receptor affinity and selectivity in quinoline tachykinin receptor antagonists. *J. Med. Chem.* **2001**, 44, 1675-1689.

40) Yu, X. Y.; Hill, J. M.; Yu, G.; Yang, Y.; Kluge, A. F.; Keith, D.; Finn, J.; Gallant, P.; Silverman, J.; Lim, A. A series of quinoline analogues as potent inhibitors of C. albicans prolyl tRNA synthetase. *Bioorg. Med. Chem. Lett.* **2001**, 11, 541-544.

41) Das, J.; Chen, P.; Norris, D.; Padmanabha, R.; Lin, J.; Moquin, R. V.; Shen, Z.; Cook, L. S.; Doweyko, A. M.; Pitt, S.; Pang, S.; Shen, D. R.; Fang, Q.; De Fex, H. F.; McIntyre, K. W.; Shuster, D. J.; Gillooly, K. M.; Behnia, K.; Schieven, G. L.; Wityak, J.; Barrish, J. C. 2-aminothiazole as a novel kinase inhibitor template. Structure-activity relationship studies toward the discovery of N-(2-chloro-6-methylphenyl)-2-[[6-[4-(2-hydroxyethyl)-1-piperazinyl)]-2-methyl-4-pyrimidinyl]amino)]-1,3-thiazole-5-carboxamide (dasatinib, BMS-354825) as a potent pan-Src kinase inhibitor. *J. Med. Chem.* **2006**, 49, 6819-6832.

42) Borzilleri, R. M.; Bhide, R. S.; Barrish, J. C.; D'Arienzo, C. J.; Derbin, G. M.; Fargnoli, J.; Hunt, J. T.; Jeyaseelan, R.; Kamath, A.; Kukral, D. W.; Marathe, P.; Mortillo, S.; Qian, L.; Tokarski, J. S.; Wautlet, B. S.; Zheng, X.; Lombardo, L. J. Discovery and evaluation of N-cyclopropyl-2,4-difluoro-5-((2-(pyridin-2-ylamino)thiazol-5-ylmethyl)amino)benzamide (BMS-605541), a selective and orally efficacious inhibitor of vascular endothelial growth factor receptor-2. *J. Med. Chem.* **2006**, 49, 3766-3769.

43) Jimonet, P.; Audiau, F.; Barreau, M.; Blanchard, J.C.; Boireau, A.; Bour, Y.; Coleno, M. A.; Doble, A.; Doerflinger, G.; Huu, C. D.; Donat, M. H.; Duchesne, J. M.; Ganil, P.; Gueremy, C.; Honor, E.; Just, B.; Kerphirique, R.; Gontier, S.; Hubert, P.; Laduron, P. M.;

Le Blevec, J.; Meunier, M.; Miquet, J. M.; Nemecek, C.; Mignani, S. Riluzole series. Synthesis and in vivo “antiglutamate” activity of 6-substituted-2-benzothiazolamines and 3-substituted-2-imino-benzothiazolines. *J. Med. Chem.* **1999**, 42, 2828-2843.

44) Schneider, C. S.; Mierau, J. Dopamine autoreceptor agonists: resolution and pharmacological activity of 2,6-diaminotetrahydrobenzothiazole and an aminothiazole analogue of apomorphine. *J. Med. Chem.* **1987**, 30, 494-498.

45) Lazer, E. S.; Miao, C. K.; Cywin, C. L.; Sorcek, R.; Wong, H. C.; Meng, Z.; Potocki, I.; Hoermann, M.; Snow, R. J.; Tschantz, M. A.; Kelly, T. A.; McNeil, D. W.; Coutts, S. J.; Churchill, L.; Graham, A. G.; David, E. Grob, P. M.; Engel, W.; Meier, H.; Trummlitz, G. Effect of structural modification of enol_carboxamide-type nonsteroidal anti-inflammatory drugs on COX-2/COX-1 selectivity. *J. Med. Chem.* **1997**, 40, 980-989.

46) Trifilieff, A.; Keller, T. H.; Press, N. J.; Howe, T.; Gedeck, P.; Beer, D.; Walker, C. CGH2466, a combined adenosine receptor antagonist, p38 mitogen-activated protein kinase and phosphodiesterase type 4 inhibitor with potent in vitro and in vivo anti-inflammatory activities. *Br. J. Pharmacol.* **2005**, 144, 1002-1010.

47) Legraverend, M.; Grierson, D. S. The purines: potent and versatile small molecule inhibitors and modulators of key biological targets. *Bioorg. Med. Chem.* **2006**, 14, 3987-4006.

48) Galons, H.; Oumata, N.; Gloulou, O.; Meijer, L. Cyclin-dependent kinase inhibitors closer to market launch? Expert Opin. Ther. Pat. **2013**, 23, 945-963.

49) Van Linden, O. P.; Kooistra, A. J.; Leurs, R.; De Esch, I. J.; De Graaf, C. KLIFS: a knowledge-based structural database to navigate kinase–ligand interaction space. *J. Med. Chem.* **2014**, 57, 249-277.

50) Ubersax, J. A.; James E.; Ferrell, J. Mechanisms of specificity in protein phosphorylation. *Nat. Rev. Mol. Cell Biol.* **2007**, 8, 530-541.

51) Tsai, C.; Nussinov, R. The molecular basis of targeting protein kinases in cancer therapeutics. *Semin. Cancer Biol.* **2013**, 23, 235-242.

52) Cohen, P. Protein kinases-the major drug targets of the twenty-first century. *Nat. Rev. Drug Discovery*. **2002**, 1, 309-315.

53) Cohen, P.; Alessi, D. R. Kinase drug discovery--what's next in the field? *ACS Chem. Biol.* **2013**, 8, 96-104.

54) Cohen, P.; Tcherpakov, M. Will the ubiquitin system furnish as many drug targets as protein kinases? *Cell.* **2010**, 143, 686-693.

55) Aktories, K.; Barbieri, J. T. Bacterial cytotoxins: targeting eukaryotic switches. *Nat. Rev. Microbiol.* **2005**, 3, 397-410.

56) Bishop, A.; Hall, A. Rho GTPases and their effector proteins. *Biochem. J.* **2000,** 348, 241-255.

57) Van Aelst, L.; D'Souza-Schorey, C. Rho GTPases and signaling networks. *Genes Dev.* **1997**, 11, 2295-2322.

58) Pan, P.; Shen, M.; Yu, H.; Li, Y.; Li, D.; Hou, T. Advances in the development of Rho-associated protein kinase (ROCK) inhibitors. *Drug Discovery Today*. **2013**, 18, 1323-1333.

59) Shi, J.; Wu, X.; Surma, M.; Vemula, S.; Zhang, L.; Yang, Y.; Kapur, R.; Wei, L. Distinct roles for ROCK1 and ROCK2 in the regulation of cell detachment. *Cell Death Dis.* **2013**, 4, e483.

60) Mueller, B. K.; Mack, H.; Teusch, N. Rho kinase, a promising drug target for neurological disorders. *Nat. Rev. Drug Discovery*. **2005,** 4, 387-398.

61) Nakagawa, O.; Fujisawa, K.; Ishizaki, T.; Saito, Y.; Nakao, K.; Narumiya, S. ROCK-I and ROCK-II, two isoforms of Rho-associated coiled-coil forming protein serine/threonine kinase in mice. *FEBS Lett.* **1996**, 392, 189-193.

62) Zhang, Y. M.; Bo, J.; Taffet, G. E.; Chang, J.; Shi, J.; Reddy, A. K.; Michael, L. H.; Schneider, M. D.; Entman, M. L.; Schwartz, R. J.; Wei, L. Targeted deletion of ROCK1 protects the heart against pressure overload by inhibiting reactive fibrosis. *FASEB J.* **2006**, 20, 916-925.

63) Lee, S. H.; Huang, H.; Choi, K.; Lee, D. H.; Shi, J.; Liu, T.; Chun, K. H.; Seo, J. A.; Lima, I. S.; Zabolotny, J. M.; Wei, L.; Kim, Y. B. ROCK1 isoform-specific deletion reveals a role for diet-induced insulin resistance. *Am. J. Physiol. Endocrinol. Metab.* **2014,** 306, E332-E343.

64) Shimizu, Y.; Thumkeo, D.; Keel, J.; Ishizaki, T.; Oshima, H.; Oshima, M.; Noda, Y.; Matsumura, F.; Taketo, M. M.; Narumiya, S. ROCK-I regulates closure of the eyelids and ventral body wall by inducing assembly of actomyosin bundles. *J. Cell Biol.* **2005,** 168, 941-953.

65) Duffy, P.; Schmandke, A.; Sigworth, J.; Narumiya, S.; Cafferty, W. B.; Strittmatter, S. M. Rho-associated kinase II (ROCKII) limits axonal growth after trauma within the adult mouse spinal cord. *J. Neurosci.* **2009**, 29, 15266-15276.

66) Thumkeo, D.; Shimizu, Y.; Sakamoto, S.; Yamada, S.; Narumiya, S. ROCK-I and ROCK-II cooperatively regulate closure of eyelid and ventral body wall in mouse embryo. *Genes Cells.* **2005**, 10, 825-834.

67) Hirooka, Y.; Shimokawa, H.; Takeshita, A. Rho-kinase, a potential therapeutic target for the treatment of hypertension. *Drug News Perspect.* **2004,** 17, 523-527.

68) Wirth, A. Rho kinase and hypertension. *Biochim. Biophys. Acta.* **2010**, 1802, 1276- 1284.

69) Yamakawa, T.; Tanaka, S.; Numaguchi, K.; Yamakawa, Y.; Motley, E. D.; Ichihara, S.; Inagami, T. Involvement of Rho-kinase in angiotensin II-induced hypertrophy of rat vascular smooth muscle cells. *Hypertension.* **2000**, 35, 313-318.

70) Kamiyama, M.; Utsunomiya, K.; Taniguchi, K.; Yokota, T.; Kurata, H.; Tajima, N.; Kondo, K. Contribution of Rho A and Rho kinase to platelet-derived growth factor-BB-induced proliferation of vascular smooth muscle cells. *J. Atheroscler. Thromb.* **2003,** 10, 117-123.

71) Uehata, M.; Ishizaki, T.; Satoh, H.; Ono, T.; Kawahara, T.; Morishita, T.; Tamakawa, H.; Yamagami, K.; Inui, J.; Maekawa, M.; Narumiya, S. Calcium sensitization of smooth muscle mediated by a Rho-associated protein kinase in hypertension. *Nature*. **1997,** 389, 990-994.

72) Takagi, Y.; Yasuda, S.; Takahashi, J.; Takeda, M.; Nakayama, M.; Ito, K.; Hirose, M.; Wakayama, Y.; Fukuda, K.; Shimokawa, H. Importance of dual induction tests for coronary vasospasm and ventricular fibrillation in patients surviving out-of-hospital cardiac arrest. *Circ J.* **2009,** 73, 767-769.

73) Kandabashi, T.; Shimokawa, H.; Miyata, K.; Kunihiro, I.; Kawano, Y.; Fukata, Y.; Higo, T.; Egashira, K.; Takahashi, S.; Kaibuchi, K.; Takeshita, A. Inhibition of myosin phosphatase by upregulated Rho-kinase plays a key role for coronary artery spasm in a porcine model with interleukin-1beta. *Circulation.* **2000,** 101, 1319 -1323.

74) Himokawa, H.; Seto, M.; Katsumata, N.; Amano, M.; Kozai, T.; Yamawaki, T.; Kuwata, K.; Kandabashi, T.; Egashira, K.; Ikegaki, I.; Asano, T.; Kaibuchi, K.; Takeshita, A. Rho-kinase-mediated pathway induces enhanced myosin light chain phosphorylations in a swine model of coronary artery spasm. *Cardiovasc. Res.* **1999,** 43, 1029-1039.

75) Yada, T.; Shimokawa, H.; Hiramatsu, O.; Kajita, T.; Shigeto, F.; Tanaka, E.; Shinozaki, Y.; Mori, H.; Kiyooka, T.; Katsura, M.; Ohkuma, S.; Goto, M.; Ogasawara, Y.; Kajiya, F. Beneficial effect of hydroxyfasudil, a specific Rho-kinase inhibitor, on ischemia/reperfusion injury in canine coronary microcirculation in vivo. *J. Am. Coll. Cardiol.* **2005**, 45, 599- 607.

76) Vahebi, S.; Kobayashi, T.; Warren, C. M.; De Tombe, P. P.; Solaro, R. J. Functional effects of Rho-kinase-dependent phosphorylation of specific sites on cardiac troponin. *Circ. Res.* **2005,** 96, 740-747.

77) Duong-Quy, S.; Bei, Y.; Liu, Z.; Dinh-Xuan, A. T. Role of Rho-kinase and its inhibitors in pulmonary hypertension. *Pharmacol. Ther.* **2013,** 137, 352-364.

78) Abe, K.; Shimokawa, H.; Morikawa, K.; Uwatoku, T.; Oi, K.; Matsumoto, Y.; Hattori, T.; Nakashima, Y.; Kaibuchi, K.; Sueishi, K.; Takeshita, A. Long-term treatment with a Rho-kinase inhibitor improves Monocrotaline-induced fatal pulmonary hypertension in Rats. *Circ Res.* **2004,** 94, 385-393.

79) Bach, L. A. Rho kinase inhibition: a new approach for treating diabetic nephropathy? *Diabetes.* **2008,** 57, 532-533.

80) Peng, F.; Wu, D.; Gao, B.; Ingram, A. J.; Zhang, B.; Chorneyko, K.; McKenzie, R.; Krepinsky, J. C. RhoA/Rho-kinase contribute to the pathogenesis of diabetic renal disease. *Diabetes.* **2008,** 57, 1683-1692.

81) An ongoing research in Dr.MacLeod lab.

82) Lin, G.; Craig, G. P.; Zhang, L.; Yuen, V. G.; Allard, M.; McNeill, J. H.; MacLeod, K. M. Acute inhibition of Rho-kinase improves cardiac contractile function in streptozotocin-diabetic rats. *Cardiovasc Res.* **2007,** 75, 51-58.

83) Loirand, G.; Guérin, P.; Pacaud, P. Rho kinases in cardiovascular physiology and pathophysiology. *Circ Res.* **2006,** 98, 322-334.

84) Bivalacqua, T. J.; Champion, H. C.; Usta, M. F.; Cellek, S.; Chitaley, K.; Webb, R. C.; Lewis, R. L.; Mills, T. M.; Hellstrom, W. J.; Kadowitz, P. J. RhoA/Rho-kinase suppresses endothelial nitric oxide synthase in the penis: a mechanism for diabetes-associated erectile dysfunction. *Proc. Natl. Acad. Sci. U S A.* **2004**, 101, 9121-9126.

85) Luscher, T. F.; Creager, M. A.; Beckman, J. A.; Cosentino, F. Diabetes and vascular disease: pathophysiology, clinical consequences, and medical therapy: part II. *Circulation.* **2003,** 108, 1655-1661.

86) Yao, L.; Romero, M. J.; Toque, H. A.; Yang, G.; Caldwell, R. B.; Caldwell, R. W. The role of RhoA/Rho kinase pathway in endothelial dysfunction. *J. Cardiovasc. Dis. Res.* **2010,** 1, 165-170.

87) Yin, H.; Ru, H.; Yu, L.; Kang, Y.; Lin, G.; Liu, C.; Sun, L.; Shi, L.; Sun, Q.; Liu, C. Targeting of Rho kinase ameliorates impairment of diabetic endothelial function in intrarenal artery. *Int. J. Mol. Sci.* **2013,** 14, 20282-20298.

88) Kanda, T.; Wakino, S.; Homma, K.; Yoshioka, K.; Tatematsu, S.; Hasegawa, K.; Takamatsu, I.; Sugano, N.; Hayashi, K.; Saruta, T. Rho-kinase as a molecular target for insulin resistance and hypertension. *FASEB J.* **2006,** 20, 169-171.

89) Wong, C. C.; Wong, C. M.; Tung, E. K.; Man, K.; Ng, I. O. Rhokinase 2 is frequently overexpressed in hepatocellular carcinoma and involved in tumor invasion. *Hepatology.* **2009**, 49, 1583-1594.

90) Vishnubhotla, R.; Sun, S.; Huq, J.; Bulic, M.; Ramesh, A.; Guzman, G.; Cho, M.; Glover, S. C. ROCK-II mediates colon cancer invasion via regulation of MMP-2 and MMP-13 at the site of invadopodia as revealed by multiphoton imaging. *Lab. Invest.* **2007**, 87, 1149-1158.

91) Kamai, T.; Tsujii, T.; Arai, K.; Takagi, K.; Asami, H.; Ito, Y.; Oshima, H. Significant association of Rho/ROCK pathway with invasion and metastasis of bladder cancer. *Clin. Cancer Res.* **2003**, 9, 2632-2641.

92) Lin, S. L.; Chang, D.; Ying, S. Y. Hyaluronan stimulates transformation of androgen-independent prostate cancer. *Carcinogenesis*. **2007**, 28, 310-320.

93) Riento, K.; Ridley, A. J. ROCKs: multifunctional kinases in cell behaviour. *Nat. Rev. Mol. Cell Boil.* **2003**, 4, 446-456.

94) Bryan, B. A.; Dennstedt, E.; Mitchell, D. C.; Walshe, T. E.; Noma, K.; Loureiro, R.; Saint-Geniez, M.; Campaigniac, J. P.; Liao, J. K.; D'Amore, P. A. RhoA/ROCK signaling is essential for multiple aspects of VEGF-mediated angiogenesis. *FASEB J.* **2010,** 24, 3186-3195.

95) Liu, S.; Goldstein, R. H.; Scepansky, E. M.; Rosenblatt, M. Inhibition of Rho-associated kinase signaling prevents breast cancer metastasis to human bone. *Cancer Res.* **2009,** 69, 8742-8751.

96) Ying, H.; Biroc, S. L.; Li, W.; Alicke, B.; Xuan, J.; Pagila, R.; Ohashi, Y.; Okada, T.; Kamata, Y.; Dinter, H. The Rho kinase inhibitor fasudil inhibits tumor progression in human and rat tumor models. *Mol. Cancer Ther.* **2006,** 5, 2158-2164.

97) Bonn, S.; Herrero, S.; Breitenlechner, C. B.; Erlbruch, A.; Lehmann, W.; Engh, R. A.; Gassel, M.; Bossemeyer, D. Structural analysis of protein kinase a mutants with Rho-kinase inhibitor specificity. *J. Biol. Chem.* **2006,** 281, 24818-24830.

98) Yamaguchi, H.; Kasa, M.; Amano, M.; Kaibuchi, K.; Hakoshima, T. Molecular mechanism for the regulation of Rho-kinase by dimerization and its inhibition by fasudil. *Structure.* **2006,** 14, 589-600.

99) Jacobs, M.; Hayakawa, K.; Swenson, L.; Bellon, S.; Fleming, M.; Taslimi, P.; Doran, J. The structure of dimeric ROCK I reveals the mechanism for ligand selectivity. *J. Biol. Chem.* **2006,** 281, 260-268.

100) Chico, L. K.; Van Eldik, L. J.; Watterson, D. M. Targeting protein kinases in central nervous system disorders. *Nat. Rev. Drug Discovery*. **2009,** 8, 892-909.

101) Huse, M.; Kuriyan, J. The conformational plasticity of protein kinases. *Cell.* **2002,** 109, 275-282.

102) Leung, I. W.; Lassam, N. The kinase activation loop is the key to mixed lineage kinase-3 activation via both autophosphorylation and hematopoetic progenitor kinase 1 phosphorylation. *J. Biol. Chem.* **2001,** 27, 1961-1967.

103) Zhang, J.; Yang, P. L.; Gray, N. S. Targeting cancer with small molecule kinase inhibitors. *Nat. Rev. Cancer.* **2009,** 9, 28-39.

104) Kufareva, I.; Abagyan, R. Type-II kinase inhibitor docking, screening, and profiling using modified structures of active kinase states. *J. Med. Chem.* **2008,** 51, 7921-7932.

105) Liao, J. J. Molecular recognition of protein kinase binding pockets for design of potent and selective kinase inhibitors. *J. Med. Chem.* **2007**, 50, 409–424.

106) Liu, Y.; Gray, N. S. Rational design of inhibitors that bind to inactive kinase conformations. *Nat. Chem. Biol.* **2006,** 2, 358-364.

107) Schindler, T.; Bornmann, W.; Pellicen, P.; Miller, W. T.; Clarkson, B.; Kuriyan, J. Structural mechanism for STI-571 inhibition of abelson tyrosine kinase. *Science.* **2000**, 289, 1938-1942.

108) Skoraa, L.; Mestanb, J.; Fabbrob, D.; Jahnkeb, W.; Grzesiek, S. NMR reveals the allosteric opening and closing of Abelson tyrosine kinase by ATP-site and myristoyl pocket inhibitors. *Proc. Natl. Acad. Sci. U.S.A.* **2013**, 110, E4437–E4445.

109) Zhao, Z.; Wu, H.; Wang, L.; Liu, Y.; Knapp, S.; Liu, Q.; Gray, N. S. Exploration of type II binding mode: a privileged approach for kinase inhibitor focused drug discovery. *ACS Chem. Biol.* **2014**, 9, 1230-1241.

110) Regan, J.; Pargellis, C. A.; Cirillo, P. F.; Gilmore, T.; Hickey, E. R.; Peet, G. W.; Proto, A.; Swinamer, A.; Moss, N. The kinetics of binding to p38MAP kinase of analogues of BIRB 796. *Bioorg. Med. Chem. Lett.* **2003,** 13, 3101-3104.

111) Gavrin, L. K.; Saiah, E. Approaches to discover non-ATP site kinase inhibitors. *Med. Chem. Commun.* **2013**, 4, 41-51.

112) Rikitake, Y.; Kim, H.H.; Huang, Z.; Seto, M.; Yano, K.; Asano, T.; Moskowit, M. A.; Liao, J. K. Inhibition of Rho kinase (ROCK) leads to increased cerebral blood flow and stroke protection. *Stroke*. **2005**, 36, 2251-2257.

113) Shimokawa, H.; Seto, M.; Katsumata, N.; Amano, M.; Kozai, T.; Yamawaki, T.; Kuwata, K.; Kandabashi, T.; Egashira, K.; Ikegaki, I.; Asano, T.; Kaibuchi, K.; Takeshita, A. Rho-kinase-mediated pathway induces enhanced myosin light chain phosphorylations in a swine model of coronary artery spasm. *Cardiovasc. Res.* **1999,** 43, 1029-1039.

114) Tamura, M.; Nakao, H.; Yoshizaki, H.; Shiratsuchi, M.; Shigyo, H.; Yamada, H.; Ozawa, T.; Totsuka, J.; Hidaka, H. Development of specific Rho-kinase inhibitors and their clinical application. *Biochim. Biophys. Acta.* **2005,** 1754, 245-252.

115) Yamaguchi, H.; Miwa, Y.; Kasa, M.; Kitano, K.; Amano, M.; Kaibuchi, K.; Hakoshima, T. Structural basis for induced-fit binding of Rho-kinase to the inhibitor Y-27632. *J. Biochem.* **2006**, 140, 305-311.

116) Iwakubo, M.; Takami, A.; Okada, Y.; Kawata, T.; Tagami, Y.; Sato, M.; Sugiyama, T.; Fukushima, K.; Taya, S.; Amano, M.; Kaibuchi, K.; Iijima, H. Design and synthesis of Rho kinase inhibitors (III). *Bioorg. Med. Chem.* **2007,** 15, 1022-1033.

117) Ray, P.; Wright, J.; Adam, J.; Bennett, J.; Boucharens, S.; Black, D.; Cook, A.; Brown, A. R.; Epemolu, O.; Fletcher, D.; Haunso, A.; Huggett, M.; Jones, P.; Laats, S.; Lyons, A.; Mestres, J.; De Man, J.; Morphy, R.; Rankovic, Z.; Sherborne, B.; Sherry, L.; Van Straten, N.; Westwood, P.; Zaman, G. Z. R. Fragment-based discovery of 6-substituted isoquinolin-1-amine based ROCK-I inhibitors. *Bioorg. Med. Chem. Lett.* **2011,** 21, 97-101.

118) Wu, F.; Buttner, F. H.; Chen, R.; Hickey, E.; Jakes, S.; Kaplita, P.; Kashem, M. A.; Kerr, S.; Kugler, S.; Paw, Z.; Prokopowicz, A.; Shih, C.; Snow, R.; Young, E.; Cywin, C. L. Substituted 2H-isoquinolin-1-one as potent Rho-kinase inhibitors. Part 1: Hit-to-lead account. *Bioorg. Med. Chem. Lett.* **2010,** 20, 3235-3239.

119) Lavogina, D.; Kalind, K.; Bredihhina, J.; Hurt, M.; Vaasa, A.; Kasari, M.; Enkvist, E.; Raidaru, G.; Uri, A. Conjugates of 5-isoquinolinesulfonylamides and oligo-D-arginine possess high affinity and selectivity towards Rho kinase (ROCK). *Bioorg. Med. Chem. Lett.* **2012,** 22, 3425-3430.

120) Nakajima, M.; Hayashi, K.; Egi, Y.; Katayama, K.; Amano, Y.; Uehata, M.; Ohtsuki, M.; Fujii, A.; Oshita, K.; Kataoka, H.; Chiba, K.; Goto, N.; Kondo, T. Effect of Wf536, a novel ROCK inhibitor, against metastasis of B16 melanoma. *Cancer Chemother. Pharmacol.* **2003,** 52, 319-324.

121) Patel, R. A.; Forinash, K. D.; Pireddu, R.; Sun, Y.; Sun, N.; Martin, M. P.; Schönbrunn, E.; Lawrence, N. J.; Sebti, S. M. RKI-1447 is a potent inhibitor of the Rho-associated ROCK kinases with anti-invasive and antitumor activities in breast cancer. *Cancer Res.* **2012,** 72, 5025-5034.

122) Boland, S.; Defert, O.; Alen, J.; Bourin, A.; Castermans, K.; Kindt, N.; Boumans, N.; Panitti, L.; Van de Veldeb, S.; Stalmans, I.; Leysen, D. 3-[2-(Aminomethyl)-5-[(pyridin-4-yl)carbamoyl]phenyl] benzoates as soft ROCK inhibitors. *Bioorg. Med. Chem. Lett.* **2013,** 23, 6442-6446.

123) Rajagopalan, L. E.; Davies, M. S.; Kahn, L. E.; Kornmeier, C. M.; Shimada, H.; Steiner, T. A.; Zweifel, B. S.; Wendling, J. M.; Payne, M. A.; Loeffler, R. F.; Case, B. L.; Norton, M. B.; Parikh, M. D.; Nemirovskiy, O. V.; Mourey, R. J.; Masferrer, J. L.; Misko, T. P.; Kolodziej, S. A. Biochemical, cellular, and anti-inflammatory properties of a potent, selective, orally bioavailable benzamide inhibitor of Rho kinase activity. *J. Pharmacol. Exp. Ther.* **2010**, 333, 707-716.

124) Li, R.; Martin, M. P.; Liu, Y.; Wang, B.; Patel, R. A.; Zhu, J. Y.; Sun, N.; Pireddu, R.; Lawrence, N. J.; Li, J.; Haura, E. B.; Sung, S. S.; Guida, W. C.; Schonbrunn, E.; Sebti, S. M. Fragment-based and structure-guided discovery and optimization of Rho kinase inhibitors. *J. Med. Chem.* **2012,** 55, 2474-2478.

125) Tokushige, H.; Inatani, M.; Nemoto, S.; Sakaki, H.; Katayama, K.; Uehata, M.; Tanihara, H. Effects of topical administration of Y-39983, a selective Rho-associated protein kinase

inhibitor, on ocular tissues in rabbits and monkeys. *Invest. Ophthalmol. Vis. Sci*. **2007,** 48, 3216-3222.

126) Chen, J.; Runyan, S. A.; Robinson, M. R. Novel ocular antihypertensive compounds in clinical trials. *Clin. Ophthalmol.* **2011,** 5, 667-677.

127) Schirok, H.; Kast, R.; Figueroa-Perez, S.; Bennabi, S.; Gnoth, M. J.; Feurer, A.; Heckroth, H.; Thutewohl, M.; Paulsen, H.; Knorr, A.; Hutter, J.; Lobell, M.; Munter, K.; Geiss, V.; Ehmke, H.; Lang, D.; Radtke, M.; Mittendorf, J.; Stasch, J. P. Design and synthesis of potent and selective azaindole-based Rho kinase (ROCK) inhibitors. *ChemMedChem.* **2008,** 3, 1893-1904.

128) Kast, R.; Schirok, H.; Figueroa-Pe´rez, S.; Mittendorf, J.; Gnoth, M. J. ; Apeler, H.; Lenz, J.; Franz, J. K.; Knorr, A.; Hu¨tter, J.; Lobell, M.; Zimmermann, K.; Mu¨nter, K.; Augstein, K. H.; Ehmke, H.; Stasch, J. P. Cardiovascular effects of a novel potent and highly selective azaindole-based inhibitor of Rho-kinase. *Br. J. Pharmacol.* **2007,** 152, 1070-1080.

129) Goodman, K. B.; Cui, H.; Dowdell, S. E.; Gaitanopoulos, D. E.; Ivy, R, L,; Sehon, C. A.; Stavenger, R. A.; Wang, G. Z.; Viet, A. Q.; Xu, W.; Ye, G.; Semus, S. F.; Evans, C.; Fries, H. E.; Jolivette, L. J.; Kirkpatrick, R. B.; Dul, E.; Khandekar, S. S.; Yi, T.; Jung, D. K.; Wright, L. L.; Smith, G. K.; Behm, D. J.; Bentley, R.; Doe, C. P.; Hu, E.; Lee, D. Development of dihydropyridone indazole amides as selective Rho-kinase inhibitors. *J. Med. Chem.* **2007,** 50, 6-9.

130) Oh, K. S.; Oh, B. K.; Park, C. H.; Seo, H. W.; Kang, N. S.; Lee, J. H.; Lee, J. S.; Ho, L. B. Cardiovascular effects of a novel selective Rho kinase inhibitor, 2-(1H-indazole-5-yl)amino-4-methoxy-6-piperazino triazine (DW1865). *Eur. J. Pharmacol.* **2013,** 702, 218-226.

131) Feng, Y.; Cameron, M. D.; Frackowiak, B.; Griffin, E.; Lin, L.; Ruiz, C.; Schröter, T.; LoGrasso, P. Structure-activity relationships, and drug metabolism and pharmacokinetic properties for indazole piperazine and indazole piperidine inhibitors of ROCK-II. *Bioorg. Med. Chem. Lett.* **2007,** 17, 2355-2360.

132) Lee, J. H.; Zheng, Y.; Von Bornstadt, D.; Wei, Y.; Balcioglu1, A.; Daneshmand, A.; Yalcin, N.; Yu, E.; Herisson, F.; Atalay, Y. B.; Kim, M. H.; Ahn, Y. J.; Balkaya, M.; Sweetnam, P.; Schueller, O.; Poyurovsky, M. V.; Kim, H. H.; Lo, E. H.; Furie, K. L.; Ayata, C. Selective ROCK2 inhibition in focal cerebral ischemia. *Ann. Clin. Transl. Neurol.* **2014,** 1, 2-14.

133) Feng, Y.; Yin, Y.; Weiser, A.; Griffin, E.; Cameron, M. D.; Lin, L.; Ruiz, C.; Schurer, S. C.; Inoue, T.; Rao, P. V.; Schroter, T, Lograsso, P. Discovery of substituted 4-(pyrazol-4-yl)-phenylbenzodioxane-2-carboxamides as potent and highly selective Rho kinase (ROCK-II) inhibitors. *J. Med. Chem.* **2008,** 51, 6642-6645.

134) Fang, X.; Yin, Y.; Chen, Y. T.; Yao, L. Wang, B.; Cameron, M. D.; Lin, L.; Khan, S.; Ruiz, C.; Schroter, T.; Grant, W.; Weiser, A.; Pocas, J.; Pachori, A.; Schurer, S.; LoGrasso, P.; Feng, Y. Tetrahydroisoquinoline derivatives as highly selective and potent Rho kinase inhibitors. *J. Med. Chem.* **2010,** 53, 5727-5737.

135) Chen , Y. T.; Vojkovsky, T.; Fang, X.; Pocas, J. R.; Grant, W.; Handy, A. M. W.; Schröter, T.; LoGrasso, P.; Bannister, T. D.; Feng, Y. Asymmetric synthesis of potent chroman-based Rho kinase (ROCK-II) inhibitors. *Med. Chem. Commun.* **2011,** 2, 73-75.

136) Yin, Y.; Lin, L.; Ruiz, C.; Cameron, M. D.; Pocas, J.; Grant, W.; Schroter, T.; Chen, W.; Duckett, D.; Schurer, S.; Lograsso, P.; Feng, Y. Benzothiazoles as Rho-associated kinase (ROCK-II) inhibitors. *Bioorg. Med. Chem. Lett.* **2009,** 19, 6686-6690.

137) Yin, Y.; Lin, L.; Ruiz, C.; Khan, S.; Cameron, M. D.; Grant, W.; Pocas, J.; Eid, N.; Park, H.; Schroter, T.; Lograsso, P. V.; Feng, Y. Synthesis and biological evaluation of urea derivatives as highly potent and selective rho kinase inhibitors. *J. Med. Chem.* **2013,** 56, 3568-3581.

138) Stavenger, R. A.; Cui, H.; Dowdell, S. E.; Franz, R. G.; Gaitanopoulos, D. E.; Goodman, K. B.; Hilfiker, M. A.; Ivy, R. L.; Leber, J. D.; Marino, J. P.; Oh, H. J.; Viet, A. Q.; Xu, W.; Ye, G.; Zhang, D.; Zhao, Y.; Jolivette, L. J.; Head, M. S.; Semus, S. F.; Elkins, P. A.; Kirkpatrick, R. B.; Dul, E.; Khandekar, S. S.; Yi, T.; Jung, D. K.; Wright, L. L.; Smith, G. K.; Behm, D. J.; Doe, C. P.; Bentley, R.; Chen, Z. X.; Hu, E.; Lee, D. Discovery of aminofurazan-azabenzimidazoles as inhibitors of Rho-kinase with high kinase selectivity and antihypertensive activity. *J. Med. Chem.* **2007,** 50, 2-5.

139) Doe, C.; Bentley, R.; Behm, D. J.; Lafferty, R.; Stavenger, R.; Jung, D.; Bamford, M.; Panchal, T.; Grygielko, E.; Wright, L. L.; Smith, G. K.; Chen, Z.; Webb, C.; Khandekar, S.; Yi, T.; Kirkpatrick, R.; Dul, E.; Jolivette, L.; Marino, J. P.; Willette, R.; Lee, D.; Hu, E. Novel Rho kinase inhibitors with anti-inflammatory and vasodilatory activities. *J. Pharmacol. Exp. Ther*. **2007**, 320, 89-98.

140) Bamford, M. J.; Alberti, M. J.; Bailey, N.; Davies, S.; Dean, D. K.; Gaiba, A.; Garland, S.; Harling, J. D.; Jung, D. K.; Panchal, T. A.; Parr, C. A.; Steadman, J. G.; Takle, A. K.;

Townsend, J. T.; Wilson, D. M.; Witherington, J. (1H-Imidazo[4,5-c]pyridin-2-yl)-1,2,5-oxadiazol-3-ylamine derivatives: a novel class of potent MSK-1-inhibitors. *Bioorg. Med. Chem. Lett.* 2**005**, 15, 3402–3406.

141) Akama, T.; Dong, C.; Virtucio, C.; Sullivan, D.; Zhou, Y.; Zhang, Y. K.; Rock, F.; Freund, Y.; Liu, L.; Bu, W.; Wu, A.; Fan, X. Q.; Jarnagin. K. Linking phenotype to kinase: identification of a novel benzoxaborole hinge-binding motif for kinase inhibition and development of high-potency rho kinase inhibitors. *J. Pharmacol. Exp. Ther.* **2013,** 347, 615-625.

142) Sessions, E. H.; Smolinski, M.; Wang, B.; Frackowiak, B.; Chowdhury, S.; Yin, Y.; Chen, Y. T.; Ruiz, C.; Lin, L.; Pocas, J.; Schroter, T.; Cameron, M. D.; LoGrasso, P.; Feng, Y.; Bannister, T. D. The development of benzimidazoles as selective Rho kinase inhibitors. *Bioorg. Med. Chem. Lett.* **2010,** 20, 1939-1943.

143) Shen, M.; Yu, H.; Li, Y.; Li, P.; Pan, P.; Zhou, S.; Zhang, L.; Li, S.; Lee, S. M.; Hou, T. Discovery of Rho-kinase inhibitors by docking-based virtual screening. *Mol. BioSyst.* **2013,** 9, 1511-1521.

144) Oh, K. S.; Mun, J.; Cho, J. E.; Lee, S.; Yi, K. Y.; Lim, C. J.; Lee, J. S.; Park, W. J.; Lee, B. H. Discovery of novel scaffolds for Rho kinase 2 inhibitor through TRFRET- based high throughput screening assay. *Comb. Chem. High Throughput Screen*. **2013**, 16, 37-46.

145) Ishizaki, T.; Uehata, M.; Tamechika, I.; keel, J.; Nonomura, K.; Narumiya, S. Pharmacological properties of Y-27632, a specific inhibitor of Rho-associated kinases. *Mol. Pharmacol.* , **2000,** 57, 976-983.

146) Wei, L.; Malhotra, S. V. Recent development of cyclic amide (pyridone/lactam) moiety containing heterocycles as protein kinase inhibitors. *Curr. Med. Chem.* **2010,** 17, 234-253.

147) Kibou, Z.; Cheikh, N.; Villemin, D.; Choukchou-Braham, N.; Mostefa-Kar, B.; Benabdallah, M. A simple and efficient procedure for a 2-pyridones synthesis under solvent-free conditions. *Int. J. Org. Chem.* **2011**, 1, 242-249.

148) Lima, L. M.; Barreiro, E. J. Bioisosterism: a useful strategy for molecular modification and drug design. Curr. Med. Chem., **2005**, 12, 23-49.

149) Knight, D. W.; Pattenden, G.; Rippon, D. E. Synthesis of the tris-oxazole ring system of ulapualides. *Synlett.* **1990**, 1, 36-37.

150) Wipf, P.; Miller, C.P. A new synthesis of highly functionalized oxazoles. *J. Org. Chem.* **1993**, 58, 3604–3606.

151) Graham, T. H. A direct synthesis of oxazoles from aldehydes. *Org. Lett.* **2010**, 12, 3614-3617.

152) Sanz-Cervera, J. F.; Blasco, R.; Piera, J.; Cynamon, M.; Ibáñez, I.; Murguía, M.; Fustero, S. Solution versus fluorous versus solid-phase synthesis of 2,5-disubstituted 1,3-azoles. preliminary antibacterial activity studies. *J. Org. Chem.* **2009**, 74, 8988-8996.

153) Wallace, E. M.; Lyssikatos, J.; Blake, J. F.; Seo, J.; Yang, H. W.; Yeh, T. C.; Perrier, M.; Jarski, H.; Marsh, V.; Poch, G.; Livingston, M. G.; Otten, J.; Hingorani, G.; Woessner, R.; Lee, P.; Winkler, J.; Koch, K. Potent and selective mitogen-activated protein kinase kinase (MEK) 1,2 inhibitors. 4-(4-bromo-2-fluorophenylamino)-1-methylpyridin-2(1H)-ones. *J. Med. Chem.* **2006,** 49, 441–444.

154) Yang, H. W.; Craven, B. M. Charge density of 2-pyridone. *Acta Crystallogr. B.* **1998**, 54, 912-920.

155) Comins, D. L.; Jianhua, G. *N*- vs. *O*-Alkylation in the Mitsunobu reaction of 2-pyridone. *Tetrahedron lett.* **1994**, 35, 2819-2822.

156) Kociensk, Ph. J. Protecting Groups, George Thieme Verlag, **2005**, 3rd Edition, p 343.

157) Grierson, D. S.; Harris, M.; Husson, H. P. 2-Cyano Δ^3 piperideines—IX1: General strategies for the synthesis of corynanthé-strychnos type indole alkaloids. *Tetrahedron.* **1983**, 39, 3683-3694.

158) Wada, M.; Mitsunobu, O. Intermolecular dehydration between alcohols and active hydrogen compounds by means of diethyl azodicarboxylate and triphenylphosphine. *Tetrahedron Lett.* **1972**, 13, 1279-1282.

159) Casasnovas, R.; Frau, J.; Ortega-Castro, J.; Salvà, A.; Donoso, J.; Muñoz, F. Absolute and relative pKa calculations of mono and diprotic pyridines by quantum methods. *J. Mol. Struct.-THEOCHEM*. **2009**, 912, 5-12.

160) Schelhaas, M.; Waldmann, H. Protecting group strategies in organic synthesis. *Angew. Chem. Int. Ed. Engl.* **1996,** 35, 2056-2083.

161) Garner, P.; Park, J. M. The synthesis and configurational stability of differentially protected β-hydroxy-α-amino aldehydes. *J. Org. Chem.* **1987**, 52, 2361-2364.

162) Van der Auwera, C.; Anteunis, M. J. O. *N*,*N*'-bis(2-oxo-3-oxazolidinyl) phosphinic chloride (BOP-Cl); a superb reagent for coupling at and with iminoacid residues. *Int. J. Peptide Protein Res.* **1987**, 29, 574-588.

163) Christian A.; Montalbetti, N.; Falque, V. Amide bond formation and peptide coupling. *Tetrahedron*. **2005,** 61, 10827–10852.

164) Phillips, A. J.; Uto, Y.; Wipf, P.; Reno M. J.; Williams, D. R. Synthesis of functionalized oxazolines and oxazoles with DAST and deoxo-fluor. *Org. Lett.* **2000**, 2, 1165-1168.

165) Wipf, P.; Miller, C. P. A short, stereospecific synthesis of dihydrooxazoles from serine and threonine derivatives. *Tetrahedron Lett*. **1992**, 33, 907–910.

166) Williams, D. R.; Lowder, P. D.; Gu, Y. G.; Brooks, D. A. Studies of mild dehydrogenations in heterocyclic systems. *Tetrahedron Lett.* **1997**, 38, 331-334.

167) Murai, K.; Takahara, Y.; Matsushita, T.; Komatsu, H.; Fujioka, H. Facile preparation of oxazole-4-carboxylates and 4-ketones from aldehydes using 3-oxazoline-4-carboxylates as intermediates. *Org. Lett.* **2010**, 12, 3456-3459.

168) Yu, Y.; Chen, H.; Wang, L.; Chen, X.; Fu, B. A facile synthesis of 2,4-disubstituted thiazoles using MnO2. *Molecules.* **2009**, 14, 4858-4865.

169) Boraa, R. O.; Dara, B.; Pradhanc, V.; Farooqui, M. [1, 2, 4]-Oxadiazoles: synthesis and biological applications. *Mini Rev. Med. Chem.* **2013**, 13, 1-15.

170) Vu, C. B.; Corpuz, E. G.; Merry, T. J.; Pradeepan, S. G.; Bartlett, C.; Bohacek, R. S.; Botfield, M. C.; Eyermann, C. J.; Lynch, B. A.; MacNeil, I. A.; Ram, M. K.; Van Schravendijk, M. R.; Violette, S.;Sawyer, T. K. Discovery of potent and selective SH2 inhibitors of the tyrosine kinase ZAP-70. *J. Med. Chem.* **1999**, 42, 4088-4098.

171) Ricardo, A. W.; Neves, F. A. A handy and solventless direct route to primary 3-[3-Aryl)-1,2,4-oxadiazol-5-yl]propionamides using microwave irradiation. *Molecules.* **2006**, 11, 318-324.

172) Patani, G. A.; LaVoie, E. J. Bioisosterism: a rational approach in drug design. *Chem. Rev.* **1996**, 96, 3147-3176.

173) Augustine, J. K.; Akabote, V.; Hegde, S. G.; Alagarsamy, P. PTSA-ZnCl2 is an efficient and mild catalyst for the synthesis of 3,5-disubstituted-1,2,4-oxadiazoles from amidoximes and organic nitriles. *J. Org. Chem.* **2009**, 74, 5640-5643.

174) Amarasinghe, K. K. D.; Maier, M. B.; Srivastava, A.; Gray, J. L. One-pot synthesis of 1,2,4-oxadiazoles from carboxylic acid esters and amidoximes using potassium carbonate. *Tetrahedron Lett.* **2006**, 47, 3629-3631.

175) Katritzky, A. R.; Shestopalov, A. A.; Suzuki, K. A convenient synthesis of chiral 1,2,4-oxadiazoles from N-protected (α-aminoacyl)benzotriazoles. *ARKIVOC.* **2005**, 2005, 36-55.

176) Olah, G. A.; Narang, S. C.; Fung, A. P.; Gupta, G. B. Cyanuric chloride, a mild dehydrating agent in the preparation of nitriles from amides. *Synthesis.* **1980**, 1980, 657-658.

177) Srivastava, R. M.; Pereira, M. C.; Faustino, W. W. M.; Coutinho, K.; Dos Anjos, J. V.; De Melo, S. J. Synthesis, mechanism of formation, and molecular orbital calculations of arylamidoximes. *Monatsh. Chem.* **2009**, 140, 1319-1324.

178) Rajeswari, S.; Jones, R. J.; Cava, M. P. A new synthesis of amides from acyl fluorides and N-silylamines. *Tetrahedron Lett.* **1987**, 28, 5099-5102.

179) Tullock, C. W.; Coffman, D. D. Synthesis of fluorides by metathesis with sodium fluoride. *J. Org. Chem.* **1960**, 25, 2016-2019.

180) Hirabayashi, T.; Itoh, K.; Sakai, S.; Ishii, Y. Insertion reactions of diethylaluminium derivatives III. Reactions of diethylaluminium dimethylamide, ethanethiolate and ethanolate with lactones or acid anyhydrides. *J. Organomet. Chem.* **1970**, 25, 33-41.

181) Basha, A.; Lipton, M.; Weinreb, M. N-Alkylation of amides and related compounds. *Tetrahedron Lett.* **1977**, 17, 1465-1468.

182) Lloyd, J.; Schmidt, J. B.; Rovnyak, G.; Ahmad, S.; Atwal, K. S.; Bisaha, S. N.; Doweyko, L. M.; Stein, P. D.; Traeger, C. S.; Mathur, A.; Conder, M. L.; DiMarco, J.; Harper, T. W.; Jenkins-West, T.; Levesque, P. C.; Normandin, D. E.; Russell, A. D.; Serafino, R. P.; Smith, M. A.; Lodge, N. J. Design and synthesis of 4-substituted benzamides as potent, selective, and orally bioavailable IKs blockers. *J. Med. Chem.* **2001**, 44, 3764-3767.

183) Dubreuil, P.; Letard, S.; Ciufolini, M.; Gros, L.; Humbert, M.; Casteran, N.; Borge, L.; Hajem, B.; Lermet, A.; Sippl, W.; Voisset, E.; Arock, M.; Auclair, C.; Leventhal, P. S.; Mansfield, C. D.; Moussy, A.; Hermine, O. Masitinib (AB1010), a potent and selective tyrosine kinase inhibitor targeting KIT. *PLoS ONE.* **2009**, 4, e7258.

184) Borzilleri, R. M.; Bhide, R. S.; Barrish, J. C.; D'Arienzo, C. J.; Derbin, G. M.; Fargnoli, J.; Hunt, J. T.; Jeyaseelan, R.; Kamath, A.; Kukral, D. W.; Marathe, P.; Mortillo, S.; Qian, L.; Tokarski, J. S.; Wautlet, B. S.; Zheng, X.; Lombardo, L. J. Discovery and evaluation of *N*-Cyclopropyl-2,4-difluoro-5-((2-(pyridin-2-ylamino)thiazol-5-ylmethyl)amino) benzamide (BMS-605541), a selective and orally efficacious inhibitor of vascular endothelial growth factor receptor-2. *J. Med. Chem*. **2006**, 49, 3766-3769.

185) Gallardo-Godoy, A.; Gever, J.; Fife, K. L.; Silber, M.; Prusiner, S. B.; Renslo, A. R. 2-aminothiazoles as therapeutic leads for prion diseases. *J. Med. Chem.* **2011**, 54, 1010-1021.

186) Williams, A.; Jencks, W. P. Urea synthesis from amines and cyanic acid: kinetic evidence for a zwitterionic intermediate. *J. Chem. Soc., Perkin Trans. 2*. **2002**, 1974, 1753-1759.

187) Congdon, W. I.; Edward, J. T. The alkaline hydrolysis of N-acylthioureas. *Can. J. Chem.* **1974**, 52, 697-701.

188) Egan, R. S.; Tadanier, J.; Garmaise, D. L.; Gaunce, A. P. Intermediates in the Hantzsch thiazole synthesis. *J. Org. Chem.* **1968**, 33, 4422-4426.

189) McTiguea, M.; Murray, B. W.; Chen, J. H.; Deng, Y. L.; Solowiej, J.; Kania, R. S. Molecular conformations, interactions, and properties associated with drug efficiency and clinical performance among VEGFR TK inhibitors. *Proc. Natl. Acad. Sci. U S A.* **2012**, 109, 18281-18289.

190) Iwakubo, M.; Takami, A.; Okada, Y.; Kawata, T.; Tagami, Y.; Ohashi, H.; Sato, M.; Sugiyama, T.; Fukushima, K.; Iijima, H. Design and synthesis of rho kinase inhibitors (II). *Bioorg. Med. Chem.* **2007**, 15, 350-364.

191) Misra, R. N.; Xiao, H.; Williams, D. K.; Kim, K. S.; Lu, S.; Keller, K. A.; Mulheron, J. G.; Batorsky, R.; Tokarski, J. S.; Sack, J. S.; Kimball, S. D.; Lee, F. Y.; Webster, K. R. Synthesis and biological activity of N-aryl-2-aminothiazoles: potent pan inhibitors of cyclin-dependent kinases. *Bioorg. Med. Chem. Lett.* **2004**, 14, 2973-2977.

192) Beletskaya, I. P.; Cheprakov, A. V. Copper in cross-coupling reactions, the post-Ullmann chemistry. *Coord. Chem. Rev.* **2004**, 248, 2337-2364.

193) Monnier, F.; Taillefer, M. Catalytic C-C, C-N, and C-O Ullmann-type coupling reactions. *Angew. Chem. Int. Ed.* **2009**, 48, 6954-6971.

194) Louie, J.; Hartwig, J. F. Palladium-catalyzed synthesis of arylamines from aryl halides. Mechanistic studies lead to coupling in the absence of tin reagents. *Tetrahedron Lett.* **1995**, 36, 3609-3612.

195) Guram, A. S.; Rennels, R. A.; Buchwald, S. L. A simple catalytic method for the conversion of aryl bromides to arylamines. *Angew. Chem. Int. Ed. Engl.* **1995**, 34, 1348-1350.

196) Schnuerch, M.; Waldner, B.; Hilber, K.; Mihovilovic, M. D. Synthesis of 5-arylated N-arylthiazole-2-amines as potential skeletal muscle cell differentiation promoters. *Bioorg. Med. Chem. Lett.* **2011**, 21, 2149-2154.

197) Slagt, V. F.; De Vries, A. M.; De Vries, J. G.; Kellogg, R. M. Practical aspects of carbon−carbon cross-coupling reactions using heteroarenes. *Org. Process Res. Dev.* **2010**, 14, 30-47.

198) Wang, J.; Liang, Y. L.; Qu, J. Boiling water-catalyzed neutral and selective N-Boc deprotection. *Chem. Commun.* **2009**, 31, 5144-5146.

199) Diez-Cecilia, E.; Kelly, B.; Rozas, I. One-step double reduction of aryl nitro and carbonyl groups using hydrazine. *Tetrahedron lett*. **2011**, 52, 6702-6704.

200) Crestey, F.; Collot, V.; Stiebing, S.; Rault, S. A new and efficient synthesis of 2-azatryptophans. *Tetrahedron*. **2006**, 62, 7772-7775.

201) Kim, S.; Rieke, R. D. Recent advance in heterocyclic organozinc and organomanganese compounds; direct synthetic routes and application in organic synthesis. *Molecules.* **2010**, 15, 8006-8038.

202) Gan, S. D.; Patel, K. R. Enzyme immunoassay and enzyme-linked immunosorbent assay. *J. Invest. Dermatol.* **2013**, 133, e12.

203) Lequin, R. M. Enzyme immunoassay (EIA)/enzyme-linked immunosorbent assay (ELISA). *Clin. Chem.* **2005**, 51, 2415-2418.

204) Schmid, J. A.; Sitte, H. H. Fluorescence resonance energy transfer in the study of cancer pathways. *Curr. Opin. Oncol.* **2003**, 15, 55-64.

205) Rahman, M. M. An introduction to fluorescence resonance energy transfer (FRET). *Sci. J. Phys*. **2012**, 2012, 2276-6367.

206) Newton, P.; Harrison, P.; Clulow, S. A novel method for determination of the affinity of protein: protein interactions in homogeneous assays. *J. Biomol. Screen.* **2008**, 13, 674-682.

207) Faller, B.; Urban, L. Hit finding and profiling for protein kinases: assay development and screening, libraries. WILEY-VCH. **2009**, p 3-39.

208) Kitagawa, D.; Yokota, K.; Gouda, M.; Narumi, Y.; Ohmoto, H.; Nishiwaki, E.; Akita, K.; Kirii, Y. Activity-based kinase profiling of approved tyrosine kinase inhibitors. *Genes Cells*. **2013**, 18, 110-122.

209) Acker, M. G.; Auld, D. S. Considerations for the design and reporting of enzyme assays in high-throughput screening applications. *Perspectives in Science.* **2014**, 1, 56-73.

210) Minor, L. K. Handbook of Assay Development in Drug Discovery. Taylor&Francis group. **2006**, first edition, p 83.

211) Copeland, R. A. Enzymes: A practical introduction to structure, mechanism and data analysis. Wiley-VCH, NY, 2nd Edition, **2000,** p 238.

212) Wu, G. Assay development: fundamentals and practices. John Wiley & Sons, 2nd Edition, **2010**, p 181.

213) Abel, U.; Deppe, H.; Feurer, A.; Graedler, U.; Goutopoulos, A.; Schwarz, M. 4-(Arylamino)pyridones as MEK1 inhibitors, their preparation, pharmaceutical compositions, and use in therapy. WO 2006056427 A1, June 1, 2006.

214) Shi, J.; Xu, G.; Zhu, W.; Ye, H.; Yang, S.; Luo, Y.; Han, J.; Yang, J.; Li, R.; Wei, Y.; Chen, L. Design and synthesis of 1,4,5,6-tetrahydropyrrolo[3,4-c]pyrazoles and pyrazolo[3,4-b]pyridines for Aurora-A kinase inhibitors. *Bioorg. Med. Chem. Lett.* **2010**, 20, 4273-4278.